TECHNISCHE UNIVERSITÄT WIEN
Vienna | Austria

PhD-Thesis

Dissertation

Onium Salts for Cationic Polymerization and Ring-opening Metathesis Polymerization

ausgeführt zum Zwecke der Erlangung
des akademischen Grades eines Doktors der technischen Wissenschaften

unter der Leitung von
Univ. Prof. Dipl.-Ing. Dr. techn. Robert Liska
und
Dipl.-Ing. Dr. techn. Patrick Knaack

Institut für Angewandte Synthesechemie

IAS
Institute of Applied Synthetic Chemistry

eingereicht an der Technischen Universität Wien
Fakultät für Technische Chemie

von
Dipl.-Ing. Roland Taschner, BSc
[redacted]
[redacted]

Wien, 13.01.2023

Dipl.-Ing. Roland Taschner

Danksagung

Zunächst möchte ich mich bei meinem Professor Robert für die Möglichkeit die Doktorarbeit in seiner Arbeitsgruppe durchführen zu können bedanken. Danke für die tolle Betreuung und alle Hilfestellungen! Deine Bürotür war stets für mich offen, egal ob die Arbeit im Labor mal gut oder schlecht gelaufen ist. Weiters möchte ich meinem Betreuer Patrick danken, der immer Zeit für mich und meine Anliegen hatte. Egal ob Arbeits- oder Privatleben, die Gespräche in deinem Büro waren immer interessant, spannend und unterhaltsam. Auch für die Gelegenheit auf vielen Konferenzen und Seminaren dabei sein zu dürfen möchte ich mich bei euch Beiden bedanken.

Außerdem möchte ich mich bei der gesamten Arbeitsgruppe Makromolekulare Chemie bedanken, die mich über die letzten 5 Jahre begleitet hat. Hierbei möchte ich mich bei meinen Univ.-Ass. Kollegen für die tolle Zeit in den Laboren bedanken. Auch möchte ich meinem Bench-Buddy Toni danke sagen, die immer mit gutem Rat und meinungsverstärkenden Utensilien zur stelle war, falls mal wieder jemand den Abzug beim flüssigen Abfall nicht fachgerecht verschlossen hat #SpaceBench! Auch ohne euch, Carola und Klausi wäre meine Arbeit an der Universität nur halb so lustig gewesen. Viele unterhaltsame Stunden habe ich bei euch in der Bench verbracht. Die Themen reichten von Laborarbeit über Wochenendpläne bis hin zu dem neuesten Klatsch und Tratsch. Sobald man angefangen hat sich über brisante Themen zu unterhalten, war auch Tina schnell zur Stelle um ihre Meinung kundzutun. Die politische Korrektheit wurde hierbei natürlich immer stets gewahrt, so wie man das vom H45 auch erwartet. Das beste Konzept das ich in unserem Labor recht erfolgreich implementieren konnte, war der schon eine Woche vorher geplante, gehypte und allseits bekannte Sushi-Friday. Den Jo haben wir aber bis heute noch nicht finden können..

Besonderer Dank gilt meinem Schulchemielehrer Professor Herbert Lang! Er hat mein Interesse an der Chemie geweckt und die Stunden sowie Module immer interessant gestaltet. Ganz besonderer Dank gilt meiner Partnerin Betti, die immer für mich da war! Und meiner ganzen Familie, besonders meinen Eltern. Ihr habt mich immer bedingungslos unterstützt und gefördert. Ohne euch 3 wäre ich nicht da, wo ich mich heute befinde!

DANKE!

ABSTRACT

3D-printing and frontal polymerization are two hot topics with a seemingly endless variety of applications. For both highly specialized technologies, cationic polymerization represents a powerful tool to produce a broad field of materials starting from various monomers. Epoxides are frequently used since this monomer class provides great adhesion to most materials, high resistance towards chemicals and well-defined material properties. Iodonium perfluorinated antimonates and tetraphenylborates are the most widespread class of photoinitiators used in frontal polymerization applications, while sulfonium equivalents excel in 3D-printing applications due to their enhanced thermal stability.

Within the *first part* of this thesis, atoms from group 14 to 16 in the periodic table of elements were explored as *novel cations in onium-based photoinitiators* since the introduction of a positive charge and the resulting transformation into onium salts is well researched and many classes are easily accessible. Using commercial epoxy resins, thiopyrylium-, bismuthonium-, and pyrylium salts show good reactivity and high epoxy group conversions in classical cationic photopolymerization. On the other hand, the introduction of bismuth- and oxygen-based onium salts, new potent initiator candidates arise for frontal polymerization. The advantage of bismuthonium-based systems is the outstanding pot life of the formulations, which can be cured at the press of a button via frontal polymerization.

The *second part* focuses on the exploration of *novel anions in onium-based photoinitiations*. Extensive research in the fields of ionic liquids and lithium ion battery electrolytes, made many borate-based superacids available. Cyanide-ligated boranes are of special interest due to lower molecular weight compared to state-of-the-art borates and less expensive commercial starting materials. The new borates outperform all commercial systems in a broad range of temperatures with excellent epoxy group conversions. The cyanide-ligated borane is exceptionally suited for frontal applications and produces transparent specimens in contrast to the tested commercial systems, which are black. Easy synthetic access, sufficient pot life of formulations, high reactivity and good frontal parameters make cyanide-ligated iodonium borates a compelling alternative to current state-of-the-art initiators.

Within the *third part* of this work, *ring-opening metathesis polymerization* ROMP and its potent curing process incorporating metal-based initiators is challenged. With a continuing shift away from heavy metals in material production, pyrylium salts are a compelling

alternative for metal-free ROMP. After modification of the state-of-the-art pyrylium photoredox mediators for ROMP, novel and highly efficient systems are obtained. The resulting alkoxylated pyrylium hexafluorophosphates show exceptional performance in metal-free ROMP of norbornene in solution achieving 98% conversion, high molecular weight and narrow polydispersities.

KURZFASSUNG

3D-Druck und Frontalpolymerisation sind zwei hochaktuelle Themen in Industrie und Wissenschaft mit schier endloser Anwendungsvielfalt. Für beide spezialisierten Technologien stellt die kationische Polymerisation ein leistungsfähiges Werkzeug dar, um ausgehend von verschiedenen Monomeren ein breites Feld von Materialien herzustellen. Epoxide werden häufig verwendet, da diese Monomerklasse eine gute Haftung auf den meisten Materialien, eine hohe Beständigkeit gegen Chemikalien und definierte Materialeigenschaften bietet. Iodoniumperfluorierte Antimonate und Tetraphenylborate sind die am weitesten verbreitete Klasse von Photoinitiatoren, die in Frontalpolymerisation verwendet werden, während die Sulfonium-Äquivalente aufgrund hoher thermischen Stabilität in 3D-Druckanwendungen hervorstechen.

Im *ersten Teil* dieser Arbeit wurden Atome aus den Gruppen 14 bis 16 des Periodensystems der Elemente als neuartige *Kationen in Onium-basierten Photoinitiatoren* untersucht, da die Einführung einer positiven Ladung und die daraus resultierende Umwandlung in Oniumsalze gut erforscht ist, viele Klassen umfasst und diese leicht zugänglich sind. Unter Verwendung handelsüblicher Epoxidharze zeigen Thiopyrylium-, Bismutonium- und Pyryliumsalze eine gute Reaktivität und hohen Epoxidgruppenumsatz in der klassischen kationischen Photopolymerisation. Andererseits ergeben sich durch die Einführung von Bismut- und Sauerstoff-basierten Oniumsalzen neue vielversprechende Initiatorkandidaten für die Frontalpolymerisation. Der Vorteil Bismuthonium-basierter Systeme liegt in der hervorragenden Lagerstabilität der Formulierungen, die per Frontalpolymerisation auf Knopfdruck ausgehärtet werden können.

Der *zweite Teil* konzentriert sich auf die Erforschung neuartiger *Anionen in Onium-basierten Photoinitiationen*. Umfangreiche Forschungen in den Bereichen ionische Flüssigkeiten und Elektrolyte für Lithium-Ionen-Batterien machten viele boratbasierte Supersäuren zugänglich. Cyanid-ligierte Borane sind von besonderem Interesse aufgrund des niedrigeren Molekulargewichts im Vergleich zu modernen Boraten und weniger teuren, kommerziellen Ausgangsmaterialien. Die neuen Borate übertreffen alle kommerziellen Systeme in einem breiten Temperaturbereich mit hervorragenden Epoxidgruppenumsätzen. Das Cyanid-ligierte Boran eignet sich hervorragend für frontale Anwendungen und ergibt transparente Proben im Gegensatz zu den getesteten kommerziellen Systemen, die schwarze Proben produzieren.

Einfacher synthetischer Zugang, ausreichende Lagerstabilität der Formulierungen, hohe Reaktivität und gute Frontalparameter machen Cyanid-ligierte Iodoniumborate zu einer überzeugenden Alternative zu aktuellen State-of-the-Art-Initiatoren.

Im *dritten Teil* dieser Arbeit wird die *ringöffnende Metathesepolymerisation* ROMP und ihr effizienter Härtungsprozess unter Anwendung metallbasierter Initiatoren herausgefordert. Mit einer anhaltenden Abkehr von Schwermetallen in der Materialherstellung sind Pyryliumsalze eine überzeugende Alternative für metallfreie ROMP. Nach Modifikation der aktuellsten Pyrylium-Photoredox-Mediatoren für ROMP werden neuartige und hocheffiziente Systeme erhalten. Die resultierenden alkoxylierten Pyryliumhexafluorphosphate zeigen eine außergewöhnliche Effizienz bei der metallfreien ROMP von Norbornen in Lösung, wobei ein Umsatz von 98 %, ein hohes Molekulargewicht und enge Polydispersitäten erreicht werden.

TABLE OF CONTENTS

×

INTRODUCTION

Photopolymerization

In photopolymerization, a liquid formulation of monomer(s) together with a photoinitiator is transformed into a solid polymer material by electromagnetic irradiation. In general, the emitted light ranges from ultraviolet light into the range of near infrared light. In addition to the most commonly utilized light spectra, different approaches based on plasma, X-rays, gamma-rays, microwaves or even electron beams can be applied to cure the liquid formulation.[1] This modern technique of monomer curing provides high energy efficiency, solvent-free formulations and low cost due to rapid through cure and usually relatively simple irradiation source equipment.[2] Since the penetration of light is directly proportional to its wavelength, thin layer applications are targeted most frequently. Hence, photopolymerization remains the perfect solution for the protective- and decorative coatings industry where thin layers need to be hardened fast, efficient and affordable. Enabling coatings consisting of a nearly endless selection of monomers on most substrates such as wood, ceramic, metal, paper or polymer materials.

Most commonly, radical or cationic photopolymerization is selected as curing mechanism for a variety of applications across a broad sector of industries. Optics, adhesives or electronics are only a few examples where photopolymerization plays a major role.[3] Beyond these nowadays fairly standard applications, more advanced use cases depend on the unique properties of photopolymerization. Research- and economic interest in dental fillings, additive manufacturing technologies and frontal polymerization is growing fast.[3, 4] Enabling long-lasting, white fillings, personalized or prototype material production and overcoming the penetration depth issues connected to classic photopolymerization. With an ever growing field of applications, photopolymerization techniques and frequent improvements on existing ones provide academia and industry with a stream of novel solutions.

Additive Manufacturing Technologies

Since the introduction of additive manufacturing technologies (AMT) in the 1980s, they greatly impacted the classic manufacturing industry by a novel approach towards building parts.[5] Describing additive manufacturing technologies with the term 3D-printing has seen a rise in popularity and is in use across many industries as well as the private sector and media.[3] AMT are based on a selective layer-by-layer approach and by stacking all the layers, producing the desired part according to a computer-generated 3-dimensional model (Figure 1). The 3D-model is created by computer-aided design (CAD) and virtually sliced into layers of a set thickness.

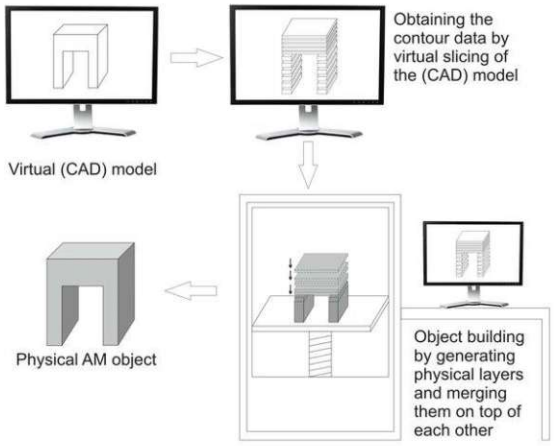

Figure 1: From virtual CAD model to physical part by AMT[6]

AMT with their layer-by-layer approach show high contrast to much older, classic manufacturing techniques. Subtractive manufacturing such as CNC milling removes selectively material from a bulk part to result in the targeted geometry. Formative manufacturing like bending, casting or forging alters the shape of a part without a change in volume. Therefore, AM enables the production of highly complex parts, while no material is wasted. Prototyping is especially interesting since no new casts or tools are needed for AM, making the process economically and ecologically favorable.[3, 5] The main drawback of AM is relatively low throughput of 3D-printing if production has to be scaled up. Therefore, individualized products, low batch sizes and highly complex parts are the main benefits of 3D-printing. Accessible to AMT are a broad range of materials, for example metals, ceramics or polymers. Polymer-based additive manufacturing represents the biggest sector with around half of the total AMT market.[7]

Considering polymer 3D-printing, two main methods of material processing are available. The first process is based on filaments or powders as inputs. The material melts and is deposited

onto a building platform layer-by-layer. The so-called fused deposition modeling (FDM) therefore works similar to an extruder and already polymeric, thermoplastic input material is necessary. The second process is fundamentally different since no polymer starting material is needed. Namely lithography-based AMT generate the polymer in situ upon irradiation with light. This technique allows for much smoother surface finishes as well as outstanding precision compared to filament- of powder-based processes.[8]

Lithography-based Additive Manufacturing Technologies

Lithography-based additive manufacturing is based on an initially liquid photopolymerizable resin in a vat, which is locally crosslinked via light. This curing process is carried out in very thin layers sometimes a few micrometers in thickness. To produce a material, all layers stack up to form the final part.[3] First, a monomer together with the printing process has to be selected. This choice highly depends on the monomer's properties such as viscosity, volatility, reactivity or functionality.[9] Lithography-based additive manufacturing technologies are defined by the type of irradiation, either digital light processing (DLP) or stereolithography (SLA). The portfolio of printable materials is mainly limited to (meth)acrylate- and epoxy-based monomers, often leading to brittle parts due to high crosslinking density.[3, 5] Therefore, the major aim of lithography-based additive manufacturing remains the production of materials with comparable thermomechanical properties compared to conventionally produced ones.[10]

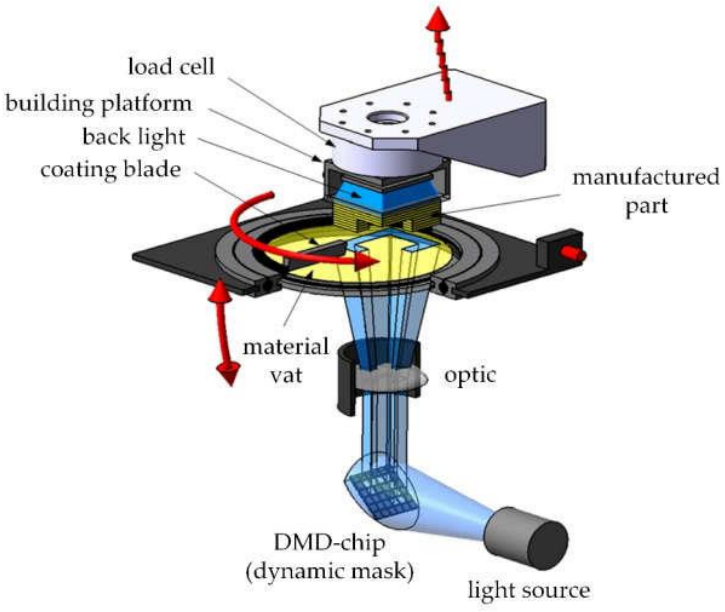

Figure 2: Scheme of a digital light processing 3D-printer[11]

DLP technology was introduced in the 1990s and uses a light source based on LEDs in combination with a digital micromirror device (DMD) chip to expose one resin layer after another to the LED light, subsequently polymerizing the resin into a part (Figure 2).[12] While irradiation takes place, the building platform moves up and a fresh layer of resin from the material vat is applied via the coating blade. Advantages of the DLP process are short build times due to the irradiation of the whole fresh layer of resin at a time. However, DLP suffers from lower lateral resolution of around 10-50 µm since the number of mirrors and subsequently pixels in the DMD chip cannot infinitely be miniaturized.[2]

Figure 3: Scheme of a stereolithography 3D-printer[13]

SLA printers manufacture a part by scanning a laser beam within a plane of the resin tank. The laser is typically emitting UV-light to enable photopolymerization. Guidance of the laser beam is achieved by tilting galvanometers which guide the focused light source across a x-y-dimensions. The layer-by-layer-built part is then together with the build platform, moved either up or down along the z-axis, depending on the printer setup. Standard SLA printers carry out subsequent layer formation via the laser light source from on top of the resin vat (top-down).[3] So-called inverted SLA printers (Figure 3) irradiate the resin from below the resin vat to eliminate possible oxygen inhibition by pulling the part out of the resin tank (bottom-up).[14, 15] Stereolithography is much slower compared to DLP, however the outstanding resolution of a few micrometers makes SLA one of the most used additive manufacturing techniques.[3, 5]

Hot Lithography

Standard lithography-based additive manufacturing technologies described in advance are often limited by the viscosity of the applied resins or suffer from poor reactivity of some monomer classes at room temperature. Both drawbacks can be eliminated by the introduction of hot lithography. Developed by "Cubicure GmbH", this process combines SLA with elevated temperatures. A heated resin reservoir enables hot lithography-based 3D-printers to produce very thin layers from highly viscous resins (Figure 4). Similar to the standard SLA technique, a UV-laser is used to cure the layers locally by scanning across the x-y-dimensions. As soon as a layer is completed, the building platform moves out of the way in z-axis, to make space for peeler and blade (coating unit). The coating unit applies a new layer of resin onto a glass plate, the building platform moves down and the resin is cured again in a bottom-up process.[16, 17] A limit for resin viscosity is in the range of 20 Pa s, rendering the technology much more versatile compared to 1 Pa s for standard lithography-based additive manufacturing.[18]

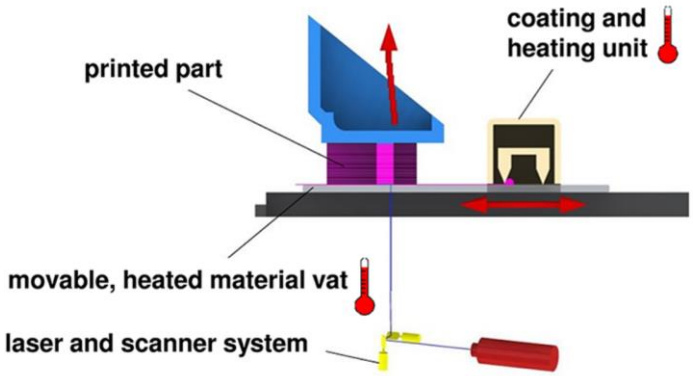

Figure 4: Scheme of hot lithography[19]

An advantageous side effect of increased temperatures, is high resin mobility on a molecular level. Printing speeds can be increased significantly in hot lithography to finally result in lower production times and more output. However, hot lithography is not well suited for classic radical polymerization since for example (meth)acrylate-based formulations suffer from thermal stability issues at 140 °C. To circumvent the thermal stability problem, cationic polymerization is introduced with a broad range of highly stable monomers.

Frontal Polymerization

Whenever a polymerization reaction occurs directionally with a local reactive zone, the term frontal polymerization (FP) is used. The local reactive zone or front propagates through the curable material. There are three types of frontal polymerization. First, a front which

propagates due to the continuing flux of radiation, for example UV photons. The second type describes a front, where the gel effect is used to produce the local reaction zone. Starting from the polymer seed, the reaction zone continuously propagates to form more polymer over time. The last type is thermal FP, where the front is driven by a combination of the temperature dependent reaction rate during an exothermic polymerization reaction and thermal diffusion.[20] Since the third type shows the greatest potential and compatibility in combination with the previously described onium salts, the focus stays on thermal frontal polymerization.

Thermal Frontal Polymerization

The benefits of thermal frontal polymerization applied in high pressure methacrylate systems were first described by Chechilo et al.[21] The classical thermal FP is highly dependent on the reaction heat generated from the exothermic polymerization of monomers. The more reactive a moiety of a monomer, the more heat of polymerization is liberated during the process. In the presence of a thermal radical initiator, the exothermic nature of the polymerization results in the cleavage of this initiator. This process can be highly localized while propagating through the monomer, therefore forming the reaction front. Due to the nature of the thermal FP, even the curing of complex parts is possible. Structures, where for example UV light cannot reach the resin, FP is a versatile option. If non-sufficient exothermicity is generated during the polymerization reaction, there is not enough heat available to cleave the thermal radical initiator, which leads to termination of the front. In the best-case scenario, a front comes to a still stand due to the complete consumption of available monomer.

Of great importance is the stability of the thermal initiator at ambient or storage temperatures of the resin. However, the reaction rate at frontal temperatures needs to be very high, to ensure a sustainably high heat release.

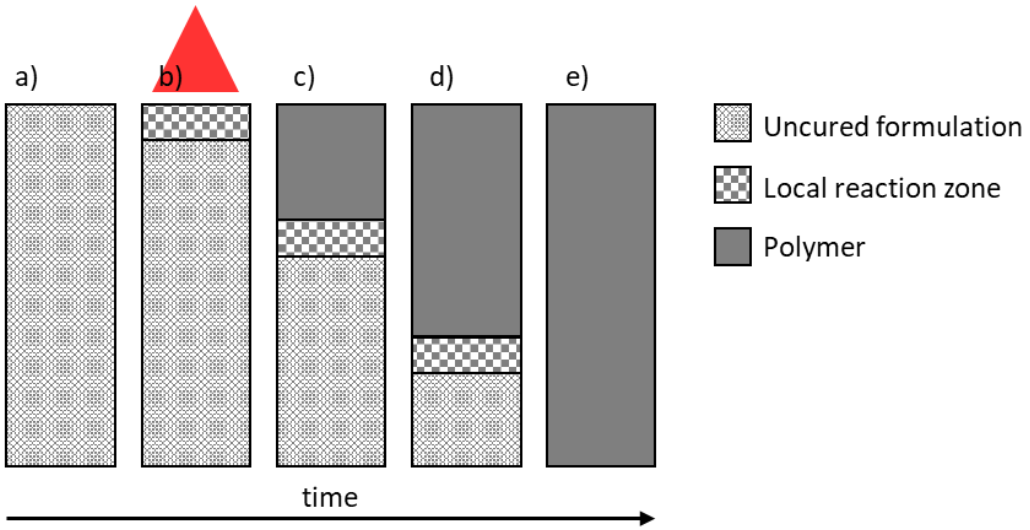

Figure 5: Schematic pathway of a thermal frontal polymerization over time

Uncured resin which contains the thermal initiator is prepared in a mold (Figure 5a). By direct heat input, the localized reaction zone is formed at the top of the mold (b). This initiation process decomposes the initiator, followed by the exothermic polymerization reaction. If the FP is sustainable, the liberated heat during the polymerization cleaves more initiator and the initiation process starts again. It is worth mentioning, that the thermal source can be removed at this point and is no longer necessary to sustain the front. Over time the front is propagating through the material, leaving cured polymer behind (c, d). Eventually, the front moves through all available material and a cured part is formed (e).

There are various different categories besides the free-radical FP[22], like atomic transfer radical polymerization (ATRP) FP[23] or ring-opening metathesis polymerization (ROMP) FP.[24] The epoxy-based FP usually results in very similar mechanical properties compared to batch-cured polymers.[25] However, a major drawback of thermal FP is the short storage stability of the formulations in the range of only a few hours. By investigating the concentration dependence of the initiator compared to the moving speed of the reactive zone in catatonically polymerizable monomers, it was found that an increase of initiator results in a faster frontal velocity as well as increased frontal temperature. However, by using a thermo-labile BF_3-amine complex the pot life of the formulations could not exceed four hours and a rather slow reaction speed.[26] A combination of thermal FP and cationic photopolymerization is very practical due to the elimination of the short storage stability problem of the formulations. Therefore, radical induced cationic FP with onium salts is a promising approach to circumvent the stability issue.[27]

Cationic Polymerization

A variety of different monomers can be polymerized cationically. They all share the property of an electron-donating group, which enables the electrophilic addition of the initiating cation. Examples for such cationically polymerizable monomers are heterocyclic and unsaturated molecules (Figure 6).

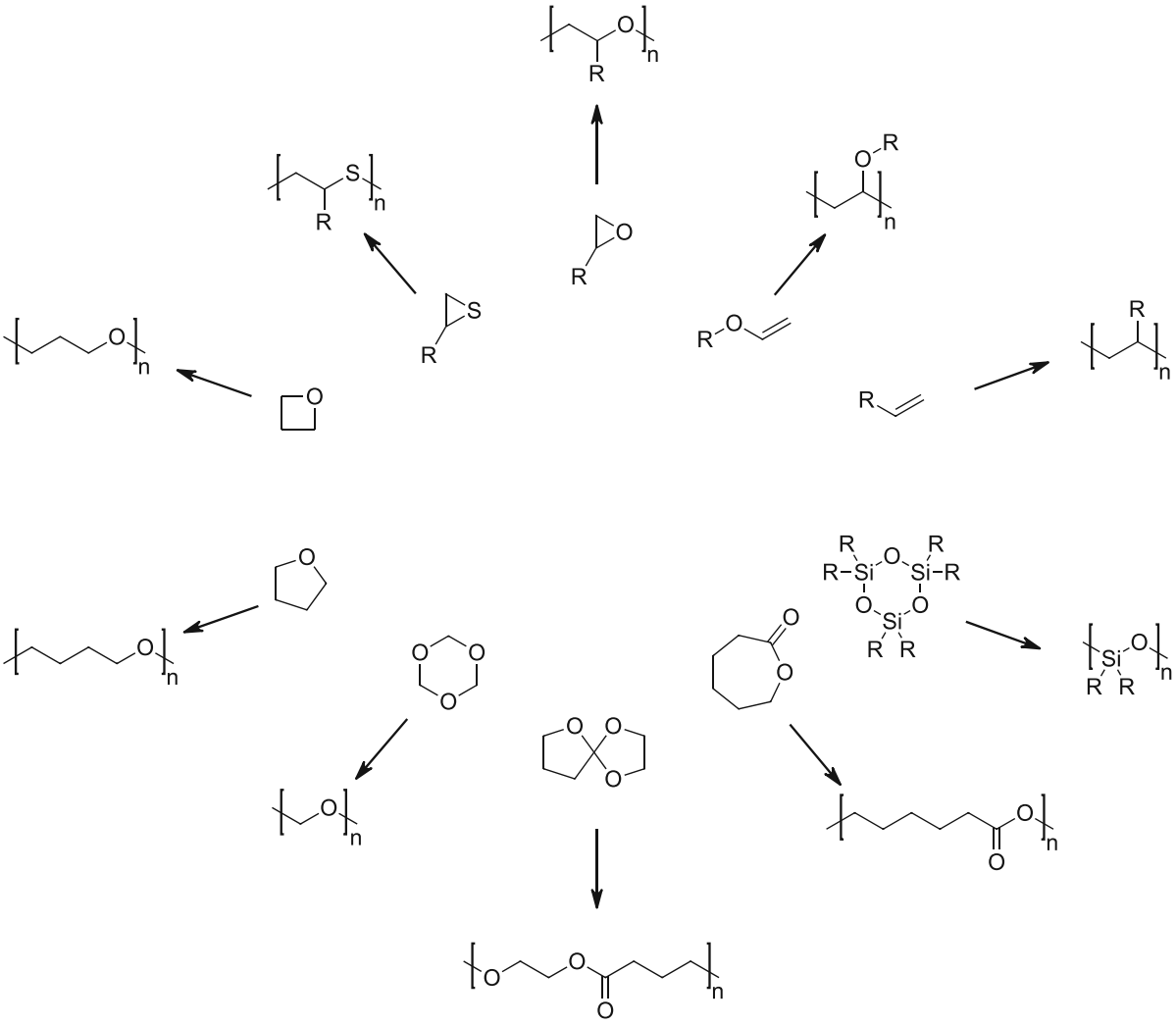

Figure 6: Monomers suitable for cationic polymerization[28]

Cationic polymerization undergoes a chain growth mechanism and consists out of five main steps. Initiation, start of the propagation reaction, propagation, chain transfer and termination. To start a cationic polymerization, a strong Brønsted or Lewis acid is necessary. These acids provide the proton or carbocation for the initiation step of the reaction. In most applications, epoxides and vinyl monomers are in use. Especially the epoxy monomers are capable of achieving material properties unlike radically polymerized resins, such as excellent adhesion and resistance against many chemicals, which is required in inks, films, coatings and

adhesives.[29] Cationic polymerization mechanism of commonly used epoxy monomers is shown in Figure 7.

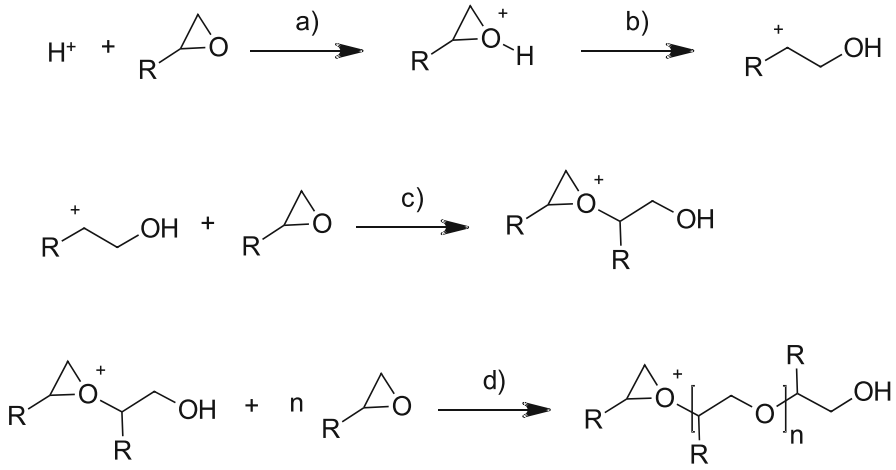

Figure 7: Cationic polymerization of an epoxy monomer

The initiation of the cationic polymerization is an exclusively thermally driven process, therefore are the kinetics highly temperature dependent and can be described as discrete steps with monomer specific, kinetic rate constants.[29] In the first step, the reaction is initiated by a strong protonic acid and the formation of a secondary oxonium cation takes place (a). Due to the instability of secondary oxonium cations, the intermediate performs an intramolecular proton shift, generating a highly reactive species, the carbocation (b). The nucleophilic epoxide monomers are now capable of S_N2 attack the carbocation, undergo a ring opening reaction and producing a tertiary oxonium cation (c). In the last step, the polymerization reaction propagates at the terminal oxonium moiety until no monomer is left or termination occurs (d).[30] The resulting molecule is a polyether, originated out of ring opened epoxides.

Cationic polymerization shows one major advantage compared to classic radical polymerization. The propagating, cationic polymer chains are not affected by oxygen inhibition in any way, therefore an inert atmosphere is not necessary during the curing process.[1] In addition, many cationic monomers are considered non-cytotoxic in contrast to acrylates for example.[31] Once the initiation reaction has taken place, there are almost no termination reactions during polymerization, which ensures high efficiency and conversion.

Even in the absence of light, the previously initiated reaction keeps polymerizing in the material due to the long-living protonic acid. The thermally promoted cationic polymerization reaction after the photoacid was generated, leads to further propagation without additional irradiation. This post-curing behavior, the so-called “dark reaction” ensures maximum

conversion of the monomer, with short irradiation times.[32, 33] Additionally, there are no recombination reactions of propagating polymer chains, like in radical polymerization, due to the natural occurring repellent force of two cations.[31]

Cationic polymerization is sensitive towards bases and functional groups, such as amines and urethanes. Additionally, thiols inhibit the propagation reaction since the protonated epoxy group adds to the thiol forming an unreactive sulfide.[34] Basic pigments, substrates or fillers can terminate the polymerization. Water and alcohols act as chain transfer agents during the chain growth reaction, therefore reducing the molecular weight of the macromolecules in the material (Figure 8). The generated protons are capable of initiating the cationic polymerization again.

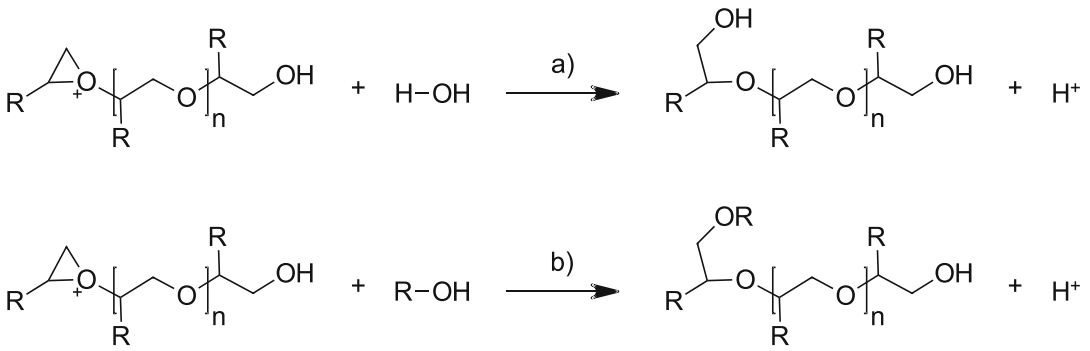

Figure 8: Chain transfer reaction with protic regulators (a) water and (b) alcohols

The cationic species are not inactivated after the curing procedure, hence acidic residuals of the cationic initiator still remain in the final product.[35]

Advantages and drawbacks of cationic photopolymerization are summarized in Table 1.[29, 35]

Table 1: Advantages and disadvantages of cationic photopolymerization

+ high reaction rates	- inhibition by bases
+ insensitive to oxygen inhibition	- inhibition by amines and urethanes
+ dark curing	- acid remains in product
+ no solvent necessary	- chain transfer by water and alcohols
+ variety of polymerizable monomers	
+ different backbone structures	

Photoacid Generators for Cationic Photopolymerization

During cationic photopolymerization, most likely a UV-photon is absorbed by the cationic initiator, forming the ion, which is capable of starting the polymerization reaction.[29] For simplicity, a cationic initiator activated via photon, is described as photoacid generator (PAG).

Ideal PAG for cationic polymerization require chromophores to absorb light of a specific wavelength in high quantum yields, in combination with the creation of the photoacid. Thermal stability in the dark to ensure long term storage and of course compatibility to the aimed system, as well as easy synthesis and a low price.[1, 35]

There are also non-ionic photoacid generators like organosilanes, latent sulfonic acids and onium salts. The last mentioned are of highest interest, due to efficient photodecomposition, high stability and easy synthetic access.[35, 36]

Onium salts consist of two ions with clearly separated roles, when it comes to absorption, stability or initiation efficiency properties (Table 2). The cation represents the chromophore and determines all photochemistry related properties. The anion affects the strength of the generated photoacid, therefore initiation efficiency and all polymer chemistry related properties.[37]

Table 2: Roles of cation and anion in onium salts[37]

Cation (photochemistry)	Anion (polymer chemistry)
absorption maximum	acid strength
molar absorption coefficient	nucleophilicity
quantum yield	initiation efficiency
thermal stability	propagation rate constant

Besides onium salts, there are organometallic photoinitiators used for a major part of cationic polymerization applications. For example ferrocenium salts are commonly used as photoacid generators.[38] They create Lewis acids for the initiation process, but due to their coordination to the monomer to the central atom, only specific types can be used with these initiators. In addition, the solubility of ferrocenium salts is limited strongly.

Onium Cations

As mentioned, onium salts are based on the synergistic concept of cation and anion to establish well photoinitiating components. The cations, representing the photochemistry properties of the salt, are the chromophore and a variety of them has been investigated over the years. Such as aryldiazonium, diaryliodonium, triarylsulfonium, triarylselenonium, dialkylphenacylsulfonium and triarylsulfoxonium cations.[35] The first efficient photoacid generators were aryldiazonium salts for cationic polymerization (Figure 9).[39]

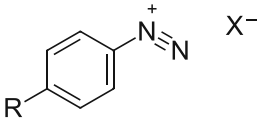

Figure 9: General structure of aryldiazonium salts

Disadvantages of these aryldiazonium salts are crucial, like insufficient thermal stability. Therefore, those salts are less storage stable and release nitrogen gas during the curing process. Also discolored products, potential interaction with pigments or fillers and the risk of explosion exclude this class of salts for the use as safe and stable cationic initiator.[1, 35]

Commonly used in industry are the onium salts, containing diaryliodonium and triarylsulfonium as cations (Figure 10). They are efficient, stable photoacid generators and without extensive effort to prepare. The inventor of those compounds was Crivello et al. in the 1970s.[36, 37, 40]

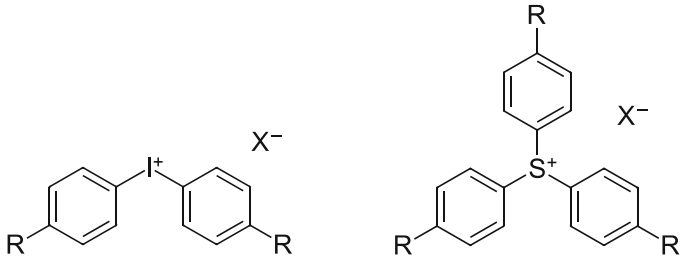

Figure 10: General structure of diaryliodonium and triarylsulfonium salts

To prepare the diaryliodonium salts, there are two general reaction routes. One for symmetrical and one for asymmetrical compounds.[36, 41] The formation of symmetrical diaryliodonium salt is induced by reacting the aromatic precursor with potassium iodate, sulfuric acid and acetic anhydride. The asymmetrical compounds are synthesized by reacting aryliodoso precursors with an aromatic compound in the presence of an acid. Some diaryliodonium salts, for example the chlorides, are commercially available and therefore directly used for an ion exchange reaction. The negative charged counterions are readily swapped via salt metathesis to give the desired colorless, stable and easy to purify product.

Triarylsulfonium salts are the second type of promising onium compounds discovered and synthesized by Crivello et al.[40] This group of onium salts is known for its uncomplicated preparation, excellent thermal and photochemical properties. Sulfonium-based salts are prepared via Friedel-Crafts reaction with benzene as starting material and sulfur monochloride, aluminum chloride and chloride as reagents. This reaction route provides differently substituted sulfonium derivatives.[42, 43] A second route leading towards high yields and additionally asymmetrical triarylsulfonium salts is the copper(II)-catalyzed reaction of diarylsulphides with diaryliodonium salts.[40, 44]

The cations photochemical reaction is determined by its ability to absorb a photon by its chromophore, leading to an excited state of the molecule. By transition from the excited state to the ground state, photoproducts are generated. These initiating decomposition products can only be created directly with the irradiation of UV-light, due to its nature being a high energy radiation source. High energy photons break bonds in the cation, followed by hydrogen abstraction from the Brønsted acid, which is responsible for the cationic initiation process.[35]

Quantum yield determines the efficiency of the initiation process. It describes the ratio of the number of molecules reacting to the number of photons absorbed by the system. The quantum yield of decomposition (Equation 1) defines excited states, that lead to decomposition reactions in ratio to absorbed photons, whereas the quantum yield of the formation of initiating species (Equation 2) describes the number of initiating species created by a certain number of photons. The overall quantum yield of photopolymerization (Equation 3) is determined by the ratio of monomers polymerized to the number of photons absorbed.[35] For photoacid generators like onium salts, the quantum yield is defined by photolysis reaction, which leads to the formation of a photoacid, compared to number of photons absorbed.

Equation 1: Quantum yield of decomposition[35]

$$\Phi_{dec} = \frac{Number\ of\ reactions\ producing\ initiating\ species}{Number\ of\ quanta\ absorbed}$$

Equation 2: Quantum yield of the formation of initiating species[35]

$$\Phi_{in} = \frac{Number\ of\ reactions\ leading\ to\ decomposition}{Number\ of\ quanta\ absorbed}$$

Equation 3: Quantum yield of photopolymerization[35]

$$\Phi_{poly} = \frac{Number\ of\ monomers\ polymerizing}{Number\ of\ quanta\ absorbed}$$

The mechanism of the photochemical excitement via UV-light of the photoacid generator, followed by homolytic or heterolytic cleavage of the carbon-heteroatom bond is illustrated for a diphenyliodonium salt in Figure 11.

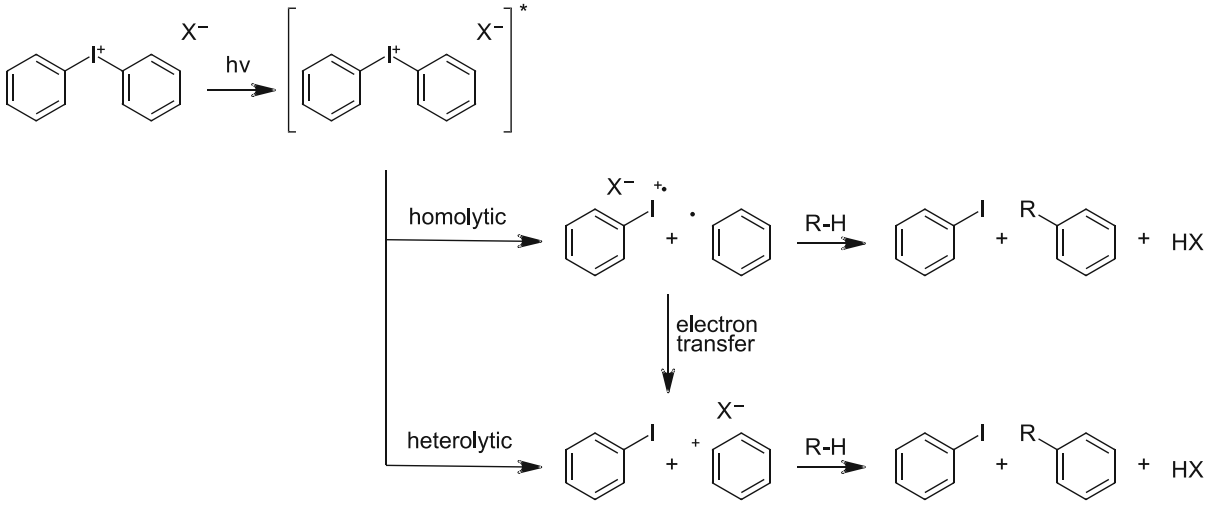

Figure 11: Photochemical decomposition of the photoacid generator (diphenyl iodonium salt)[45]

Irradiation with UV-light leads to absorption of photons by the chromophore of the photoacid generator. This leads to excitement of the molecule towards its singlet state. From there on, the decomposition can happen homolytically or heterolytically.[45] During this cleavage, various products like radical-cations, radicals, cations and arylhalides are formed. If the cleavage occurs homolytically, there is the possibility to convert the decomposition products to the heterolytically ones via electron transfer. In the last step the radical, formed in the homolytic pathway, performs a hydrogen abstraction from the monomer or possibly the solvent to form the Brønsted acid (HX) and a neutral aryl species. In the case of heterolytic cleavage, the phenyl cation performs an electrophilic attack on the monomer or solvent, forming the Brønsted acid (HX) and a neutral aryl species again. The Brønsted acid is in both cases the essential species, capable of initiating the cationic polymerization.[30, 37]

Perfluorometallate Anions

After the Brønsted acid formed, the anion defines the polymer chemistry. The essential requirement for those anions is non-nucleophilicity, therefore a well masked charge towards its environment. Considering the acid catalyzed mechanism of cationic polymerization (Figure 7), the stronger the formed acids, the more efficient the initiation process occurs. Due to this fact, the strongest acids are desired. If an acid, is stronger compared to 100% sulfuric acid, it is defined as superacid.[46] To measure the strength of those superacids, the pH-value is not

suitable due to the need of aqueous environment. Therefore, the Hammett acidity is introduced for such superacids (Equation 4).

Equation 4: Hammett acidity calculation

$$H_0 = pK_{BH^+} - log\frac{[BH^+]}{[B]}$$

H_0…Hammett acidity [ ]
pK_{BH^+}…acid dissociation constant [ ]
[BH^+]…concentration of the conjugated acid [mol L^{-1}]
[B]…concentration of the base [mol L^{-1}]

Given dissociation constant of the conjugated acid and the logarithmic ionization ratio, the Hammett acidity can be calculated. With exemplary values for sulfuric acid and the combination of HF and BF_3 ($HF + BF_3 \rightleftharpoons BF_4^-$) represented in a table inspired by Gurney (Table 3).[47] Therefore, perfluorometallates are of high interest as anions, due to their acid strength. Highly interesting are therefore acidities between -15 and -30 to initiate the cationic polymerization as efficient as possible.[48]

Table 3: Selection of Hammett superacids and their corresponding acidity including literature

Compound	**H_0 [ ] & Lit.**		**Compound**	**H_0 [ ] & Lit.**	
$HAlCl_4$	-24.5	[49]	HSO_3CF_3	-14.1	[50]
$HSbF_6$	-23.6	[51]	$HSO_3C_2F_5$	-14.0	[52]
HBF_4	-22.7	[51]	$HSO_3C_4F_9$	-13.2	[52]
$HN(SO_3CF_3)_2$	-19.0	[51]	$HSO_3C_6F_{13}$	-12.3	[52]
$HClO_4$	-16.1	[51]	HSO_3Cl	-13.8	[50]
HSO_3F	-15.1	[51]	H_2SO_4	-12.0	[51]
HF	-15.1	[50]	HCl	-11.2	[51]

The Hammett superacidity scale relies such as classic Brønsted acids on H^+ protons to determine a value experimentally. However, a different approach has to be made for Lewis superacids. Fluoride ions exhibit high basicity and basically react with all Lewis acids which makes them a suitable reference for further considerations. Due to fluoride ions small size, steric effects are negligible. Fluoride ion affinity (FIA) is defined as the binding enthalpy of the ion with a Lewis acid in the gas phase (Equation 5).[53] Due to its exothermic behavior, the FIA exhibits a negative value. However, they are usually converted into positive values in literature.

Equation 5: Schematic reaction of the Lewis acid with the fluoride ion

$$LA + F^- \xrightarrow{FIA} [LA - F]^-$$

LA…Lewis acid [ ]
F^-…Fluoride ion [ ]
FIA…Fluoride ion affinity [kJ mol^{-1}]

FIA is pretty elaborate to determine experimentally, thus computational methods are usually applied.[54] Therefore, the shortcomings of FIA are the scattered range of values due to different calculation methods and a neglection of solvation effects which lower the theoretically calculated FIA values.[55] In addition to a collection of calculated, inverted FIA values (Table 4), a more extensive table was published by Greb et al. including modeling of the FIA-lowering effects of solvation.[55]

Table 4: Selection of Lewis superacids and their corresponding FIA(-1) including literature*

Compound	**FIA [kJ mol^{-1}] & Lit.**		**Compound**	**FIA [kJ mol^{-1}] & Lit.**	
$As(OTeF_5)_5$	593	[56]	$Al(SO_3CF_3)_3$	474	[54]
$P(SO_3CF_3)_5$	557	[55]	$Ga(N(C_6F_5)_2)_3$	472	[57]
$B(CF_3)_3$	556	[58]	$B_2(C_6F_5)_2(C_6F_4)_2$	471	[56]
$Al(OTeF_5)_3$	552	[54]	$B(C_6H_3(CF_3)_2)_3$	471	[56]
$B(OTeF_5)_3$	552	[58]	$B(C_{10}F_7)_3$	469	[59]
$Al(OC(CF_3)_3)_3$	543	[58]	$P(OC(CF_3)_3)_5$	453	[55]
$Al(OR^F)$	537	[56]	$B(C_6F_5)_3$	452	[58]
$Al(C_6F_5)_3$	536	[58]	$B(C_{12}F_9)_3$	447	[59]
$B(SO_3CF_3)_3$	530	[54]	AsF_5	426	[56]
$Al(C_6F_5)_3$	530	[59]	$B(OC_6F_5)_3$	419	[55]
$1,2\text{-}((C_6F_5)_2B)_2C_6F_4$	510	[56]	PF_5	394	[56]
$B(p\text{-}CF_3\text{-}C_6F_4)_3$	499	[60]	BF_3	338	[56]
SbF_5	489	[56]	$P(OC(CF_3)_3)_3$	319	[55]

For example, SbF_6^-, AsF_6^-, PF_6^- or BF_4^- are commonly used counter ions for oxonium cations.[37] Their Hammett acidity inversely depends on the nucleophilicity of the anion. Low nucleophilicity is desired for the initiation and propagation reaction. In an ideal system, the interaction of the propagating cation and the anion would be negligible. Therefore a low nucleophilicity is directly related to a high rate of polymerization.[29]

If the same photoinitiating cation was used for these different counter ions, the amount of correlating superacid produced would be the same. But despite this fact, the acid strength and rate of polymerization is strongly determined by the anion used for the superacid generation. The reactivity of the used system corresponds to the degree of separation of the cationic polymer chain and the anion, as well as the stability of the anion itself. A fluoride abstraction for example would lead to the Lewis acid BF_3, therefore quenching the cationic polymerization (Figure 12a). The second termination reaction occurs, if a base is present in the formulation. For example, chloride anions act as strong bases due to their high nucleophilicity (Figure 12b).

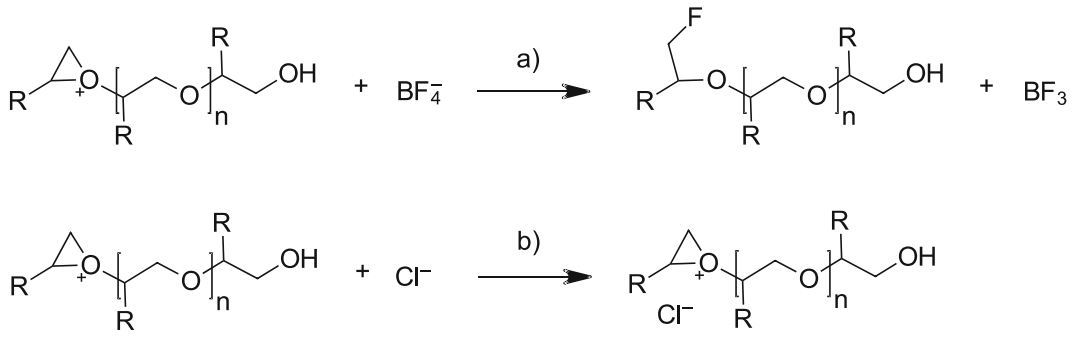

Figure 12: Possible termination reaction

Beside acid strength and non-nucleophilicity, also stability is desired for efficient polymerization.[35] By arranging a few exemplary anions according to their nucleophilicity, a reactivity ranking can be obtained (Figure 13). The theoretical considerations are proven in various experiments such as the anion dependent maximum curing speed of a thin film on a conveyor belt.[35]

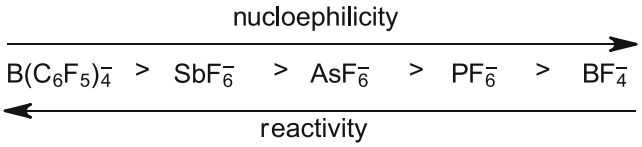

Figure 13: Nucleophilicity vs. reactivity of different perfluorometallates decreasing in size from left to right

Obviously, the disadvantage of those anions is their high toxicity, due to their acidic nature. Also, heavy metal containing counter ions, like SbF_6^- and AsF_6^-, and the possibility to liberate fluoric acid limit their applications, for example in the health sector. Especially the heavy-metal-based hexafluoro antimonite is a wide-spread counter ion in industry.

Radical Induced Decomposition of Onium Salts

It is known, that stable onium compounds undergo cleavage, if suitable radical initiators are present in the system.[61] The formed radicals can either result from photo- or thermal radical initiators. For example diaryliodonium salts could be cleaved radical induced by acylphosphine oxides as radical photoinitiators.[62] For this system to work, abstractable protons, provided by the monomer for example, are necessary (Figure 14).

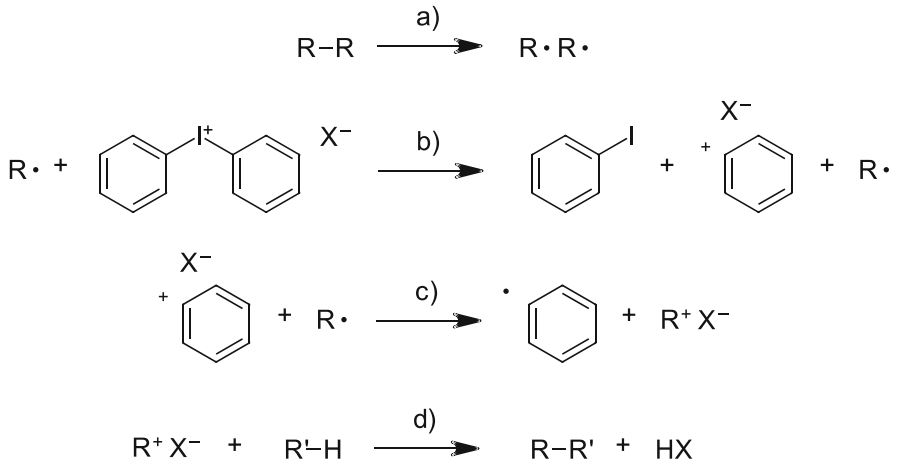

Figure 14: Radical induced decomposition of diphenyl iodonium salt

In the first step, the radical initiator undergoes photo- or thermal, homolytic cleavage (a). The formed radicals are capable of decomposing the photoacid generator (b), followed by an oxidation of the radical to a carbocation (c). In the final step the essential hydrogen is abstracted, leading to a recombination product and the superacid HX (d). By the liberation of the superacid, cationic polymerization initiates, without the irradiation of the photoacid generator by UV-light. The initiation process after the acid generation was described previously in Figure 7. Also humidity in the surrounding atmosphere can act as the proton source for the superacid generation.[63]

Radical induced Cationic Frontal Polymerization

RICFP is able to prevent the limitation of the thermal-only FP in terms of pot life and low reactivity. In addition, the initiation mechanism can be either thermal or by irradiation with UV-light. By using cationic photoinitiators, in contrast to thermal-only FP a reaction rate difference between ambient and frontal temperatures is not needed. The polymerization rate of the cationic initiator in the resin is neglectable, once irradiated, the high reactivity combined with a high rate of polymerization can be “switched on” on demand. Additionally,

the front can be started with conventional thermal sources too, due to the combination of thermal FP and radical induced cationic polymerization (RICP).

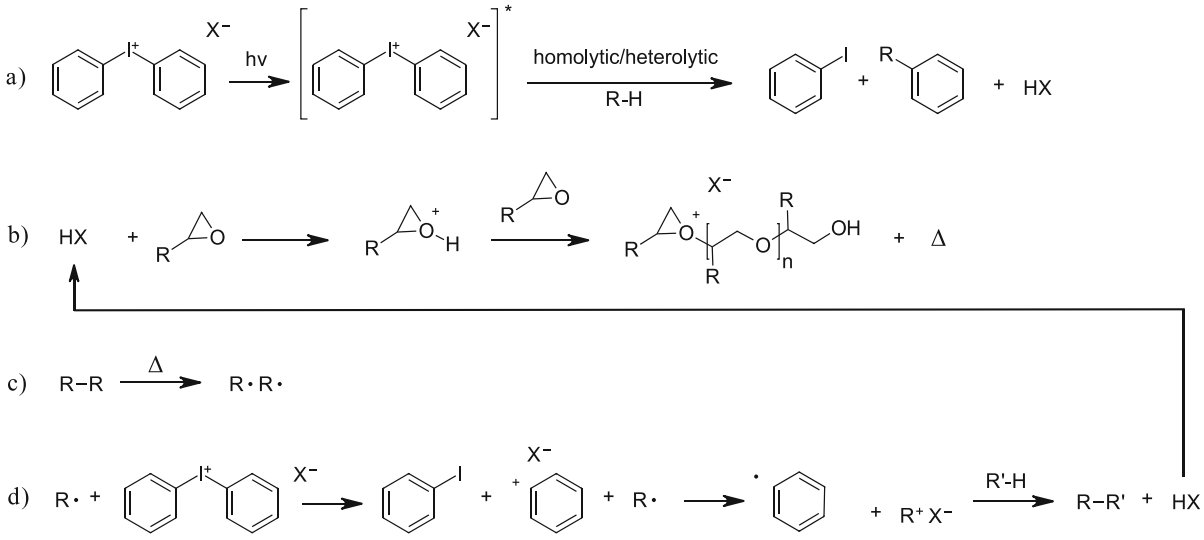

Figure 15: Schematic reaction pathway of the UV light initiated RICFP of an epoxy monomer[61, 64, 65] a) photochemical decomposition of onium salts; b) polymerization reaction; c) radical thermal initiator cleavage; d) radical induced decomposition of onium salts

The mechanism behind the RICFP is well known, since it is a combination of the previously described RICP and a thermal FP propagating through the material. The requirements for such a formulation are a catatonically curable monomer, a radical thermal initiator and the photoacid generator. First, the iodonium salt is excited with UV photons and cleaves either homolytically or heterolytically, followed by the abstraction of a hydrogen. This step was already described in detail in Figure 11. The crucial step for initiation of the cationic polymerization is the liberation of the superacid HX (Figure 15a). This superacid is able to attach its hydrogen to an epoxy group of a monomer, where classical cationic polymerization takes place. During the polymerization reaction of the reactive epoxides, a major amount of heat Δ is liberated (b). The liberated thermal energy is able to cleave the thermal radical initiator (c). The radical decomposition of onium salts was already described in detail in Figure 14. These generated radicals can decompose the iodonium salt and by the abstraction of a hydrogen, the superacid HX is formed once again (d). After the formation of HX, another epoxy-group can be protonated, hence initiate the cationic polymerization and the cycle (back to step b) is repeated. This also means, that the UV irradiation source can be switched off immediately after the frontal temperature is reached and from there on, the self-sustaining front is formed. If any of the mentioned steps a) to d) are suppressed ore occur prematurely, the RICFP cannot take place as expected.

Sensitization of Onium Salts

The penetration depth of an electromagnetic wave such as light is strongly dependent on its wavelength. Therefore, it is advantageous to irradiate with lower-energy, long wavelength light to improve penetration depth. Most onium salts used for cationic polymerization show their absorption maximum below 350 nm, which makes them rather unsuitable for the irradiation by low energy light. A shift of the absorption maximum can be achieved by substituting the aromatic moieties of the onium salts. However this modification of the aromatic rings shows limited success, bathochromically shifting the maximum around 20 nm.[35] Hence nearly the same issue stays present. To solve this problem, onium salts can be cleaved by sensitization using a suitable molecule with a significantly shifted absorption maximum to longer wavelength.[66] It does so by either transferring energy of its excited state (most common in radical systems) or by using electron transfer (most common in cationic systems). The sensitizer molecule, usually consisting out of several aromatic rings and is consumed in the initiation process (Figure 16).

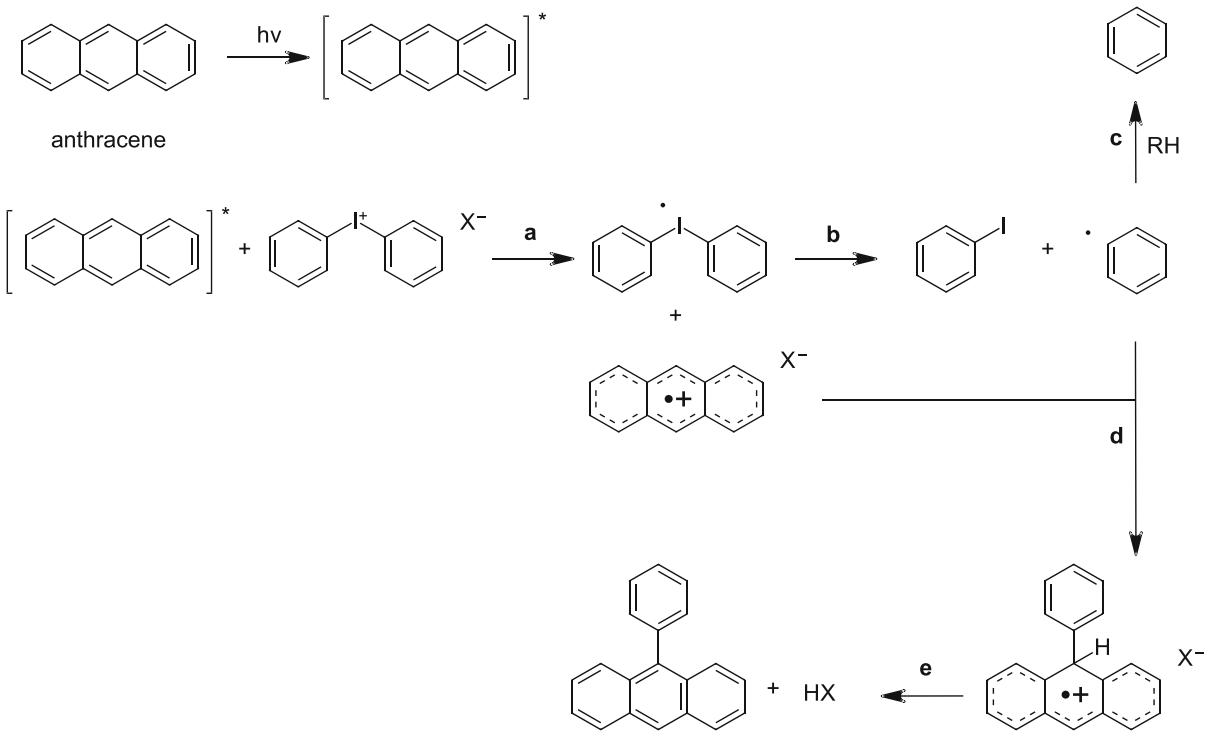

Figure 16: Sensitization of an onium salt (diphenyl iodonium) by anthracene resulting in the liberation of the super acid HX[44]

Anthracene is promoted into its excited state via irradiation. The sensitized anthracene reacts with the iodonium salt to generate a radical species of the onium salt as well as the anthracene radical cation (a). After this step the iodonium salt decomposes into iodobenzene and a benzyl radical (b). The benzyl radical can either abstract a hydrogen form a hydrogen source nearby

(c), or arylate the radical cation (d). In the last step the superacid is liberated and the arylated anthracene is formed (e).[44]

Considering common photoacid generators such as diaryliodonium and triarylsulfonium salts, the iodonium ones are much more prone to sensitization compared to sulfonium salts. This circumstance can be explained by taking a closer look at the redox potential of the sensitization compounds (Figure 17).

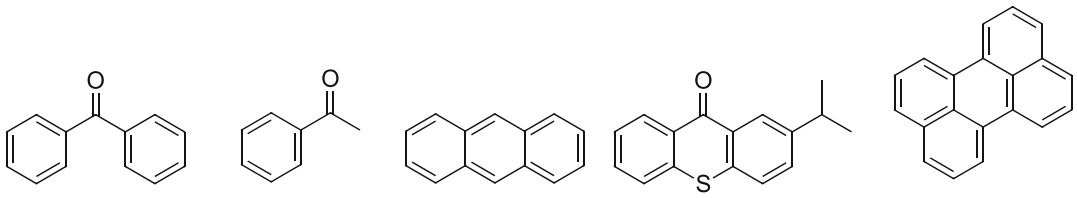

Figure 17: Sensitizers benzophenone, acetophenone, anthracene, 2-isopropylthioxanthone and perylene

Sulfonium salts experience a reduction potential of around 1.2 eV, while iodonium salts take up an electron at 0.2 eV. Therefore iodonium and sulfonium salts can be sensitized with a variety of compounds (Table 5).[66]

Table 5: Various sensitizers including their absorption maxima and ability to sensitize iodonium and sulfonium salts (+ … sensitization possible; - … sensitization not possible)

Sensitizer	Absorption [nm]	Iodonium Salts	Sulfonium Salts
Benzophenone	254	+	-
Acetophenone	278	+	+
Anthracene	376	+	+
ITX	383	+	-
Perylene	410	+	+

Ring-opening Metathesis Polymerization

Ring-opening metathesis polymerization (ROMP) is a powerful and broadly used tool in generating macromolecular materials. Developed in the 1950s, this method transforms olefins via mostly transition-metal catalysts into polymers. Further development, especially the investigation of the key intermediates, enabled the production of more complex polymers and material architectures.[67-71] Alkene metathesis can be described as metal-mediated carbon-carbon double bond exchange process.[72] Modern ROMP catalysts show a certain tolerance towards functional groups, which leads to different polymerizable monomers (Figure 18).

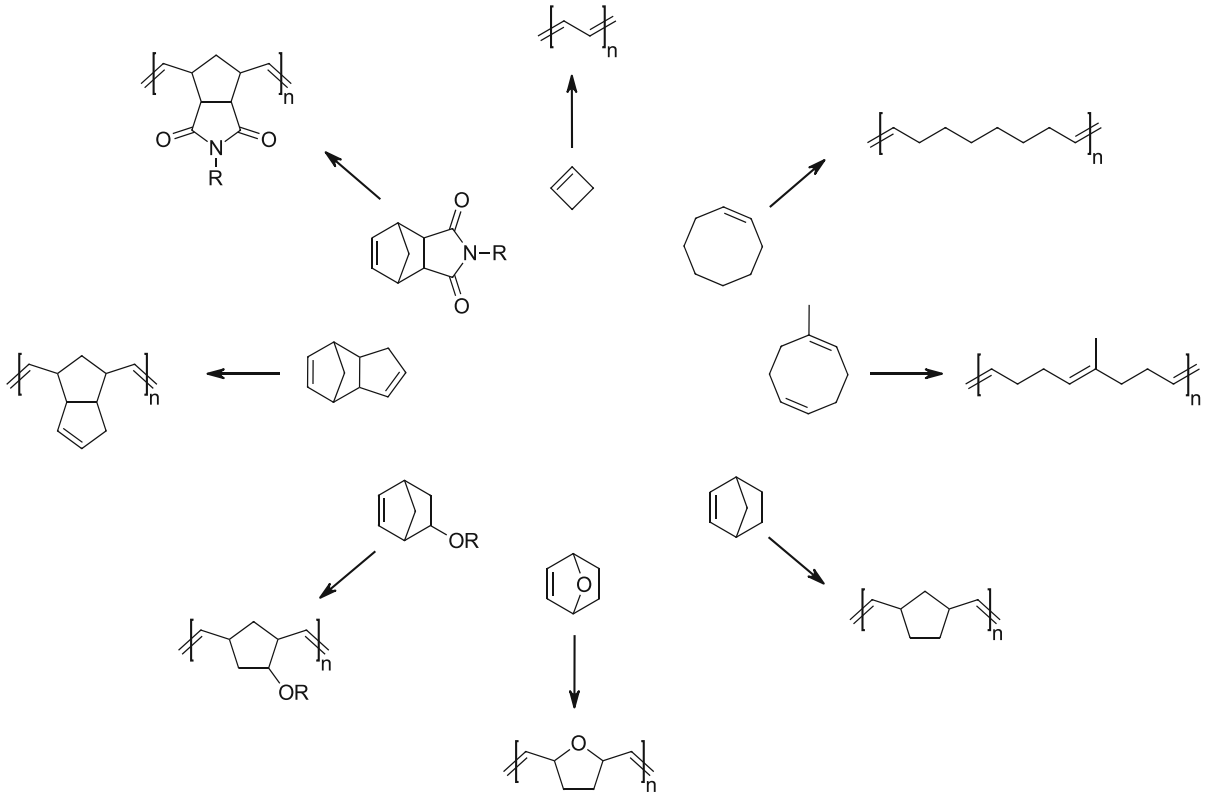

Figure 18: Monomers suitable for ROMP[73]

In contrast to classic alkene additions, the conversion from monomer to polymer via ROMP, conserves unsaturated moieties in the final material. Ring-opening metathesis polymerization benefits from the high ring-strain within the cyclic monomers, which is released during the ring-opening process of cyclic alkenes. Most ROMP monomers like cyclobutene, cyclooctene, norbornene or dicyclopentadiene show notable ring-strain. Cyclohexene is worth mentioning due to its negligible ring-strain, hence this monomer is hard to undergo ROMP.[74] Since the ring-opening is an enthalpy driven process, ROMP reactions have a celling temperature at given concentrations. If the concentration or temperature is too high, the released energy by ring-opening is not sufficient and polymerization will not take place. Therefore, ROMP

processes at high monomer concentrations and the lowest possible temperature work well.[75] In general, higher temperatures lead to increased Đ and lower yields.[76]

The mechanism of a classic ROMP process undergoes three basic steps. Initiation, followed by propagation and finally termination (Figure 19).

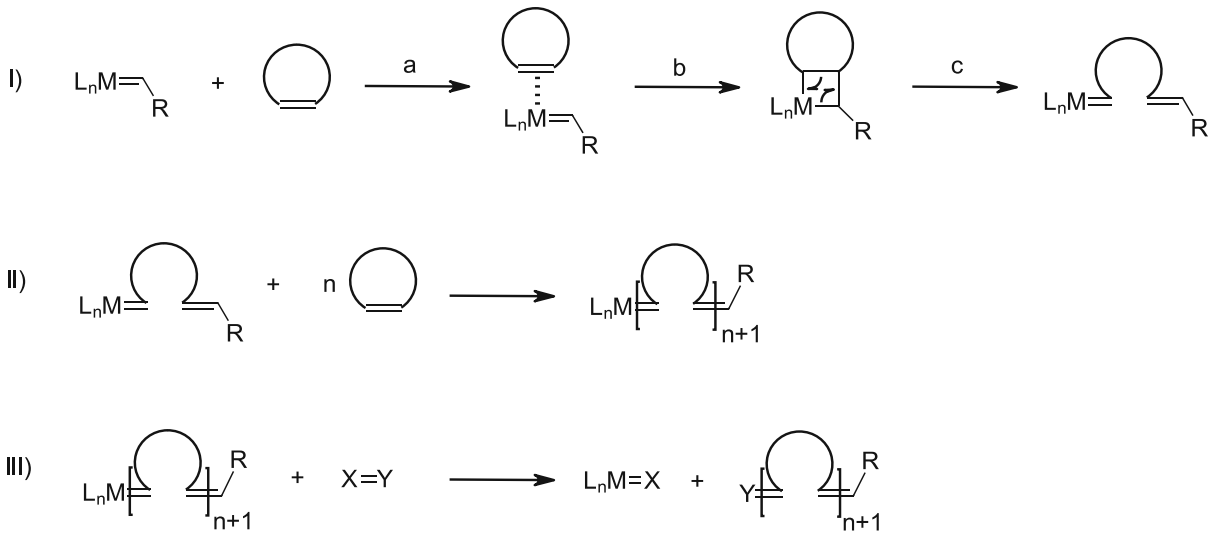

Figure 19: Three general steps of ROMP: I) Initiation, II) Propagation and III) Termination[77, 78]

The transition-metal center coordinates with the alkene to form an alkylidene complex as the first initiation step (Ia). After coordination, a [2+2]-cycloaddition takes place to form a four-membered intermediate state, which is able to start the polymerization reaction (Ib). The metallacyclobutane undergoes cycloreversion to finally yield a metal alkylidene again (Ic). The once covalently bond metal alkylidene and organic moiety R are now separated by the growing chain. In the second step, propagation occurs and nearby monomer is incorporated into the growing polymer chain (II). If all available monomer is consumed, an equilibrium is reached or termination occurs, the propagation step comes to an end. In living ROMP, a quenching agent is added on purpose to terminate the polymerization reaction (III). The agent is either removing or deactivating the transition metal at the end of the chain or replacing it with a functional group of choice. Such quenching agents are for example ethyl vinyl ether or benzaldehyde.[77, 78] Of course all steps described above are reversable, since ROMP reactions take place as equilibrium between monomer addition and subtraction.

During the chain-growth step, additional inter- and intramolecular chain transfers take place (Figure 20). Since these are chain transfer reactions, the number of active metal-alkylidene centers remains constant. Therefore, broadening the polydispersity of the final material.

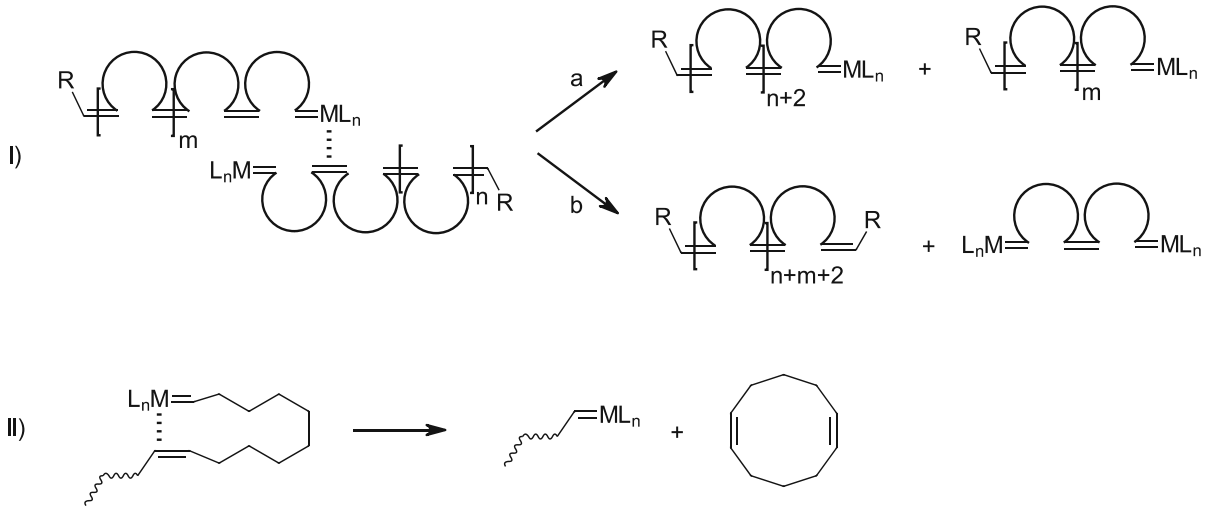

Figure 20: I) Intermolecular chain transfer and II) intramolecular chain transfer[77]

During intermolecular chain transfer (I), a growing polymer chain with an active metal alkylidene at the end can interact with double bonds of other chains. Despite the total number of chains remaining constant, molecular weights increase or decrease accordingly. If an active metal alkylidene at the end of a growing chain reacts with a double bond in the same polymer molecule, this process is called intramolecular chain transfer (II). As depicted in the illustration above, this chain transfer releases a cyclic polymer and a still active metal alkylidene terminated chain with a lower molecular weight. However, formation of cyclic polymers occurs more frequently at high temperatures and low concentrations.[77, 79, 80]

To be classified as "living" ring-opening metathesis polymerization, fast and complete initiation by the catalyst has to be ensured. Additionally, a linear relation between degree of polymerization and monomer consumption as well as a polydispersity (Đ) below 1.5 is necessary.[81] Therefore, living ROMP reactions can lead to very well-defined polymer architectures like block- or graft-copolymers and narrow polydispersity.[82]

Polymers produced on an industrial scale are mainly polynorbornenes and polycyclopentadienes. There are two possible pathways to metathesis polymers via ROMP. Either heterogeneous- or homogeneous-catalysts are used for polymer production. Heterogenous catalysis is known for the use of two synergistic compounds, the ill-defined catalyst and co-catalyst. The much more modern process is homogeneous catalysis with the application of well-defined metal complexes as catalysts for material production.

Metal Catalysts for ROMP

Effective metal catalysts in combination with co-catalysts for the initiation of heterogenous ROMP reactions were first developed by Ziegler and Natta in the 1950s.[83, 84] Across the next decade, a massive amount of research was performed towards optimizations in metal-carbene complexes.[85] Such catalysts have to show a variety of properties to be ideal for ROMP. First of all, after an efficient initiation process the monomer should be converted into polymer rapidly and quantitatively. Inter- and intramolecular chain transfers as well as terminations have to be kept at a minimum. In addition, the catalysts and the corresponding termination agents should be affordable to synthesize and well soluble in most non-polar and polar solvents. Due to practicality, a moisture- and air-stable compound is preferred.[77]

To sustain a ROMP reaction with living characteristics, a shift from metal chlorides to metal complexes with organic ligands was observed. These catalysts react in a much more controlled and homogeneous manner. The first reported catalysts for homogeneous ROMP without the need of a co-catalysts, were tungsten-carbene complexes by Fischer.[86] A variety of metal-carbene catalysts were investigated in the following years with specific central atoms: titanium,[87] tantalum,[88] tungsten,[89] molybdenum[90] and ruthenium.[91, 92]

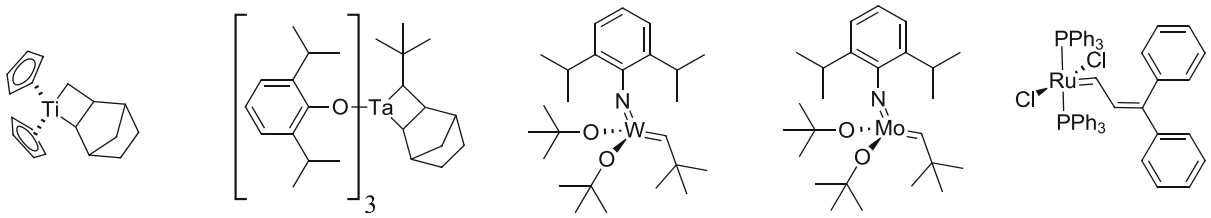

Figure 21: First single-component complexes based on titanium, tantalum, tungsten, molybdenum and ruthenium[93]

Titanacyclobutane and tantalacyclobutane complexes (Figure 21) are the first single-component catalysts for living ROMP based on titanium and tantalum. Narrow Đ and a linear relation between the Đ and monomer consumption are observed. However, both catalysts face challenges, since they are incompatible with most heteroatom-containing groups.[94]
Well-defined catalyst complexes based on tungsten are able to catalyze living ROMP in norbornenes for example. A tolerance towards ester groups is noticeable.[95]

Molybdenum-based complexes are noticeably compatible with most functionalities. Esters, amides, imides, ketals, ethers, cyan groups and halogens in monomers for Mo-catalyzed ROMP work well.[90]

Ruthenium complexes and their low oxophilicity as well as outstanding compatibility with most functional groups lead to the development of countless catalysts for living ROMP. Such Ru-catalysts are much more tolerant towards polar functionalities compared to Ti, Ta, W and Mo.[77] The first well-defined single-component catalyst based on ruthenium is depicted in Figure 21.[96]

Nowadays, a variety of ruthenium-based carbene complexes are broadly commercially available. One of the most successful catalysts in metathesis reactions is the Grubbs 1st generation Ru-complex (Figure 22). Due to its relatively easy synthesis[97] and high tolerance of functional groups, the catalyst remains an important piece in metathesis chemistry.

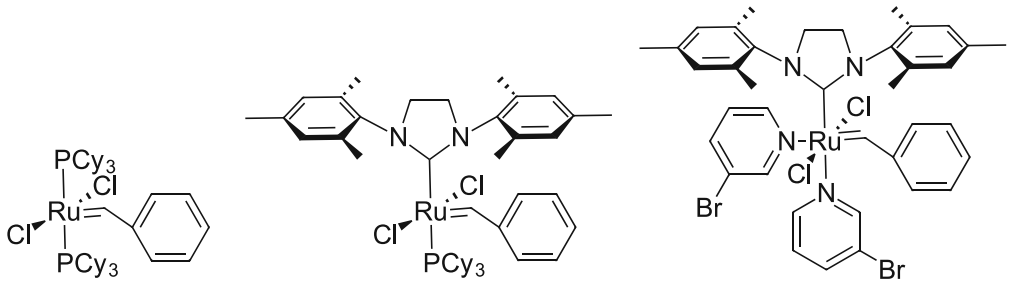

Grubbs 1st Gen. Grubbs 2nd Gen. Grubbs 3rd Gen.

Figure 22: Different generations of Grubbs catalysis

The shift from cyclohexyl phosphine groups to better sigma donors like nitrogen-heterocyclic carbenes (NHCs) resulted in higher stability of the complex. The second generation of Grubbs catalysts exhibits extraordinary reactivity in ROMP due to its enhanced dissociation properties of the ruthenium center and the phosphine ligand. A drawback of the Grubbs 2nd generation catalyst is its inability to generate polymers with narrow Đ.[98] The polydispersity problem is solved by the introduction of the third generation.[99] The strong NHC ligand as well as the weakly coordinating, brominated pyridines result in high reactivity due to the labile pyridines. This generation of catalysts provides narrow Đ and especially high reaction rates.[100]

Late transition metals like ruthenium are more stable towards polar functionalities compared with early transition metals (Table 6). Via modification and optimization of the ligands, the

activity in ROMP reactions of late transition metals can be comparable to the early transition metals.[77]

Table 6: Tolerance of functional groups of various catalysts; the further up in the table, the more reactive is the catalyst towards stated functionalities[77]

Ti	Ta	W	Mo	Ru
acids	acids	acids	acids	alkenes
alcohols	alcohols	alcohols	alcohols	acids
aldehydes	aldehydes	aldehydes	aldehydes	alcohols
ketones	ketones	ketones	alkenes	aldehydes
esters/amides	esters/amides	alkenes	ketones	ketones
alkenes	alkenes	esters/amides	esters/amides	esters/amides

Photoinitiated ROMP

The photoinitiated polymerization of norbornene with ruthenium-based sandwich complexes was performed even in polar protic solvents like alcohol-water mixtures. Irradiation with a mercury lamp of the complex lead to Ru(II) ions in solution, which are able to initiate the metathesis reaction (Figure 23).[101]

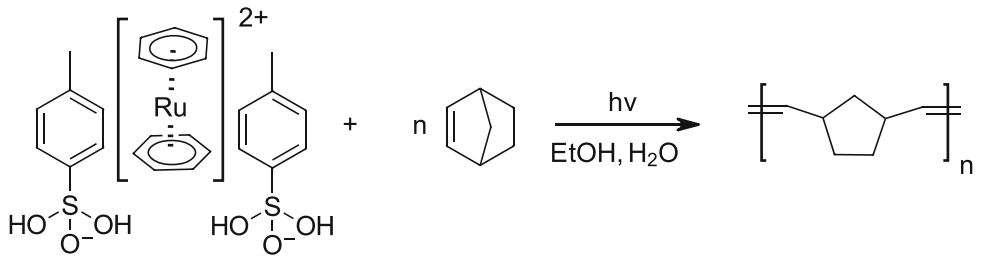

Figure 23: Photoinitiated ROMP reaction in aqueous media[68]

A completely different approach was investigated using ruthenium catalysts with sulfur-based ligands. A ruthenium NHC complex is chelated with a sulfur atom, which bridges between the benzylidene and an aromatic moiety (Figure 24). This special circumstance allows the complex to be activated via light. If the aromatic moiety is replaced with a CF_3-group, a latent catalyst at room temperature with high reactivity if activated is obtained.[102]

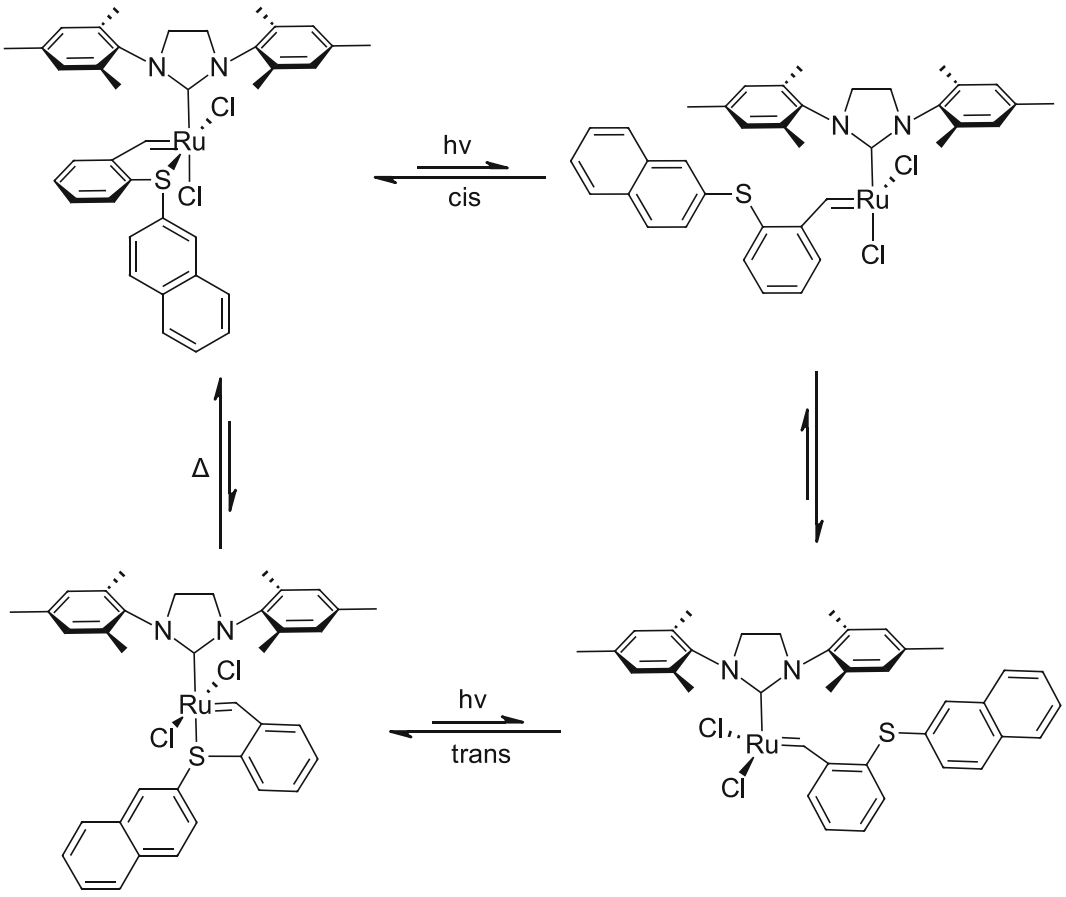

Figure 24: Light-switchable photoisomerization[102]

The sulfur-chelated ruthenium complex remains in its *cis*-form until irradiation leads to the unstable cis-transition state. This intermediate quickly rearranges to the more stable *trans*-state, followed by a transition to the sulfur-chelated trans-species. Deactivation is achieved by thermal energy input. Heating to around 80 °C leads to the formation of the inactive *cis*-state again. Therefore, it is possible to switch on the catalyst by irradiation and switch it off by heating.

(Photo)redox-mediated Metal-Free ROMP

In general, ROMP catalysts are based on rather expensive transition metals like ruthenium, molybdenum or tungsten. Despite low molar ratios of catalyst needed for the successful ROMP reaction of most monomers, industrial scale production of metathesis polymers leads to high consumption of those precious metals. In addition, metal-based catalysts usually remain in the final material due to either covalent bonds to the polymer or inability to diffuse out of the fibers or networks sufficiently. This is especially problematic for biomedical applications since the limit remains at < 5 ppm in the European Union since 2008.[103] Attempts to reduce the transition metal content in the final material are mainly chromatographical

removals,[104] chemical transformations,[105] removing of ruthenium via the tenfold amount of phosphines[106] and many more.[107] Obviously, those drawbacks of an additional purification step are not feasible for most commercial processes, since they increase cost and process duration.[108]

Therefore, research in metal-free (MF) ROMP is of high interest. In the 2000s it was noticed, that cross metathesis of enol ethers and terminal alkenes via electrochemical intermolecular cross coupling was possible.[109] They form a four-membered intermediate state, which resembles the metallacyclobutane intermediate from metal-mediated ROMP reactions.[110] The formed radical cation can undergo reduction to cyclobutene or fragment to give a alkene and an enol ether radical cation (Figure 25).

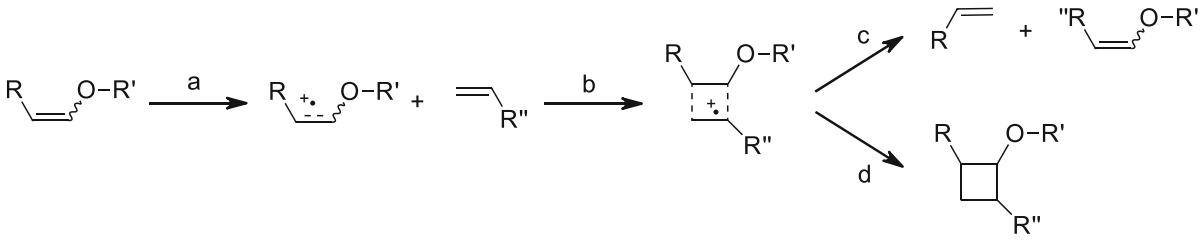

Figure 25: Electrochemical enol ether metathesis (c) and reduction (d)[111]

In the first step, a enol ether is oxidized by removing one electron to form its radical cation species (a). By ring formation reaction with a second alkene, a cyclobutene radical cation intermediate is formed (b). This cyclic intermediate state can either lead to metathesis reaction resulting in an exchange of organic moieties R and R'' (c), or be reduced intentionally or unintentionally (d).[111]

Redox-mediated MF-ROMP exhibits the same steps involved in conventional ROMP reaction. Initiation, followed by propagation and finally termination (Figure 26).

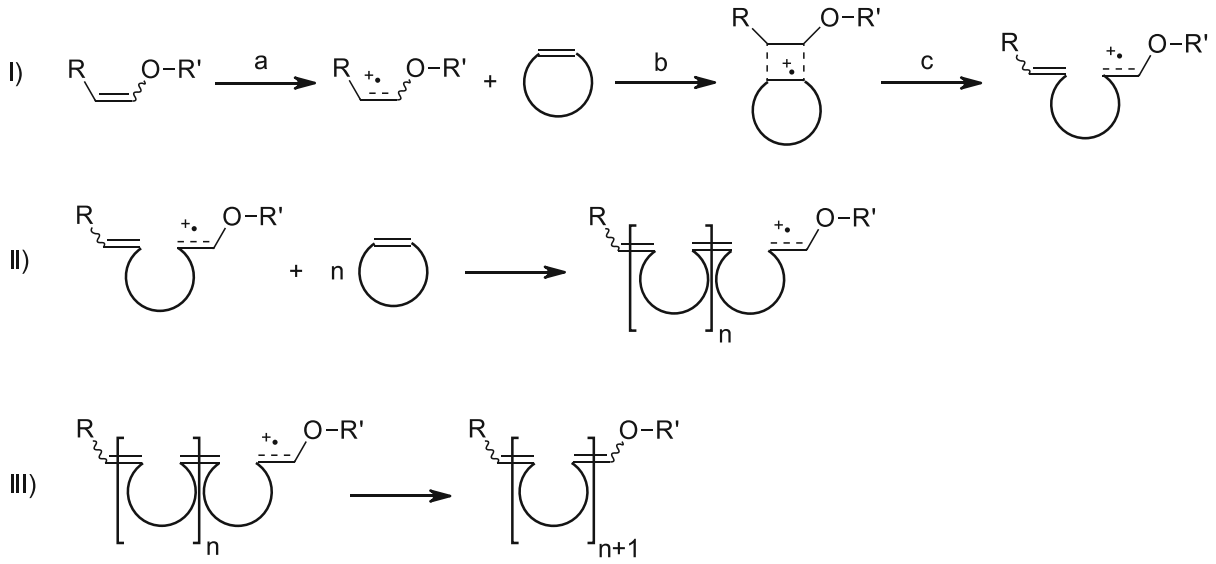

Figure 26: Three general steps of redox-mediated metal-free ROMP: I) Initiation, II) Propagation and III) Termination[111]

The initiation step consists of the reduction of the enol ether and the formation of a radical cation (Ia). In a second step, a strained cyclic alkene reacts with the radical cation to form a four-membered intermediate state (Ib). With the release of ring strain, the cyclobutene radical cation undergoes ring opening (Ic). During propagation, more monomers experience ring opening to form a growing polymer chain (II). Termination can be triggered intentionally by adding a reduction agent or unintentionally by impurities for example (III).[111]

To successfully initiate photoredox-mediated MF-ROMP, a photo-oxidation agent and an initiator are needed. Pyrylium- and thiopyrylium salts show promising capabilities as such agents. In combination with enol ethers as initiators, cyclic alkenes like norbornene or cyclopentadiene can be polymerized.[112] However, the photoredox-mediated MF-ROMP is not quite tolerant in terms of functional groups.[111]

Frontal Ring-opening Metathesis Polymerization

A rather recently emerged topic is the frontal ROMP or FROMP.[113] In 2001 the first report was published on the FROMP of solid dicyclopentadiene (DCPD) with triphenylphosphine as retardant and a ruthenium-based catalyst. Maximum frontal temperatures of 204 °C and frontal velocities of around 2.6 cm min^{-1} are measured.[24] The pot life of those formulations was improved to 20 to 30 min by the addition of toluene to keep the formulation in its liquid state.[114] A major step towards industrial application was the extension of the formulations pot

life to up to 30 h by using *endo*-DCPD as monomer and 8 eq. of tributylphosphite (Figure 27).[115]

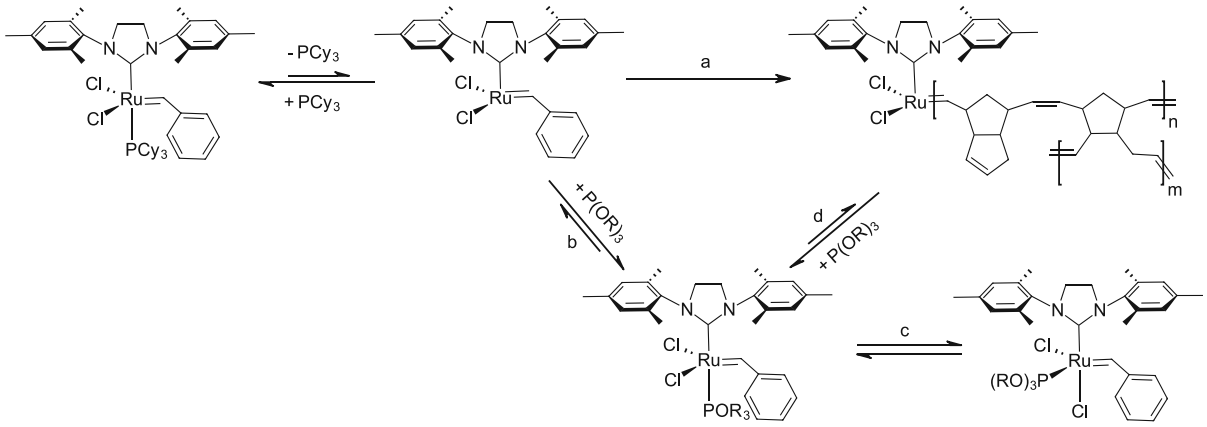

Figure 27: Formation of the latent ruthenium-phosphite complex and ROMP process of DCPD at room temperature[115]

The ruthenium-based catalyst exhibits an equilibrium reaction to its form without the tricyclohexyl phosphine ligand. As soon as the PCy_3-ligand is cleaved, the catalyst is in its active form to initiate the ROMP process (a). However, an equilibrium favoring its latent form with the POR_3 ligand is observed at 25 °C, since phosphites are known to bind strongly to metal centers (b).[116] The latent form itself can rearrange the phosphite ligand (c). In addition, the chain growth is able to be inhibited by the coordination of a phosphite to the ruthenium catalyst at the chain end (d). Therefore, the inactive species is generated inhibiting further ROMP.

To manually trigger the ROMP reaction, a thermal stimulus has to be applied on the formulation containing mainly latent phosphite-ligated catalyst. The phosphite ligand starts to leave the complex as temperature rises. The equilibrium shifts drastically to a point where mainly active ruthenium catalyst is present, able to polymerize the monomer efficiently. Since the ring strain of each monomer molecule is released during the ROMP process, temperature of the formulations rises significantly to around 200 °C for DCPD-based formulations. The temperature increase leads to more phosphite ligands decoupling from the complex, therefore creating a moving reactive zone. Ideally the FROMP process terminates as soon as the monomer is fully consumed.

OBJECTIVE

The main objective of this thesis is the creation of novel cationic initiators for their application in 3D-printing and frontal polymerization. Since onium salts are fundamentally derived from a cation and an anion with specific roles in cationic polymerization, both building blocks need to be focused on separately. For the cation part a variety of different central atoms and structural features are available due to excessive research already performed in the field of onium salts. In terms of anions a broad selection of non-nucleophilic anions is available due to the fast progress in lithium ion battery research. With the acquired knowledge from both topics, a combination of existing and novel building blocks should be synthesized and tested.

Within the first part of this thesis, an especially accessible class of onium salts should be focused on, the tetrafluoroborates in combination with a selection of cations. The salts should then be tested in terms of redox-potential, thermal stability and reactivity. A specific set of the best-performing (photo)acid generators should be paired with less nucleophilic anions to form new types of efficient cationic (photo)initiators. Additionally, their application in frontal polymerization should be tested and frontal parameters determined.

For the second part, novel anions for the best performing cations should be prepared. The final onium salt should be then obtained by using a metathesis reaction and examined in comparative studies with current state-of-the-art iodonium- and sulfonium salts. All onium salts should be analyzed regarding thermal stability and reactivity. The most suitable onium salts are then applied in radical induced cationic frontal polymerization. Frontal polymerization parameters such as the maximum front temperature, front starting time and frontal velocity should be determined in combination with epoxy group conversion. A selection of temperature stable onium salts should be mixed with an epoxy resin and applied in hot lithography. The quality of the final 3D-printed parts should be investigated via optical microscopy and scanning electron microscopy.

The third part of this work should investigate state-of-the-art onium salts for photoredox-mediated metal-free ROMP, shich are mainly based on the pyrylium cation. Therefore, novel pyrylium mediators should be prepared and their photochemical and reactivity properties determined. The onium salts should be mixed with commercial ROMP monomers such as norbornene, dicyclopentadiene and derivatives. In these systems, conversion and molecular weight should be monitored over time to compare the selected pyrylium salts.

I. The Cationic Species of Photoacid Generators

1. State of the Art

The most important class of photoacid generators as initiators for cationic polymerization are onium salts. These ionic species consisting of a center cation stabilized by a weakly coordinating, negative charged counterion. Onium compounds for cationic polymerization need sufficient thermal and hydrolysis stability, good solubility and high reactivity towards monomers. Still state of the art and most commonly used in industry are diaryliodonium salts and triarylsulfonium salts, which were prepared and characterized by Crivello et al. back in the 1970s.[36, 37, 40]

Diaryliodonium Salts

This class of photoinitiators is highly efficient, shows excellent photochemical behavior and is easy to obtain via synthesis. Responsible for the photochemical properties is the aromatic nature of the diaryliodonium salts. The absorption maximum of the unsubstituted diphenyliodonium salt is at 227 nm, while achieving impressive quantum yields up to 0.9.[37] Additionally, there is a broad absorption at 318 nm, making it suitable for most mercury lamp-based irradiation systems. Only a slight bathochromic shift can be achieved by substituting the phenyl rings of the iodonium salt with chromophores. This substitution process is beneficial, if the absorption maximum has to be more in line with the emission spectrum of a light source. The drawback of unsubstituted diphenyliodonium compounds is the limited solubility in certain monomers and the release of benzene upon irradiation. However, this can be easily solved by the introduction of a long aliphatic chain to improve solubility in non-polar media. Many commercially available iodonium salts show these features like substituents to improve photochemical properties as well as alkyl chains to solve potential solubility issues (Figure 28).

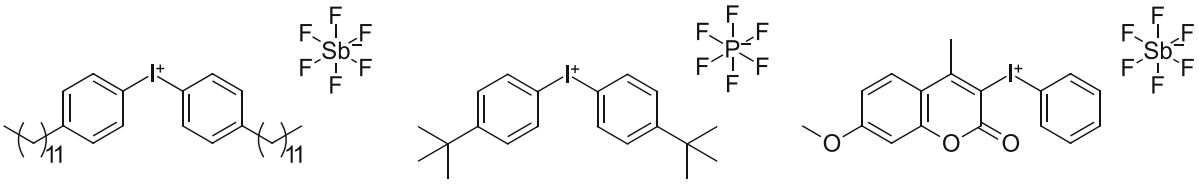

Figure 28: Examples for iodonium-based photoacid generators (SpeedCure 937, SpeedCure 938 and Sylanto 7M-S)

Most commonly used in industry are salts incorporating hexafluoroantimonate or hexafluorophosphate as counterions. They are very cheap to synthesize and in combination with phenyl substituted iodonium cations the preferred absorption and solubility requirements are met. A drawback of the fluorinated antimonate and phosphate anions is the relatively low reactivity compared to much less non-nucleophilic state-of-the-art anions like the tetrakis(pentafluorophenyl)borate or tetra(nonafluoro-tert-butoxy)aluminate (Figure 29). The absorption maxima of the four mentioned, commercially available iodonium salts are in the narrow range of 230 to 245 nm.

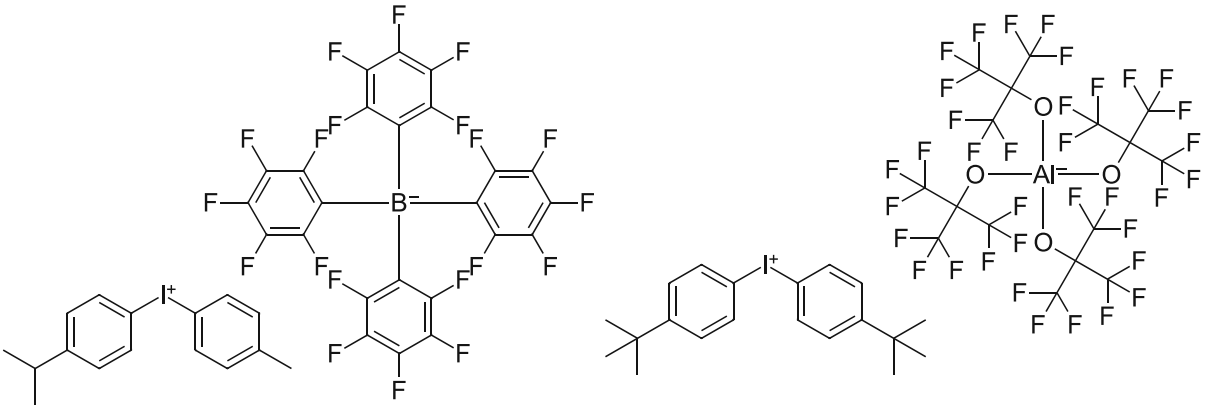

Figure 29: Examples for better performing, but more expensive iodonium-based photoacid generators (SpeedCure 939 and bis[4-(tert-butyl)phenyl]iodonium tetra(nonafluoro-tert-butoxy)aluminate)

The reactivity is great for the borate and outstanding for the aluminate in epoxy-based systems. Additionally, there are the possibilities to sensitize the iodonium salts with anthracene or to decompose it with radicals (RICP).[117, 118] In both cases the rather low absorption maximum of iodonium salts can be circumvented by the absorption range of the sensitizer or the radical generating species.

Triarylsulfonium Salts

The second class of commercially used photoacid generators are the sulfonium-based cations, which can be readily synthesized, show excellent absorption behavior and are much more thermally stable compared to the iodonium salts. The increased thermal stability emerges from the relatively high redox potential of sulfonium salts. This property additionally leads to better storage stability over an extended period of time.[37] The absorption maximum of the unsubstituted triphenylsulfonium compound is at 230 nm. Unlike iodonium salts, the maxima can be bathochromically shifted to around 280 nm without any problems by substitution of the phenyl rings. Considering the quantum yield in this absorption range, sulfonium salts

archive values of around 0.7. If substituted with the right chromophores, the sulfonium-based cations can easily achieve absorptions of 1 x 10^3 times higher at 313 nm compared to the unsubstituted derivative. This is the crucial property to give sulfonium salts an advantage over iodonium-based ones. Standard mercury lamps can be used to induce the cleavage of the sulfonium-cation. Similar to the iodonium-based species, the solubility can be enhanced by the introduction of aliphatic groups (Figure 30).

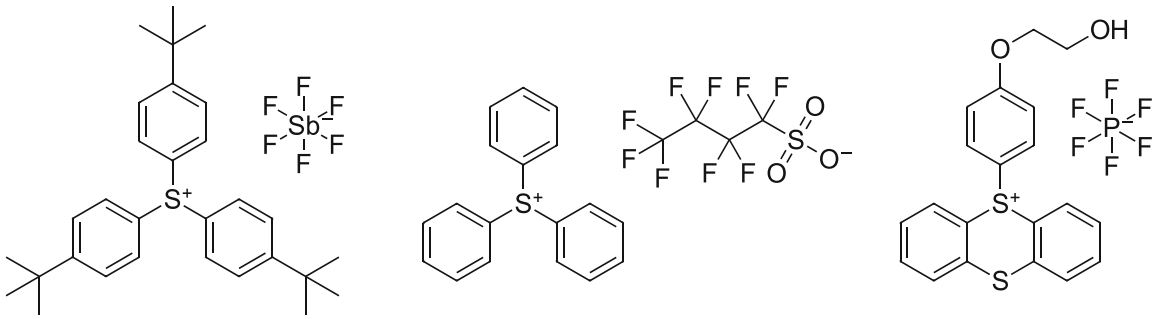

Figure 30: Examples for sulfonium-based photoacid generators (Tris(4-tert-butylphenyl)sulfonium hexafluoro antimonate, Triphenylsulfonium perfluoro-1-butanesulfonate and Esacure 1187)

Industry standard sulfonium-based acid generators often use antimonates or sulfonates as counterions. Sulfonium salts are also commercially available in their bis-onium derivative, which improves the absorption properties even more due to the increased cross-section of the molecule (Figure 31). Worth to mention is the poor solubility in nonpolar media of the bis-sulfonium photoacid generator. Therefore, it is available in a mixture containing 50 wt% propylene carbonate. In combination with a common epoxy-based monomer the photoinitiator solution can be homogenized much more efficiently, leading to time and energy savings.

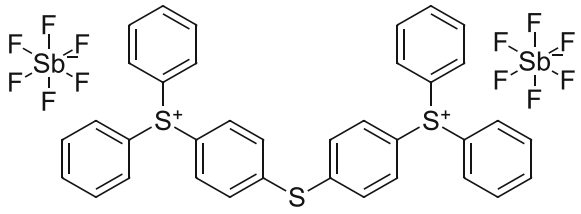

Figure 31: Examples for bis-sulfonium-based photoacid generators (SpeedCure 967)

Overall sulfonium and iodonium salts suffer from relatively poor solubility in organic media. Despite the introduction of alkyl groups, the solubility in non-polar monomers can be tricky. Therefore many applications use the cheaper, unsubstituted onium salts rather than expensive better soluble derivatives, and mix them with 30 to 50 wt% of propylene carbonate.[35, 119]

Role of Cations in Frontal Polymerization

Due to the versatility of FP in general, a lot of research is performed towards creating frontal polymerizations in various monomer systems with suitable initiators. For example, in thermally triggered (meth)acrylate-based FP with commercial peroxides acting as initiators.[120, 121] In addition, those (meth)acrylate FP can be triggered on demand via UV-light, using a commercial type I photoinitiator to start the reaction, whereas a difunctional peroxide represents the thermolabile initiator to ensure stable propagation.[122] Cationic monomers, like epoxides and composites can be cured by FP as well. In general, an iodonium- or sulfonium salt acts as photoinitiator and starts the polymerization reaction. The liberated exothermicity then cleaves a C-C labile molecule or peroxide, which is able to decompose the initiator to create a sustainable cycle.[64, 65] In addition, cyclic monomers like dicyclopentadiene can be cured in bulk by a ring opening metathesis FP, using a ruthenium Grubb's catalyst and triphenylphosphine as additive.[24]

Radical Induced Cationic Frontal Polymerization

State-of-the-art systems are based on epoxy monomers and iodonium salts as photoacid generators. However, the selection of the thermal radical initiator shows differences between the researchers.

The research of Marani et al. states the use of a cycloaliphatic epoxy system in combination with the thermal radical initiator dibenzoylperoxide (Figure 32).

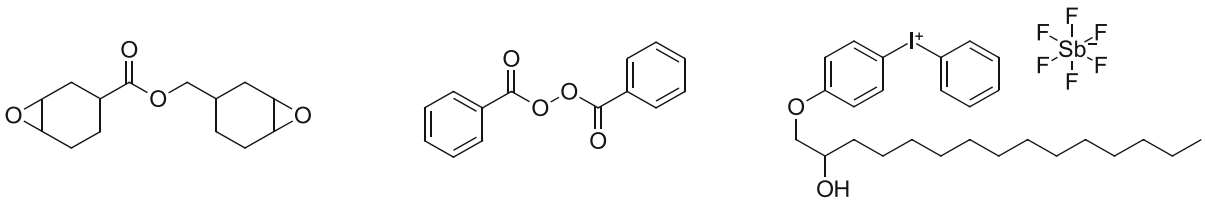

Figure 32: RICPF of ECC with the thermal radical initiator BP and the iodonium salt HOPH as photoacid generator

As photoacid generator, a substituted iodonium salt was used. However, the reported front parameters state 230 °C to 300 °C frontal temperature and a maximum frontal velocity of 6 cm min^{-1}. A major drawback of this setup is the intensive gas formation during the RICFP, which leads to very porous polymers.[27]

For Zhou et al., it was possible to cure epoxy resins via UV initiated FP. Formulations based on cycloaliphatic epoxides were used in combination with the thermo-labile BF_3-amine complex. To be able to initiate the RICFP via UV light, a small amount of triarylsulfonium salt was added to the initial reaction zone (Figure 33).

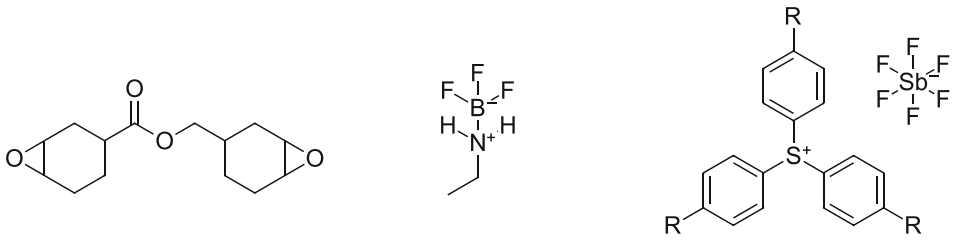

Figure 33: RICFP in ECC with the thermo-labile BF_3-amine complex and a mixture of triarylsulfonium salts as photoacid generator

The reported frontal parameters reached temperatures of 164 °C to 212 °C and velocities of around 2-3 cm min^{-1}. Bubble formation was not an issue with this monomer-initiator-photoacid generator system. The major drawback remains relatively poor pot life of the formulations.[123]

In the work by Lecompère et al. Pyrylium salts with vinyl ethers are used as coinitiators for cationic thermal frontal polymerization. It has been found that the presence of a vinyl ether can dramatically increase the reactivity of pyrylium salts as initiators for cationic polymerization (Figure 34).

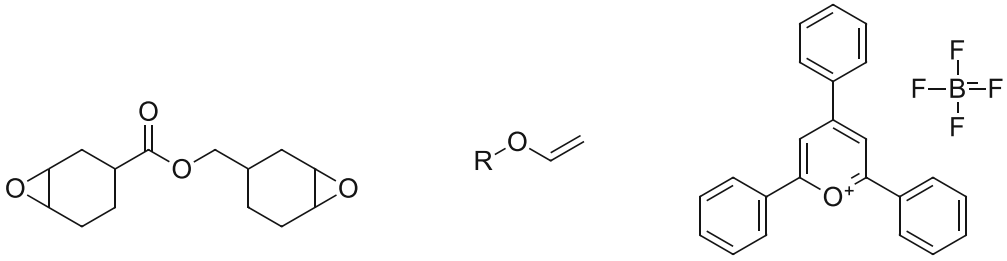

Figure 34: RICFP in ECC with the vinyl ether – pyrylium salt co-initiator system

Cycloaliphatic epoxides were investigated as monomers, with the vinyl ethers also subsequently being able to polymerize as comonomers. The coinitiator system of pyrylium salts and vinyl ethers offers, versatile applications for the polymerization of epoxides due to the possibility of initiating the frontal polymerization both thermally and photochemically. However, storage stability of the formulations is limited.[124]

Probably the most reactive system is based on the research of Bomze et al. The radical induced cationic frontal polymerization of epoxy monomers, such as bisphenol-A-diglycidylether (BADGE) or 1,6-hexanediol diglycidylether (HDDGE) is applied as a curing method for bifunctional epoxides. (4-Octyloxyphenyl) phenyliodonium hexafluoroantimonate was used as the onium salt and 1,1,2,2-tetraphenyl-1,2-ethanediol (TPED) was used as the radical starter (Figure 35).

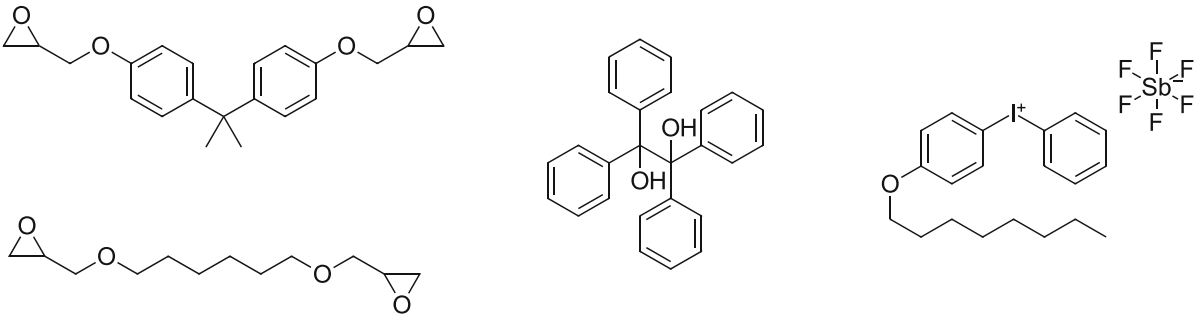

Figure 35: RICFP in BADGE/HDDGE with the thermal radial initiator TPED and the photoacid generator 4-octoxyphenyl phenyl iodonium hexafluoroantimonate

A major advantage compared to other formulations is the absence of bubble formation during the FP. The frontal polymerization can be started thermally or by irradiation with UV light. The maximum front temperature and the front speed are strongly dependent on the monomers used and on the initiator concentration. For example, a maximum front temperature of 173 °C and a front speed of 2.7 cm min^{-1} were measured in bisphenol-A-diglycidylether with 1 mol% of the thermal radical initiator and photoacid generator.[125] However, a more reactive system was developed based on a iodonium salt with a different counterion, the alkoxy aluminate.[117]

2. Potential Cations as new (Photo)Acid Generators

When it comes to new cations as photoacid generators, there are several options to focus on. Besides the commercially used diaryliodonium and triarylsulfonium salts in industry, phosphonium, selenonium, oxonium, telluronium, stibonium and many more are highly interesting, to investigate as new (photo)acid generators.[126] The aim was the preparation of similar substituted onium compounds, containing different central atoms (Figure 36). Iodine- and sulfur-based state of the art initiators are present in the nonmetals part of group 16 and 17. Additionally, nonmetals and transition metals of groups 14, 15, 16 and 17 were of special interest, due to their relatively easy conversion into onium salts.

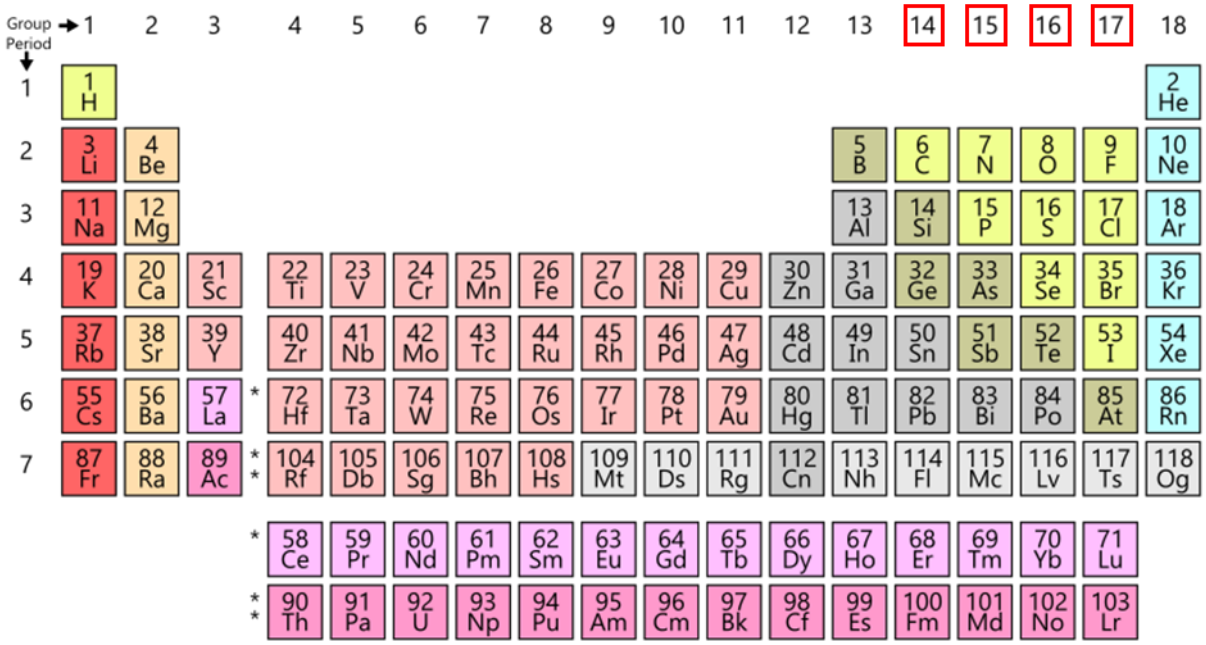

Figure 36: Simple periodic table chart including element numbers and abbreviations[127]

At first, tetrafluoroborate was chosen to function as counterion in all synthesized species, due to the broad commercial availability and easy synthetic access of this specific anion. The aimed salts were divided into four categories, state of the art initiators and group 14, 15 and 16 (Figure 37). Therefore, the introduction of the tetrafluoroborate during every synthesis was aimed to guarantee a fair comparison in the tests afterwards. This limitation to only one anion is crucial to exclude every possible effect of different counterions and only cations are benchmarked in later experiments against each other. Additionally, there are many tetrafluoroborates commercially available.

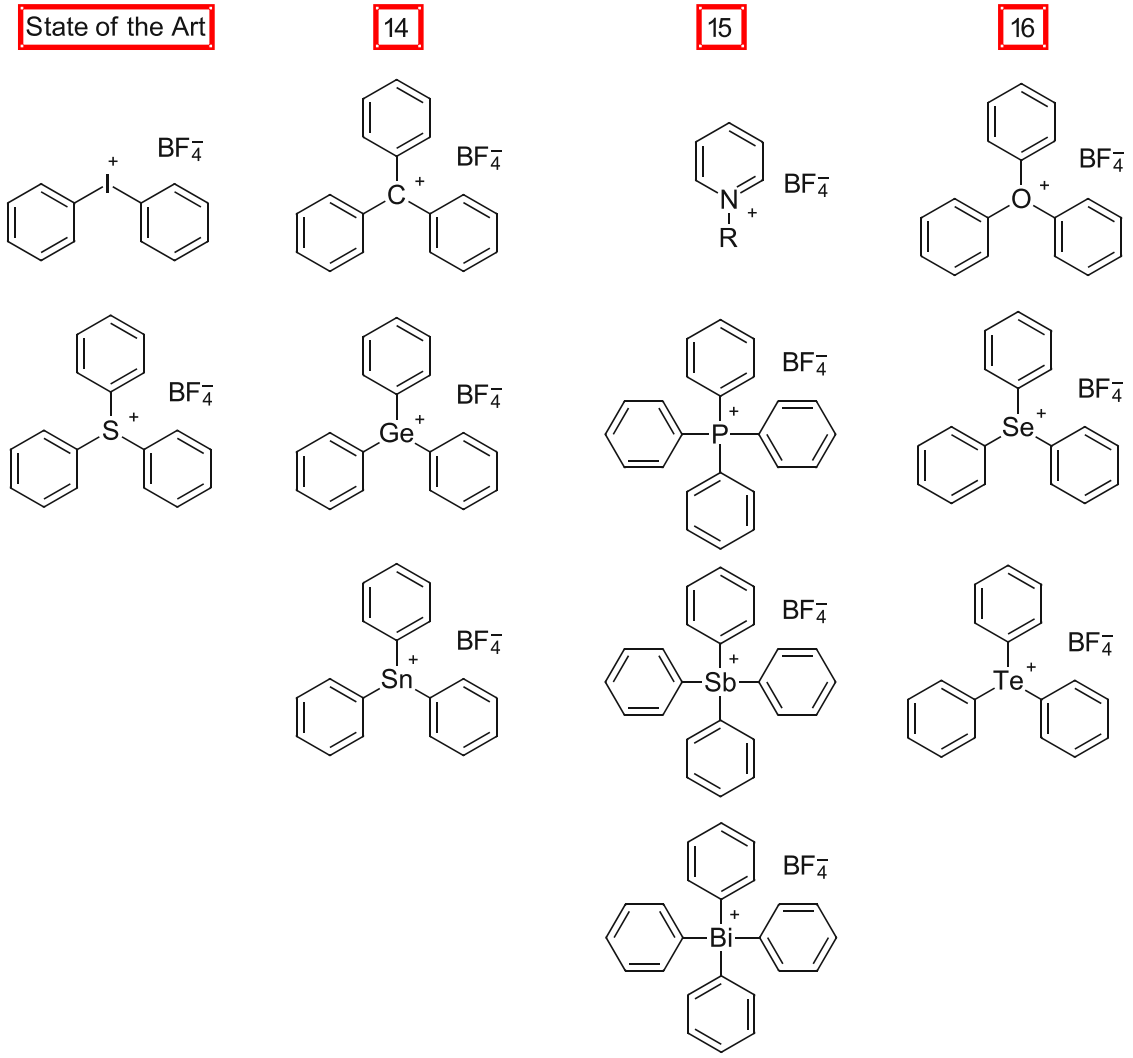

Figure 37: examples for iodonium, sulfonium, methylium, germanonium, stanonium, pyridinium, phosphonium, stibonium, bismuthonium, oxonium, selenonium and telluronium salts

Once synthesized, the target molecules mentioned above, should be mixed with a commercially available resin for the studies. Despite possible solubility issues of non-substituted phenyl rings in onium salts, the phenyl-only molecules were targeted. Simplicity was preferred over good solubility in nonpolar monomers, due to the usually more complex synthesis of asymmetric onium compounds. Additionally, the solubility issues can be prevented by using formulations containing propylene carbonate as a polarity increasing component. Comparison of redox potential, reactivity and stability of the (photo)acid generators to already established sulfonium and iodonium compounds was planned.

3. Onium Tetrafluoroborates

3.1. Synthesis

The synthesis of a variety of onium tetrafluoroborates was aimed for. As already stated, group 14, 15 and 16 of the periodic table of elements was focused in addition to state-of-the-art cations.

3.1.1. State of the Art Cations

3.1.1.1. Iodonium Salts

The inventor of iodonium salts were Crivello et al.[40] in the 1970s. The preparation of symmetrical diaryliodonium is performed by reacting the aromatic precursor with potassium iodate, sulfuric acid and acetic anhydride.[36] The counterion can later be exchanged to the desired anion easily via salt metathesis.

3.1.1.1.1. Diphenyl Iodonium Tetrafluoroborate

At first, diphenyl iodonium tetrafluoroborate was selected to be prepared. Iodonium is state of the art cations when it comes to cationic photopolymerization. Therefore, the simplest derivative, the diphenyl iodonium tetrafluoroborate, was the target compound. The first batch was synthesized according to Korwar et al.[128] This more modern route compared to Crivello et al.[40] includes the BF_3-etherate promoted reaction of phenylboronic acid with diacetoxyiodo benzene at low temperatures (Figure 37).

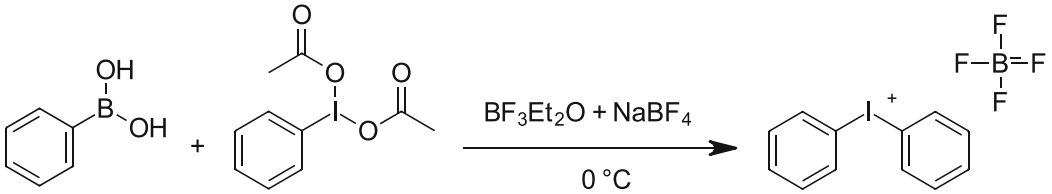

I1-B
27%

Figure 38: Synthesis of diphenyl iodonium tetrafluoroborate (I1-B)

The intermediate product is the diphenyl iodonium acetate is generated and transformed into the tetrafluoroborate via salt metathesis.

3.1.1.2. Sulfonium Salts

Triarylsulfonium salts were also discovered and synthesized by Crivello et al.[40] This group of onium salts can be prepared via Friedel-Crafts reaction with benzene as starting material and sulfur monochloride, aluminum chloride and chloride as reagents. This reaction route provides differently substituted sulfonium derivatives.[42, 43] A second route towards asymmetrical

triarylsulfonium salts in high yields is the copper(II)-catalyzed reaction of diarylsulfides with diaryliodonium salts.[40, 44]

3.1.1.2.1. Triphenyl Sulfonium Tetrafluoroborate

As a second representative of state of the art photoinitiators for cationic polymerization is the sulfonium-based onium salt. The symmetric triphenyl sulfonium salt was targeted (Figure 39).

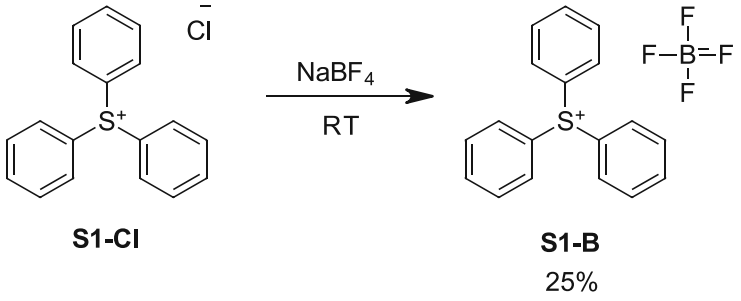

S1-Cl **S1-B**
25%

Figure 39: Synthesis of triphenyl sulfonium tetrafluoroborate (S1-B)

Due to the easy access to commercially available triphenyl sulfonium chloride, a salt metathesis similar to Li et al.[129] was aimed. This reaction route involves an ion exchange from chloride to tetrafluoroborate using sodium tetrafluoroborate as reagent. The less polar tetrafluoroborate precipitates of an aqueous solution.

3.1.1.2.2. 2,4,6-Triphenyl Thiopyrylium Tetrafluoroborate

Unlike normal trivalent sulfonium salts, the thiopyrylium class is based on a positive charged thiophene ring. The sulfur cation is directly built into the aromatic ring structure, instead of phenyl substituents directly attached to it. This structural change may lead to different photochemical behavior in terms of absorption and reactivity (Figure 40).

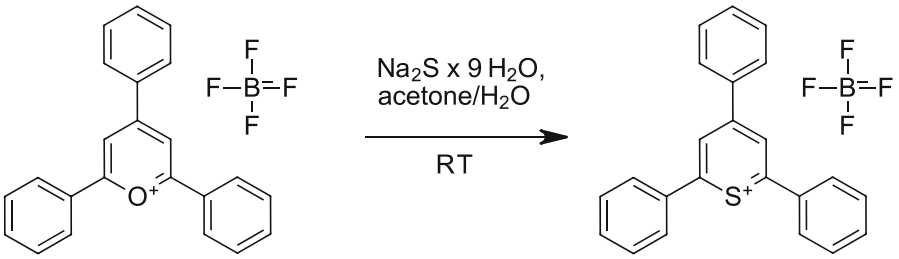

O4-B **S2-B**
24%

Figure 40: Synthesis of 2,4,6-triphenylthiopyrylium tetrafluoroborate (S2-B)

By reacting 2,4,6-triphenyl pyrylium tetrafluoroborate with sodium sulfide, the desired product can be directly obtained according to a route published by Michaudel et al.[130]

3.1.2. Group 14 Cations

3.1.2.1. Methylium Salts

In the 1930s Meerwein et al. came across the existence of trivalent, positively charged carbon atoms while studying the kinetics of the rearrangement of camphene hydrochloride.[131] While the methylium ion was only an intermediate step during the rearrangement. Much more stable compounds were introduced later.

3.1.2.1.1. Triphenyl Methylium Tetrafluoroborate

For an instance triphenyl methylium salts (Figure 41) which are especially stable due to the distribution of the positive charge over 10 carbon atoms (center atom, *para*- and *ortho*-carbon atoms). The most commonly used synthesis routes are the reaction of tritylchloride with either tetrafluoroboric acid or silver tetrafluoroborate. However the stability of triphenyl methylium is great under inert conditions, the hydrolysis stability of methylium compounds is known to be limited.[132]

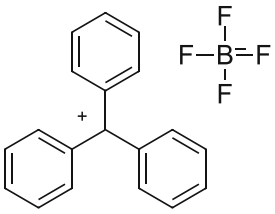

C1-B

Figure 41: Triphenyl methylium tetrafluoroborate (C1-B)

Due to the commercial availability of the triphenyl methylium salts, the compound was acquired and used as received for further testing.

Preliminary tests of the methylium salt hinted major hydrolysis issues while mixing with commercial monomers like BADGE. The residual water content in monomers was enough to hydrolyze the majority of the onium compound, hence generating decomposition products. A dark solid was obtained after a few seconds exposed to air or commercial monomers.

3.1.2.1.2. Tris(4-methoxyphenyl) Methylium Tetrafluoroborate

To overcome the mentioned stability issues of methylium salts, a derivative was chosen to tackle the problem. By the introduction of an alkoxy group the positive charge of the central carbon atom is even better distributed due to the strong mesomeric effect of alkoxy functionalities. Therefore, the para-substituted methoxy derivative was aimed, starting from the commercially available chloride (Figure 42). The synthesis rout was based on the work of Karim et al.[133]

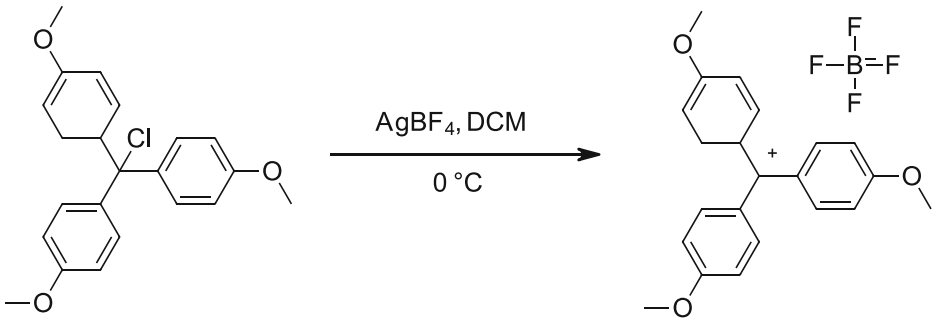

Figure 42: Synthesis to achieve tris(4-methoxyphenyl) methylium tetrafluoroborate (C2-B)

In addition, the stability against hydrolysis in air and water was checked via NMR. After around one minute, the result of the water stability test was negative. Direct exposure to water hydrolyzes the C2-B very quickly. However, the experiment conducted in air was positive. There was no noticeable hydrolysis after 1 h of exposure of the product to ambient air. Additionally, a halogen test was performed to verify the absence of residual chloride anions.

3.1.2.2. Germanonium Salts

The ability to convert germanium center atoms into germanonium cations with bromide as counterion was performed by Kraus et al.[134] However not all substituents or counterions are possible for those salts. For an instance the chemically very similar silicone in its trialkyl configuration is not able to form a stable salt with perfluorometallated anions like hexafluoroantimonate at room temperature.[135]

3.1.2.2.1. Triphenyl Germanonium Tetrafluoroborate

Nevertheless the synthesis approach was carried out according to Kraus et al.[134] Forming the symmetrical triphenyl germanonium bromide by reacting tetraphenyl germanium with bromine. During the course of the reaction, bromobenzene is liberated. Once synthesized, the bromide was tried to transform into the tetrafluoroborate via salt metathesis similar to the work of Li et al.[129]

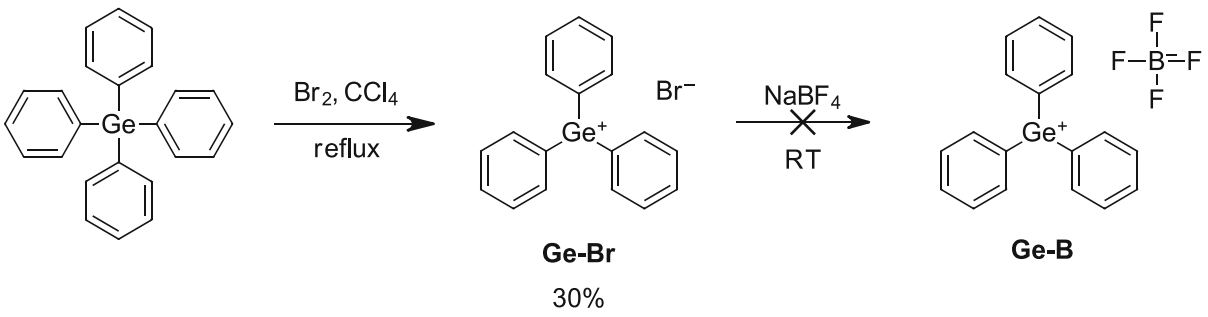

Figure 43: Synthesis route to achieve triphenyl germanonium tetrafluoroborate (Ge-B)

For the second step, 1 eq. of triphenyl germanonium bromide was dissolved in deionized water. After the educt was completely dissolved, 1.1 eq. of sodium tetrafluoroborate, dissolved in deionized water, were added. No precipitate was formed. A change of the solvent to mostly methanol did also not lead to the desired product. Additionally, a different route with silver tetrafluoroborate in acetonitrile was carried out with no evidence of the aimed tetrafluoroborate product after removal of the solvent.

According to literature, Edlund et al. suggests the evidence of organotin cations with weakly coordinating anions only in solution.[136] Due to the high similarity of tin and germanium, the observed results are very compatible with the literature claims.

3.1.2.3. Stanonium Salts

Tin-based onium salts can be either prepared by direct formation of the perfluorometallated version by reacting triarytin hydride with the corresponding silver salt (for example the trifluoromethanesulfonate)[137] or by synthesizing the triphenyltin bromide[138] and try a salt metathesis later.

3.1.2.3.1. Triphenyl Stanonium Tetrafluoroborate

Similar to the idea of the germanium-based initiator, a tin-based tetrafluoroborate was prepared. The well-known bromide was synthesized according to Chambers et al.[138] was preferred over the direct synthesis pathway due to the easier handling of the educts (Figure 44). The commercially available triphenyl tin hydroxide is a known herbicide and reacted with hydrobromic acid to give the desired bromide. Once synthesized, the bromide was tried to transform into the tetrafluoroborate via salt metathesis similar to the work of Li et al.[129]

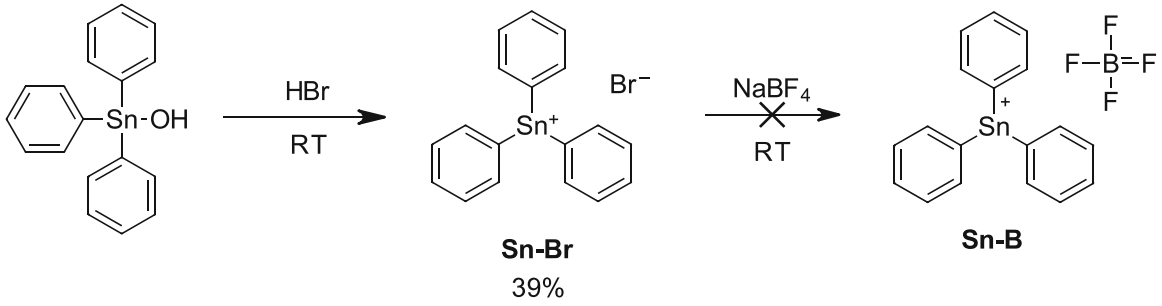

Figure 44: Synthesis route to achieve triphenyl stanonium tetrafluoroborate (Sn-B)

For the salt metathesis, 1 eq. of triphenyl germanonium bromide was dissolved in deionized water. After the starting material was completely dissolved, 1.1 eq. of sodium tetrafluoroborate, dissolved in deionized water, were added. A white precipitate was formed immediately, and the mixture was further stirred. Next, the dispersion was filtrated and

washed with deionized water, followed diethyl ether. The solid, white powder was then dried, yielding a greyish powder. The powder was not able to dissolve in any commonly used laboratory solvents, as well as in rather unconventional solvents like hexafluoroisopropanol. It was most likely a mixture of oxides and other decomposition products, indicated by a melting point higher than 400 °C. According to literature, Edlund et al. suggests the evidence of organotin cations with weakly coordinating anions only in solution.[136]

3.1.3. Group 15 Cations

3.1.3.1. Azonium Salts

The very broad term azonium ions includes a variety of different substance classes. Ammonium-,nitrosonium- or diazonium-ions are common examples just to name a few.[139] Since diazonium compounds are thermally very instable and release nitrogen gas upon irradiation (either thermal- or UV-photons), their application as cationic photoacid generators is not of interest. Additionally, the free electron pair of diazonium- and nitrosonium-compounds can act as an inhibiting base, therefore interferes with the propagating, positive charged chain end during cationic polymerization. This leads to ammonium salts as suitable substance class due to the thermal stability and absence of free electron pairs.

3.1.3.1.1. 1-Butyl-4-methyl Pyridinium Tetrafluoroborate

Pyridinium salts (Figure 45) are a subclass of quaternary ammonium ions. They are used as herbicides or in Friedel-Craft acylation. The preparation includes the reaction of pyridine with a corresponding acid and a salt metathesis to receive the desired counterion.[140]

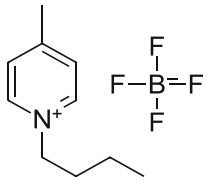

N-B

Figure 45: 1-butyl-4-methyl pyridinium tetrafluoroborate (N-B)

Since pyridinium tetrafluoroborates are commercially available, the 1-butyl-4-methyl derivative was acquired from commercial sources and used for further testing.

3.1.3.2. Phosphonium salts

Tetravalent phosphor-based compounds were introduced in the early 1960s by Sasse et al.[141] Quaternary phosphonium cations are generally produced by alkylation of organophosphines (for example triphenylphosphine) with iodides.[142] This reaction route leads to stable

phosphonium salts which are known for obtaining in high yields and easy purification. Due to the high thermal stability, phosphonium salts show low potential as thermal initiators. Investigation of this behavior was performed by Takuma et al. and lead to the assumption, that phosphonium hexafluoroantimonates can act as a latent thermal initiator for cationic polymerization of epoxides.[143] When irradiated directly at their absorption maximum at 268 nm, the phosphonium salts are unable to generate reactive species to induce cationic polymerization. However, irradiation at a bathochromically shifted peak including the tail-out region seems more promising.[144]

3.1.3.2.1. Butyl Triphenyl Phosphonium Tetrafluoroborate

As the first representative of the phosphonium compounds, a classic approach towards butyl triphenyl phosphonium tetrafluoroborate was targeted (Figure 46), due to its well-known preparation and easy synthesis.

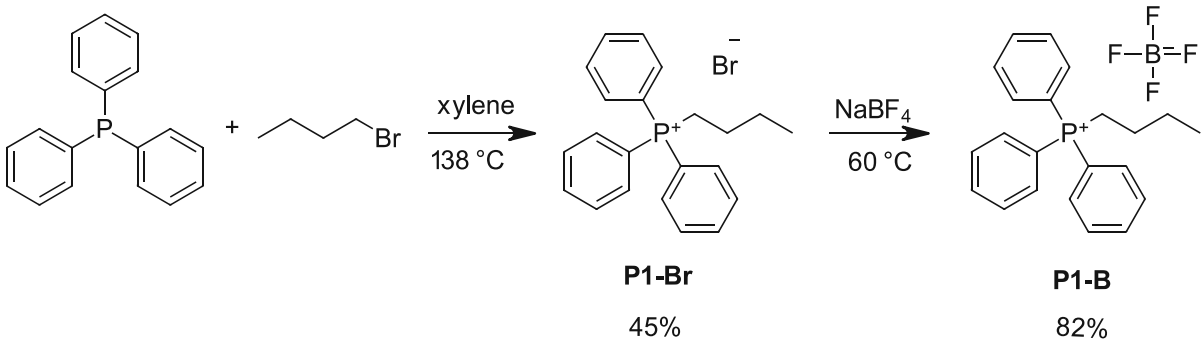

Figure 46: Synthesis route to achieve butyl triphenyl phosphonium tetrafluoroborate (P1-B)

The reaction route was performed according to a patent by Kusumoto et al.[145] with triphenylphosphine as precursor and 1-bromobutane as reagent. A general review by Virieux et al.[146] was also taken into account for the synthesis route planning. In the second step, an ion exchange reaction similar to the work of Li et al.[129] was performed, which converts the bromine into the tetrafluoroborate.

3.1.3.2.2. Tetraphenyl Phosphonium Tetrafluoroborate

To access the most similar molecule to the diphenyl iodonium and triphenyl sulfonium cations, a symmetrical, tetraphenyl substituted phosphonium salt was prepared (Figure 47).

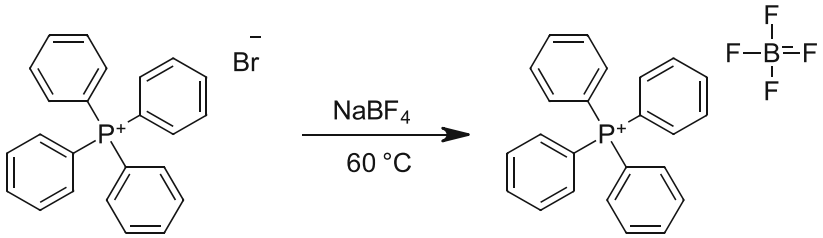

P2-Br **P2-B**

87%

Figure 47: Synthesis of tetraphenyl phosphonium tetrafluoroborate (P2-B)

A salt metathesis similar to Li et al.[129] was performed to convert the commercially available bromide into the tetrafluoroborate.

3.1.3.2.3. Benzyl Triphenyl Phosphonium Tetrafluoroborate

To obtain a variety of phosphonium salts with different substituents and solubility, the benzyl triphenyl phosphonium was prepared via salt metathesis according to Li et al.[129] (Figure 48).

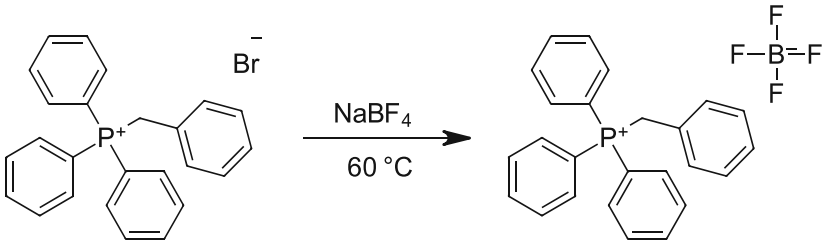

P3-Br **P3-B**

84%

Figure 48: Synthesis of butyl triphenyl phosphonium tetrafluoroborate (P3-B)

The bromide educt was transformed into the tetrafluoroborate by using sodium tetrafluoroborate as reagent.

3.1.3.2.4. Cyclopropyl Triphenyl Phosphonium Tetrafluoroborate

As a last representative of the aryl-phosphonium salts, the cyclopropyl triphenyl derivative was aimed (Figure 49).

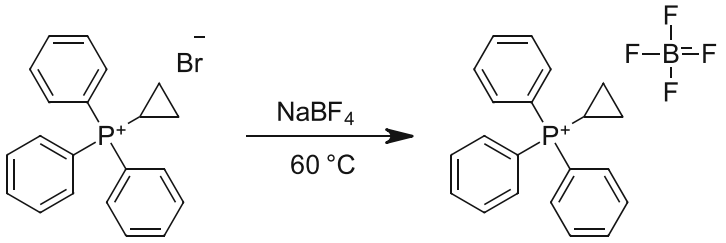

P4-Br **P4-B**

73%

Figure 49: Synthesis of cyclopropyl triphenyl phosphonium tetrafluoroborate (P4-B)

Again an ion exchange procedure similar to Li et al.[129] was performed with the commercially available bromine educt to give the desired product upon mixture with sodium tetrafluoroborate.

3.1.3.2.5. Tetraethyl Phosphonium Tetrafluoroborate

By using the commercially available tetraethyl phosphonium tetrafluoroborate as representative of alkylated phosphonium salts, the difference in reactivity and photosensitivity can be investigated (Figure 50).

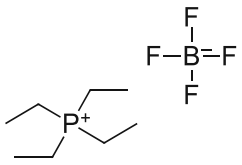

P5-B

Figure 50: Tetraethyl phosphonium tetrafluoroborate (P5-B)

Low solubility in non-polar monomers was expected for this alkyl-based compound due to its high polarity. Due to its low cost and broad availability the acquisition of P5-B was easy and the onium salt was used as received from the supplier.

3.1.3.3. Stibonium Salts

Similar to tetravalent phosphor and arsenic compounds, there is the possibility to synthesize antimony-based onium salts. Stibonium hexafluoroantimonates were used to polymerize THF with triethyl silane as an additive.[147] Therefore the photochemical properties and reactivity of such compounds is very interesting.

3.1.3.3.1. Tetraphenyl Stibonium Tetrafluoroborate

Antimony-based onium salts should be able to initiate cationic polymerization. Therefore, the compound tetraphenyl stibonium tetrafluoroborate was aimed (Figure 51).

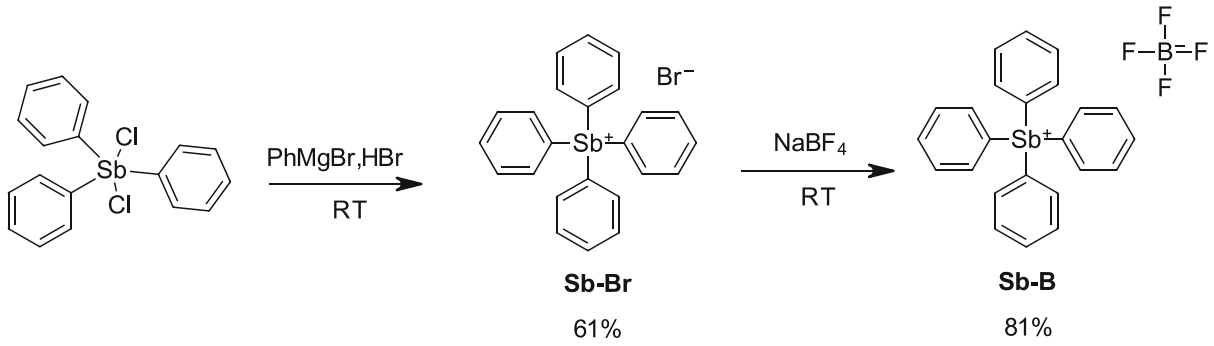

Figure 51: Synthesis route to achieve tetraphenyl stibonium tetrafluoroborate (Sb-B)

A reaction route according to Ma et al.[148] was carried out to synthesize the bromide out of dichlorotriphenyl antimony and phenyl magnesium bromide in a Grignard reaction. Once the Sb-Br is synthesized, a salt metathesis to the tetrafluoroborate was performed similar to Li et al.[129]

3.1.3.4. Bismuthonium Salts

Bismuth-based onium salts comprise the property of being classified as a metal, rather than non-metals and transition metals like phosphonium or stibonium salts. This circumstance makes them an interesting onium class on their own. Previous research conducted by Matano et al. shown the good photochemical behavior of bismuthonium hexafluoroantimonates in epoxy-based systems as a photoacid generator.[149]

3.1.3.4.1. Tetraphenyl Bismuthonium Tetrafluoroborate

The triphenyl bismuth difluoride starting material was prepared first, starting from triphenyl bismuth. The chloride was synthesized similar to Solyntjes et al. using sulfonyl chloride as reagent (Figure 52).[150]

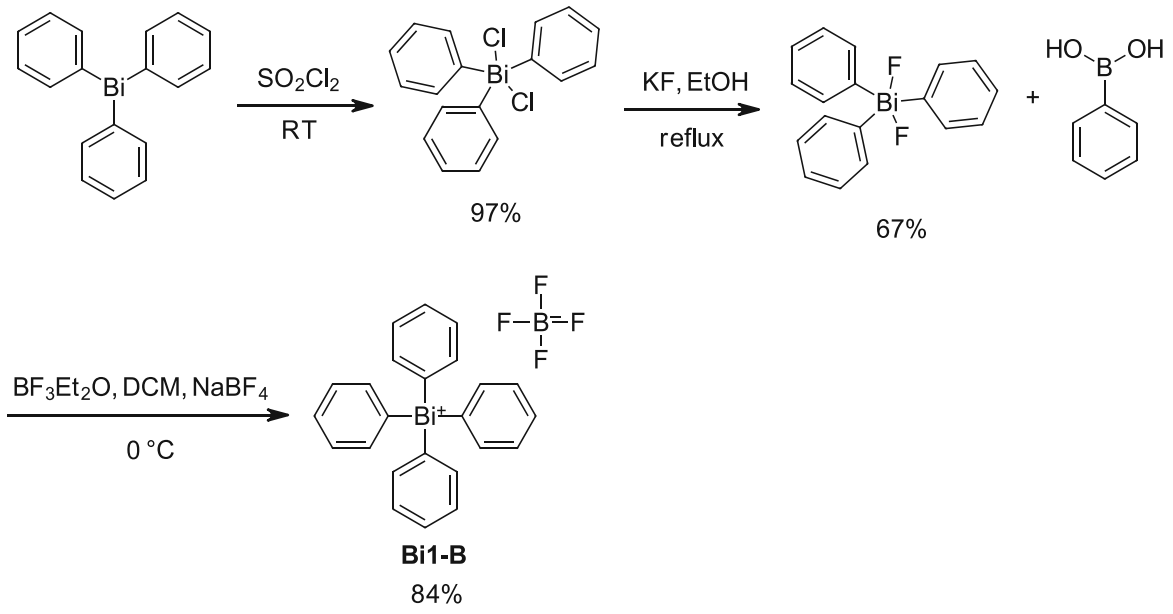

Figure 52: Synthesis of tetraphenyl bismuthonium tetrafluoroborate (Bi1-B)

According to the work of Challenger et al.[151] the dichloride was fluorinated via KF. To further synthesize the bismuthonium-based tetrafluoroborate, a synthesis route according to Matano et al.[152] was carried out. This route involves the BF_3-etherate-promoted reaction of the triphenyl bismuth difluoride with phenylboronic acid.

3.1.4. Group 16 Cations

3.1.4.1. Oxonium Salts

When oxonium compounds are mentioned, usually Meerwein salts[153] are the topic of most interest. Trivalent alkyl oxonium salts are generally used in organic chemistry. Tri(m)ethyl oxonium tetrafluoroborates for example are highly efficient alkylation agents. However, they suffer from thermal instability and hydrolysis at room temperature. Interestingly, positive charged oxygen atoms bond to phenyl rings experience rather unexpected stability towards temperature and moisture. Triphenyl oxonium salts were first investigated by Nesmeyanov et al.[154] by the reaction of diphenyl ether with benzene diazonium tetrafluoroborate, while nitrogen gas is released. The rather low yield of the reaction can be improved by forcing an intramolecular nitrogen release instead of an intermolecular one. However the educt for this improved route is more complicated to obtain.[155] All mentioned oxonium salts to this point

were symmetrical ones, however there is the possibility to generate asymmetric oxonium salts in-situ like aryl-dialkyl or diaryl-alky substituted compounds. The problem of asymmetric oxonium compounds is their instability above -70 °C in solution. Therefore, such salts are not able to be isolated due to their immense reactivity towards trans-alkylation.[156, 157]

3.1.4.1.1. Tri(m)ethyl Oxonium Tetrafluoroborate

Despite their temperature and moisture sensitivity, trimethyl oxonium tetrafluoroborate and triethyl oxonium tetrafluoroborate were included in the tested compounds too (Figure 53).

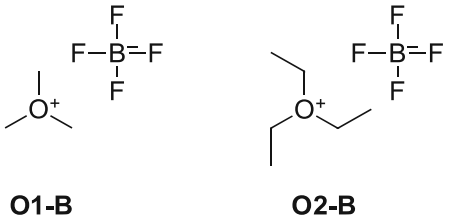

Figure 53:Trimethyl oxonium tetrafluoroborate (O1-B) and triethyl oxonium tetrafluoroborate (O2-B)

Due to the fact that these two alkyl-oxonium salts are often used as alkylation agents, they are very cheap to acquire and broadly commercially available. Upon mixing with 50 wt% of propylene carbonate to increase the solubility in nonpolar media like epoxy-based monomers like BADGE, the formulations started to harden after a few seconds for the O1-B at room temperature. It took around one minute for O2-B to harden, while homogenizing the mixture and holding the vial during the process. Body temperature transfer to the vial was enough to liberate the superacid and polymerize the epoxy monomer. This makes the alkyl oxonium salts unable to perform in storage stable pre-mixed formulations for cationic polymerization.

3.1.4.1.2. Triethyl Oxonium Hexafluorophosphate

To investigate the influence of the counter ion of alkyl-substituted oxonium compounds and consequently the thermal stability as well as reactivity. It is generally known that the strong acid replaces the weaker acid in salts easily. Therefore, a counter ion exchange was performed by liberating the tetrafluoro boric acid to prepare the triethyl oxonium hexafluorophosphate (Figure 54).

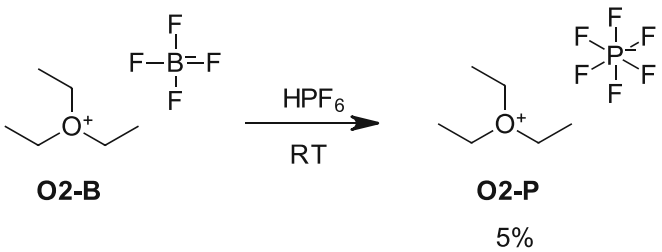

Figure 54: Synthesis of triethyl oxonium tetrafluoroborate (O2-P)

First tests with 50 wt% of propylene carbonate as additive and BADGE as monomer, lead to hardened samples after a few seconds at ambient temperatures. Additionally, contact with water leads to decomposition of the O2-P into mainly diethyl ether and ethanol besides other decomposition products. Due to the weaker coordination of anion and cation compared to the educt O2-B, the Hexafluorophosphate decomposes faster in water.

Due to the fact, that no alkyl oxonium salt is suitable for the preparation of a storage stable epoxy-based formulation, more stable oxonium salts were aimed (Figure 55).

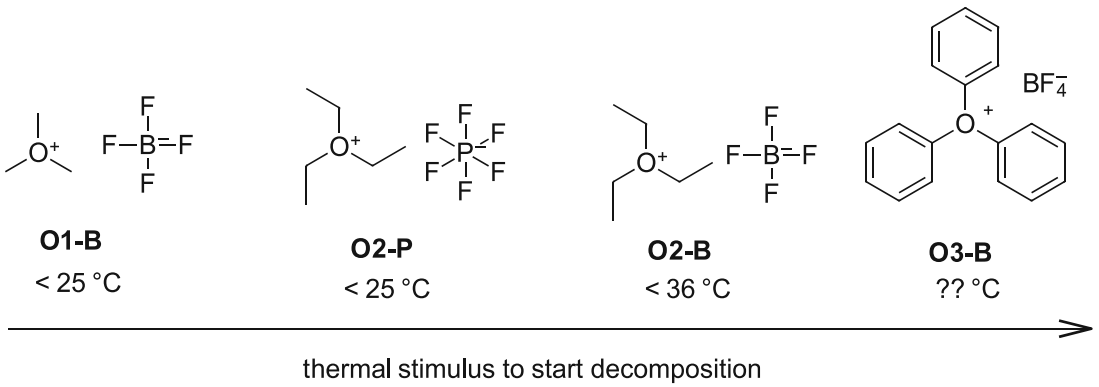

Figure 55: Temperatures at which the different oxonium salts thermally decompose and form a superacid

The already known triphenyl oxonium tetrafluoroborate for example seems to be a promising candidate to solve the stability issues (decomposition temperature is above 200 °C).[154]

3.1.4.1.3. Triphenyl Oxonium Tetrafluoroborate

For better comparison to other phenyl-substituted onium salts synthesized previously, the triphenyl oxonium tetrafluoroborate was aimed to prepare (Figure 56). This molecule is promising to be a stable oxonium compound with benzene diazonium tetrafluoroborate and diphenyl ether as starting materials. The diazonium salt is freshly prepared in advance very similar to the work of Flood et al.[158] One exception to the original procedure was made. Instead of the hydrochloric acid, tetrafluoroboric acid was used in the first step, therefore skipping the salt metathesis afterwards. The yield of this synthesis is expected to be approximately 2% according to the work of Nesmeyanov et al.[154]

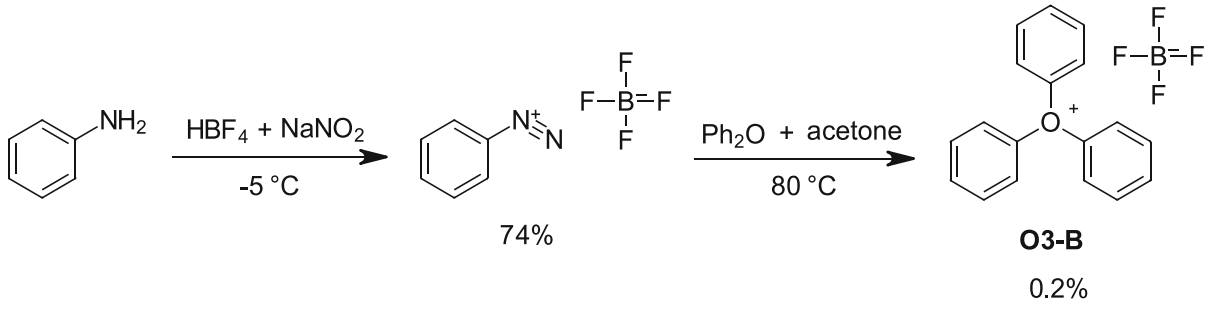

Figure 56: Synthesis route to achieve triphenyl oxonium tetrafluoroborate (O3-B)

First tests of the triphenyl oxonium salt indicate good preliminary storage stability of formulations containing the oxonium salt, propylene carbonate and the epoxy-based monomer BADGE. Thermally-driven decomposition at 36 °C followed by initiation, like it was the case with all tested alkyl oxonium salts, did not occur with O3-B. The low yield of the O3-B can easily be explained due to a very dominant occurring side reaction, the azo-coupling. The color change of the diphenyl ether solution during the addition of the benzene diazonium tetrafluoroborate (electrophile) from colorless to yellow to red is caused by the formation of azo-dyes (Figure 57).

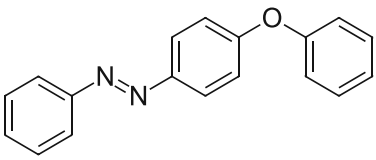

Figure 57: Azo-coupling of benzene diazonium tetrafluoroborate with diphenyl ether (example structure)

In this case the electrophile attacks the *para*-position of the electron rich aromatic ring of the diphenyl ether, followed by the liberation of HBF_4. This is only one possible product which can be formed due to the activation of *ortho*- and *para*-positions of the diphenyl ether. But less steric hindrance allows the *para*-positions to be more reactive compared to the *ortho*-position.

3.1.4.1.4. 2,4,6-Triphenyl Pyrylium Tetrafluoroborate

Unlike normal oxonium salts, where the positive charge is carried by a central oxygen atom, pyrylium salts distribute this charge along at least one aromatic ring. The base molecule is a six-membered ring including the oxonium ion (Figure 58). The triphenyl pyrylium tetrafluoroborate shown reactivity towards cationically polymerizable resins with vinyl ethers as coinitiators.[159]

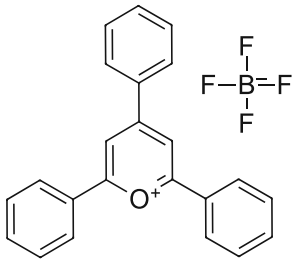

O4-B

Figure 58: Triphenyl pyrylium tetrafluoroborate (O4-B)

Triphenyl pyrylium tetrafluoroborate is a commercially available pyrylium salt, therefore used as received in further testing.

3.1.4.1.5. 2,6-Di-tert-butyl-4-methyl Pyrylium Tetrafluoroborate

To compare the influence of different substituents at the pyrylium structure, the di-tert-butyl-methyl pyrylium trifluoromethanesulfonate (Figure 59) was converted into its tetrafluoroborate derivative via salt metathesis similar to the patent of Hovione Inter. LTD.[160]

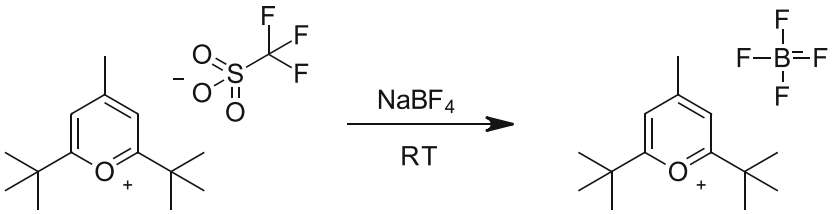

O5-S **O5-B**

51%

Figure 59: Synthesis of 2,6-di-tert-butyl-4-methyl pyrylium tetrafluoroborate (O5-B)

This route involves O5-S and excess sodium tetrafluoroborate as ion exchange reagent at room temperature.

3.1.4.1.6. 2,4,6-Trimethyl Pyrylium Tetrafluoroborate

The commercially available pyrylium salt trimethyl pyrylium tetrafluoroborate was considered as potential candidate as cationic initiator as well (Figure 60).

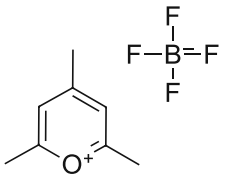

O6-B

Figure 60: Trimethyl pyrylium tetrafluoroborate (O6-B)

Since the tetrafluoroborate anion is already present in the O6-B, no additional salt metathesis had to be performed. The compound was used as received for further testing.

3.1.4.2. Selenonium Salts

The preparative aspects of selenonium and other group 16 cations have been compiled in a review by Irgolic et al.[161] Additionally, Crivello et al.[162] investigated the photochemical properties of selenonium salts and its potential of acing as an acid generator. Therefore, this class of onium compound was included in the studies.

3.1.4.2.1. Triphenyl Selenonium Tetrafluoroborate

To get access to a selenonium-based photoacid generator, the triphenyl substituted one was synthesized (Figure 61).

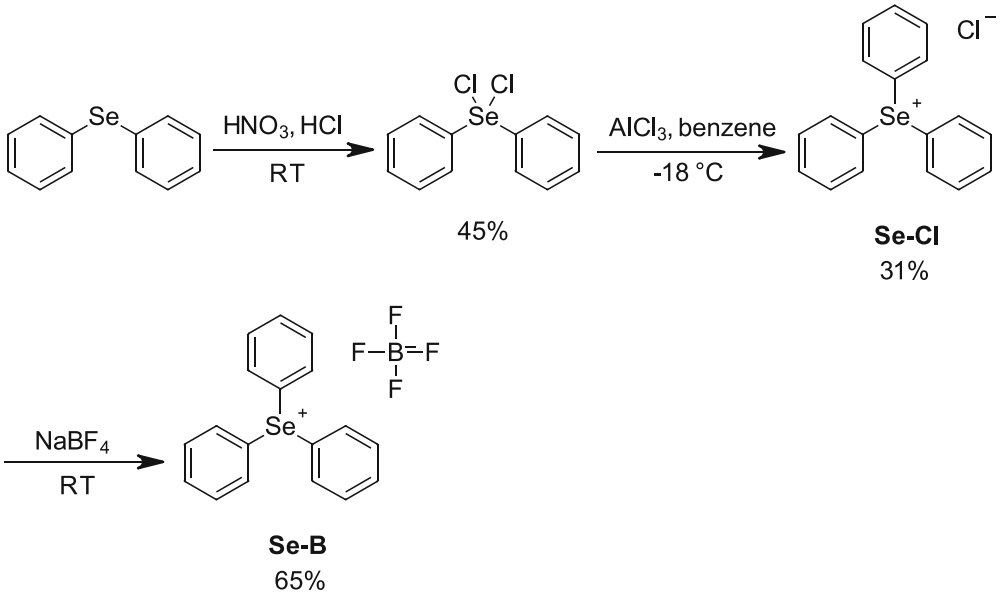

Figure 61: Synthesis route to achieve triphenyl selenonium tetrafluoroborate (Se-B)

As stated in the paper of Crivello et al.[162] this compound is light sensitive, therefore a candidate as (photo)acid generator for cationic polymerization.

3.1.4.3. Telluronium Salts

In contrast to group 15 nonmetals, for example sulfonium and selenonium salts, the telluronium compounds are part of the transition metals located in the fifth period of the periodic table of elements. Therefore, the photochemical properties are expected to change due to the more metal like behavior of telluronium salts. This makes them an interesting component of the selected compounds for further testing. Synthesis of tellurium-based onium salts is a well understood procedure and possible in high yields.[161]

3.1.4.3.1. Triphenyl Telluronium Tetrafluoroborate

The synthesis was performed similar to the research of Gunther et al.[163] A Lewis acid catalyzed reaction of the tellurium tetrachloride with aluminum chloride in benzene was carried out (Figure 62).

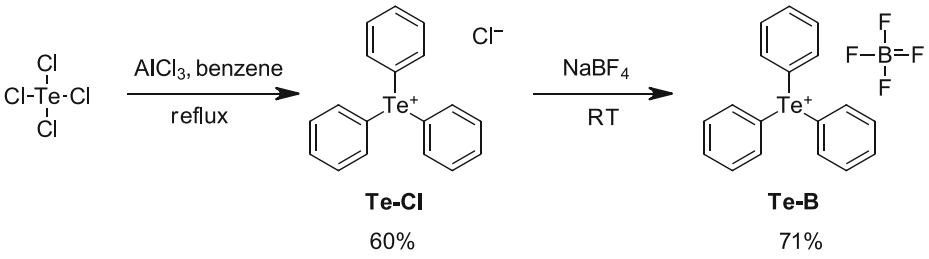

Te-Cl 60%

Te-B 71%

Figure 62: Synthesis route to achieve triphenyl telluronium tetrafluoroborate (Te-B)

The obtained triphenyl telluronium chloride was then used in a salt metathesis reaction similar to Li et al.[129]

3.2. Characterization of Onium Tetrafluoroborates

3.2.1. Selection of the Onium Tetrafluoroborate Compounds

Since synthesis of most aimed onium salts was successfully executed, the selection for the testing phase was performed. Therefore, the potential of each initiator can be determined under various conditions, for example thermal- or photo-stimuli to potentially start cationic polymerization (Figure 63).

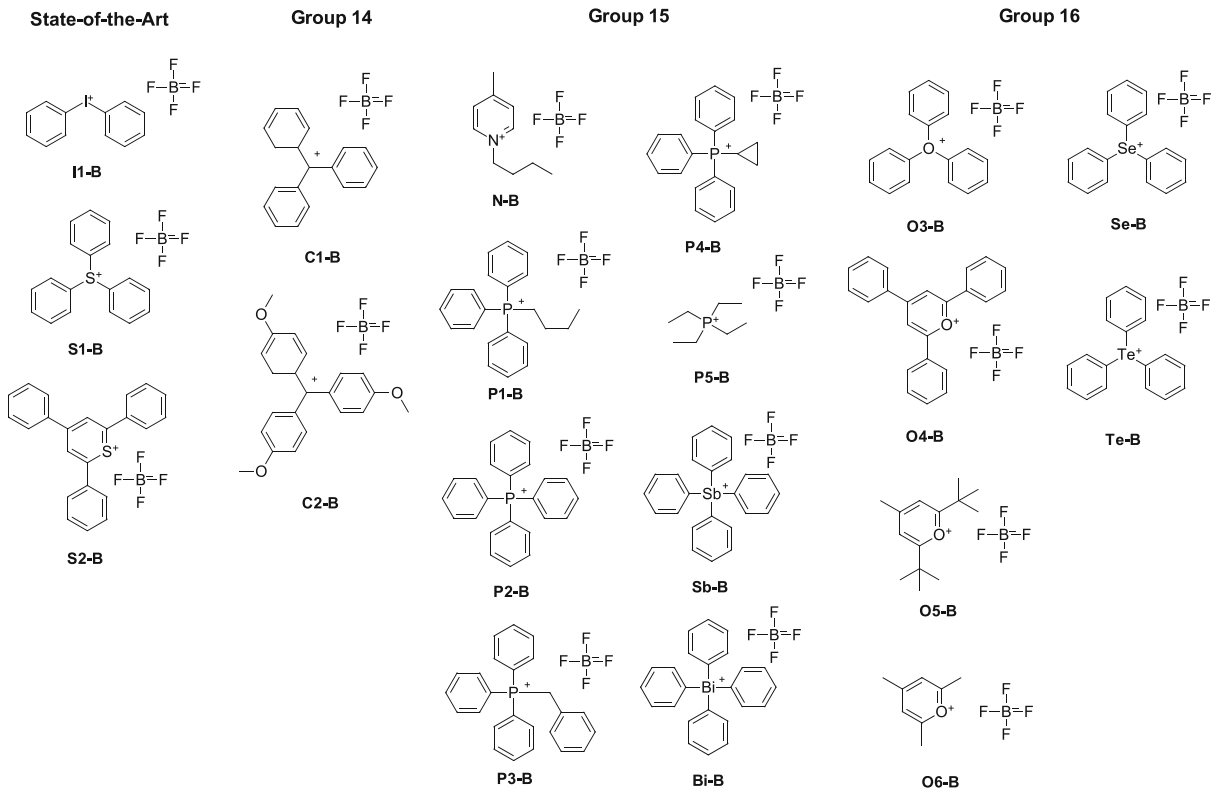

Figure 63: Selection of the onium tetrafluoroborates for further analysis

From every mentioned subcategory of onium salt at least one compound was selected, except for alkyl oxonium and unsubstituted pheny methylium compounds due to their severe stability issues. Alkylated oxonium salts turned out to be rather unstable, if mixed with a commercial epoxy-based resin, hence hardening of the formulation was happening in the matter of seconds. Triphenyl methylium tetrafluoroborate hydrolyzed during the mixing process with the commercially available epoxy monomers due to residual moisture in such monomers. Despite those rare exceptions, a broad collection of onium-based molecules could be tested in terms of photochemical behavior, redox potential and reactivity.

3.2.2. Verifying the Absence of Strong Bases

To ensure a well propagating cationic polymerization, no (Lewis-)bases, such as chloride- or bromide-ion traces from starting materials, are allowed in the formulations. Since halogens are strong nucleophiles, they bind strongly to the cationic end of the polymer. Due to this ionic bond formation, the positive charge of the chain end is shielded and unable to attack further monomer molecules, quenching cationic polymerization. Therefore, all onium compounds were tested, to ensure the absence of halogens (Table 7).

Table 7: Results of the test for strong bases (chloride and bromide ions)

Compound	Result	Compound	Result
I1-B	negative	P5-B	negative
S1-B	negative	Sb-B	negative
S2-B	negative	Bi1-B	negative
C2-B	negative	O1-B	negative
N-B	negative	O3-B	negative
P1-B	negative	O4-B	negative
P2-B	negative	O5-B	negative
P3-B	negative	Se-B	negative
P4-B	negative	Te-B	negative

The procedure consisted of dissolving the onium compound in a 1:1 vol% mixture of water and methanol and adding silver nitrate solution in the same mixture of solvents. Due to solubility issues, some onium salts were dissolved in DMSO with a slight amount of water. All mixtures were allowed to react for 5 minutes after mixing. If the test outcome was positive, a clearly visible, white silver halogenate precipitate had settled or was dispersed in solution according to the equation (Figure 64).

Figure 64: Precipitation reaction of a positive halogen test (A^+…onium ion; X^-…halogen counter ion (Cl^-, Br^-, I^-))

A clear solution with the absence of solids indicated the aimed negative test result.

3.2.3. Absorption Spectra determined via UV-VIS Experiments

3.2.3.1. Onium Salts

During the photochemical analysis, the ultraviolet (UV) and visible light (VIS) absorption spectra of the onium compounds were determined. The scanned wavelength window ranges from 260 nm to 600 nm. This analysis enables the appropriate selection of a light source and wavelength filter for further experiments. Samples were dissolved in dry acetonitrile. Depending on the absorption of the onium salt, concentrations of 1×10^{-4} mol L^{-1} or 1×10^{-5} mol L^{-1} were used. The solution was transferred into 10 mm quartz cells and absorption was measured at the photometer.

3.2.3.1.1. State of the Art Cations

The first set of the selected onium tetrafluoroborates, state-of-the-art compounds were subject of UV-VIS measurements.

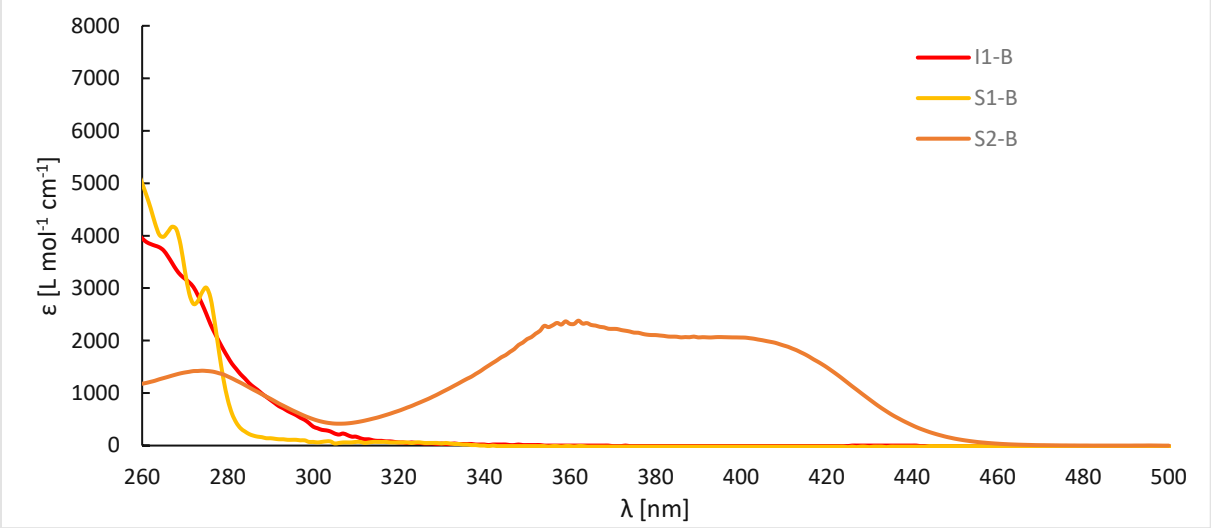

Figure 65: Wavelength dependence of the molar extinction coefficient for state of the art iodonium, sulfonium and thiopyrylium salts

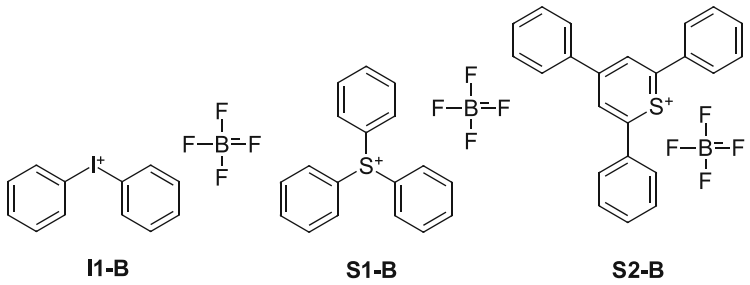

As illustrated in the absorption spectra above (Figure 65), the commercially used S1-B shows two maxima at 268 nm and 276 nm with a tail-out region to around 320 nm (Figure 65). I1-B shows an absorption starting around 320 nm. Only the thiopyrylium-based S2-B showed broad absorption behavior starting at 460 nm with its peak at 361 nm.

3.2.3.1.2. Group 14 Cations

Secondly, all methylium-based onium salts were measured in acetonitrile to determine the wavelength-dependent extinction coefficient.

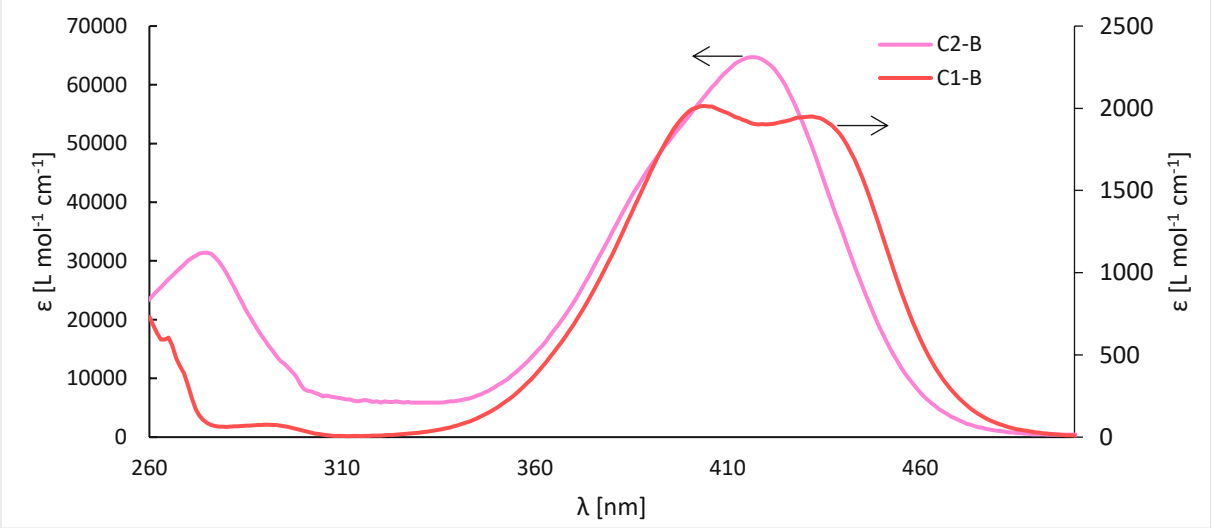

Figure 66: Wavelength dependence of the molar extinction coefficient for tris(4-methoxyphenyl) methylium tetrafluoroborate (primary axis) and triphenyl methylium tetrafluoroborate (secondary axis)

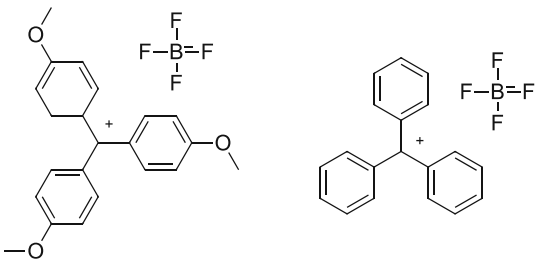

Methylium tetrafluoroborates (Figure 66) show interesting absorption behavior compared to nearly all other onium salts tested. The quite bathochromic shift of the absorption maxima at 418 nm for the C2-B and 435 nm as well as 406 nm for the C1-B. In addition, there are peaks in the deeper UV-range too. To be precise, 277 nm for the methoxy-substituted methylium and around 290 nm for the phenylated methylium salt. The shifted maximum as well as the decreased overall extinction coefficient of C2-B is the result of the increased mesomeric stabilization in combination with the electron withdrawing effect of three methoxy moieties.

3.2.3.1.3. Group 15 Cations

Next, the nitrogen-based onium salt together with all 7 differently substituted phosphorus-based salts were investigated.

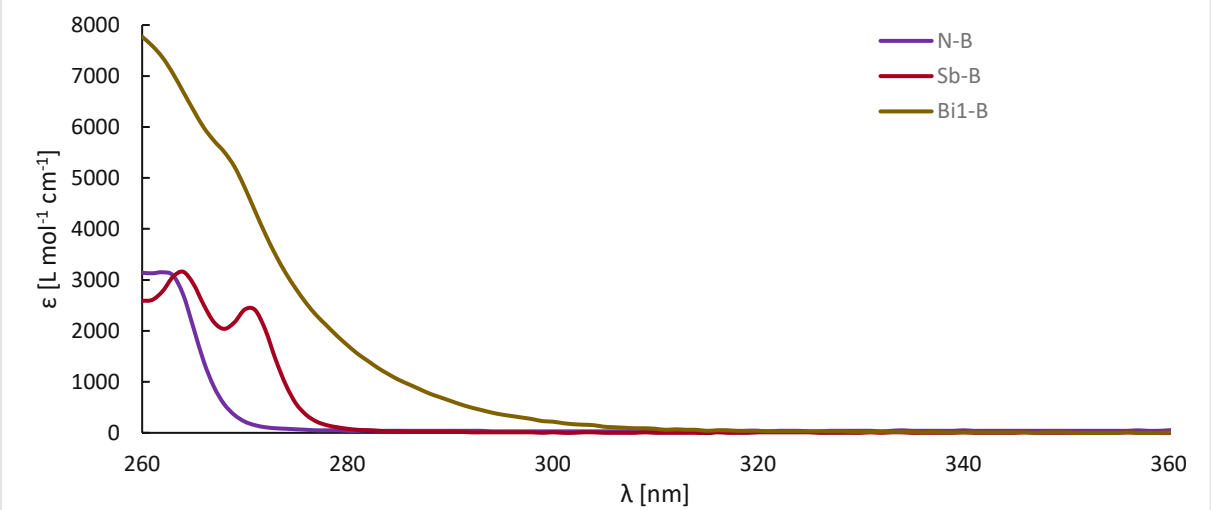

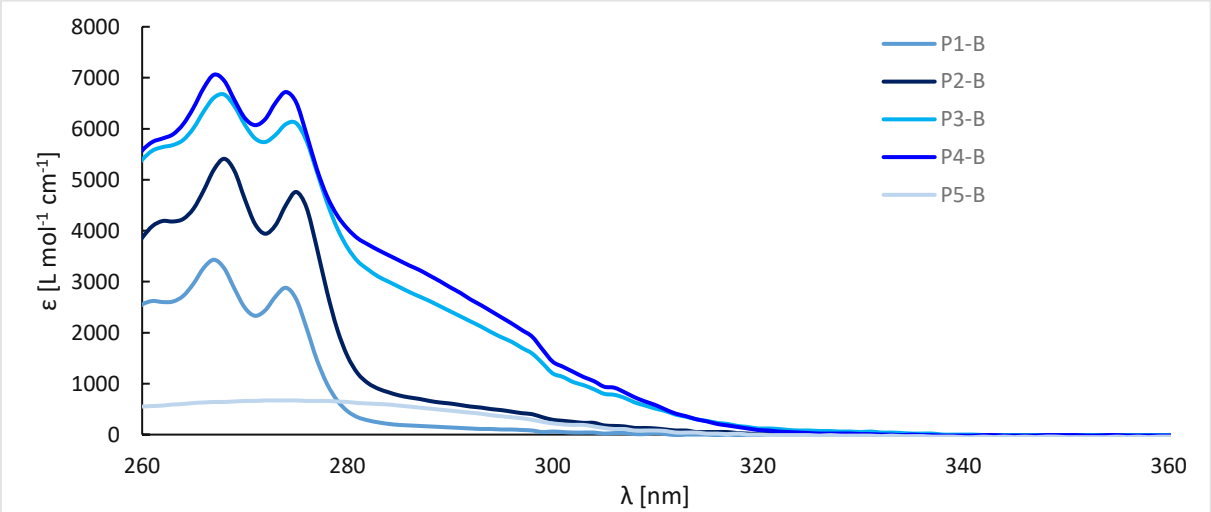

Figure 67: Wavelength dependence of the molar extinction coefficient for pyridinium, phosphonium, stibonium and bismuthonium compounds

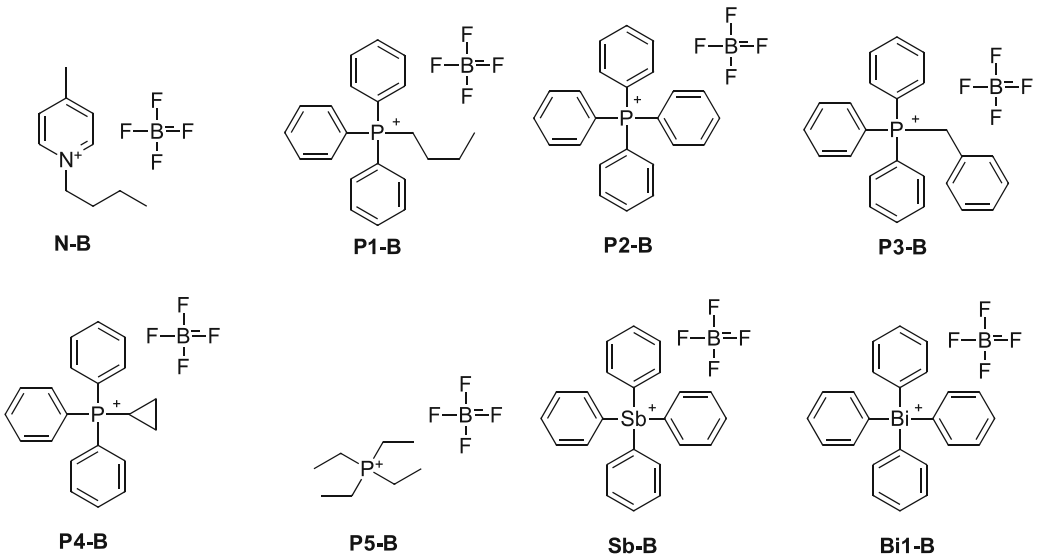

The pyridinium-based salt shows a small peak at 263 nm, while the regions above 280 nm show no absorption at all. Considering the phosphor-based onium salts one can clearly notice the similar absorption behavior according to their shared chemical structure (Figure 67). As expected, the highest extinction coefficient is reached by the highly aromatic P2-B, followed by the P3-B and the phosphonium compounds with alkyl substituents P1-B and P4-B. The phosphonium chromophore shows peaks at approximately 270 nm, which is also in accordance to literature.[144] Only the purely alkyl-based P5-B show no absorption peak in the scanned wavelength area, however there is a noticeable increase while scanning from 260 nm down to 310 nm. The data obtained for the solutions containing Sb-B, shows two absorption maxima in the measured range (264 and 2671 nm) with extinction coefficients above 2400 L mol^{-1} cm^{-1}. The bismuth-based onium salt shows no absorption peak in the measured range, however at lower wavelengths, starting at around 310 nm, a strong absorption is obtained.

3.2.3.1.4. Group 16 Cations

The last group of UV-VIS measured onium salts contains all oxygen-based compounds such as pyrylium and oxonium salts.

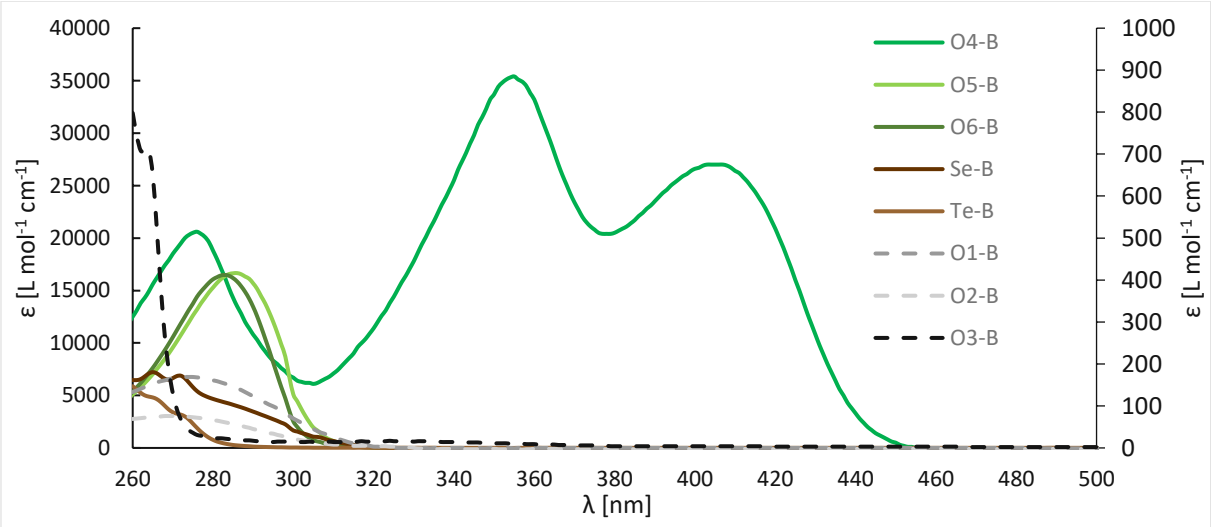

Figure 68: Wavelength dependence of the molar extinction coefficient for pyrylium, selenonium and telluronium compounds (primary axis) and alkyl/phenyl-oxonium compounds (secondary axis)

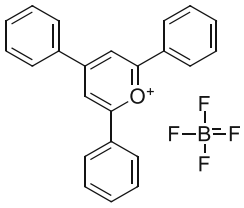

O4-B

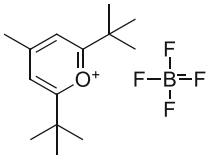

O5-B

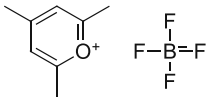

O6-B

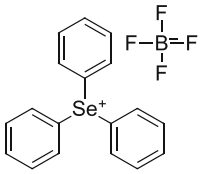

Se-B

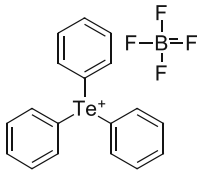

Te-B

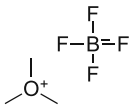

O1-B

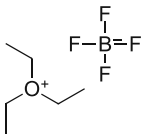

O2-B

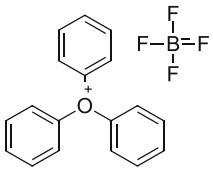

O3-B

The absorption maxima for the pyrylium-based salts show a very similar behavior at wavelengths of approximately 285 nm (Figure 68). As expected the O4-B with its four aromatic rings reaches the highest value in terms of molar extinction coefficient. In addition, its two peaks at 357 nm and 409 nm are quite bathochromically shifted compared to the other onium salts. The pyrylium compounds, O6-B and O5-B, act very similar and show their single maximum at 285 nm and 286 nm respectively. With a molar extinction below 200 L mol^{-1} cm^{-1} both O1-B and O2-B show their maximum at around 270 nm. The absorption maximum for O3-B in the measured range is visible at 264 nm with an extinction coefficient of around 700 L mol^{-1} cm^{-1}. The selenium-based compound shows its maximum at 319 nm and 267 nm, while the tellurium-based onium salt shows no peak in the scanned region.

3.2.3.2. Sensitizers

Sensitizers comprise the ability to transfer absorbed energy from photons directly to onium salts. This process can lead to cleavage of the onium compound and consequently to the liberation of the superacid which is crucial for the initiation step. To investigate the absorption properties of the sensitizers, a UV-VIS study was performed (Figure 69). Similar to the section considering onium compounds, the samples were measured in concentration of 1 x 10^{-4} mol L^{-1} or 1 x 10^{-5} mol L^{-1}.

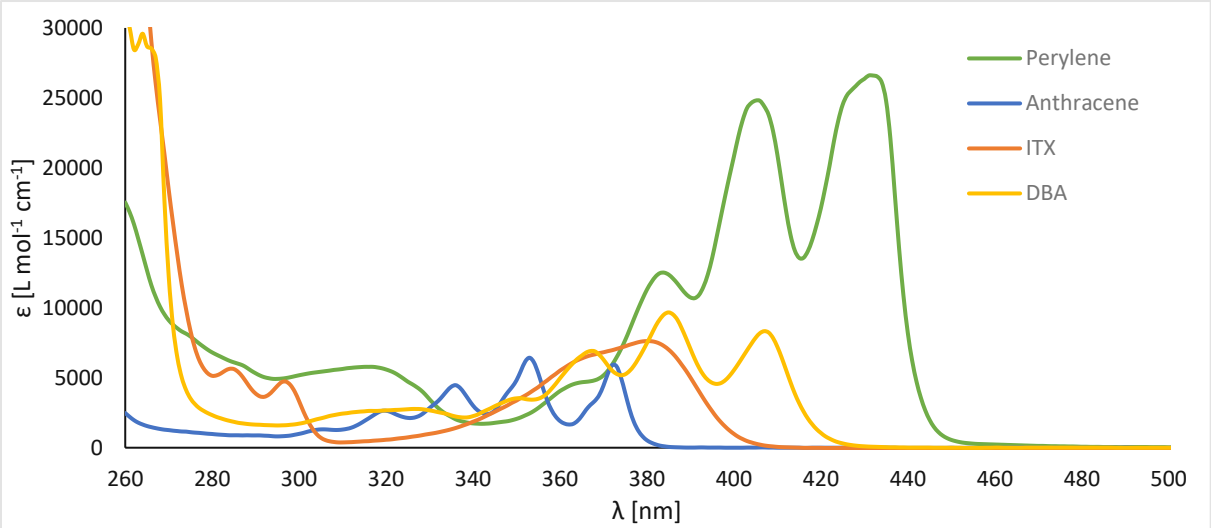

Figure 69: Wavelength dependence of the molar extinction coefficient for the sensitizers

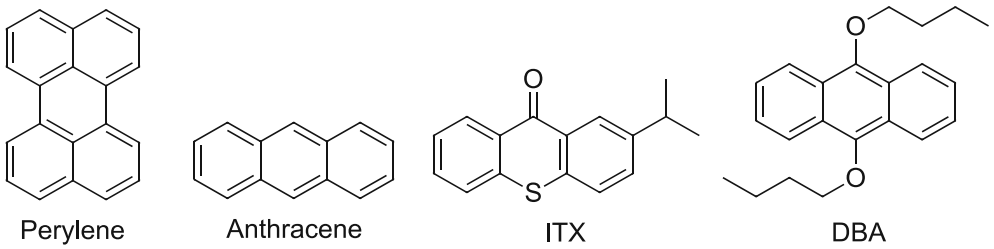

According to the aromaticity of all sensitizers tested, their extinction coefficients are rather high with a maximum of around 27,000 L mol^{-1} cm^{-1} (Figure 69). Therefore, making them perfectly suitable as potential sensitizing molecules to transfer the charge to the onium compounds. Perylene has of course the highest value in terms of extinction, as well as the maximum at the highest wavelength (431 nm). The remaining maxima for perylene are besides the most hypsochromic shifted maximum at 316 nm, at 384 nm and 405 nm. Anthracene has four distinct maxima ranging from 320 to 372 nm, making it a versatile sensitizer for UV-applications. By comparing the anthracene to its dibutoxylated derivative DBA, a clear bathochromic shift of all maxima can be observed, with a tail-out region up to 430 nm. The benzophenone derivative ITX (2-Isopropylthioxanthone) shows a broad absorption maximum at 380 nm. For further testing, perylene was excluded from the set of sensitizers, due to a strong extinction coefficient resulting from its intense coloration, since transparent, non-colored samples were aimed for. Anthracene, in contrast to ITX was preferred as sensitizer, due to anthracenes inability to generate radicals upon irradiation. In addition, the performance of ITX and anthracene are nearly the same for iodonium- and sulfonium salts in cationic polymerization with only a slight advantage for the ITX.[4, 118] The anthracene derivative DBA shows superior absorption properties and better solubility

compared to standard anthracene. However, was not used in preliminary tests, due to its much higher price. Therefore, anthracene was selected for all upcoming sensitization experiments.

3.2.4. Reduction Potentials measured by Cyclic Voltammetry

To investigate the reduction and oxidation potentials, cyclic voltammetry (CV) was selected. By sweeping the applied potential on a sample, a change in current flow is detected. Therefore, the CV can determine at which potentials reactions or changes of the sample occur. In the case of CV, two potentials are chosen and the applied current changes back and forth between those set values (Figure 70).

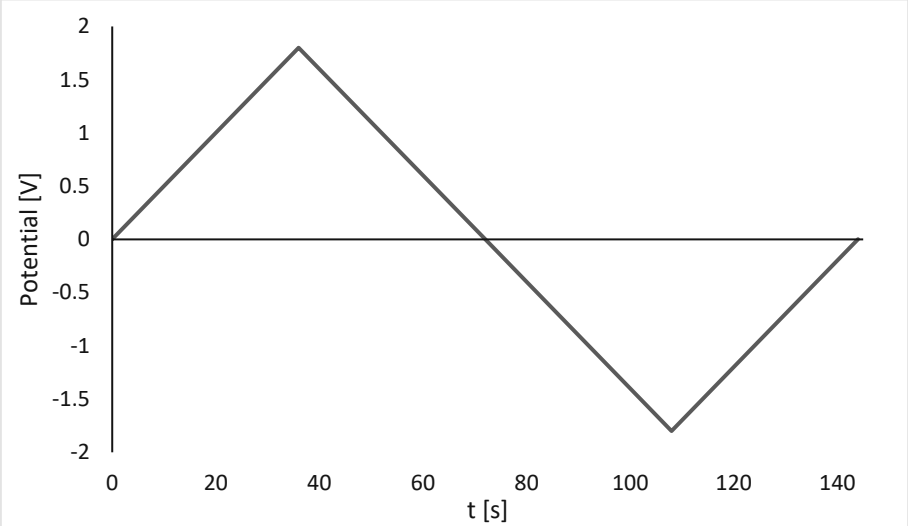

Figure 70: Programmed potential sweeping cycles from 0 V to +1.8 V, to -1.8 V, back to 0 V at a rate of 50 µV s^{-1}

The values for the two aimed potentials have to be considered wisely, due to dependence of the sample used and the critical potential for the solvent, at which it starts to decompose. If the reactions or processes are reversible, this measurement method is repeatable. Peak potentials in the voltammogram can be reduction potentials ($E_{p,c}$) or oxidation potentials ($E_{p,a}$) and together they can form the half-wave potential of a redox couple (Equation 6). A reversible voltammogram is independent of the applied scan rate, due to a normalizing procedure. The values for the peak potentials $E_{p,c}$ and $E_{p,a}$ stay the same by dividing with the square route of the scan rate.

Equation 6: Calculation of the half-wave potential of a reversible redox reaction couple

$$E_{1/2} = \frac{E_{p,c} + E_{p,a}}{2}$$

$E_{p,c}$ … maximum reduction potential [V]

$E_{p,a}$ … maximum oxidation potential [V]

If a reaction is not reversible, the obtained voltammogram contains only one peak, which either is an oxidation or reduction potential. This can be the observed, if a compound is decomposing due to the applied voltage. Another characteristic of irreversible reactions is the dependence of the peak potentials on the scan rate. Therefore, scan rate needs to be constant across all experiments. CV measurements only provide relative values for an electron transfer on a platinum surface. Therefore, it is important to measure samples like onium compounds, sensitizers and other redox active molecules under the same experimental conditions as well as with the use of a standardization compound like ferrocene. The sample solutions were purged with argon gas to replace the oxygen in solution and all measurements were conducted under light protection, if not explicitly stated otherwise. The obtained reduction and oxidation peak-voltages are normalized by refering them to the half-wave potential of ferrocene. Due to this normalization step all obtained values are compareable to each other. Thanks to normalization, measurement data is unaffected by a different batch of solvents as well as the usage of new electrodes, as long as they are made of the same material with constant surface area. The half-wave potential of ferrocene in acetonitrile at scan rate of 50 µV s^{-1} at room temperature (298.15 K) according to literature is $E_{1/2}$ = 0.992 V.[164] For the same measurement parameters in dichloromethane the half-wave potential of ferrocene is $E_{1/2}$ = 1.121 V.[164]

As soon as the half wave potential of a redox couple is measured, the free energy change (ΔG) can be calculated. If ΔG is negatice, an electron transfer is thermodynamically favourable. The simplified version of the Rehm-Weller equation does not accout for solvent effects (Equation 7). The factor 23.06 arises from the energy needed to separate two ion pairs in a rather polar solvent to a point where partically no electrostatic interaction occurs together with the Faraday constant.[165] Since acetonitrile is in use for all onium salts and sensitizers, a sufficiently large dielectric constant is given due to the polar nature of the solvent. Therefore, the ion pairs are seperated beyond theier respective Couombic fields and any solvent effects can be neglected.[165]

Equation 7: Simplified Rehm-Weller equation to calculate free energy change

$$\Delta G = 23.06 * E_{1/2} - E_S$$

ΔG … free energy change [kJ mol^{-1}]

$E_{1/2}$ … excitation energy of the reactive state of the sensitizer [kJ mol^{-1}]

$E_{1/2}$ … half wave potential [ ]

If the redox potentials of onium salt and sensitizer result in a free energy change of below -42 kJ mol^{-1}, an efficient electron transfer can usually occur.[166]

3.2.4.1. Onium Salts

Cyclic voltammetry was performed with all onium-based molecules to investigate their reduction potential for further studies involving sensitization or radical induced decmoposition. This experiment involved a buffer of tetraethylammonium tetrafluoroborate in dry acetonitrile as an electrolyte. Additionally an alredy known redox system was measured, to reproduce and compare in future experiaments, due to the normalization of every measured potential to ferrocenes half-wave potential (Figure 71). The scan was performed from 0 V to +1.8 V, from there to -1.8 V and finally back to 0 V at a rate of 50 µV s^{-1}.

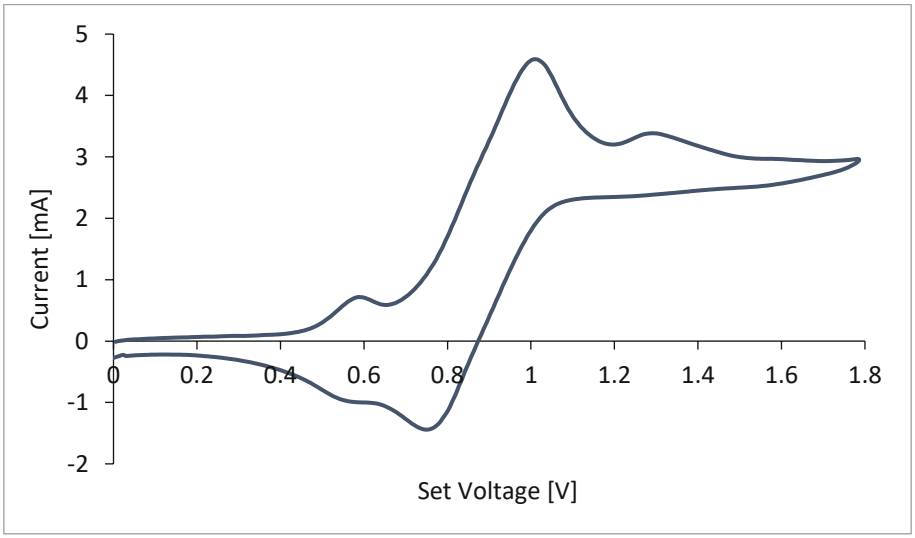

Figure 71: Voltammogram of Ferrocene (0 V -> +1.8 V -> -1.8 V -> 0 V at 50 µV s^{-1}) in dry acetonitrile

The oxidation of ferrocene occurs at 1.00 V, while the redcution peak is at 0.76 V, resulting in an half-wave potential of 0.88 V. Additionally, already known iodonium salts were measured to ensure the reproducability and reliability of the analysis method (Figure 72).

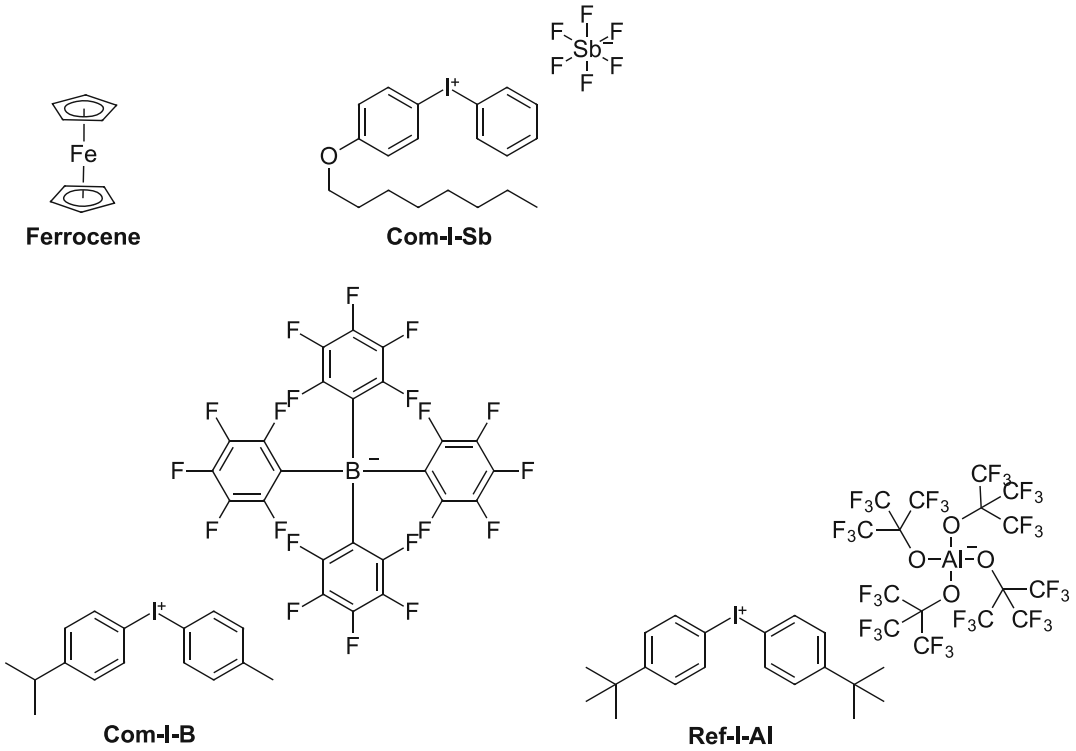

Figure 72: Ferrocen, diaryliodonium hexafluoroantimonate (Com-I-Sb); (4-butoxyphenyl)(phenyl)iodonium hexafluoroborate (Com-I-B) and bis(4-(tert-butyl)phenyl)iodonium tetrakis((1,1,1,3,3,3-hexafluoro-2-(trifluoromethyl)propan-2-yl)oxy)aluminate (Ref-I-Al)

All sample solutions were measured within the same series, with the exception of Ref-I-Al, which was measured twice. The second time a different reference electrode was used, while electrode material and surface area stayed constant.

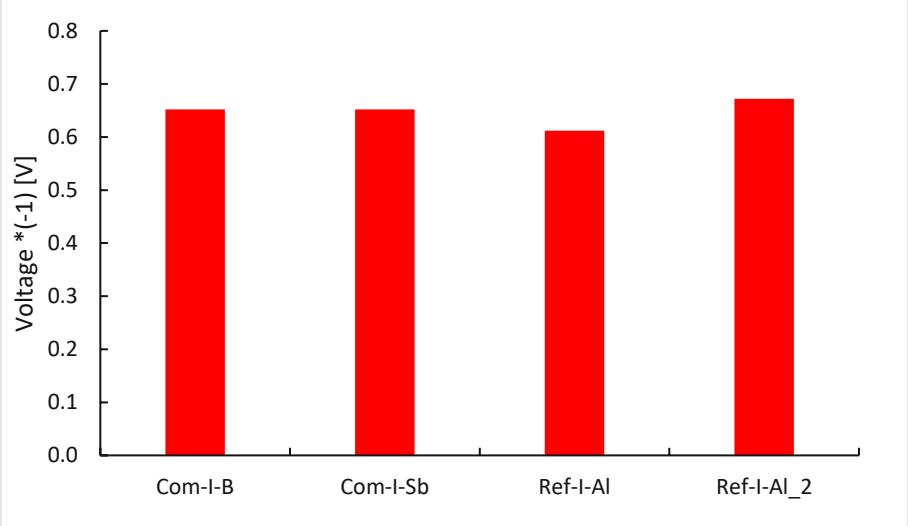

Figure 73: Inverted reduction potential of the iodonium compounds (0.01 M) measured in dry acetonitrile buffer (0.5 M tetraethylammonium tetrafluoroborate) CV: (0 V -> +1.8 V -> -1.8 V -> 0 V at 50 µV s^{-1})

As expected, the reduction potential of the iodonium salts differs only slightly, due to the common positively charged iodine as central atom, despite radically different anions (Figure 73). The positive charge is canceled irreversibly if the voltages reach +0.61 V to +0.67 V. At this

point the reduction potential of iodonium is reached, therefore not affected by the counterion and unnoticeably by the substituents at the phenyl rings. Additionally, the change of the setup to another standardized reference electrode did not change the results significantly (Ref-I-Al_2). After this evaluation, it is safe to say counterions are not affecting the reduction potential of onium compounds, neither do new electrodes. The analysis method is reproducible and reliable, due to minor differences in reduction potentials across all measured iodonium salts.

After establishing of the analysis method, the remaining onium salts were analyzed by cyclic voltammetry too.

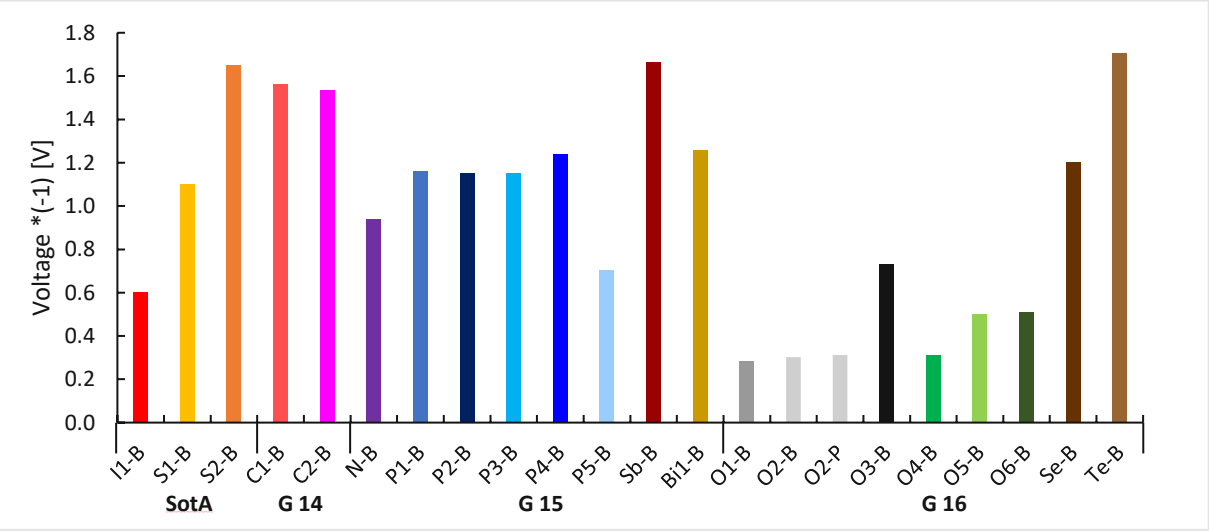

Figure 74: Inverted reduction potential of the onium salts (0.01 M) measured in dry acetonitrile buffer (0.5 M tetraethylammonium tetrafluoroborate) CV: (0 V -> +1.8 V -> -1.8 V -> 0 V at 50 µV s^{-1})

The resulting reduction potentials give basic information of how hard it is for an electron to be uptaken by the tested molecule (Figure 74). A higher reduction potential leads to an increased effort to make this electron-uptake happen. The lowest reduction potential is achieved by the alkly-oxonium compunds and the O4-B at around 0.3 V. Non-phenylated pyrylium salts (O5-B and O6-B) show a reduction potential of around 0.5 V, followed by iodonium salts with 0.65 V. O3-B and the alkyl-based P5-B show values around 0.7 V. The nitrogen based pyridinium salt reaches a reduction potential of 0.9 V, while state of the art sulfonium compounds exhibit 1.1 V of reduction potential. Phenylated phosphonium compunds are generally in the range of around 1.2 V, together with the selenium-based molecule. Bi1-B shows an reduction potential of around 1.3 V. The highest voltage values are obtained by measuring C1-B, Te-B, Sb-B and S2-B with reduction potentials of 1.6 to 1.7 V.

3.2.4.2. Sensitizers

The cyclic voltammetry experiments were also performed with the sensitizers to quanify their oxidation potential. In theory a sensitizer with a equal or higher oxidation potential compared to the reduction potential of the onium compound, should be able to oxidize the cation. Again, all measured potentials were referred to the half-wave potential of ferrocene to ensure reproducability and compareability (Figure 75).

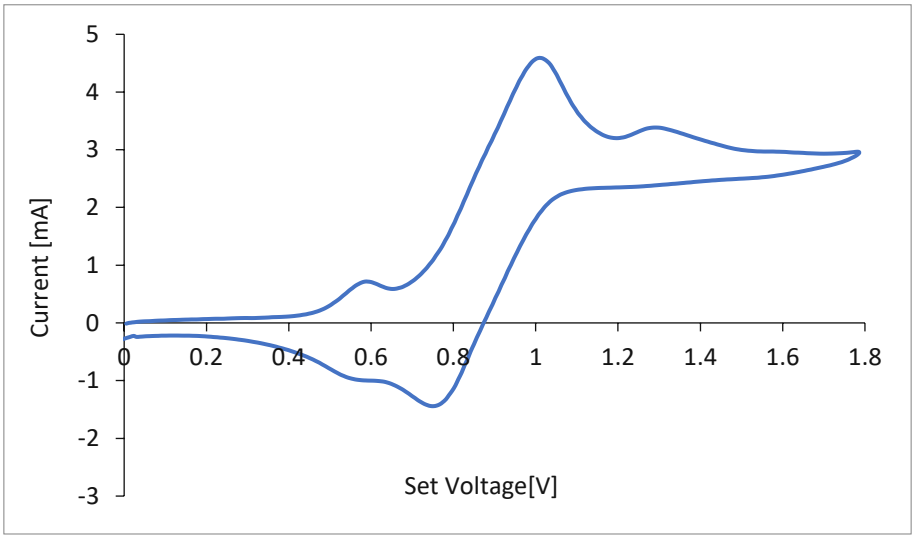

Figure 75: Voltammogram of Ferrocene (0 V -> +1.8 V -> 0 V at 50 µV s^{-1}) in dry dichloromethane

According to the measurements performed with the onium compounds, ferrocene shows a reduction at 1.02 V and its oxidation at 0.76 V. Resulting in a half-wave potential of 0.89 V. This half-wave potential was now standardized to the literiature value of 1.121 V.[164] Therefore after this normalization step, all measured oxidation potentials are increased by 0.231 V. All sensitizers were measured in a buffer consisting of tetrabutylammonium tetrafluoroborate in dry dichloromethane (Figure 76).

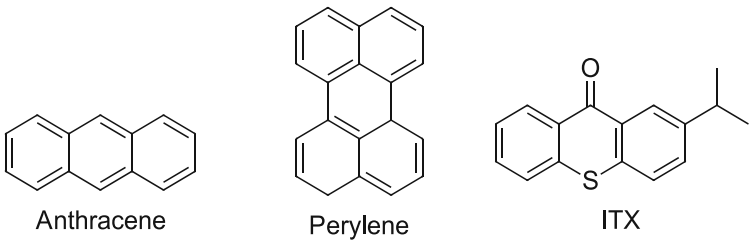

Figure 76: Sensitizers perylene, anthracene and ITX (2-Isopropylthioxanthone)

In addition, the solutions were measured a second time, but with UV-light exposure during the cyclic voltammetry experiment. Irradiation was perfomred with a 365 nm LED with a distance of 10 cm between the LED and the solution surface resulting in around 60 mW cm^{-2}.

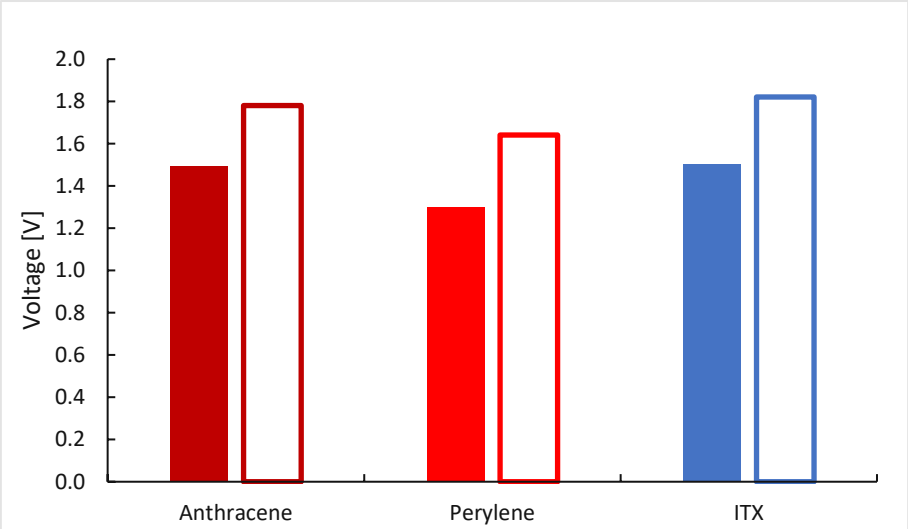

Figure 77: Oxidation potential of the sensitizers (0.01 M) measured in dry dichloromethane buffer (0.1 M tetraethylammonium tetrafluoroborate); without LED (full columns); with LED irradiation (framed columns; CV: (0 V -> +1.8 V -> 0 V at 50 µV s^{-1})

The determined oxidation potentials of the sensitizers quantify the effort needed to remove an electrone from the molecule. This electron transfer to an electrode or another molecule is crutial for a redox pair to function properly. High oxidation potentials are advantageous, due to the ability to oxidize a broader range of substances. Perylene achieves the lowest oxidation potential of around 1.3 V, followed by anthracene and ITX with approximately 1.5 V. If irradiated during the experiment, the sensitizers show increased oxidation potentials ranging from 1.6 V for perylene up to 1.8 V for anthracene and ITX. Therefore, anthracene and ITX are potent reduction agents for the onium compounds.

Together with the reduction potentials of the measured onium salts, the half wave potential of the redox couple can be calculated. The excitation energy of the reactive state of the sensitizer E_S was set according to literature for anthracene, perylene and ITX.[165] By applying the Rehm-Weller Equation on all onium salt-sensitizer couples the free energy change is obtained and with it the tendency to form funcioning redox pairs (Table 8).

Table 8: Free energy change ΔG of redox coupes: onium salt - sensitizer

Onium Salt	Anthracene	Perylene	ITX
	ΔG [kJ mol^{-1}]		
I1-B	-218	-185	-175
S1-B	-194	-161	-151
S2-B	-167	-134	-125
C1-B	-171	-139	-129
C2-B	-173	-140	-130
N-B	-201	-169	-159
P1-B	-191	-158	-148
P2-B	-191	-158	-149
P3-B	-191	-158	-149
P4-B	-187	-154	-144
P5-B	-213	-180	-171
Sb-B	-166	-134	-124
Bi1-B	-186	-153	-144
O1-B	-233	-201	-191
O2-B	-232	-200	-190
O2-P	-232	-199	-189
O3-B	-211	-179	-169
O4-B	-232	-199	-189
O5-B	-223	-190	-180
O6-B	-222	-189	-180
Se-B	-189	-156	-146
Te-B	-164	-131	-122

Since all changes in free energy below -42 kJ mol^{-1} are thermodynamically favorable,[166] all selected sensitizers are more than sufficient to transfer an electron to any of the onium salts. However, anthracene perfomes best since the gains in free energy are the most compared with perylene and ITX. Therefore, anthracene represents a capable sensizizer for further studies.

3.2.4.3. Radical Photoinitiators

Additionally, the cyclic voltammetry was performed with radical photoinitiators to quanify their oxidation potential (Figure 78). In theory a generated radical with a equal or higher oxidation potential compared to the reduction potential of the onium compound, should be able to oxidize the cation. In consequence the superacid is liberated, which is able to initiate the cationic polymerization. All measured potentials were referred to the half-wave potential of ferrocene to ensure reproducability and compareability ($E_{1/2}$ = 0.992 V).[164] The solutions were measured with UV-light exposure during the cyclic voltammetry experiment.

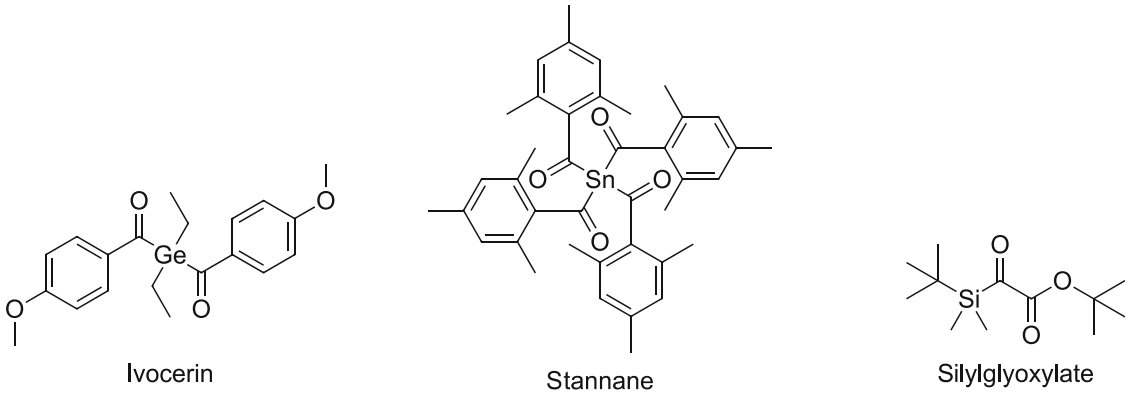

Figure 78: Radical photoinitiators Ivocerin® ((diethylgermanediyl)bis((4-methoxyphenyl)methanone)), Stannane (stannanetetrayltetrakis(mesitylmethanone)) and Silylglyoxalate (tert-butyl 2-(tert-butyldimethylsilyl)-2-oxoacetate)

Irradiation was perfomred with a 365 nm LED with a distance of 10 cm between the LED and the surface of the solution resulting in 60 mW cm^{-2}.

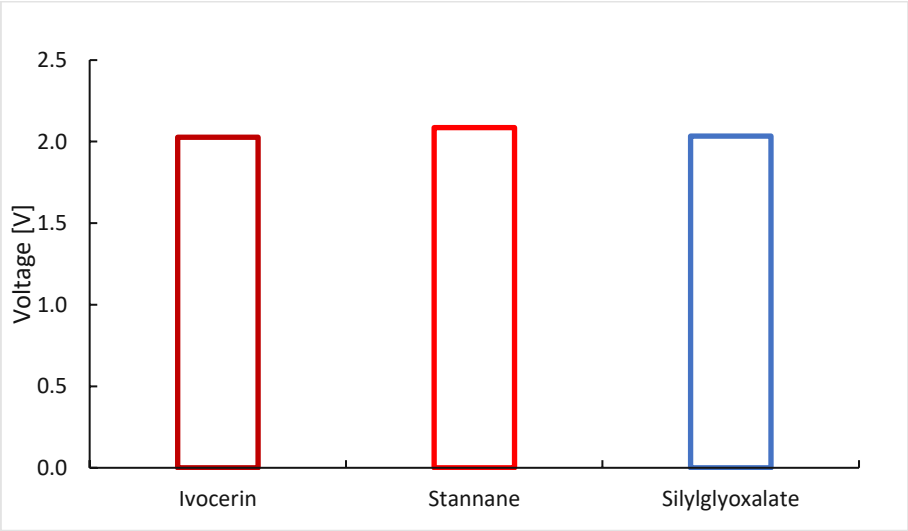

Figure 79: Oxidation potential of the radical photoinitiators (0.01 M) measured in dry acetonitrile buffer (0.5 M tetraethylammonium tetrafluoroborate) with LED irradiation; CV: (0 V -> +1.8 V -> 0 V at 50 µV s^{-1})

As expected the oxidation potentials of the generated radicals are quite high at ≥ 2 V for every sample (Figure 79). There was not significant difference between the tested photoinitiators, since all of them already reach the limit of this CV method using acetonitrile as solvent. Therefore, all three tested systems are more than sufficiently qualified as oxidation reagents for the onium salts. Ivocerine was used in all further experiments due to its commerical avaliablilty.

For all of the three radical photoinitiators no excitarion energy E_S is avaliable in literature at the time of writing. Therefore, the Rehm-Wellers equation cannot be applied on the measreud data and free energy change cannot be calculated.

3.3. Reactivity of Onium Tetrafluoroborates

3.3.1. Formulations based on BADGE/PC & ECC/PC

For the upcoming reactivity studies, appropriate formulations had to be prepared. Mixtures based on either the aromatic bisphenol-A-diglycidylether (BADGE) or the cycloaliphatic 3,4-epoxycyclohexylmethyl-3',4'-epoxycyclo-hexancarboxylat (ECC) were targeted. To ensure good solubility of the rather polar photo acid generator in the non-polar monomer matrix, propylene carbonate (PC) was used as a reactive polarity adjusting agent (Figure 80).

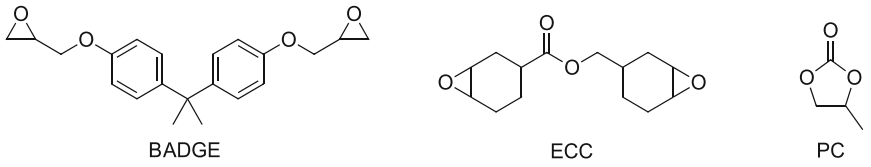

Figure 80: Monomers BADGE, ECC and additive PC

The onium salts were used in 1.16 mol% based on epoxy groups referred to BADGE and 0.84 mol% referred to the more reactive monomer ECC. This difference in onium salt concentration is based on the reactivity of the monomers themselves. ECC-based formulations are more reactive compared to the BADGE-based ones. Selected onium salts also were used with a tetrafluoroborate counterion only, to ensure a fair comparison throughout the upcoming reactivity studies (Figure 81).

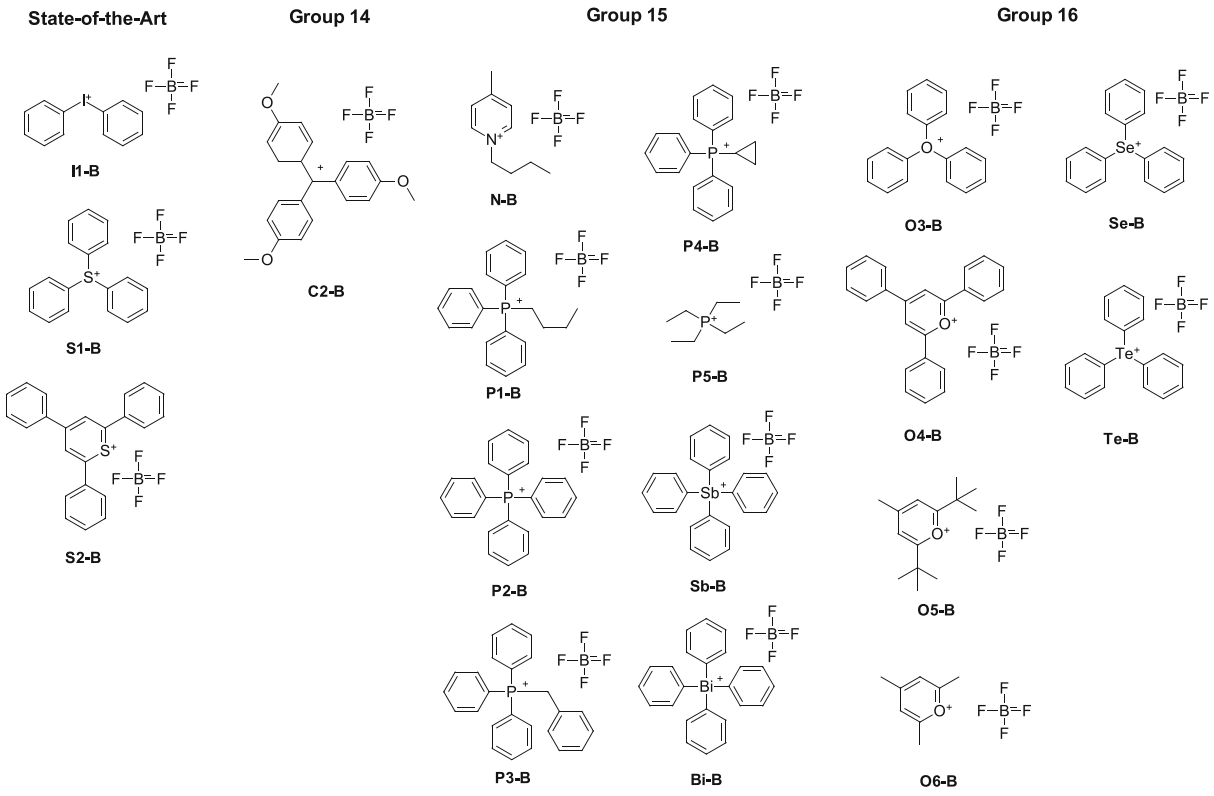

Figure 81: Selected onium tetrafluoroborates for reactivity tests

Due to solubility issues in the monomers alone, a master-mix was prepared consisting out of 22 wt% of PC and 78 wt% monomer. This improvement in polarity lead to completely homogeneous samples after treatment in an ultrasonic bath at 40 °C for 30 min. In some cases, the formulations were carefully heated to around 60 °C via heat gun to dissolve the salts completely.

Methylium and pyrylium salts were not able to be mixed with ECC/PC, due to their high reactivity. The formulations gelled a few minutes after mixing of the components.

3.3.2. Thermal Behavior of Onium Salts determined via DSC

3.3.2.1. Thermal-Induced Decomposition of Onium Salts

The thermal stability of every onium salts is limited. Therefore, the decomposition process appears at a certain onset temperature. All onium salts were exposed to a rising temperature gradient to investigate the decomposition temperature in different epoxy resins prepared in chapter I, 3.3. Once the onium salts decompose, their superacid is liberated and able to initiate cationic polymerization. The exothermic polymerization reaction is picked up by a DSC sensor during the differential scanning calorimetry (DSC) and plotted against time or temperature under nitrogen atmosphere.

Fist, an evaporation test was performed to gather data about the weight decrease during the heating of the formulations. ECC (b.p.: 362 °C) and BADGE (b.p.: 487 °C) boil at quiet high temperatures, in contrast to PC (b.p.: 242 °C) which starts to strongly evaporate above 200 °C (Figure 82).

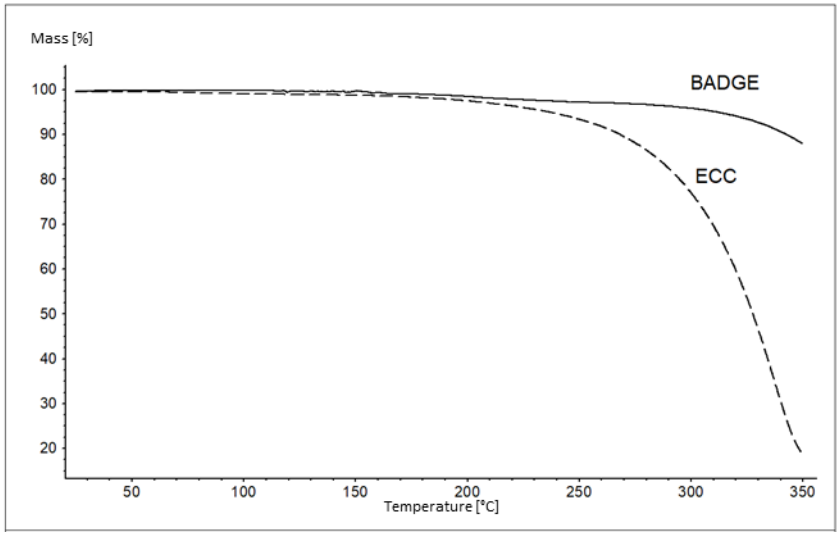

Figure 82: Change in mass of the monomers BADGE + PC (solid line) an ECC + PC (dashed line) during temperature gradient

Around 15 wt% of the formulations are already evaporated at 250 °C, however some onium salts underwent pre-tests and show decomposition temperatures of well above 300 °C. Therefore, the starting temperature was chosen to be 25 °C and the device heated up to 350 °C. The samples were weighed into aluminum crucibles, which were sealed by a punctured lid to allow volatiles to evaporate unhindered. Once the temperature peak of 350 °C is reached at a rate of 10 K min^{-1}, liquid nitrogen is used to cool down at 20 K min^{-1} back to 25 °C. The last sequence consists of an isothermal phase for 20 min at room temperature. Two determinations were made per formulation.

The temperature at which the highest exothermicity occurs is called T_{max}. Additionally, the temperature at which temperature the polymerization started called T_{onset} was evaluated. The polymerization rate R_P correlates with the curing rate (Equation 12). Higher values result in higher reactivities of the system. The epoxy group conversion EGC was determined by the ratio of the experimentally determined area under the DSC curve to the theoretical heat of polymerization of the epoxy system (Equation 11).

BADGE/PC Formulations

First, all selected onium salts were measured in the mixture of BADGE and PC to evaluate their thermal stability.

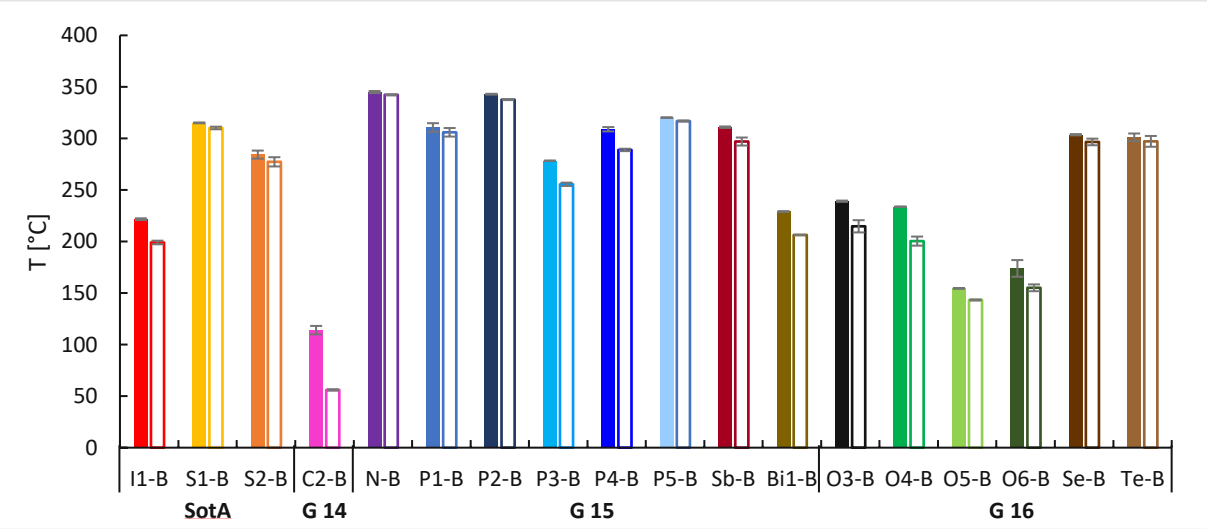

Figure 83: Temperature at the highest exothermicity (T_{max} - full) and polymerization onset temperature (T_{onset} - framed) in BADGE/PC with the onium tetrafluoroborates

Most noticeable is the quite low onset temperature of the carbon-based C2-B with 56 °C. This metric defines a very low thermal stability of the compound (Figure 83). Low T_{onset} values were achieved by the systems containing pyrylium salts as well. Ranging from 143 °C for the O5-B to the most stable pyrylium salt O4-B at 200 °C onset temperature. The commercial iodonium

salt reaches an onset temperature of 199 °C, while sulfonium-based one reaches 310 °C. The highest onset temperature is obtained with a formulation containing the pyridinium-based initiator N-B with 342 °C. Since the temperatures at the highest exothermicity are just above the onset temperatures, the T_{max} values are not discussed further.

ECC/PC Formulations

Next, the same selection of compounds was subject of a thermal stability study in the cycloaliphatic monomer ECC together with PC.

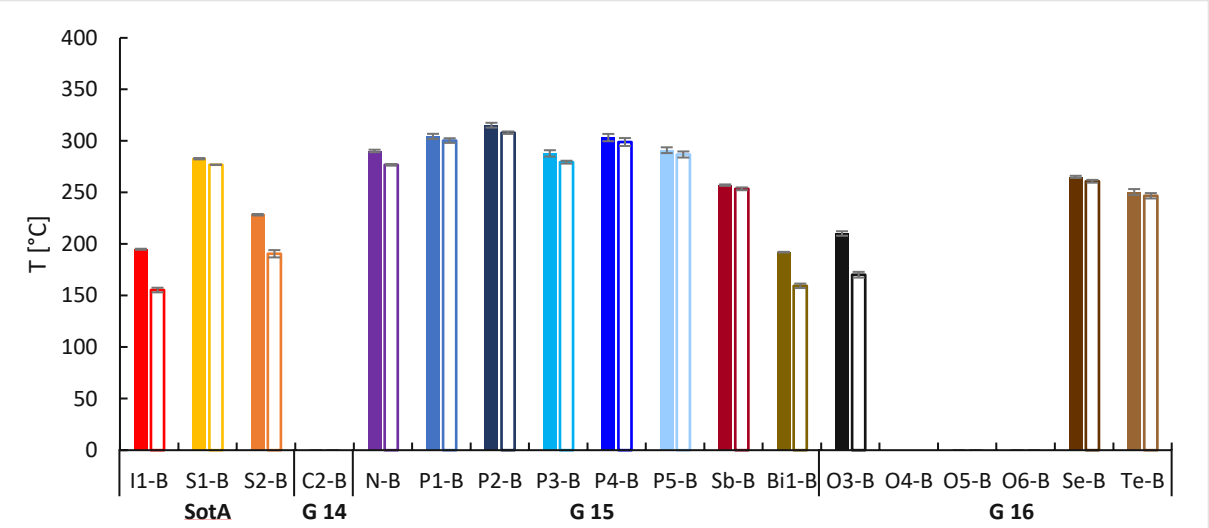

Figure 84: Temperature at the highest exothermicity (T_{max} - full) and polymerization onset temperature (T_{onset} - framed) in ECC/PC with the onium tetrafluoroborates

Due to the increased reactivity of the epoxy-based monomer ECC, the onset temperatures as well as the T_{max} values are lower compared to the BADGE-based samples (Figure 84). The onium salts follow a similar trend, with the exception of methylium and pyrylium salts. These initiators were not able to be measured, due to their high reactivity as mentioned previously.

3.3.2.2. Thermal-Induced Radical Decomposition of Onium Salts

Besides the thermal-only decomposition, onium compounds are known to decompose by thermally generated radicals from C-C labile compounds.[125] By exposure to a fixed temperature gradient, the thermal initiator TPED will start to decompose and forming the radicals. The thermal radicals are able to attack the acid generator, which is liberating the super acid, and finally initiate polymerization of the resin (Figure 85).

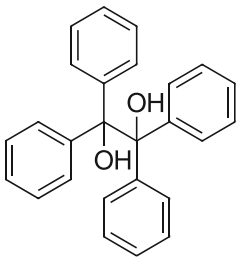

Figure 85: Radical thermal initiator TPED

This investigation was necessary to know exactly, above which onset temperature polymerization can occur in combination with TPED. In contrast to the DSC experiments without TPED, in this series of measurements two additional parameters R_P and EGC can be evaluated. The radical thermal initiator ensures at its onset temperature a potential decomposition of the onium salts and enables a better comparison between the onium salts. The formulations preparation was described in chapter I, 3.3. To all formulations containing the epoxy resin in combination with the onium compounds, an equimolar amount of TPED was added (1.16 mol% for BADGE/PC and 0.84 mol% for ECC/PC based on epoxy groups). All DSC experiments with TPED as C-C labile compound were conducted from 25 °C to 250 °C, since overall lower values are expected compared to the formulations without any TPED.

BADGE/PC Formulations

At first, all onium salts together with TPED were tested in BADGE/PC to determine thermal stability in presence of a radical thermal initiator.

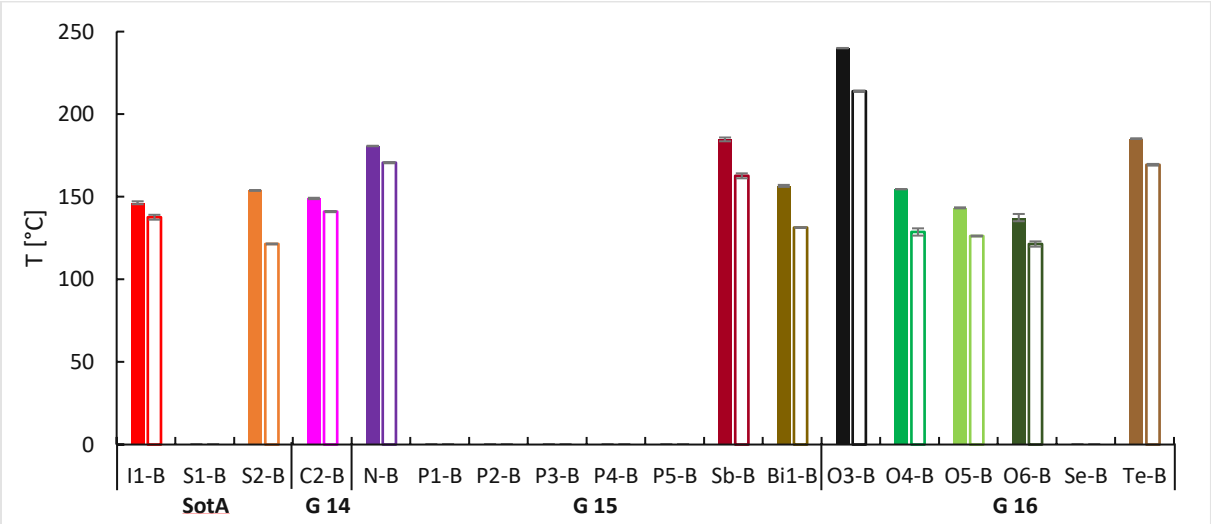

Figure 86: Temperature at the highest exothermicity (T_{max} - full) and polymerization onset temperature (T_{onset} - framed) in BADGE/PC with TPED and the onium tetrafluoroborates

State-of-the-art iodonium salt shows an onset temperature of 140 °C and a T_{max} value of 150 °C (Figure 86). The triphenyl oxonium-based acid generator shows the highest temperature at

the highest exothermicity and onset temperature, both above 210 °C. On the lower end, the pyrylium salts range from 120 to 130 °C. Interestingly, none of the phosphonium salts show a radical induced decomposition by TPED in the measured temperature range. This circumstance suggests the phosphonium salt-TPED redox couple does not match at the cleavage temperature of TPED.

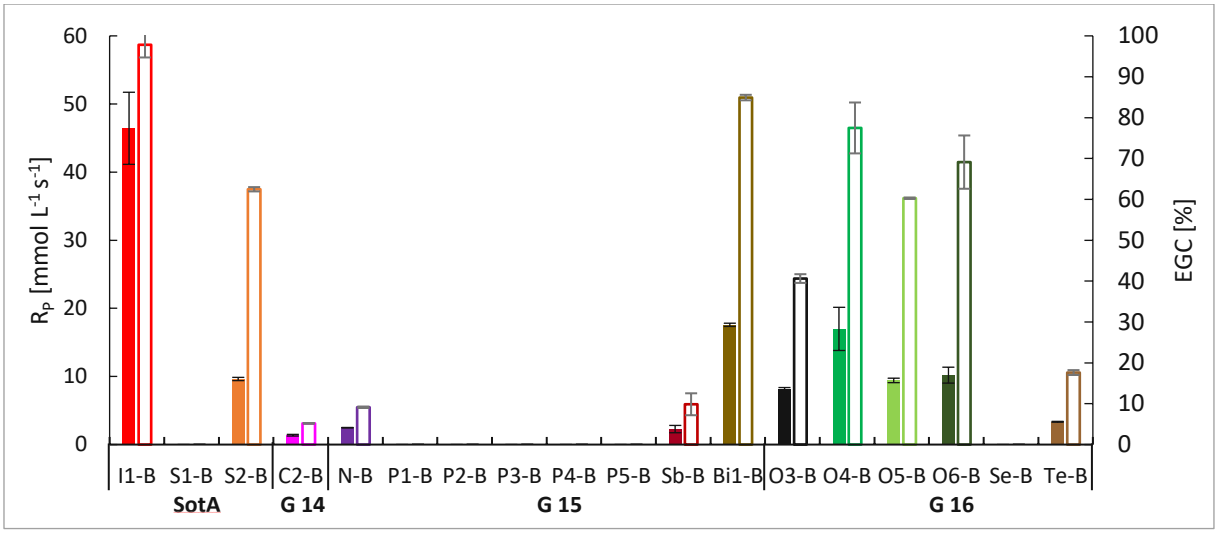

Figure 87: Rate of polymerization (R_P - full) and epoxy group conversion (EGC – framed) in BADGE/PC with TPED and the onium tetrafluoroborates

Considering the rate of polymerization (Figure 87), one can clearly notice the advantageous behavior of the iodonium-based salt. The closest values to this benchmark are Bi1-B as well as O4-B. Conversions reach up to 98% for the iodonium-based I1-B. With 88% conversion, Bi1-B performs quite well in BADGE. The pyrylium salts O4-B and O6-B reach around 80% conversion.

ECC/PC Formulations

Analogously, the second series was performed in ECC and PC mixed with the onium compounds and the thermolabile molecule TPED.

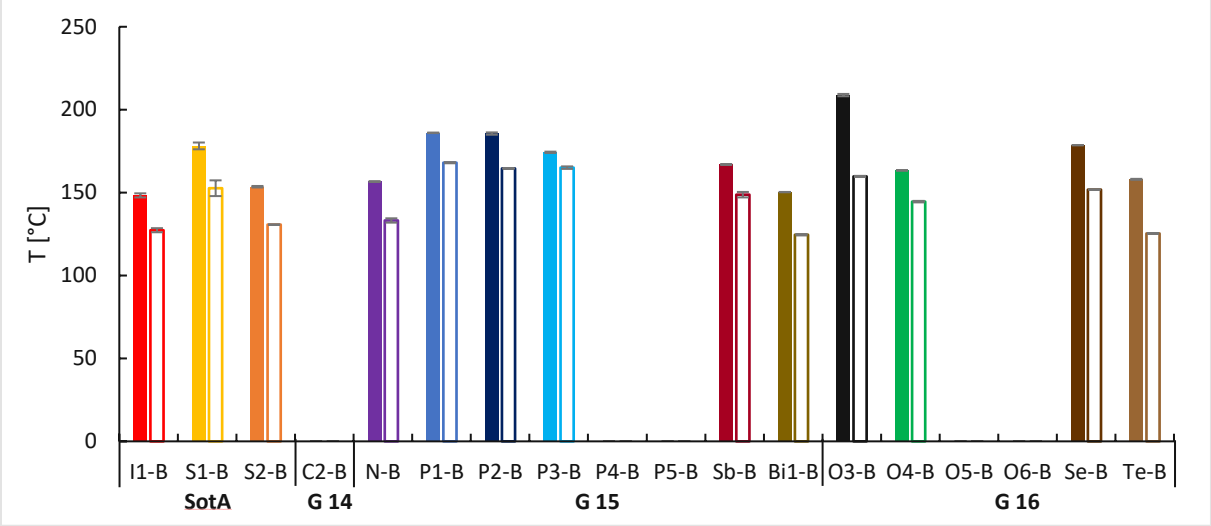

Figure 88: Temperature at the highest exothermicity (T_{max} - full) and polymerization onset temperature (T_{onset} - framed) in ECC/PC with TPED and the onium tetrafluoroborates

By comparing the BADGE onset temperatures to the ECC ones (Figure 88), the decreased T_{onset} and T_{max} values in the aliphatic monomer can be seen immediately. Onset temperatures range from 125 °C for Bi1-B up to 170 °C for phosphonium-based salts.

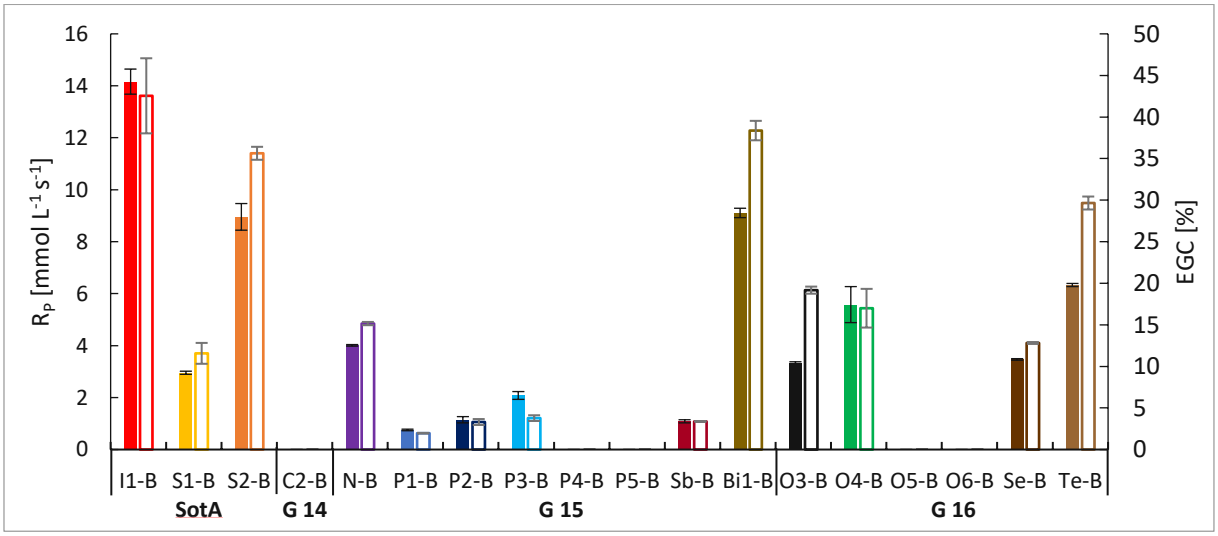

Figure 89: Rate of polymerization (R_P - full) and epoxy group conversion (EGC – framed) in ECC/PC with TPED and the onium tetrafluoroborates

Considering the rate of polymerization values (Figure 89) obtained during the DSC analysis, the best performance is delivered by the iodonium-based salt in combination with TPED (14 mmol L^{-1} s^{-1}). In ECC, lower overall polymerization rates are measured compared to BADGE. The second highest polymerization rate is achieved by the bismuth-based salt,

followed by S2-B, O4-B and Te-B. All other onium salts do not react at all or reached values of or below 4 mmol L^{-1} s^{-1}. In the aliphatic epoxy monomer ECC the 2P-O-BF_4 reaches values of 57%, closely followed by the bismuth-based salt at 52%. S2-B reaches 48% and Te-B a conversion of 40%. The residual onium salts stay below 26%, therefore not reaching practical conversion values.

Compared to the iodonium-based salt, none of the synthesized molecules can achieve the same reactivity and in performance in general. Overall, the onium salts show low to moderate potential for radical induced cationic polymerization in combination with TPED. The best candidates, which achieve at least similar performance are Bi1-B and O4-B in BADGE and Bi1-B and S2-B in ECC.

3.3.3. Photoreactivity determined via Photo-DSC

3.3.3.1. Photoinitiation Study

A photoinitiation study was carried out to to investigate the efficiency of the potential photoacid generators. The main objective was to investigate the potentials of all onium salts as photoacid generators. Since the UV-VIS experiments indicated a broad range of absorption across the tested onium compounds, a broad-band mercury lamp was used as irradiation source (Figure 90). The emission spectrum ranges from around 250 nm to 650 nm.

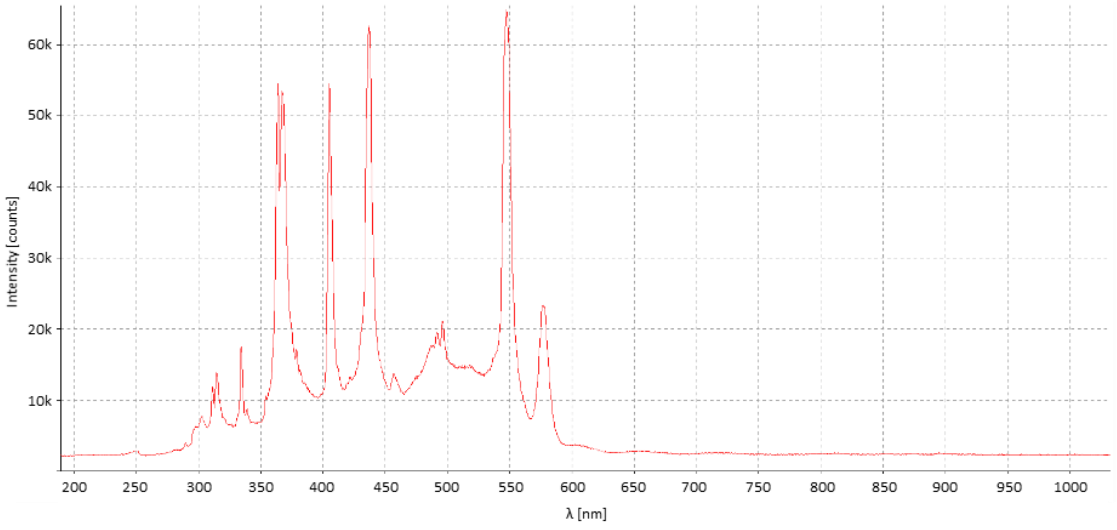

Figure 90: Wavelength versus intensity of a broad-band mercury lamp without a wavelength filter

The formulations described in the previous chapter I, 3.3 were used for this study without any additives. To finally result in 1.16 mol% onium salt in BADGE/PC and 0.84 mol% in ECC/PC.

BADGE/PC Formulations

Considering the performance in BADGE/PC, the state-of-the-art iodonium salt does outstandingly well (Figure 91).

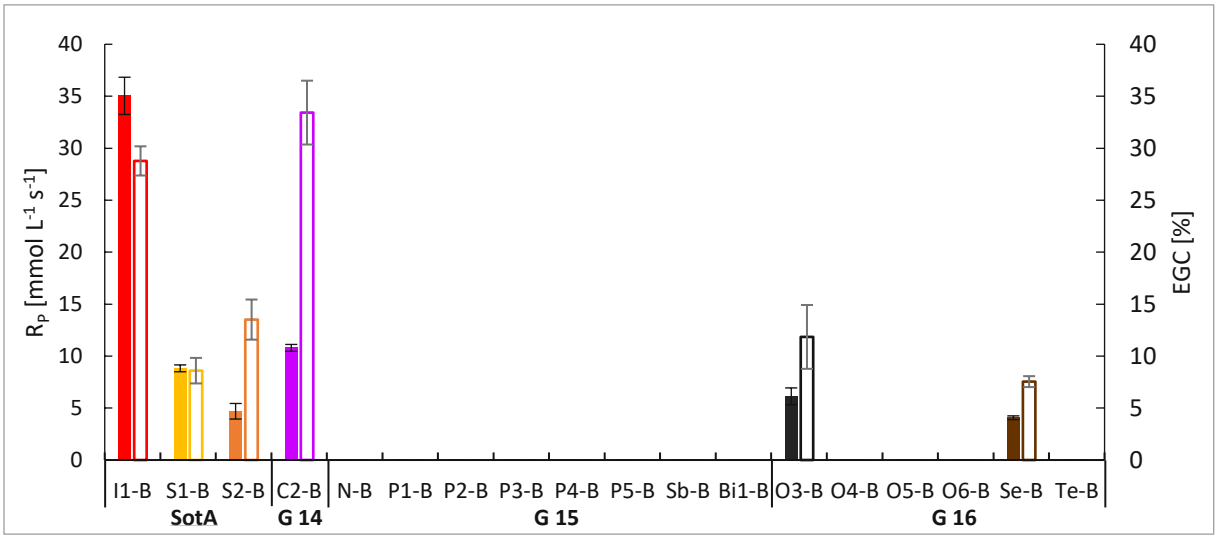

Figure 91: Rate of polymerization (R_P - full) and epoxy group conversion (EGC – framed) in BADGE/PC with the onium tetrafluoroborates (Photoinitiation); The time-based parameters t_{max} and $t_{95\%}$ are located in the attachment (Figure 259)

Its rate of polymerization is more than double compared with the second-best onium salt C2-B in this study. However, most onium salts do not show any exothermic behavior. Interestingly, the bismuth-based Bi1-B and the tellurium-based Te-B do show a very strong endothermic behavior during the polymerization, which could not be explained trivially. The samples were totally hardened after irradiation. However, no exothermic peak could be obtained in several measurements. The conversion of the carbon-based onium salt exceeds the value of the iodonium salt by 3%. All other onium salts measured conversions below 9%.

ECC/PC Formulations

Next, the series of measurements in ECC/PC was carried out to evaluate the reactivity of the onium salts.

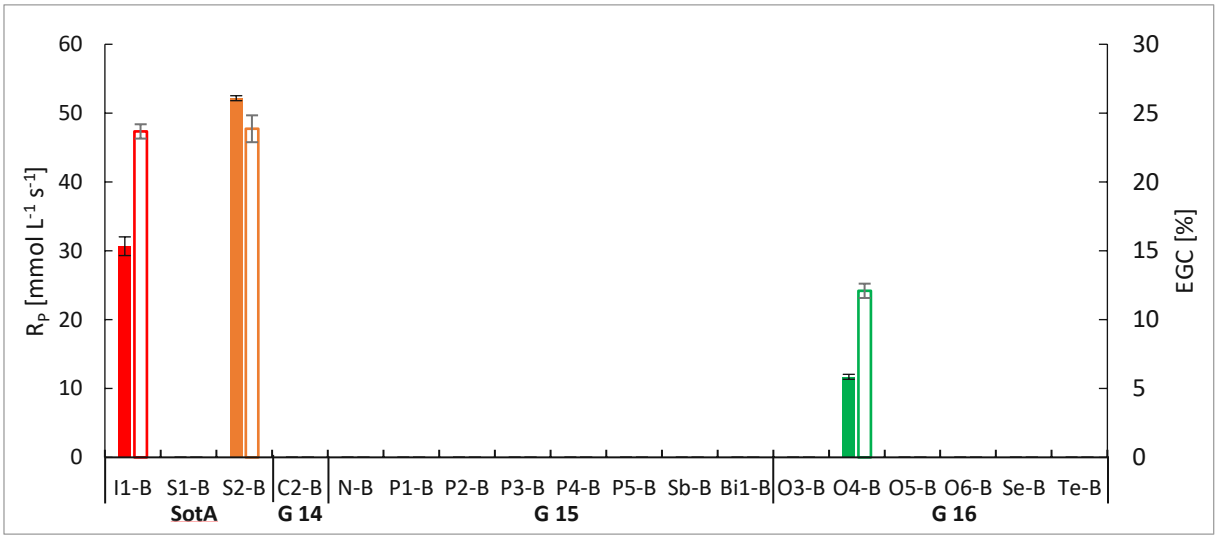

Figure 92: Rate of polymerization (R_P - full) and epoxy group conversion (EGC – framed) in ECC/PC with the onium tetrafluoroborates (Photoinitiation); The time-based parameters t_{max} and $t_{95\%}$ are located in the attachment (Figure 260)

The rate of polymerization in ECC/PC shows a clear difference to the BADGE/PC-based samples. This time only pyrylium and thiopyrylium salts show exothermic behavior. Even outperforming the iodonium tetrafluoroborate with the thiopyrylium compound (Figure 92). Similar to the BADGE/PC-based formulations, bismuthonium and telluronium salts show strong endothermic behavior during the DSC measurements, despite resulting in cured samples after irradiation. In terms of conversion, I1-B and S2-B reach pretty similar results at around 19%. The pyrylium salt stays below 10%.

3.3.3.2. Sensitization of Onium Salts

To investigate the efficiency of the potential sensitizers, a Photo-DSC study was performed with the onium salts and anthracene as sensitizing compound. The series of measurements should give basic information about the reactivity. The more reactive an initiator-sensitizer system behaves, the better for the overall initiation efficiency and curing of the material. Anthracene shows its absorption maxima from 320 to 370 nm, with a tail-out region reaching up to 380 nm. Therefore, an UV-source with a 320-500 nm filter was used in this series of experiments. The formulations described in the previous chapter I, 3.3 were modified with the addition of an equimolar amount of anthracene (Figure 93).

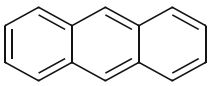

Figure 93: Anthracene sensitizer

To result in 1.16 mol% anthracene for BADGE/PC and 0.84 mol% for ECC/PC based on epoxy groups.

BADGE/PC Formulations

The first sensitization study of the onium salts was conducted in the aromatic epoxy monomer BADGE together with PC.

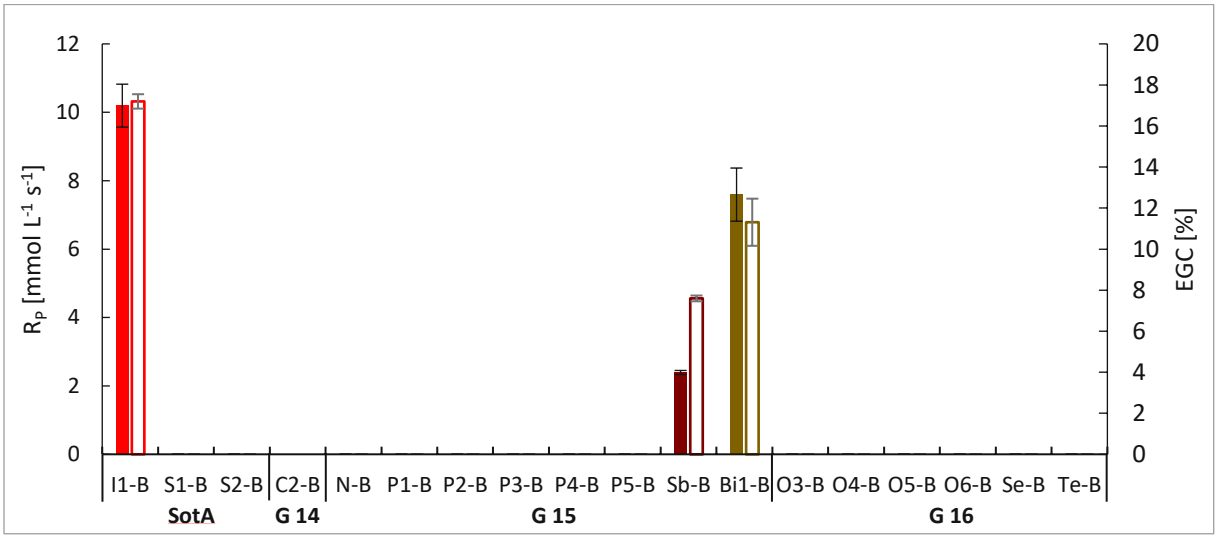

Figure 94: Rate of polymerization (R_P - full) and epoxy group conversion (EGC – framed) in BADGE/PC with the onium tetrafluoroborates (sensitized by anthracene); The time-based parameters t_{max} and $t_{95\%}$ are located in the attachment (Figure 255)

Comparing the reactivity of the onium salts one can clearly see the advantage of using the commercially established iodonium compound (Figure 94). The second highest rate is obtained in a formulation containing the bismuth-based Bi1-B. The only other onium compound, to achieve an exothermic behavior at all, besides the iodine- and bismuth-based one, is the chemically very similar (same group in periodic table of elements) Sb-B with a rather low rate of polymerization of around 2 mmol L^{-1} s^{-1}. Considering the overall epoxy conversion, one can clearly see the benefit of iodonium salts at around 11% conversion, compared to the 7% for Bi1-B and 5% for the antimony-based salt.

ECC/PC Formulations

Secondly, the same selection of onium salts mixed with anthracene as sensitizer were evaluated in ECC/PC formulations.

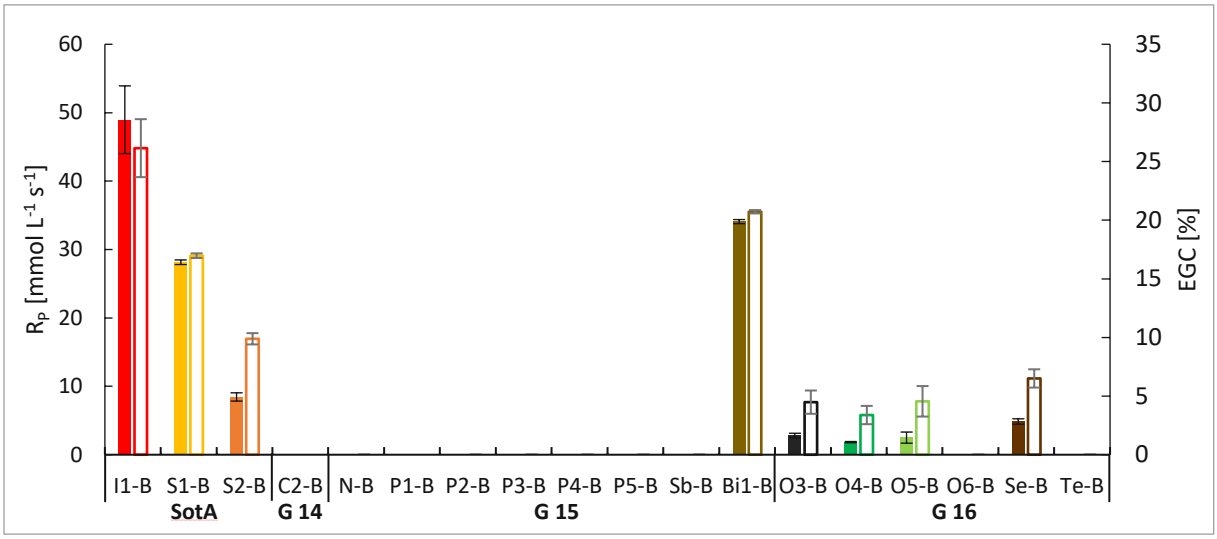

Figure 95: Rate of polymerization (R_P - full) and epoxy group conversion (EGC – framed) in ECC/PC with the onium tetrafluoroborates (sensitized by anthracene); The time-based parameters t_{max} and $t_{95\%}$ are located in the attachment (Figure 256)

As expected, the ECC based formulations achieve higher values in reactivity compared to formulations based on BADGE (Figure 95). Sulfonium and iodonium compounds achieve quite high reactivities. However, the second highest rate of polymerization is achieved by the bismuth-based Bi1-B. The residual onium salts do not show significant reactivity in ECC. The conversion of the iodonium-based initiator reaches the highest conversion at around 21%, followed by the Bi1-B at 17%. The sulfonium-salt reaches a conversion of around 14%, while all other onium compounds fell below 8% conversion.

Overall, the Bi1-B is the only onium salt, which provides sufficient performance to come close to the reactivity of the state of the art iodonium salts. Therefore, this bismuth-based salt can be further investigated due to its good performance with sensitizers like anthracene.

3.3.3.3. Photo-Induced Radical Decomposition of Onium Salts

To investigate the efficiency of the radical starters, a Photo-DSC study was performed with the onium salts and a photoinitiator to decompose the onium compound by the formed radicals. This series of measurements should provide information about the reactivity of the system if the onium salts are decomposed by photochemically generated radicals. The more reactive an initiator-radical generator system behaves, the better for the overall initiation efficiency and curing of the material. Ivocerin® shows its absorption maxima from 390 to 445 nm.

Therefore, an UV-source with a 400-500 nm filter was used in this series of experiments (Figure 96).

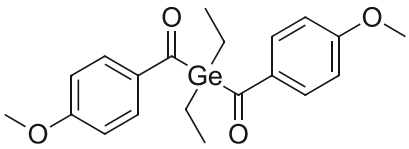

Figure 96: Ivocerin® structure

The formulations described in the previous chapter I, 3.3 were modified with an equimolar amount of the germanium-based photoinitiator Ivocerin. To finally result in 1.16 mol% Ivocerin in BADGE/PC and 0.84 mol% in ECC/PC based on epoxy groups.

BADGE/PC Formulations

First, all onium salts mixed with Ivocerin in the monomer BADGE/PC were measured to get a selection of potential candidates for photo-induced radical decomposition.

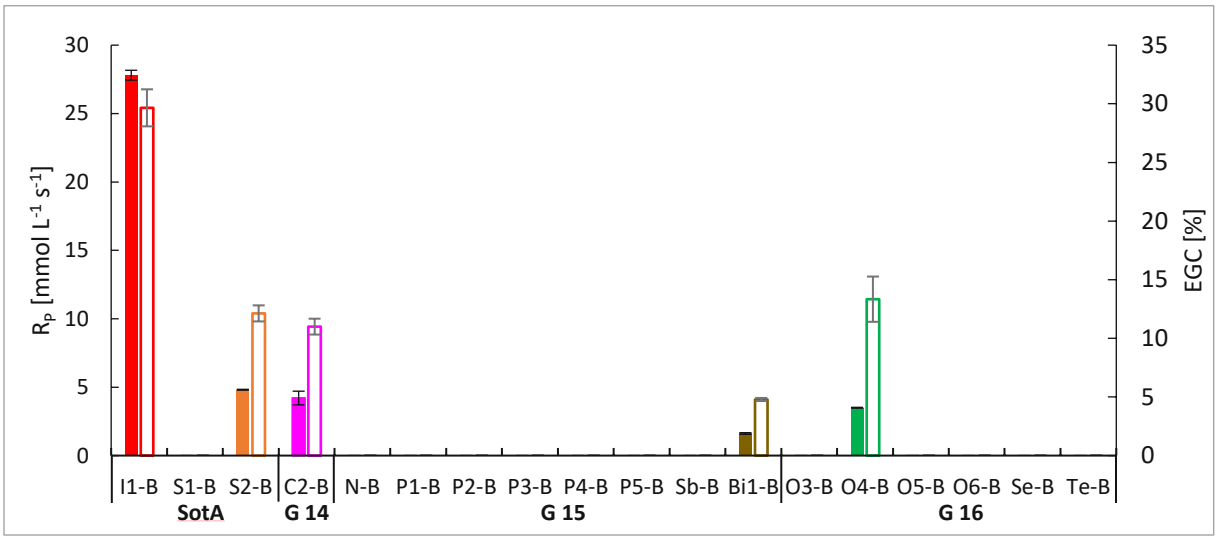

Figure 97: Rate of polymerization (R_P - full) and epoxy group conversion (EGC – framed) in BADGE/PC with the onium tetrafluoroborates (photo-induced decomposition by Ivocerin); The time-based parameters t_{max} and $t_{95\%}$ are located in the attachment (Figure 257)

The only sufficient reactivity is achieved with the idodonium-based I1-B (Figure 97). All remaining onium compounds show less than 7 mmol L^{-1} s^{-1}. The same trend can be applied to the conversion. Idonium shows the hightest value at around 19%, followed by the pyrylium-based O4-B at 9%.

ECC/PC Formulations

The iodonium-based salt I1-B in combination with the radical photoinitiator shows the highest reactivity in ECC/PC (Figure 98).

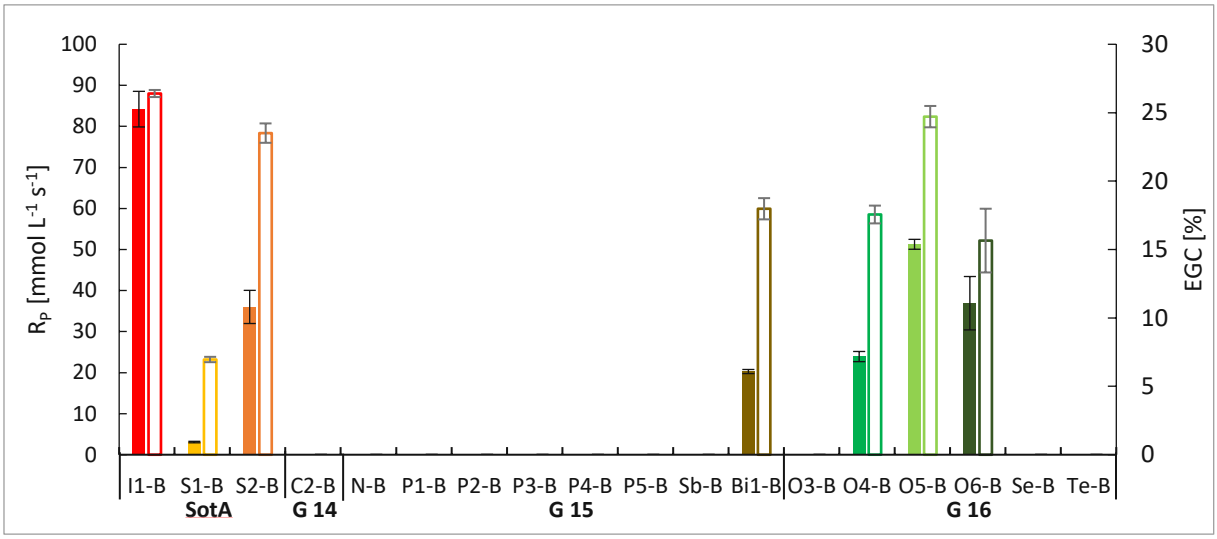

Figure 98: Rate of polymerization (R_P - full) and epoxy group conversion (EGC – framed) in ECC/PC with the onium tetrafluoroborates (photo-induced decomposition by Ivocerin); The time-based parameters t_{max} and $t_{95\%}$ are located in the attachment (Figure 258)

However, the pyrylium- and thiopyrylium-based onium salts show high rates too. O5-B represents the most reactive pyrylium-system in this series with the bismuthonium salt achieving slightly lower polymerization rates. Considering the conversion achieved by the onium salts, the iodonium initiator shows the highest conversion with approximately 21%, followed by the pyrylium/thiopyrylium compounds with up to 20% for the O5-B. However, the Bi1-B performers well, due to 14% epoxy conversion.

Since the radical photoinitaitor Ivocerin decomposes the oniuim salt to potentially start RICP, similar experimental conditions like in the DSC series based on the radical thermal initiator TPED are present. Therefore, the results share similarities as well. Overall, the iodonium-based salt delivers the highest reactivity. However, pyrylium and thiopyrylium salts show medium reactivity and good conversions in ECC. Comparing the results in BADGE, I1-B is clearly dominating. Unlike in the TPED series, Ivocerin is not able to initiate RICP with nitrogen-, selenium- or tellurium-based salts.

To conclude, the performance of established iodonium salts during the photoinitiation study is unmatched in BADGE/PC. However, switching to ECC/PC measurements, the data shows a clear advantage for the thiopyrylium salt S2-B, outperforming all onium salts in the series.

4. Onium Hexafluoroantimonates

4.1. Synthesis

4.1.1. Unmodified Cations

After reactivity screening of all onium tetrafluoroborates, it was finally time to use more reactive counterions. Previous reactivity data gathered from various DSC measurements suggested the application of the bismuth-, carbon- and pyrylium-based onium salts as potentially new cationic initiators and good candidates for RCFP. These three onium compounds were selected for further investigation. The commercial systems to benchmark against, are iodonium hexafluoroantimonates which show great reactivity in cationically polymerizable resins, as well as in frontal polymerization applications.[4, 35] Therefore, the hexafluoroantimonates of the selected cations were aimed to synthesize (Figure 99). The SbF_6^- counterion is less nucleophilic compared to the already tested tetrafluoroborates, which should result in a significant boost of reactivity.

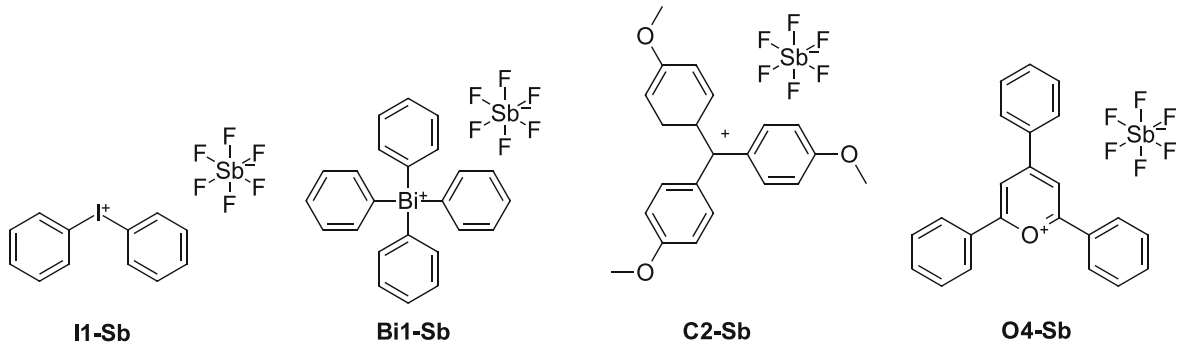

Figure 99: Aimed compounds: iodonium, bismuthonium, methylium and pyrylium hexafluoroantimonate

By using hexafluoroantimonate as counterion in all aimed compounds, a fair comparison is ensured in the upcoming analysis.

4.1.1.1. Diphenyl Iodonium Hexafluoroantimonate

The diphenyl iodonium hexafluoroantimonate was the first compound to be synthesized. It represents one of the most used cationic initiators in industry. A quit simple reaction route was chosen (Figure 100).

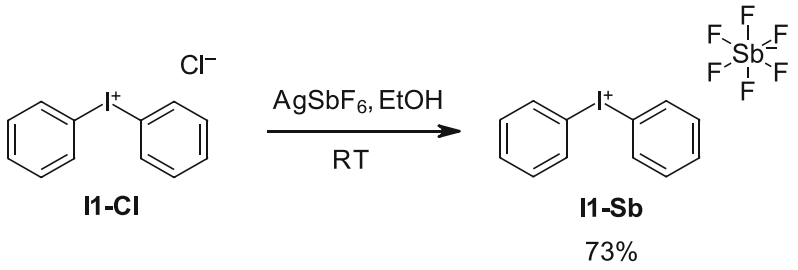

Figure 100: Synthesis route to achieve diphenyl iodonium hexafluoroantimonate (I1-Sb)

Starting with the chloride, a salt metathesis was performed with silver hexafluoroantimonate according to Watanabe et al.[167]

4.1.1.2. Tetraphenyl Bismuthonium Hexafluoroantimonate

Very similar to the synthesis of the tetrafluoroborate in chapter I, 3.1.3.4.1 starting from the triphenyl bismuth, the triphenyl bismuth dichloride was obtained in 97% yield and afterwards converting it into the difluoride at 67% yield. The reaction route to obtain the hexafluoroantimonate was a variation of the work of Matano et al. (Figure 101).[152] With the exception of using $NaSbF_6$ instead of $NaBF_4$ and therefore a different workup. This route involves the BF_3-etherate-promoted reaction of the triphenyl bismuth difluoride with phenylboronic acid.

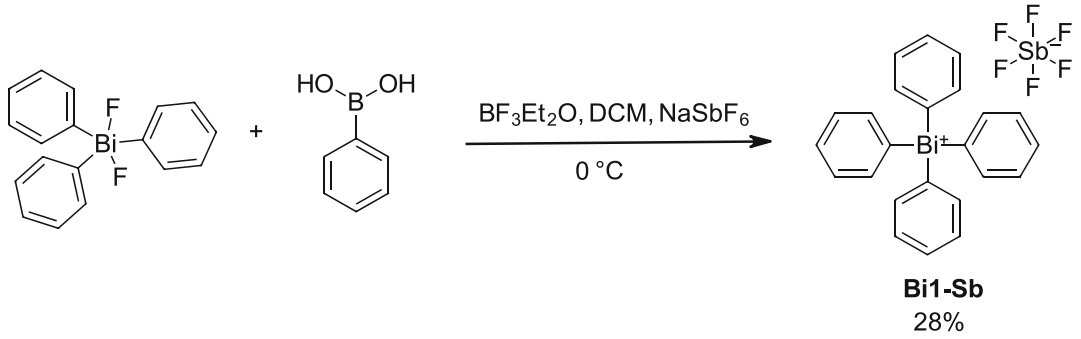

Figure 101: Synthesis route to achieve tetraphenyl bismuthonium hexafluoroantimonate (Bi1-Sb)

The quite low yield of 28% can be significantly improved to above 90% by adding 2 eq. of the commercially available hexafluoroantimonic acid (65-70% in water) instead of the sodium hexafluoroantimonate after the 2 h of reaction time. This dramatically shifts the equilibrium of BF_4 : SbF_6 due to the much lower H_0-value of $HSbF_6$. The fundamental concept behind this circumstance is the replacement of weaker acid salts by stronger acids, while liberating the weaker acid in form of HBF_4.

4.1.1.3. Tris(4-methoxyphenyl) Methylium Hexafluoroantimonate

To prepare the hexafluoroantimonate of the para-substituted methylium compound, a reaction route based on Karim et al.[133] was chosen. The chloride starting material (Figure 102) was reacted with silver hexafluoroantimonate to give the onium salt in high yields.

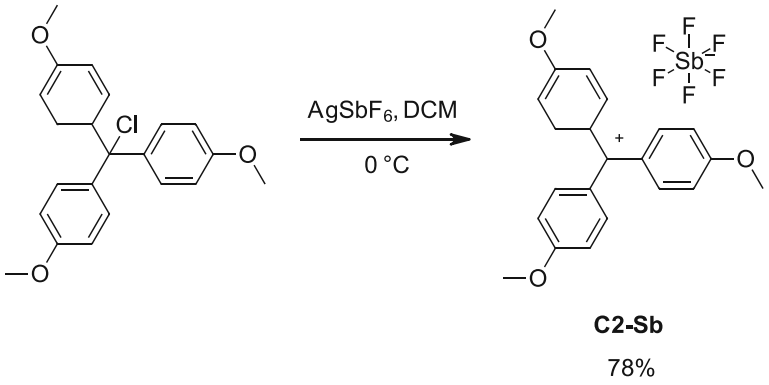

Figure 102: Synthesis route to achieve tris(4-methoxyphenyl) methylium hexafluoroantimonate (C2-Sb)

In addition, the stability against hydrolysis in air and water was checked via NMR. After around one minute, the result of the water stability test was negative. Direct exposure to water hydrolyzes the C2-Sb very quickly. However, the experiment conducted in air was positive. There was no noticeable hydrolysis after 1 h of exposure of the product to ambient air. Upon addition to monomers mixtures like BADGE/PC, ECC/PC or HDDGE, a stability issue was noticed. The formulations started to solidify during mixing of the components after a few minutes, except for the BADGE/PC-based ones. Unfortunately, this stability issue of the methylium salt prevents the compound from being practically applied in reactive epoxy formulations.

4.1.1.4. 2,4,6-Triphenyl Pyrylium Hexafluoroantimonate

To synthesize the pyrylium-based hexafluoroantimonate, a synthesis route in accordance to the work of Fortage et al.[168] was carried out (Figure 103).

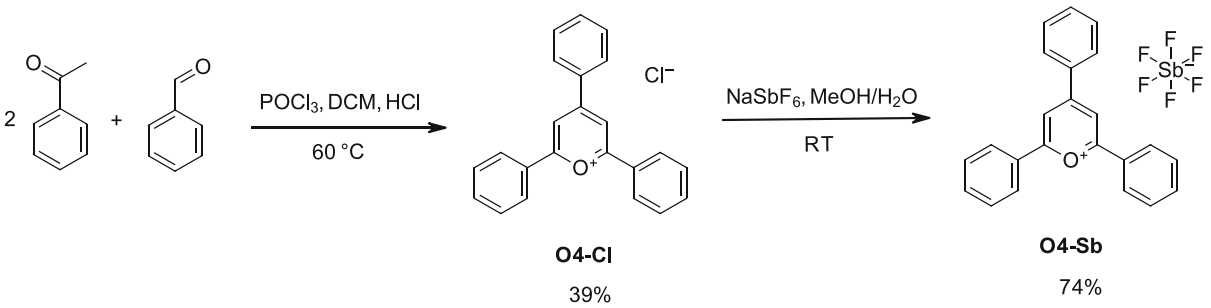

Figure 103: Synthesis route to achieve 2,4,6-triphenyl pyrylium hexafluoroantimonate (O4-Sb)

Starting with easily available benzaldehyde and acetophenone, the pyrylium-ring formation is promoted by the addition of an oxophile, the phosphoryl chloride. After the first step, a simple metathesis reaction similar to the work of Li et al.[129] was performed to exchange the chloride ions to hexafluoroantimonate ones.

4.1.2. Alkoxylation of the Cations to improve Solubility

After the three aimed SbF_6-salts were synthesized and ready for analysis, the first solubility tests of the hexafluoroantimonates in various monomers were carried out. Despite being soluble in BADGE/PC and ECC/PC mixtures like in previous tests, to be a real candidate for cationic frontal polymerization, the presence of propylene carbonate in formulations has to be avoided. PC leads to major issues during RICFP, due to the strong bubble formation along the process. Unfortunately, none of the synthesized onium salts dissolved in commercial epoxy-based monomers like BADGE, ECC or HDDGE. Usually epoxy-monomers offer a non-polar environment which is not well suited to dissolve rather polar onium salts. Even the iodonium initiator I1-Sb showed significant solubility issues in the monomers mentioned above.

The common solution to this problem is the introduction of alkoxy groups into the iodonium salts, as used in industry.[169] A frequently used iodonium salt (Com-I-Sb) is modified with a *para*-octoxy substituent at one of the phenyl rings (Figure 104). An additional advantage of the substituted iodonium salt is its broad commercial availability, therefore this compound does not need to be synthesized. This approach was used to modify Bi1-Sb and O4-Sb as well.

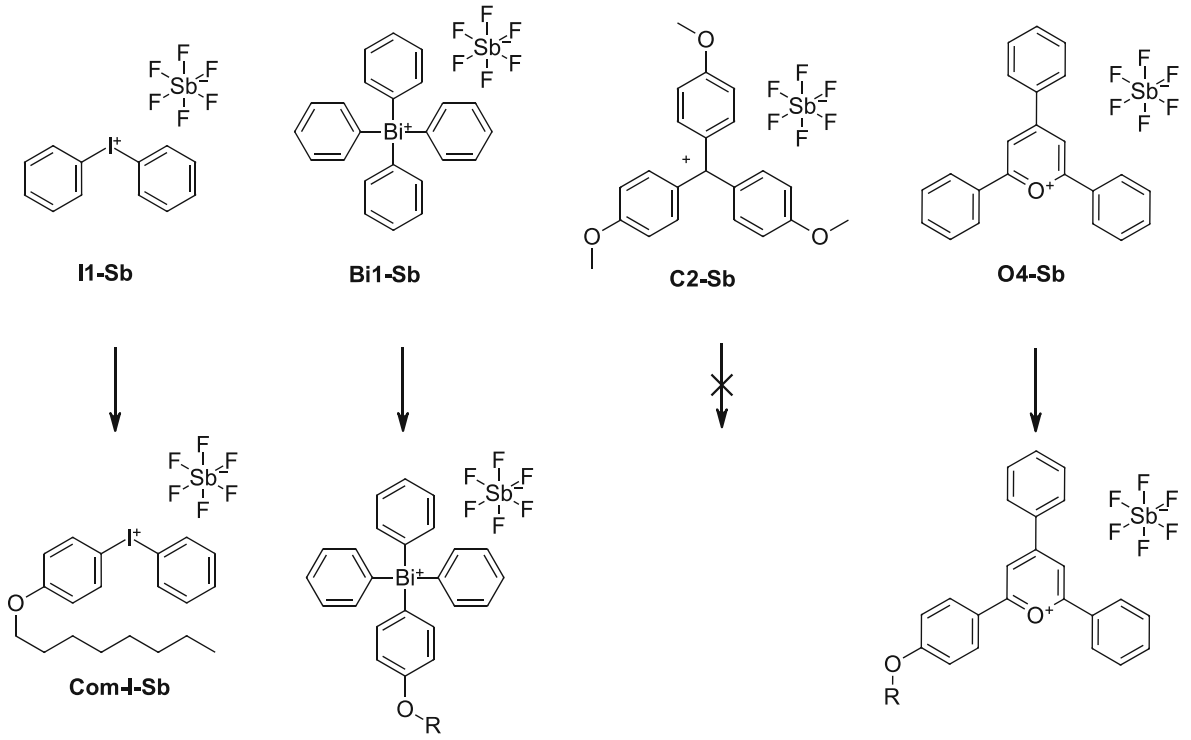

Figure 104: Schematic substitution of one aromatic ring to enhance solubility properties

The carbon-based C2-Sb was not considered for modification, since solidification of the samples during mixing with ECC and HDDGE occurred within one minute. Additionally, the samples containing BADGE as monomer gelled after a few hours at room temperature, rendering the initiator rather useless in epoxy monomers.

4.1.2.1. 4-Hexyloxyphenyl Triphenyl Bismuthonium Hexafluoroantimonate

First, a commercial derivative of the phenylboronic acid was searched to modify the bismuth-based onium salt. Finally, the hexoxylated phenylboronic acid was used to react with triphenyl bismuth difluoride (Figure 105). To yield the desired product Bi2-Sb, a reaction route similar to Matano et al.[152] was carried out. The intermediate salt during this route is a bismuthonium tetrafluoroborate. By addition of hexafluoroantimonic acid, an equilibrium reaction takes place. Strong acids replace weak acid salts easily, while liberating the weaker acid. The equilibrium is practically only on the side of the hexafluoroantimonate due to the orders of magnitude higher H_0-acidity value of $HSbF_6$ compared to HBF_4. Therefore, tetrafluoroboric acid is liberated and the bismuthonium hexafluoroantimonate formed.

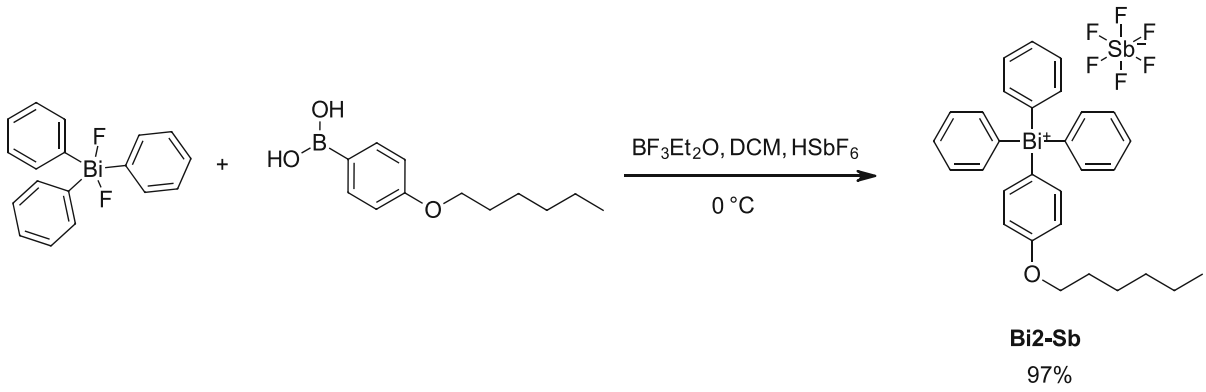

Figure 105: Synthesis route to achieve 4-hexyloxyphenyl triphenyl bismuthonium hexafluoroantimonate (Bi2-Sb)

The sticky appearance of the bismuthonium salt is a great indicator for much better solubility due to less crystallinity, introduced by the alkoxy chain.

4.1.2.2. 4(4-Decyloxyphenyl)-2,6-Diphenyl Pyrylium Hexafluoroantimonate

In the first step the pyrylium chloride has to be synthesized. There are two possibilities to accomplish the introduction of an alkoxy chain during the synthesis, similar to the work of Fortage et al. (Figure 106).[168]

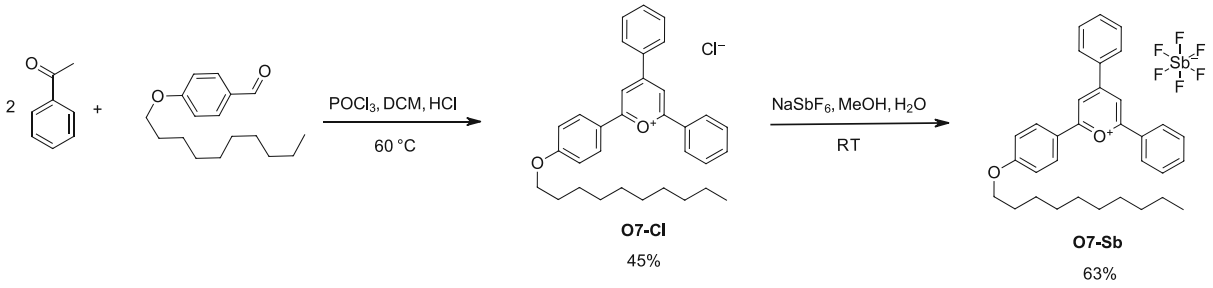

Figure 106: Synthesis route to achieve 4(4-decyloxyphenyl)-2,6-diphenyl pyrylium hexafluoroantimonate (O7-Sb)

The first possibility is to use a *para*-alkoxylated benzaldehyde derivative, while the second variant is an acetophenone derivative. The first approach would introduce one alkoxy chain into the molecule, whereas the second one would introduce a total of two. Since a decyloxy benzaldehyde is commercially available, this 10-carbon atom long chain should provide enough lipophilicity to dissolve the final pyrylium salt in rather non-polar monomers like BADGE, ECC or HDDGE. The single-alkoxylated pyrylium salt then underwent a salt metathesis similar to the work of Li et al.[129] to result in the pyrylium hexafluoroantimonate.

4.2. Characterization of Onium Hexafluoroantimonates

4.2.1. Selection of the Onium Hexafluoroantimonate Compounds

In addition to the unmodified onium salts Bi1-Sb and O4-Sb, the onium salts were prepared in their alkoxylated hexafluoroantimonate version. Therefore, the now modified bismuth- and pyrylium-based salts were ready to compete against the state-of-the-art iodonium salt, which was commercially acquired in its alkoxylated form (Figure 107). The carbon-based salt was not tested any further, since major stability issues arose during preliminary tests in epoxy-resins BADGE, ECC and HDDGE.

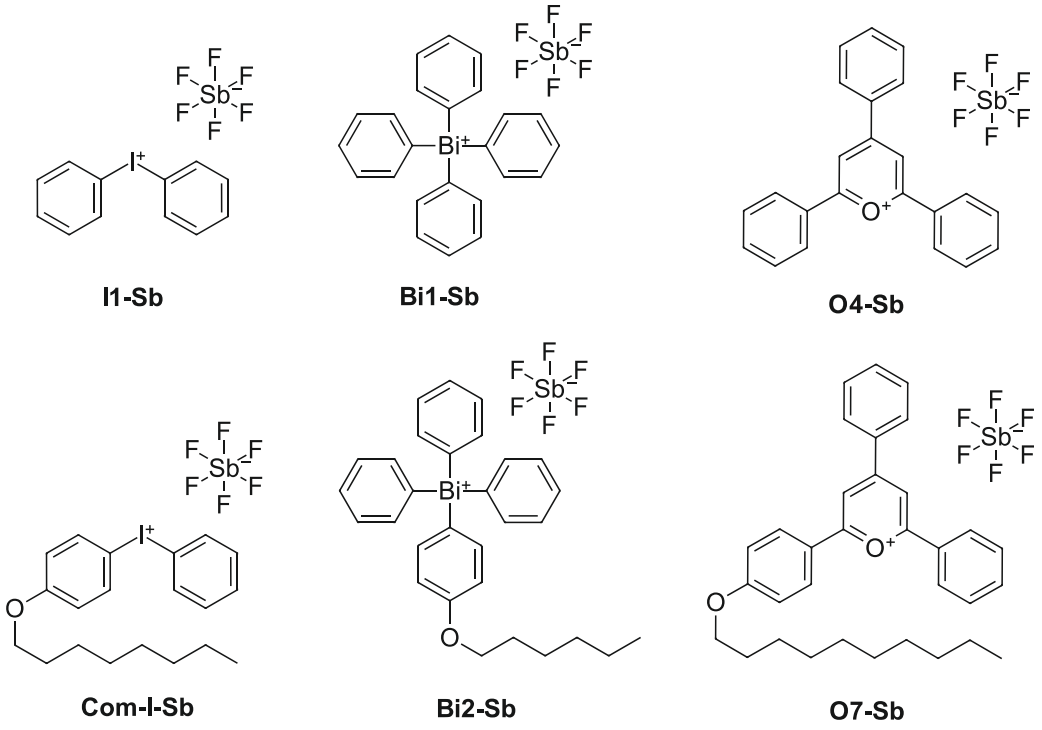

Figure 107: Selection of onium hexafluoroantimonates for further analysis

Additionally, all onium salts were tested negative on any residual halogens like chlorides. Strong bases inhibit cationic polymerization by forming a strong ion pair with the positively charged growing chain, therefore their absence must be verified with a silver nitrite test (see chapter I, 3.2.2).

4.2.2. Absorption Spectra determined via UV-VIS Experiments

According to chapter I, 3.2.3 the absorption spectra of the onium compounds were determined to select an appropriate light source for further testing. The wavelength scan ranges from 250 nm to 600 nm. Samples were dissolved in dry acetonitrile. Depending on the absorption of the onium salt, concentrations of 1 x 10^{-4} mol L^{-1} or 1 x 10^{-5} mol L^{-1} were used. The unmodified onium salts as well as the alkoxylated derivatives were measured.

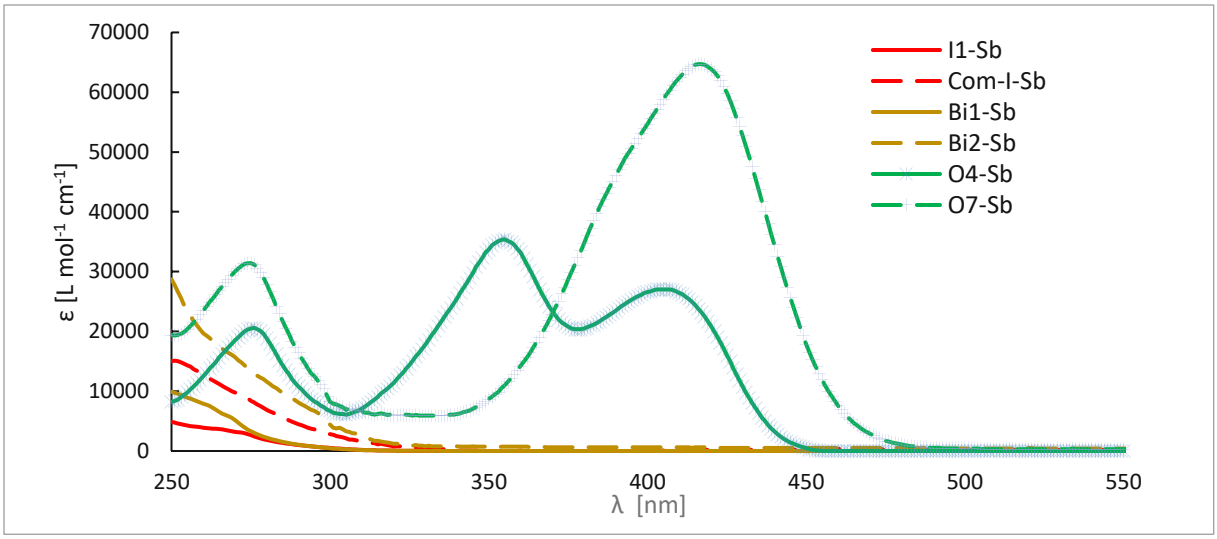

Figure 108: Wavelength dependence of the molar extinction coefficient for iodonium, bismuthonium and pyrylium salts

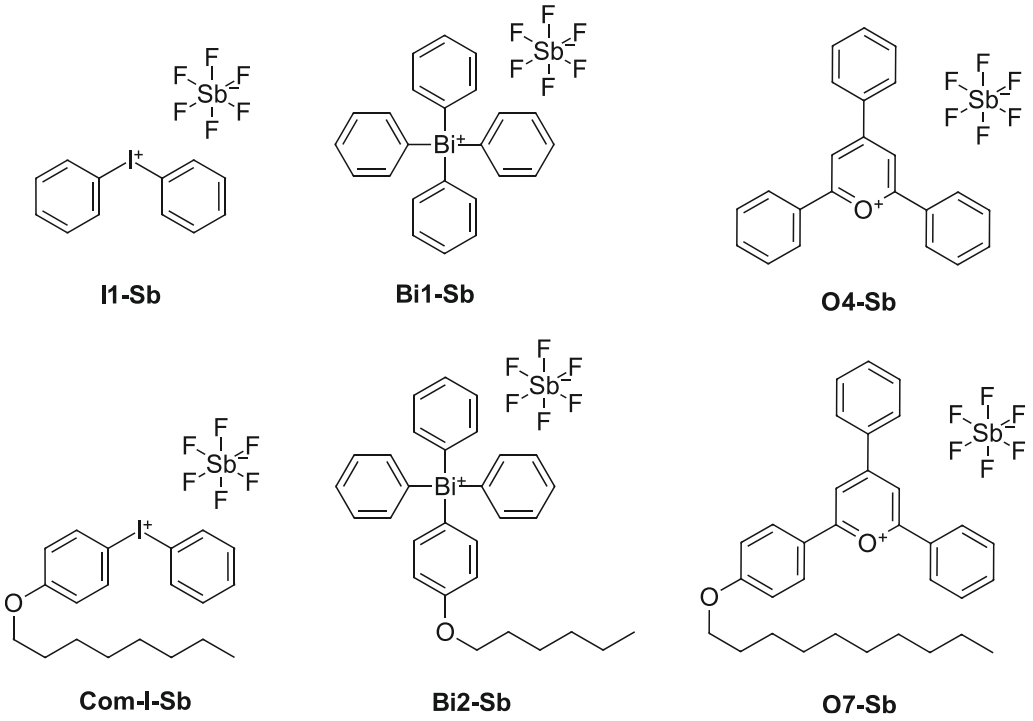

There is a clear trend visible, if comparing the unmodified onium salts based on iodonium, bismuthonium and pyrylium (Figure 108). The presence of an alkoxy chain is responsible for increasing the extinction coefficient significantly. Iodonium- and bismuthonium hexafluoroantimonates show no absorption maximum in the scanned range, however their extinction increases by a factor of around three at 275 nm. The pyrylium-based onium salt shows a different behavior, if modified with the decyloxy moiety. The originally two maxima at 357 nm and 408 nm, merge into one maximum at 419 nm with an extinction coefficient of around 64000 L mol^{-1} cm^{-1}. In addition, the tail-out region shifts from 450 nm to 480 nm for the O7-Sb.

4.3. Reactivity of the Onium Hexafluoroantimonates

4.3.1. Formulations based on BADGE/HDDGE

Since the unmodified onium hexafluoroantimonates were not soluble in the aimed monomer mixture of BADGE and HDDGE, only the alkoxylated onium salts were used. Finally removing any undesired propylene carbonate from the formulations. Therefore, the iodonium-, bismuthonium- and pyrylium-based hexafluoroantimonates could be homogeneously dissolved in a mixture of 80 mol% BADGE and 20 mol% HDDGE (1,6-hexanediol diglycidylether) (Figure 109).

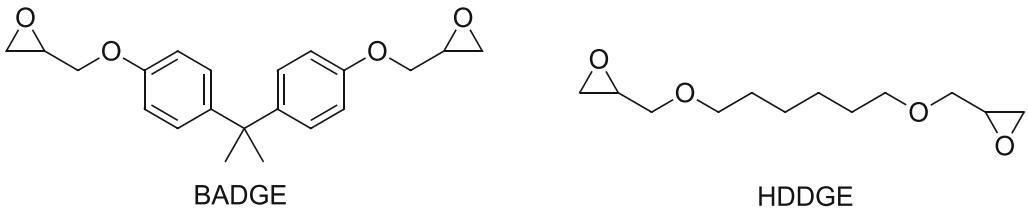

Figure 109: Monomers BADGE and HDDGE

The epoxy-based monomer HDDGE represents the reactive diluent in the formulations, conveniently lowering the viscosity. In addition, solubility for the onium salts enhanced compared to pure BADGE. The selected onium salts Com-I-Sb, Bi2-Sb and O7-Sb were dissolved in the resins (Figure 110).

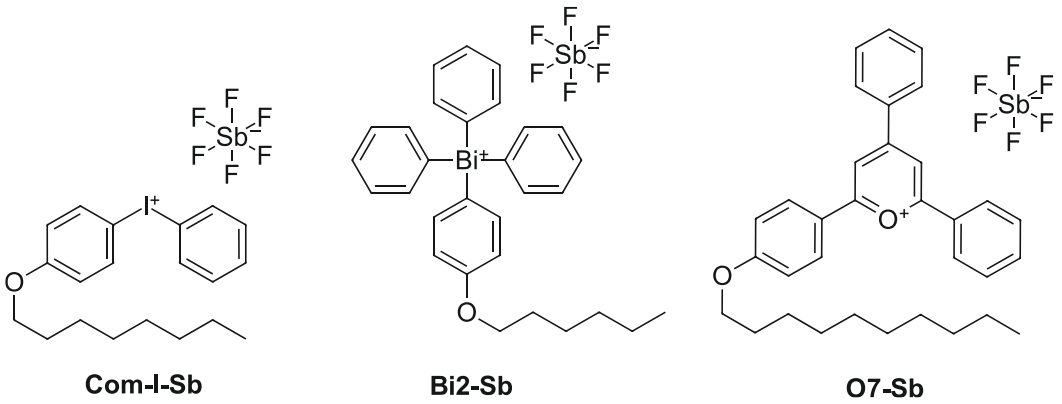

Figure 110: Selected alkoxylated-onium hexafluoroantimonates for reactivity tests

All alkoxylated onium salts were used in 0.5 mol% based on epoxy groups.

4.3.2. Thermal Behavior of Onium Salts determined via DSC

4.3.2.1. Thermal-Induced Decomposition of Onium Salts

To gather information regarding temperature stability of the onium salts, a simultaneous thermal analysis was performed. Analogous to chapter I, 3.3.2, the onium salts were exposed

to a temperature gradient starting at 25 °C with a temperature ramp to 350 °C. Once the onium salts decompose, their superacid is liberated and able to initiate cationic polymerization. The exothermic polymerization reaction is picked up by a DSC sensor during the measurement and plotted against temperature. Formulations based on BADGE/HDDGE with 1 mol% onium salt prepared in chapter I, 4.3.1 were used for the experiments.

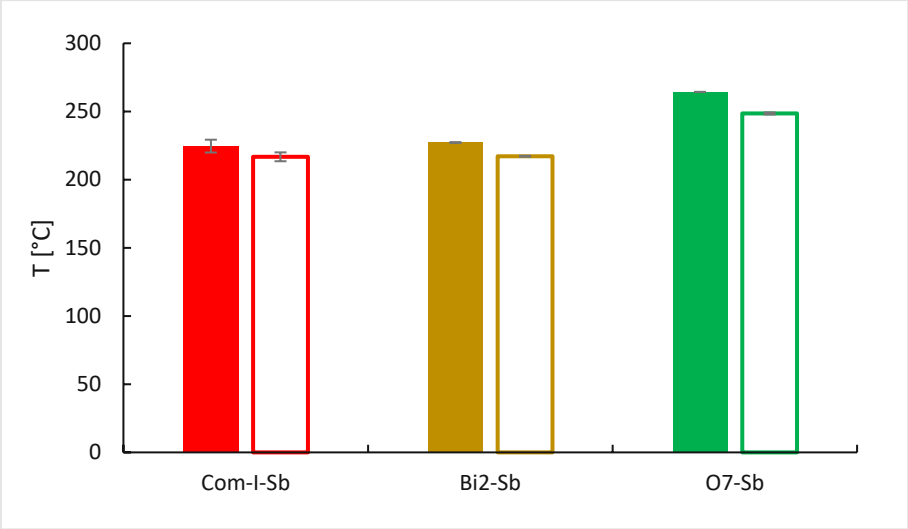

Figure 111: Temperature at the highest exothermicity (T_{max} - full) and polymerization onset temperature (T_{onset} - framed) in BADGE/HDDGE with the alkoxylated onium hexafluoroantimonates

Onset temperatures reach up to 217 °C for the iodonium- and bismuthonium salt (Figure 111). The pyrylium salt delivers an onset temperature of nearly 249 °C. The corresponding values for the temperature at the highest exothermicity follow the same pattern.

4.3.2.2. Thermal-Induced Radical Decomposition of Onium Salts

Besides the thermal decomposition of pure onium salts, the onium hexafluoroantimonates were mixed with the C-C labile compound TPED to determine their onset temperatures together with the temperatures at maximum exothermicity. Expected are overall lower temperatures, since the radical thermal imitator TPED is present. By exposure to the fixed temperature gradient (25 °C to 350 °C), TPED cleaves and its radicals attack the onium salt. The formulations preparation was described in chapter I, 4.3.1. To all formulations based on 0.5% onium salt for BADGE/HDDGE based on epoxy groups were modified with an equimolar amount of TPED.

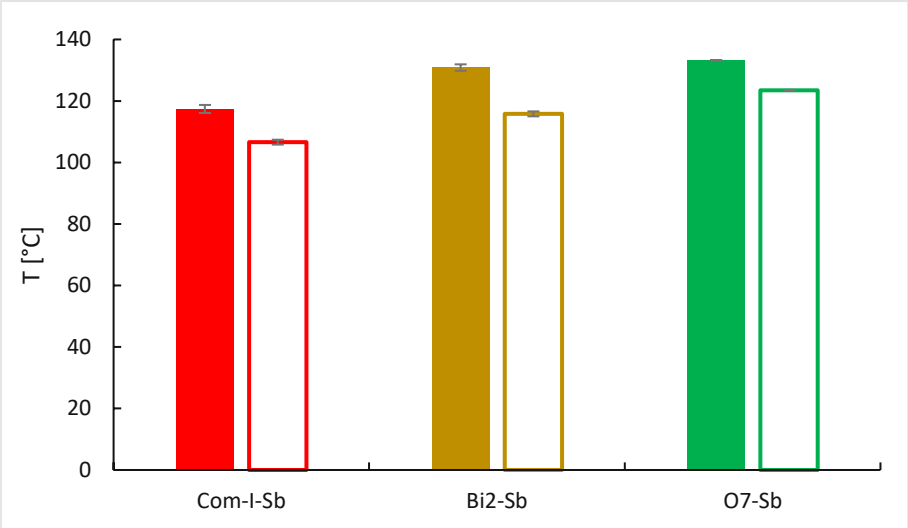

Figure 112: Temperature at the highest exothermicity (T_{max} - full) and polymerization onset temperature (T_{onset} - framed) in BADGE/HDDGE with TPED and the alkoxylated onium hexafluoroantimonates

Considering onset temperatures, one can see the steady increase by around 10 °C, if starting with the iodonium salt and ending with the pyrylium initiator (Figure 112). A similar trend is visible for the T_{max} values. Therefore, the iodonium-based salt requires the least amount of energy to start the superacid liberation.

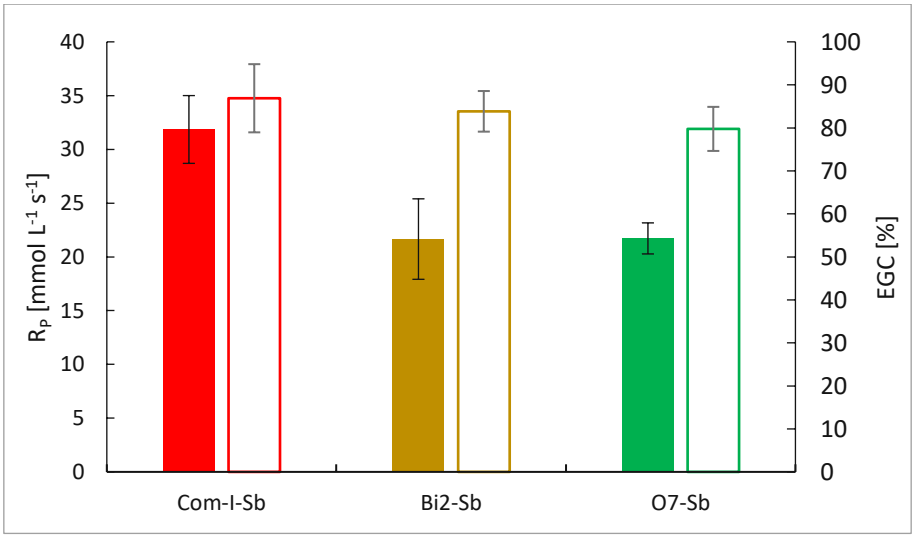

Figure 113: Rate of polymerization (R_P - full) and epoxy group conversion (EGC – framed) in BADGE/HDDGE with TPED and the alkoxylated onium hexafluoroantimonates

The slight reactivity advantage of the commercial iodonium salt is present (Figure 113). Second place is achieved by the bismuthonium- and pyrylium salt at 68% of the reactivity of the iodonium initiator. As seen in previous experiments in BADGE-based formulations, the conversions reach pretty similar values. A significant improvement of the absolute values is simply achieved by removing the PC from the formulations and replacing in with HDDGE. Therefore, a boost from 40% in BADGE/PC to above 80% in BADGE/HDDGE is obtained.

Iodonium salts still show the best results, however the bismuthonium- and pyrylium initiators show great potential as well. Generally, bismuth- and pyrylium-based salts are potent candidates for thermal-induced radical decomposition.

4.3.3. Photoreactivity determined via Photo-DSC

4.3.3.1. Photoinitiation Study

Analogously to the tetrafluoroborates, a UV study without the use of a wavelength filter was performed for the hexafluoroantimonates as well. A broad-band mercury lamp was used as irradiation source. The emission spectrum ranges from around 250 nm to 650 nm. The formulations described in the previous chapter I, 4.3.1 were used for this study without any additional compounds. To finally result in 0.5 mol% onium salt in BADGE/HDDGE.

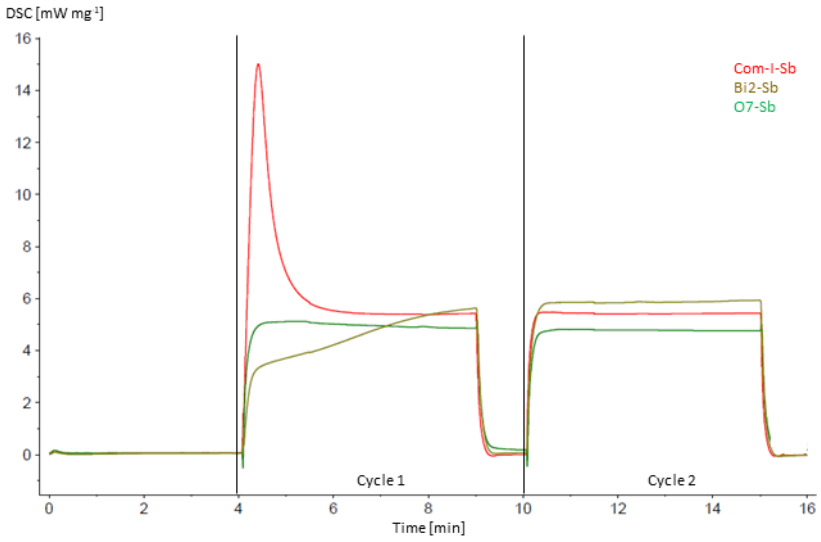

Figure 114: Photo-DSC data in BADGE/HDDGE with the alkoxylated onium hexafluoroantimonates (Photoinitiation)

Considering the obtained reactivity data, one can see the advantage in polymerization rate with the commercial iodonium salt (Figure 114). Reaching 59 mmol L^{-1} s^{-1} and 48% EGC. The pyrylium salt did not show any signs of polymerization, since the samples were liquid after irradiation. Interestingly, the bismuthonium salt shows significant endothermic behavior during the curing procedure and the samples were completely solid afterwards. The iodonium salt measured 48% epoxy conversion in the photoinitiation experiments. Since the pyrylium salt stayed liquid and the bismuthonium salt's DSC-data was endothermic, no rate of polymerization or conversion can be calculated for the two initiators.

During the photoinitiation tests, the commercial state-of-the-art initiator Com-I-Sb outperforms the bismuthonium- and pyrylium salt. Pyrylium salts do not work in epoxy-based

systems under UV light and bismuth-based ones show a distinct endothermicity in the data every single time irradiated with UV light. Many investigative measurements were conducted due to this strange endothermic behavior of the bismuthonium salts. First, it was assumed that reliable pre-measurement crystallization of BADGE containing Bi2-Sb in the aluminum crucibles leads to an endothermic melting peak which overlaps with the exothermic polymerization peak, resulting in an overall negative area. However, this proposed theory is problematic due to a lack of crystal formation within the formulation. Storing the samples in aluminum crucibles for a few hours under light protection and within the nitrogen-flushed photo-DSC chamber without irradiation does not result in crystallized formulations. Additionally, measurements with a light-reflecting aluminum lid on top of the sample crucible were carried out with the expectation to see only the endothermic behavior since no light-induced polymerization is able to take place. Neither an exothermic nor an endothermic peak was obtained in this series of measurements. Unfortunately, only a proposed theory but no clarifying results were obtained for the unexpected endothermic behavior of Bi2-Sb in epoxy resins.

4.3.3.2. Sensitization of Onium Salts

To investigate the efficiency of sensitization for the hexafluoroantimonates, a Photo-DSC study analogously to chapter I, 3.3.3 was performed with the onium salts and anthracene as sensitizing compound. The formulations containing 0.5 mol% onium salt in BADGE/HDDGE based on epoxy groups described in the previous chapter I, 4.3.1 were modified with an equimolar amount of anthracene. Anthracene shows its absorption maxima from 320 to 370 nm, with a tail-out region reaching up to 380 nm. Therefore, an UV-source with a 320-500 nm filter was used in this series of experiments.

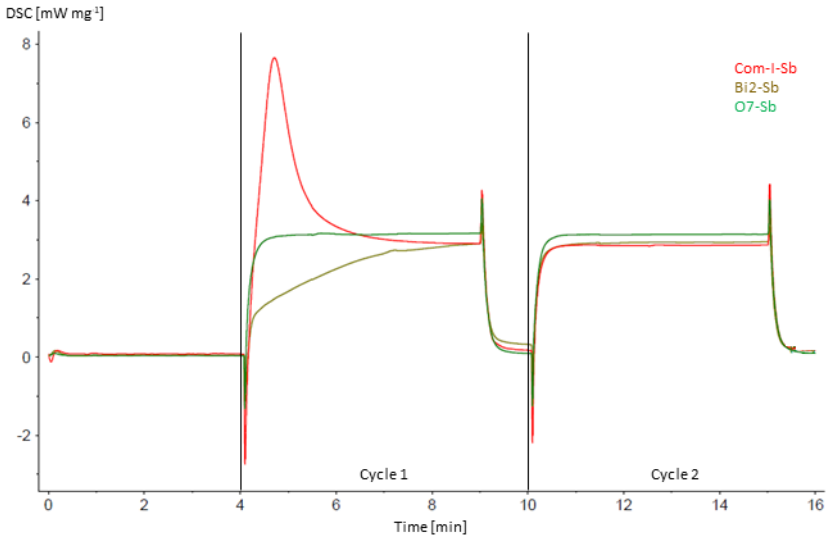

Figure 115: Photo-DSC data in BADGE/HDDGE with the alkoxylated onium hexafluoroantimonates (sensitized by anthracene)

The raw DSC curves are segmented into three parts (Figure 115). The four minute long isotherm phase at the start, followed by two cycles of 5 min irradiation plus 1 min isotherm phase. By subtracting cycle two from cycle one, usually a positive area value for reactive initiators and zero for non-reactive initiators is obtained. Unexpectedly, the endothermic behavior (negative area value) of the bismuthonium-based samples prevents any determination of Photo-DSC parameters. However, all bismuth containing samples were fully cured after the exposure in the photo-DSC. This behavior is highly unusual for DSC measurements, since cationic polymerization of epoxy resins inevitably leads to exothermicity. Therefore, only the iodonium salt's reactivity can be evaluated with a rate of polymerization of 27 mmol L^{-1} s^{-1} an epoxy group conversion of 48%. O7-Sb samples do not solidify during the experiments.

To sum all data obtained during the photo-DSC experiments with anthracene up, the advantages of the iodonium initiator are clearly visible. Bismuthonium salts show endothermic behavior in BADGE-based formulations during the measurements, despite producing hardened samples after irradiation.

4.3.3.3. Photo-Induced Radical Decomposition of Onium Salts

After the sensitization experiments, a Photo-DSC study was performed with the onium salts and a photoinitiator to decompose the onium compound by the formed radicals. The formulations based on 0.5 mol% onium salt in BADGE/HDDGE described in the previous chapter I, 4.3.1 were modified with an equimolar amount of the germanium-based photoinitiator Ivocerin. Ivocerin® shows its absorption maxima from 390 to 345 nm. Therefore, an UV-source with a 400-500 nm filter was used in this series of experiments.

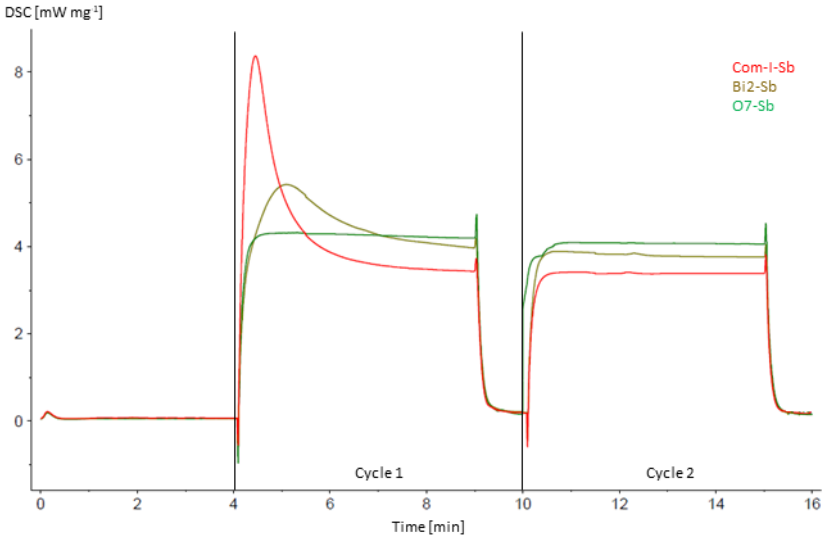

Figure 116: Photo-DSC data in BADGE/HDDGE with the alkoxylated onium hexafluoroantimonates (photo-induced decomposition by Ivocerin)

As expected, the highest reactivity is achieved by the iodonium-Ivocerin couple (Figure 116) with a rate of polymerization reaching 370 mmol L^{-1} s^{-1}. The bismuth-based initiator shows only a little reactivity with Ivocerin. The pyrylium salt did not show any exothermicity at all, however the samples solidified during the irradiation period in the Photo-DSC. EGC reaches 82% for the iodonium salt.

The combination of Ivocerin and the iodonium hexafluoroantimonate results in a highly effective initiator pair. Unfortunately, Bi2-Sb and O7-Sb did not reach significant reactivity in this study.

4.4. Radical Induced Cationic Frontal Polymerization

4.4.1. Selection of the Compounds

The selection of onium salts for the radical induced cationic frontal polymerization experiments was justified by measured reactivity in BADGE/HDDGE via DSC. In addition, the solubility of the onium salts in the epoxy system was crucial. Propylene carbonate cannot be

used in frontal polymerization, since it would lead to severe bubble formation. The evaporation of PC is a result of a rather low boiling point of 242 °C for frontal polymerization, since frontal temperatures reach well above 180 °C and sometimes even 275 °C.[125] Therefore, both new alkoxylated hexafluoroantimonates were considered for frontal polymerization. Bi2-Sb and O7-Sb were readily soluble in the monomer mixture BADGE/HDDGE and could therefore be compared with the state-of-the-art onium salt Com-I-Sb (Figure 117).

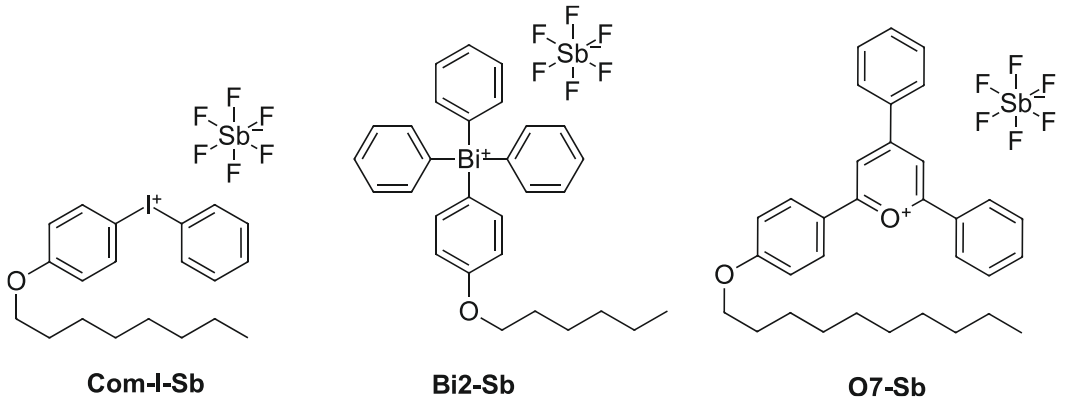

Figure 117: Selection of alkoxylated onium hexafluoroantimonates for RICFP

Additionally, TPED was added for the initiation of the frontal polymerization, since the synthesized onium salts had reactivities comparable to Com-I-Sb in the previously carried out DSC study.

4.4.2. Storage Stability Tests

One major advantage of the radical induced cationic frontal polymerization compared to other curing techniques is the enhanced pot life of the formulations. All necessary compounds for RICFP are mixed in advance and can usually be stored over several days, even weeks without decreasing the performance significantly.[125] Therefore, a storage stability study was carried out at a constant storage temperature of 50 °C under light protection for the iodonium-, bismuthonium- and pyrylium salts. The formulations contained 80 mol% BADGE and 20 mol% HDDGE with 0.5 mol% iodonium salt and 1.5 mol% bismuthonium- and pyrylium salt referred to epoxy groups. All formulations were prepared with an equimolar amount of TPED compared to the onium salt.

The focused-on metric in terms of stability of a formulation was the viscosity, which was measured with a rheometer. The viscosity was determined at a shear rate of 100 s^{-1} and the gap size between stamp and plate was 48 µm. The lower the change in viscosity over time, the better is the storage stability of a formulation.

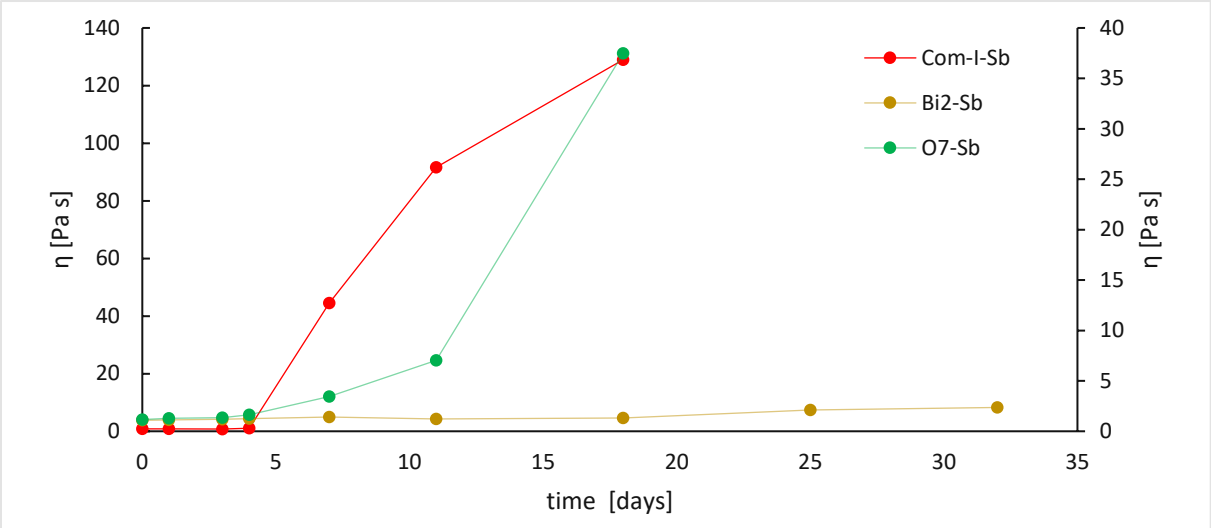

Figure 118: Time dependent viscosity of the BADGE/HDDGE-based formulations at a storage temperature of 50 °C under light protection. Primary axis: Com-I-Sb/TPED was used in 0.5 mol%. Secondary axis: Bi2-Sb/TPED and O7-Sb/TPED were used in 1.5 mol%

At the start of the pot life experiments, the iodonium-based formulation shows around 0.8 Pa s, while the bismuthonium- and pyrylium-based formulations measure approximately 1.1 Pa s (Figure 118). This starting difference can be easily explained, due to the triple amount of onium salt and TPED dissolved in the more viscous samples. Pyrylium hexafluoroantimonate shows a storage stability of around 3 to 4 days, before the viscosity starts ton rapidly increase. A similar trend can be observed for the commercial iodonium salt in BADGE/HDDGE, since the viscosity increase is clearly visible after 3 to 4 days. After 11 days the viscosity of the Com-I-Sb formulation already surpassed 9 Pa s, which represents an increase in viscosity by a factor of 115. Interestingly, the formulations containing Bi2-Sb experience a completely different viscosity pattern. The change in viscosity is rather low, even after 32 days the viscosity increased by a factor of only 2. Therefore, the bismuthonium salt shows a clear advantage over the iodonium salt in terms of storage stability. However, the increase of the viscosity to around 2.4 Pa s suggests some small amount of polymer formed due to the cleavage of TPED and further on the bismuthonium salt.

4.4.3. RICFP

First, the onium salts and the TPED were dissolved in various concentrations in a monomer mixture of 80 mol% BADGE and 20 mol% HDDGE. Formulations starting with 0.5 mol% and ranging up to 2.0 mol% of the respective onium salts (Com-I-Sb, Bi2-Sb, O7-Sb) with the same concentration of TPED based on the epoxy groups of the monomers. The formulations were then poured into a Teflon mold and irradiated with a focused infrared source. This source

heated the formulation at the edge of the mold and, due to the temperature sensor, switched off the IR source automatically as soon as 190 °C were reached. The frontal polymerization reaction was then observed using a thermal imaging camera (Figure 119).

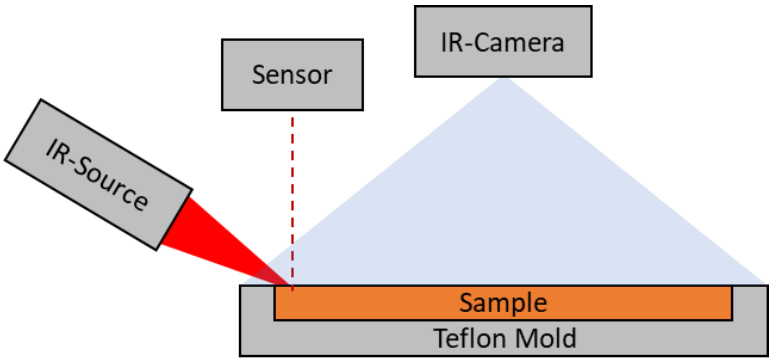

Figure 119: Schematic illustration of the RICFP setup

With the thermal imaging camera information obtained, both the front speed and the maximum front temperature could be calculated. For the samples that showed a well-functioning and stable frontal polymerization, three measurements were carried out. Important parameters of frontal polymerization are frontal velocity v_F, correlating with the speed with which the local reactive zone spreads, and the maximum front temperature T_F.

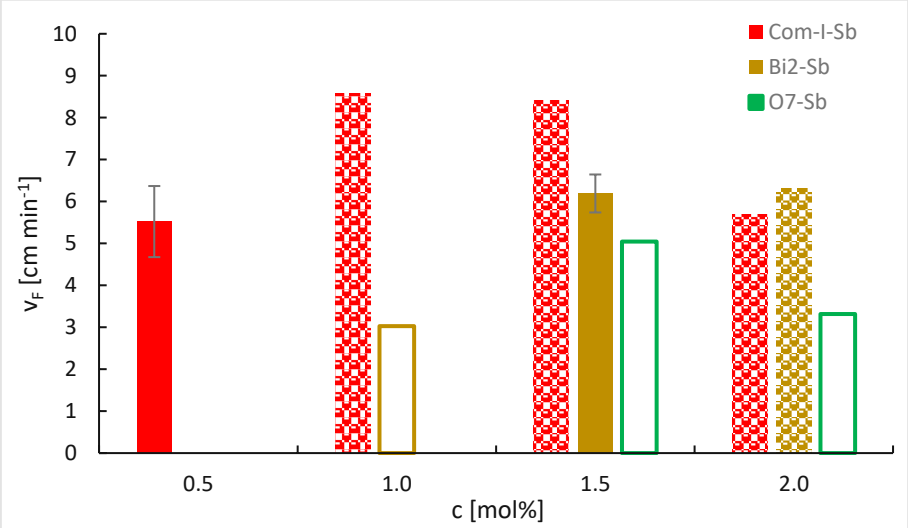

Figure 120: Frontal velocity v_F versus the concentration of the alkoxylated onium hexafluoroantimonates and TPED in BADGE/HDDGE (full bars – stable front; empty framed bars – non-stable front; patterned bars – bubble formation during frontal polymerization)

The iodonium-based initiator was the only one of the three analyzed onium salts in which a stable, functioning frontal polymerization can be observed at 0.5 mol% based on the epoxy groups (Figure 120). From 1.0 mol% and rising, Com-I-Sb is already too reactive, so that very strong bubble formation occurs during the frontal polymerization. It is interesting that with increasing Com-I-Sb and TPED concentrations, the front velocity appears to increase first, and

then decreases again. This behavior can be explained with the massive bubble formation in the sample at 2.0 mol%, therefore decreasing the stability of the front and subsequently its velocity.

In the case of the formulations with the bismuthonium salt, the potential for frontal polymerization becomes visible starting from 1.0 mol%. However, the 1.0 mol% frontal polymerizations remain too instable and terminated sometimes. Reproduceable and stable fronts are achieved with 1.5 mol%. At 2.0 mol%, bubble formation is observed due to excessively high reactivity.

The pyrylium hexafluoroantimonate shows potential for frontal polymerization at the concentrations of 1.5 mol% and 2.0 mol%. However, the fronts created by these samples are very unstable and hardly reproducible. A further increase in the concentration of the initiator was no longer carried out due to the increasingly poor solubility of that much initiator and TPED in BADGE/HDDGE.

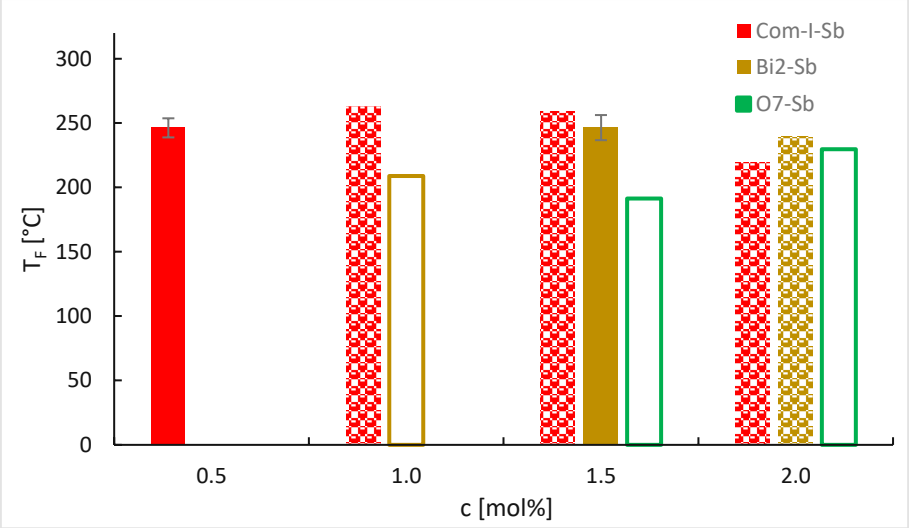

Figure 121: Frontal temperature T_F versus the concentration of the alkoxylated onium hexafluoroantimonates and TPED in BADGE/HDDGE (full bars – stable front; empty framed bars – non-stable front; patterned bars – bubble formation during frontal polymerization)

Regarding to the maximum front temperature (Figure 121), as expected significantly lower temperatures were measured for the non-stable fronts compared to the working ones. Eventually the frontal polymerization has come to a standstill due to insufficient exothermicity. Considering the two stable fronts, Com-I-Sb at 0.5 mol% and Bi2-Sb at 1.5 mol%, a very similar frontal temperature of 246 °C is obtained. The specimens produced via RICFP are depicted in Figure 122.

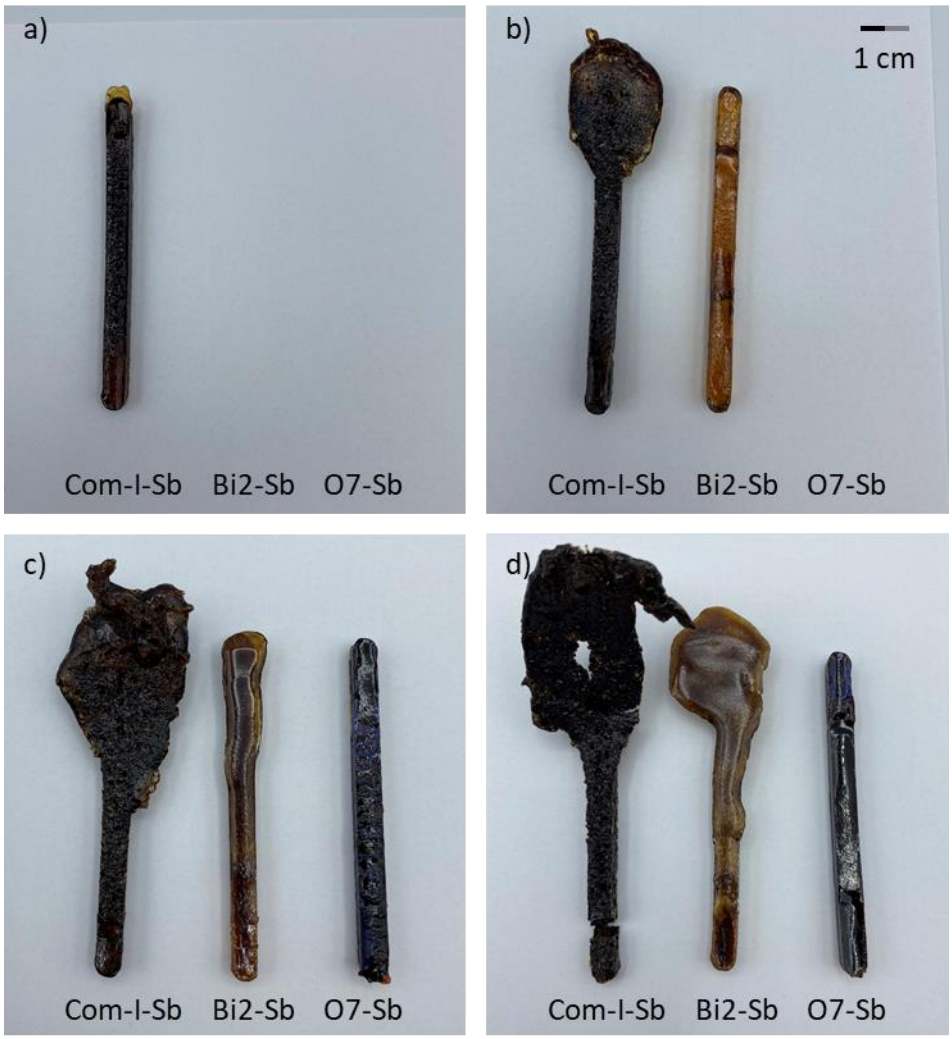

Figure 122: Specimens produced via RICFP of BADGE/HDDGE with the onium salt/TPED concentration of: a) 0.5 mol%; b) 1.0 mol%; c) 1.5 mol%; d) 2.0 mol% based on epoxy groups; The samples, in which the frontal polymerization was not stable and stopped frequently, were fully cured by repeated exposure to the IR source

The cured specimens show the various onium salts in four different concentrations. It is immediately obvious which samples contained too much initiator due to excessive bubble formation and resulting porosity of the specimens.

Since TPED is a thermal radical initiator, it is going to decompose to some degree at 50 °C over an extended period of time. To ensure a still applicable formulation for frontal polymerization, the bismuth-based initiator had to be tested after the 32 days. If successful, the experiment would provide evidence for a very long pot life of the bismuthonium-based formulation.

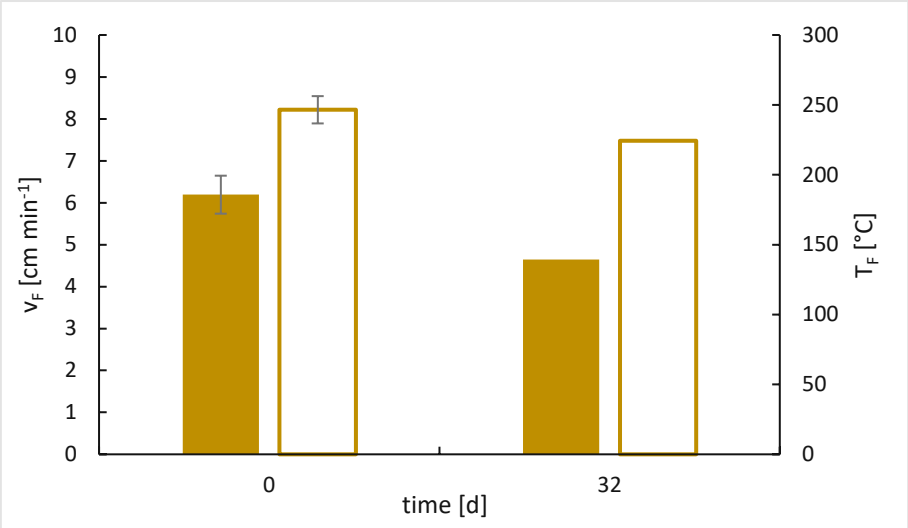

Figure 123: Frontal velocity vF (primary axis, full columns) and frontal temperature TF (secondary axis, framed columns) versus storage time at 50 °C of 1.5 mol% Bi2-Sb /TPED in BADGE/HDDGE

According to the obtained data, the formulation containing Bi2-Sb as initiator perform surprisingly well (Figure 123). After around one month of storing the formulation at 50 °C, the necessary reactivity for RICPF is still present. Overall the frontal parameters noticeably decreased, which suggests already cleaved TPED and some minor amount of polymer formed, due to the 2x increase in viscosity. Reaching approximately 74% of the initial 6.2 cm min^{-1} is a noticeable drop in frontal velocity, however the specimen could be cured nominally without any issues. In addition to lower frontal velocity, the frontal temperature is decreased from around 247 °C to 224 °C after 32 days of storage at elevated temperatures. This circumstance is not dramatic, however an over 20 °C lower frontal temperature can be responsible for interrupting the ongoing frontal polymerization due to insufficient exothermicity at some point. Nevertheless, this could not be observed during this experiment using the 5 mm deep Teflon mold.

4.4.4. RICFP of thin Layers

In addition to standard RICFP experiments, thin layers were polymerized as well. The property is especially useful in practical applications, due to the determination of the minimum part thickness. The minimum layer thickness (MTL) of a sample was determined in the following experiments. The thinner the layer, in which a stable frontal polymerization is possible, the more reactive is a system. With the well-performing formulations of Com-I-Sb with 0.5 mol% and of Bi2-Sb with 1.5 mol%, an ascending Teflon mold (Figure 124) was used to measure the

minimum layer thickness at which the frontal polymerization stops. Three samples were analyzed per formulation.

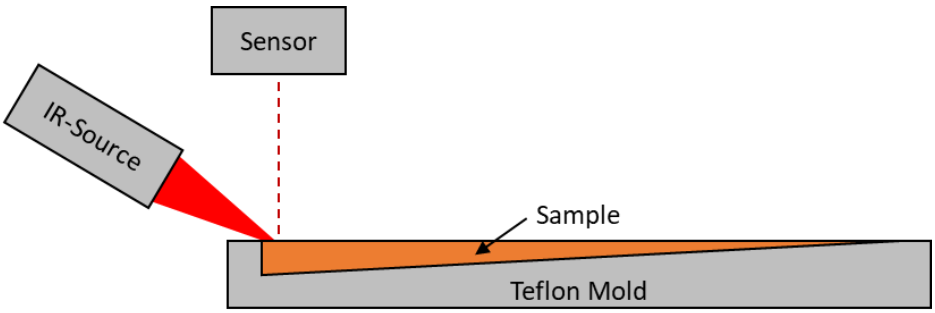

Figure 124: Schematic illustration of the RICFP minimum layer thickness setup

When comparing the minimum layer thicknesses at which the frontal polymerization terminates, it is noticeable that the formulation containing 1.5 mol% of the bismuthonium salt has approximately the same MLT as the reference formulation with 0.5 mol% iodonium hexafluoroantimonate (Table 9).

Table 9: Minimum layer thickness (MLT) of the samples containing different amounts of onium salt/TPED

Onium Salt	c [mol%]	MLT [mm]
Com-I-Sb	0.5	2.8 ± 0.1
Bi2-Sb	1.5	3.0 ± 0.1

This data demonstrates the advantages of commercial iodonium salts, due to the increased reactivity. By tripling the amount of bismuthonium salt and TPED in a formulation, still a 7% increase in MLT is obtained compared to the iodonium salt.

II. The Anionic Species of Photoacid Generators

1. State of the Art

The most accessible class of anions is represented by perfluorinated boron, antimony and arsenic atoms. Examples for this well performing class in photopolymerization are tetrafluoroborates, hexafluoroantimonates, hexafluorophosphates and hexafluoroarsenates as weakly coordinating anions (WCAs). Despite comprising a rather high nucleophilicity, those anions are broadly commercially available and usually easy to obtain as counterions of onium salts via metathesis reactions. However, much less nucleophilic anions are available for onium salts such as perfluorinated borates[170] and aluminates[117] (Figure 125).

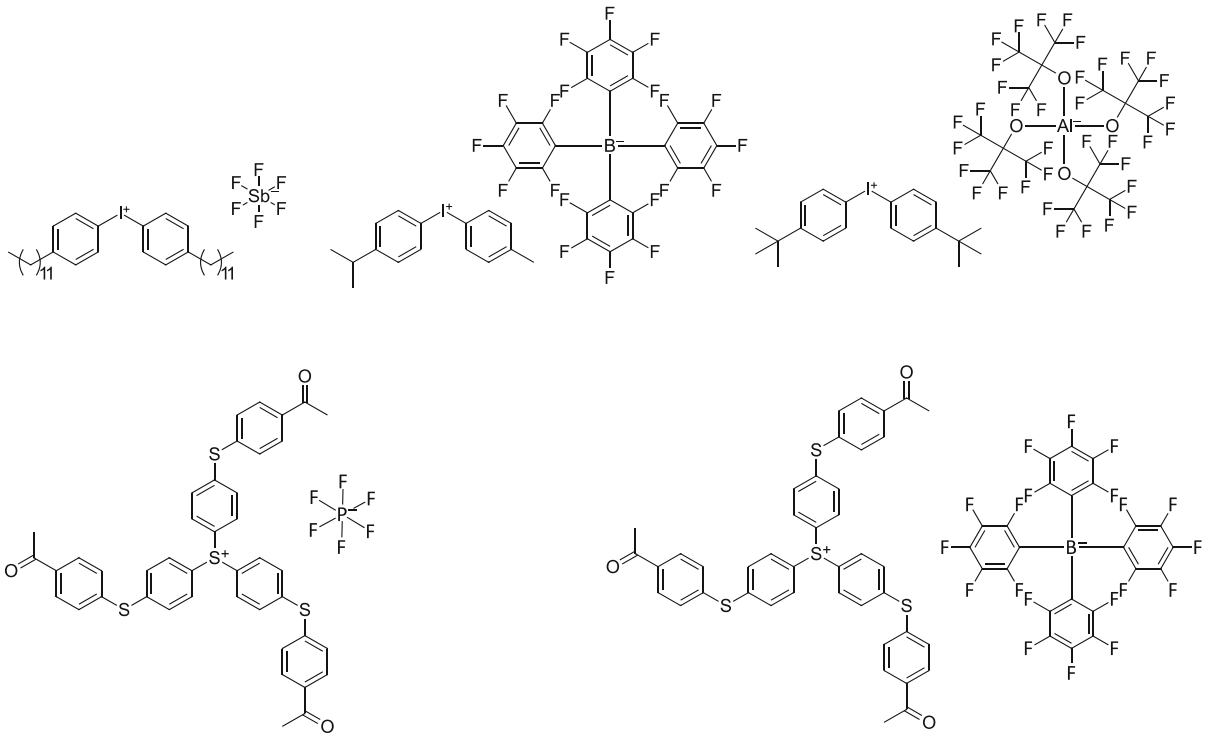

Figure 125: Examples for iodonium- and sulfonium-based PAGs with WCAs (SpeedCure 937, SpeedCure 939 and Bis[4-(tert-butyl)phenyl]iodonium Tetra(nonafluoro-tert-butoxy)aluminate as well as Omnicat 270 and Irgacure 290)

Other stable WCAs with low nucleophilicity are represented by trifluomethanesulfonamides, teflate-based anions, or bridged alkoxy aluminates and borates.[171, 172] Generally, the size of the anion is amongst other factors, directly responsible for lower nucleophilicity, due to better charge distribution across the anion (Figure 126).

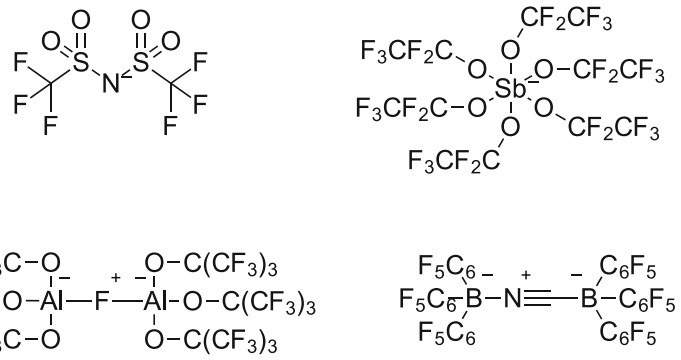

Figure 126: Example structures for sulfonamides, teflates and bridged aluminates/borates

The highly electron-withdrawing sulfonyl groups of the trifluoromethanesulfonamide are responsible for the ion's stability and its superacidic behavior.[173] This class of WCA is usually applied as ionic liquid, electrolyte or catalyst.[174, 175] To further increase the charge delocalization of hexafluoroantimonate, the teflate group can be introduced. The result is a WCA showing less nucleophilicity, however a major drawback is its high sensitivity to moisture. One of the most promising WCAs is the bridged, perfluorinated alkoxy aluminate. Compared to the non-bridged aluminate, it shows better stability if electrophiles are present, as well as much lower coordinative binding strength.[176] The cyanide-bridged borane is a large and well performing WCA, capable of polymerizing ethene.[177, 178]

For applications in cationic photo- and frontalpolymerization, WCAs in combination with onium salts need to demonstrate low coordinative strength. Additionally, WCAs ideally show a certain tolerance towards moisture, due to the usage of industrial monomers. Generally, such monomers measure a small water content.

Lithography-based Additive Manufacturing Technologies

The first cationic systems based on vinyl ethers were printed via SLA in the 1980s using a laser light source.[179] However, shape distortion was observed at the produced parts. This problem was solved with the introduction of epoxy-vinyl hybrid systems. The vinyl ether monomers were polymerized with light at the 3D-printer, while only a few epoxy monomers cured due to their rather low reactivity at room temperature. After the SLA, the "green" part was thermally cured to crosslink all residual epoxy groups, therefore creating the final part with low overall shrinkage.[180] A similar technique is still applied in many state-of-the-art processes, for example in the work of Crivello et al. investigating these epoxy-vinyl resins.[181] However, the approach of printing parts via SLA at room temperature severely limits the selection of monomers. Highly viscous and low reactive monomers such as BADGE cannot be applied in

their pure form, since literature states a general limit of around 0.5 - 1 Pa s.[18, 182] Any further increase in viscosity would lead to problems while applying a fresh resin layer onto the polymerized structure. Severely limiting part quality due to inhomogeneously applied layers as well as increase manufacturing time.

Therefore, a rather new approach towards 3D-printing highly viscous monomers is introduced. Using SLA printers at elevated temperatures drastically increases the scope of monomers, since viscosity decreases with temperature significantly.[183] The so-called hot lithography process is already used for many applications in research and industry due to the high processing temperatures of up to 140 °C, enabling the SLA of viscous state-of-the-art monomers.[184] For example, hot lithography allows for 3D-printing of low reactive monomers and high viscosity resins such as pure BADGE, which cannot be printed at room temperature by standard SLA or DLP.[185]

2. Potential new Anions for Photoacid Generators

In the first chapter, cations with a selection of different central atoms were tested regarding their ability to effectively and efficiently initiate cationic polymerization. The most compelling option is represented by state-of-the-art iodonium salts and sulfonium salts (Figure 127). Usually, one or both of the aromatic rings of the iodonium cation are modified with an alkoxy or alkyl moiety to ensure good solubility in rather non-polar media such as most commercial epoxide monomers. Sulfonium cations are frequently substituted with three aromatic moieties in para-position to achieve a bathochromic shift of their absorption maximum as well as increase solubility in non-polar media.

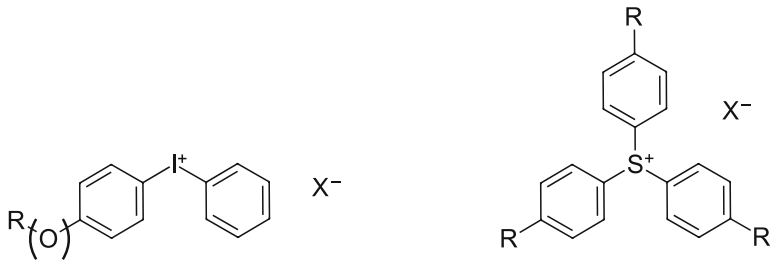

Figure 127: General structure of an alkoxylated/alkylated iodonium salt and an arylated sulfonium salt (X^-... non-nucleophilic anion)

Use cases in cationic polymerization range from simple cleavage upon UV-light or thermal exposure, to more complex initiation mechanisms like sensitization or radical induced cationic polymerization. The shared outcome of all described cases is the resulting superacid liberation

to initiate the polymerization reaction. A much more special application is radical induced cationic frontal polymerization (RICFP). Iodonium salts perform especially well in frontal polymerization due to their suiting redox potential together with TPED, low onset temperatures, high reaction rates and subsequently increased frontal velocities.[125] Sulfonium salts on the other hand are well suited for specialized 3D-printing processes such as hot lithography, since they show increased stability towards high temperature compared to their iodonium counterparts.[186]

Stable WCAs with low nucleophilicities are for example the classical anions formed by lewis acids, carboranes, alkoxymetallates, teflates, fluorinated borates, trisphate- and phosphate-based anions or oxalatoborates.[171, 172] Various anions with boron as central atom were targeted (Figure 128).

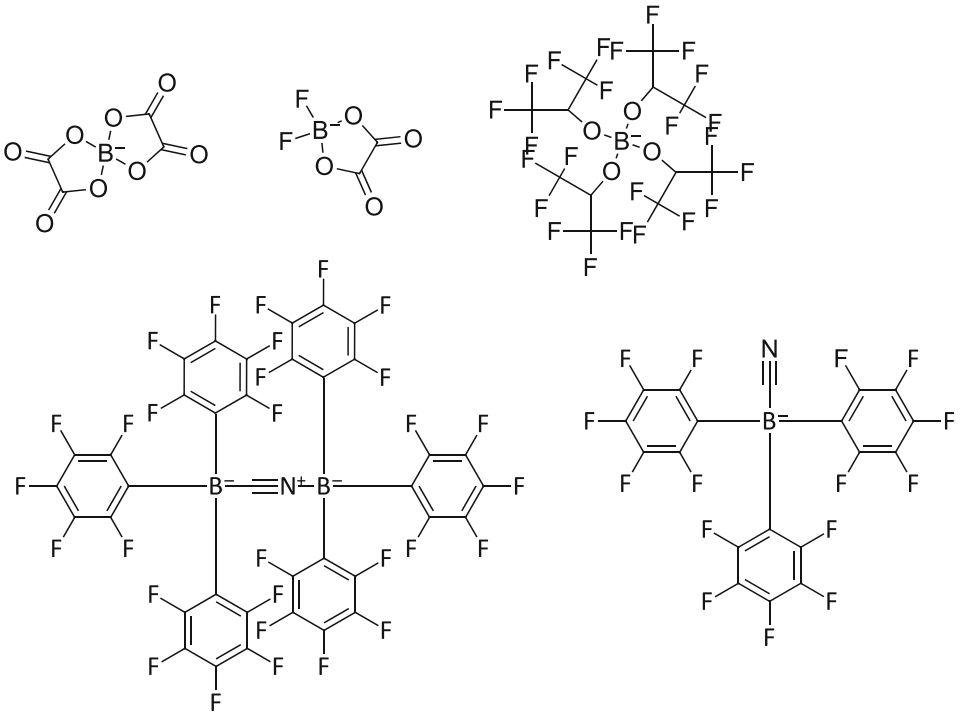

Figure 128:Non-fluorinated and fluorinated oxalatoborates, aliphatic borates as well as cyanide-bridged borane and cyanide-ligated borane

The target anions described above, should be synthesized with lithium, sodium or potassium cations. Afterwards, a metathesis reaction should be carried out to result in the aimed iodonium- and sulfonium salts. The onium salts then should be mixed with a commercially available resin for the studies. Comparison of reactivity, versatility and stability of the produced photoacid generators was planned.

3. Iodonium Borates

3.1. Synthesis

The targeted iodonium tosylate (I-Ts) represents the starting material for all further metathesis reactions, since its anion can be easily exchanged to a different one (Figure 129).

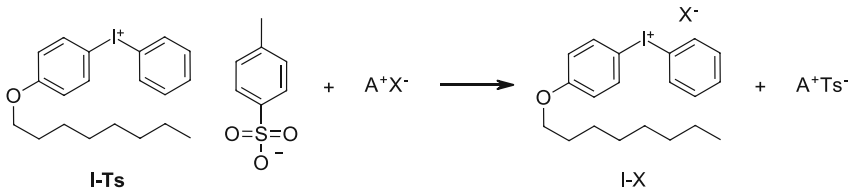

Figure 129: Schematic salt metathesis reaction starting from iodonium tosylate (I-Ts) and alkali metal salt (A^+X^-), resulting in the aimed iodonium salt (I-X) and the precipitating alkali metal tosylate (A^+Ts^-)

In a classic metathesis reaction, an alkali metal cation (A^+) paired to the target anion (X^-) is reacted with the iodonium tosylate in solution, to form the desired iodonium salt (I-X). During this process either lithium-, sodium- or potassium-tosylate (A^+Ts^-) precipitates out of solution to shift the equilibrium to the aimed product.

For both iodonium salts, it is very important to remove all residual alkali metal tosylate as well as remaining I-Ts from the product. Any residues are going to inhibit cationic polymerization, since both anions are not weakly coordinating and eventually start to form a strong ionic bond to the positively charged chain end during polymerization.

3.1.1. (4-Octoxyphenyl) Phenyl Iodonium Tosylate

First, the iodonium-based starting material I-Ts for all following metathesis reactions had to be synthesized. The best option is to synthesize an alkoxylated iodonium salt with a tosylate counter ion, since this molecule is well known in literature and easy to obtain. In addition, the tosylate is not a WCA and will not able to initiate cationic polymerization.

In the first step, octyl phenyl ether was prepared in a classic ether synthesis according to a patent by Castellanos et al. (Figure 130).[187]

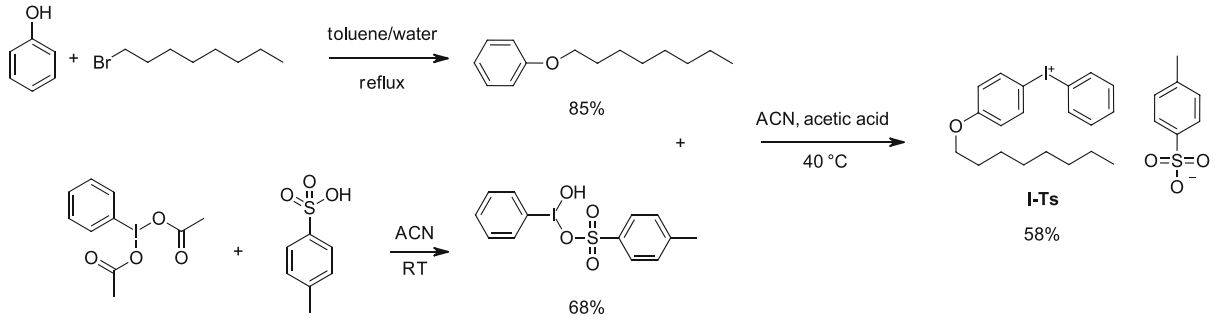

Figure 130:Synthesis pathway to achieve (4-octoxyphenyl) phenyl iodonium tosylate (I-Ts)

Then, hydroxy tosyloxy iodobenzene was synthesized with iodobenzene diacetate and para-toluolsulfonic acid according to the work of Cross et at.[188] Finally, the two freshly prepared compounds were reacted to form (4-octoxyphenyl) phenyl iodonium tosylate similar to a patent of Castellanos et al.[187]

3.1.2. (4-Octoxyphenyl) Phenyl Iodonium Bis(trifluoromethane) Sulfonimide

Sulfonimides are stable WCAs, which are broadly commercially available in their free acid form or as alkali metal salt (Figure 131).

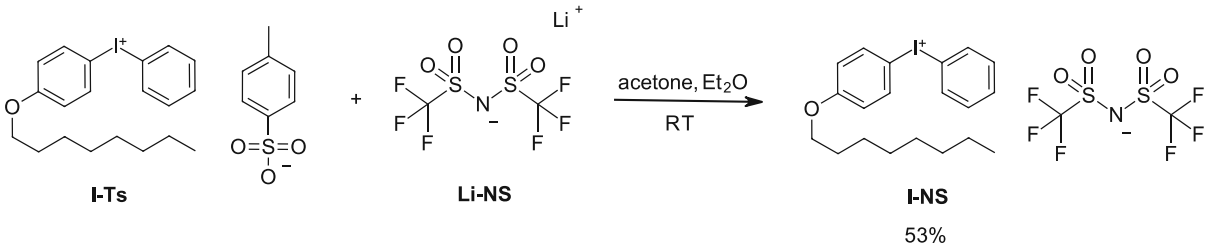

Figure 131: Synthesis of (4-octoxyphenyl) phenyl iodonium bis(trifluoromethane) sulfonimide (I-NS)

Therefore, the lithium salt of the compound (Li-NS) was acquired from a supplier and reacted with the I-Ts in a metathesis reaction to form I-NS similar to Castellanos et al.[187] During this reaction, lithium tosylate will form as a byproduct. Iodonium sulfonimides are known to initiate cationic polymerization in epoxy systems.[189]

3.1.3. (4-Octoxyphenyl) Phenyl Iodonium Bis(oxalato)borate

Oxalatoborates are relatively new WCAs and mainly used in lithium-ion battery research, as they are relatively cheap and perform well as electrolytes and as ionic liquids.[190, 191] In the first reaction step, boric acid was reacted with oxalic acid and lithium hydroxide to form the desired Li-B1 (Figure 132).

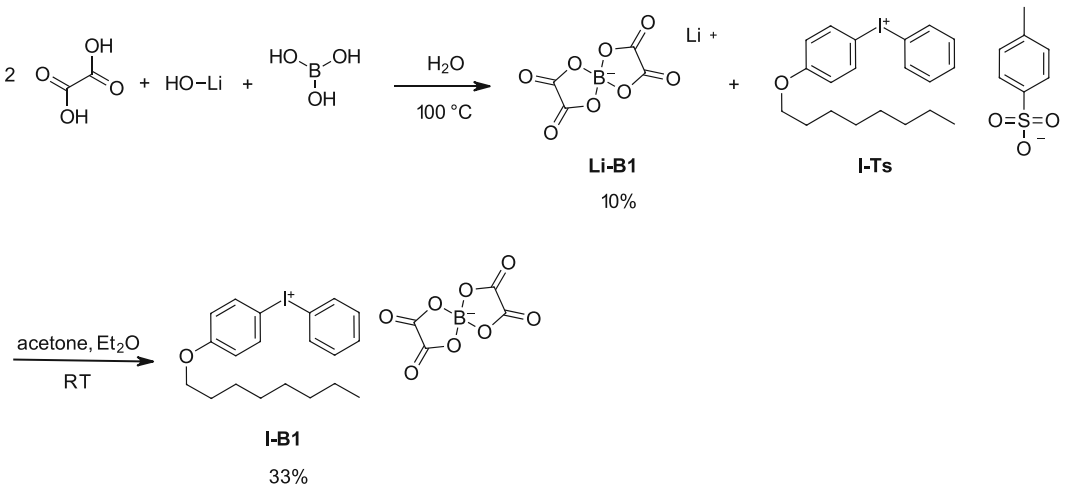

Figure 132: Synthesis pathway to achieve (4-octoxyphenyl) phenyl iodonium bis(oxalato)borate (I-B1)

The synthesis was carried out according to a patent by Lischka et at.[192] In a second step, a metathesis reaction was performed similar to the work of Castellanos et al.[187] I-Ts was reacted with Li-B1 in solution, to result in I-B1 and lithium tosylate as byproduct.

3.1.4. (4-Octoxyphenyl) Phenyl Iodonium Difluoro(oxalato)borate

Fluorinated oxalato borates are used as stabilizing additives in electrolytes for lithium-ion batteries.[193] In the first reaction step, oxalic acid is reacted with boric acid according to a patent by Zhang et al.[194] to form lithium difluoro (oxalato) borate (Figure 133).

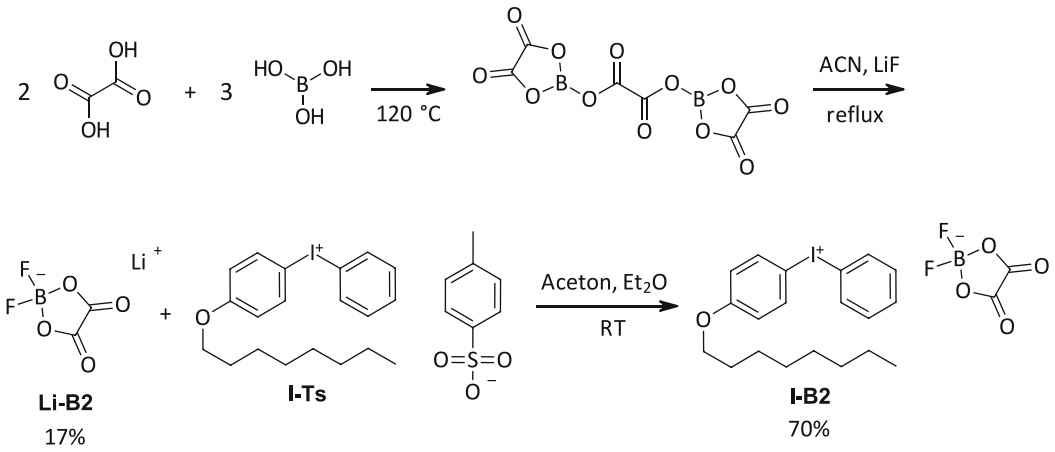

Figure 133: Synthesis pathway to achieve (4-octoxyphenyl) phenyl iodonium difluoro(oxalato)borate (I-B2)

In the second step, a metathesis reaction according to a patent by Castellanos et al.[187] was carried out starting with I-Ts to give the desired product I-B2 and lithium tosylate as a by-product.

3.1.5. (4-Octyloxyphenyl) Phenyl Iodonium Tetrakis((1,1,1,3,3,3-hexafluoro-propan-2-yl)oxy)borate

Oxyborates are used in particular as high-performance anodes in lithium-ion batteries.[195, 196] In the first reaction step, sodium borohydride is reacted with hexafluoroisopropanol according to a paper by Kaliner et al.[197] to form sodium tetrakis((1,1,1,3,3,3-hexafluoropropan-2-yl)oxy)borate (Figure 134).

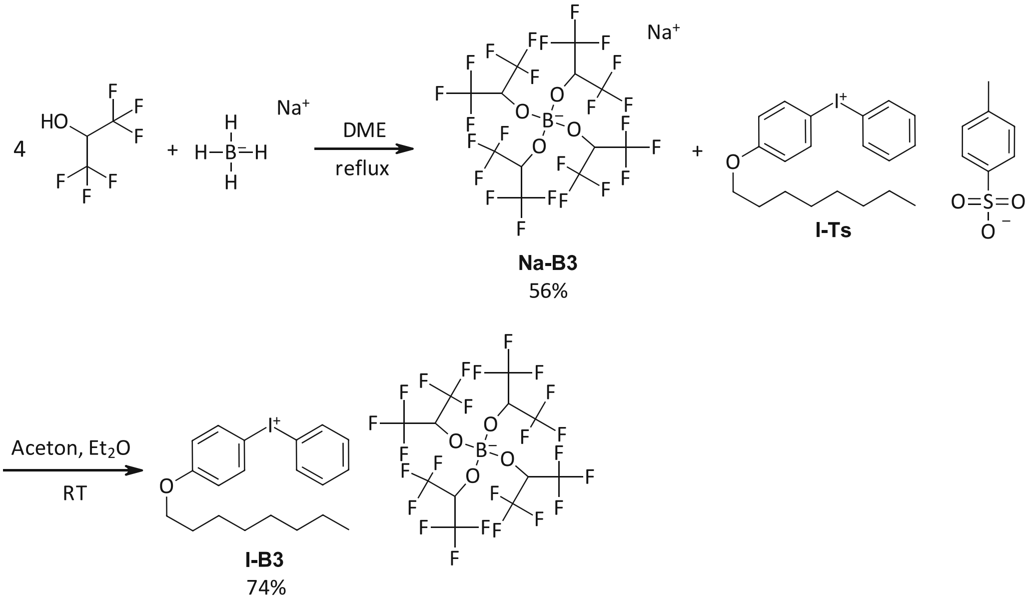

Figure 134: Synthesis pathway to achieve (4-octyloxyphenyl) phenyl iodonium tetrakis((1,1,1,3,3,3-hexafluoro-propan-2-yl)oxy)borate (I-B3)

In the second step, a metathesis reaction according to a patent by Castellanos et al.[187] was carried out with I-Ts to give the desired product I-B3 and sodium tosylate as a by-product.

3.1.6. (4-Octyloxyphenyl) Phenyl Iodonium CN-Bis[Tris(pentafluorophenyl)borane]

Cyanide-bridged boranes represent very weakly coordinating anions, which can be used as potential counterions for the iodonium salts.[178] In the first reaction step, bromopentafluorobenzene was converted to the trisborane, followed by the second step to yield K-B4 based on the work of Fischer et al.[198] and Zhou et al.[199] (Figure 135).

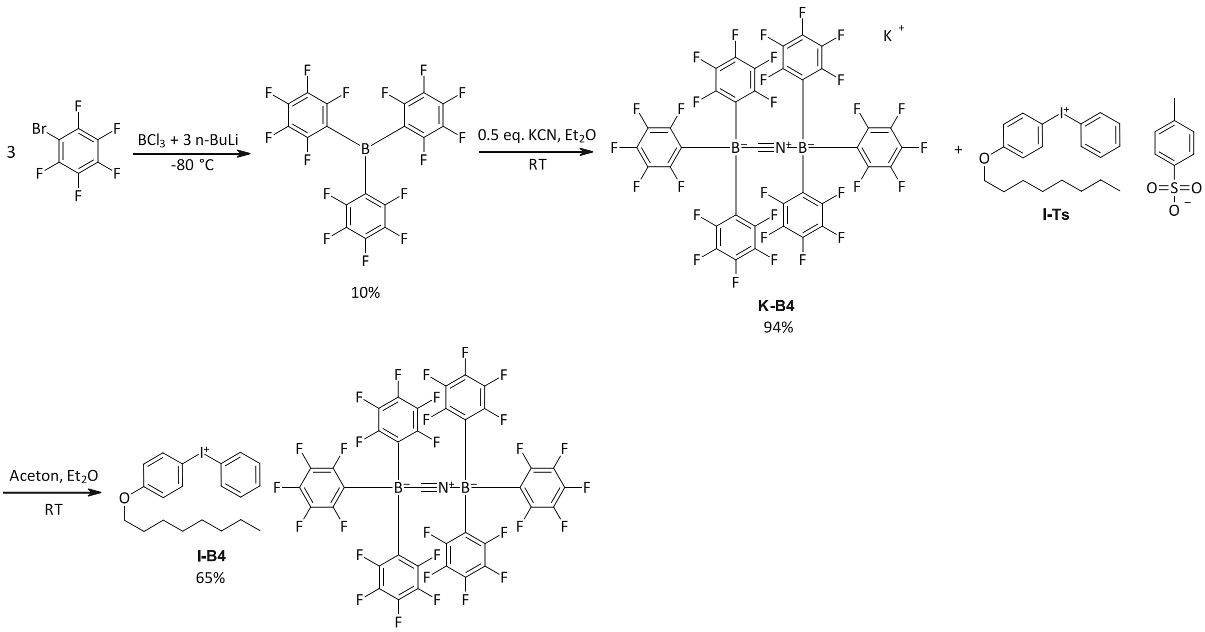

Figure 135: Synthesis pathway to achieve (4-octyloxyphenyl) phenyl iodonium CN-bis[tris(pentafluorophenyl)borane] (I-B4)

In the third step, a metathesis reaction according to a patent by Castellanos et al.[187] was carried out with I-Ts to yield the desired cyanide-bridged product I-B4 and potassium tosylate as a by-product.

3.1.7. (4-Octyloxyphenyl) Phenyl Iodonium CN-[Tris(pentafluorophenyl)borane]

Very similar to the cyanide-bridged borane I-B4 the cyanide-ligated form I-B5 was aimed for next. In the first reaction step, K-B5 was synthesized based on the work of Zhou et al.[199] (Figure 136). Afterwards, a metathesis reaction according to a patent by Castellanos et al.[187] was carried out with I-Ts to yield the desired product I-B4 and potassium tosylate as a by-product.

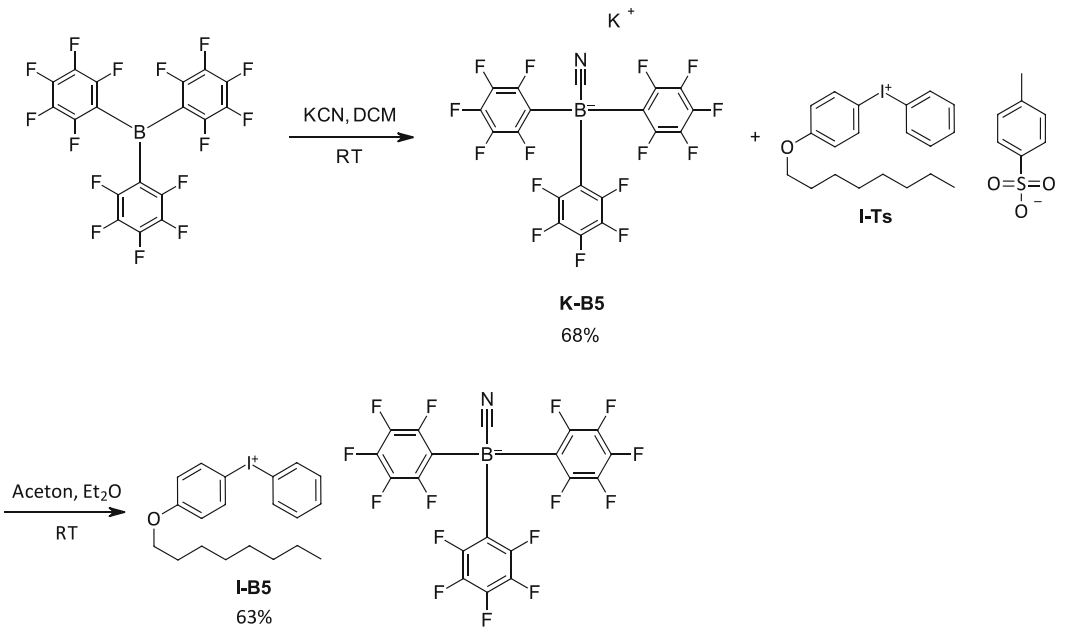

Figure 136: Synthesis pathway to achieve (4-octyloxyphenyl) phenyl iodonium CN-[tris(pentafluorophenyl)borane] (I-B5)

The workup can be simplified in some cases where a high yield is preferred over high purity. Since the K-B5 is a precursor for iodonium and sulfonium salts, a high yield was aimed for usually. The simplified workup skips the water addition and the extraction process entirely. After the 16 h of stirring, the solvents were evaporated to result in a viscous liquid. To remove any residual water faster, dichloromethane was added to the viscous liquid and evaporated quickly. This workup leads to K-B5 as a white solid in a yield of 99%.

3.2. Characterization of Iodonium Borates

3.2.1. Selection of the Iodonium Compounds

Since synthesis of most aimed iodonium salts was successfully executed, the selection for the testing phase was performed. Therefore, the initiators can now be decomposed by thermal-, radical- or photo-stimuli to start cationic polymerization (Figure 63).

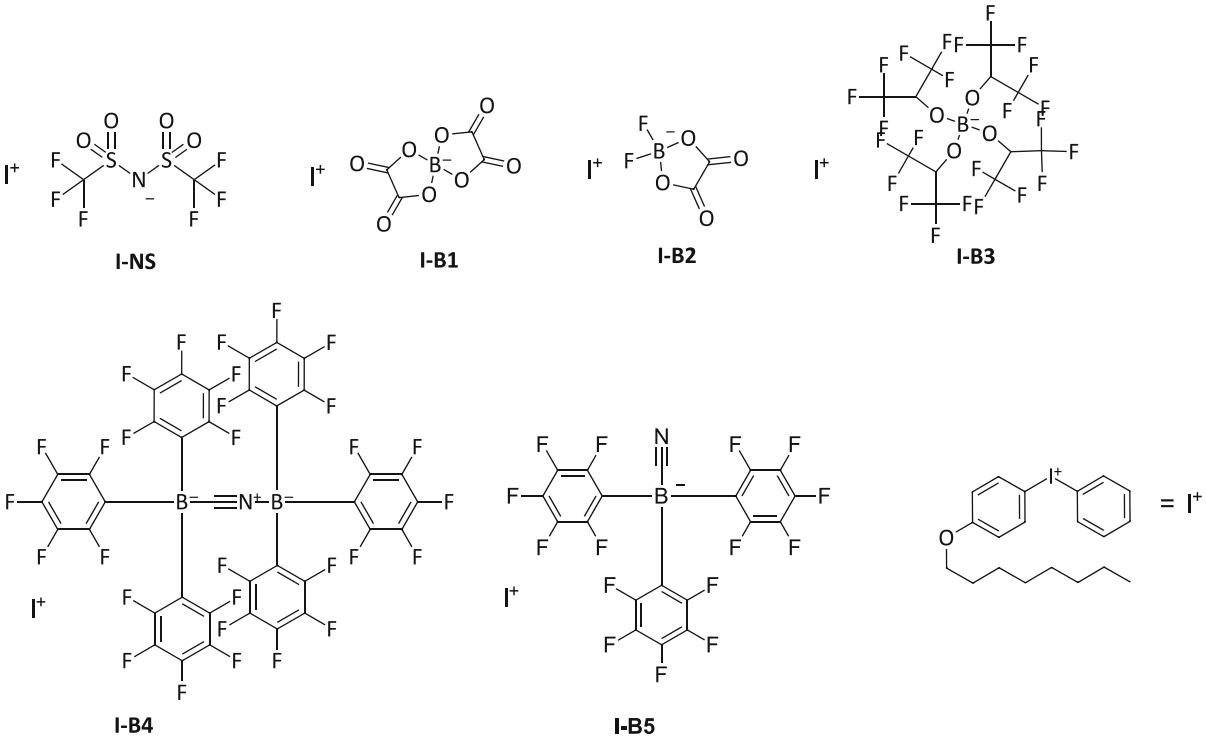

Figure 137: Selection of the synthesized iodonium salts I-NS, I-B1, I-B2, I-B3, I-B4 and I-B5 for further analysis

All synthesized alkoxylated iodonium salts paired with different WCAs were ready to be benchmarked against commonly used iodonium hexafluoroantimonates in industry and much more reactive state-of-the-art salts such as iodonium tetrakis(2,3,4,5,6-pentafluorophenyl)borate and iodonium tetrakis[2,2,2-trifluoro-1,1-bis(trifluoromethyl)-ethoxy]aluminate (Figure 138). Due to broad availability, the iodonium salts Com-I-Sb, Com-I-B and Ref-I-Al were acquired from commercial suppliers.

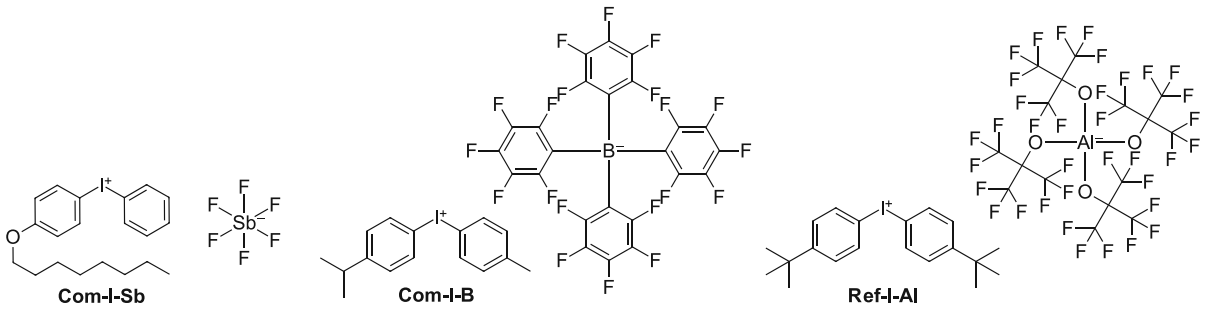

Figure 138: Selection of the acquired state-of-the-art iodonium salts Com-I-Sb, Com-I-B and Ref-I-Al for further analysis

Comparative studies of synthesized and acquired iodonium salts were carried out in terms of photochemical behavior, reactivity and stability in cationically polymerizabl resins.

3.2.2. Absorption Spectra determined via UV-VIS Experiments

During the photochemical analysis, the ultraviolet (UV) and visible light (VIS) absorption spectra of the onium compounds were determined. The wavelength scan ranges from 250 nm to 500 nm. Onium salt and concentrations of 1 x 10^{-5} mol L^{-1} were used.

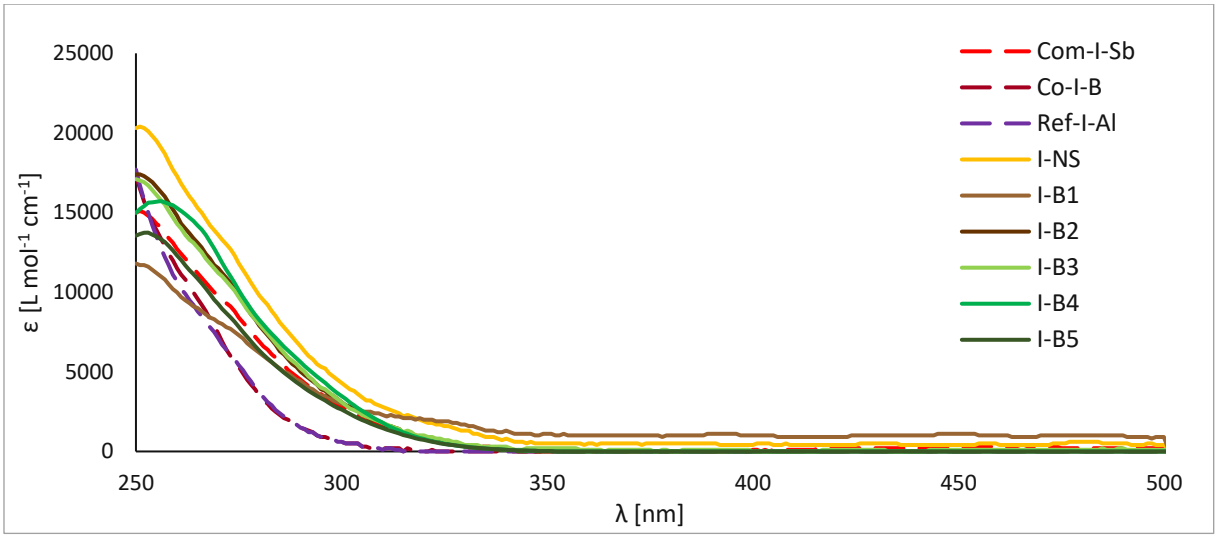

Figure 139: Wavelength dependence of the molar extinction coefficient for synthesized and acquired iodonium salts

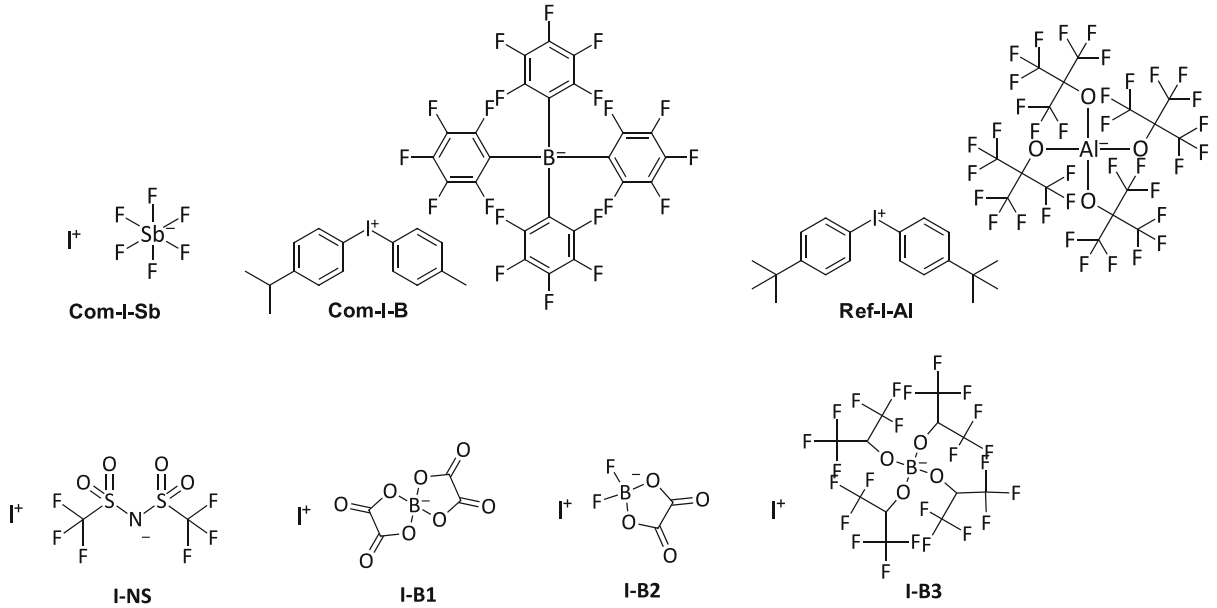

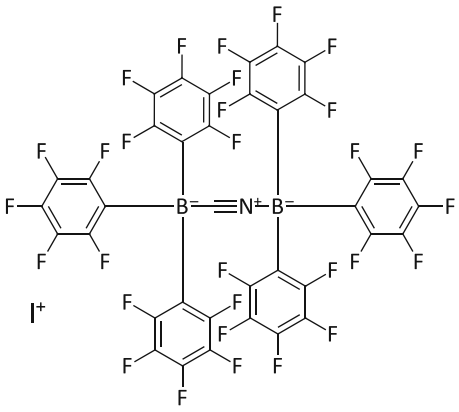

I-B4

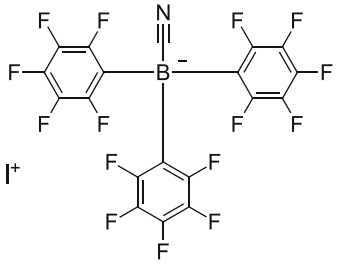

I-B5

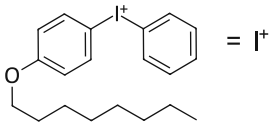

Considering onium salts in general, the cation is responsible for the photochemical properties such as absorption (Figure 65). Therefore, the difference between the selected compounds is rather small, due to high similarities of the iodonium cation. The compounds Com-I-Sb, I-NS, I-B1, I-B2, I-B3, I-B4 and I-B5 all contain the same alkoxylated cation and consequently show very similar absorption behavior, tailing out at around 350 nm. In addition, Com-I-B and Ref-I-Al consist of a very similar cation and therefore show related spectra. All samples show es expected for iodonium salts, an absorption maximum in the range of 250 nm. Com-I-Sb shows the lowest molar extinction coefficient (ε_{251} = 15100 L mol^{-1} cm^{-1}), while I-NS shows the highest one (ε_{250} = 20100 L mol^{-1} cm^{-1}).

3.3. Reactivity of Iodonium Borates

3.3.1. Formulations based on BADGE and ECC

For the upcoming reactivity studies, formulations based on epoxy-based monomers had to be prepared (Figure 80). This mixture's main component was either the aromatic bisphenol-A-diglycidylether (BADGE) or the cycloaliphatic 3,4-epoxycyclohexyl-methyl-3',4'-epoxycyclo-hexancarboxylat (ECC).

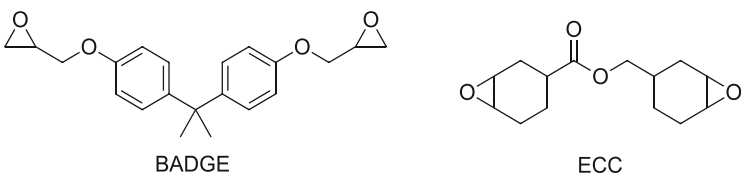

BADGE ECC

Figure 140: Monomers BADGE and ECC

The onium salts were used in 1.0 mol% based on epoxy groups referred to BADGE and ECC. Selected iodonium salts, originating from either synthesis or acquisition were used in the upcoming studies (Figure 81).

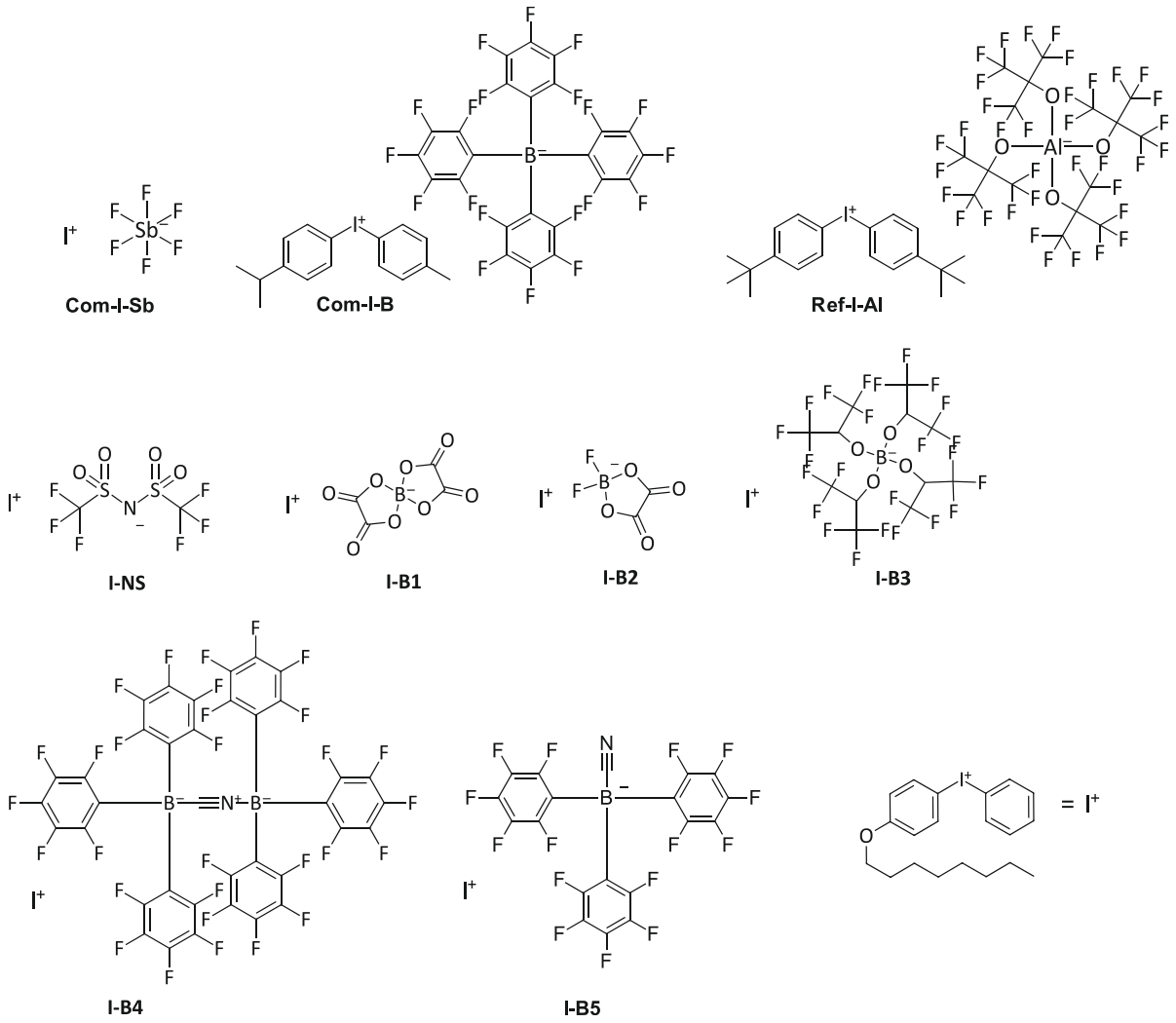

Figure 141: Selected iodonium salts for reactivity tests

Treatment in an ultrasonic bath, with the exception of I-B4 containing samples, at 40 °C of epoxy resin and iodonium initiator leads to completely homogeneous samples after 30 min.

3.3.2. Storage Stability Tests

The stability of a cationically curable formulation is of great importance. As soon as the initiator is mixed into the resin, there is a possibility of undesired side reactions and degradations happening. This circumstance usually leads to premature curing of the resin. Therefore, a storage stability study was carried out at a constant storage temperature of 50 °C for all iodonium salts under light protection. The formulations described in Chapter II, 3.3.1. contained either BADGE or ECC with 1.0 mol% iodonium salt and TPED based on epoxy groups. The focused-on metric of a formulation was the viscosity, which was measured with a rheometer. The viscosity was determined at a shear rate of 100 s^{-1} and the gap size between

stamp and plate was 48 µm. The lower the change in viscosity over time, the better is the storage stability of a formulation.

BADGE Formulations

The formulations containing various synthesized and acquired iodonium salts based on BADGE were tested first.

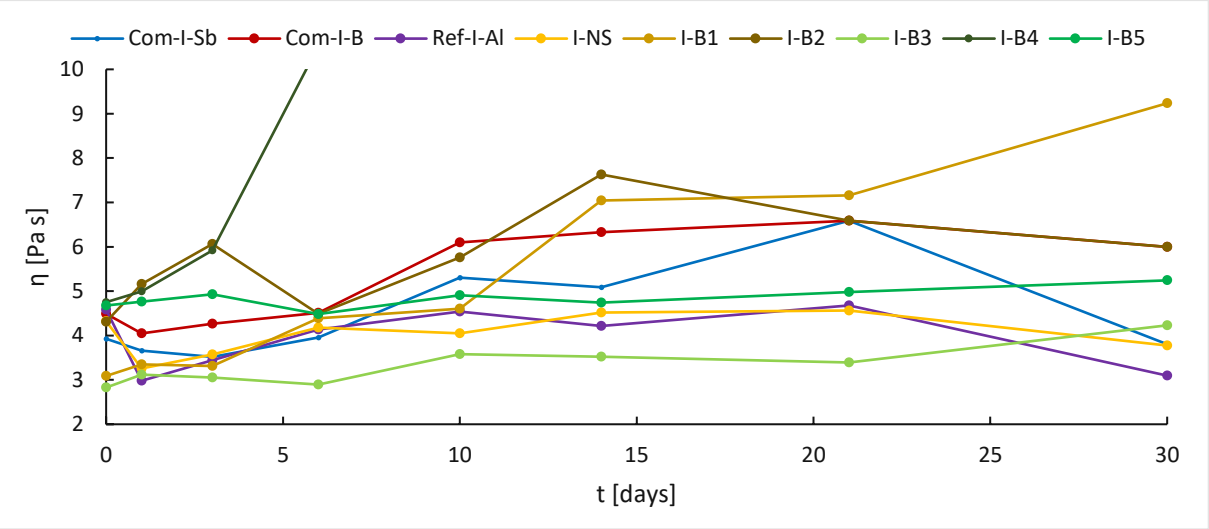

Figure 142: Time dependent viscosity of the BADGE-based formulations with 1.0 mol% iodonium salt at a storage temperature of 50 °C under light protection

The BADGE-based formulations show initial viscosities ranging from 2.8 up to 4.7 Pa s depending on the initiator (Figure 142). The highest increase in viscosity from 3.1 to 9.2 Pa s or 200% is measured with formulations containing I-B1 as initiator. Formulations containing the remaining boron-based initiators Com-I-B, I-B2, I-B3 and I-B5 show an increase of around 12% to 50% of the initial viscosity. The initiator Com-I-Sb shows an increase in viscosity by 68%. The best performing initiators in BADGE are Ref-I-Al and I-NS with around 2% to 6% increase after 21 days. None of the samples gelled over the course of the 30-day study with the exception of I-B4, which is only stable for around 3 days.

ECC Formulations

Second, the same selection of iodonium salts was subject to a storage stability study in the monomer system ECC.

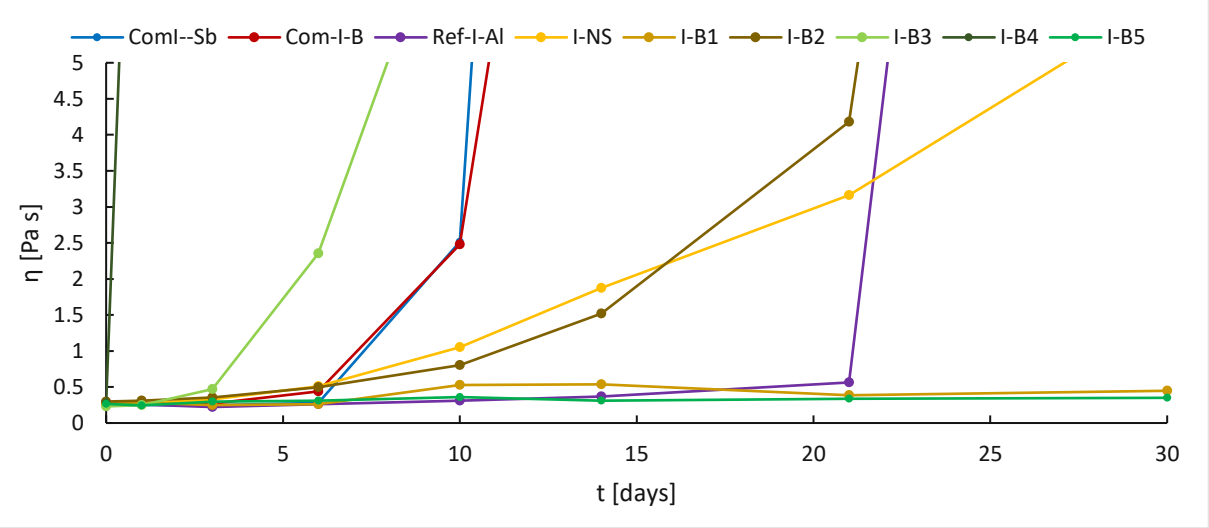

Figure 143: Time dependent viscosity of the ECC-based formulations with 1.0 mol% iodonium salt at a storage temperature of 50 °C under light protection

Initial viscosities are around 0.25 Pa s for all initiators mixed with the cycloaliphatic monomer ECC (Figure 143). In contrast to BADGE-based formulations, six out of the nine samples (I-B4, I-B3, Com-I-Sb, Com-I-B, I-B2 and Ref-I-Al) reach incredibly high viscosities over the course of the storage stability study with gel-like textures or completely solid samples on day 30. The sulfonimide I-NS remains the third still liquid sample at day 30 with a viscosity of 5.9 Pa s or an 22x increase compared to its initial viscosity. The best performing initiators are I-B5 with an increase of 32% followed by I-B1 with an 64% increase in viscosity. Surprisingly, I-B5 shows no signs of thermal decomposition at 50 °C over 30 days despite premature polymerization at the Photo-DSC at 90 °C within a few minutes.

3.3.3. Thermal Behavior of Iodonium Salts determined via DSC

3.3.3.1. Thermal-Induced Decomposition of Iodonium Salts

The thermal stability of every iodonium salts is limited, hence a decomposition process appears at a certain onset temperature. To gather information regarding temperature stability of the iodonium compounds, a DSC was performed from 25 °C up to 300 °C. Formulations based on BADGE and ECC containing 1 mol% iodonium salt prepared in chapter II, 3.3.1 were used.

BADGE Formulations

The first set of thermal stability measurements included selected iodonium salts in the monomer BADGE.

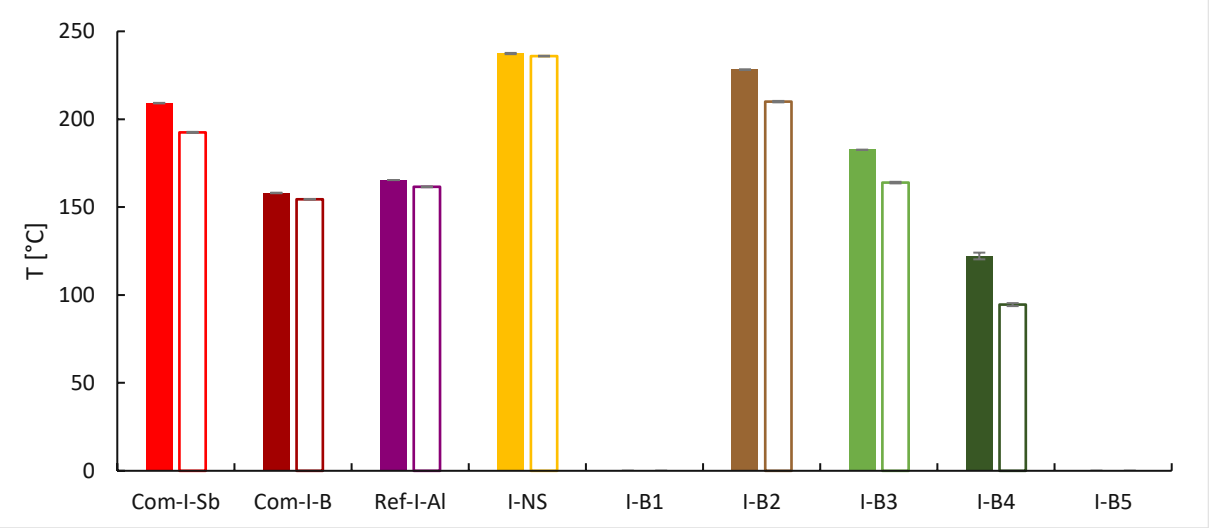

Figure 144: Temperature at the highest exothermicity (T_{max} - full) and polymerization onset temperature (T_{onset} - framed) in BADGE with the iodonium salts

Onset temperatures of the commercially available iodonium salts Com-I-Sb, Com-I-B and Ref-I-Al as well as those of the newly produced I-B3 are below 200 °C (Figure 144) except two I-NS and I-B2, which are above 200 °C. A similar trend can be observed for the temperatures at the highest exothermicity. The cyanide-bridged borane I-B4 shows the lowest temperatures measured in the experiment. The iodonium salts I-B1 and I-B5 are missing in the diagrams due to insufficient exothermicity.

ECC Formulations

The next study was based on the same selection of state-of-the-art and self-synthesized iodonium salts in ECC.

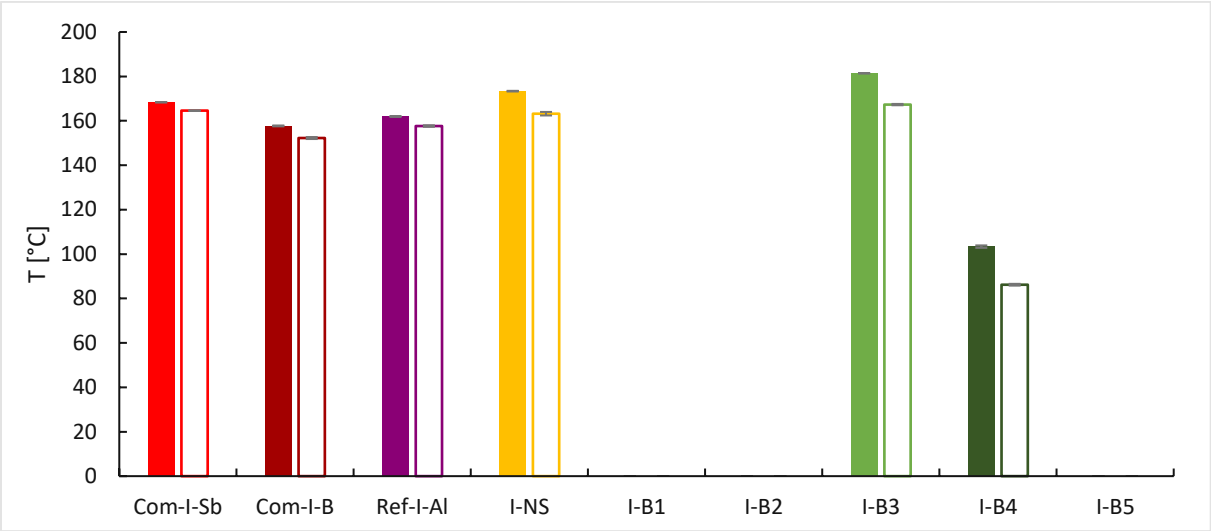

Figure 145: Temperature at the highest exothermicity (T_{max} - full) and polymerization onset temperature (T_{onset} - framed) in ECC with the iodonium salts

As expected, the start temperatures of the polymerization for all iodonium salts in ECC-based formulations are significantly lower compared to the BADGE-based samples (Figure 145). With the exception of I-B4, all iodonium salts are in the range of 170 °C – 180 °C, due to higher reactivity of the aliphatic monomer. The newly synthesized I-B4 shows by far the lowest starting temperature with 86 °C. The temperatures at the highest exothermicity show similar trends. The iodonium salts I-B1, I-B2 and I-B5 are missing in the diagrams due to insufficient exothermicity.

3.3.3.2. Thermal-Induced Radical Decomposition of Iodonium Salts

Besides purely thermal decomposition, onium compounds are known to decompose by thermally generated radicals from C-C labile compounds.[125] By exposure to a fixed temperature gradient, the thermal initiator TPED will start to decompose and forming the radicals. The thermal radicals are able to attack the acid generator, which is liberating the super acid, and finally initiate polymerization of the resin (Figure 85). This mechanism is exceptionally similar to the propagation step in RICFP and therefore necessary to investigate. Additionally, a fair comparison of polymerization parameters such as R_P and EGC can be stated since all onium salts can be cleaved at TPED's onset temperature.

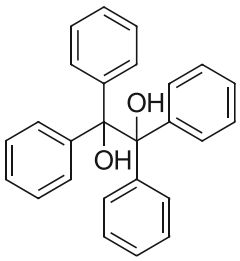

Figure 146: Thermal radical initiator TPED

This investigation was necessary to know exactly, above which onset temperature polymerization can occur in combination with TPED. The formulations preparation was described in chapter II, 3.3.1. All formulations contain 1.0 mol% onium salt in BADGE and ECC based on epoxy groups. Additionally, an equimolar amount of TPED was added compared to the onium salt. All DSC experiments with TPED as C-C labile compound were conducted from 25 °C to 300 °C.

BADGE Formulations

Thermal-induced radical decomposition of all iodonium salts together with TPED was investigated first in the monomer BADGE.

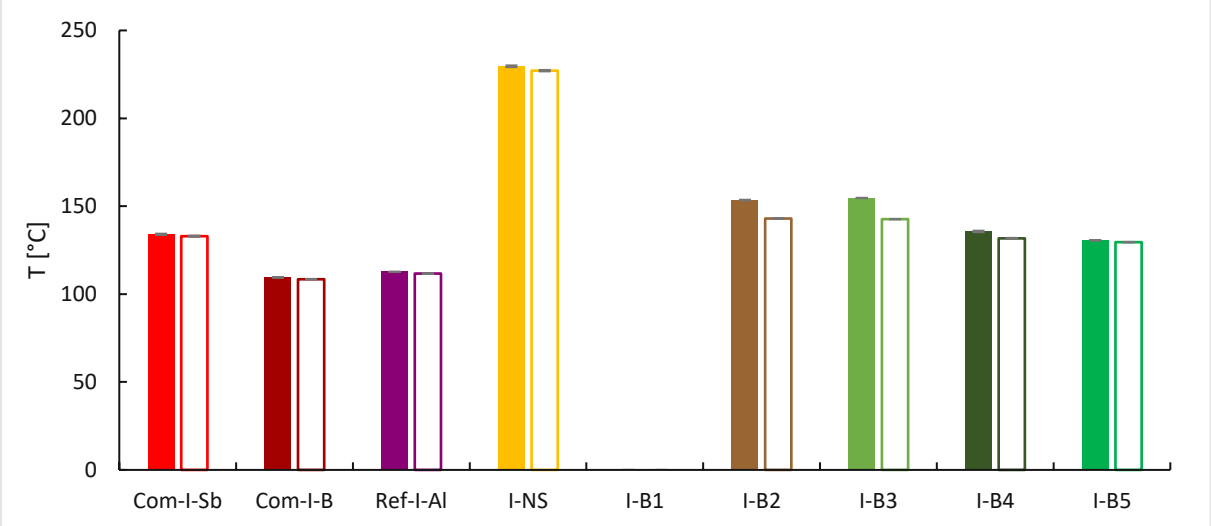

Figure 147: Temperature at the highest exothermicity (T_{max} - full) and polymerization onset temperature (T_{onset} - framed) in BADGE with the iodonium salts and TPED

As expected, the onset temperatures of the polymerization are decreased significantly as a result of TPED addition (Figure 147). The commercially available and five of the newly synthesized iodonium salts have starting temperatures below 144 °C. I-NS has by far the highest starting temperature at 227 °C and is different from the other iodonium salts. This exception is a result of the non-functioning redox couple I-NS and TPED. Therefore, no decomposition of the iodonium salt is achieved at TPED's decomposition temperature. The

temperatures at the maximum exothermicity show the same trend. The iodonium salt I-B1 is missing in the following diagrams due to insufficient exothermicity.

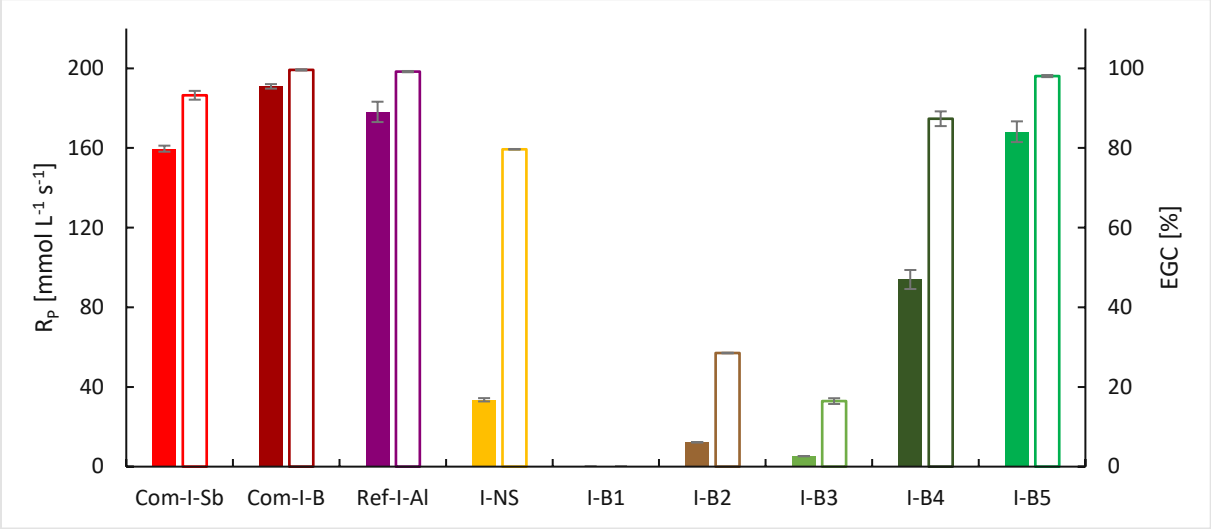

Figure 148: Rate of polymerization (R_P - full) and epoxy group conversion (EGC – framed) in BADGE with the iodonium salts and TPED

The commercial iodonium salts show the highest polymerization rates (Figure 148). The iodonium borates I-B5 and I-B4 clearly stand out from the remaining newly synthesized iodonium salts. The iodonium salts Com-I-B and Ref-I-Al show conversions of around 99% in BADGE with TPED. The newly synthesized iodonium salt I-B5 achieves an EGC of 98%. I-NS and I-B4 show a conversion of above 79%, but I-B2 and I-B3 only achieve below 30% EGC.

ECC Formulations

Secondly, the thermal stability of the iodonium salts in presence of the radical thermal initiator TPED was measured in ECC.

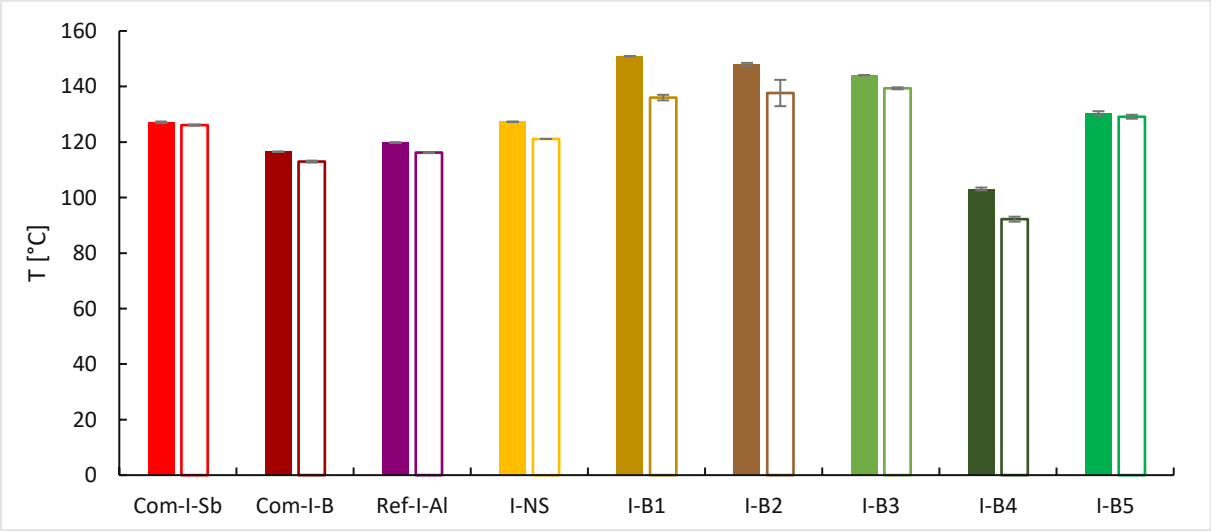

Figure 149: Temperature at the highest exothermicity (T_{max} - full) and polymerization onset temperature (T_{onset} - framed) in ECC with the iodonium salts and TPED

The starting temperatures of the commercially available salts and the synthesized I-NS have values are below 130 °C (Figure 149). The starting temperatures of the remaining synthesized iodonium salts are all in the range of 136 °C to 143 °C. As expected, the onset temperatures are significantly lower than for the formulations without the radical thermal initiator TPED. The temperatures at the maximum exothermicity show the same trend.

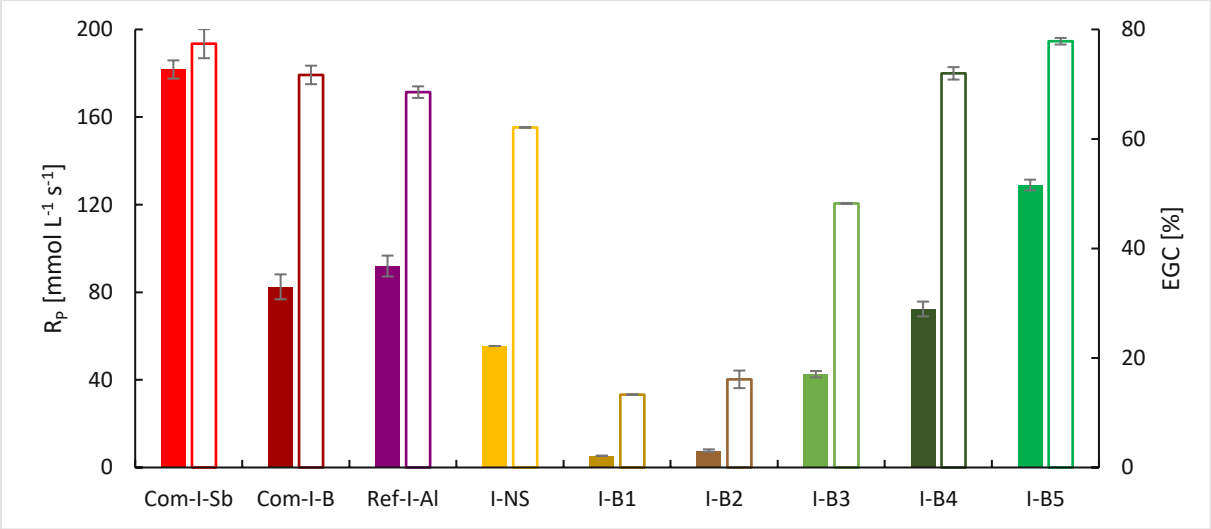

Figure 150: Rate of polymerization (R_P - full) and epoxy group conversion (EGC – framed) in ECC with the iodonium salts and TPED

In particular, the commercial iodonium salt Com-I-Sb stands out from all other PAGs with a high polymerization rate (Figure 150). But I-B5 also clearly stands out from the synthesized iodonium salts and outperforms the other two commercial products Com-I-B and Ref-I-Al. The commercial iodonium salts in ECC with TPED show conversions between 69% and 78%. The newly synthesized iodonium salts I-B5 and I-B4 also have high EGC values of 78% to 72%. The small initiators I-B1 and I-B2 only achieve conversions below 20%.

In the series using BADGE as monomer together with TPED, the cyanide-ligated borane I-B5 shows great reactivity data, reaching similar R_P values as Com-I-B, Com-I-Sb and Ref-I-Al. Additionally, I-B4 shows high reactivity with TPED as thermal radical initiator. Switching the monomer to the cycloaliphatic ECC, I-B5 comes in second right after the commercial Com-I-Sb in terms of reactivity together with high epoxy group conversions. I-B4 shows high EGC and reactivity as well.

3.3.4. Photoreactivity determined via Photo-DSC

3.3.4.1. Photo-Induced Radical Decomposition of Onium Salts

To investigate the efficiency of the radical starters, a Photo-DSC study was performed with the iodonium salts and a radical photoinitiator to decompose the onium compound by the formed radicals. The formulations described in the previous chapter II, 3.3.1. were modified with an equimolar amount of the germanium-based photoinitiator Ivocerin (Figure 96). To result in 1.0 mol% Ivocerin in BADGE and ECC based on epoxy groups.

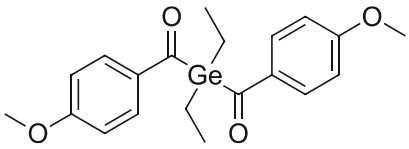

Figure 151: Ivocerin® structure

This series of measurements should provide information about the reactivity of the system if the onium salts are decomposed by photochemically generated radicals. The more reactive an initiator-radical generator system behaves, the better for the overall initiation efficiency and curing of the material. Ivocerin® shows its absorption maxima from 390 to 445 nm. Therefore, an UV-source with a 400-500 nm filter was used in this series of experiments.

BADGE Formulations

At first, all iodonium salts were tested together with the photo radical initiator Ivocerin in BADGE.

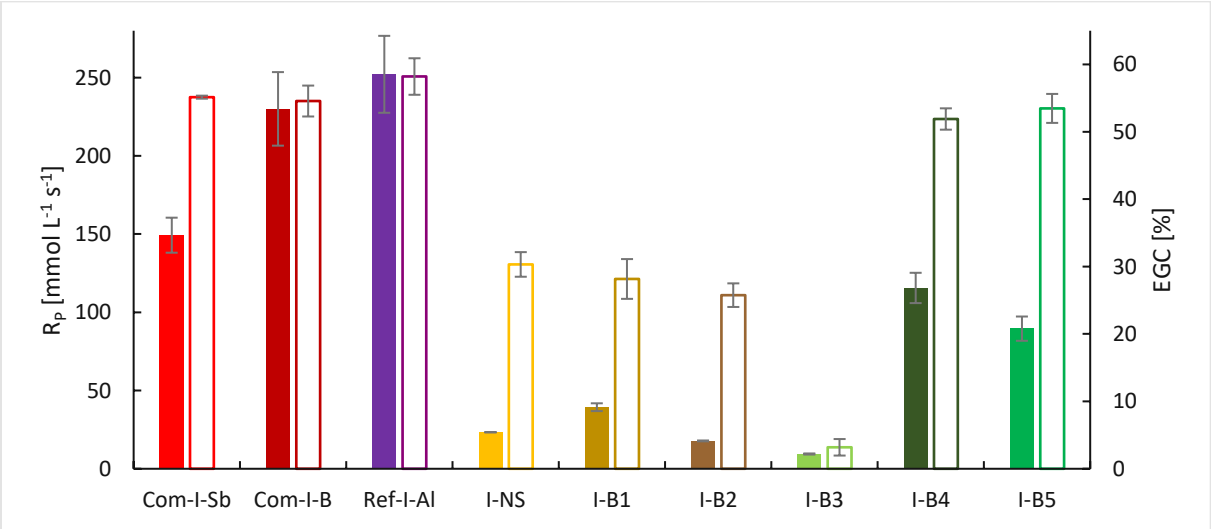

Figure 152: Rate of polymerization (R_P - full) and epoxy group conversion (EGC – framed) in BADGE with the iodonium salts (photo-induced decomposition by Ivocerin); The time-based parameters t_{max} and $t_{95\%}$ are located in the attachment (Figure 261)

The commercial iodonium salts achieve high rates of polymerization followed by the newly synthesized iodonium salts with the best performance delivered by I-B5 (Figure 152).

Interestingly I-B5 and I-B4 achieve similarly high conversions compared to the commercial products.

ECC Formulations

Next up, the same selection of iodonium salts together with Ivocerin was subject to investigation in the cycloaliphatic monomer ECC.

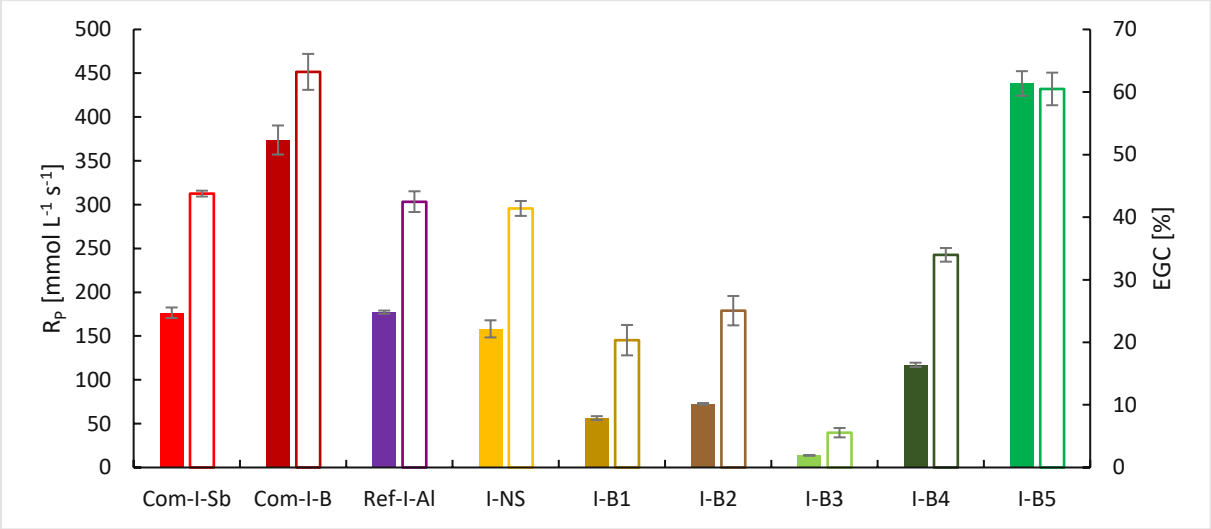

Figure 153: Rate of polymerization (R_P - full) and epoxy group conversion (EGC – framed) in ECC with the iodonium salts (photo-induced decomposition by Ivocerin); The time-based parameters t_{max} and $t_{95\%}$ are located in the attachment (Figure 262)

As expected, both radical induced cationic polymerization studies with TPED and Ivocerin share similarities within the results. However, Ivocerin as radical photoinitiator in combination with the well performing iodonium salts achieves higher absolute polymerization rates. What is striking when looking at polymerization rates is the high value of the newly synthesized I-B5. (Figure 153) which clearly stands out from all the iodonium salts investigated. The only comparably high value is provided by the commercial iodonium salt Com-I-B with 85% of the reactivity. Both the commercial Com-I-B and the newly synthesized I-B4 show EGC of above 60%. The conversions of the remaining iodonium salts are all below 45%.

As expected, both radical induced cationic polymerization studies with TPED and Ivocerin share similarities within the results. However, Ivocerin as radical photoinitiator in combination with the well performing iodonium salts achieves higher absolute polymerization rates. In terms of reactivity, the cyanide-ligated and -bridged borane I-B5 as well as I-B4 show good reactivity and even better EGC in BADGE together with Ivocerin. In the cycloaliphatic monomer ECC, I-B5 even outperforms all tested initiators by a significant margin for the EGC and rate of polymerization, marking it as a very efficient cationic initiator.

3.3.4.2. Photoinitiation Study

In addition to the sensitization and photo-induced radical cationic polymerization experiments, a photoinitiation study was carried out. The main objective was to investigate the potentials of all iodonium salts as photoacid generators since this measurement series resembles conditions at the initiation step of RICFP. UV-VIS experiments indicated very similar absorption spectra across the tested iodonium compounds, an irradiation source equipped with a 320-500 nm filter was used. The formulations based on 1.0 mol% iodonium salt in BADGE and ECC described in the previous chapter II, 3.3.1. were used for this study without any additives.

BADGE Formulations

Firstly, the selection of iodonium salts in absence of any additives was measured in the epoxy monomer BADGE.

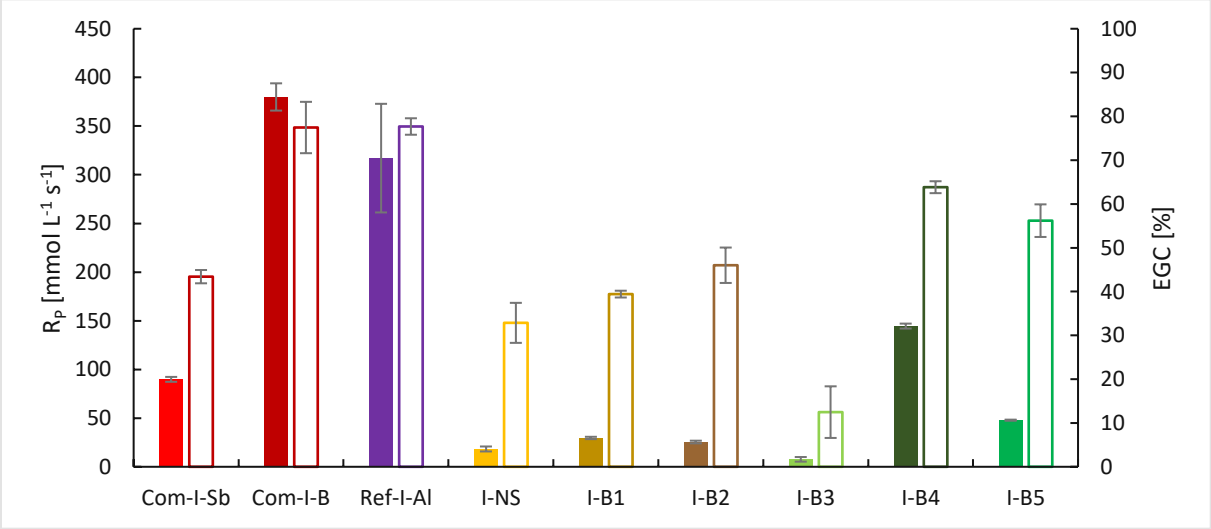

Figure 154: Rate of polymerization (R_P - full) and epoxy group conversion (EGC – framed) in BADGE with the iodonium salts (Photoinitiation); The time-based parameters t_{max} and $t_{95\%}$ are located in the attachment (Figure 263)

The commercial iodonium salts show high polymerization rates with Com-I-B delivering the best results in terms of reactivity (Figure 154). EGC for the commercial salts are in the range of 43% to 78%. The synthesized iodonium salts show comparatively low reactivity except I-B4 and I-B5 reaching up to 6% EGC and medium R_P.

ECC Formulations

Secondly, all iodonium salts were measured in the cycloaliphatic epoxy monomer ECC with no additives in the formulation.

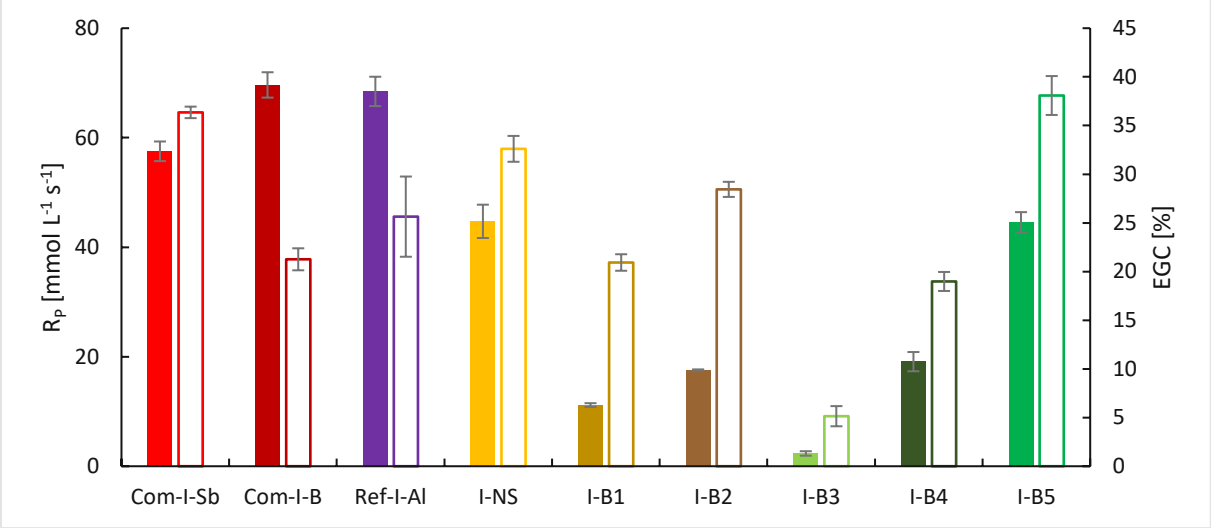

Figure 155: Rate of polymerization (R_P - full) and epoxy group conversion (EGC – framed) in ECC with the iodonium salts (Photoinitiation); The time-based parameters t_{max} and $t_{95\%}$ are located in the attachment (Figure 264)

The commercial iodonium compounds show high polymerization rates with Com-I-B at the top (Figure 155). However, I-NS and I-B5 achieve the highest polymerization rate of all newly synthesized compounds. I-B5 shows the highest EGC amongst all iodonium salts in ECC with 38%.

For the formulations based on BADGE, I-B4 represents the best self-synthesized initiator reaching higher reactivity compared to the industry used Com-I-Sb. However, Com-I-B and Ref-I-Al show even more reactivity. Switching the monomer to ECC, the sulfonimide I-NS together with I-B5 show very promising results similar to the commercial and reference initiators.

3.3.4.3. Temperature-dependent Photoreactivity with 1 wt% Iodonium Salt

To better compared the much less expensive to produce and small molecular weight initiators, especially I-B1 and I-B2, a study referred to initiator weight was carried out. Previous Photo-DSC experiments were utilizing formulations with 1 mol% (chapter II, 3.3.1.) of iodonium salt based on epoxy groups. Most industrial applications, use for sake of simplicity and more straight forward comparability regarding price, formulations containing a set percentage of initiating species referred to weight. For the whole study, an irradiation source equipped with a 320-500 nm filter was used. The formulations consist out of 1 wt% of iodonium-based photoacid generator combined with the monomers BADGE and ECC. Additionally, the

temperature dependence was investigated to draw a comparison between each of the initiators at RT, 50 °C, 70 °C and 90 °C. A study at different temperatures is especially insightful due to a sharp drop in viscosity at increased temperatures of highly viscous resins like BADGE. Therefore, formulations based on BADGE were tested first.

BADGE Formulations

At first, the iodonium salts were irradiated without any additives in formulations based on BADGE.

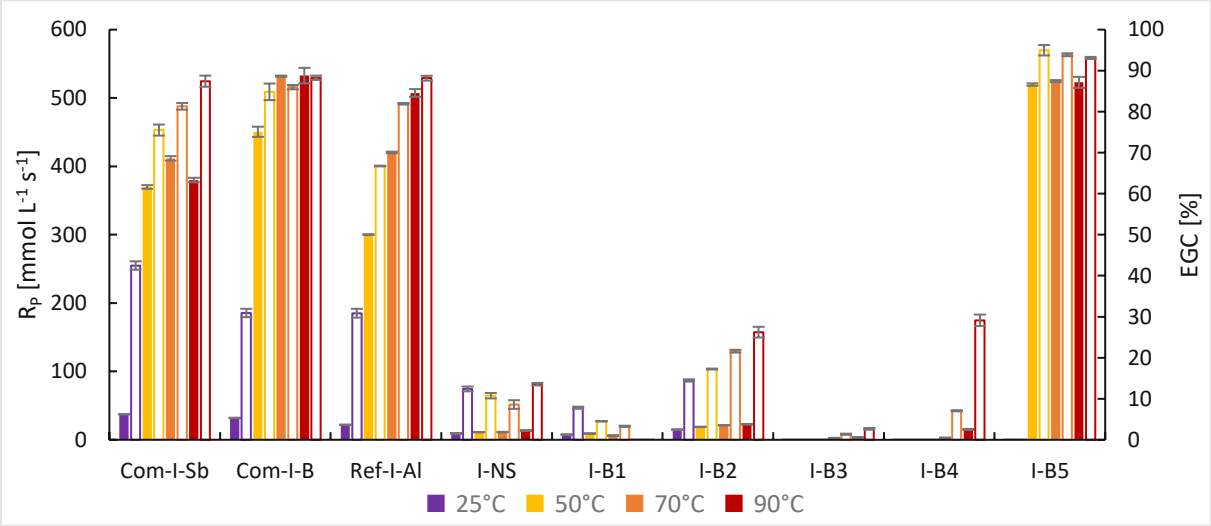

Figure 156: Rate of polymerization (R_P - full) and epoxy group conversion (EGC – framed) in BADGE with 1 wt% of iodonium salt at 25 °C, 50 °C, 70 °C and 90 °C (Photoinitiation); The time-based parameters t_{max} and $t_{95\%}$ are located in the attachment (Figure 265)

As expected, a clear trend towards increased rates of polymerization and EGC as temperature rises is present across all initiator systems (Figure 156). A good example is presented by the commercial systems like the borate Com-I-B, which increases its R_P from 32 mmol L^{-1} s^{-1} at 25 °C up to 533 mmol L^{-1} s^{-1} at 90 °C. Most of the self-synthesized iodonium salts, do not show great reactivity across any temperature investigated in the study. If comparing the performance of the cyanide-bridged borane I-B4 to the study with 1 mol% in BADGE (Figure 154), the clear disadvantage of such high-molecular weight initiators in this 1 wt% study can be seen compared to iodonium salts with lower weight counter ions. However, the exception is represented by the cyanide-ligated I-B5 which provides significant reactivity, even outperforming all commercial systems at 50 °C with a R_P of 520 mmol L^{-1} s^{-1}. This polymerization rate is 41%, 15%, and an astonishing 470% higher compared to Com-I-Sb, Com-I-B and Ref-I-Al respectively. The I-B5 system starts to stagnate and even decrease slightly in reactivity at 70 °C and 90 °C. Its striking, that I-B5 as an initiator system reaches increased EGC

compared to the commercial systems at 86% up to 97%. Interestingly, I-B5 samples at 25 °C turn out to be solid after the irradiation procedure. However, no rate of polymerization can be calculated due to no exothermic behavior during the DSC experiments. This odd behavior can be explained by the reliable crystallization of BADGE at room temperature if mixed with I-B5. Therefore, the melting of the monomer causes significant endothermicity.

ECC Formulations

Nest, the same selection of iodonium compounds was investigated in terms of reactivity in the monomer ECC.

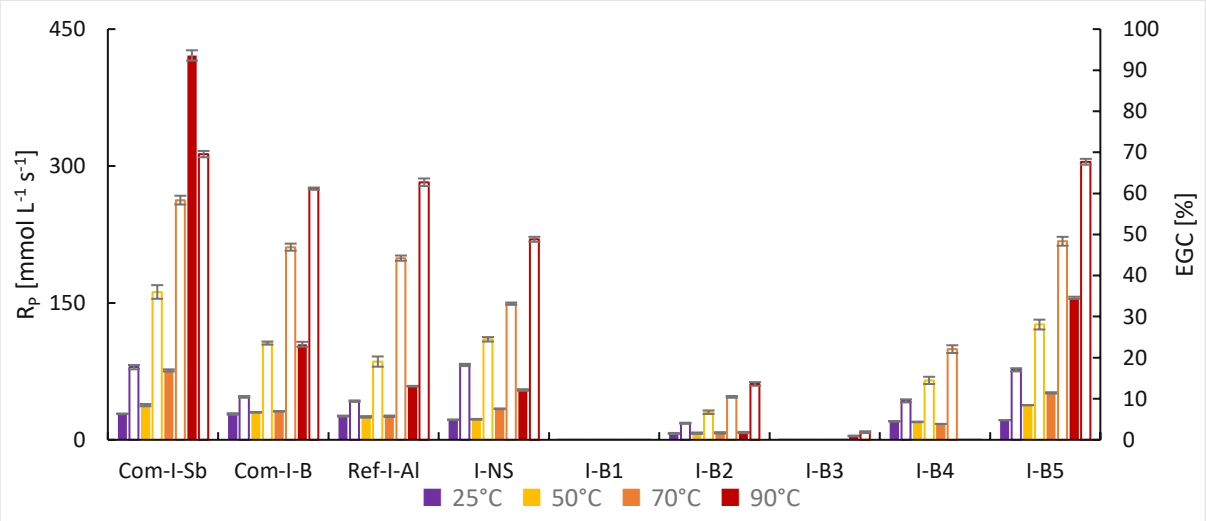

Figure 157: Rate of polymerization (R_P - full) and epoxy group conversion (EGC – framed) in ECC with 1 wt% of iodonium salt at 25 °C, 50 °C, 70 °C and 90 °C (Photoinitiation); The time-based parameters t_{max} and $t_{95\%}$ are located in the attachment (Figure 266)

Switching the monomer from BADGE to ECC, a different behavior of the initiators is observed (Figure 157). The by far best results are seen in formulations containing the commercial antimony-based Com-I-Sb across all temperatures, especially at 90 °C with a R_P of 421 mmol L^{-1} s^{-1}. However, the second-best performer across the measured temperatures is I-B5 with its peak reactivity at 90 °C achieving 156 mmol L^{-1} s^{-1} with great EGC. Therefore, the new I-B5 outperforms the commercial Com-I-B and Ref-I-Al systems in all metrics. Unfortunately, I-B5 cannot unfold its full potential at 90 °C in the cycloaliphatic monomer ECC, since a non-negligible amount of the polymerization takes place as soon as the sample is inserted into to measurement chamber at 90 °C. Therefore, the stability of formulations containing I-B5 in ECC is not sufficient at this high temperature.

3.3.4.4. Temperature-dependent Photoreactivity with 1 mol% Iodonium Salt

The main objective of this photoinitiation study was to investigate the difference in reactivity if exact molar amounts or percent by weight are used. With the focus of the work shifting towards RICFP, the epoxy monomer ECC was no longer been used. The formulations consist out of 1 mol% of iodonium-based PAG combined with the monomer BADGE according to chapter II, 3.3.1. A comparison between each of the initiators at 25 °C, 50 °C, 70 °C and 90 °C was aimed for. Since I-NS, I-B2, I-B3 and I-B4 at 1 wt% did not show significant reactivity in BADGE, they were not included in this study.

BADGE Formulations

The first set of tests was conducted with the iodonium salts only. As a monomer, the aromatic epoxy-based BADGE was used.

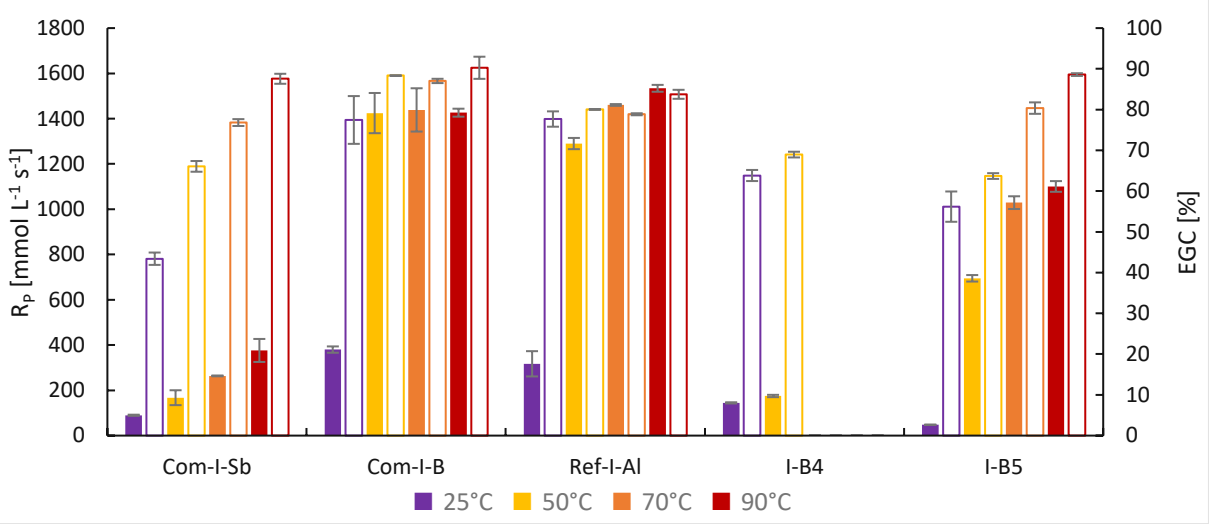

Figure 158: Rate of polymerization (R_P - full) and epoxy group conversion (EGC – framed) in BADGE with 1 mol% of iodonium salt at 25 °C, 50 °C, 70 °C and 90 °C (Photoinitiation); The time-based parameters t_{max} and $t_{95\%}$ are located in the attachment (Figure 267)

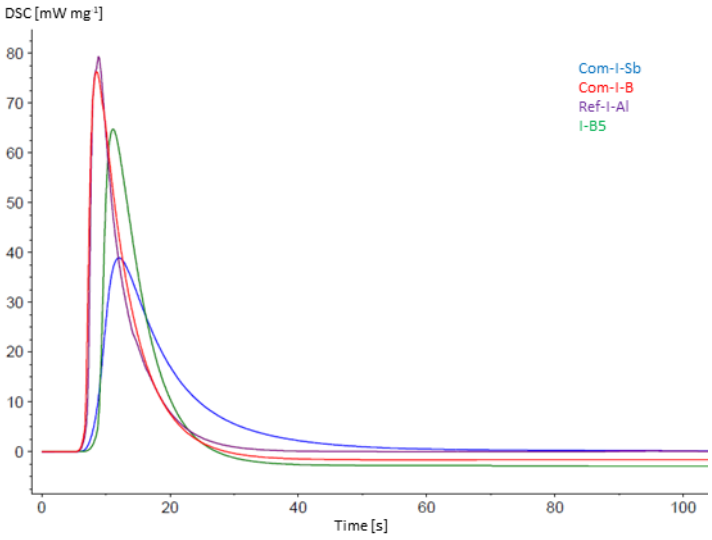

Figure 159: First 100 s of Photo-DSC data in BADGE with 1 mol% of iodonium salt at 90 °C (Photoinitiation)

By comparing the data obtained by the photo-DSC measurements at four different temperatures, clear trends in reactivity can be seen (Figure 158). Generally, the higher the temperature the more reactive an initiator system behaves. Com-I-B and Ref-I-Al together with the new cyanide-ligated borane I-B5 demonstrate high reactivity across a broad range of temperatures. I-B5 reaches 71% of the reactivity of the best performing reference Ref-I-Al. The reactive nature of I-B5 can be seen well by both the peak height as well as its narrow width (Figure 159). Interestingly, the cyanide-bridged borane I-B4 shows a rapid drop in reactivity starting at 70 °C due to thermolability. Polymerization of I-B4 samples takes place as soon as the sample is inserted into the preheated DSC chamber, therefore no more significant exothermicity can be recorded during the irradiation period. Comparing the EGC of all initiator systems, a clear trend can be obtained of most samples. With the exception of I-B4, the EGC at 90 °C is between 90% and 84% across all systems with the best performance demonstrated by the commercial Com-I-B and I-B5.

3.4. Radical Induced Cationic Frontal Polymerization

3.4.1. Selection of the Compounds and Formulations for RICFP

The application of all iodonium borate initiators in frontal polymerization was investigated next. The choice of iodonium salts for the radical induced cationic frontal polymerization experiments was decided by one main factor. Reactivity of the photoacid generators in cationically polymerizabl resins in combination with the thermal radical generator TPED. All commercial products Com-I-Sb, Com-I-B and Ref-I-Al as well as the self-synthesized iodonium

salts show low to very high reactivity during the previous thermal DSC study in monomers BADGE and ECC (Figure 160).

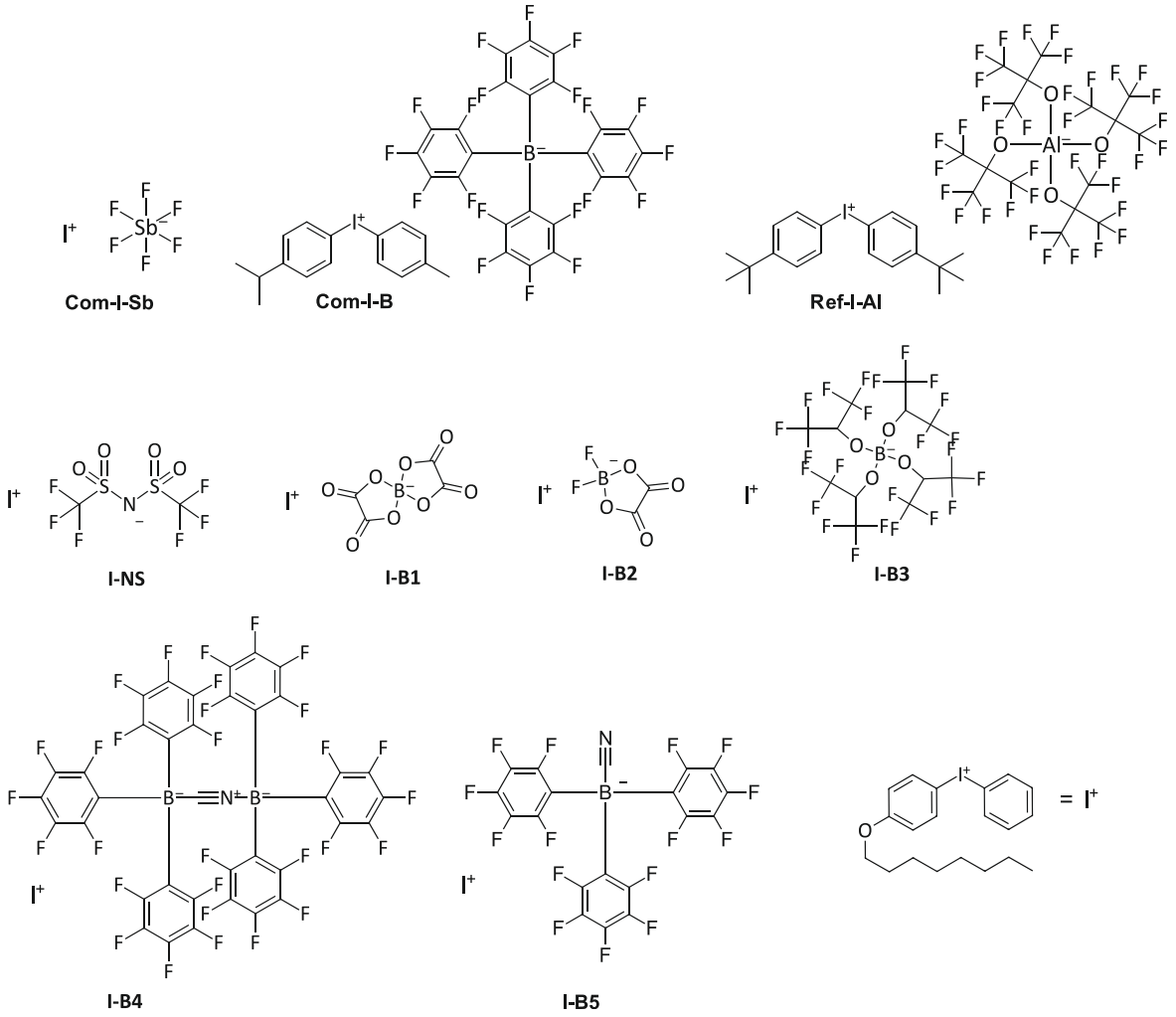

Figure 160: Selection of iodonium salts for RICFP

Therefore, all iodonium compounds were tested for frontal polymerization capabilities. Previously, the iodonium salts were tested in BADGE and ECC environments. However, for the RICFP experiments, pure BADGE resins usually need highly reactive initiator systems, whereas ECC is often too reactive and can lead to undesired bubble formation. Therefore, all iodonium salts were homogeneously dissolved in a mixture of 80 mol% BADGE and 20 mol% HDDGE (1,6-hexanediol diglycidylether) (Figure 161).

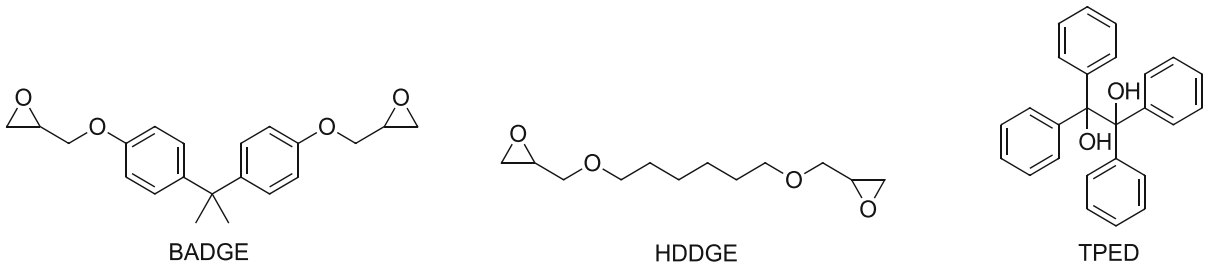

Figure 161: Monomers BADGE, HDDGE and the thermal radical initiator TPED

Previous research suggests BADGE/HDDGE mixtures as well suitable epoxy resin for RICFP.[200] The role of HDDGE in the formulations is mainly an increase in reactivity. In addition, the viscosity of the formulations is decreased, as well as the solubility for the iodonium salts enhanced compared to pure BADGE. All iodonium salts (Figure 160) were used in 0.1, 0.25, 0.5 and 2.0 mol% based on epoxy groups and an equimolar amount of TPED was added.

3.4.2. Storage Stability Tests

One major advantage of the radical induced cationic frontal polymerization compared to other epoxy-curing techniques is the enhanced pot life of the formulations. There is no need for a two component system, since all the necessary compounds for RICFP are mixed in advance and can usually be stored over several days without decreasing the performance significantly.[125] Therefore, a storage stability study was carried out at a constant storage temperature of 50 °C for all iodonium salts under light protection.

The formulations described in Chapter II, 4.3.1. contained 80 mol% BADGE and 20 mol% HDDGE with 0.5 mol% iodonium salt and TPED based on epoxy groups. The focused-on metric in terms of stability of a formulation was the viscosity, which was measured with a rheometer. The viscosity was determined at a shear rate of 100 s^{-1} and the gap size between stamp and plate was 48 µm. The lower the change in viscosity over time, the better is the storage stability of a formulation.

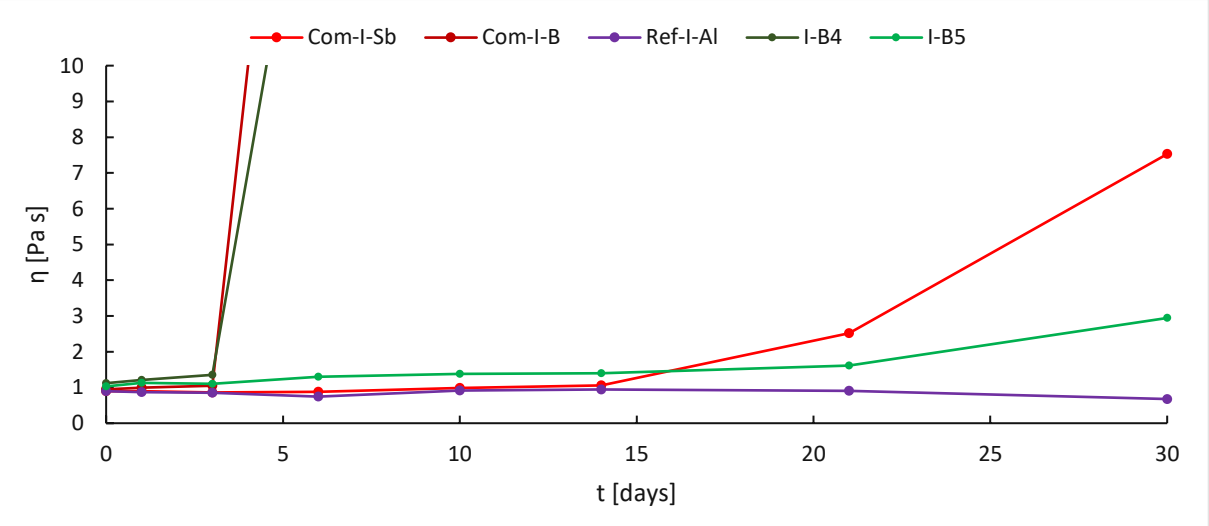

Figure 162: Time dependent viscosity of the BADGE/HDDGE-based formulations with 0.5 mol% iodonium salt and TPED at a storage temperature of 50 °C under light protection

Storage stability results in BADGE/HDDGE containing the thermal radical initiator TPED show as expected higher viscosity increases over time compared to the pure BADGE-based samples

tested in advance (Figure 162). Initial viscosity for all formulations is around 1 Pa s. Outstanding is the poor shelf life of the boron-based Com-I-B and I-B4 at 50 °C. After 3 days, the viscosity starts to increase rapidly to finally result in a gel-like state on day 6. The remaining samples based on Com-I-Sb, Ref-I-Al and I-B4 show much better stability. The best performing salt is the aluminate Ref-I-Al with a peak-increase of only 6% at day 10, before the viscosity is slightly decreasing until day 30. The commercial Com-I-Sb shows a significant increase starting after 2 weeks and reaching 7.5 Pa s after one month. Interestingly the bridged borane I-B5 shows much better performance compared to the commercial boron-based salts Com-I-B or the structurally very similar I-B4 with 2.9 Pa s after 30 days.

3.4.3. RICFP

3.4.3.1. Frontal Polymerization Experiments

With a frontal polymerization test setup, the capabilities of the iodonium initiators could be determined. Formulations based on iodonium salt and TPED in 80 mol% BADGE and 20 mol% HDDGE described in Chapter II, 4.3.1. were used. The formulations were then poured into a Teflon mold (Figure 163).

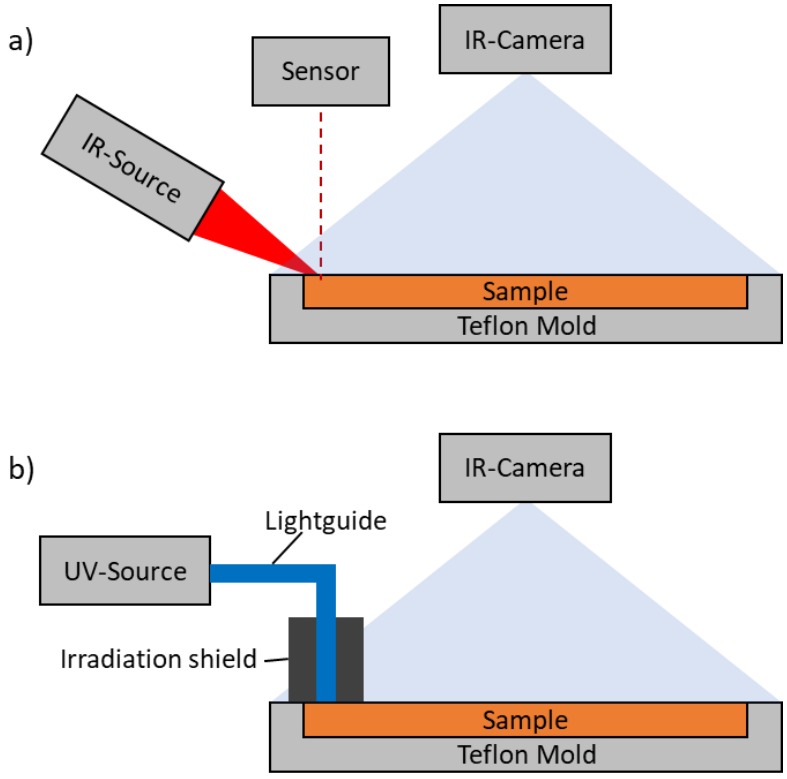

Figure 163: Schematic illustration of the a) thermally-initiated RICFP setup; b) photochemically-initiated RICFP setup

An IR-source heated the formulation at the edge of the mold and a temperature sensor switched off the IR source automatically as soon as 190 °C were reached. The frontal

polymerization reaction was then observed using a thermal imaging camera (Figure 163a). In a second series of experiments, the formulations in the Teflon molds were initiated via UV-light (Figure 163b).

With the thermal imaging camera information obtained, front speed, maximum front temperature and front starting time could be calculated. Three measurements were carried out for each formulation.

No potential for frontal polymerization at 2 mol% iodonium salt and TPED was noticed with formulations containing the salts I-NS, I-B1 and I-B3. Therefore, they are missing in the following diagrams. The self-synthesized I-B2 is also partially polymerized at a concentration of 2 mol%, however a stable front did not develop. The iodonium salts I-B5 and I-B4 turn out to be the only self-synthesized iodonium salt which showed sufficient reactivity to form a stable front. However, I-B5 and I-B4 in combination with the 3 commercial salts Com-I-Sb, Com-I-B and Ref-I-Al were measured in concentrations starting from 0.1 mol% up to 0.5 mol%. As expected, 1 mol% and above lead to bubble formation due to excessive reactivity and was not considered an appropriate concentration for the more reactive iodonium salts.

Important parameters of frontal polymerization are the frontal velocity v_F, correlating with the speed with which the local reactive zone spreads, and the maximum front temperature T_F. For the UV-initiated RICFP, the front starting time $t_{F,s}$ was calculated to evaluate the plainness of the formulations to start a frontal polymerization.

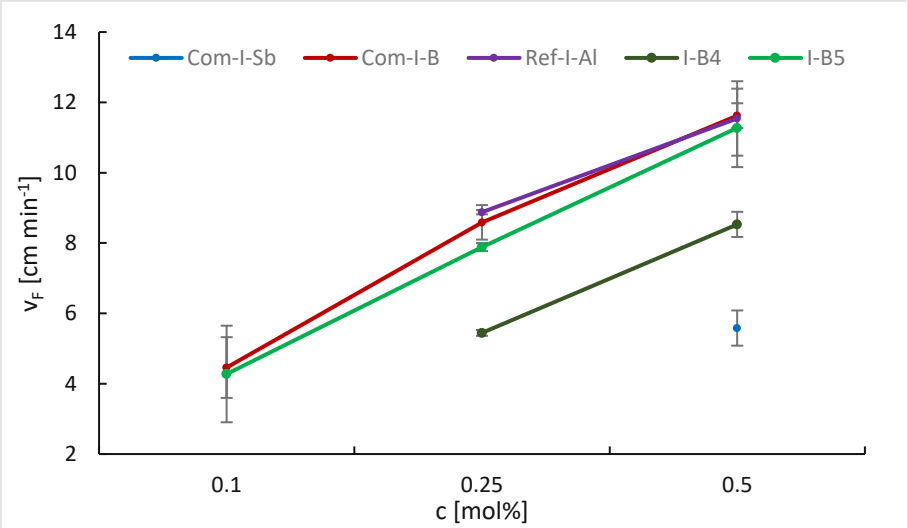

Figure 164: Frontal velocity v_F versus the concentration of the iodonium salts and TPED in BADGE/HDDGE

The cyanide-ligated borane I-B5 performs all at the same level compared to the commercial iodonium salts Com-I-Sb, Com-I-B and Ref-I-Al with a maximum velocity of around 11.5 cm min^{-1} at a concentration of 0.5 mol% (Figure 164). The next best compound is the

cyanide-bridged borate I-B4, reaching frontal velocities of 8.5 cm min^{-1}. Even at the lower concentration of 0.1 and 0.25 mol%, the frontal polymerization obtained by I-B5 reaches similar velocities compared to the state-of-the-art borate Com-I-B.

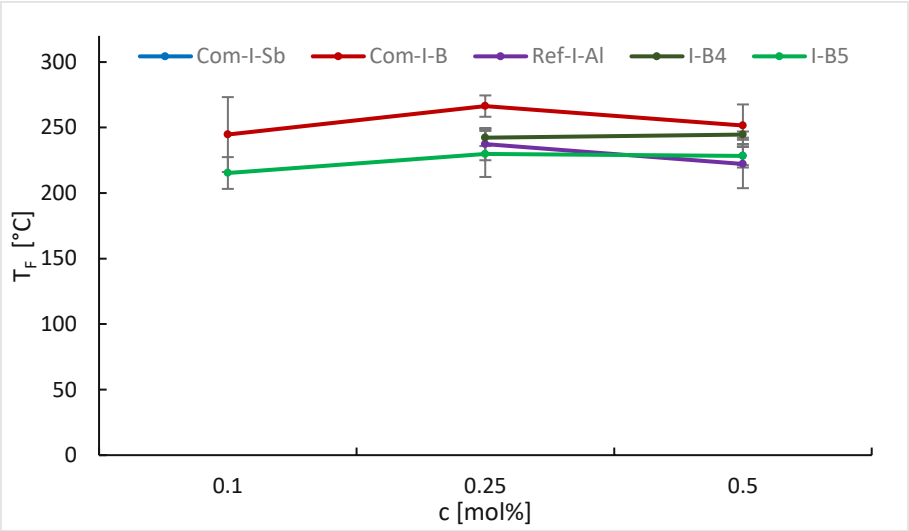

Figure 165: Frontal temperature v_F versus the concentration of the iodonium salts and TPED in BADGE/HDDGE

Considering the maximum front temperature T_F of all tested iodonium salts, a range can be obtained starting from 215 °C to 266 °C regardless of concentration (Figure 165). However, I-B5 samples shows slightly lower values compared to commercial products of 215 °C at 0.1 mol% and 230 °C at 0.25 and 0.5 mol%. The highest temperatures are measured within the Com-I-B samples at a maximum of 266 °C at 0.25 mol% initiator.

A visual inspection of the specimens after frontal polymerization revealed some bubble formation of the samples with 0.5 mol% Com-I-B, Ref-I-Al and I-B5 (Figure 166). Therefore, those initiator loadings are too high to form dense, bubble-free specimens. Samples with a concentration of 0.25 mol% show no visible bubbles to the naked eye. At a concentration of 0.1 mol% I-B5, a bubble-free, clear specimen can be obtained. However, the specimen shows slight stickiness at its surface, while Com-I-B and Ref-I-Al samples show slightly better curing behavior at such low loadings at the surface. Missing sample specimens like the Com-I-Sb at 0.1 mol% indicate a non-successful frontal polymerization at that concentration. If the RICFP was successfully initiated, however stops due to insufficient reactivity, the short specimens are represented. Examples for such a prematurely interrupted frontal polymerization are Com-I-Sb at 0.25 mol% and Ref-I-Al at 0.1 mol% loading. In addition, due to lower frontal temperatures the I-B5-based formulations produce yellowish samples, in contrast to the other commercial compounds. I-B4 specimens, despite being structural very similar to I-B5 on a

molecular level, show a completely different coloring. The cyanide-bridged borane I-B4 produces brown to black specimens, which are lighter in color at the IR-lasers irradiation spot.

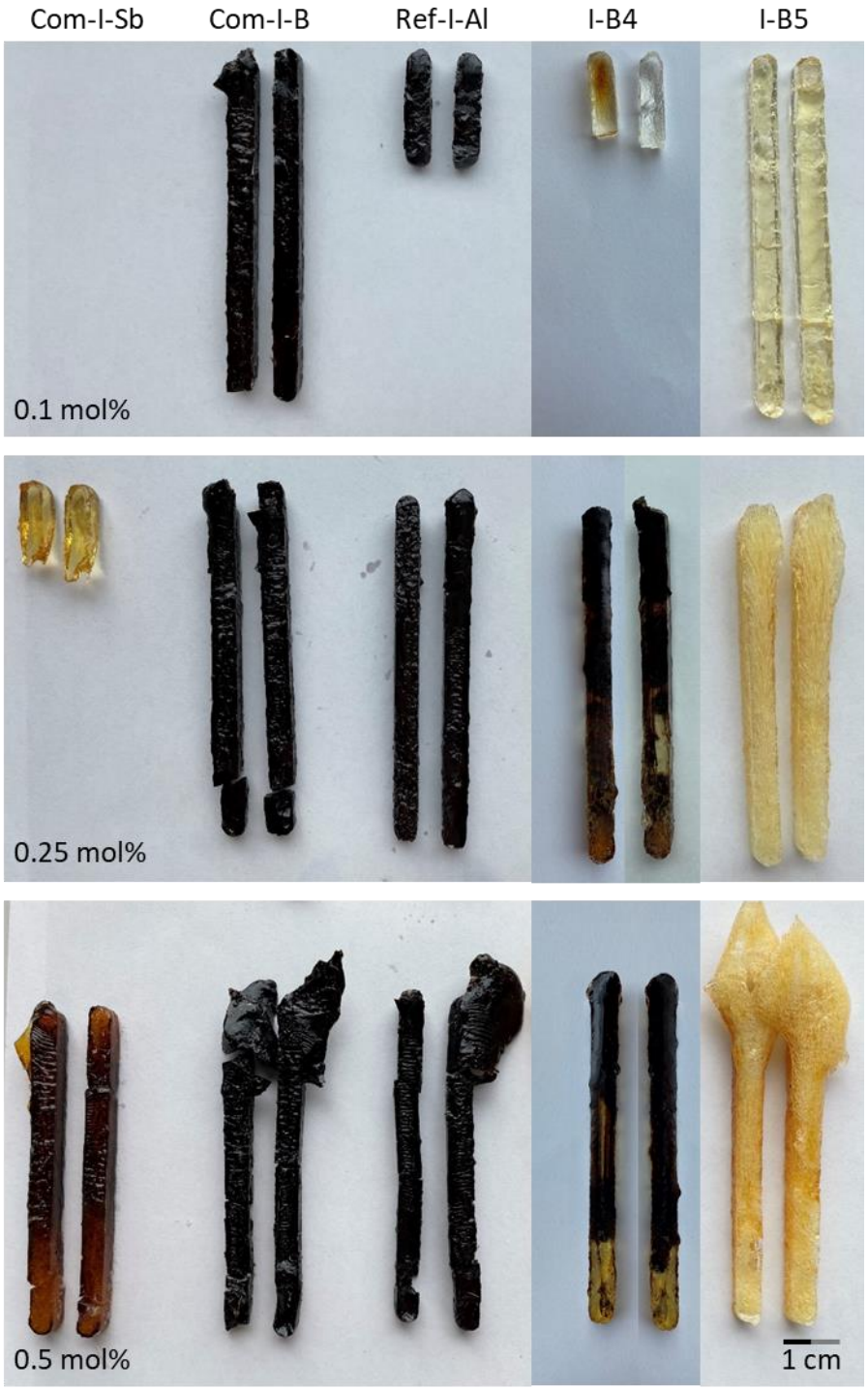

Figure 166: Specimens produced via thermally-initiated RICFP of BADGE/HDDGE with the iodonium salt/TPED concentration of 0.1 mol, 0.25 mol% and 0.5 mol% based on epoxy groups; Ref-I-Al (0.1 mol%), I-B4 (0.1 mol%) and Com-I-Sb (0.25 mol%) are shorter due to non-stable FP

After the thermally-initiated RICFP experiments, the same formulations were subject to UV-initiated RICFP. The frontal parameters such as frontal velocity, frontal temperature and epoxy group conversion for working frontal polymerization do not change compared to the

thermally-initiated systems (Figure 167, Figure 168 and Figure 169). This circumstance originates due to the frontal parameters of a formulations being an inherent property of the system. As soon as a stable front is established, it propagates unchanged no matter if initiated thermally or photochemically.

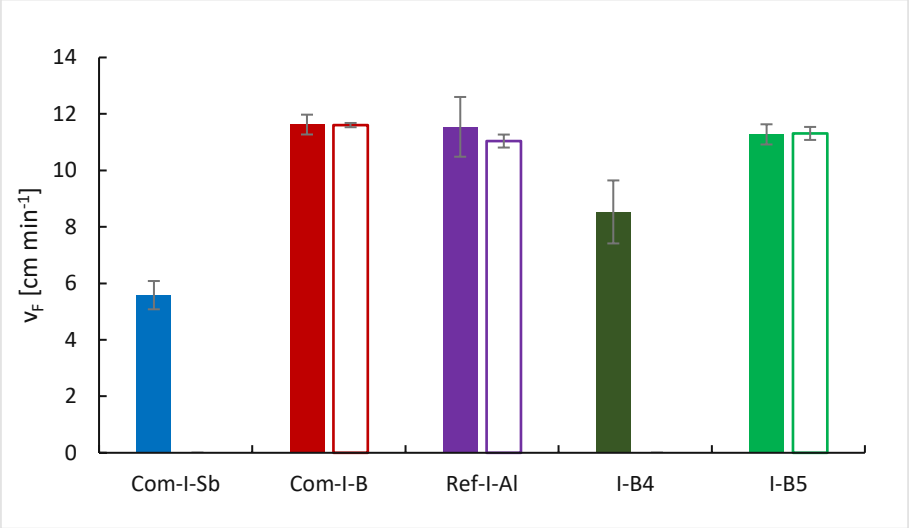

Figure 167: Thermally-initiated RICFP (full bars) vs. photochemically-initiated RICFP (framed bars): Frontal velocity (v_F) of the iodonium salt with TPED in BADGE/HDDGE

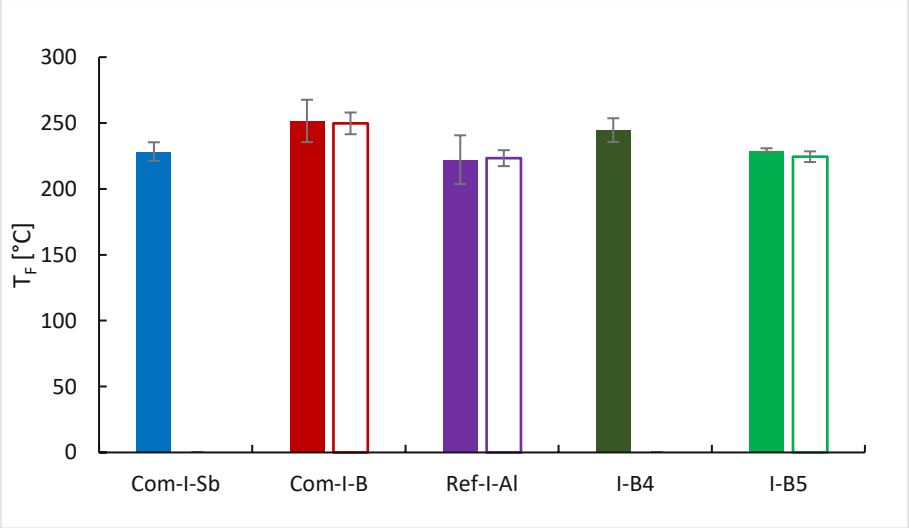

Figure 168: Thermally-initiated RICFP (full bars) vs. photochemically-initiated RICFP (framed bars): Frontal temperature (T_F) of the iodonium salt with TPED in BADGE/HDDGE

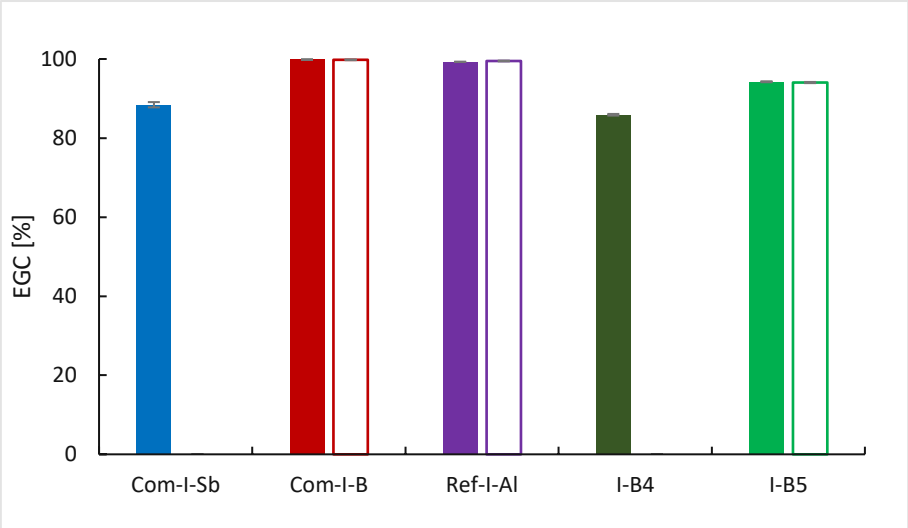

Figure 169: Thermally-initiated RICFP (full bars) vs. photochemically-initiated RICFP (framed bars): Epoxy group conversion (EGC) of the specimens after RICFP of the iodonium salt with TPED in BADGE/HDDGE

Interestingly, the commercial antimonate Com-I-Sb as well as the self-synthesized I-B4 do not show the potential for photochemically-initiated frontal polymerization (Figure 167-Figure 169). The reason behind this behavior can be explained with the nature of the initiation sources used in both experiments. The focused IR-source has a rated power output of 150 W at a focal point a few millimeters in diameter whereas the UV-source delivers 2.5 W cm^{-1} to the surface of the sample. For UV-applications the seemingly low power output is actually very high and usually in the mW range as stated in the Photo-DSC section. However, both Com-I-Sb and I-B4 samples are not able to reach sufficient exothermicity to cleave enough TPED during polymerization to sustain a frontal polymerization. An increase in concentration can lead to stable frontal polymerization for initiation systems.[125]

With the UV-initiated RICFP the front starting time can be calculated. The front starting time ($t_{F,s}$) represents the time interval from start of the UV-irradiation until a stable frontal polymerization is established.[125]

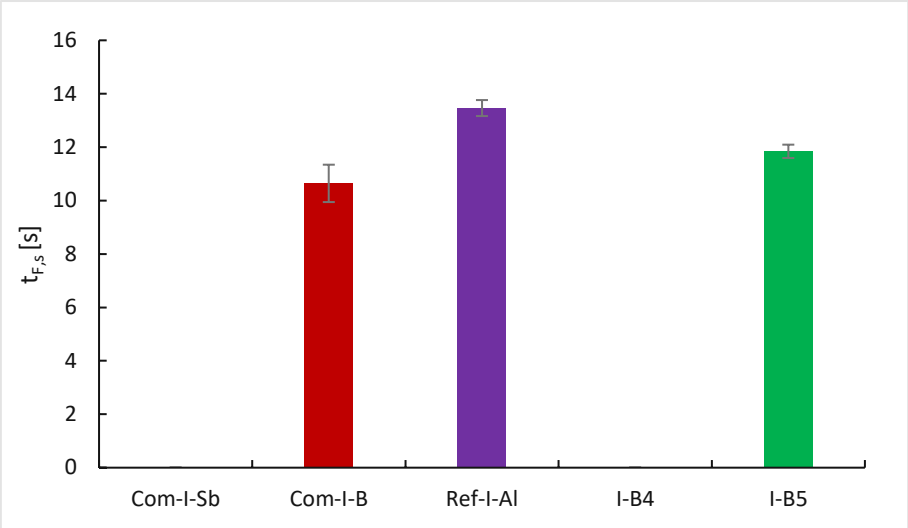

Figure 170: Photochemically-initiated RICFP: front starting time ($t_{F,s}$) of the iodonium salts and TPED in BADGE/HDDGE

The front starting times for Com-I-B, Ref-Al and I-B5 are quite similar in the range of 10.6 s for Com-I-B up to 13.5 s for Ref-I-Al (Figure 170). The self-synthesized BCN performs better compared to the aluminate and nearly on pair with the commercial borate.

3.4.3.2. Epoxy Group Conversion determined via ATR-FTIR

After successful frontal polymerization experiments, the epoxy group conversion (EGC) of the specimens cured by RICFP was determined using ATR-FTIR spectroscopy. The IR spectrum of the specimens was measured in the range of 4000 to 600 cm^{-1}. The epoxy group conversion was calculated by the difference of epoxy band integral before and after polymerization takes place. The band representing the epoxy group itself is located at a wavenumber of 914 cm^{-1}. The amount in decrease in area of this band correlates with the EGC value (Equation 10). The chemical reaction responsible for the decrease in area is the ring opening of the epoxide moiety, resulting in an aliphatic ether. To qualify as a reference, the area of the band is not allowed to change between the initial and the final spectrum to compare with. Therefore, no chemical reaction, such as ring opening for example, takes place at the reference bands. Additionally, no overlapping with the target band is preferred. As reference bands, the aromatic ring of the monomer BADGE (828 cm^{-1}) and the phenyl ether of BADGE (1183 cm^{-1}) were chosen. Three measurements for each specimen were carried out at three different locations across the sample.

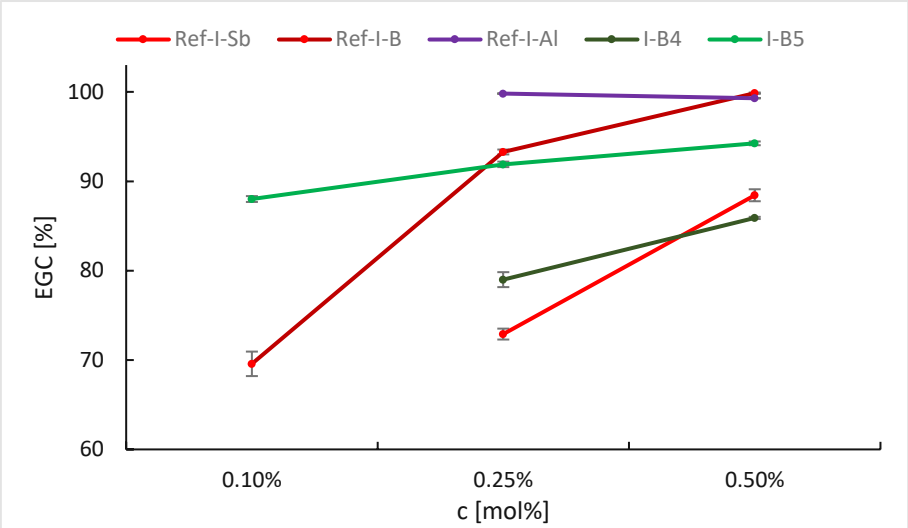

Figure 171: Epoxy group conversion of the specimens after RICFP for different concentrations of iodonium salt and TPED

A clear trend in EGC can be obtained for all samples after RICFP. As expected, higher initiator loadings lead to an increase in epoxy group conversion (Figure 171). The highest overall EGC is achieved by iodonium aluminate Ref-I-Al at 99% for all tested concentrations, even for the 0.1 mol% sample where the FP came to a halt and therefore was not successful. The Com-I-Sb specimens can achieve EGC of 88% if a concentration of 0.5 mol% of initiator is used. The borate Com-I-B reaches 70% to 99% conversion depending on the initiator loading. The cyanide-bridged borane I-B4 delivers EGC of 79% to 86% for both specimens where the FP is working. The best performing self-synthesized iodonium salt is I-B5 achieves EGC of 88% to 94%.

3.4.3.3. RICPF of thin Layers

The minimum layer thickness (MTL) of a sample was determined in the following experiments. The thinner the layer, in which a stable frontal polymerization is possible, the more reactive is a system. In addition, this property is very useful in practical applications, due to the determination of the minimum part thickness. An ascending Teflon mold (Figure 124) was used to measure the minimum layer thickness at which the frontal polymerization stops.

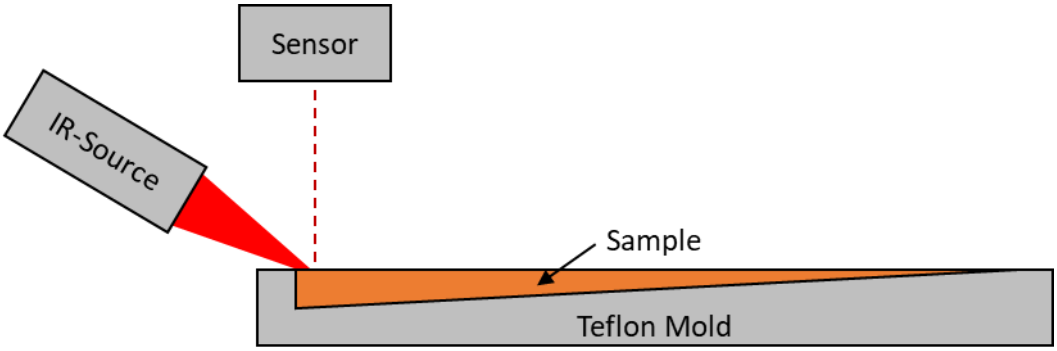

Figure 172: Schematic illustration of the RICFP minimum layer thickness setup

The well-performing formulations with low initiator loadings (0.1 mol% and 0.25 mol%) were tested containing the iodonium salts Com-I-B, Ref-I-Al, I-B5 and I-B4. Three samples were analyzed per formulation.

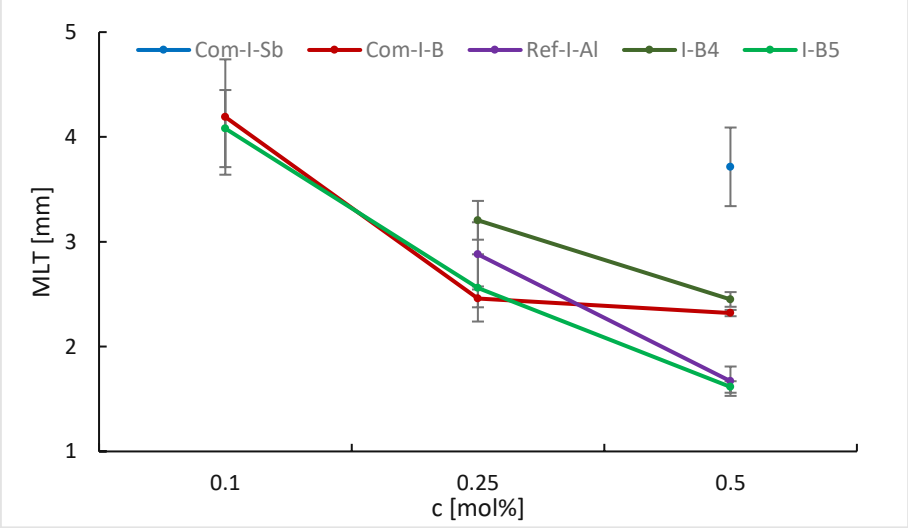

Figure 173: Minimum layer thickness (MLT) of the samples containing different amounts of onium salt/TPED

It can be clearly seen that very similar MLTs are achieved by the self-synthesized I-B5 compared to the state-of-the-art salts Com-I-B and Ref-I-Al at around 4.1 mm (Figure 173). When the concentrations of the iodonium salt and thermal radical generator TPED are increased to 0.25 mol%, the minimum layer thicknesses shrink as expected. Within small deviation, all initiators deliver 3.2 mm down to 2.5 mm of MLT. Best performers at 0.25 mol% are the commercial borane Com-I-B and the cyanide-ligated borane I-B5 with 2.5 mm MLT

(Figure 174). By increasing the concentration to 0.5 mol% the best performance is obtained with samples containing I-B5 and Ref-I-Al at around 1.7 mm MLT. Interestingly, Com-I-B stagnates regarding MLT performance from 0.25 mol% to 0.5 mol% initiator concentration. This counterintuitive observation can be explained by significant bubble formation at 0.5 mol% with Com-I-B leading to heat dissipation and an overall higher MLT.

Figure 174: Specimen produced via RICFP of BADGE/HDDGE with I-B5/TPED concentration of 0.25 mol% based on epoxy groups

The data obtained in the RICFP experiments demonstrates the performance of the single ligated borane I-B5, due to the on-pair reactivity in frontal formulations compared to state-of-the-art salts. Achieving non-black samples with the same frontal velocity, lower frontal temperature and similar MLT values compared to the best performing commercial counterparts.

4. Sulfonium Borates

4.1. Synthesis

Sulfonium salts

Regarding sulfonium salts, the starting material is represented by the commercial sulfonium chloride (S-Cl) which can be readily exchanged to any other anion via metathesis reaction (Figure 175).

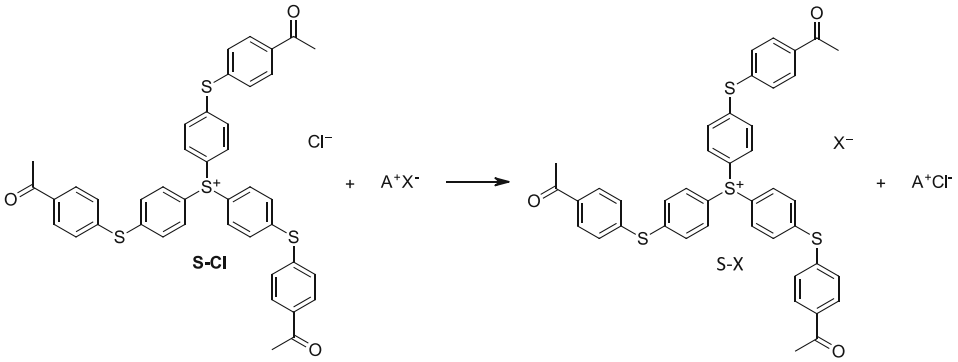

Figure 175: Schematic salt metathesis reaction starting from sulfonium chloride (S-Cl) and alkali metal salt (A^+X^-), resulting in the aimed sulfonium salt (S-X) and the precipitating alkali metal chloride (A^+Cl^-)

An alkali metal cation (A^+) paired to the target anion (X^-) is reacted with the sulfonium chloride in solution, to form the desired iodonium salt (S-X). During this process either lithium-, sodium- or potassium-chloride (A^+Cl^-) precipitates out of solution to shift the equilibrium to the aimed product.

For sulfonium salts, it is very important to remove all residual chloride as well as remaining S-Cl from the product. Any residues are going to inhibit cationic polymerization, since both anions are not weakly coordinating and eventually start to form a strong ionic bond to the positively charged chain end during polymerization.

4.1.1. Tris(4-((4-acetylphenyl)thio)phenyl) Sulfonium Sulfonimide

The first synthesized sulfonium salt is represented by the sulfonimide S-NS (Figure 176).

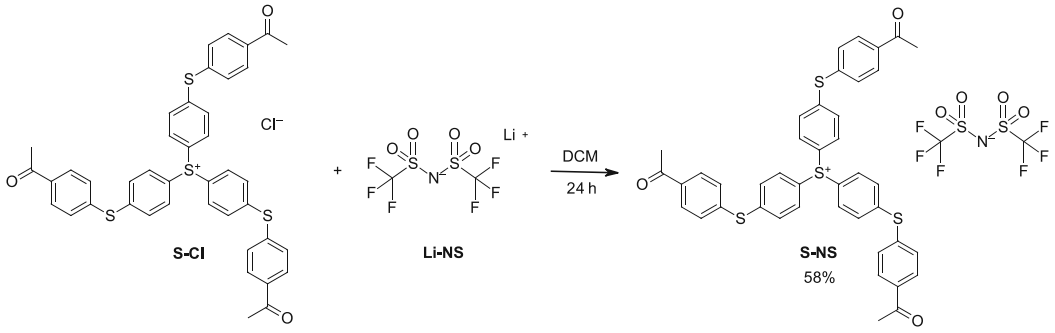

Figure 176: Synthesis of tris(4-((4-acetylphenyl)thio)phenyl) sulfonium sulfonimide (S-NS)

To synthesize tris(4-((4-acetylphenyl)thio)phenyl) sulfonium sulfonimide, a metathesis reaction according to a paper of Klikovits et al.[117] was carried out.

4.1.2. Tris(4-((4-acetylphenyl)thio)phenyl) Sulfonium Bis(oxalatoborate)

Analogously to the iodonium salt synthesized previously, the sulfonium bis(oxalatoborate) was targeted next (Figure 177).

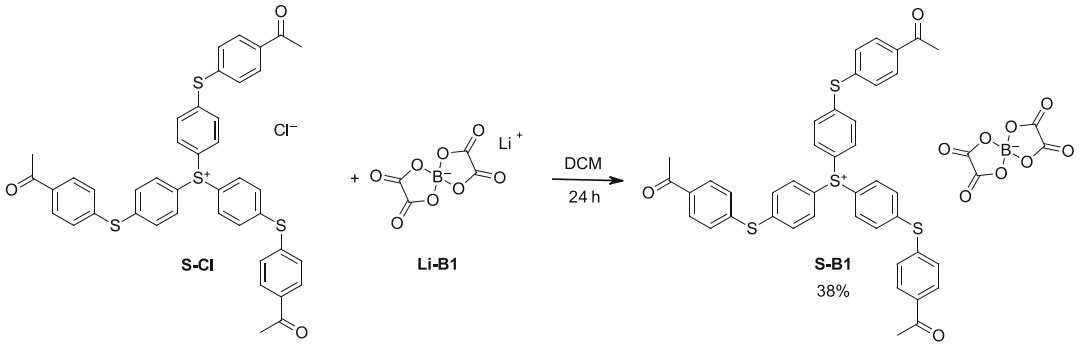

Figure 177: Synthesis of tris(4-((4-acetylphenyl)thio)phenyl) sulfonium bis(oxalatoborate) (S-B1)

To synthesize tris(4-((4-acetylphenyl)thio)phenyl) sulfonium bis(oxalatoborate), a metathesis reaction according to a paper of Klikovits et al.[117] was carried out.

4.1.3. Tris(4-((4-acetylphenyl)thio)phenyl) Sulfonium Difluoro(oxalato)borate

Next, the sulfonium difluoro(oxalate)borate was targeted next (Figure 178).

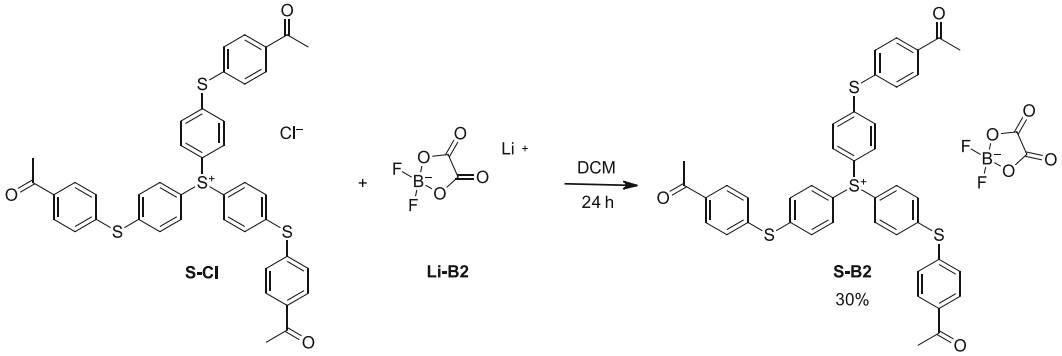

Figure 178: Synthesis of tris(4-((4-acetylphenyl)thio)phenyl) sulfonium difluoro(oxalato)borate (S-B2)

To synthesize tris(4-((4-acetylphenyl)thio)phenyl) sulfonium difluoro(oxalato)borate, a metathesis reaction according to a paper of Klikovits et al.[117] was carried out.

4.1.4. Tris(4-((4-acetylphenyl)thio)phenyl) Sulfonium CN-bis[Tris(pentafluorophenyl)borane]

Analogously to the iodonium salt, the sulfonium derivative was targeted next (Figure 179).

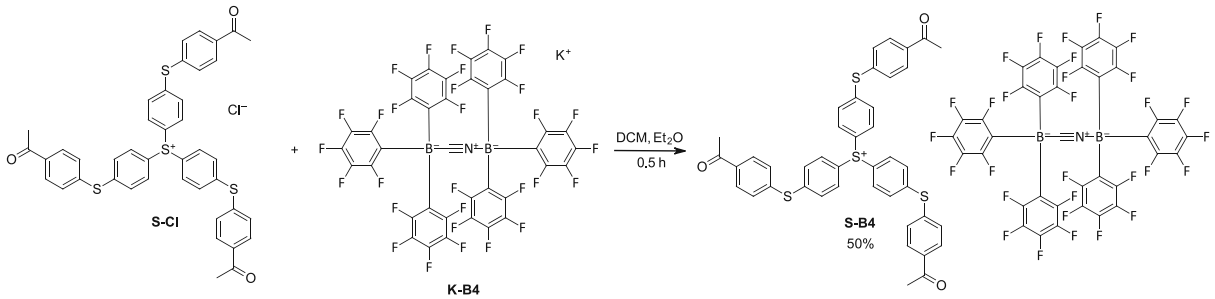

Figure 179: Synthesis of tris(4-((4-acetylphenyl)thio)phenyl) sulfonium CN-bis[tris(pentafluorophenyl)borane] (S-B4)

To synthesize tris(4-((4-acetylphenyl)thio)phenyl) sulfonium CN-bis[Tris(pentafluorophenyl)borane], a metathesis reaction according to a paper of Klikovits et al.[117] was carried out.

4.1.5. Tris(4-((4-acetylphenyl)thio)phenyl) Sulfonium CN-[Tris(pentafluorophenyl)borane]

After the synthesis of the iodonium salt derivative produced previously, the sulfonium cyanide-ligated borane was targeted next (Figure 180).

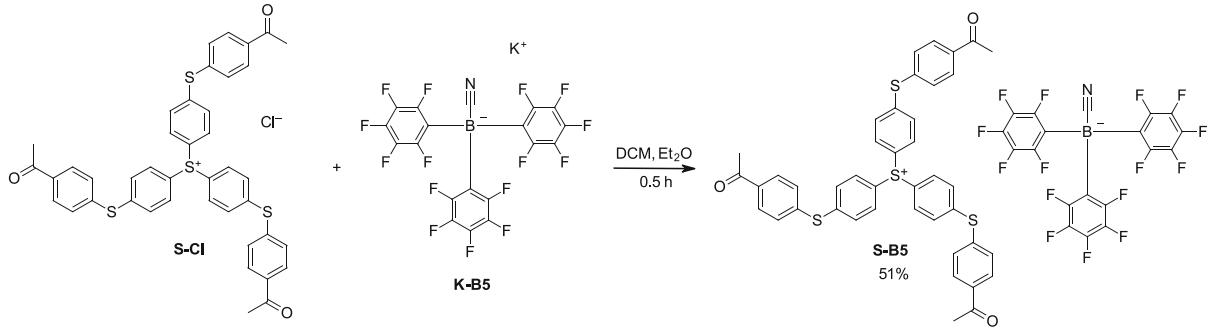

Figure 180: Synthesis of tris(4-((4-acetylphenyl)thio)phenyl) sulfonium CN-[tris(pentafluorophenyl)borane] (S-B5)

To synthesize tris(4-((4-acetylphenyl)thio)phenyl) sulfonium CN-[tris(pentafluorophenyl)borane], a metathesis reaction according to a paper of Klikovits et al.[117] was carried out.

4.2. Characterization of Sulfonium Borates

4.2.1. Selection of the Sulfonium Compounds

Synthesis of all aimed sulfonium salts was a success. Therefore, the initiators can now be decomposed by thermal- or photo-stimuli to start cationic polymerization analogously to the iodonium salts (Figure 181). However, the final purpose for the sulfonium salts is aimed at 3D-printing via hot lithography rather than RICFP compared to the iodonium salts.

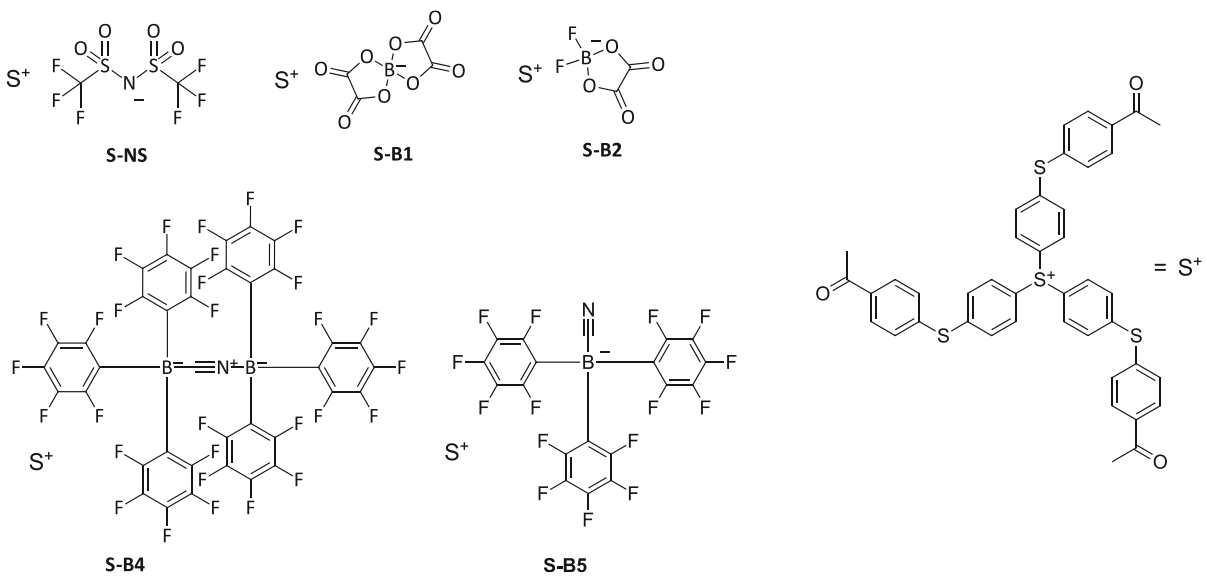

Figure 181: Selection of the synthesized sulfonium salts S-NS, S-B1, S-B2, S-B4 and S-B5 for further analysis

All synthesized sulfonium salts paired with different WCAs were ready to be benchmarked against commonly used sulfonium hexafluorophosphates in industry and much more reactive state-of-the-art salt, sulfonium tetrakis(2,3,4,5,6-pentafluorophenyl)borate (Figure 182). The sulfonium salts Com-S-P and Com-S-B were acquired from commercial sources.

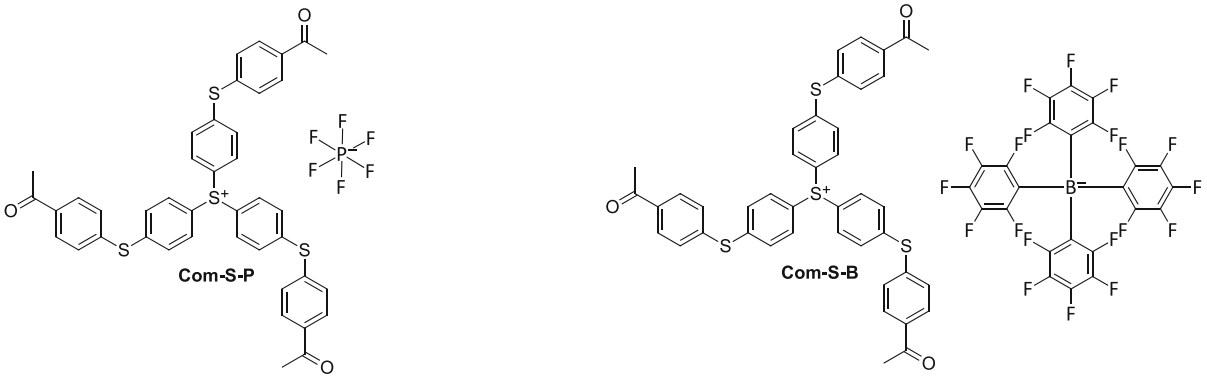

Figure 182: Selection of the acquired state-of-the-art sulfonium salts Com-S-P and Com-S-B for further analysis

Comparative studies of synthesized and acquired sulfonium salts were carried out in terms of photochemical behavior, reactivity in cationically polymerizabl resins and stability.

4.2.2. Absorption Spectra determined via UV-VIS Experiments

Similar to the iodonium salt, the absorption was determined for all sulfonium salts as well to know which light source is appropriate for further measurements. During the photochemical analysis, the ultraviolet (UV) and visible light (VIS) absorption spectra of the onium compounds were determined. The wavelength scan ranges from 250 nm to 500 nm. Onium salt and concentrations of 1 x 10^{-5} mol L^{-1} were used.

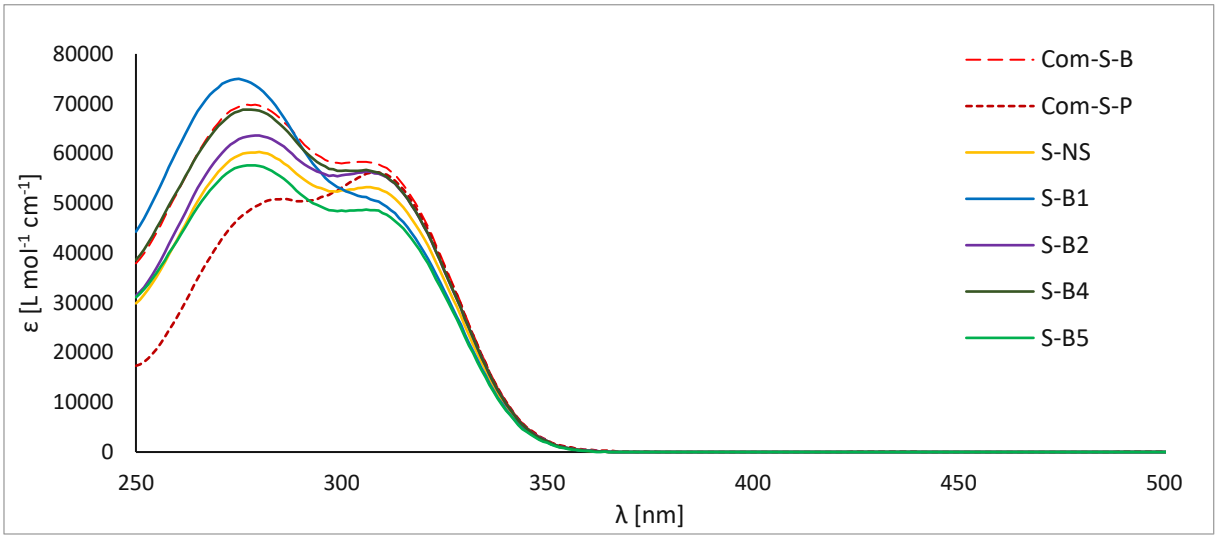

Figure 183: Wavelength dependence of the molar extinction coefficient for synthesized and acquired sulfonium salts

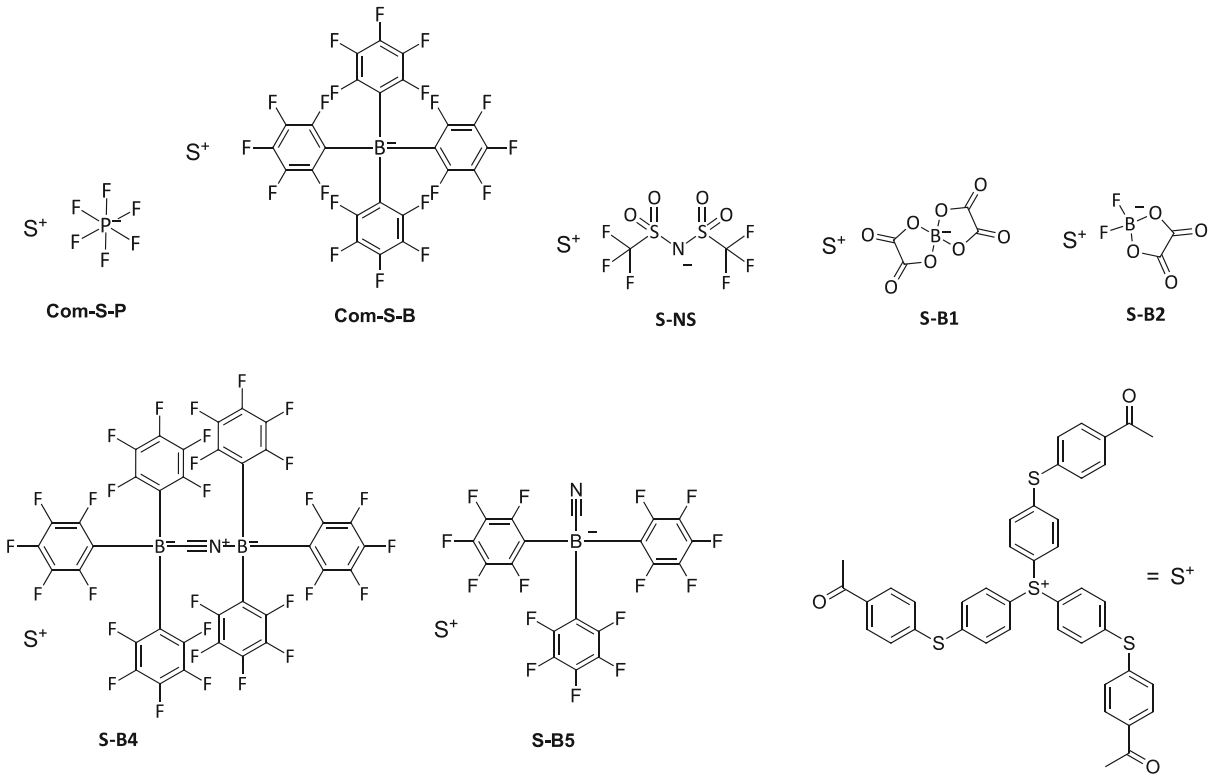

Considering onium salts in general, the cation is responsible for the photochemical properties such as absorption (Figure 183). Therefore, the difference between the selected compounds

is rather small, due to high similarities of the sulfonium cation. Two distinct maxima are obtained for all sulfonium salts, one at 278 nm and the other one at 311 nm. The molar extinction coefficients range from 48000 up to 55000 L mol^{-1} cm^{-1} at 311 nm.

4.3. Reactivity of Sulfonium Borates

4.3.1. Formulations based on BADGE and ECC

For the upcoming reactivity studies, formulations based on a cationically polymerizable epoxy-based monomer had to be prepared (Figure 184). This mixture's main component was either the aromatic bisphenol-A-diglycidylether (BADGE) or the cycloaliphatic 3,4-epoxycyclohexyl-methyl-3',4'-epoxycyclo-hexancarboxylat (ECC).

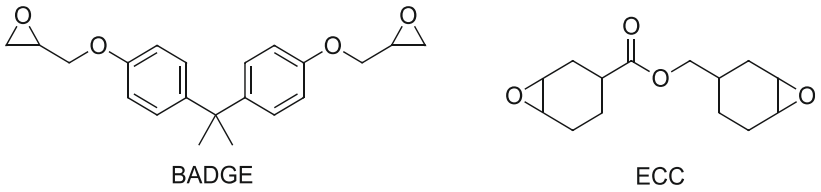

Figure 184: Monomers BADGE and ECC

The onium salts were used in 1.0 mol% based on epoxy groups referred to BADGE and ECC. Selected iodonium salts, originating from either synthesis or acquisition were used in the upcoming studies (Figure 185).

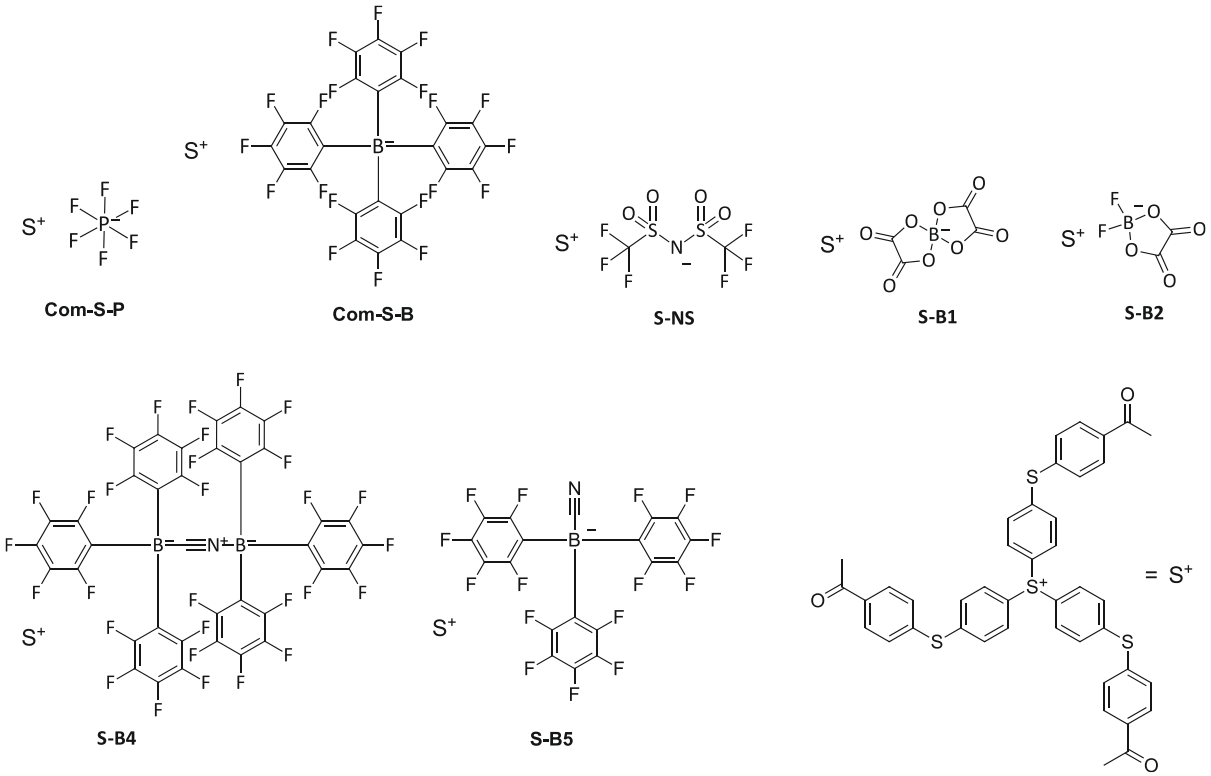

Figure 185: Selected sulfonium salts for reactivity tests

At first, heating shortly to around 80 °C and swirling of the formulations on a vortex device was performed. Afterwards, a treatment in an ultrasonic bath at 40 °C leads to completely homogeneous samples after 30 min. Unfortunately, S-B4 formulations are unstable due to residual moisture in commercial resins like BADGE and ECC. The anion is prone to hydrolysis, therefore reducing the pot life of the formulations significantly to around one hour.

4.3.2. Storage Stability Tests

The stability of a formulation for 3D-printing is deceive, since premature or uncontrolled solidification of the resin would definitely harm the printer's vat. Therefore, a storage stability study was carried out at a constant temperature of 50 °C for all sulfonium salts under light protection. The formulations described in Chapter II, 4.3.1. contained either BADGE or ECC with 1.0 mol% sulfonium salt referred to epoxy groups.

The focused-on metric of a formulation was the viscosity, which was measured with a rheometer. The viscosity was determined at a shear rate of 100 s^{-1} and the gap size between stamp and plate was 48 µm. The lower the change in viscosity over time, the better is the pot life of a formulation.

BADGE Formulations

First, the sulfonium salts were subject of a storage stability study in the monomer BADGE.

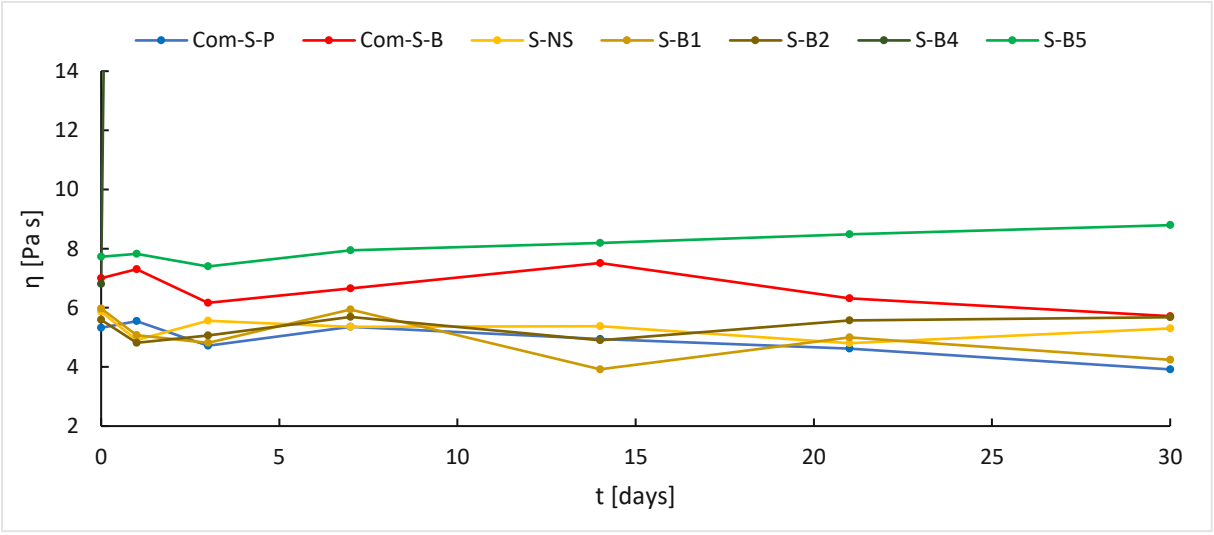

Figure 186: Time dependent viscosity of the BADGE-based formulations with 1.0 mol% sulfonium salt at a storage temperature of 50 °C under light protection

The results in BADGE over 30 d period, show a quite linear trend for most sulfonium salts (Figure 186). As expected from previous formulation preparations, the cyanide-bridged borane S-B4 was liquid at the start of the test, however started to gel rapidly within the first

24 h. Surprisingly, the structurally very similar S-B5 measures nearly constant viscosity with a slight increase of 14% from start to day 30.

ECC Formulations

Next, the same selection of sulfonium-based salts were tested in the cycloaliphatic monomer ECC.

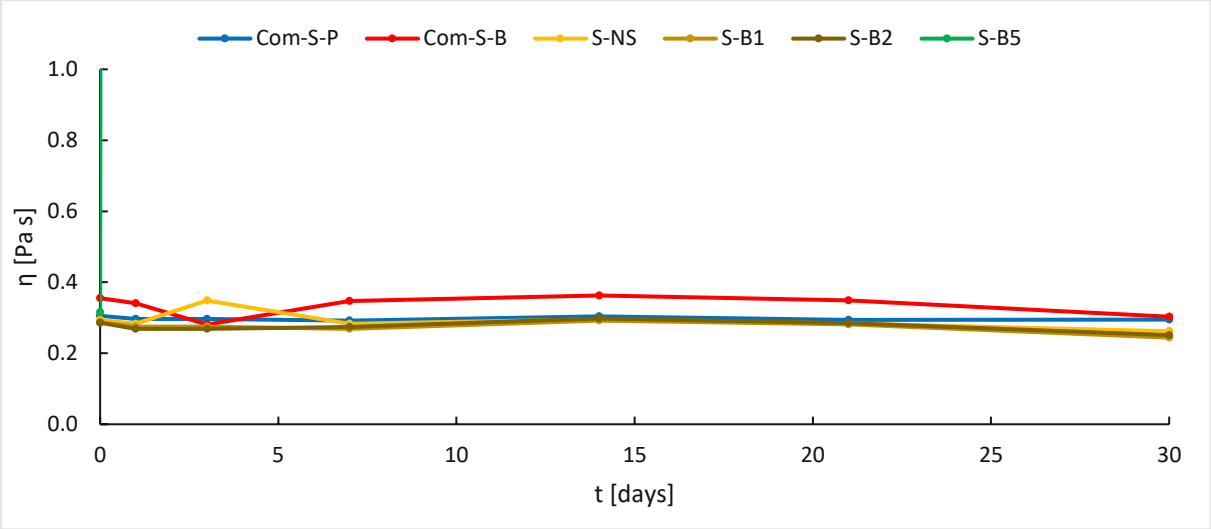

Figure 187: Time dependent viscosity of the ECC-based formulations with 1.0 mol% sulfonium salt at a storage temperature of 50 °C under light protection

Switching to the more reactive cycloaliphatic monomer ECC, a similar trend of the viscosities can be observed (Figure 187). The commercial compounds as well as S-NS, S-B1 and S-B2 show a practically constant viscosity over 30 d. S-B4 did gel during the formulation preparation and was therefore not measured at the rheometer. The cyanide-ligated borane S-B5 was a liquid formulation at the start of the study, however within the first 24 h the sample gelled.

4.3.3. Thermal Stability of Sulfonium Salts determined via DSC

The thermal stability of every sulfonium salt is limited, hence a decomposition process appears at a certain onset temperature. This is especially important for the aimed hot lithography-based 3D-printing process, since the sulfonium salts need a high tolerance towards temperatures up to 110 °C. Therefore, high onset temperatures with a suitable safety margin above the final processing temperature are preferred.

The samples were weighed into aluminum crucibles, which were sealed by a punctured lid to allow volatiles to evaporate unhindered. All sulfonium salts were exposed in a DSC measurement to a rising temperature gradient to investigate the decomposition temperature

in epoxy resins BADGE and ECC prepared in chapter II, 4.3.1. The starting temperature was chosen to be 25 °C and the device heated up to 450 °C

BADGE Formulations

The thermal stability of all sulfonium salts was investigated in the monomer BADGE first.

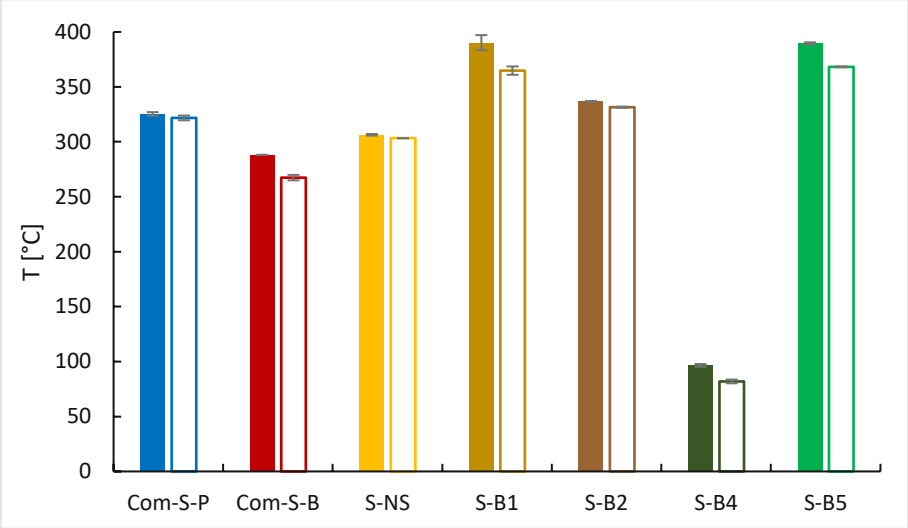

Figure 188: Temperature at the highest exothermicity (T_{max} - full) and polymerization onset temperature (T_{onset} - framed) in BADGE with the sulfonium salts

As expected, S-B4 onset temperature is unusually low at 82 °C due to the unstable anion incorporated in the salt (Figure 188). All remaining salts show onset temperatures above 267 °C with S-B1 and S-B5 achieving the highest thermal stability at 365 °C and 368 °C onset temperature respectively. The T_{max} values show the same trend.

ECC Formulations

After the BADGE-based testes, the stability of the sulfonium salts in ECC was determined.

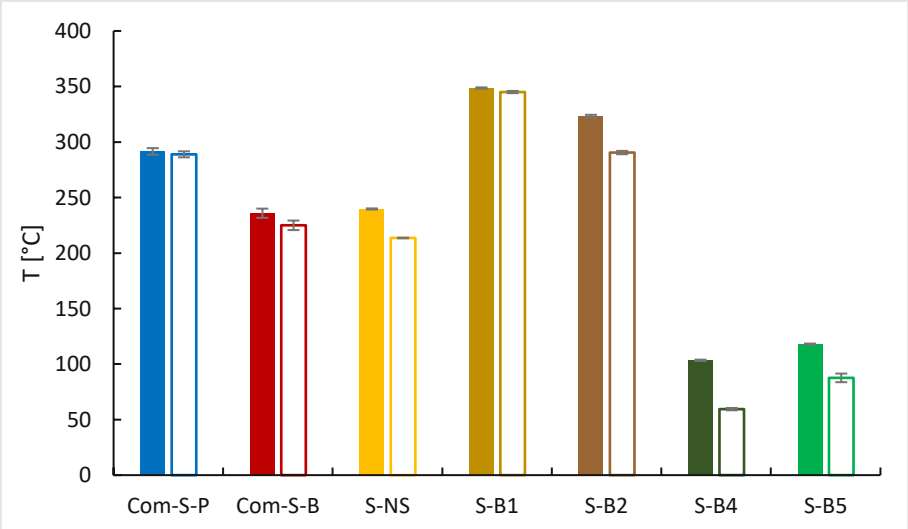

Figure 189: Temperature at the highest exothermicity (T_{max} - full) and polymerization onset temperature (T_{onset} - framed) in ECC with the sulfonium salts

As expected, the start temperatures of the polymerization for all iodonium salts in ECC-based formulations are generally lower compared to the BADGE-based samples (Figure 189). Surprisingly, the cyanide-bridged S-B4 and the cyanide-ligated borane S-B5 show rather low onset temperatures of 60 °C and 88 °C respectively. The data for S-B5 finally resolves the thermal stability issues of the formulations in ECC at the Photo-DSC at 90 °C despite being storage stable for 30 days at 50 °C. The remaining sulfonium salts show thermal stability upwards of 213 °C.

By comparing the results of the thermal stability study, there are many suitable candidates for further 3D-printing experiments. With the exception of S-B4 in BADGE as well as S-B4 and S-B5 in ECC, all tested sulfonium salts pass the requirements in terms of thermal stability. Reaching up to 368 °C as onset temperature for the cyanide-ligated borane S-B5 in BADGE. Interestingly, the S-B5 remains highly temperature stable in BADGE, whereas in ECC stability is limited to below 90 °C.

4.3.4. Photoreactivity determined via Photo-DSC

4.3.4.1. Temperature-dependent Photoreactivity with 1 mol% Sulfonium Salt

The main objective of the photoinitiation study was to investigate the potentials of all sulfonium salts as photoacid generators for 3D-printing. The formulations consist out of 1 mol% of sulfonium-based PAG combined with the monomer BADGE. The formulations described in the previous chapter II, 4.3.1. were used for this study without any additives. To finally result in 1.0 mol% sulfonium salt in BADGE and ECC. Additionally, the temperature dependence was investigated to draw a comparison between each of the initiators at 25 °C, 50 °C, 70 °C, 90 °C and 110 °C. A study at different temperatures is especially interesting due to the rise of technologies like hot lithography that enable the application of highly viscous resins like BADGE. A benefit, that comes alongside with the drop in viscosity is the increase in reactivity of the resin at elevated temperatures. Since the UV-VIS experiments indicated very similar absorption spectra across the tested sulfonium compounds, an irradiation source equipped with a 320-500 nm filter was used.

BADGE Formulations

At first, the reactivity of all sulfonium salts was tested in the monomer BADGE without any additives.

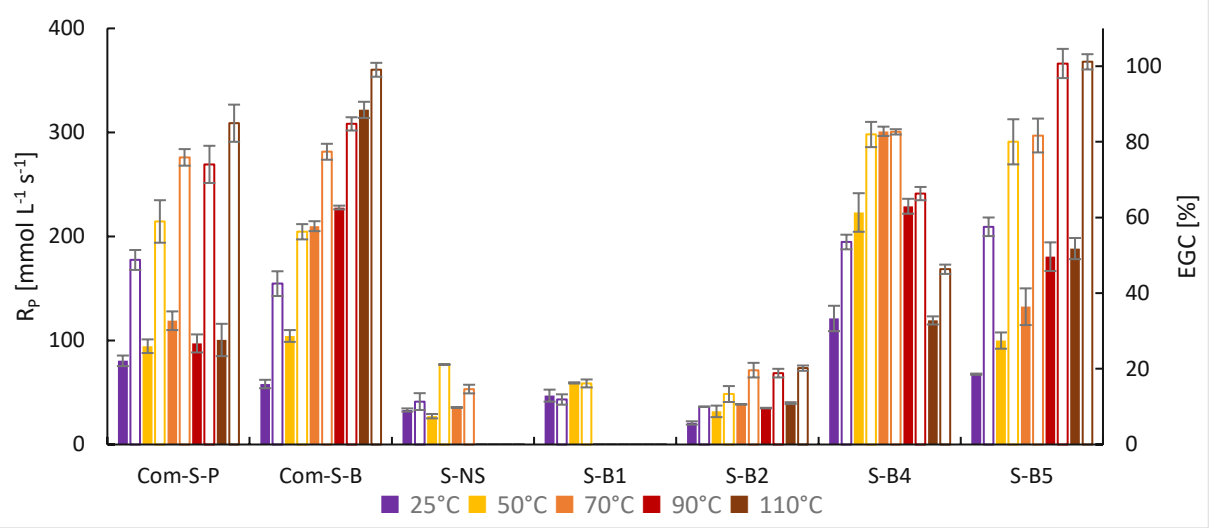

Figure 190: Rate of polymerization (R_P - full) and epoxy group conversion (EGC – framed) in BADGE with 1 mol% of sulfonium salt at 25 °C, 50 °C, 70 °C, 90 °C and 110 °C (Photoinitiation); The time-based parameters t_{max} and $t_{95\%}$ are located in the attachment (Figure 268)

The reactivity of the newly synthesized S-B4 outperforms all commercial sulfonium salts at 50 °C and 70 °C with up to 301 mmol L^{-1} s^{-1} (Figure 190). This correlates to a 43% increased reactivity compared to the commercial phosphate Com-S-P and 153% for the commercial borate Com-S-B at 70 °C. Interestingly, peak reactivity for S-B4 is at 70 °C and starts to decrease at elevated temperatures. The labile behavior of S-B4 anion leads to pre-polymerization in the photo-DSC measurement chamber starting at 90 °C. Therefore, the polymerization reaction is already finished in the isothermal phase, leaving a significantly lower number of reactive epoxy-groups for the irradiation phase, where the exothermic peak usually occurs. Evaluating the new cyanide-ligated borane S-B5 and Com-S-B, increased reactivity by rising temperatures can be observed. The two sulfonium salts show their maximum reactivity at 110 °C.

Comparing the EGC of all systems, the new S-B5 demonstrates great potential for high conversions. Starting at room temperature, already 58% of the epoxy groups react and a rising EGC-trend continues up to full conversion at 90 °C and 110 °C. Additionally, S-B4 outperforms both commercial systems at 25 °C, 50 °C and 70 °C significantly before becoming too unstable at higher temperatures.

ECC Formulations

Second, the same selection of sulfonium compounds was subject of a reactivity study in ECC.

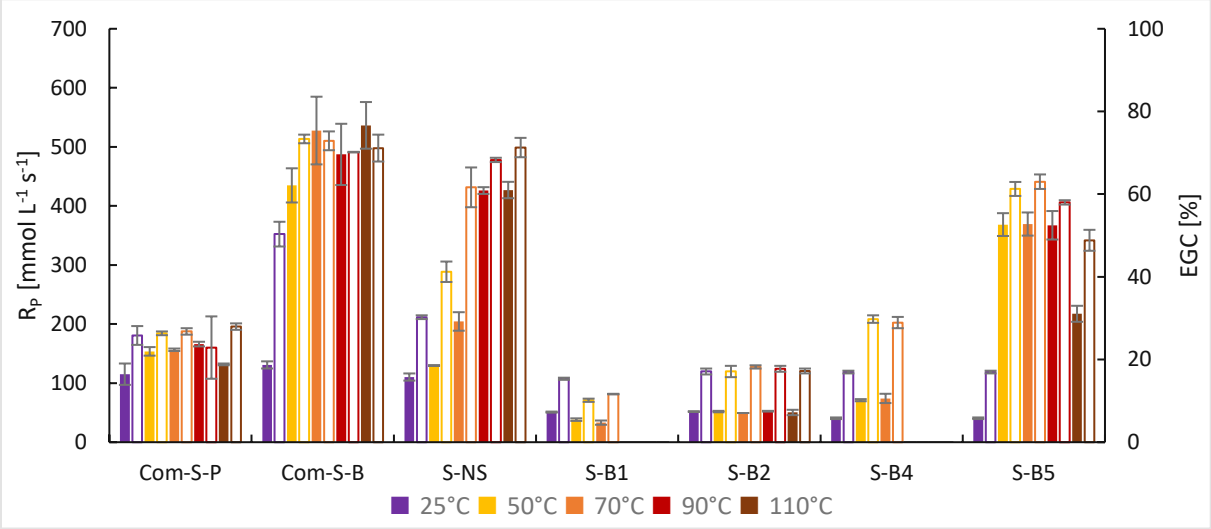

Figure 191: Rate of polymerization (R_P - full) and epoxy group conversion (EGC – framed) in ECC with 1 mol% of sulfonium salt at 25 °C, 50 °C, 70 °C, 90 °C and 110 °C (Photoinitiation); The time-based parameters t_{max} and $t_{95\%}$ are located in the attachment (Figure 269)

With a more reactive monomer system like ECC, higher polymerization rates are achieved compared to the BADGE-based samples (Figure 191). The commercial borate Com-S-B demonstrates high reactivity at 110 °C. However, the sulfonium borate starts to stagnate in performance as soon as 70 °C is reached. The second-best performance is delivered by S-NS, which performs significantly better in ECC compared to BADGE. The cyanide-ligated borane S-B5 shows high reactivity all the way up to 90 °C. As expected, the reactivity of S-B4 at 90 °C and 110 °C cannot be calculated correctly in a more reactive system such as ECC due to pre-polymerization in the preheated DSC-chamber.

Comparing the EGC of all sulfonium salts, the highest values are measured in samples containing the commercial borate Com-S-B, followed by the sulfonimide S-NS and the self-synthesized borate S-B5. EGC of up to 73%, 62% and 63% are achieved at 70 °C respectively.

The overall best performing sulfonium salt as cationic initiator remains the state-of-the-art Com-S-B. However, the newly synthesized S-B5 shows great potential in BADGE, outperforming the industrial initiator Com-S-P by a significant margin and Com-S-B in many conditions as well.

4.3.4.2. Temperature-dependent Sensitization of Sulfonium Salts

The main objective of the sensitization experiments is to resemble the 3D-printing conditions as close as possible. Since the 3D-printer is equipped with a 405 nm laser as irradiation source, the sulfonium salts themselves do not absorb photons at this wavelength as demonstrated in the UV-VIS section. Therefore, a sensitizer is necessary to absorb light at 405 nm and transfer the energy to the sulfonium salt. ECC was not further investigated, since BADGE is much more applicable in hot lithography due to its high viscosity. The formulations based on BADGE and 1 mol% sulfonium salt described in the previous chapter II, 4.3.1. were used for this study. In addition, the anthracene-derivative DBA was used in 0.35 mol% and the superacid scavenger EDAB was used in 0.12 mol% based on epoxy groups according to literature (Figure 192).[201] The di-butoxylated anthracene was selected over standard anthracene, due to better solubility in monomers like BADGE and its superior absorption properties with a tail-out region up to 430 nm (Figure 69). The acid scavenger's purpose is to prevent overpolymerization during the printing process by neutralizing the migrating superacid. This acid-base mechanism of the sulfonium salts' superacid and EDAB enhances resolution of the printed part significantly.[201]

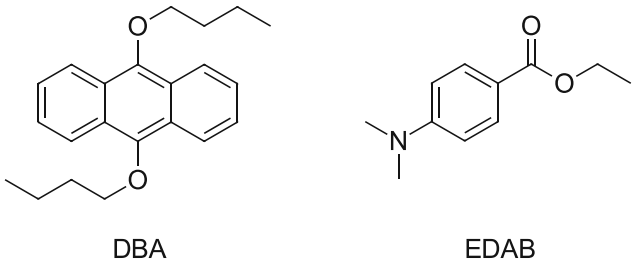

Figure 192: Sensitizer 9,10-Dibutoxyanthracene (DBA) and superacid scavenger Ethyl 4-(dimethylamino)benzoate (EDAB)

Since the performance of some sulfonium salts in the previous reactivity study was quite impressive, their performance with the addition of DBA was investigated next. The following photo-DSC study was performed to obtain the best suiting printing temperature for hot lithography. Therefore, reactivity of the sulfonium salts was measured at 25 °C, 50 °C, 70 °C, 90 °C and 110 °C. To imitate the 405 nm laser of the printer, a mercury lamp was used as irradiation source, equipped with a 400 – 500 nm filter. The cyanide-bridged initiator S-B4 was not investigated further, due to low storage stability of the formulations. S-B4-based formulations risk uncontrolled polymerization of the 3D-printer's material vat, which would be catastrophic.

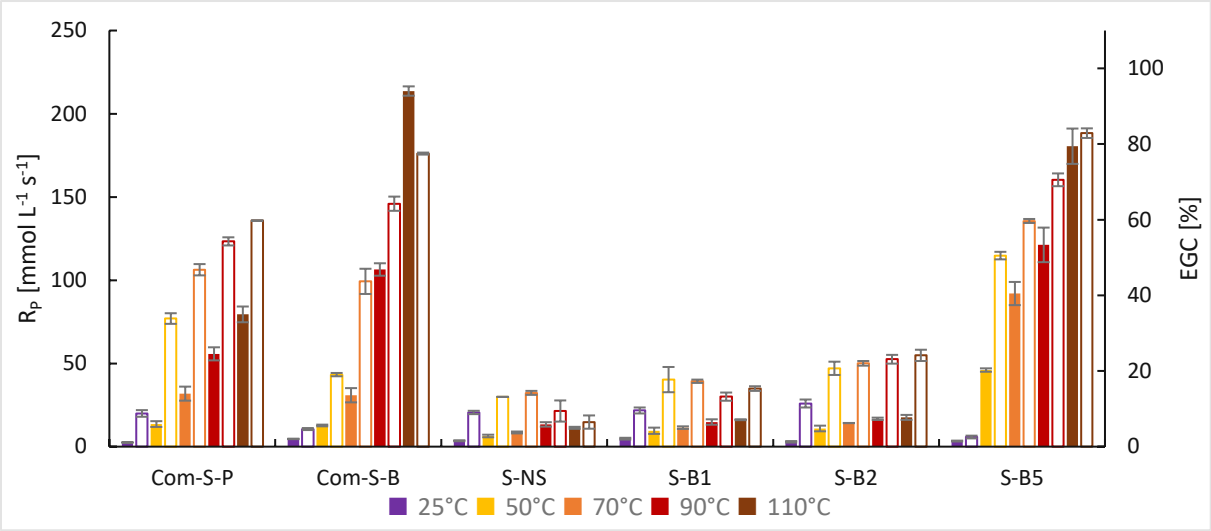

Figure 193: Rate of polymerization (R_P - full) and epoxy group conversion (EGC – framed) in BADGE with 1 mol% of sulfonium salt, 0.35 mol% DBA and 0.12 mol% EDAB at 25 °C, 50 °C, 70 °C, 90 °C and 110 °C (sensitization by DBA); The time-based parameters t_{max} and $t_{95\%}$ are located in the attachment (Figure 270)

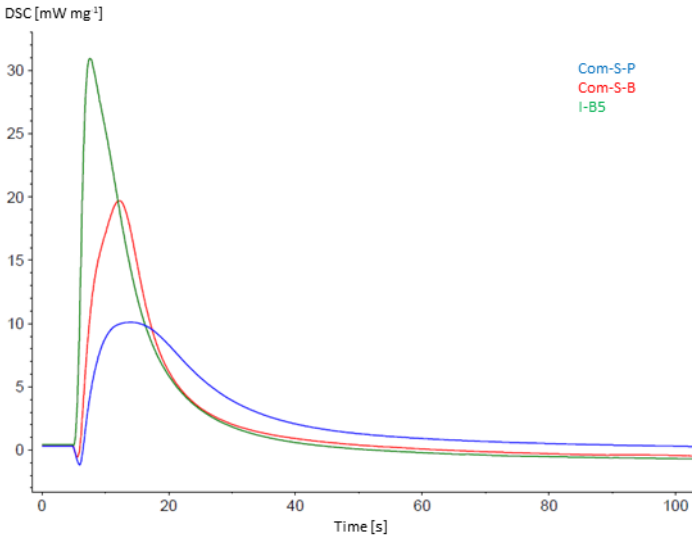

Figure 194: First 100 s of Photo-DSC data in BADGE with 1 mol% of sulfonium salt at 90 °C (sensitization by DBA)

The cyanide-ligated borane S-B5 demonstrates surprisingly high reactivity if sensitized by DBA in BADGE (Figure 193). Especially at 90 °C, S-B5 outperforms all commercial systems since the appearance of its peak is both higher and sharper (Figure 194). With a rate of polymerization of 121 mmol L^{-1} s^{-1} it performs much better compared with the state-of-the-art compounds Com-S-B and Com-S-P significantly. The commercial borane and phosphate reach only 88% and 46% of the R_P of S-B5. In addition to a high rate of polymerization, the newly synthesized S-B5 reaches the highest values in terms of epoxy group conversion with 71%. Com-S-B and Com-S-P achieve 64% and 54% EGC respectively.

Overall, the newly synthesized initiator S-B5 demonstrates extraordinary reactivity and high epoxy group conversions if sensitized by DBA in BADGE. Outperforming the commercial

sulfonium salts Com-S-B and Com-S-P in all polymerization parameters. This photo-DSC study represents the proof of concept for the following 3D-printing experiments.

4.4. Hot Lithography

4.4.1. Selection of the Compounds and Formulations for Hot Lithography

Since hot lithography represents a 3D-printing process at elevated temperatures, only temperature and storage stable sulfonium salts are suitable. A second criteria is reactivity. Exclusively sulfonium salts with sufficient reactivity in the photo-DSC experiments are selected (Figure 195).

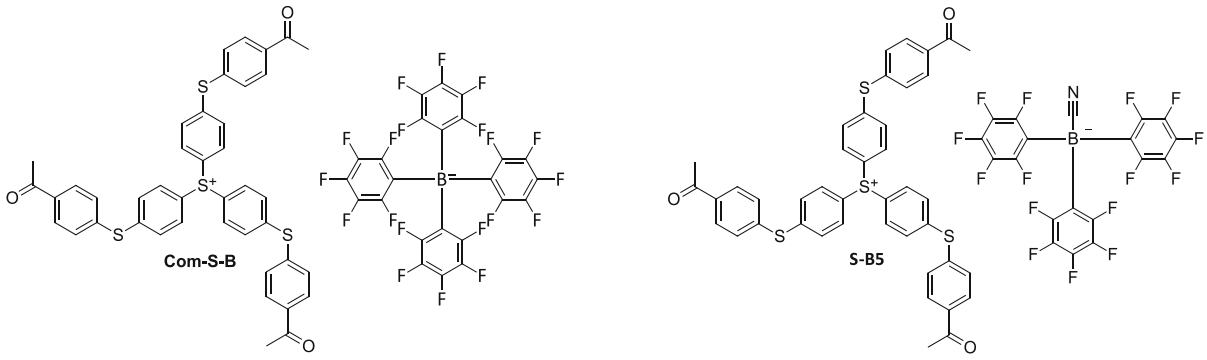

Figure 195: Selected sulfonium salts for hot lithography

Since S-B4 shows major stability issues, it was excluded from the experiments. Unfortunately, the self-synthesized components S-NS, S-B1 and S-B2 do not show sufficient reactivity in catatonically curable resins like BADGE and ECC. Therefore, the two most reactive salts were used. On one side, the commercial borate Com-S-B and on the other side the new cyanide-ligated borane S-B5.

The formulations were based on the aromatic monomer BADGE, since it is perfectly suitable for hot lithography due to its high viscosity and comparatively low reactivity at room temperature. Based on the epoxy groups of BADGE, 1 mol% sulfonium salt, 0.35 mol% DBA as sensitizer and 0.12 mol% EDAB as superacid scavenger were used (Figure 196).[201]

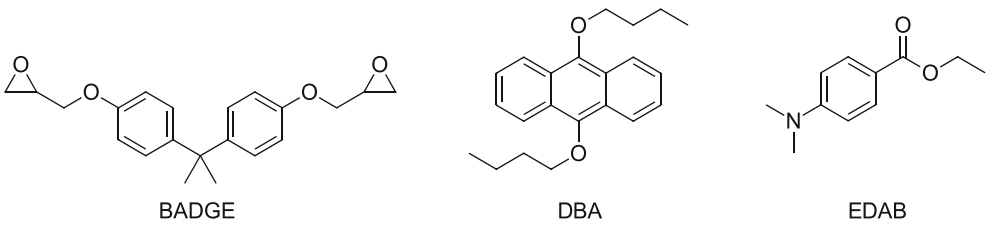

Figure 196: Monomer BADGE, sensitizer DBA and superacid scavenger EDAB

The anthracene derivative DBA is used for electron transfer to the sulfonium salts and EDAB prevents overpolymerization during 3D-printing.

4.4.2. Hot Lithography Experiments

All previous tests indicate that S-B5 is a very capable initiator for hot lithography. Subsequently, 3D-printing of the formulations prepared in chapter II, 4.4.1. was targeted. To fabricate of the targeted three-dimensional structures, the 3D models were created via CAD (Figure 197). Discs, hexagonal pyramids and hollow quadratic pyramids were prepared virtually and the resulting STL files sliced into layers.

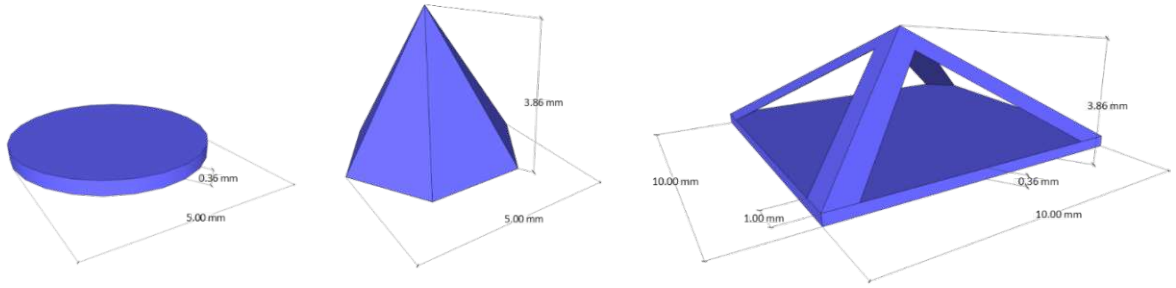

Figure 197: 3D models of the disc, the hexagonal pyramid and the hollow quadratic pyramid including dimensions

The disc model was sliced into 8 layers and both pyramids into 78 layers. Since the first layer height was set to 10 µm and all following layers were cured in 50 µm thickness, the resulting part heights of discs and pyramids are 0.36 mm and 3.86 mm respectively. Two separate sets of parts were printed on a Caligma 200 UV printer. The first set of the BADGE-based formulations contains the reference sulfonium borate Com-S-B and the second set the best-performing self-synthesized initiator S-B5. All parts with direct resin contact were heated to 90 °C to enable the additive manufacturing of the highly viscous BADGE. The light source during the printing process is represented by a 405 nm LED laser with a spot diameter of 18 µm at the surface of the material. This laser beam scans a 2-dimensional plane step by step to produce the 3-dimensional part with a layer thickness of 50 µm. However, the thickness of the first layer was set to 10 µm and it was irradiated twice to increase the cured resins adhesion to the building platform. The glass plate was equipped with a transparent Teflon foil to prevent any cured resins sticking to it. Energy intensity of the LED laser was set to 1936 mJ cm^{-1} at scan speed of 2 m s^{-1}. After successful printing of the parts, post processing was required to remove residual resin sticking to the specimens. Therefore, all parts were suspended in acetone and ultrasonicated for one minute. The acetone was poured off and the clean parts obtained (Figure 198).

Figure 198: BADGE-based discs fabricated via hot lithography by the use of initiator S-B5 and Com-S-B (photographed around 10 h after printing)

The fabricated parts show good printing quality and no signs of BADGE overpolymerization. Therefore, the implementation of EDAB as overpolymerization prevention additive is successful. Interestingly, the coloration of the parts is vastly different depending on the applied initiator. Samples printed by the use of the commercial Com-S-B appear much darker in color compared with S-B5. Lighter colors are advantageous since discoloration prevents application in several fields, where esthetics and optical properties are of interest. The hollow quadratic pyramid shape successfully printed to proof the concept of fabricating complex parts via hot lithography.

However, the removal of the parts from the metal building platform was challenging. The brittle nature of pure BADGE polymers increases the odds of breaking or cracking a part during the removal procedure. Such a crack can be seen in the base of the hollow quadratic pyramid, running from the left corner upwards in the direction of the right corner. Nevertheless, mechanical and material properties are not the focus of this work due to the investigation of S-B5 as new initiator for hot lithography compared with the commercial Com-S-B.

4.4.3. Characterization of the 3D-Printed Parts

4.4.3.1. Post-Curing and Coloration of the 3D-Printed Parts

In the next step, post curing of all parts was performed since a dark curing effect is present in all cationic photopolymerization. The liberated superacid remains in the final material and is able to increase the conversion over time, if stored at an appropriate temperature. To investigate the epoxy group conversions as well as color at different post-curing stages, a selection of parts was stored for 6 days at temperatures of 25 °C, 50 °C, 90 °C, 150 °C and 200 °C respectively. The rather long time period was selected to make sure no further increase

in EGC nor change in color would occur. After 72 h of post-curing, already no noticeable change in color was observed for the higher temperatures.

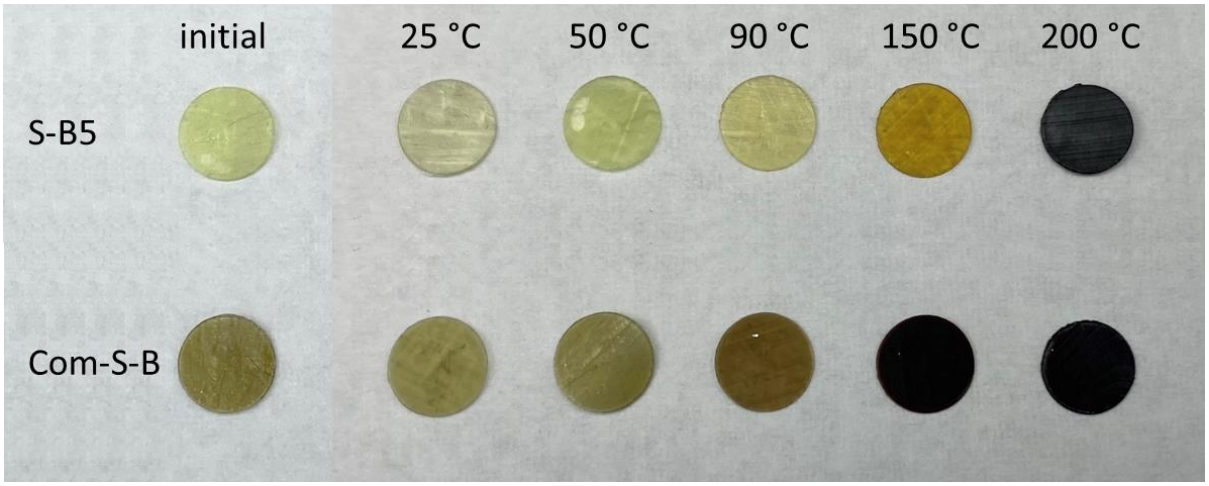

Figure 199: S-B5- and Com-S-B-based 3D printed discs after post-curing at different temperatures for 6 days

A distinct color difference of the initial S-B5 and Com-S-B discs was already noticed, however this trend continues as post-curing temperature is increased (Figure 199). Specifically, at 90 °C and 150 °C the difference in appearance is significant. Whereas S-B5 starts to slowly shifts towards brown, Com-S-B already produces brown and black parts. Compared to the initial printed parts, the set of discs post-cured at 25 °C and 50 °C do not show a significant discoloration. For S-B5, even the disc stored at 90 °C remains at its initial color. At 200 °C all specimens are already slightly degraded at the surface and completely back (Figure 200).

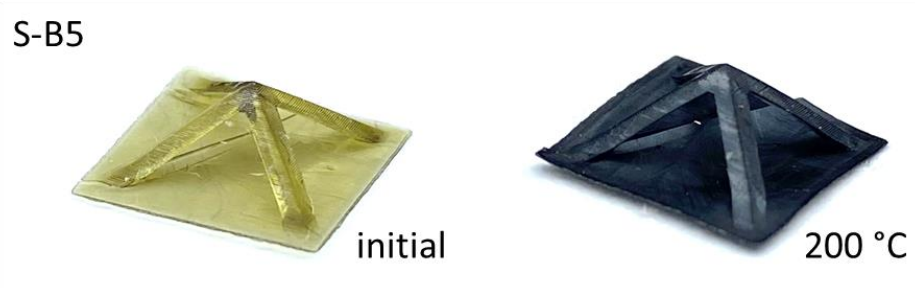

Figure 200: Color difference of the initially printed hollow quadratic pyramid and the post-cured one at 200 °C for 6 days

This circumstance can also be observed for the pyramid stored at such high temperatures.

4.4.3.2. Epoxy Group Conversion determined via ATR-FTIR

The epoxy group conversion (EGC) of the 3D-printed parts was determined using ATR-FTIR spectroscopy. The IR spectrum of the specimens was measured in the range of 4000 to 600 cm^{-1}. The epoxy group conversion was calculated by the difference of epoxy band integral before and after polymerization takes place. The band representing the epoxy group itself is located at a wavenumber of 914 cm^{-1}. The amount in decrease in area of this band correlates

with the EGC value (Equation 10). As reference bands, the aromatic ring of the monomer BADGE (828 cm^{-1}) and the phenyl ether of BADGE (1183 cm^{-1}) were selected. Three measurements for each specimen were carried out at three different locations across the sample surface.

The first layer of all bottom-up 3D printed specimens was cured twice to ensure good adhesion to the building platform, whereas all subsequent layers were only scanned once by the laser. Since the layer-by-layer printing of the parts was not performed homogeneously across the height of the parts, two different EGC values are obtained depending on the orientation of the disc on the ATR crystal. A slightly increased value is measured for the bottom layer of all parts since curing was more efficient due to double laser scanning. On average, the initial EGC determined 10 h after printing, starting from the bottom layer is around 5 - 10% higher compared with the one measured from the top of the discs. This on demand increase in EGC by irradiating twice can be useful for the fabrication thin supporting structures, which need higher strength compared to the remaining part. Therefore, the more representative EGC measured, starting from the top layer of the fabricated parts was only accounted for.

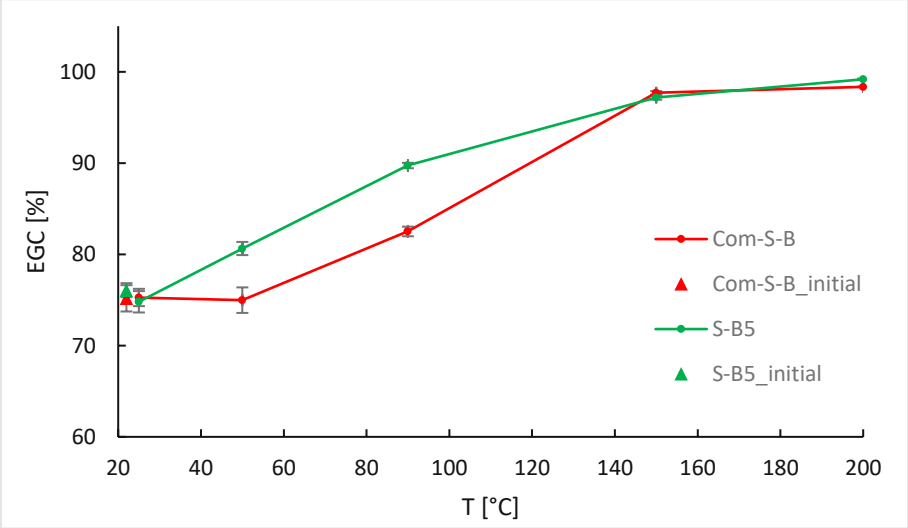

Figure 201: Epoxy group conversion versus post-curing temperature measured on the top layer surface of the discs stored for 6 days

The initial EGC are referred to the conversions present around 10 h after the 3D-print was finished and the parts collected. These initial conversion values are 75% for Com-S-B and 76% for the new borate S-B5 (Figure 201). Since BADGE represents a difunctional epoxy monomer, such high EGC already suggests that all monomer molecules are covalently bound statistically. Interestingly, post-curing at 25 °C for 6 days leads to no increase in EGC compared with the initial values. However, the borate S-B5 already outperforms the commercial Com-S-B

significantly if increased post-curing temperatures are applied. By achieving 81% at 50 °C and even 90% at 90 °C, S-B5 significantly outperforms the commercial initiator which measures much lower conversions of 75% and 83% at respective temperatures. Post-curing at 150 °C already equalizes the prior advantage of S-B5 since both sulfonium salts reach 97% conversion. With above 99% EGC, post-curing at 200 °C leads to practically full conversion. However, a major drawback remains the partial degradation of the part surface at such high temperatures. Recorded IR-spectra of the parts prove the optically suggested degradation. Therefore, post-curing at 200 °C is not recommended for BADGE-based parts due to degradation issues. Much more advantageous are temperatures ranging from 50 °C up to 150 °C depending on the desired EGC.

4.4.3.3. Layer Quality determined by Light Microscopy

Sufficient layer quality and precision as well as no overpolymerization is desired for high quality 3D-printed objects. Therefore, the hexagonal pyramids printed via hot lithography were post-cured at a selection of temperatures and the around 50 µm thin layers analyzed via light microscopy. Microscopy was performed on a Keyence VHX-S550E digital multi scan microscope equipped with a lens system capable of x200 up to x2000 magnification.

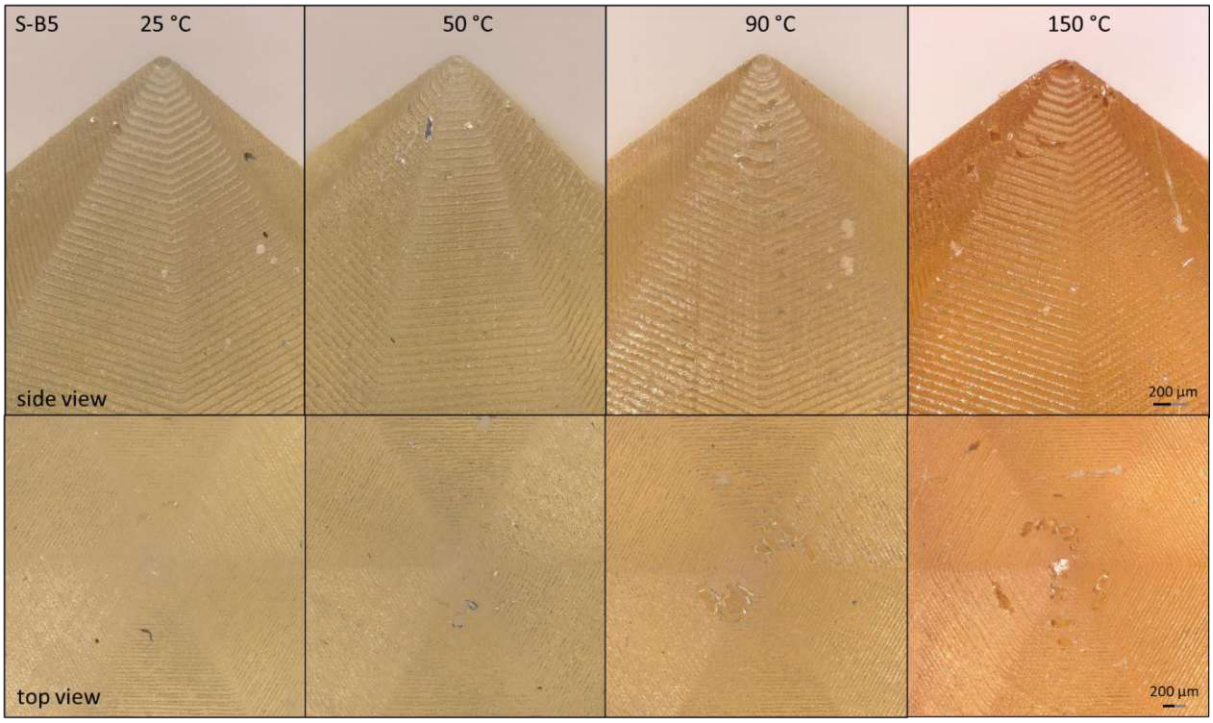

Figure 202: S-B5-based 3D-printed hexagonal pyramids after post-curing at different temperatures for 6 days in side view (40 ° tilt) and top view

The hexagonal pyramids fabricated by hot lithography were photographed from side and top view (Figure 202). As expected, S-B5 produces lightly colored parts and only starts to discolor towards orange at 150 °C post curing temperature. By analyzing the individual layers of the pyramids, a regular layer distribution at high quality can be obtained. At this magnification, overpolymerization is not present. At some locations, artifacts originating from the 3D-printing job are detected with a tendency of being more frequent at increased storage temperatures. However, those irregularities can be avoided by fine tuning the printing conditions and are not related to S-B5's performance as initiator. The hollow quadradic pyramid was imaged next (Figure 203 & Figure 204).

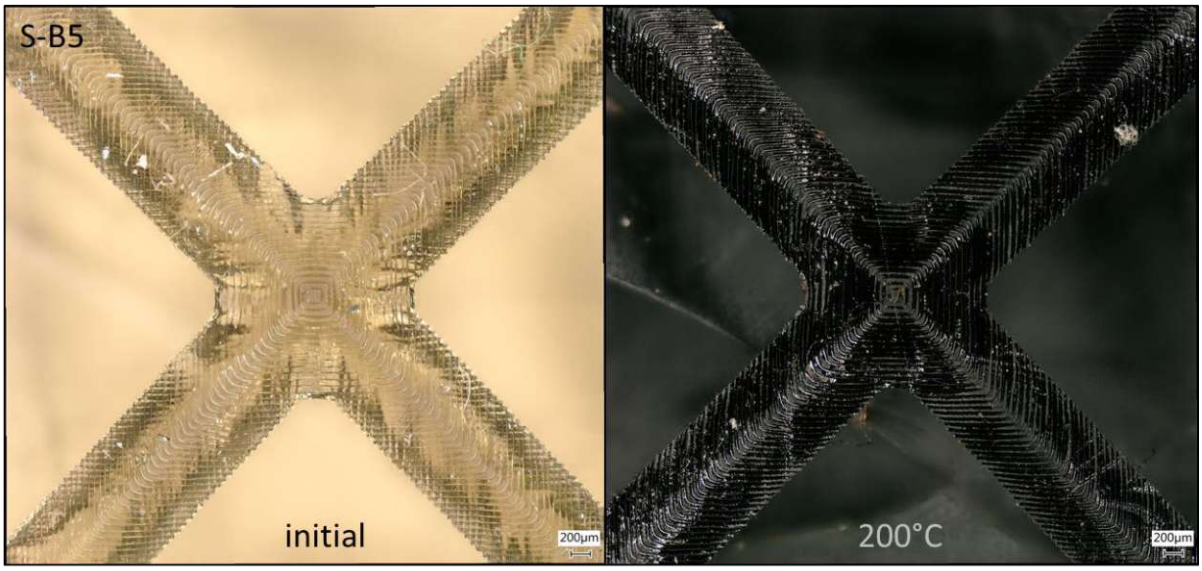

Figure 203: Initial S-B5-based 3D-printed quadratic hollow pyramid and after post-curing at 200 °C for 6 days in top view

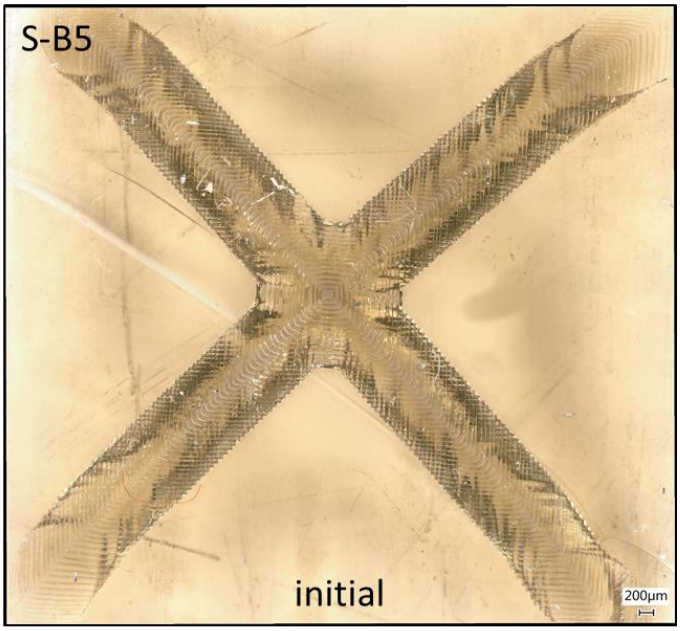

Figure 204: Initial S-B5-based 3D-printed quadratic hollow pyramid in top view

By analyzing the top part of the quadratic hollow pyramid from top view, high quality layers are visible without any artifacts. In addition, a picture of the entire pyramid was taken.

4.4.3.4. Layer Quality determined by SEM

The 3D printed parts were characterized via scanning electron microscopy (SEM) to determine layer quality. Prior to imaging with a Phillips XL-30, the parts were coated with a thin gold layer via sputtering to ensure electrical conductivity or the polymer samples. Images in the range of x19 to x500 magnification were taken.

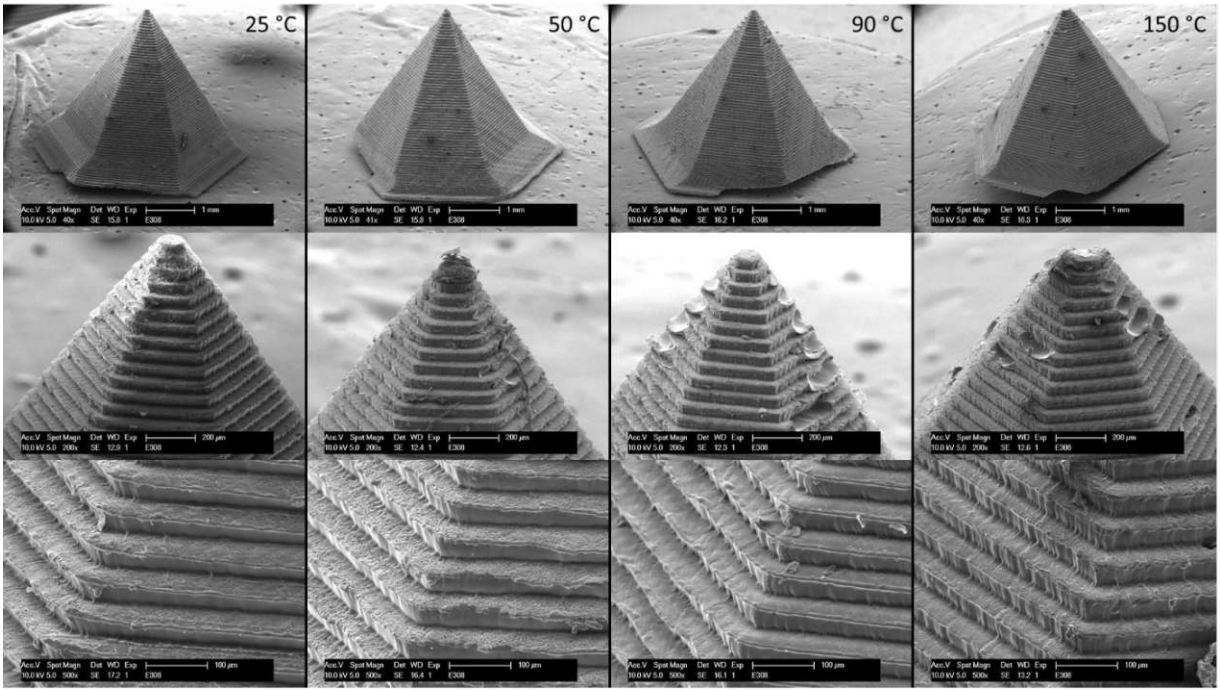

Figure 205: S-B5-based 3D-printed hexagonal pyramids after post-curing at different temperatures for 6 days in three different magnification modes (x40, x200 and x500)

The hexagonal pyramids stored at 25 °C and 50 °C show the lowest number of artefacts on the surface (Figure 205). Parts post-cured at 90 °C and 150 °C tend to have more of those irregularities, especially at the tip of the pyramid, detectable in the x200 magnification images. By investigating the x500 magnifications, well-defined and high quality layers are obtained in all four parts. However, the samples stored at increased temperatures show slightly enhanced interlayer fusion.

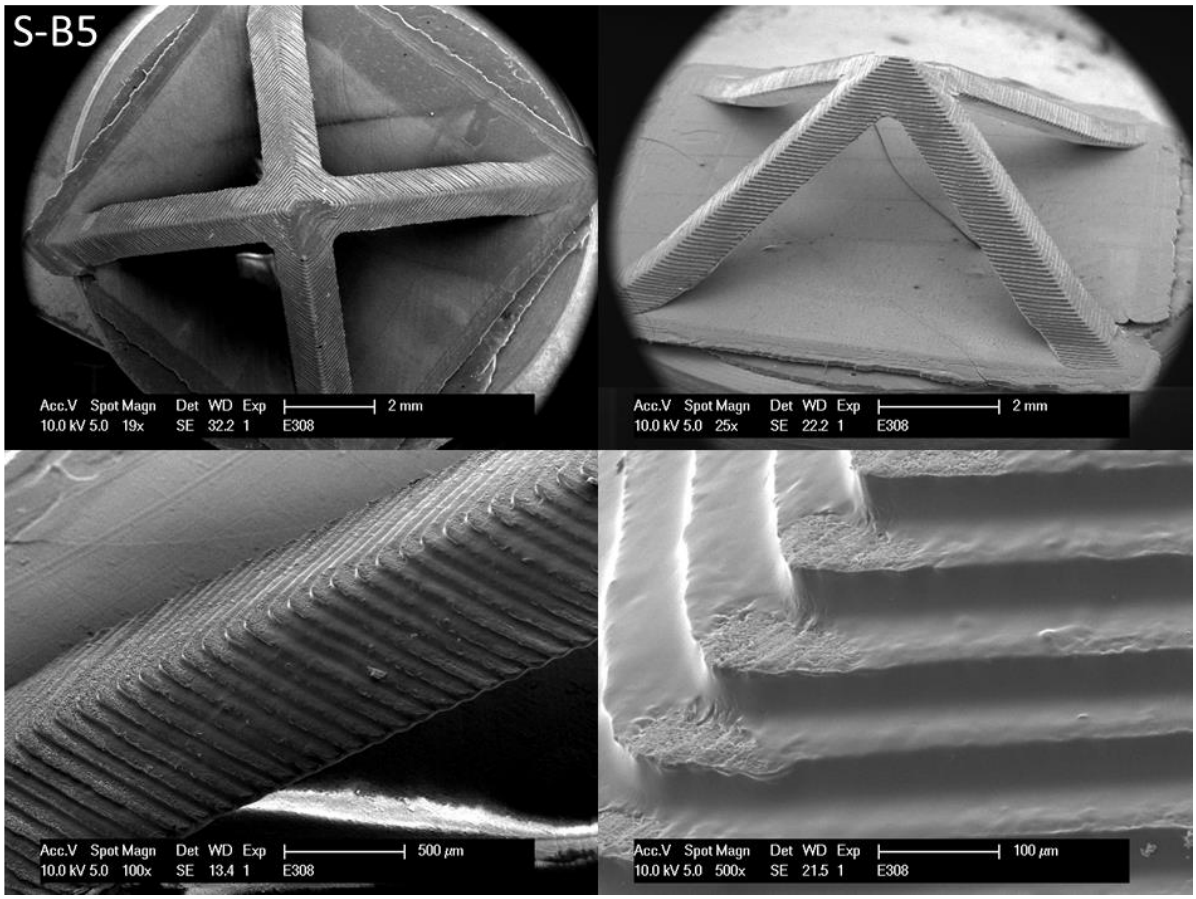

Figure 206: Initial S-B5-based 3D-printed quadratic hollow pyramid in selected views at four different magnification modes (x19, x25, x100 and x500)

By imaging the quadratic hollow pyramid via SEM, high quality and well-defined layers can be seen especially in the x100 and x500 magnifications (Figure 206). Overall, imaging via SEM of the successfully printed parts show no overpolymerization, proofing the positive effect of small amounts of the additive EDAB in the formulations.

III. Metal-Free Ring-Opening Metathesis Polymerization

1. State of the Art

Ruthenium catalysts are highly active metathesis catalysts with tolerance towards most functional groups as well as moisture- and oxygen-resistance (Figure 207). Additionally, ruthenium-based high active catalysts are suitable for aqueous ROMP reactions.[202]

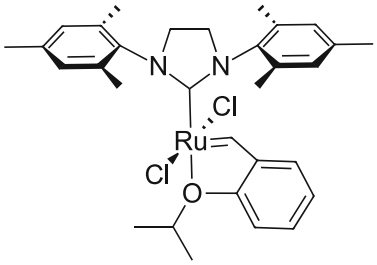

Figure 207: Ruthenium-based highly stable catalyst for aqueous media[202]

For applications in photoinitiated ROMP, ruthenium-based NHC complexes with sulfur-chelates and phosphite ligands represent highly active, light-switchable catalysts (Figure 208). Capable of polymerizing various alkenes such as norbornenes, cyclooctenes, norbornenes or other nitrogen-based heterocycles with reactive double bonds. Conversions above 90% are reached with many different monomers. However, ROMP reactions are performed with 0.5 M monomer in dichloromethane or toluene after several hours of irradiation with UV-light.[102]

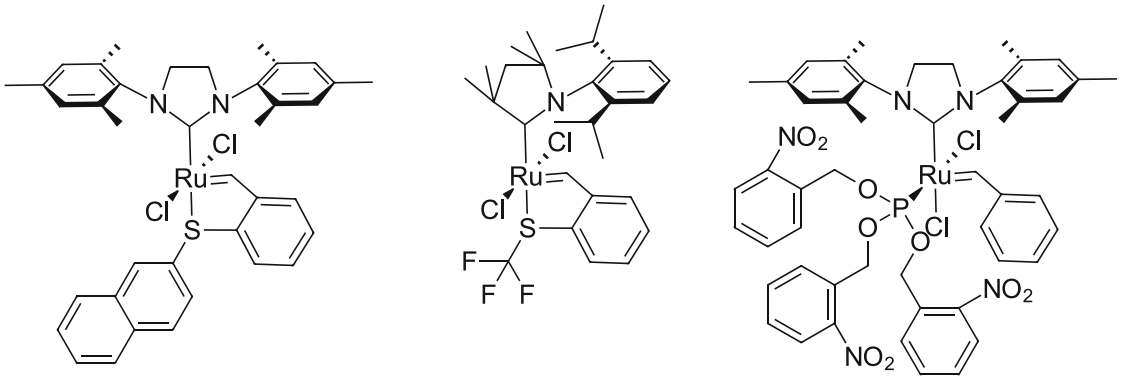

Figure 208: Sulfur-chelated and phosphite-ligated photoactive metathesis catalysts[102]

Very similar ruthenium catalysts with phosphite ligands, as well as a commercial catalyst named HeatMet were tested by Legzizamon et al. in combination with photo-sensitizers such as the thioxanthone ITX (Figure 209).[203] These cyclopentadiene-based, photoinitiatable formulations show promising results in terms of reactivity, mechanical properties of the specimens and are even applied in 3D-printing.

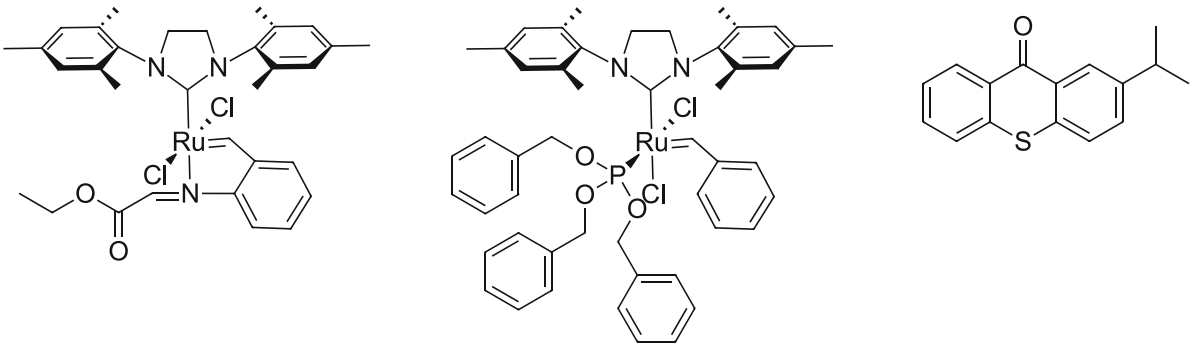

Figure 209: Nitrogen-chelated (HeatMet) and phosphite-ligated ruthenium catalyst and the sensitizer ITX[203]

Compared to formulations without the photosensitizer, exposure times to achieve a stable cured material were in the range of 30 to 60 s. By adding ITX and ruthenium catalyst HeatMet to DCPD and irradiating it with an UV-source (365 nm LED), a gelation of the formulations can be achieved after less than 5 seconds. This significant improvement in reactivity lead to much faster printing speeds.

In photoredox-mediated MF-ROMP, the state-of-the-art mediators are based on methoxylated pyrylium- and thiopyrylium tetrafluoroborates (Figure 210). Enol ethers are used as initiators to start the chain-growth reaction via oxidation by the mediator. Conversions up to 84% and Đ of around 1.5 in norbornene and a mixture of norbornene and methoxy norbornene are reached in under 2 hours. The irradiation source was a blue LED light and the ROMP reaction was conducted in a dichloro methane solution.[111, 112]

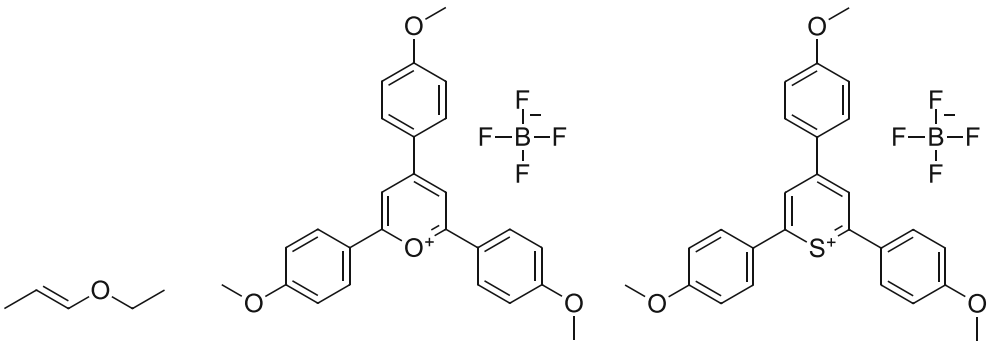

Figure 210: Ethyl propenyl ether, pyrylium- and thiopyrylium tetrafluoroborate

Metal-free catalysts for ROMP have to ensure high conversions and low Đ. Additionally, the tolerance towards functional groups has to be enhanced, since the metal-based counterparts generally show high compatibility with a variety of functionalities.

2. Potential new Initiators for Photoredox-mediated ROMP

The target molecules are photoactive compounds which upon irradiation with a suitable light source oxidize enol ethers. The pyrylium photoredox mediator is able to perform this oxidation reaction multiple times until it is fragmented by undesired side reactions, discoloring the reaction solution slowly over time (Figure 211).[111]

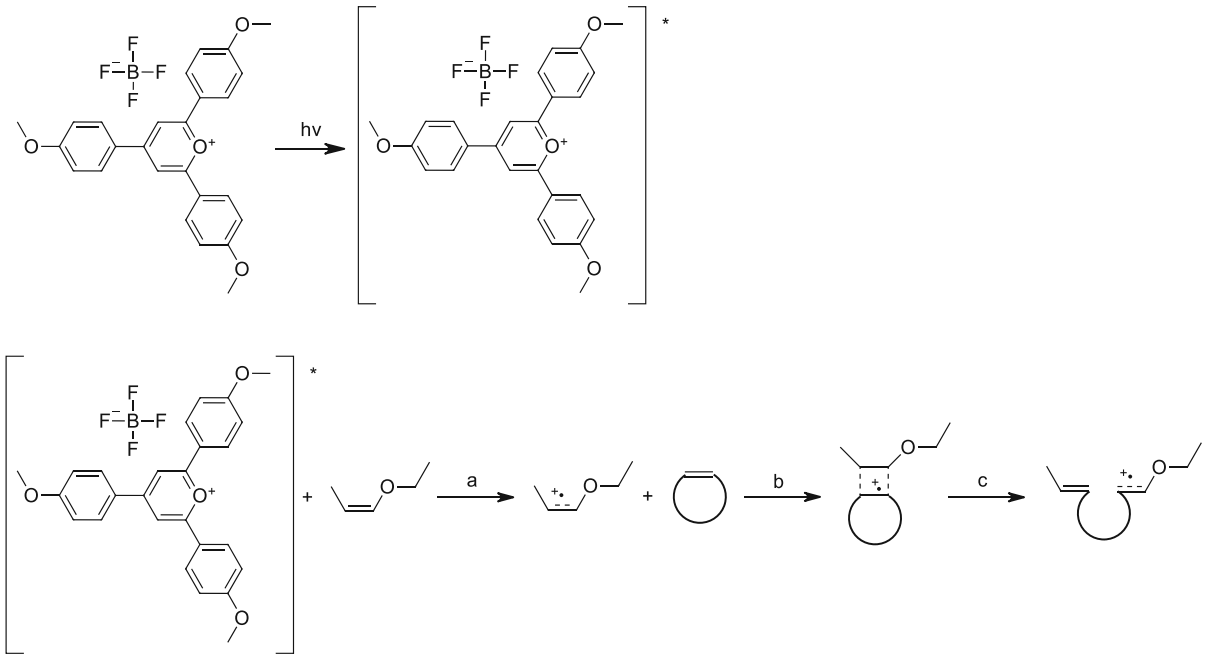

Figure 211: Generation of the excited state of the pyrylium salt and photoredox-mediated metal-free ROMP initiation step with ethyl propenyl ether

Upon irradiation the pyrylium salt enters its excited state and is able to perform an electron transfer. The initiation step consists of the reduction of the enol ether and the formation of a radical cation (a). In a second step, a strained cyclic alkene reacts with the radical cation to form a four-membered intermediate state (b). With the release of ring strain, the cyclobutene radical cation undergoes ring opening (c). Afterwards, more monomer molecules are added and the growing chain is propagating until termination occurs.[111] According to the state-of-the-art mediators for photoredox-mediated MF-ROMP, pyrylium salts are the targeted mediator class (Figure 212).

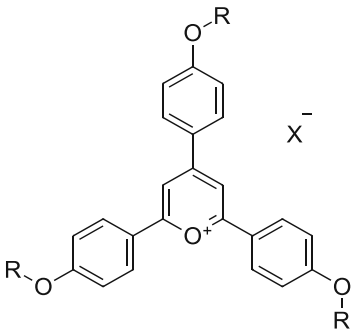

Figure 212: General structure of an alkoxylated pyrylium salt (X^-… non-nucleophilic anion)

Alkoxylation of the phenyl rings is advantageous, since pyrylium salts are quite polar molecules despite their abundant aromatic moieties. Solubility is tremendously enhanced by the introduction of long and preferably branched alkoxy chains. The counter ion X is represented by a non-nucleophilic anion, due to lower coordination with the positively charged pyrylium center. Tetrafluoroborates are low toxicity, broadly commercially available and low cost. Thereby BF_4 is a compelling counterion for the target molecules.

Once synthesized the targeted pyrylium salts described above should be mixed with ROMP monomers for further studies. Comparison of reactivity, functional group tolerance and stability of the resulting formulations in solution are pursued.

3. ROMP Monomers

3.1. Synthesis

In advance of the photoredox mediator synthesis, commercially available ROMP monomers were acquired (Figure 213). Broadly used norbornene and dicyclopentadiene as well as norbornene derivatives were added to the portfolio. The following multifunctional monomers were selected due to easy access to modification after polymerization. The remaining double bonds in the final ROMP polymer material can be subject to cross-lining, vulcanization or sulfonation for example.[204]

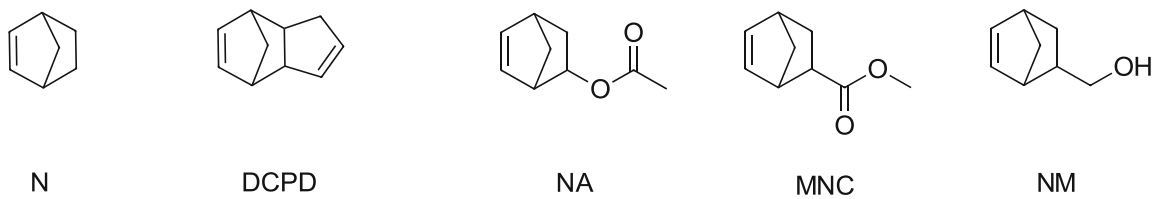

Figure 213: Norbornene (N), dicyclopentadiene (DCPD), norbornene acetate (NA), methyl norbornene carboxylate (MNC) and norbornene methanol (NM)

In addition to the purchased monomers, selected norbornene ethers were synthesized. The expectation is better compatibility with the pyrylium-based mediators, since they are not known for their tolerance towards many functionalities.

3.1.1. 5-(Butoxymehtyl)-2-norbornene

First, the butoxymethyl derivative of norbornene was synthesized. According to Liu et al. a synthesis pathway was planned (Figure 214).[205]

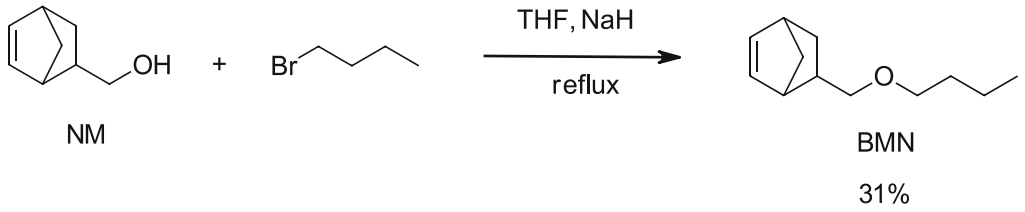

Figure 214: Synthesis of 5-(Butoxymehtyl)-2-norbornene (BMN)

Therefore, a classic ether synthesis with norbornene methanol as starting material and 1-bromobutane was carried out.

3.1.2. 5-(Methoxymethyl)-2-norbornene

Since butoxymethyl norbornene BMN has a bulky butoxy group, which may lead to problems during the ROMP reaction, a norbornene derivative with a shorter chain was aimed for (Figure 215).

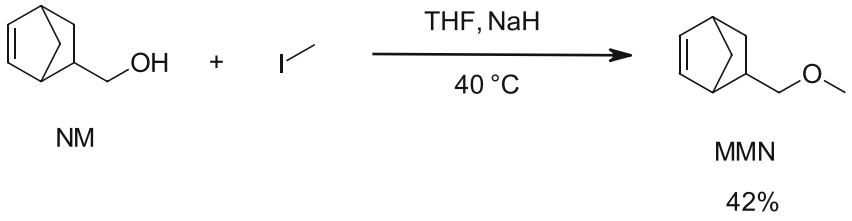

Figure 215: Synthesis of 5-(Methoxymethyl)-2-norbornene (MMN)

A procedure similar Lu et al.[111] was carried out. NM was reacted with iodomethane to result in MMN.

4. Photoredox-Mediators

4.1. Synthesis

Since a well-known pyrylium-based photoredox mediator is commercially available, the Com-P-B compound was acquired (Figure 216). However, the trimethoxy pyrylium tetrafluoroborate shows poor solubility in extremely non-polar monomers like norbornene.

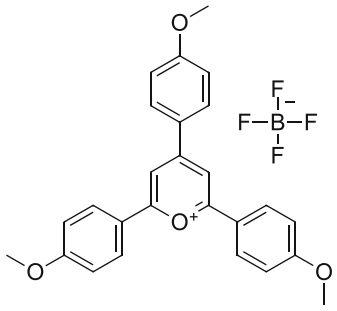

Figure 216: 2,4,6-Tris(4-methoxyphenyl) pyrylium tetrafluoroborate (Com-P-B)

Due to already mentioned solubility issues in common ROMP monomers, a strategy towards less polar pyrylium salts was established. In a first approach, polarity is decreased by exchangeing the anion with a bulkier and/or weaker coordinating one. A second approach introduces longer and branched alkoxy moieties instead of methoxy groups. Therefore, polarity is decreased significantly as well. Hence, a selection of differently alkoxylated pyrylium salts paired with a variety of counterions were targeted to be synthesized. As a consequence, the influence of different pyrylium cations as well as the influence of various anions on MF-ROMP can be investigated.

4.1.1. Pyrylium Tetrafluoroborates

4.1.1.1. 4(4-Declyoxyphenyl)-2,6-(4-methoxyphenyl) Pyrylium Tetrafluoroborate

The first targeted molecule was a pyrylium salt with an alkoxy chain attached to one of its aromatic moieties to enhance solubility (Figure 217).

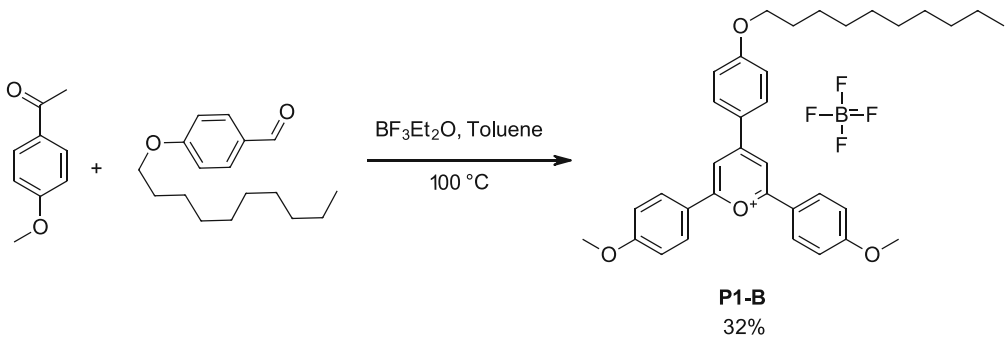

Figure 217: Synthesis of 4(4-decyloxyphenyl)-2,6-(4-methoxyphenyl) pyrylium tetrafluoroborate (P1-B)

The common solution to this problem is the introduction of alkoxy groups into the iodonium salts, as used in industry.[169] By reacting 4-methoxy acetophenone with 4-decyloxy benzaldehyde similar to a procedure from Breder et al.,[206] the desired pyrylium salt P1-B was obtained.

4.1.1.2. 4(4-Declyoxyphenyl)-2,6(4-ethylhexanoxyphenyl) Pyrylium Tetrafluoroborate

Despite the non-polar decyloxy chain introduction, the P1-B cation still suffered from poor solubility in ROMP monomers such as norbornene or methoxymethyl norbornene. Therefore, another approach towards non-polar substituents was carried out. To introduce even more non-polar moieties to the photoredox mediator molecule, a new pyrylium salt was aimed for. An acetophenone precursor was targeted to later be converted into a pyrylium salt. To achieve a decrease in polarity in the final photoredox-mediator, a 2-ethyl-hexyl moiety was introduced. Therefore, a synthesis similar to Hudkins et al. was carried out.[207] By reacting ethylhexyl acetophenone with decyloxy benzaldehyde similar to a synthesis by Fortage et al. the highly alkoxylated product P2-Cl was targeted (Figure 218).[168]

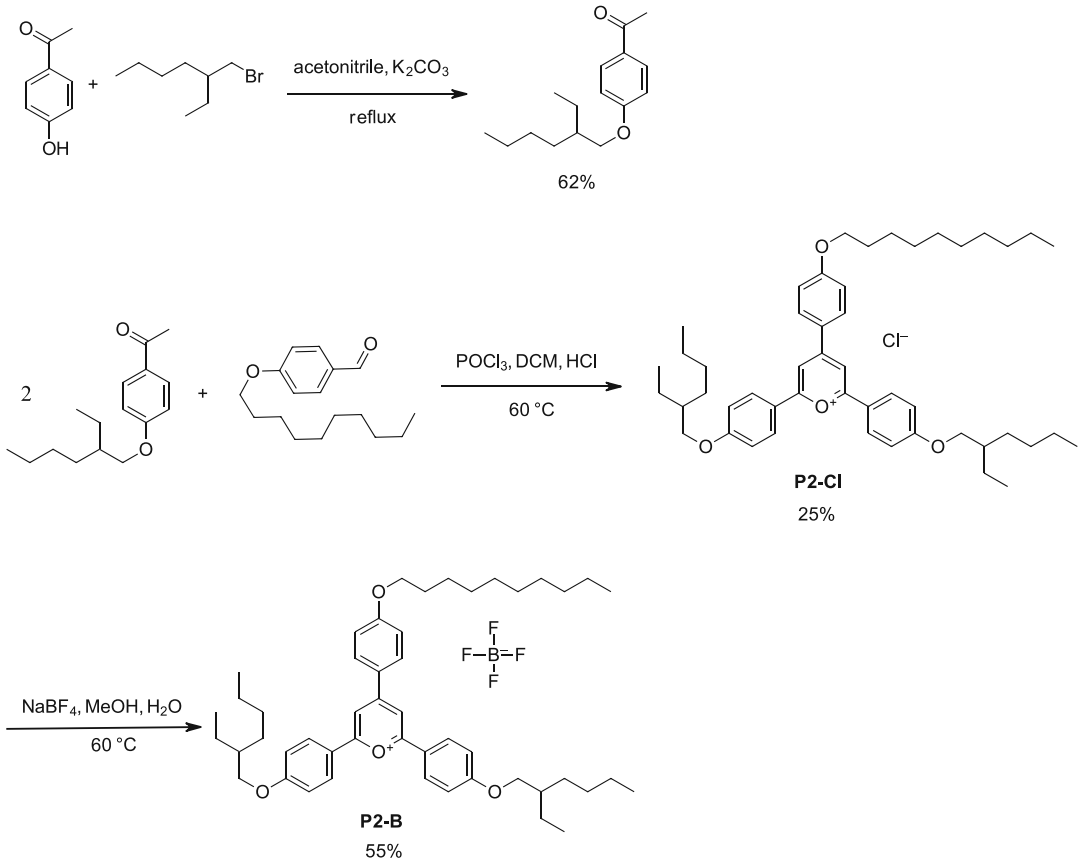

Figure 218: Synthesis pathway to achieve 4(4-declyoxyphenyl)-2,6(4-ethylhexanoxyphenyl) pyrylium tetrafluoroborate (P2-B)

In a second step a metathesis reaction to the tetrafluoroborate similar to Li et al. was aimed for.[129] The resulting product P2-B shows extremely high non-polarity. Solubility in monomers

like norbornene or MMN should be enhanced significantly compared to previously synthesized pyrylium salts.

4.1.2. Pyrylium Hexafluoroantimonates and Tetraphenylborates

4.1.2.1. 4(4-Decyloxyphenyl)-2,6(4-methoxyphenyl) Pyrylium Hexafluoroantimonate

Similar to the previously synthesized P1-P, the SbF_6 salt was targeted (Figure 219). Less nucleophilicity leads to lower coordination strength to the cationic chain end of the fast-growing MF-ROMP polymer, therefore the propagation can take place more efficiently. Therefore, perfluorinated anions such as hexafluorophosphates and hexafluoroantimonates were targeted. The easy to access P1-Sb broadens the selection of P1-based pyrylium salts to compare the anions influence later on.

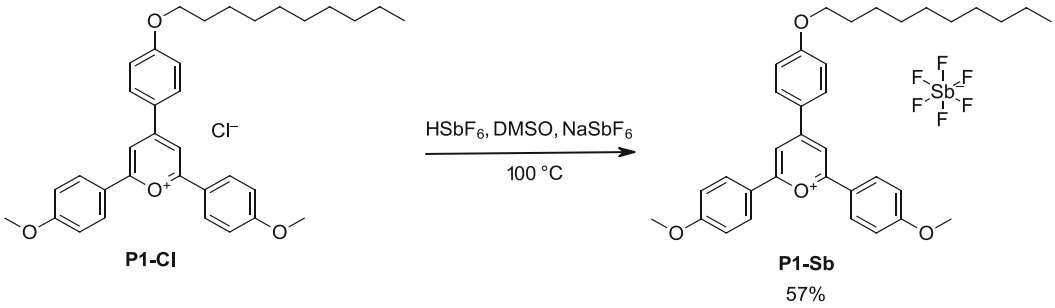

Figure 219: Synthesis of 4(4-decyloxyphenyl)-2,6(4-methoxyphenyl) pyrylium hexafluoroantimonate (P1-Sb)

4(4-decyloxyphenyl)-2,6(4-methoxyphenyl) pyrylium hexafluoroantimonate was synthesized similar to a patent of Tavares. et al.[160]

4.1.2.2. 4(4-Decyloxyphenyl)-2,6(4-methoxyphenyl) Pyrylium Tetraphenylborate

To better investigate the influence of the anion, to the selection of already synthesized salts a tetraphenylborate was added. This salt promises even better solubility in non-polar monomers due to its four aromatic moieties present in the anion (Figure 220).

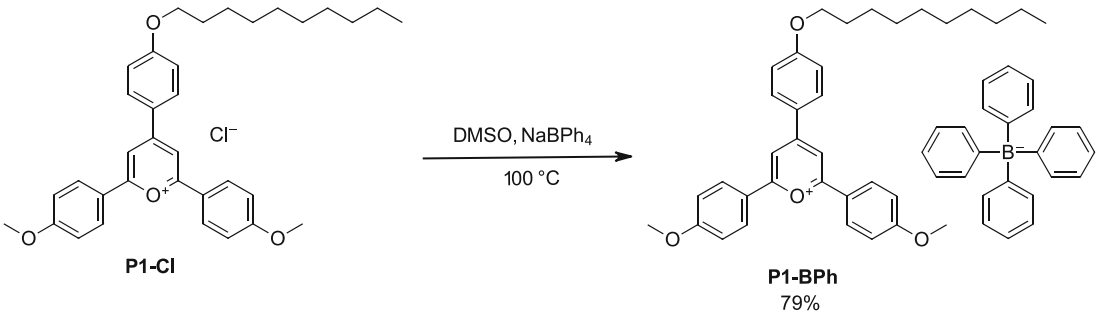

Figure 220: Synthesis of 4(4-decyloxyphenyl)-2,6(4-methoxyphenyl) pyrylium tetraphenylborate (P1-BPh)

4(4-decyloxyphenyl)-2,6(4-methoxyphenyl) pyrylium tetraphenylborate was synthesized similar to the work of Li et al.[129]

4.1.3. Pyrylium Hexafluorophosphates

4.1.3.1. 4(4-Decyloxyphenyl)-2,6(4-methoxyphenyl) Pyrylium Hexafluorophosphate

Next, a hexafluorophosphate together with the P1 cation was targeted. 4(4-Decyloxyphenyl)-2,6(4-ethylhexanoxyphenyl) pyrylium chloride was synthesized as a precursor in accordance to the work of Fortage et al. (Figure 221).[168]

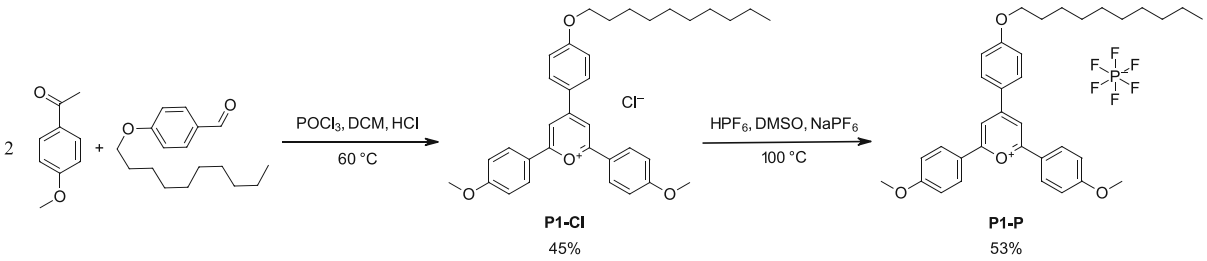

Figure 221: Synthesis pathway to achieve 4(4-decyloxyphenyl)-2,6(4-methoxyphenyl) pyrylium hexafluorophosphate (P1-P)

The subsequent hexafluorophosphate was synthesized similar to a patent of Tavares. et al.[160]

4.1.3.2. 4(4-Decyloxyphenyl)-2,6(4-ethylhexanoxyphenyl) Pyrylium Hexafluorophosphate

In addition to the already synthesized P2-B tetrafluoroborate, the less nucleophilic PF_6 salt P2-P was aimed for (Figure 222). Subsequently broadening the variation of cations and anions further.

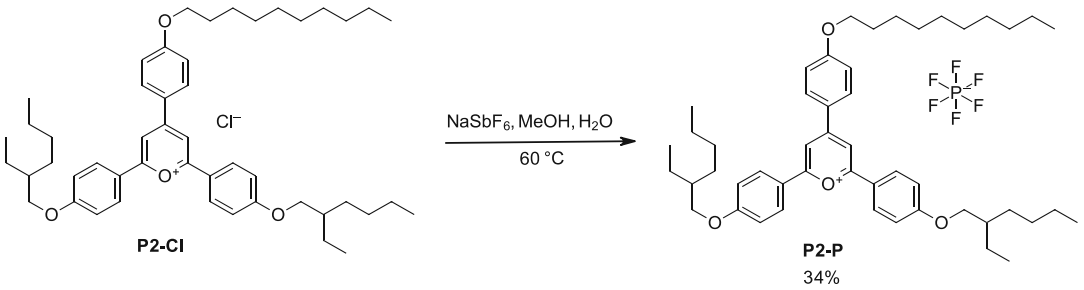

Figure 222: Synthesis of 4(4-decyloxyphenyl)-2,6(4-ethylhexanoxyphenyl) pyrylium hexafluorophosphate (P2-P)

4(4-decyloxyphenyl)-2,6(4-ethylhexanoxyphenyl) pyrylium hexafluorophosphate was synthesized similar to the work of Li et al.[129]

4.1.3.3. 4(4-Octadecyloxyphenyl)-2,6(4-methoxyphenyl) Pyrylium Hexafluorophosphate

A final approach to obtain highly non-polar pyrylium salts was pursued. Similar to the already synthesized decoxylated cation P1, an even longer alkoxy chain was targeted. 4(4-Octadecyloxyphenyl)-2,6(4-methoxyphenyl) pyrylium chloride was synthesized as a precursor similar to the work of Fortage et al. (Figure 223).[168]

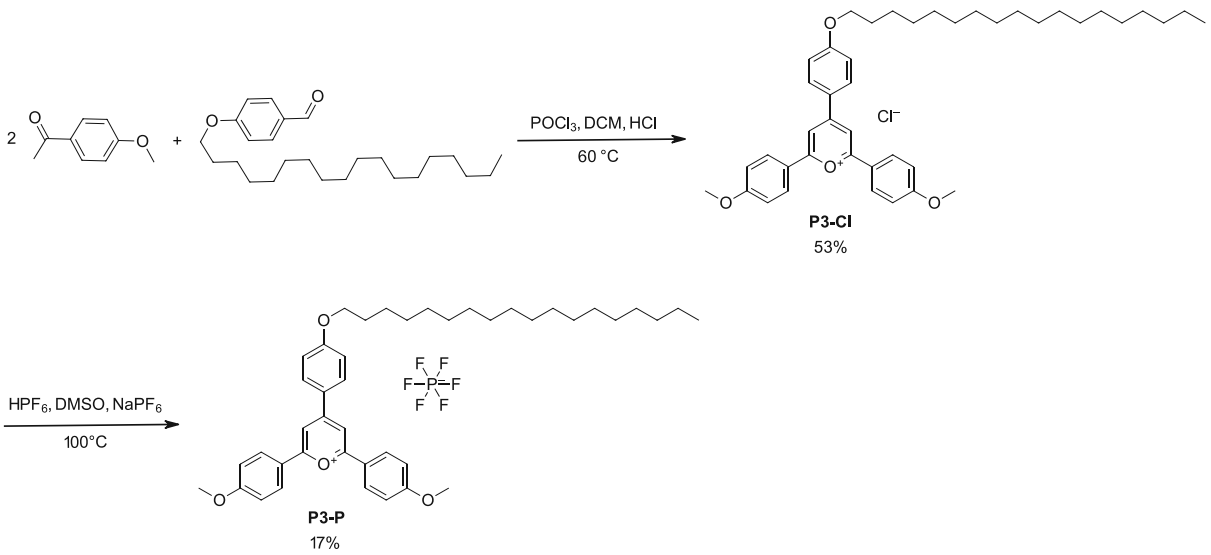

Figure 223: Synthesis pathway to achieve 4(4-octadecyloxyphenyl)-2,6(4-methoxyphenyl) pyrylium hexafluorophosphate (P3-P)

The hexafluorophosphate salt was synthesized in a metathesis reaction similar to a patent of Tavares. et al.[160]

4.2. Characterization of Photoredox-Mediators based on Pyrylium Salts

4.2.1. Selection of the Photoredox-Mediators and ROMP Monomers

Since synthesis of all aimed pyrylium salts was successful, a selection of the compounds was conducted (Figure 63). Additionally, the purchased reference molecule Com-P-B for MF-ROMP was added to the selection. The selection provides many versions of mediators including two differently substituted tetrafluoroborates pyrylium salts to be compared directly to the reference compound. Influences of the counterions can also be investigated further, since the P1 cations are paired with a total of four distinct anions. The two remaining salts P2-P and P3-P represent the most promising candidates for MF-ROMP since they share a weakly coordinating, non-heavy metal-containing hexafluorophosphate anion as well as high alkoxylation.

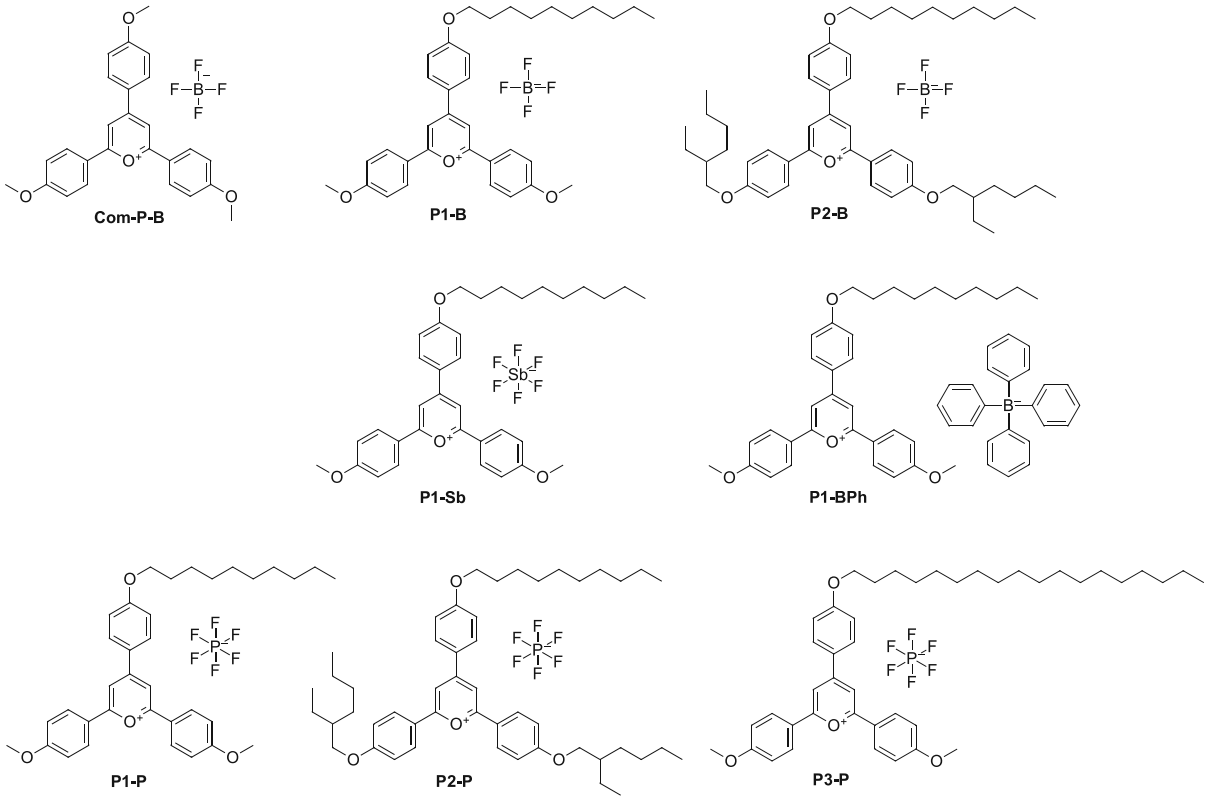

Figure 224: Selection of pyrylium-based photoredox-mediators

The two aimed norbornene-based monomers BMN and MMN were synthesized in high yields and selected together with commercially acquired ROMP-monomers for further testing (Figure 225).

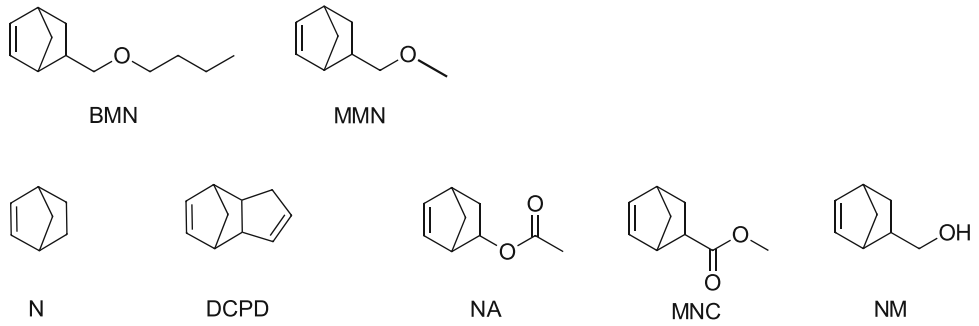

Figure 225: Selection of the ROMP monomers

The collection of monomers and metal-free ROMP mediators can be used for preparation of formulations. Those formulations are then tested regarding reactivity, stability and tolerance towards functional groups of the mediators.

4.2.2. Absorption Spectra determined via UV-VIS Experiments

First, the absorption behavior of the photoredox mediators was investigated. During the photochemical analysis, the ultraviolet (UV) and visible light (VIS) absorption spectra of the onium compounds were determined. The wavelength range to scan started at 800 nm and went down to 250 nm. Onium salt and concentrations of 1 x 10^{-5} mol L^{-1} were used.

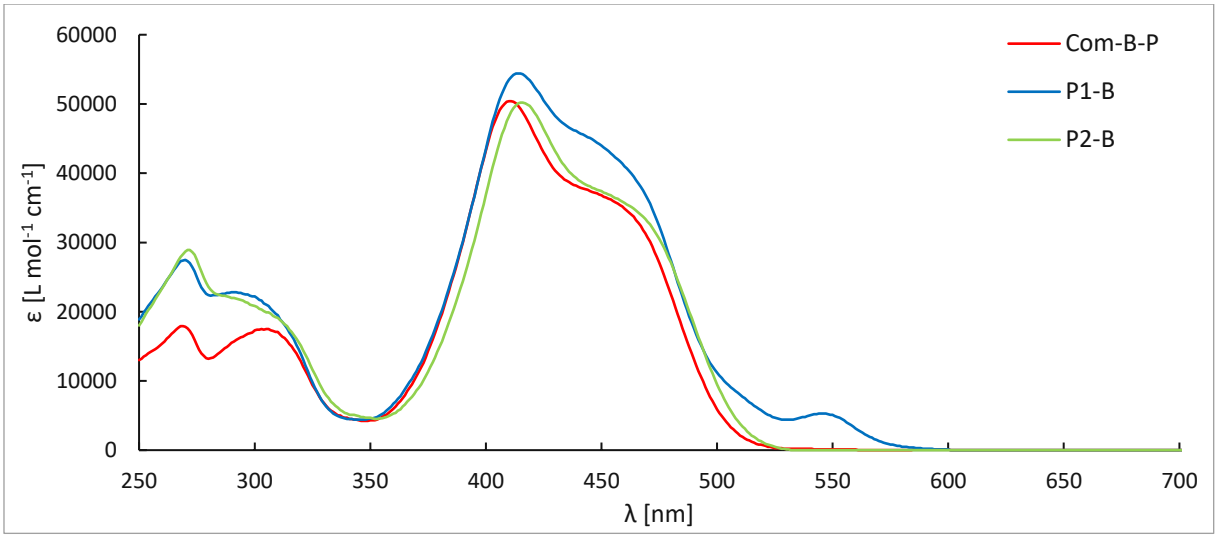

Figure 226: Wavelength dependence of the molar extinction coefficient for the pyrylium tetrafluoroborates

As expected by comparing the different pyrylium tetrafluoroborates, no practical difference in the spectra can be observed (Figure 65). The absorption maximum is for all three salts in the 413 nm to 417 nm at an extinction coefficient of around 50,000 L mol^{-1} cm^{-1}. All selected pyrylium salts share nearly the same chromophores in the cation, resulting in a spectrum with little distinctions. Altering the alkyl chains at the alkoxy site(s) of the pyrylium molecule with non-chromophores only shifts absorption maxima by a minor amount.

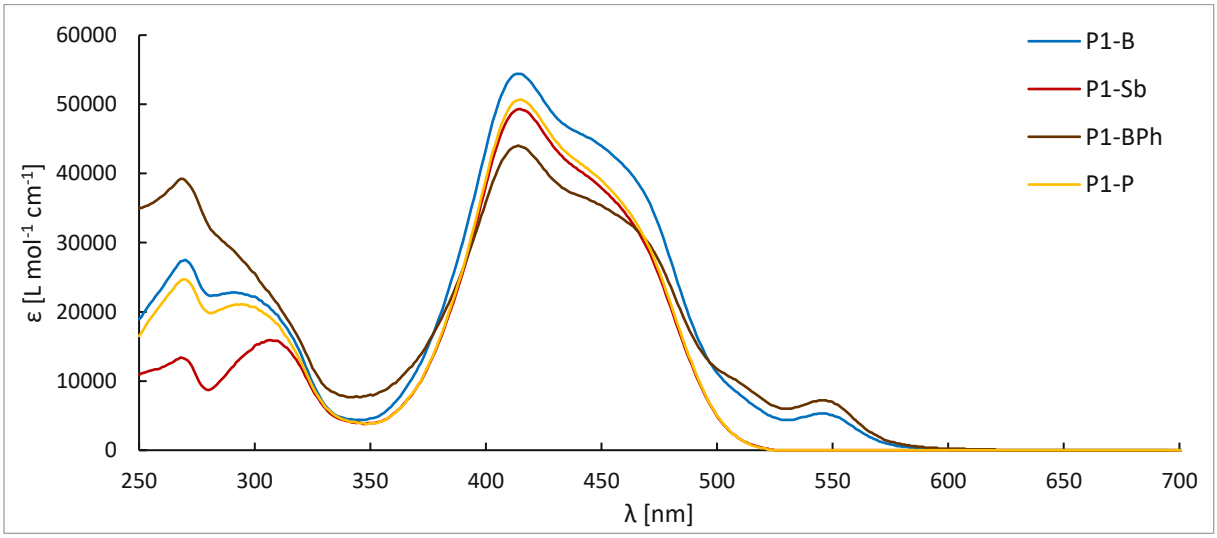

Figure 227: Wavelength dependence of the molar extinction coefficient for the 1De2Me-P pyrylium cation paired with different anions

By comparing the pyrylium salts regarding their paired counterion, a similar result is observed (Figure 227). The detected maxima in the scanned range are between 415 nm and 417 nm with very similar extinction coefficient values. It is known, that anions do not influence the photochemistry of onium salts, therefore proofing a point with this series of measurements.[37]

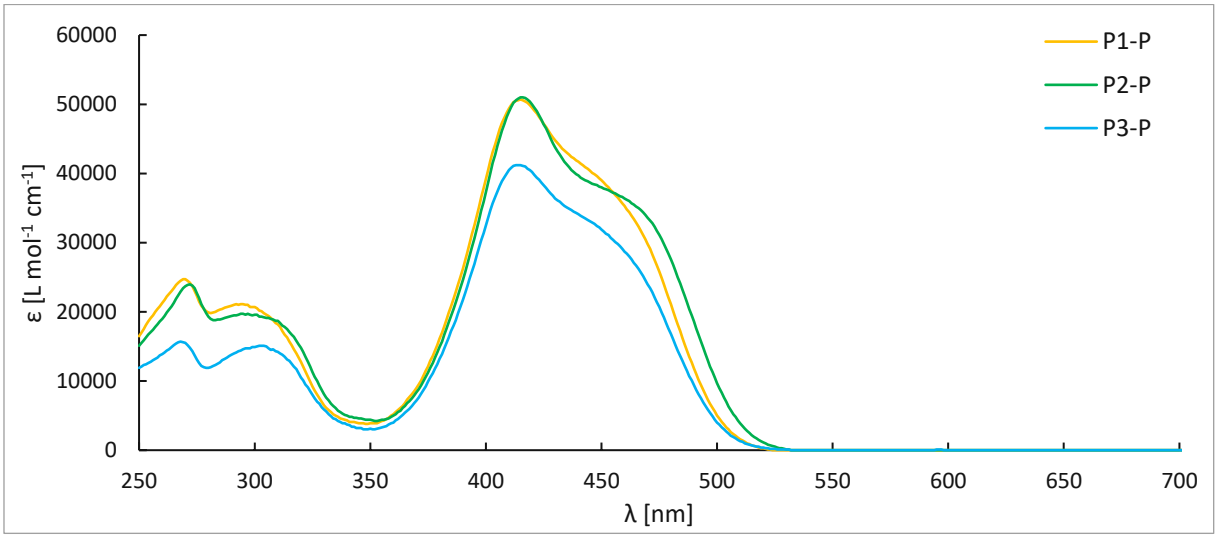

Figure 228: Wavelength dependence of the molar extinction coefficient for the pyrylium hexafluorophosphates

By comparing the pyrylium hexafluorophosphates, their different degree of alkoxylation only results in little variation of the spectra (Figure 228). All three salts exhibit their highest extinction of around 50,000 L mol^{-1} cm^{-1} in the very slim wavelength window of 416 nm to 418 nm.

With the absorption spectra of all selected pyrylium salts recorded, an appropriate light source can be selected for the following photochemical experiments.

4.3. Photoredox-mediated MF-ROMP in Solution

4.3.1. Preparation of the Formulations

To investigate the ROMP efficiency of the initiator-mediator pair, appropriate formulations were prepared, based on selected ROMP monomers in combination with the pyrylium mediators. The initiating species is represented by enol ethers such as ethyl propenyl ether EPE and to undergo ROMP, combined with selected pyrylium salts (Figure 229). The selected solvent for the polymerization experiments in solution is deuterated dichloromethane to make NMR analysis during the polymerization progress straighter forward.

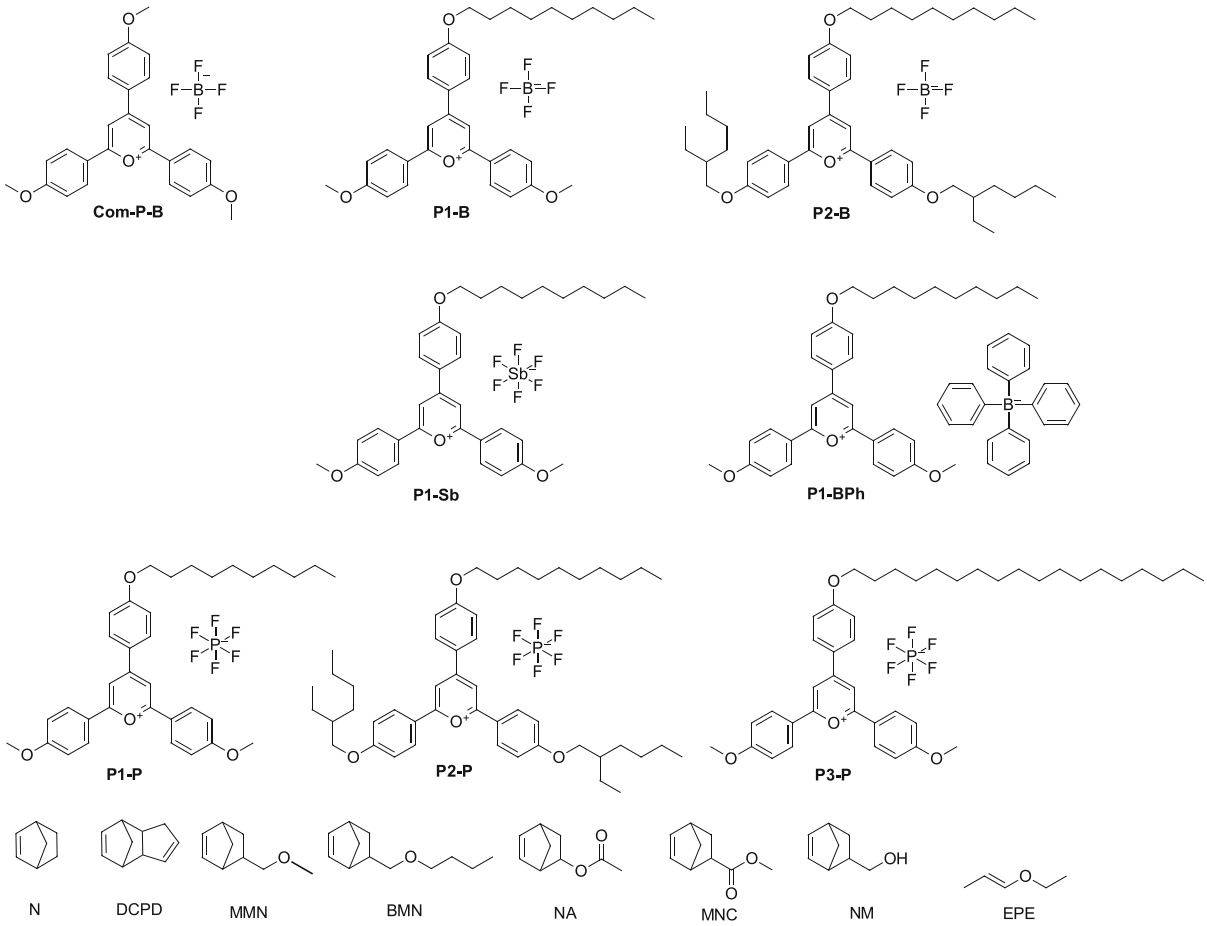

Figure 229: Photoredox-mediators, ROMP monomers N, DCPD and MMN as well as the enol ether-based initiator EPE

The norbornene-based monomers BMN, NA, MNC and NM include functionalities such as esters, bulky ethers and hydroxy groups, which turn out to be unsuitable for MF-ROMP. However, the non-tolerance of pyrylium photoredox-mediators towards mentioned functional groups is described in literature.[111] The molar ratios of mediator to initiator to monomer was set to 0.03 : 1 : 100 respectively for homopolymerization experiments. For the copolymerization experiments of norbornene and MMN, the molar ratio of mediator to initiator to monomer to comonomer was set to 0.03 : 1 : 90 : 10 respectively. These ratios mentioned above are known to function best in 1.9 M dichloromethane solutions.[112] Since halogens are highly nucleophilic bases, none of the synthesized pyrylium chlorides can be used for MF-ROMP in solution. Their high coordinative strength would lead to ROMP inhibition immediately.

4.3.2. Homo- and Copolymerization of ROMP Monomers

The formulations prepared in chapter III, 4.3.1. were transferred into the photoreactor. The initial mass of all components in the formulation was noted and the final mass transferred via syringe into the photoreactor was recorded as well. Irradiation was performed with a mercury lamp using a 320 – 500 nm wavelength filter. The irradiation intensity is set to 64 mW cm^{-2} at the surface of the solution, and was carried out under magnetic stirring at constant temperature set to 25 °C (Figure 230). Room temperature was selected, since if successful ROMP can be carried out, a broad field of applications is available.

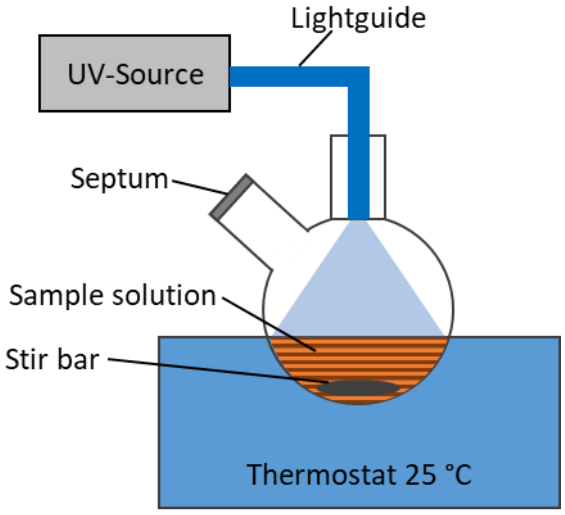

Figure 230: Schematic setup of the photoreactor

The progress of the MF-ROMP over time was monitored at certain time intervals. Those time intervals were set to 0, 10, 30 and 60 min respectively. During the precisely timed sample collection of the solution via the septum, a distinct increase in viscosity was noticed over time. The mass of each sample removed from the photoreactor was noted. The two monomers N and DCPD were tested in their ability to undergo homopolymerization, while N mixed with MMN were used as monomers in the copolymerization experiments. Finally, all collected samples were analyzed via GPC and ^{1}H-NMR to gather information about the ROMP polymer at each time interval.

4.3.3. Determination of the Conversion via ^{1}H-NMR

To calculate the conversions of the ROMP-monomers, nuclear magnetic resonance spectra were recorded of the samples taken from the photoreactor at distinct time intervals. The sample measured in advance of any irradiation (t=0) represents no conversion in the NMR spectrum and is used as reference. For all subsequent spectra (t=10, 30 and 60) distinct

changes in the integrals of specific peaks are noticed. The first photoreactor series was carried out with norbornene as monomer and the NMR spectra were interpreted (Figure 231).

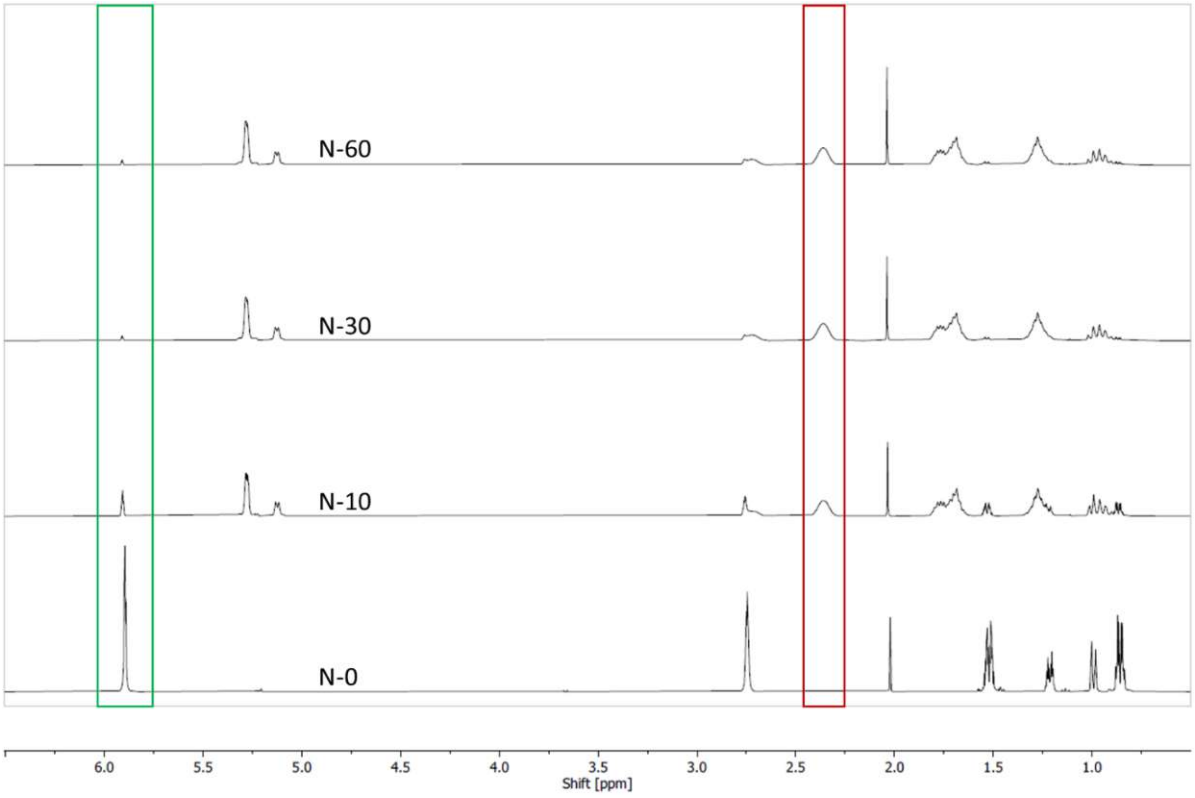

Figure 231: ^{1}H-NMR Spectra of the photoreactor with the formulation containing 0.03 : 1 : 100 molar equivalents of P1-P : EPE : N in deuterated dichloromethane at 0, 10, 30 and 60 min in the photoreactor

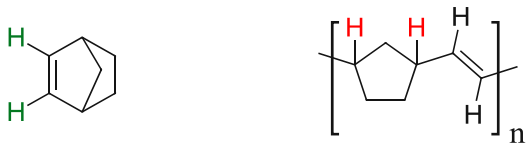

Figure 232: Norbornene hydrogens and it's ring-opened form's hydrogens for integration in ^{1}H-NMR

For the calculation of the monomer conversion to its ring-opened form, one distinct peak from the norbornene and a specific peak from the ring-opened product is necessary (Figure 232). The two hydrogens of the norbornene double bond at 6 ppm are perfectly suited for integration. For the ring-opened polyN, the two hydrogens in the backbone of the five-membered ring at 2.4 ppm are selected for integration. Since the hydrogen ratio of N and its ring-opened product remain constant, no additional correction is needed for the calculations (Table 11).

For the second homopolymerization series, DCPD was used together with the initiator and the pyrylium salts and NMR spectra were recorded (Figure 233).

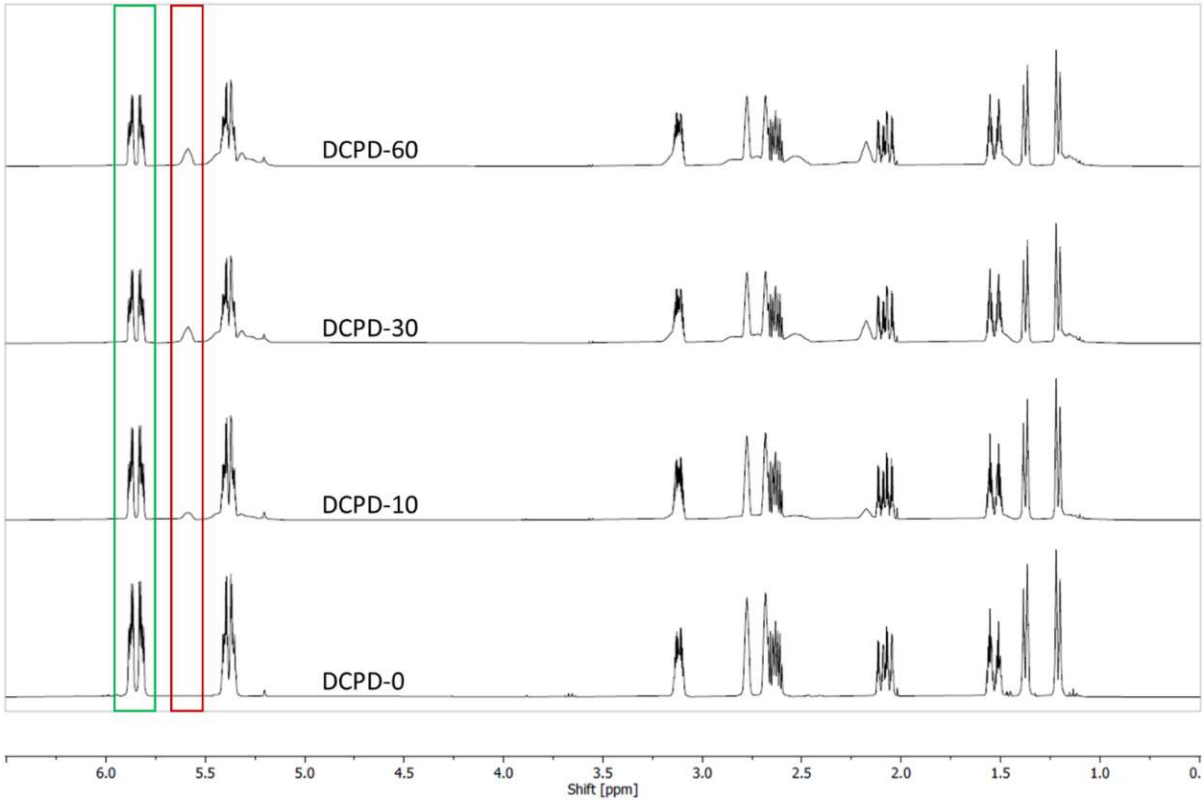

Figure 233: ^{1}H-NMR Spectra of the photoreactor with the formulation containing 0.03 : 1 : 100 molar equivalents of P1-P : EPE : DCPD in deuterated dichloromethane at 0, 10, 30 and 60 min in the photoreactor

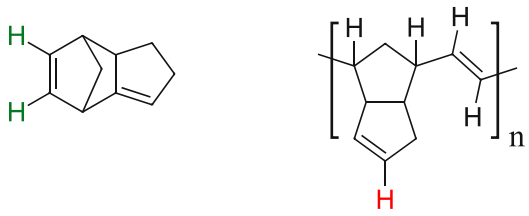

Figure 234: Dicyclopentadiene hydrogens and it's ring-opened form's hydrogen for integration in ^{1}H-NMR

The multiplet at 5.8 ppm corresponding to the two hydrogens at the DCPD double bond (Figure 234). For the ring-opened polyDCPD the broad polymer-peak at 5.6 ppm is integrated representing the single hydrogen at the second DCPD double bond. For the ratio of monomer to polymer, the ratio of integrated hydrogens in the NMR has to be considered.

Copolymerization was carried out with the monomers N and MMN. The corresponding NMR spectra were analyzed (Figure 235).

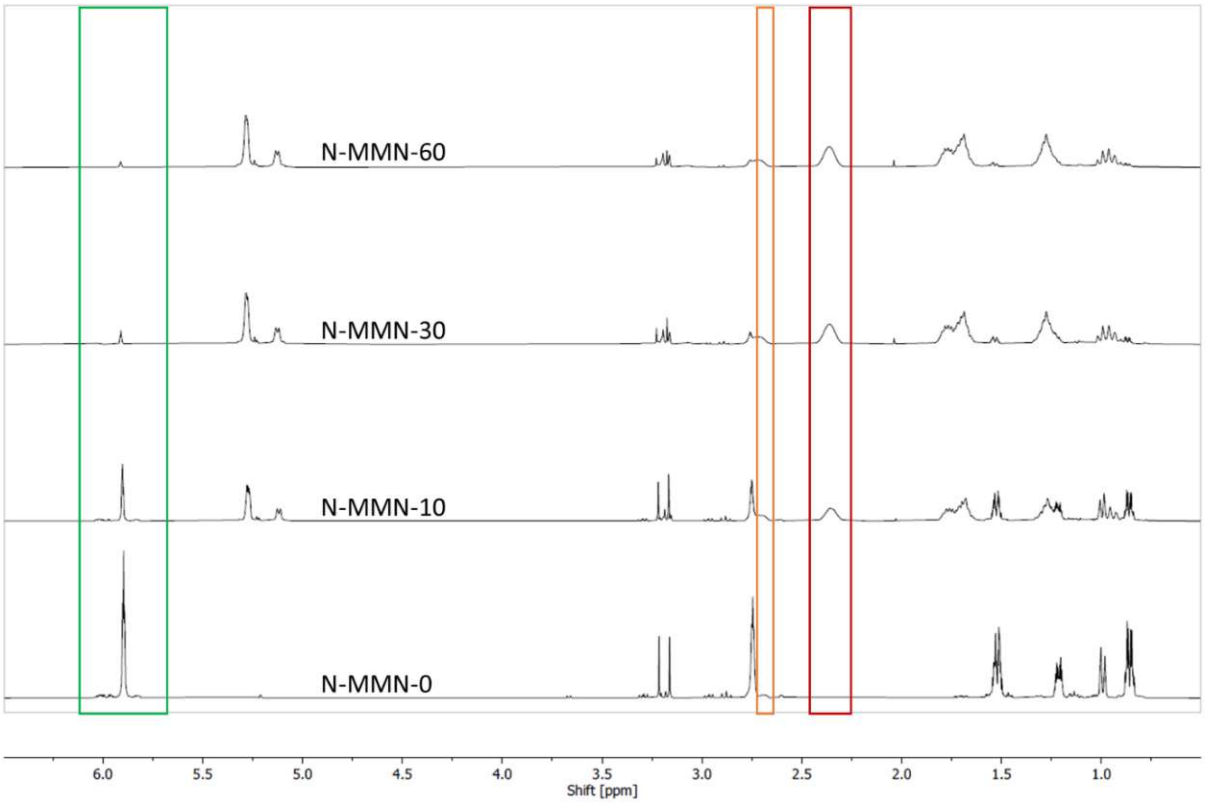

Figure 235: ^{1}H-NMR Spectra of the photoreactor with the formulation containing 0.03 : 1 : 10 : 90 molar equivalents of P1-P : EPE : MMN : N in deuterated dichloromethane at 0, 10, 30 and 60 min in the photoreactor

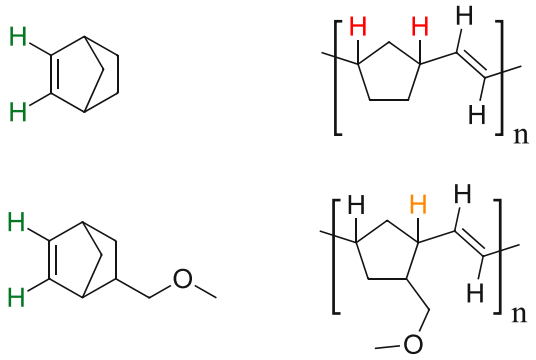

Figure 236: Norbornene and MMN hydrogens and their ring-opened form's hydrogens for integration in ^{1}H-NMR

Copolymerization complicates the situation slightly, due to overlapping hydrogens of the starting monomers N and MMN at 6 ppm (Figure 236). However, the ring-opened polymer of N and MMN are separated enough in ^{1}H-NMR to perform the necessary calculations for conversion. The broad polymer peak at 2.4 ppm is selected for the two hydrogens of polyN and the peak at 2.6 ppm for the single hydrogen of polyMMN. For the molar ratio of monomer to polymer, the ratio of integrated hydrogens in the NMR has to be considered.

Finally, the conversions can be calculated. The mass of each component in the formulations, the actually transferred mass into the photoreactor as well as the mass of each sample removed from the reactor are known. Hence, the mass and molar amount of each component

at any point in time are available, except for the ring-opened polymer. Therefore, the molar amount of monomer at 0, 10, 30 and 60 min was used to conclude the molar amount of ring-opened product via the NMR-integrals. With this crucial ratio of monomer to polymer, absolute conversion values could be calculated (Equation 8 and Equation 9).

Influence of the Cation on Conversion

At first a subset of the selected pyrylium salts were tested in the photoreactor to better understand the influence of the pyrylium cations on conversion.

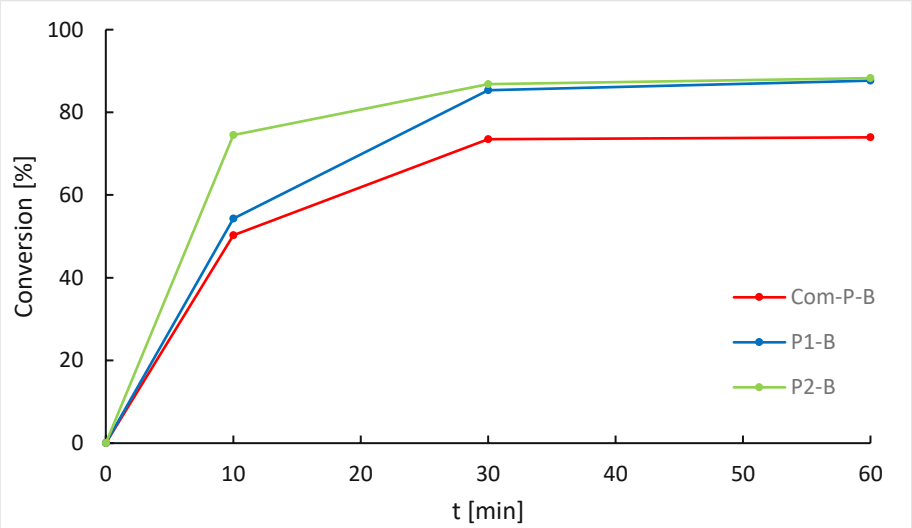

Figure 237: Conversions over time of pyrylium tetrafluoroborates, homopolymerization of N in d2-DCM solution

At first, different pyrylium tetrafluoroborates and their corresponding conversions are analyzed (Figure 237). Com-P-B, P1-B and P2-B only differ in the carbon chain lengths of the alkoxy groups in the pyrylium cation. The reference salt Com-P-B shows the lowest reactivity in ROMP, since all conversion levels at any point in time remain lower compared to the decoxylated P1-B and the even higher alkoxylated P2-B. With a norbornene conversions of 75% and 88% after 10 and 60 min respectively, P2-B is the best performer across the tetrafluoroborates in N. However, P1-B achieves the same final conversion after 60 min.

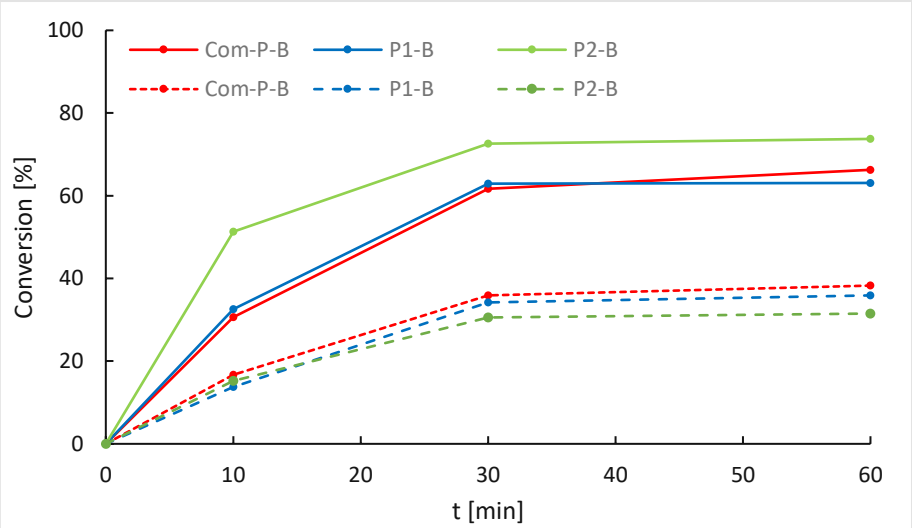

Figure 238: Conversions over time of pyrylium tetrafluoroborates, copolymerization of N-MMN (full lines) and homopolymerization of DCPD (dashed lines) in d2-DCM solution

Unfortunately, the copolymerization of N and MMN by the pyrylium tetrafluoroborates did not work as well as the homopolymerization of N (Figure 238). Conversion values of 74% at most for the highly alkoxylated P2-B are achieved. An even lower conversion is reached if DCPD is homopolymerized, maxing out at 38% for the commercial pyrylium salt Com-P-B.

Influence of the Anion on Conversion

Secondly, all P1-based pyrylium salts were subject of investigation. This study aims for the clarification of the anions influence on conversion.

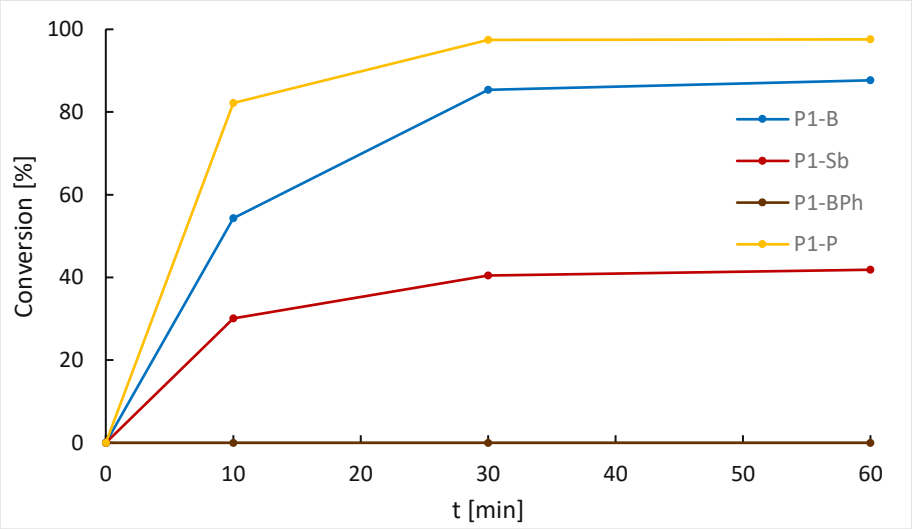

Figure 239: Conversions over time of pyrylium salts, homopolymerization of N in d2-DCM solution

To investigate the anion's influence on conversion, a series of different pyrylium salts were tested (Figure 239). The cation of all salts in this series is the decoxylated pyrylium. The best performance is clearly delivered by the hexafluorophosphate P1-P, which achives an astonishing 82% conversion after only 10 min and practically full conversion of 98% after

60 min. Tetrafluoroborate P1-B comes in second with 88%, and the hexafluoroantimonate P1-Sb third with a conversion of 42% after 60 min. Unfortunately, the tetraphenylborate P1-BPh does not show any reactivity and subsequently no conversion. The reason for the non-existent reactivity for P1-BPh is due to its high coordinative strength compared to the other perfluorometallates, inhibiting ROMP.

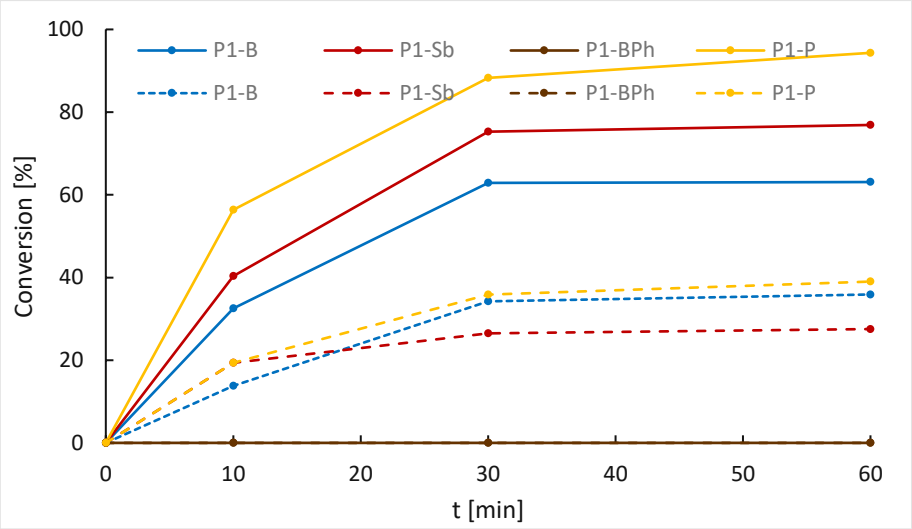

Figure 240: Conversions over time of pyrylium salts, copolymerization of N-MMN (full lines) and homopolymerization of DCPD (dashed lines) in d2-DCM solution

After the homopolymerization of norbornene, MMN and N were copolymerized in solution (Figure 239). The clear advantage of P1-P can be measured. With 94% conversion it achieves the highest conversion across all pyrylium salts in the copolymerization series. Surprisingly, the weak performing hexafluoroantimonate P1-Sb comes in second right after the tetrafluoroborate P1-B at 77% and 63% respectively. By switching to the polyDCPD conversions, a similar trend can be observed. However, with only 39% conversion by P1-P none of the pyrylium salts achieve high values. As expected, P1-BPh experiments were without success and no (co)polymer was formed in both series.

Best Performers - Pyrylium Hexafluorophosphates

Finally, the conversions of the best performing pyrylium hexafluorophosphates was determined in the photoreactor.

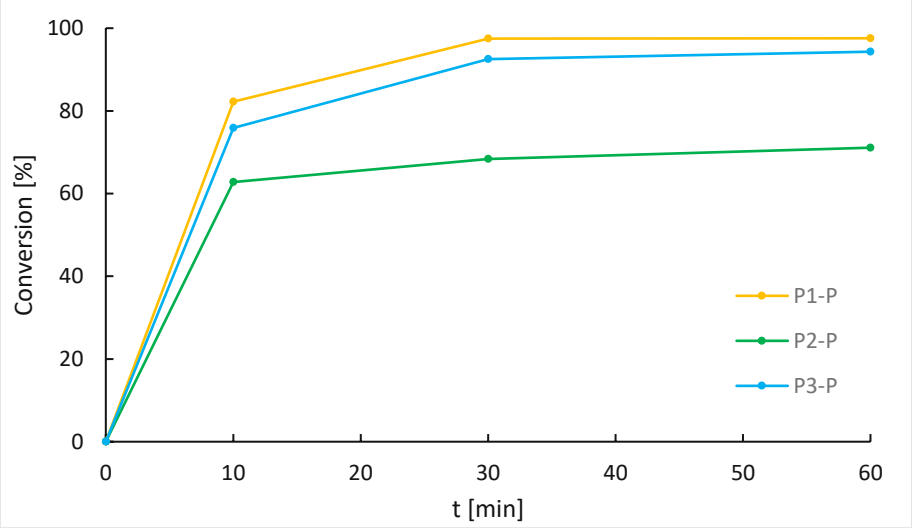

Figure 241: Conversions over time of pyrylium hexafluorophosphates, homopolymerization of N in d2-DCM solution

Since the pyrylium hexafluorophosphate P1-P achieved by far the best reactivity and conversion across all tested pyrylium salts including the commercial reference, more hexafluorophosphates were tested (Figure 241). The pyrylium cations were once again altered to investigate their influence on ring-opening conversion. The previously tested P1-P remains the best performing salt across the hexafluorophosphates with excellent conversions of up to 98%. The highly alkoxylated P-2P achieves slightly lower conversion with up to 94% and the pyrylium salt with the C_{18}-alkoxy chain comes in last with up to 71% conversion.

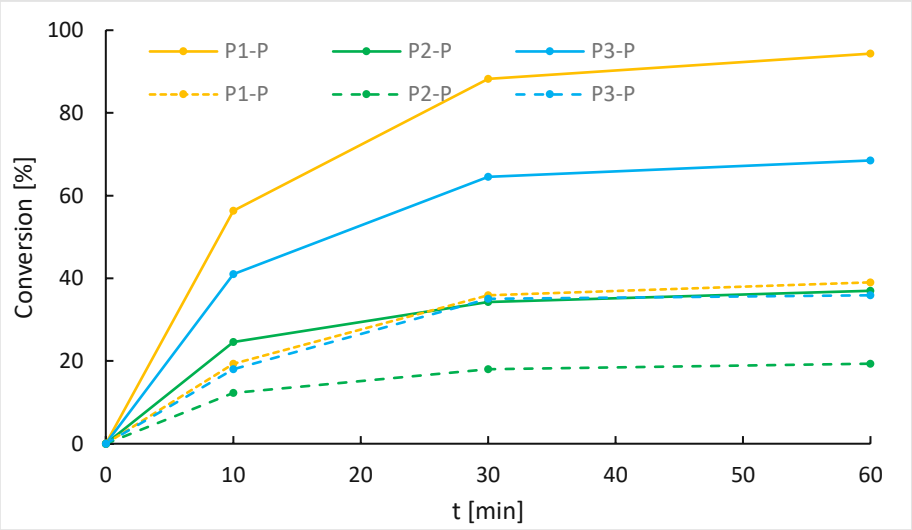

Figure 242: Conversions over time of pyrylium hexafluorophosphates, copolymerization of N-MMN (full lines) and homopolymerization of DCPD (dashed lines) in d2-DCM solution

Switching to different monomer systems, the same trend compared to the polyN series can be observed (Figure 242). In copolymerization experiments P1-P achieves with its 94% conversions, 25 and 58 percentage points more compared to P3-P and P2-P respectively. A similar observation can be made in the homopolymerization of DCPD. However, P1-P and P3-P deliver around the same curve progression over time.

With all NMR spectra evaluated and the conversion calculated for each pyrylium salt over time, a clear winner in terms of performance can be stated. The decoxylated pyrylium hexafluorophosphate P1-P significantly outperforms the commercial tetrafluoroborate Com-P-B as well as all self-synthesized pyrylium salts regardless of cation or anion. In addition, P1-P shows the highest conversions across all monomer systems N, N-MMN and DCPD. However, the overall conversion in DCPD remains rather low for all tested pyrylium photoredox mediators. Overall, a high degree long alkoxy chains in the pyrylium cation as well as the use of hexafluoroantimonates as counterions are advantageous if conversions are considered.

4.3.4. Gel Permeation Chromatography of the MF-ROMP Polymers

The molecular weight and polydispersity Đ of the obtainedROMP-polymers was determined by gel permeation chromatography (GPC). The samples taken from the photoreactors at 10, 30 and 60 min were diluted in dry THF containing BHT as stabilizer and dry THF as eluent at 35 °C. Concentrations were set to 2-3 mg mL^{-1}. A relative average molecular weight was determined with conventional calibration using a calibration curve of 11 narrow polystyrene standards with an average molecular weight M_w ranging from 375 g mol^{-1} to 177000 g mol^{-1}. Finally, the molecular weights M_n of the polymers was calculated by the ratio of measured M_w to Đ. The polydispersities for all experiments are in the range of 1.5 up to 2.6 (Table 10).

Table 10: Polydispersities Đ of all samples after a specific time in the photoreactor

ROMP-System	Com-P-B	P1-B	P2-B	P1-Sb	P1-BPh	P1-P	P2-P	P3-P
N-t_{10}	1.5	1.6	1.4	2.5	-	1.5	1.8	1.5
N-t_{30}	1.5	1.6	1.4	2.4	-	1.7	1.9	1.7
N-t_{60}	1.4	1.7	1.4	2.2	-	1.8	2.0	1.8
N-MMN-t_{10}	1.6	1.6	1.5	1.8	-	1.5	2.4	1.5
N-MMN-t_{30}	1.6	1.8	1.5	1.9	-	1.6	2.5	1.5
N-MMN-t_{60}	1.6	1.9	1.5	2.1	-	1.7	2.3	1.5
DCPD-t_{10}	2.2	2.0	2.0	2.3	-	1.8	2.1	1.6
DCPD-t_{30}	1.8	2.0	1.6	2.4	-	2.0	2.5	2.1
DCPD-t_{60}	2.0	2.0	2.0	2.6	-	2.2	2.1	2.1

Influence of the Cation on Molecular Weight

At first, the influence of the pyrylium cations on the final polymers molecular weight was investigated.

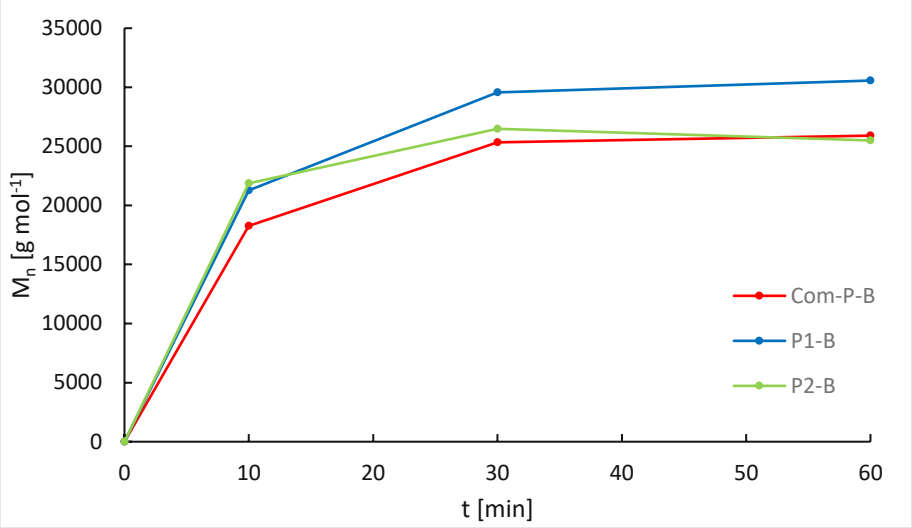

Figure 243: Molecular weight M_n over time of pyrylium tetrafluoroborates, homopolymerization of N in d2-DCM solution

By accessing the influence of the three tested pyrylium cations on the molecular weight over time, the highest M_n was obtained with the photoredox-mediator P1-B at around 30500 g mol^{-1} after 60 min (Figure 243). The commercial Com-B-P and highly alkoxylated P2-B achieve slightly lower values at around 26000 g mol^{-1}.

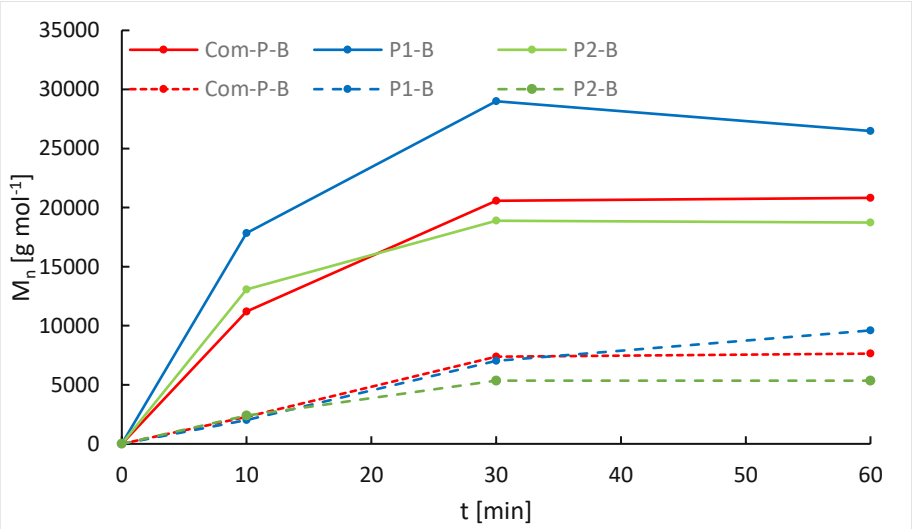

Figure 244: Molecular weight M_n over time of pyrylium tetrafluoroborates, copolymerization of N-MMN (full lines) and homopolymerization of DCPD (dashed lines) in d2-DCM solution

Switching the monomer system from pure norbornene to the N-MMN and DCPD, significantly lower molecular weights are obtained (Figure 244). P1-B remains the best performing mediator in this series of measurements with M_n-values of 26500 g mol^{-1} and 9600 g mol^{-1} after 60 min respectively.

Influence of the Anion on Molecular Weight

Second, the conversions of the subset of P1-based pyrylium salts paired with various anions was determined.

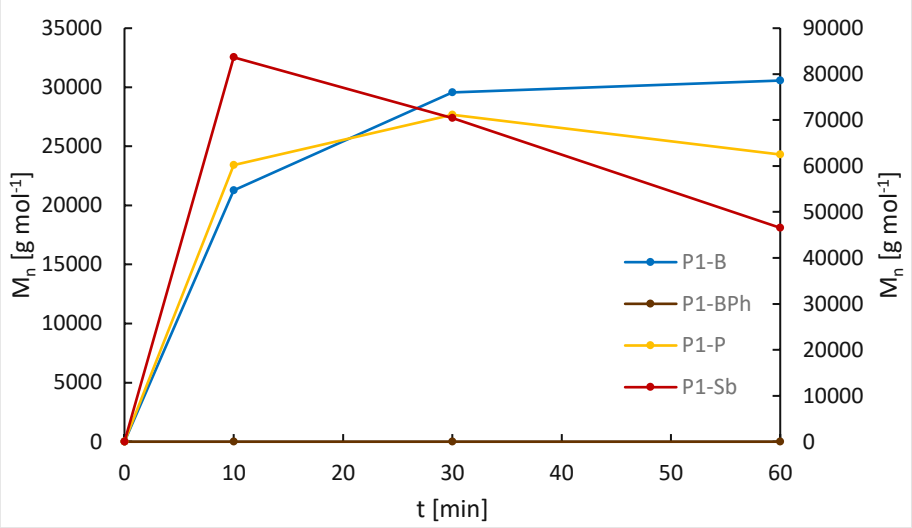

Figure 245: Molecular weight M_n over time of pyrylium salts P1-B, P1-BPh and P1-P (primary y-axis) and P1-Sb (secondary y-axis), homopolymerization of N in d2-DCM solution

The selection of the anion for photoredox-mediators is crucial, since it is responsible for all ionic interactions with the photoredox-mediator and the radical cation at the growing polymer chain. Surprisingly, the tetrafluoroborate P1-B shows the smoothest molecular weight curve over time, reaching 30600 g mol^{-1} (Figure 245). The hexafluorophosphate P1-P achieves its peak in M_n at 30 min, while the tetraphenylborate P1-BPh did not produce any polymers in solution. Interestingly, the highest molecular weight of 83700 g mol^{-1} is achieved by the hexafluoroantimonate P1-Sb after only 10 min. However, molecular weight decreases steadily over time and overall conversions remain rather low for the salt.

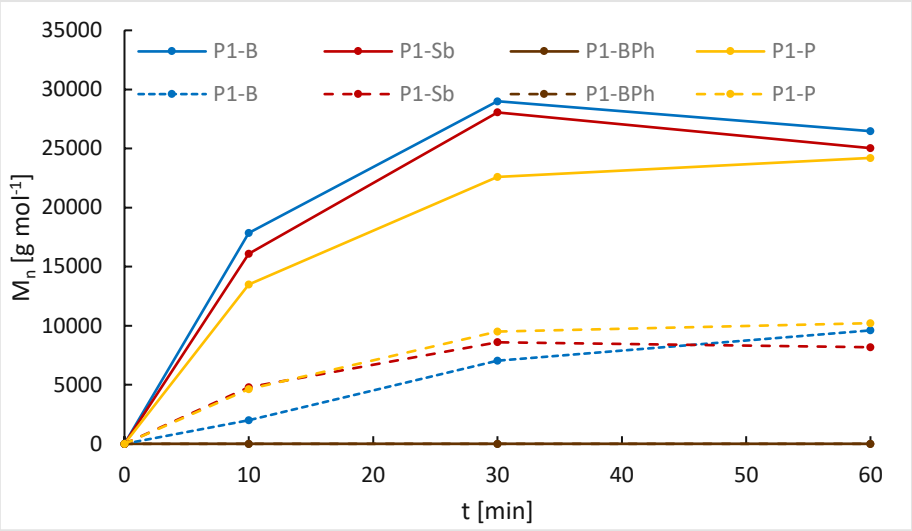

Figure 246: Molecular weight M_n over time of pyrylium salts, copolymerization of N-MMN (full lines) and homopolymerization of DCPD (dashed lines) in d2-DCM solution

By investigating the copolymerization experiments of N-MMN and the homopolymerization of DCPD, a clear trend towards lower molecular weights after 30 min can be seen for P1-B and P1-Sb (Figure 246). P1-P is the only candidate in both series, achieving a steady increase in M_n as expected for ROMP polymerizations monitored over time.

Best Performers - Pyrylium Hexafluorophosphates

At last, the molecular weight of the best performing hexafluoroantimonates was compared.

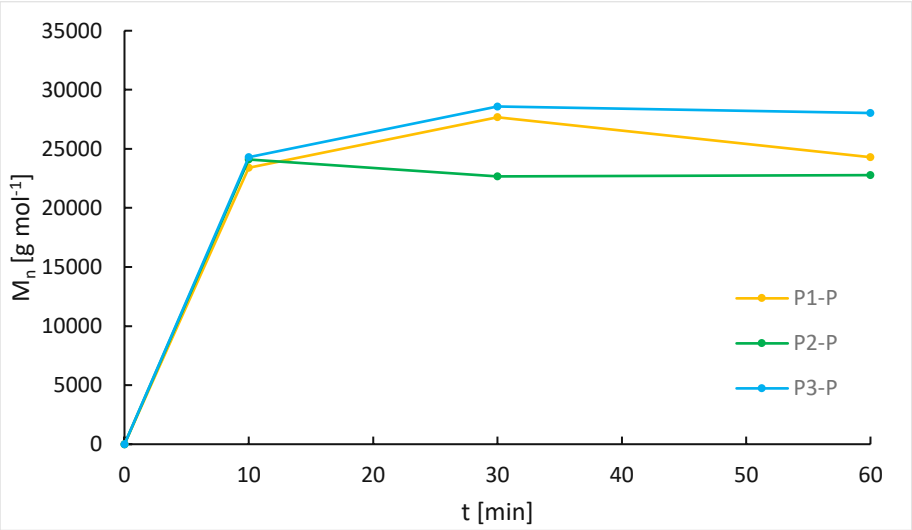

Figure 247: Molecular weight M_n over time of pyrylium hexafluorophosphates, homopolymerization of N in d2-DCM solution

The best performing pyrylium salts regarding conversion are the hexafluorophosphates as shown in previous studies. The same trend cannot be stated for the molecular weights (Figure 247). All pyrylium hexafluorophosphates remain below 30000 g mol^{-1} after 60 min in the photoreactor.

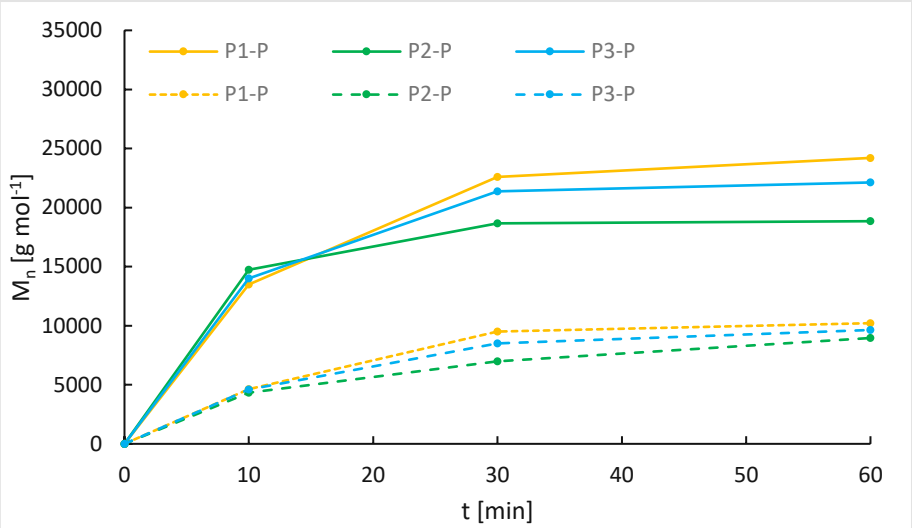

Figure 248: Molecular weight M_n over time of pyrylium hexafluorophosphates, copolymerization of N-MMN (full lines) and homopolymerization of DCPD (dashed lines) in d2-DCM solution

Interestingly, the molecular weight seems to decrease from 30 min to 60 min for the N-MMN series for most tested pyrylium salts, except all hexafluorophosphates (Figure 248). In addition, P1-P achieves the highest overall Mn across all tested salts in DCPD at 9600 g mol^{-1}. Molecular weight trends over time vary a lot depending on the complex interactions of pyrylium cation and their corresponding counterion. The homopolymerization of N works best for all photoredox mediators, achieving high M_n and narrow Đ of as low as 1.4. The copolymerization series of N-MMN shows overall worse results regarding molecular weight. The highest Đ of up to 2.6 are obtained in DCPD as monomer, achieving M_n of below 10000 g mol^{-1} across all tested pyrylium salts.

SUMMARY AND CONCLUSIONS

To conclude, cationic polymerization is a powerful tool when it comes to adhesive, coating and bulk material production. A variety of monomers is suitable for the cationic polymerization, however epoxy-based systems are used in many applications, due to their high reactivity and versatility. With the introduction of the onium salt, a highly efficient approach to photopolymerize cationic monomers was made. Additionally, radical induced cationic polymerization and sensitization are possible with onium salts, opening an even broader field of applications. The main focus of this thesis is the synthesis of a new onium salt, suitable for radical induced cationic frontal polymerization (RICFP), a hot topic in recent years, due to its very fast and energy efficient curing of monomers. The challenge to produce a new, highly efficient photoacid generator like the commercial iodonium- and sulfonium salts was quite difficult, since a lot of basic research in this topic was already performed.

I. The Cationic Species of Photoacid Generators

The overall aim of the first part of this thesis is the investigation of a variety of different onium salts for the application in cationic polymerization and subsequently RICFP. After a screening of many group 14 to 16 elements, which could be transformed into their onium species rather easily, a few promising candidates could be obtained during the work of this thesis. The first goal was the synthesis of the onium tetrafluoroborates, due to the broad commercial availability and simple synthesis of this weakly coordinating anion. The main issue during the investigation of the cations was the solubility in nonpolar media like most epoxides. Therefore, a quite high amount of propylene carbonate had to be used to completely dissolve the onium salts in the cationically polymerizable monomers. Mainly bismuthonium-, methylium- and pyrylium salts showed promising results during the first reactivity tests and were compared to the state-of-the-art iodonium salt. With the bismuth-based Bi1-B reaching up to 74% of the reactivity compared to the iodonium tetrafluoroborate reference I1-B in epoxy-based monomers like ECC and BADGE with the thermal radical initiator TPED and quite good reactivity in formulations containing the sensitizer anthracene (64% of the reactivity of the iodonium salt). Experiments with formulations based on ECC and BADGE, containing the photo radical initiator Ivocerin, showed quite high reactivity of the pyrylium tetrafluoroborate initiator (up to 82% compared to the iodonium salt). Besides the very interesting absorption

behavior of methylium salts, their high reactivity in cationic monomers is known. However, the carbon-based C2-B initiator showed mediocre reactivity during the Photoinitiation study in BADGE-based samples, since the mixing with ECC and monomers with similar reactivity resulted in the prematurely polymerization of the formulations during homogenization.

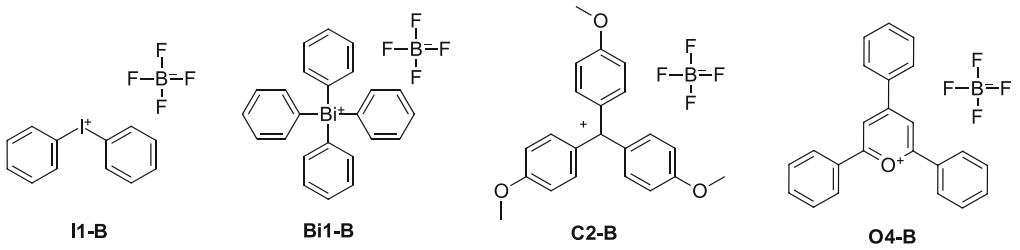

I1-B Bi1-B C2-B O4-B

Since tetrafluoroborates are quite low reactive compared to other low nucleophilic anions, a more practical and industry-related counterion was chosen. The hexafluoroantimonate provides lower coordination strength and therefore an expected increased reactivity.

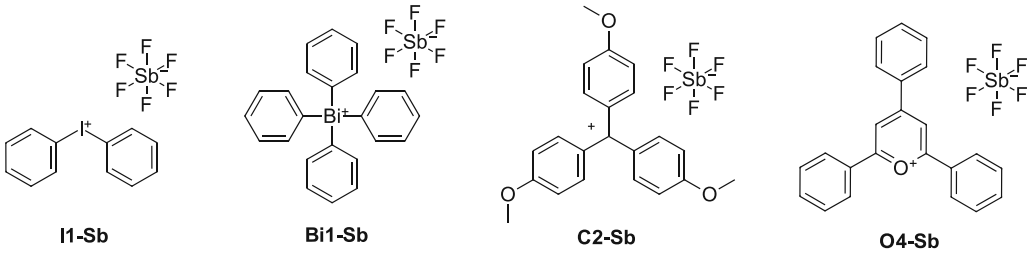

I1-Sb Bi1-Sb C2-Sb O4-Sb

However, with the focus of the work now shifting towards the RICFP of epoxides, the solubility issue became very dominant. Prior, the polarity difference between the rather polar onium salts and the nonpolar monomers was solved with the addition of high amounts of propylene carbonate. Since propylene carbonate exhibits a rather low boiling point, bubble formation during frontal polymerization is a major problem. This would ultimately lead to porous polymers with poor mechanical properties compared to specimens cured with common curing techniques. Therefore, alkoxy groups were introduced to modify the solubility properties of the cations. This change in molecular structure eventually lead to the possibility of producing formulations without the propylene carbonate, hence a bubble-free bulk polymerization of the resins.

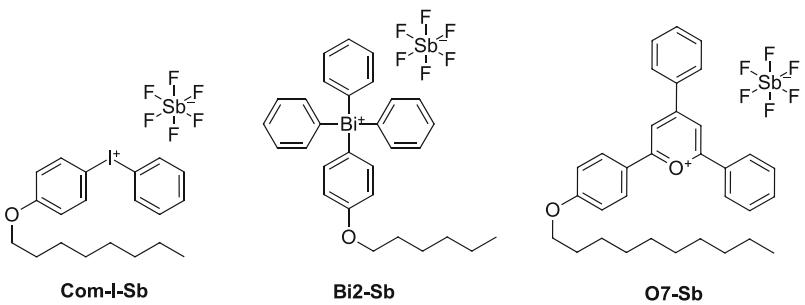

Com-I-Sb Bi2-Sb O7-Sb

However, one component, the methylium salt, had to be excluded from further testing. Problematic was its premature polymerization during the homogenization step in high reactive epoxy monomers like HDDGE. For the alkoxylated bismuthonium and pyrylium salt, HDDGE represents no issue at all. However, pure or too much HDDGE in the formulation would lead to undesired bubble formation due to its high reactivity. Therefore, a BADGE/HDDGE-based system was chosen, since it represented a good compromise between reactivity, viscosity and polarity.

With every component ready for frontal polymerization, the frontal parameters for BADGE/HDDGE formulations were determined. The front velocity (v_F), frontal temperature (T_F) as well as the minimal layer thickness (MLT) was investigated in dependence on the concentration of onium salt and thermal radical initiator TPED. During the RICFP experiments, the three alkylated onium salt showed good results, however neither the bismuthonium- nor the pyrylium salt were able to outperform the iodonium hexafluoroantimonate. With a concentration of 0.5 mol% referred to epoxy groups, the iodonium salt delivered a highly reactive and well performing system. Reaching 5.5 cm min^{-1} and a frontal temperature of 246 °C. The alkoxylated bismuthonium salt did achieve a stable front with 1.5 mol% and an equimolar amount of TPED. Despite good performance as a cationic initiator in ECC, the pyrylium salt was not very well performing in the frontal experiments. Due to its low reactivity, 1.5 mol% and even 2.0 mol% of onium salt and TPED were not enough to establish a stable frontal polymerization, due to the high onset temperature of the pyrylium front. Continuously the front was interrupted and an increase in initiator concentration was not an option due to the poor solubility above 2.0 mol% in BADGE/HDDGE. Considering the minimum layer thickness (MLT) of the front, despite one third of onium salt and TPED concentration, the iodonium hexafluoroantimonate achieved 2.8 mm in average, while the bismuthonium compound measured a minimum layer thickness (MLT) of 3.0 mm. However, the pot life of bismuthonium-based formulations is remarkable.

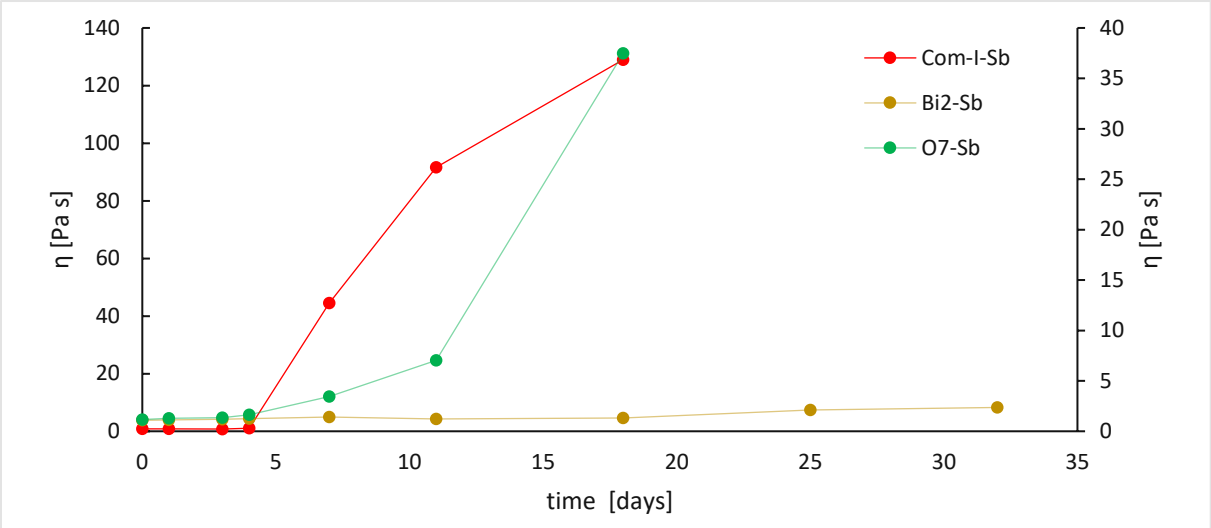

*Figure 249: Time dependent viscosity of the BADGE/HDDGE formulations at a storage temperature of 50 °C under light protection. Primary axis: Com-I-Sb/*TPED *was used in 0.5 mol%. Secondary axis: Bi2-Sb/TPED and O7-Sb/TPED were used in 1.5 mol%*

Storing the formulations, used for the working frontal experiments, at 50 °C, the obtained data provides a good overview considering storage stability (Figure 249). Iodonium- and pyrylium salts start to increase the viscosity rapidly after approximately 3 to 4 days. After one week, the viscosity increased by a factor of 44 for the iodonium salt. Only the bismuthonium-based formulations showed a very stable trend. Even after one month of storage, the viscosity increase was only around 2x to around 2.4 Pa s. This behavior is a clear advantage over the commercial iodonium salts, if the RICFP-ready resins have to be transported, stored or are exposed to non-temperature regulated container over an extended period of time. Additionally, a working frontal polymerization could be carried out with slightly worse frontal parameters using the formulations stored for 32 days at 50 °C.

II. The Anionic Species of Photoacid Generators

Iodonium Salts

Iodonium salts represent one of the best performing initiator classes in cationic polymerization and are therefore broadly available and used in a variety of applications across many industries. Hence, novel iodonium initiators were aimed to be synthesized and investigated. By utilizing the synthesized alkali salt anions, the corresponding diaryliodonium salts were obtained in a metathesis reaction in overall high yields to form the desired iodonium-based initiators.

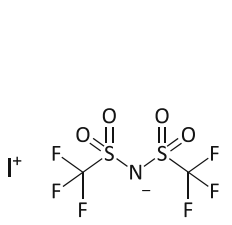

I-NS

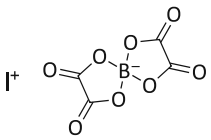

I-B1

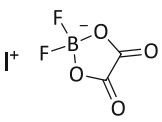

I-B2

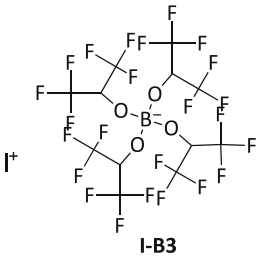

I-B3

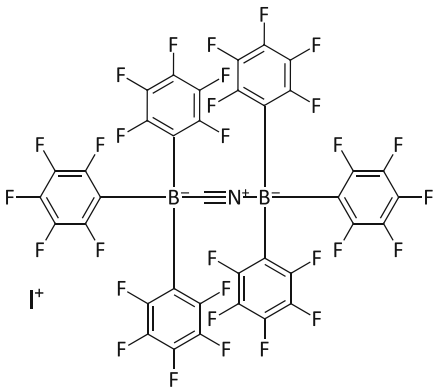

I-B4

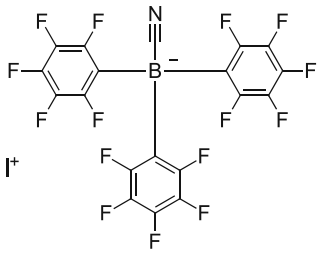

I-B5

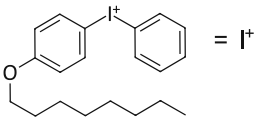

These newly synthesized photo acid generators were mixed with commercially available epoxy monomers BADGE and ECC to determine their reactivity via various DSC experiments. Their performance was compared with commercial products. The iodonium hexafluoroantimonate Com-I-Sb and the iodonium tetraphenylborate Com-I-B as well as a state-of-the-art reference iodonium aluminate Ref-I-Al.

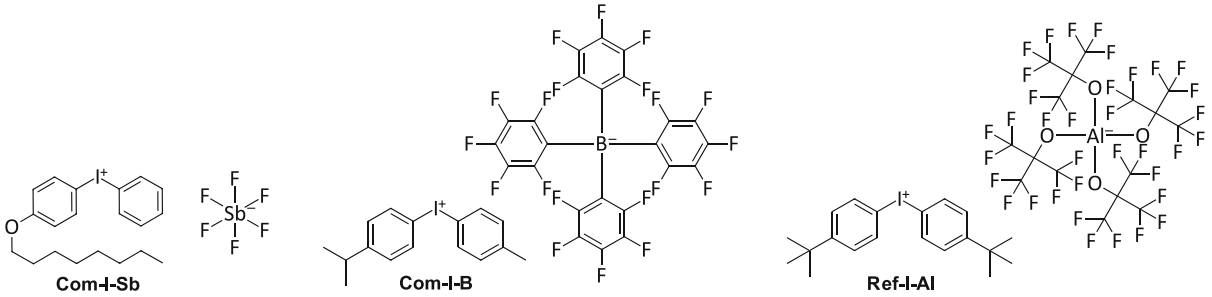

Comparing the 1 mol% photo-DSC data of the initiators, the new borate I-B5 demonstrates high reactivity. Completely outperforming the most frequently used commercial antimonate Com-I-Sb and even reaching up to 77% of the reactivity compared to Com-B and Ref-I-Al. By evaluating the more industry relevant 1.0 wt% PAG formulations at four temperatures at the photo-DSC, the stunning performance of I-B5 in BADGE across a broad range of temperatures can be seen. Even outperforming any commercial system tested in terms of reactivity and EGC at 50 °C. To determine the thermal stability as well as propagation properties, an DSC was performed. The cyanide-ligated borane I-B5 achieves nearly on pair reactivity compared to the commercial borate Com-I-B.

By comparing the front starting times of photochemically-initiated RICFP using TPED as thermal radical initiator, I-B5 performs as well as Com-I-B and event better than Ref Al in both experiments. Both I-B5 and I-B4 are well suited for the application in thermally-initiated RICFP. Es expected, the frontal parameters frontal velocity v_F, frontal temperature TF and EGC do not regardless of the initiation source. Stable and reproducible fronts could be obtained for all investigated concentrations 0.5 mol% down to 0.1 mol% for I-B5. Even at the very low concentration of 0.1 mol% based on the epoxy groups, I-B5 remains highly reactive and achieves together with Com-I-B the highest fontal velocities. Out of all three commercial salts, only Com-I-B could still show a stable frontal polymerization at the concentration of 0.1 mol%. The optical advantages of the polymerized I-B5 samples compared to the black, non-transparent commercial initiator-based front samples are striking.

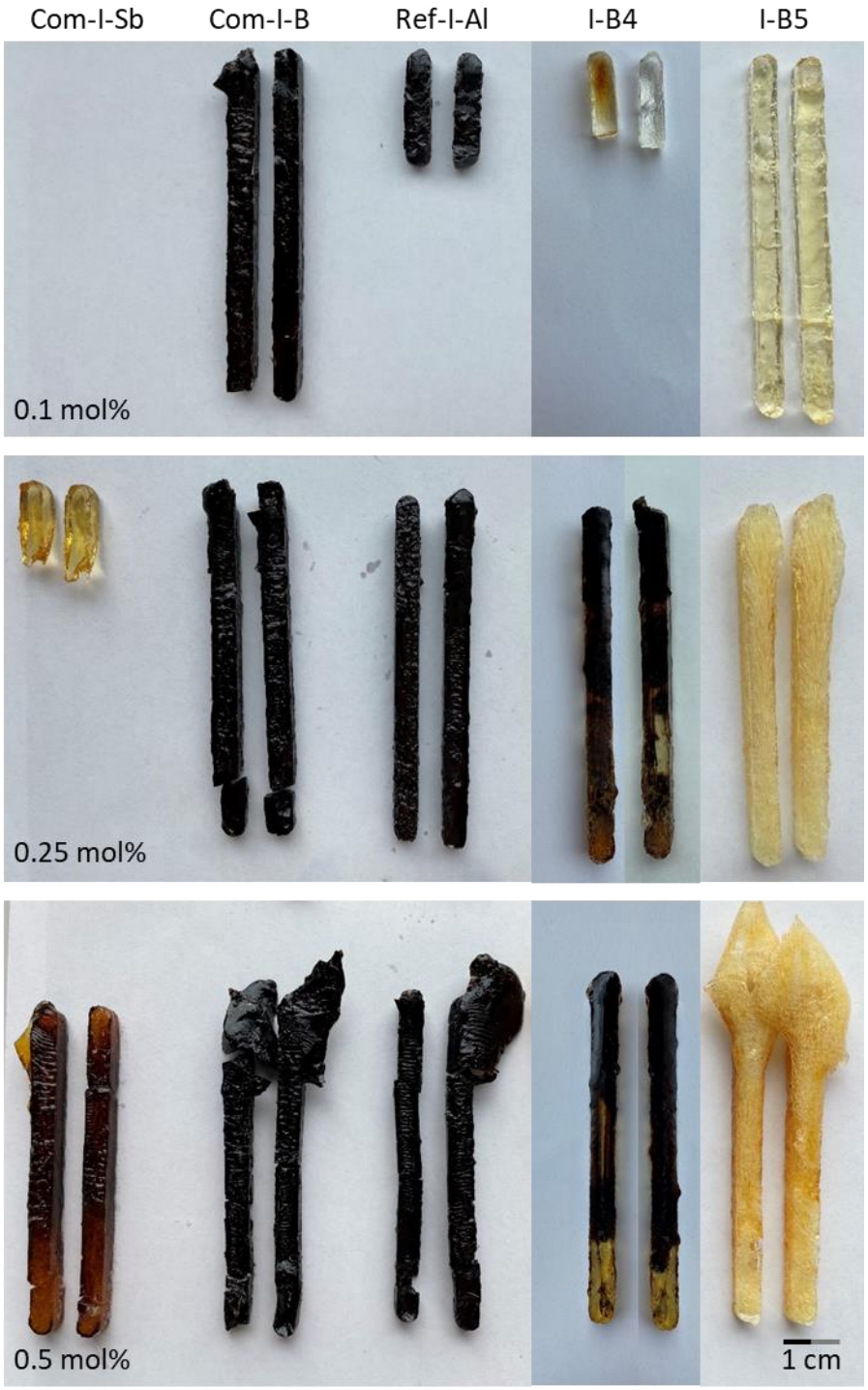

Figure 250: Specimens produced via thermally-initiated RICFP of BADGE/HDDGE with the iodonium salt/TPED concentration of 0.1 mol, 0.25 mol% and 0.5 mol% based on epoxy groups; Ref-I-Al (0.1 mol%), I-B4 (0.1 mol%) and Com-I-Sb (0.25 mol%) are shorter due to non-stable FP

After curing, the I-B5 samples appear transparent and slightly yellowish at a concentration of 0.1 mol% (Figure 250). This observation can be explained with low frontal temperatures of I-B5 compared to the commercial and reference systems. Storage stability studies show the best performing synthesized salt is I-B5 together with the reference aluminate Ref-I-Al

showing much better performance compared to the commercial boron-based salt Com-I-B and the most commonly used antimonate Com-I-Sb.

The new boron-based cationic initiator I-B5 shows on pair or even better performance in terms of reactivity compared to its commercial counterpart Com-I-B. However, the molecular weight of the cyanide-ligated anion in I-B5 is 21% and 44% lower compared to the state-of-the-art PAGs Com-I-B and Ref-I-Al respectively. This advantage of lower molecular mass as well as easy synthetic access in combination with its high reactivity in all tested systems, leaves I-B5 as a novel, highly interesting initiator for cationic polymerization and RICFP.

Sulfonium Salts

Since sulfur-based onium salts represent a well performing initiator class in high temperature applications in cationic polymerization, a variety of new compounds were targeted. New anions for sulfonium-based cationic initiators were prepared and characterized successfully in a range of low to high yields depending on the product. Starting from the synthesized anions, the corresponding sulfonium salts were successfully obtained in high yields.

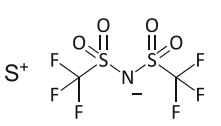

S-NS

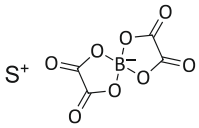

S-B1

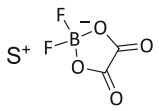

S-B2

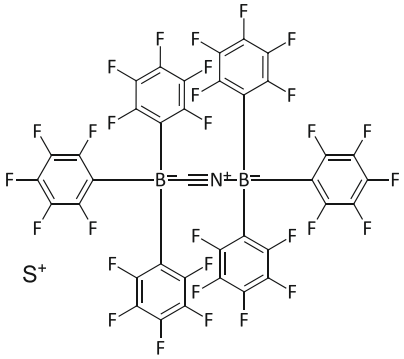

S-B4

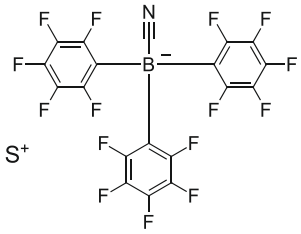

S-B5

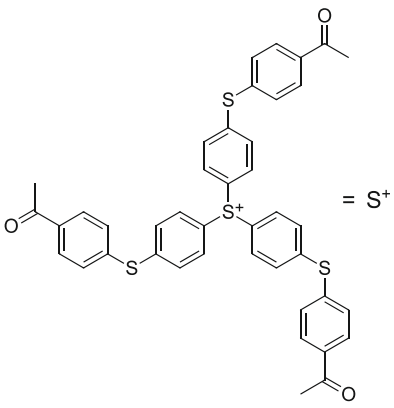

The sulfonimide and the remaining borates were compared to state-of-the-art sulfonium initiators to evaluate their applicability in reactivity studies. Therefore, the most commonly used initiators in industry, the sulfonium hexafluorophosphate Com-S-P and the sulfonium tetraphenylborate Com-S-B are introduced.

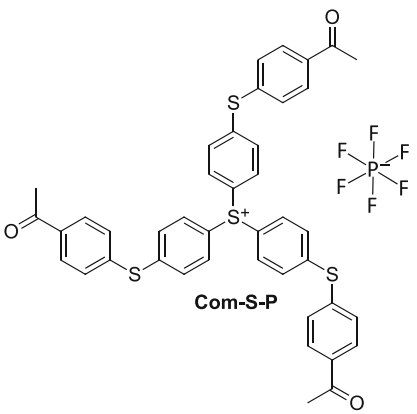

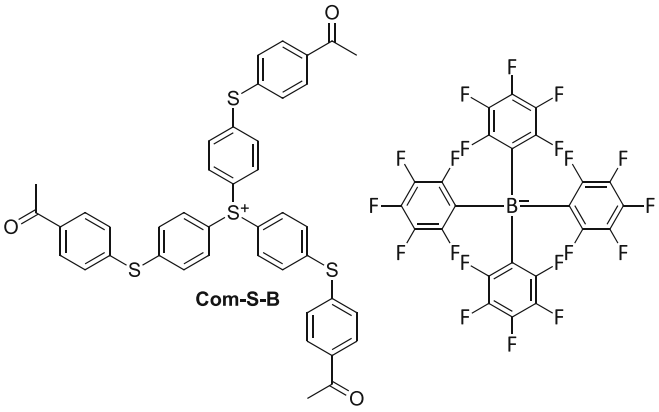

Thermal stability studies of all selected compounds indicate stability issues for the cyanide-bridged borane S-B4 in BADGE as well as S-B4 and S-B5 in the more reactive cycloaliphatic monomer ECC. Interestingly, the cyanide-ligated borane S-B5 is stable in BADGE up to around 370 °C. Photo-DSC experiments in BADGE including 1 mol% of sulfonium initiator show a clear advantage of S-B5 compared to both commercial salts. The cyanide-ligated borane outperforms Com-S-P and Com-S-B up to 70 °C in terms of polymerization rate and epoxy group conversion of up to 83%.

To evaluate the applicability of the new well performing sulfonium salt S-B5 in additive manufacturing technologies such as hot lithography, a study at the Photo-DSC was performed with the anthracene derivative DBA as sensitizer and the organic base EDAB as acid scavenger to mimic the 3D-printing conditions as close as possible. Surprisingly, S-B5 measures significantly higher rates of polymerizations and epoxy group conversions of 70% compared to the commercial salts at up to 90 °C, marking the new sulfonium initiator as well suitable for hot lithography applications.

Since the storage stability of S-B5 formulations is sufficient for 30 days at elevated temperatures, 3D-printing was performed at 90 °C. The fabricated parts show clear trend towards darker colors the higher the post curing temperature is set. However, S-B5 containing samples show much lighter colors compared to the commercial tetraphenylborate reference Com-S-B (Figure 251).

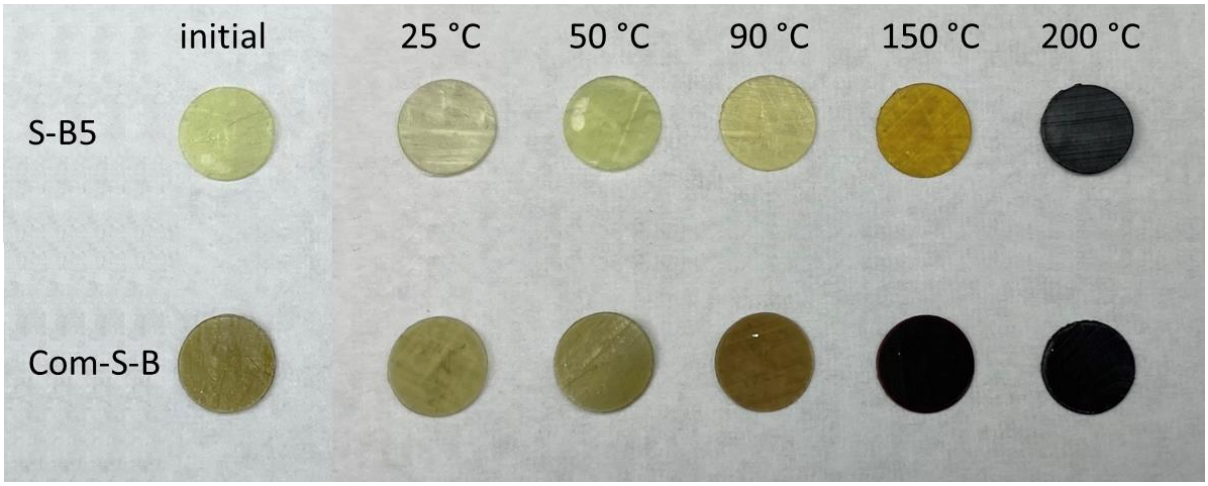

Figure 251: S-B5- and Com-S-B-based 3D printed discs after post-curing at different temperatures for 6 days

The epoxy group conversions after post curing are clear in favor of S-B5, due to overall higher or equal values compared to Com-S-B. The cyanide-ligated borane achieves 90% EGC at 90 °C and full conversion at 150 °C post curing temperature. At 200 °C, some of the BADGE-based parts already start to decompose, rendering this temperature not suitable for post curing. By investigating the layer quality of the 3D-printet parts by S-B5, evenly spaced out and high-quality layers are observed (Figure 252).

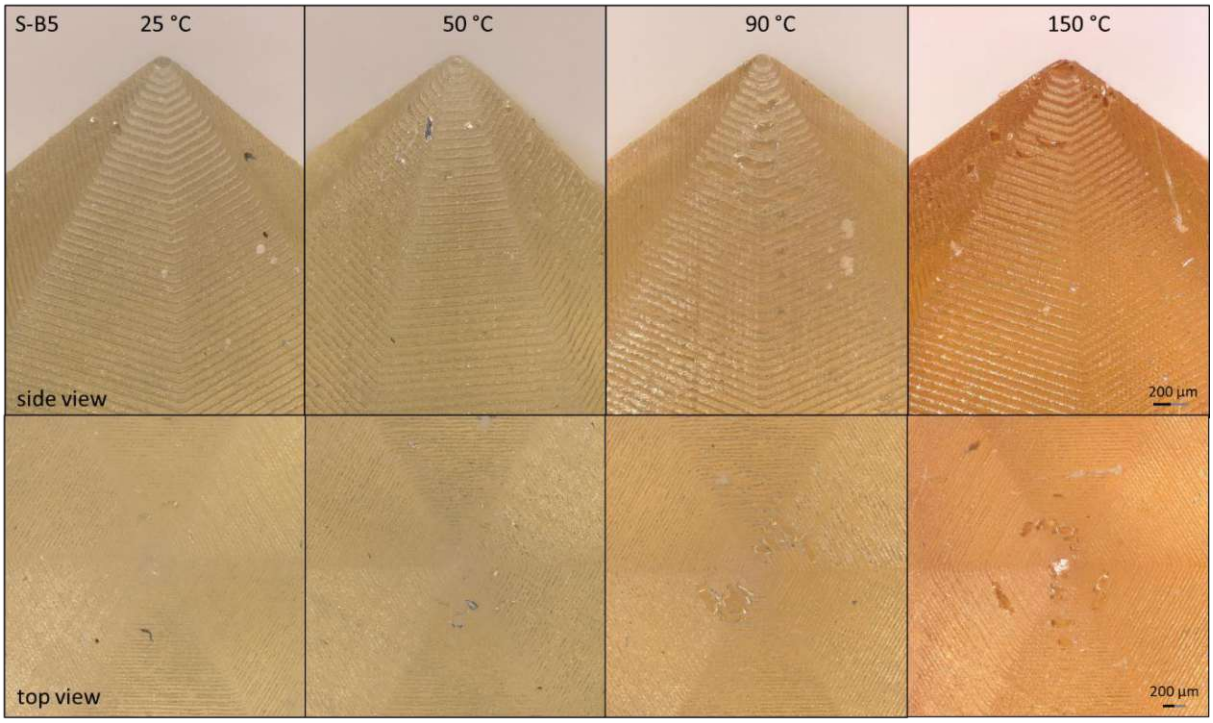

Figure 252: S-B5-based 3D printed hexagonal pyramids after post-curing at different temperatures for 6 days in side view (40 ° tilt) and top view

Due to high reactivity in epoxy-based resins, sufficient storage stability of the formulations as well as high epoxy group conversions across various different measurements proof the

applicability of the novel sulfonium salt S-B5 as cationic initiator. In combination with less discoloration of the fabricated parts and high-quality layers make S-B5 a viable initiator for hot lithography, broadening the field of applications due to lighter colors at equal conversions compared to the reference system. The slightly lower molecular weight of the B5 anion compared to the perfluorinated tetraphenylborate anion of Com-S-B leads to lower initiator cost at the same or better performance level. Overall, S-B5 represents a highly reactive, efficient and novel sulfonium salt for a broad field of possible applications. In addition, the 3D printed parts were characterized via SEM to determine layer quality (Figure 253).

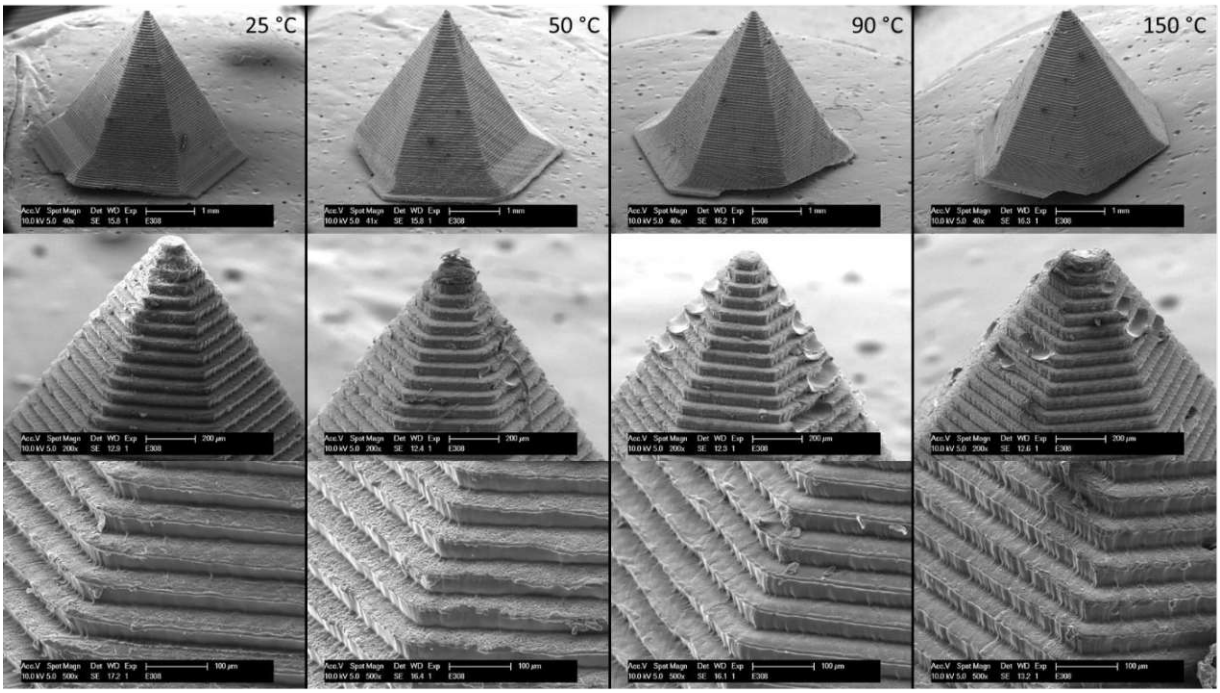

Figure 253: S-B5-based 3D-printed hexagonal pyramids after post-curing at different temperatures for 6 days in three different magnification modes (x40, x200 and x500)

By investigating the x500 magnifications, well-defined and high quality layers are obtained in all four parts. However, the samples stored at increased temperatures show slightly enhanced interlayer fusion. Overall, imaging via SEM of the successfully printed parts show no overpolymerization.

III. Metal-Free Ring-Opening Metathesis Polymerization

Besides applications in cationic polymerization, onium salts can be utilized as mediators in ring-opening metathesis polymerization (ROMP). Generally, ROMP is conducted with ruthenium-based metal complexes acting as catalysts to polymerize a variety of monomers. However, those heavy-metal-based complexes remain in the final material and are notoriously hard to remove. With the introduction of photoredox-mediated metal-free (MF) ROMP, an alternative heavy-metal free approach towards ROMP polymer materials was created. However, it is challenging to replace the metal-based catalyst entirely, due to some shortcomings of pyrylium salts as photoredox-mediators used in MF-ROMP. The suffer from poor solubility if used outside of polymerization in solution and are not nearly as tolerant towards functionalities in monomers compared to their metal-based counterparts. MF-ROMP with pyrylium salts as mediator and ethyl propenyl ether EPE as initiator is only known to work with norbornene-based monomers N, DCPD or a mixture of N and MMN in solution.

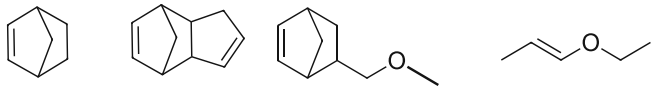

N DCPD MMN EPE

This work mainly focuses the synthesis of novel onium salts for MF-ROMP based on the pyrylium cation as well as the investigation of the produced compounds. After successful synthesis of some monomers and many targeted pyrylium photoredox-mediators, the influence of the differently substituted pyrylium cations and a selection of anions were investigated. The prevailing analytical tool for MF-ROMP in solution remains the photoreactor. Unfortunately, none of the newly-synthesized pyrylium salts can be used as photoredox-mediator for monomers other than N, DCPD or a mixture of N and MMN in solution. As a consequence of various degrees of alkoxylation of the pyrylium cations using the same tetrafluoroborate anion, a clear trend towards higher conversions in obtained with the pyrylium tetrafluoroborates P1-B and P2-B compared to the commercial pyrylium tetrafluoroborate Com-P-B.

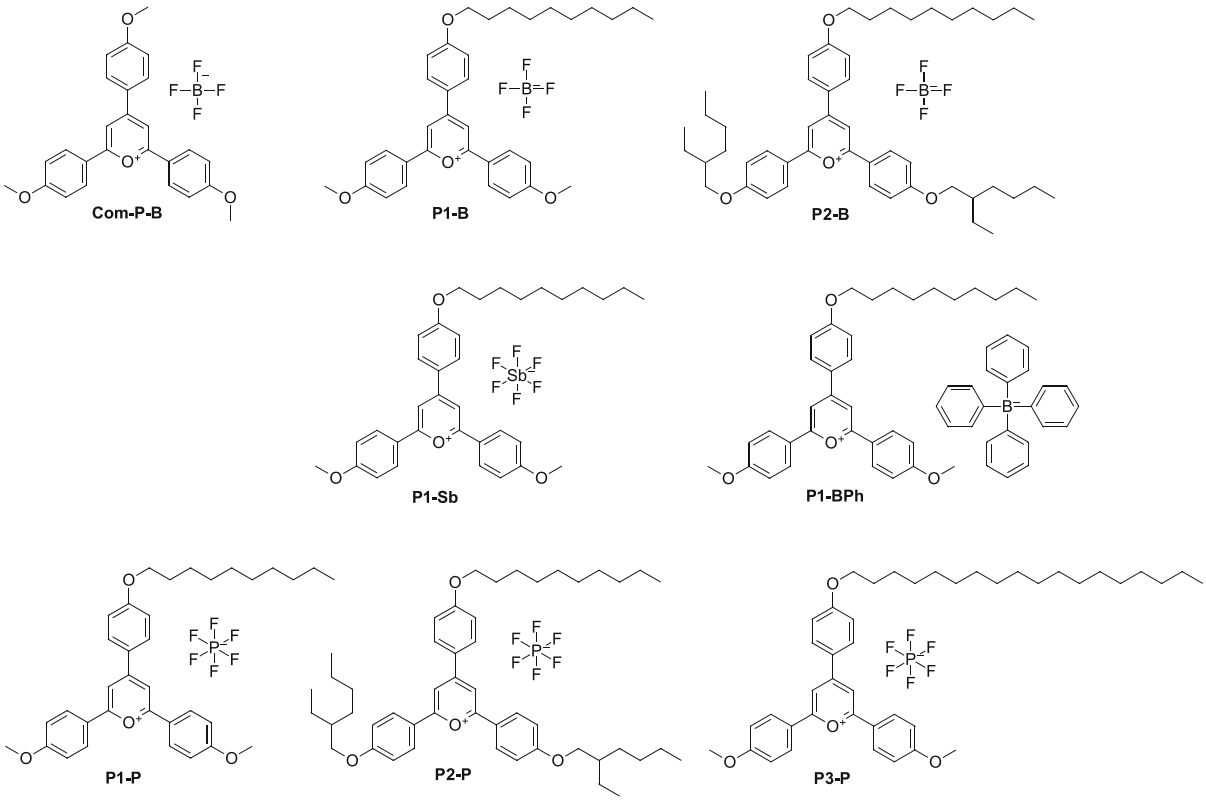

Longer, branched alkoxy chains and the resulting decrease in polarity subsequently lead to better solubility as well as much more efficient interaction between the photoredox-mediator, initiator and monomer. The best performing salt across the tetrafluoroborates with conversions of up to 88%, molecular weight of above 30000 g mol^{-1} and narrow dispersity Đ is clearly P1-B. By comparing pyrylium salts containing only different anions, an advantageous behavior of hexafluoroantimonates can be measured.

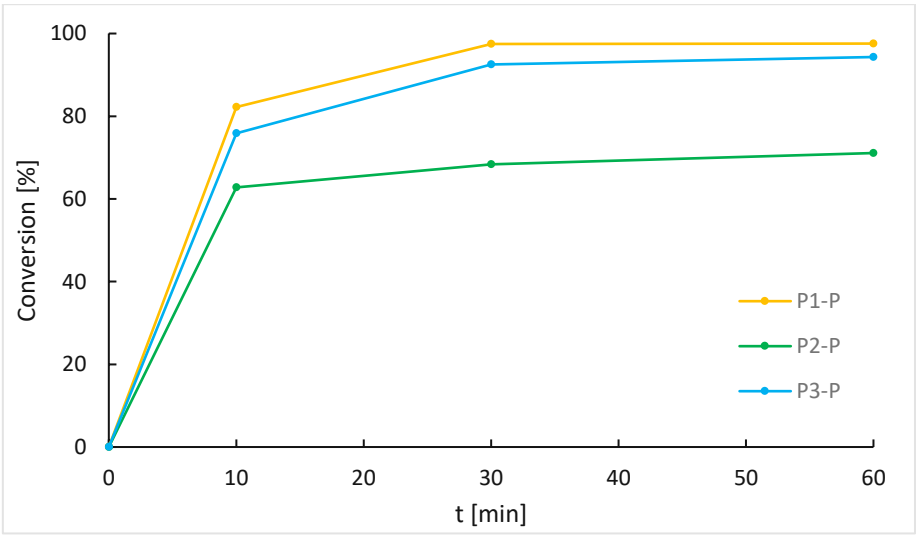

Figure 254: Conversions over time of pyrylium hexafluorophosphates, homopolymerization of N in d2-DCM solution

With astonishing conversions of 98% and a molecular weight of around 24000 g mol^{-1}, the new pyrylium hexafluorophosphate photoredox-mediator P1-P performs surprisingly well in

MF-ROMP of norbornene in solution (Figure 254). Significantly outperforming the commercial pyrylium compound Com-P-B which only achieves 74% conversion and similar M_n values in N. Polydispersities Đ of as low as 1.5 in N lead to narrowly distributed chain lengths during MF-ROMP with P1-P. In addition to the best performer P1-P with its decyloxy-chain, the even less polar P2-P with its two bulky ethyl-hexyloxy groups near its active O^+-center already suffers from steric hindrance. The smooth interaction between photoredox-mediator, initiator and monomer has to be ensured, hence P2-P only achieves 71% conversion of N. It is advantageous to introduce the long carbon-chains at the opposite site of the pyrylium cation to ensure the accessibility of the active pyrylium center. The third synthesized hexafluoroantimonate P3-P, which structurally shows the longest alkoxy chain with 18 carbon atoms compared to the 10 of P1-P remains a highly efficient mediator as well. The near doubling in chain length leads to much better solubility, however slightly lower conversions of 94% and reduced molecular weights with similar Đ. Nevertheless, the novel photoredox-mediators P2-B, P1-P and P3-P for MF-ROMP represent highly compelling alternatives to the state-of-the-art pyrylium salt Comp-P-B.

EXPERIMENTAL PART

I. The Cationic Species of Photoacid Generators

3. Onium Tetrafluoroborates

3.1. Synthesis

3.1.1. State of the Art Cations

3.1.1.1. Iodonium Salts

####### 3.1.1.1.1. Diphenyl Iodonium Tetrafluoroborate

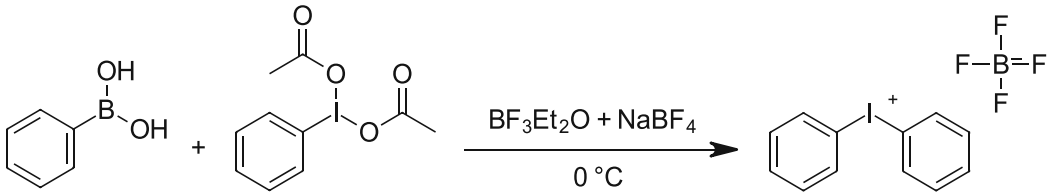

I1-B

27%

To synthesize I1-B, a reaction route according to Korwar et al.[128] was carried out. At first, 1 eq. (0.359 g, 3 mmol) of phenylboronic acid and 15 mL of dichloromethane were weighed into a 50 mL flask, which was purged with argon gas and cooled with an ice bath to 0 °C. The flask was equipped with a septum and set under argon atmosphere. To this clear solution 1.1 eq. (0.4 mL, 3.3 mmol) of boron trifluoride etherate, were added dropwise over 5 min. The solution was stirred for 15 min. After this step, 1 eq. (1.056 g, 3 mmol) of diacetoxyiodo benzene dissolved in 10 mL of dichloromethane was added and the mixture stirred for 1.5 h at 0 °C. In the last step, 3.5 mL of saturated sodium tetrafluoroborate solution in water was added and the mixture stirred for 30 min. Then, 50 mL of deionized water were added to the reaction mixture, the layers separated and the organic layer was washed twice with 50 mL of water afterwards and discarded. The aqueous layer was evaporated to a volume of approximately 4 mL and extracted with 25 mL of dichloromethane. The organic layer was dried and a white precipitate was received, which was washed with a mixture of 3:1 hexanes and dichloromethane. The white powder was washed with 3 x 20 mL of hexanes and then dried at the rotary evaporator, yielding 0.291 g (27% of theory/68% of lit.) of I1-B. The diphenyl iodonium tetrafluoroborate was characterized via melting point determination and various NMR measurements. The product was stored in the dark at 2 °C.

Analytics:

Melting point: 137.6 – 139.7 °C (lit. 135 – 136 °C)[208]

^{1}H-NMR (400 MHz, $CDCl_3$): 8.02 (d, 4H, 4x C-CH), 7.64 (t, 2H, 2x C-CH-CH-CH), 7.48 (t, 4H, C-CH-CH), 7.26 (s, $CDCl_3$)

^{13}C-NMR (100 MHz, $CDCl_3$): 135.5 (s, 4x C-CH), 133.1 (s, 2x P-C-CH-CH-CH), 132.8 (s, 4x C-CH-CH), 112.3 (s, 2x C), 77.2 (t, $CDCl_3$)

^{19}F-NMR (376 MHz, $CDCl_3$): -150.18 (s, BF_4), -150.24 (s, BF_4)

3.1.1.2. Sulfonium Salts

3.1.1.2.1. Triphenyl Sulfonium Tetrafluoroborate

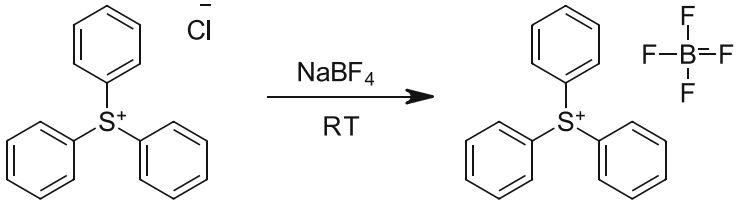

S1-Cl **S1-B**

25%

To synthesize S1-B, an ion exchange similar to Li et al.[129] was performed. At first, 1 eq. (0.508 g, 1.7 mmol) of S1-Cl and 10 mL of deionized water were weighed into a 50 mL flask. To this clear solution 1.1 eq. (0.206 g, 1.9 mmol) of sodium tetrafluoroborate, dissolved in 2 mL of deionized water, were added. A white precipitate was formed immediately. The mixture was stirred for 45 min. Next the dispersion was filtrated by a glass frit and washed with 2 x 25 mL of deionized water, followed by 1 x 25 mL of diethyl ether. The white solid was then dried at the rotary evaporator, yielding 0.148 g (25% of theory/32% of lit.) of S1-B. The triphenyl sulfonium tetrafluoroborate was characterized via melting point determination and various NMR measurements. The product was stored in the dark at 2 °C.

Analytics:

Melting point: 191.3 – 193.4 °C (lit. 186 – 187 °C)[209]

^{1}H-NMR (600 MHz, $CDCl_3$): 7.78-7.75 (m, 3H, 3x S-C-CH-CH-CH), 7.73-7.69 (m, 12H, 6x S-C-CH-CH & 6x S-C-CH), 7.26 (s, $CDCl_3$)

^{13}C-NMR (150 MHz, $CDCl_3$): 134.9 (s, 3x S-C-CH-CH-CH), 131.9 (s, 6x S-C-CH-CH), 131.4 (s, 6x S-C-CH), 124.6 (d, 3x S-C), 77.2 (t, $CDCl_3$)

^{19}F-NMR (376 MHz, $CDCl_3$): -150.27 (s, BF_4), -150.32 (s, BF_4)

3.1.1.2.2. 2,4,6-Triphenyl Thiopyrylium Tetrafluoroborate

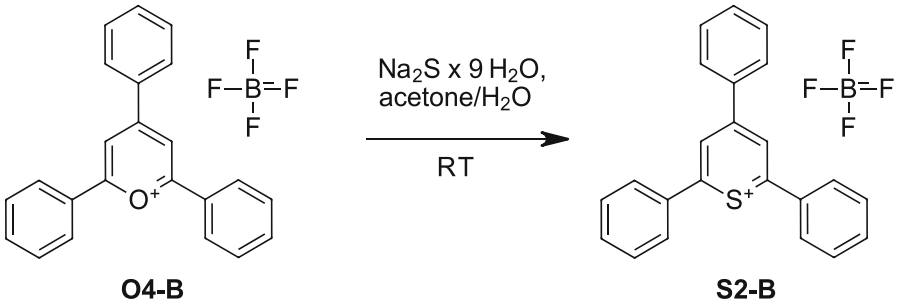

O4-B **S2-B**

24%

To synthesize S2-B, a reaction route according to Michaudel et al.[130] was carried out. At first, 1 eq. (1.128 g, 2.8 mmol) of O4-B was weighed into a flask and dissolved in 15 mL of acetone by gently applying heat. In a separate container, 4 eq. (3.70 g, 11.2 mmol) of sodium sulfide nonahydrate were dissolved in 10 mL of deionized water. The clear solution of sodium sulfide was added to a stirred clear solution of 2,4,6-triphenylpyrylium tetrafluoroborate. During the addition, the solution turned from yellow to red and was stirred for 1 h. Afterwards the red solution was added to 50 mL of stirred tetrafluoroboric acid (50 wt% in water) in an Erlenmeyer flask. A yellow precipitate started to form immediately and after 1 h of stirring, the yellow solid was filtrated via a glass frit and washed with 20 mL of diethyl ether. The product (around 0.7 g) was then dried in vacuum and afterwards recrystallized from 3 mL of acetonitrile. Due to insoluble parts, the dispersion was hot filtrated and the filtering paper purged with another 3 mL of acetonitrile to contain as much product as possible. By applying heat to the flask, the volume of acetonitrile was reduced to around 3 mL. The flask was allowed to cool down to room temperature, before being transferred to a colder environment at 2 °C. Yellow needles had formed over the course of a few hours. The crystals were filtrated via a glass frit and dried in vacuum to finally yield 0.302 g (24% of theory/63% of lit.) of 2,4,6-triphenylthiopyrylium tetrafluoroborate as yellow crystals. The S2-B was characterized via melting point determination and various NMR measurements. Additionally, a halogen test was performed to verify the absence of chloride anions by dissolving the product in a 1 : 1 mixture of methanol and deionized water and in a different container $AgNO_3$ crystals in the same mixture of solvents. The solution stayed transparent and no precipitate was formed. The product was stored in the dark at 2 °C.

Analytics:

Melting point: 193.6 – 197.8 °C (lit. 195 – 199 °C)[210]

^{1}H-NMR (600 MHz, CD_3CN): 9.01 (s, 2H, 2x S-C-CH), 8.21-8.17 (m, 2H, 2x S-C-CH-C-C-CH), 8.12-8.09 (m, 4H, 4x S-C-C-CH), 7.86-7.73 (m, 9H, 6x C-C-CH-CH; 3x C-C-CH-CH-CH), 7.26 (s, $CDCl_3$)

^{13}C-NMR (150 MHz, CD_3CN): 171.0 (s, 2x S-C), 163.5 (s, S-C-CH-C), 138.0 (s, S-C-CH-C-C), 135.5 (s, 2x S-C-C), 135.3 (s, 2x S-C-CH), 135.0 (s, S-C-CH-C-C-CH-CH-CH), 132.6 (s, 2x S-C-C-CH-CH-CH), 131.7 (s, 4x S-C-C-CH), 131.4 (s, 2x S-C-CH-C-C-CH), 131.1 (s, 2x S-C-CH-C-C-CH-CH), 130.2 (s, 4x S-C-C-CH-CH), 118.7 (s, CD_3CN), 1.4 (sep, CD_3CN)

^{19}F-NMR (564 MHz, CD_3CN): -151.79 (s, BF_4), -151.84 (s, BF_4)

3.1.2. Group 14 Cations

3.1.2.1. Methylium Salts

3.1.2.1.2. Tris(4-methoxyphenyl) Methylium Tetrafluoroborate

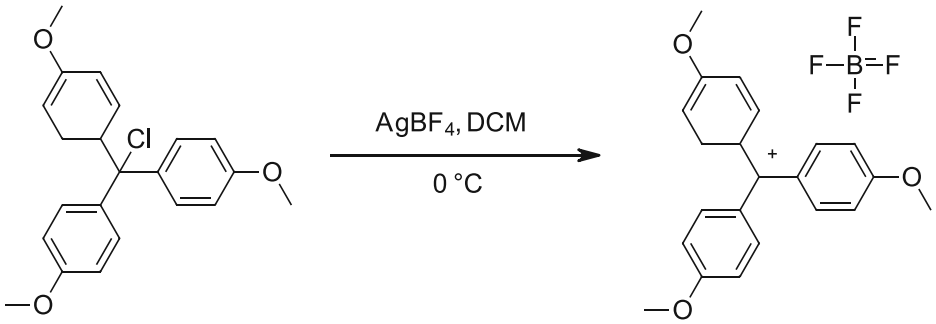

C2-B

80%

In order to produce C2-B, a synthesis route based on Karim et al.[133] was chosen. The first step was to weigh the starting materials in oven dried glass vials in the glove box. 1 eq. of $AgBF_4$ (0.293 g, 1.5 mmol) and 1 eq. of tris (4-methoxypenyl) methyl chloride (0.555 g, 1.5 mmol) were each dissolved in 5 mL of dry dichloromethane. The orange tris (4-methoxyphenyl) methyl chloride solution was added dropwise to the magnetically stirred $AgSbF_6$ solution at 0 °C and the vial washed with a further 2 mL of dichloromethane to ensure quantitatively transfer of the educt to the silver salt. When added dropwise, a white solid (AgCl) precipitated. After 2 h the reaction was stopped and the precipitate was centrifuged at 20 °C. The solution was decanted off and the solvent removed under argon atmosphere. In total the reaction yielded 0.508 g (80% of theory/123% of lit.) of tris (4-methoxyphenyl) methylium tetrafluoroborate as a deeply red colored solid. C2-B was characterized by various NMR measurements and a melting point determination. In addition, the stability against hydrolysis in air and water was checked via NMR. After around one minute, the result of the water stability test was negative. Direct exposure to water hydrolyzes the C2-B very quickly.

However, the experiment conducted in air was positive. There was no noticeable hydrolysis after 1 h of exposure of the product to ambient air. Additionally, a halogen test was performed to verify the absence of residual chloride anions by dissolving the product in methanol and in a different container $AgNO_3$ crystals in methanol with a minimal amount of deionized water to achieve a clear solution. Upon mixing, no precipitate (AgCl) was formed. The product was then stored at 2 °C in the dark under argon gas.

Analytics:

Melting point: 194.0 – 196.0 °C (slow discoloration starting at 140 °C) (lit. -)

^{1}H-NMR (400 MHz, CD_2Cl_2): 7.57 (d, 6H, 6x O-C-CH-CH), 7.28 (d, 6H, 6x O-C-CH), 5.32 (t, CD_2Cl_2), 4.10 (s, 9H, 3x O-CH_3)

^{13}C-NMR (150 MHz, CD_2Cl_2): 193.0 (s, C^+), 171.1 (s, 3x O-C), 143.4 (s, 6x O-C-CH-CH), 132.6 (s, 3x O-C-CH-CH-C), 117.0 (s, 6x O-C-CH), 57.6 (s, 3x CH_3), 54.0 (qui, CD_2Cl_2)

^{19}F-NMR (376 MHz, CD_2Cl_2): -153.27 (s, BF_4), -153.22 (s, BF_4)

3.1.2.2. Germanonium Salts

3.1.2.2.2. Triphenyl Germanonium Tetrafluoroborate

Triphenyl Germanonium Bromide

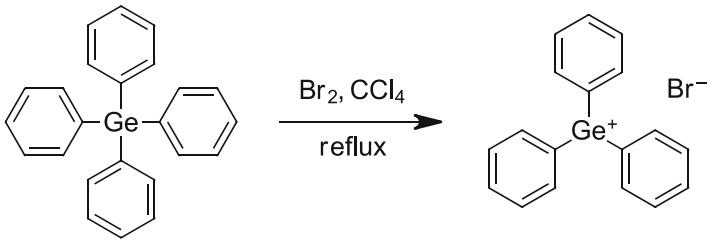

Ge-Br

30%

To synthesize Ge-Br, a reaction route according to Kraus et al.[134] was carried out. At first, 1 eq. (1.642 g, 4.3 mmol) of tetraphenyl germanium was weighed into a 25 mL flask and dissolved in carbon tetrachloride under argon atmosphere. The germanium educt was reacted with 1.1 eq. (0.24 mL, 4.7 mmol) of bromine and refluxed for 7 h at 77 °C. Afterwards the solvent was evaporated and the product dried in vacuum for 5 h at 0.1 mbar. Then the crude product was heated to 150 °C in a sublimation apparatus at 0.1 mbar to crystallize on the cooled surface. The first crystal layer was removed as soon as the apparatus reached the aimed temperature of 150 °C. Fraction 1 still contained a significant amount of impurities. In an interval of one hour, three fractions (2, 3 and 4) were collected and analyzed. Fraction 5 was collected after another 3 h. The fractions were analyzed via melting point determination and

various NMR measurements. Additionally, a halogen test was performed with silver nitrite to form, upon mixing with the Ge-Br in a methanol-water mixture, the insoluble white precipitate silver bromide. As expected fraction 1 had a melting interval of 102 – 125 °C and therefore was discarded. Fractions 4 and 5 (melting intervals of 135 – 150 °C) indicated some tetraphenyl germanium (lit. 230 – 235 °C), due to the long period of sublimation, despite its rather low volatility and high melting point. Only fraction 2 (melting interval of 133.1 - 138.5 °C) and fraction 3 (melting interval of 136.6 -138.8 °C) were pure enough for the next step and yielded in combination 0.596 g (30% of theory/61% of lit.) of the Ge-Br as white crystals. The product was stored in the dark at 2 °C.

Analytics:

Melting point: 136.6 – 138.8 °C (lit. 138.7 °C)[134]

^{1}H-NMR (400 MHz, $CDCl_3$): 7.66 – 7.61 (m, 6H, 6x C-CH), 7.49 – 7.41 (m, 9H, 6x C-CH-CH, 3x C-CH-CH-CH), 7.26 (s, $CDCl_3$)

^{13}C-NMR (100 MHz, $CDCl_3$): 134.8 (s, 3x Ge-C), 134.4 (s, 6x C-CH), 130.6 (s, 3x C-CH-CH-CH), 127.8 (s, 6x C-CH-CH), 77.2 (t, $CDCl_3$)

3.1.2.3. Stanonium Salts

3.1.2.3.2. Triphenyl Stanonium Tetrafluoroborate

Triphenyl Stanonium Bromide

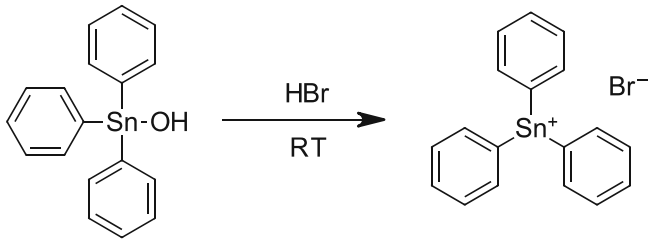

Sn-Br

39%

To synthesize Sn-Br, a reaction route according to Chambers et al.[138] was carried out. At first, 1 eq. (1.468 g, 4 mmol) of triphenyl tin hydroxide was weighed into a 200 mL beaker and dissolved in 150 mL of diethyl ether and 50 mL of chloroform. Afterwards the tin educt was shaken with 9 eq. (6 mL, 36 mmol) of hydrobromic acid (50 wt% in water). The layers were separated and the ether phase evaporated. The brownish solid powder was recrystallized from around 10 mL of diethyl ether and dried at the rotary evaporator under vacuum. Finally, 0.805 g (39% of theory/78% of lit.) of the Sn-Br were obtained as white crystals. The triphenyl stanonium bromide was characterized via melting point determination and various NMR

measurements. Additionally, a halogen test was performed with silver nitrite to form, upon mixing with the Sn-Br in a methanol-water mixture the insoluble white precipitate, silver bromide. The product was stored in the dark at 2 °C.

Analytics:

Melting point: 222.8 – 225.0 °C (lit. 220 – 221 °C)[138]

^{1}H-NMR (400 MHz, $CDCl_3$): 7.78 – 7.58 (m, 6H, 6x C-CH), 7.54 – 7.43 (m, 9H, 6x C-CH-CH, 3x C-CH-CH-CH), 7.26 (s, $CDCl_3$)

^{13}C-NMR (100 MHz, $CDCl_3$): 137.0 (s, 3x Sn-C), 136.2 (t, 6x C-CH), 130.4 (t, 3x C-CH-CH-CH), 129.2 (t, 6x C-CH-CH), 77.2 (t, $CDCl_3$)

^{119}Sn-NMR (149 MHz, $CDCl_3$): - 60.5 (s, Sn)

3.1.3. Group 15 Cations

3.1.3.1. Phosphonium Salts

3.1.3.1.2. Butyl Triphenyl Phosphonium Tetrafluoroborate

Butyl Triphenyl Phosphonium Bromide

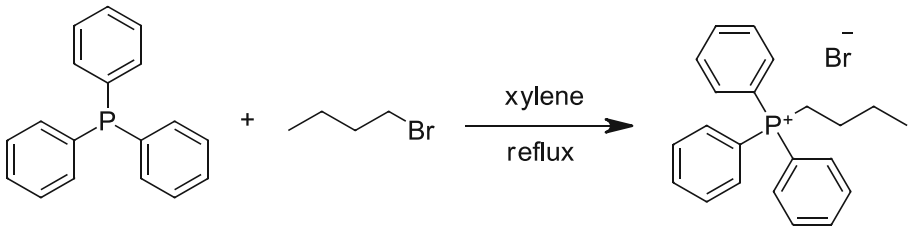

P1-Br

45%

At first, 1 eq. (2.979 g, 11.35 mmol) of triphenyl phosphine and 10 mL of xylene were weighed into a 25 mL two necked flask, equipped with a condenser and a septum. After the educt was completely dissolved, 0.98 eq. (1.2 mL) of 1-bromobutane were added. To avoid hydrolysis of the alkyl halide, a drying tube, filled with calcium chloride, was attached to the condenser and the whole apparatus was purged with argon gas once. Now the mixture was refluxed for 17 h. Shortly after the clear reaction mixture reached 60 °C, a white precipitate started to form. After cooling the dispersion to room temperature, the precipitate was filtered by a glass frit. The solid product was washed three times with 20 mL of xylene to remove unreacted educts. Using a rotary evaporator, the powder was dried, yielding 2.029 g of P1-Br (45% of theory/46% of lit.) as white crystals. The product was characterized via melting point determination and various NMR measurements.

Analytics:

Melting point: 241.3 – 243.0 °C (lit. 240 – 241 °C)[211]

^{1}H-NMR (400 MHz, $CDCl_3$): 7.85-7.75 (m, 9H, 6x P-C-CH-CH, 3x P-C-CH-CH-CH), 7.71-7.66 (m, 6H, 6x P-C-CH), 7.26 (s, $CDCl_3$), 3.79-3.72 (m, 2H, P-CH_2), 1.71-1.62 (m, 2H, P-CH_2-CH_2), 1.61-1.52 (m, 2H, P-CH_2-CH_2-CH_2), 0.88 (t, 3H, P-CH_2-CH_2-CH_2-CH_3)

^{13}C-NMR (100 MHz, $CDCl_3$): 135.2 (d, 3x P-C-CH-CH-CH), 133.8 (d, 6x P-C-CH-CH), 130.6 (d, 6x P-C-CH), 118.5 (d, 3x P-C), 77.2 (t, $CDCl_3$), 24.8 (d, P-CH_2-CH_2-CH_2), 23.8 (d, P-CH_2-CH_2), 22.8 (d, P-CH_2), 13.9 (s, P-CH_2-CH_2-CH_2-CH_3)

^{31}P-NMR (162 MHz, $CDCl_3$): 24.4 (s, 1P)

Butyl Triphenyl Phosphonium Tetrafluoroborate

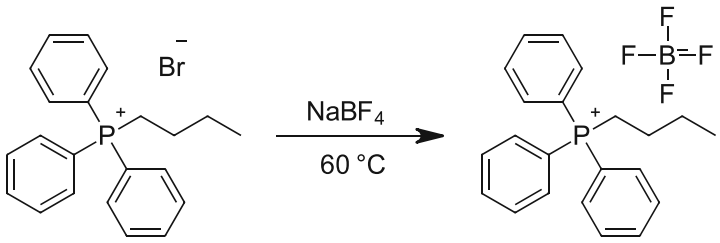

P1-Br **P1-B**

82%

To synthesize the tetrafluoroborate, an ion exchange similar to Li et al.[129] was performed. In a second step, 1 eq. (0.967 g, 2.5 mmol) of P1-Br and 10 mL of deionized water were weighed into a 50 mL flask, which was attached to a condenser. The mixture was magnetically stirred and heated to 60 °C, achieving a clear solution. After the educt was completely dissolved, 1.1 eq. (0.304 g, 2.8 mmol) of sodium tetrafluoroborate, dissolved in 1 mL of deionized water, were added. A white precipitate was formed immediately. The heating bath was removed and the mixture was allowed to cool down to room temperature, where it was further stirred for 4.5 h. Next the dispersion was filtrated by a glass frit and washed with 2 x 25 mL of deionized water, followed by 25 mL of diethyl ether. The solid, white powder was then dried at the rotary evaporator, yielding 0.832 g (82% of theory/106% of lit.) of P1-B. The butyl triphenyl phosphonium tetrafluoroborate was characterized via melting point determination and various NMR measurements. The product was stored in the dark at 2 °C.

Analytics:

Melting point: 159.5 – 162.8 °C (lit. -)

^{1}H-NMR (400 MHz, $CDCl_3$): 7.82-7.76 (m, 3H, 3x P-C-CH-CH-CH), 7.73-7.67 (m, 12H, 6x P-C-CH, 6x P-C-CH-CH), 7.26 (s, $CDCl_3$), 3.30-3.21 (m, 2H, P-CH_2), 1.63-1.54 (m, 4H, P-CH_2-CH_2-CH_2), 0.90 (t, 3H, P-CH_2-CH_2-CH_2-CH_3)

^{13}C-NMR (100 MHz, $CDCl_3$): 135.3 (d, 3x P-C-CH-CH-CH), 133.6 (d, 6x P-C-CH-CH), 130.7 (d, 6x P-C-CH), 118.3 (d, 3x P-C), 77.2 (t, $CDCl_3$), 24.7 (d, P-CH_2-CH_2-CH_2), 23.8 (d, P-CH_2-CH_2), 21.9 (d, P-CH_2), 13.7 (s, P-CH_2-CH_2-CH_2-CH_3)

^{31}P-NMR (162 MHz, $CDCl_3$): 23.8 (s, 1P)

^{19}F-NMR (376 MHz, $CDCl_3$): -150.70 (s, BF_4), -150.75 (s, BF_4)

3.1.3.1.3. Tetraphenyl Phosphonium Tetrafluoroborate

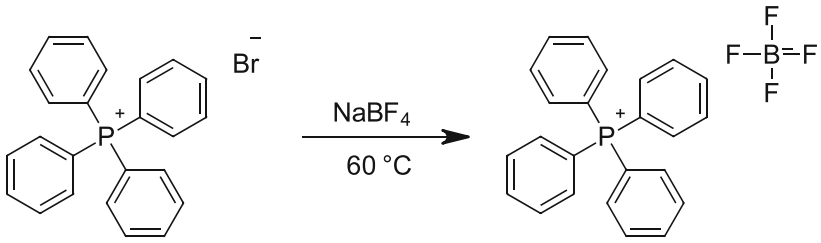

P2-Br **P2-B**

87%

To synthesize P2-B, an ion exchange similar to Li et al.[129] was performed. At first, 1 eq. (1.048 g, 2.5 mmol) of P2-Br and 20 mL of a mixture of methanol and deionized water (1:3) were weighed into a 50 mL flask, equipped with a condenser. The dispersion was magnetically stirred and heated to 60 °C, until the educt was completely dissolved. To this clear solution 1.1 eq. (0.304 g, 2.8 mmol) of sodium tetrafluoroborate, dissolved in 1 mL of deionized water, were added. A white precipitate was formed immediately. The heating bath was removed and the mixture was allowed to cool down to room temperature, where it was further stirred for 2 h. Next the dispersion was filtrated by a glass frit and washed with 2 x 25 mL of a mixture of methanol and deionized water (1:3), followed by 25 mL of diethyl ether. The solid, white powder was then dried at the rotary evaporator, yielding 0.925 g (87% of theory/113% of lit.) of P2-B. The tetraphenyl phosphonium tetrafluoroborate was characterized via melting point determination and various NMR measurements. The product was stored in the dark at 2 °C.

Analytics:

Melting point: 351.1 – 353.8 °C (lit. 350.5 °C)[209]

^{1}H-NMR (400 MHz, $CDCl_3$): 7.91-7.86 (m, 4H, 4x P-C-CH-CH-CH), 7.80-7.75 (m, 8H, 8x P-C-CH-CH), 7.67-7.62 (m, 8H, 8x P-C-CH), 7.26 (s, $CDCl_3$)

^{13}C-NMR (100 MHz, $CDCl_3$): 135.9 (d, 4x P-C-CH-CH-CH), 134.7 (d, 8x P-C-CH-CH), 130.9 (d, 8x P-C-CH), 117.4 (d, 4x P-C), 77.2 (t, $CDCl_3$)

^{31}P-NMR (162 MHz, $CDCl_3$): 23.1 (s, 1P)

^{19}F-NMR (376 MHz, $CDCl_3$): -150.71 (s, BF_4), -150.75 (s, BF_4)

3.1.3.1.4. Benzyl Triphenyl Phosphonium Tetrafluoroborate

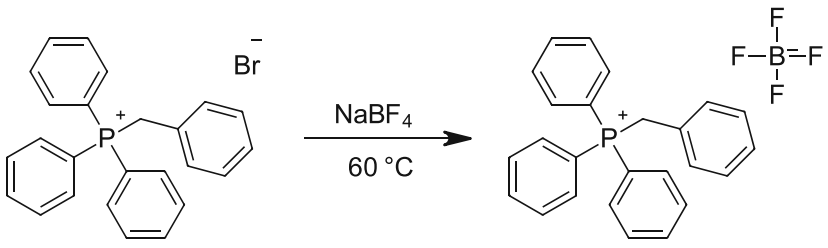

P3-Br **P3-B**

84%

To synthesize P3-B, an ion exchange similar to Li et al.[129] was performed. At first, 1 eq. (1.099 g, 2.5 mmol) of P3-Br and 40 mL of a mixture of methanol and deionized water (1:3) were weighed into a 50 mL flask, equipped with a condenser. The dispersion was magnetically stirred and heated to 60 °C, until the educt was completely dissolved. To this clear solution 1.1 eq. (0.304 g, 2.8 mmol) of sodium tetrafluoroborate, dissolved in 1 mL of deionized water, were added. A white precipitate was formed immediately. The heating bath was removed after 1 h and the mixture was allowed to cool down to room temperature, where it was further stirred for 2.5 h. Next the dispersion was filtrated by a glass frit and washed with 2 x 25 mL of a mixture of methanol and deionized water (1:3), followed by 25 mL of diethyl ether. The solid, white powder was then dried at the rotary evaporator, yielding 0.926 g (84% of theory/109% of lit.) of P3-B. The benzyl triphenyl phosphonium tetrafluoroborate was characterized via melting point determination and various NMR measurements. The product was stored in the dark at 2 °C.

Analytics:

Melting point: 209.4 – 211.1 °C (lit. 209 – 210 °C)[212]

^{1}H-NMR (400 MHz, $CDCl_3$): 7.80-7.74 (m, 3H, 3x P-C-CH-CH-CH), 7.65-7.60 (m, 6H, 6x P-C-CH-CH), 7.58-7.53 (m, 6H, 6x P-C-CH), 7.26 (s, $CDCl_3$), 7.25-7.21 (m, 1H, P-CH_2-C-CH-CH-CH), 7.12 (t, 2H, 2x P-CH_2-C-CH-CH), 6.95-6.92 (m, 2H, 2x P-CH_2-C-CH), 4.73 (d, 2H, P-CH_2)

^{13}C-NMR (100 MHz, $CDCl_3$): 135.3 (d, 3x P-C-CH-CH-CH), 134.3 (d, 6x P-C-CH-CH), 131.4 (d, 2x P-CH_2-C-CH), 130.4 (d, 6x P-C-CH), 129.2 (d, 2x P-CH_2-C-CH-CH), 128.8 (d, P-CH_2-C-CH-CH-CH), 126.9 (d, P-CH_2-C), 117.6 d, 3x P-C), 77.2 (t, $CDCl_3$), 30.5 (d, P-CH_2)

^{31}P-NMR (162 MHz, $CDCl_3$): 22.8 (s, 1P)

^{19}F-NMR (376 MHz, $CDCl_3$): -150.68 (s, BF_4), -150.74 (s, BF_4)

3.1.3.1.5. Cyclopropyl Triphenyl Phosphonium Tetrafluoroborate

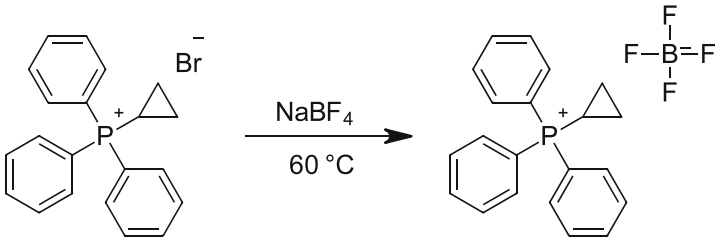

P4-Br **P4-B**

73%

To synthesize P4-B, an ion exchange similar to Li et al.[129] was performed. At first, 1 eq. (0.968 g, 2.5 mmol) of P4-Br and 20 mL of deionized water were weighed into a 50 mL flask, equipped with a condenser. The dispersion was magnetically stirred and heated to 60 °C, until the educt was completely dissolved. To this clear solution 1.1 eq. (0.306 g, 2.8 mmol) of sodium tetrafluoroborate, dissolved in 1 mL of deionized water, were added. A white precipitate was formed immediately. The heating bath was removed and the mixture was allowed to cool down to room temperature, where it was further stirred for 2 h. Next the dispersion was filtrated by a glass frit and washed with 2 x 25 mL of deionized water, followed by 25 mL of diethyl ether. The solid, white powder was then dried at the rotary evaporator, yielding 0.714 g (73% of theory/95% of lit.) of P4-B. The cyclopropyl triphenyl phosphonium tetrafluoroborate was characterized via melting point determination and various NMR measurements. The product was stored in the dark at 2 °C.

Analytics:

Melting point: 131.6 – 134.6 °C (lit. -)

^{1}H-NMR (400 MHz, $CDCl_3$): 7.82-7.66 (m, 15H, Ar-H), 7.26 (s, $CDCl_3$), 2.64-2.55 (m, 1H, P-CH), 1.74-1.66 (m, 2H, P-CH-CH_2), 0.67-0.59 (m, 2H, P-CH-CH_2)

^{13}C-NMR (100 MHz, $CDCl_3$): 135.5 (d, 3x P-C-CH-CH-CH), 133.9 (d, 6x P-C-CH-CH), 130.6 (d, 6x P-C-CH), 118.4 (d, 3x P-C), 77.2 (t, $CDCl_3$), 5.0 (d, 2x P-CH-CH_2), 0.0 (d, P-CH)

^{31}P-NMR (162 MHz, $CDCl_3$): 28.9 (s, 1P)

^{19}F-NMR (376 MHz, $CDCl_3$): -150.70 (s, BF_4), -150.74 (s, BF_4)

3.1.3.3. Stibonium Salts

3.1.3.3.1. Tetraphenyl Stibonium Tetrafluoroborate

Tetraphenyl Stibonium Bromide

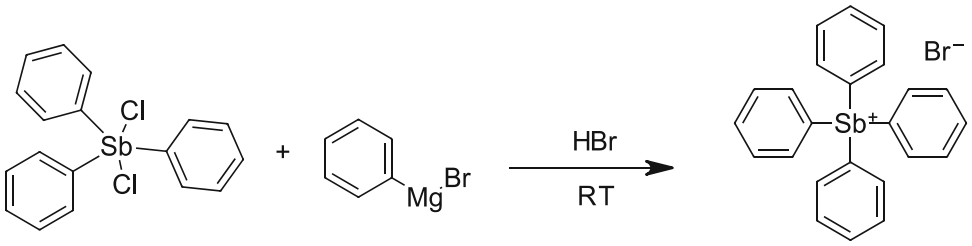

Sb-Br

61%

To synthesize Sb-Br, a reaction route according to Ma et al.[148] was carried out. At first, 1 eq. (1.950 g, 4.6 mmol) of triphenyl antimony dichloride was weighed into a 50 mL two-necked flask in a glove box to avoid hydrolysis of the precursor. Afterwards the antimony educt was dissolved in 12.3 mL of dry diethyl ether and 6.1 mL of dry toluene. The obtained solution was kept under argon for later use. In the meantime, 3 eq. (4.6 mL, 13.8 mmol) of phenyl magnesium bromide (3 M in diethyl ether) and 24.6 mL of dry diethyl ether were transferred into a 100 mL two necked-flask under Schlenk line conditions and stirred magnetically. Then the triphenyl antimony dichloride solution was added dropwise over 10 min to the phenyl magnesium bromide solution while stirring vigorously. By the use of a water bath, room temperature was maintained over the course of the reaction. After around 5 min the clear solution started to form some precipitate. The resulting dispersion was stirred for 8 days. Then 1.7 g of ice and 2.2 mL of hydro bromic acid (40% in water) were added and the mixture stirred overnight. The yellowish precipitate was filtered off by using a glass frit and washed with 30 mL of a 1 : 2 mixture of toluene and diethyl ether. The solid powder was recrystallized from 10 mL of a 3 : 2 mixture of water and ethanol. After filtration, washing with diethyl ether and drying in vacuum, 1.662 g (61% of theory/113% of lit.) of Sb-Br as white crystals were obtained. The tetraphenyl stibonium bromide was characterized via melting point determination and various NMR measurements. The product was stored in the dark at 2 °C.

Analytics:

Melting point: 209.1 – 212.9 °C (lit. 210 – 215 °C)[148]

^{1}H-NMR (400 MHz, $CDCl_3$): 7.81 – 7.78 (m, 8H, 8x C-CH), 7.56 – 7.46 (m, 12H, 8x C-CH-CH, 4x C-CH-CH-CH), 7.26 (s, $CDCl_3$)

^{13}C-NMR (100 MHz, $CDCl_3$): 135.5 (s, 8x C-CH), 131.5 (s, 4x C-CH-CH-CH), 129.8 (s, 8x C-CH-CH), 127.1 (s, 4x Sb-C), 77.2 (t, $CDCl_3$)

Tetraphenyl Stibonium Tetrafluoroborate

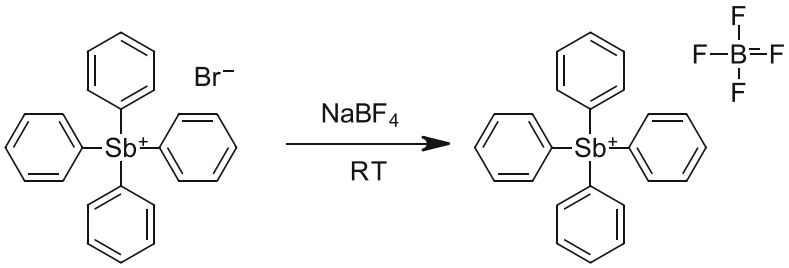

Sb-Br **Sb-B**
81%

Sb-Br was used in a procedure similar to Li et al.,[129] for an ion exchange reaction. To prepare Sb-B, at first 1 eq. (0.589 g, 1 mmol) of Sb-Br was dissolved in 16 mL of a 5 : 3 mixture of deionized water and methanol by gently applying heat to result in a clear solution. In the meantime, 3 eq. (0.346 g, 3 mmol) of sodium tetrafluoroborate were dissolved in 4 mL of a 5 : 3 mixture of deionized water and methanol. A clear solution was obtained after heating the mixture slightly. After both solutions were allowed to cool down to room temperature, their transparency was checked before moving on to the next step. The clear sodium tetrafluoroborate solution was added dropwise into the clear tetraphenyl stibonium bromide solution. A white precipitate started to form immediately and after 15 min of reaction time the reaction mixture was transferred into a tube which was centrifuged at 35 °C. The elevated temperature was used to keep possibly remaining educt (Sb-Br) for sure in solution. The fluid phase was discarded and the solid mixed with 18 mL of a 5 : 4 mixture of deionized water and methanol to remove excess sodium tetrafluoroborate. The mixture was centrifuged again at 35 °C and the washing fluid was discarded. The remaining solid white powder was dissolved in 10 mL of methanol and the solvent was evaporated at the rotary evaporator. After drying in vacuum, the Sb-B yielded 0.483 g (81% of theory/-) as a white powder. The tetraphenyl stibonium tetrafluoroborate was characterized via melting point determination and various NMR measurements. The product was stored in the dark at 2 °C.

Analytics:

Melting point: 274.7 – 277.0 °C (lit. -)

^{1}H-NMR (400 MHz, DMSO): 7.83 – 7.75 (m, 8H, 8x C-CH), 7.74 – 7.63 (m, 12H, 8x C-CH-CH, 4x C-CH-CH-CH), 2.5 (s, DMSO)

^{13}C-NMR (100 MHz, DMSO): 135.2 (s, 8x C-CH), 132.4 (s, 4x C-CH-CH-CH), 130.4 (s, 8x C-CH-CH), 128.8 (s, 4x Sb-C), 39.5 (sep, DMSO)

^{19}F-NMR (376 MHz, DMSO): -148.27 (s, BF_4), -148.32 (s, BF_4)

3.1.3.4. Bismuthonium Salts

3.1.3.4.1. Tetraphenyl Bismuthonium Tetrafluoroborate

Triphenyl Bismuth Dichloride

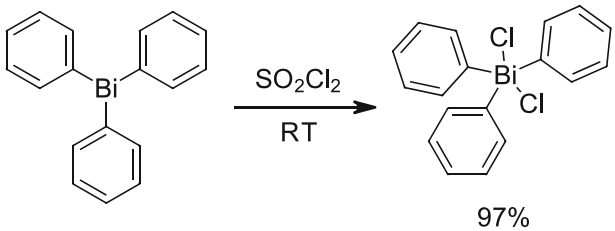

97%

To synthesize the triphenyl bismuth dichloride, a reaction route according to Solyntjes et al.[150] was carried out. First, 1 eq. of triphenyl bismuth (2.815 g, 6.4 mmol) was dissolved in 36 mL of dry dichloro methane. The mixture was magnetically stirred in a 50 mL round bottom flask equipped with a septum and was set under argon back pressure. Then 1.4 eq. of sulfonyl chloride (0.72 mL, 9 mmol) were added dropwise over 5 min. During the addition, SO_2 gas was formed. The mixture was stirred for 1 h. The solvent and residual sulfonyl chloride were evaporated at 50 °C and the remaining whitish solids were used in the next step without further purification. The reaction yielded 3.161 g (97% of theory/97% of lit.) of triphenyl bismuth dichloride. The triphenyl bismuth dichloride was characterized via melting point determination and various NMR measurements. In addition, a chloride test with $AgNO_3$ in DMSO was carried out, which was positive. Therefore, silver chloride precipitated out of solution. This qualitative analysis proved that the product contained chloride ions.

Analytics:

Melting point: 136.8 – 140.5 °C (lit. 149 – 150 °C)[213]

^{1}H-NMR (400 MHz, DMSO): 7.53 (d, 6H, 6x C-CH), 6.93 (t, 6H, 6x C-CH-CH), 6.78 (t, 3H, 3x C-CH-CH-CH), 2.50 (s, DMSO)

^{13}C-NMR (100 MHz, DMSO): 156.2 (s, 4x Bi-C), 129.7 (s, 8x C-CH), 127.7 (s, 8x C-CH-CH), 127.2 (s, 4x C-CH-CH-CH), 39.51 (sep, DMSO)

Triphenyl Bismuth Difluoride

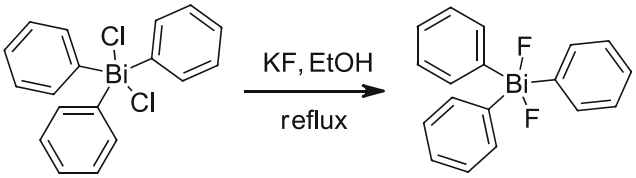

67%

To synthesize the difluoride, a reaction route according to Challenger et al.[151] was carried out. First, 1 eq. of triphenyl bismuth dichloride (7.233 g, 14.2 mmol) and 3 eq. of potassium fluoride (2.466 g, 42.5 mmol) were weighed into a 250 mL one-necked round bottom flask equipped with a condenser. The starting materials were dispersed in 100 mL of ethanol and 1 mL of deionized water. The mixture was refluxed for 20 h. The solids were filtered off with a glass frit and discarded. The filtrate was evaporated to dryness in vacuo to give a yellowish-beige solid, which was washed with 3x 20 mL of hot deionized water. Purification was carried out by washing the product with 20 mL of -20 °C cold diethyl ether. The beige solid was dried in vacuum and yielded 4.505 g (67% of theory/-) of triphenyl bismuth difluoride. The triphenyl bismuth difluoride was characterized via melting point determination and various NMR measurements. In addition, a chloride test with $AgNO_3$ in DMSO was carried out for all fractions, which was always negative. Therefore, no silver chloride precipitated out of solution. This proved that the product no longer contained any impurities of triphenyl bismuth dichloride.

Analytics:

Melting point: 155.3 – 162.1 °C (lit. 159 – 161 °C)[214]

^{1}H-NMR (400 MHz, DMSO): 8.10 (d, 6H, 6x C-CH), 7.74 (t, 6H, 6x C-CH-CH), 7.58 (t, 3H, 3x C-CH-CH-CH), 2.50 (s, DMSO)

^{13}C-NMR (100 MHz, DMSO): 144.0 (s, 4x Bi-C), 135.7 (s, 8x C-CH), 131.6 (s, 8x C-CH-CH), 131.4 (s, 4x C-CH-CH-CH), 39.51 (sep, DMSO)

^{19}F-NMR (376 MHz, DMSO): -153.4 (s, 2x Bi-F)

Tetraphenyl Bismuthonium Tetrafluoroborate

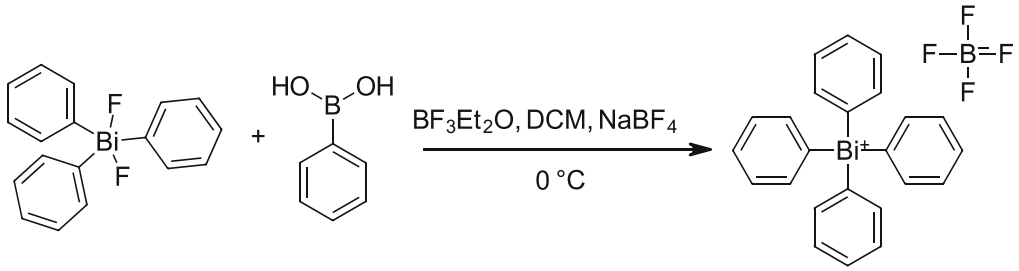

Bi1-B
84%

To synthesize Bi1-B, a reaction route according to Matano et al.[152] was carried out. The starting materials were weighed out in the glove box in order to avoid hydrolysis of the precursor. At first, 1 eq. of triphenyl bismuth difluoride (0.478 g, 1 mmol) and 1 eq. of benzene boronic acid (0.122 g, 1 mmol) were suspended in 10 mL of dry dichloromethane. The suspension was set under an argon atmosphere, cooled to 0 °C and magnetically stirred. Then 1 eq. of BF_3 diethyl etherate (0.125 mL, 1 mmol) was slowly added dropwise to the suspension, which resulted in a clear solution. After the addition, the ice bath was removed and the reaction solution was further stirred at room temperature. During the course of the reaction, intermediately some white precipitate started to form, which dissolved after some time again. After a total of 2 h of reaction time, a solution of 9.1 eq. of $NaBF_4$ (1.001 g, 9.1 mmol) in 40 mL of deionized water was added dropwise to the reaction solution. The mixture was then stirred vigorously for 0.5 h. The layers were then separated and the aqueous layer extracted twice with 10 mL of dichloromethane. The combined organic layers were dried with Na_2SO_4, filtered (filter washed with additional 5 mL of dichloromethane) and the solvent was removed at the rotary evaporator. The crude product resulted in 0.588 g of white crystals which were purified by recrystallization (31 mL with a ratio of 1 : 1.5 of diethyl ether : ethanol). The solution was allowed to cool down to room temperature and then stored at 2 °C. The crystals were filtrated via a glass frit (washed with additional 2 mL of ethanol) and dried in vacuum to finally yield 0.460 g of tetraphenyl bismuthonium tetrafluoroborate as white crystals in the first fraction. Additionally, the residual solution was concentrated in vacuum to yield further 0.049 g of Bi1-B. Hence a total yield of 0.509 g (84% of theory/127% of lit.) were obtained as pure tetraphenyl bismuthonium tetrafluoroborate. The Bi1-B was characterized via melting point determination and various NMR measurements. The product was stored in the dark at 2 °C.

Analytics:

Melting point: 246.0 – 248.0 °C (lit. 243 – 244 °C)[152]

^{1}H-NMR (400 MHz, $CDCl_3$): 7.80 (d, 8H, 8x C-CH), 7.68 (t, 8H, 8x C-CH-CH), 7.62 (t, 4H, 4x C-CH-CH-CH), 7.26 (s, $CDCl_3$)

^{13}C-NMR (100 MHz, $CDCl_3$): 137.8 (s, 4x Bi-C), 136.1 (s, 8x C-CH), 132.7 (s, 8x C-CH-CH), 132.6 (s, 4x C-CH-CH-CH), 77.23 (t, $CDCl_3$)

^{19}F-NMR (376 MHz, $CDCl_3$): -149.65 (s, BF_4), -149.70 (s, BF_4)

3.1.4. Group 16 Cations

3.1.4.1. Oxonium Salts

3.1.4.1.2. Triethyl Oxonium Hexafluorophosphate

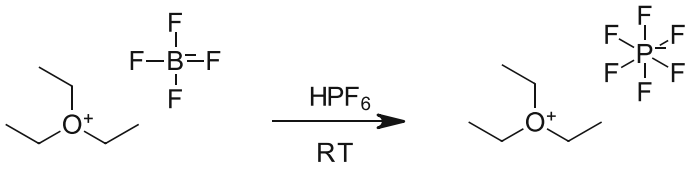

O2-B **O2-P**

5%

As generally known, the strong acid replaces the weaker acid in salts easily. Therefore, a counter ion exchange was performed by liberating the tetrafluoro boric acid. First, 1 eq. (0.986 g, 5.1 mmol) O2-B was dissolved in 5 mL of deionized water. Afterwards reacted by dropwise addition with 1.1 eq. (0.76 mL, 5.6 mmol) of hexafluoro phosphoric acid (65 wt% in H_2O) under cooling by using a water bath to around 15 °C. Immediately a white solid precipitated out of the clear solution. After 10 min of stirring, the precipitate was filtered off and washed with 3 x 1 mL of cold deionized water. The remaining solid was quickly transferred into a flask and purged with argon. Then the product was dried under reduced pressure (0.1 mbar) for 6 h. During the drying process, a noticeable amount of the white crystals evaporated, yielding 0.058 g (5% of theory/-) O2-P as a white powder. Characterization was performed via DSC analysis (O2-B has a decomposition temperature of 140 °C) and various NMR measurements. The product was stored in the dark at -18 °C.

Contact with water leads to decomposition of the O2-P into mainly diethyl ether and ethanol besides other decomposition products. Due to the weaker coordination of anion and cation compared to the educt O2-B, the Hexafluorophosphate decomposes faster in water.

Analytics:

Decomposition temperature: > 173 °C (lit. -)

^{1}H-NMR (600 MHz, $CDCl_3$): 7.26 (s, $CDCl_3$), 4.45 (q, 6H, 3x O-CH_2-CH_3), 1.66 (t, 9H, 3x O-CH_2-CH_3)

^{13}C-NMR (150 MHz, $CDCl_3$): 77.2 (t, $CDCl_3$), 66.2 (s, 3x O-CH_2-CH_3), 15.5 (s, 3x O-CH_2-CH_3)

3.1.4.1.3. Triphenyl Oxonium Tetrafluoroborate

Benzenediazonium Tetrafluoroborate

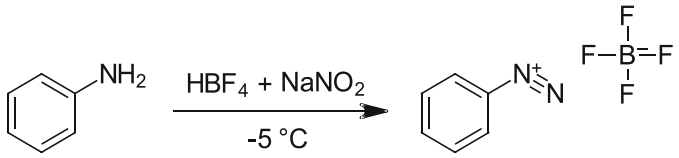

74%

Benzenediazonium tetrafluoroborate was synthesized according to Flood et al.[158] with the exception of using directly the tetrafluoroboric acid instead of the hydrochloric acid in the first step and therefore skipping the ion exchange afterwards. At first 2.1 eq. (26 mL, 105 mmol) of tetrafluoroboric acid (50 wt% in water) and additional 12 mL of deionized water were cooled down to -5 to -10 °C in a three-necked flask with a sodium chloride ice bath. The fluid was mechanically stirred due to the formation of a white, thick magma after the addition of 1 eq. (4.85 mL, 50 mmol) of distilled aniline. After the mixture was stirred for 15 min, 1.05 eq. (3.622 g, 52.5 mmol) of sodium nitrite were dissolved in 10 mL of distilled water, cooled down to -5 °C and added dropwise over 1 h. During this step the mixture was not allowed to reach a temperature above 0 °C. The slightly yellow-orange magma was then stirred for 1 h at -5 °C and afterwards the precipitated filtered by using a glass frit. The solids were washed with 50 mL of iced deionized water, followed by 50 mL of cold methanol, 50 mL of cold diethyl ether and finally 50 mL of cold hexanes. After the washing procedure the solid white powder was pre-dried in the glass frit by sucking air through the funnel for around 5 min. The benzenediazonium tetrafluoroborate yielded 7.1 g (74% of theory/89% of lit.) as a white powder. A quick approach to verify the presence of diazonium salts is the formation of nitrogen gas bubbles in around 10 to 20 min if exposed to sunlight in a DMSO solution in a small-diameter tube sitting at an angle. The product was used directly for the next reaction step after the 5 min drying procedure in the glass frit even though it was slightly wet due to the hexanes which were not removed completely during the process. For the NMR analysis, a small part of the diazonium salt was dried overnight in the desiccator while applying a slight vacuum (800 mbar). To characterize the product, various NMR measurements were performed.

Analytics:

^{1}H-NMR (400 MHz, acetone-d_6): 8.82 (d, 2H, 2x C-CH), 8.37 (t, 1H, C-CH-CH-CH), 8.07 (t, 2H, 2x C-CH-CH), 2.05 (q, acetone)

^{13}C-NMR (100 MHz, acetone-d_6): 206.8 (s, acetone), 155.3 (s, C), 129.9 (s, 2x C-CH-CH), 120.6 (s, C-CH-CH-CH), 115.3 (s, 2x C-CH), 29.9 (sept, acetone)

^{19}F-NMR (376 MHz, acetone-d_6): -150.79 (s, BF_4), -150.84 (s, BF_4)

Triphenyl Oxonium Tetrafluoroborate

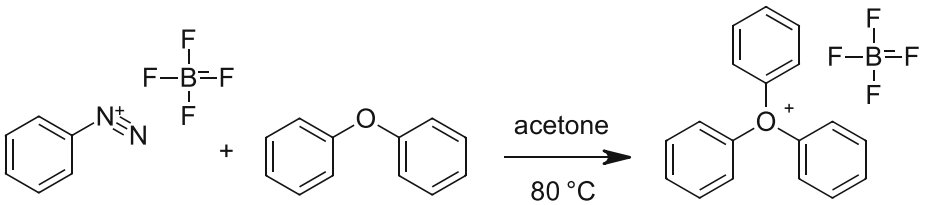

O3-B

0.2%

To synthesize O3-B, an reaction similar to the work of Nesmeyanov et al.[154] was carried out. In this paper an excess of diphenyl ether was reacted with a benzenediazonium tetrafluoroborate solution. 1 eq. of the benzyl diazonium tetrafluoroborate (7 g, 36.5 mmol) was dissolved in 300 mL of cold distilled acetone and kept in a beaker in a sodium chloride ice bath at -5 °C. It was reacted dropwise over 1 h with 16 eq. of diphenyl ether (99.9 g, 584 mmol) which were preheated to 80 °C in a flak under argon atmosphere. During the addition of the diazonium salt the solution turned from colorless to yellow to red. After refluxing for 0.5 h, the mixture was cooled to room temperature and stirred overnight. The acetone was evaporated at the rotary evaporator. Afterwards 20 mL of a 1 : 1 mixture of acetone and deionized water were added and the layers separated. The extraction was performed again with another 20 mL of the acetone-water mixture. The acetone-water layers were combined and extracted with 40 mL of diethyl ether and the layers were separated. The evaporation of the acetone-water layer should result in the precipitation of the oxonium salt after the acetone is removed due to the insolubility of oxonium salts in water. This did not happen during the acetone evaporation. Therefore, the residual aqueous layer was combined with the residues of the evaporated diethyl ether layer to perform a different workup. This time 80 mL of hexanes were added and a white precipitate started to form at the phase boundary. The white solids were filtrated by a glass frit and washed with 20 mL of deionized water. Then the solid powder was dissolved in 40 mL of distilled acetone and transferred into

a flask, where the solvent was evaporated at the rotary evaporator. The whitish crystals were dried at the high vacuum pump of 10 min. After the workup of fraction 1, additional white solids precipitated out of the aqueous layer after around 15 min (where the 80 mL of hexanes were added previously). The solids were filtrated, washed with water and transferred with acetone into a flask where the solvents were evaporated and the crystals dried in high vacuum, resulting in fraction 2. For purification the two fractions were combined and dissolved in 2 mL of distilled acetone in a centrifuge tube just to be precipitated by the addition of 3 mL hexanes. After 5 min of centrifuging at 10 °C (5000 rpm) the solvent was decanted off and kept in another centrifuge tube. This precipitation was executed again to improve the purity of the triphenyl oxonium tetrafluoroborate even more before drying the white crystals in vacuum. Therefore fraction 1 was obtained as white crystals (21 mg, m_p = 241.9 °C decomp.). The combined decanted solvents (acetone-hexanes) were stored at 2 °C and lead to additional precipitate after 30 min. The dispersion was centrifuged and the solvent decanted off into another centrifuge tube. Fraction 2 was dried in vacuum and yielded white crystals (5 mg, m_p = 240.7 °C decomp.). Afterwards the acetone-hexanes from were stored at -18 °C overnight. Again, additional crystals started to form and were centrifuged. Fraction 3 was dried in vacuum and yielded white crystals (4 mg, m_p = 236.4 °C decomp.). In combination a total yield of 30 mg (0.2% of theory/20% of lit.) of triphenyl oxonium tetrafluoroborate was obtained as white crystals. The O3-B was characterized via melting point determination and various NMR measurements. Triphenyl oxonium tetrafluoroborate is insoluble in water and hexanes but well soluble in acetone. It is stable at room temperature and in acetone solution for several days at least. Also, small amounts of water (in the acetone solution for example) do also not hydrolyze the O3-B. The product was stored in the dark at 2 °C.

Analytics:

Melting point: 241.9 °C (decomposition) (lit. 226 °C decomp.)[154]

^{1}H-NMR (600 MHz, acetone-d_6): 8.13 (d, 6H, 6x C-CH), 7.81 (t, 6H, 6x C-CH-CH), 7.75 (d, 3H, 3x C-CH-CH-CH), 2.05 (q, acetone)

^{13}C-NMR (150 MHz, acetone-d_6): 206.8 (s, acetone), 161.6 (s, 3x C), 133.2 (s, 6x C-CH-CH), 132.4 (s, 3x C-CH-CH-CH), 121.5 (s, 6x C-CH), 29.9 (sept, acetone)

^{19}F-NMR (565 MHz, acetone-d_6): -151.26 (s, BF_4), -151.31 (s, BF_4)

3.1.4.1.5. 2,6-Di-tert-butyl-4-methyl Pyrylium Tetrafluoroborate

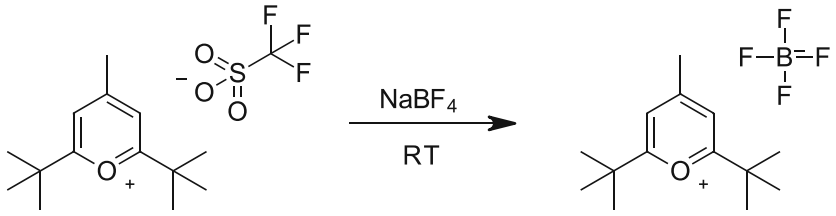

O5-S **O5-B**

59%

To synthesize O5-B, an ion exchange similar to a patent by Hovione Inter. LTD[160] was performed. At first, 12 eq. (6.5912 g, 60 mmol) of sodium tetrafluoroborate were dissolved in 60 mL of deionized water and 1 eq. of O5-S was dissolved in 30 mL of dichloromethane. Afterwards the organic layer was washed six times with 10 mL of the 1 N tetrafluoroborate solution. The organic layer was then evaporated resulting in a green powder. Yielding 0.869 g (59% of theory/72% of lit.) of O5-B. The 2,6-di-tert-butyl-4-methyl pyrylium tetrafluoroborate was characterized via decomposition temperature determination (melting point of educt: 170.0 – 173.5 °C) and various NMR measurements. The product was stored in the dark at 2 °C.

Analytics:

Decomposition temperature: > 190 °C (lit. -)

^{1}H-NMR (600 MHz, $CDCl_3$): 7.79 (s, 2H, 2x O-C-C<u>H</u>), 7.26 (s, $CDCl_3$), 2.86 (s, 3H, O-C-CH-C-C<u>H</u>$_3$), 1.53 (s, 18H, 6x O-C-C-C<u>H</u>$_3$)

^{13}C-NMR (150 MHz, $CDCl_3$): 186.0 (s, 2x O-<u>C</u>), 176.9 (s, O-C-CH-<u>C</u>), 120.5 (s, 2x O-C-<u>C</u>H), 77.2 (t, $CDCl_3$), 39.1 (s, 2x O-C-<u>C</u>), 28.3 (s, 6x O-C-C-<u>C</u>H$_3$), 24.9 (s, O-C-CH-C-<u>C</u>H$_3$)

^{19}F-NMR (376 MHz, $CDCl_3$): -151.17 (s, B<u>F</u>$_4$), -151.22 (s, B<u>F</u>$_4$)

3.1.4.2. Selenonium Salts

3.1.4.2.5. Triphenyl Selenonium Tetrafluoroborate

Dichloro Diphenyl Selenide

45%

At first, 1 eq. (2.543 g, 11 mmol) of diphenyl selenide was added into a 25 mL round bottom flask, which was cooled by a bath of cold water. Then 11 eq. (5 mL, 121 mmol) of concentrated nitric acid were added, resulting in an exothermic gas formation. After magnetically stirring for 30 min, 9 eq. (3 mL, 99 mmol) of concentrated hydrochloric acid were added, leading to

an immediate formation of a yellow precipitate. The dispersion was stirred for 5 min and filtrated by a glass frit. Resulting in a solid, yellow product, which was further washed with 70 mL of deionized water. Using a rotary evaporator, the product was dried, yielding 1.844 g of dichloro diphenyl selenide as yellow powder. Due to a broad melting interval, the purity of the product was improved via recrystallization from about 14 mL dry benzene. The crystals were washed with 25 mL of cold methanol, dried at the rotary evaporator and yielded 1.490 g (45% of theory/67% of lit.) as yellowish crystals. The dichloro diphenyl selenide was characterized via melting point determination and ^{1}H- / ^{13}C-NMR measurements.

Analytics:

Melting point: 180.2 – 183.6 °C (lit. 181 – 183 °C)[215]

^{1}H-NMR (400 MHz, $CDCl_3$): 8.06–7.99 (m, 4H, 4x Se-C-CH), 7.60-7.51 (m, 6H, 4x Se-C-CH-CH, 2x Se-C-CH-CH-CH), 7.26 (s, $CDCl_3$)

^{13}C-NMR (100 MHz, $CDCl_3$): 142.7 (s, 2x Se-C), 132.0 (s, 2x Se-C-CH-CH-CH), 131.5 (s, 4x Se-C-CH), 130.0 (s, 4x Se-C-CH-CH), 77.2 (t, $CDCl_3$)

Triphenyl Selenonium Chloride

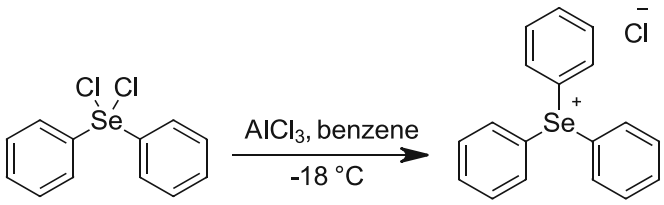

Se-Cl
31%

In the second step, 4.5 eq. (2.957 g, 22.1 mmol) of aluminum chloride were weighed into a 50 mL three-necked round bottom flask and dispersed by 22.5 eq. (10 mL, 110 mmol) of dry benzene. The flak was equipped with a condenser, which was attached to a drying tube filled with calcium chloride and was purged with argon once. The mixture was magnetically stirred and cooled to -18 °C via a sodium chloride-ice bath. Over 10 min, 1 eq. (1.490 g, 4.9 mmol) of dichloro diphenyl selenide was added to the dispersion, resulting in a red-brown solution. To quantitatively transfer the remaining of the selenide into the flask, another 22.5 eq. (10 mL, 110 mmol) of dry benzene were used. After the addition of the selenide was complete, the cooling-bath was removed and the mixture was allowed to heat up to room temperature, continuously stirring for 4 h. Now 40 mL of deionized water were added cautiously

(exothermic reaction) and two phases formed in the flask. The upper benzene layer was discarded and the aqueous layer was extracted three times with 40 mL of dichloromethane. The combined organic layers were evaporated at the rotary evaporator. The residue was a yellowish oil, which begun to foam in the flask. The solvent evaporation was interrupted, 75 mL of diethyl ether were added and the flask was stored at -18 °C for 18 h. On the next day the diethyl ether was discarded and the product was dried again at the rotary evaporator. This time no foam building occurred during the process. After the drying procedure, Se-Cl yielded 0.529 g (31% of theory/ 39% of lit.) as a yellowish powder. The triphenyl selenonium chloride was characterized via melting point determination and ^{1}H- / ^{13}C-NMR measurements.

Analytics:

Melting point: 217.6 – 221.6 °C (lit. -)

^{1}H-NMR (400 MHz, $CDCl_3$): 7.77-7.73 (m, 6H, 6x Se-C-CH), 7.66-7.54 (m, 9H, 6x Se-C-CH-CH, 3x Se-C-CH-CH-CH), 7.26 (s, $CDCl_3$)

^{13}C-NMR (100 MHz, $CDCl_3$): 133.1 (s, 3x Se-C-CH-CH-CH), 131.8 (s, 6x Se-C-CH), 131.3 (s, 6x Se-C-CH-CH), 128.7 (s, 3x Se-C), 77.2 (t, $CDCl_3$)

Triphenyl Selenonium Tetrafluoroborate

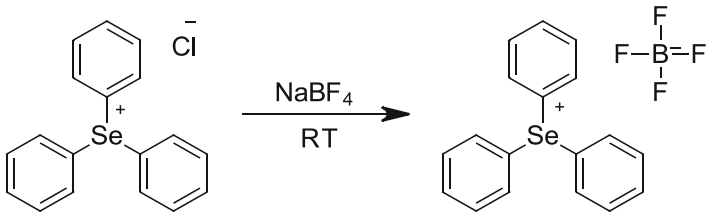

Se-Cl **Se-B**

65%

In the last step, 1 eq. (0.529 g, 1.53 mmol) of Se-Cl was weighed into a 50 mL round bottom flask and diluted with 6.2 mL of deionized water. Then 1 eq. (0.170 g, 1.53 mmol) of a sodium tetrafluoroborate solution in 1.7 mL of deionized water was added dropwise, under vigorous, magnetically stirring, into the flask. A yellowish precipitate formed immediately and the dispersion was stirred for 5 min, before filtrating the solid product by a glass frit. The product was washed two times with 10 mL of deionized water and once with 10 mL of cold diethyl ether. After removing the solvent residues at the rotary evaporator, the product Se-B was achieved as a yellowish powder, yielding 0.397 g (65% of theory/94% of lit.). The triphenyl

selenonium tetrafluoroborate was characterized via melting point determination and ^{1}H- / ^{13}C-NMR measurements and stored in a dry, dark environment at 2 °C.

Analytics:

Melting point: 184.3 – 186.4 °C (lit. 183 – 185 °C)[162]

^{1}H-NMR (400 MHz, $CDCl_3$): 7.74-7.69 (m, 3H, 3x Se-C-CH-CH-CH), 7.67-7.59 (m, 12H, 6x Se-C-CH, 6x Se-C-CH-CH), 7.26 (s, $CDCl_3$)

^{13}C-NMR (100 MHz, $CDCl_3$): 133.9 (s, 3x Se-C-CH-CH-CH), 131.8 (s, 6x Se-C-CH), 131.4 (s, 6x Se-C-CH-CH), 126.6 (s, 3x Se-C), 77.2 (t, $CDCl_3$)

^{19}F-NMR (376 MHz, acetone-d_6): -147.41 (s, BF_4), -147.46 (s, BF_4)

3.1.4.3. Telluronium Salts

3.1.4.3.5. Triphenyl Telluronium Tetrafluoroborate

Triphenyl Telluronium Chloride

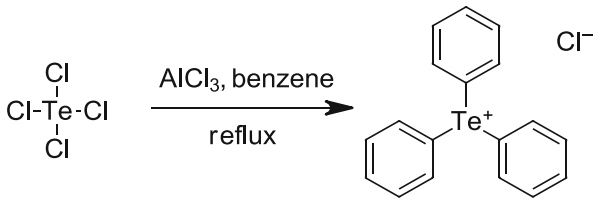

Te-Cl
60%

To synthesize 4P-Te-Br, a Lewis acid catalyzed reaction of the tellurium educt with benzene similar to Gunther et al.[163] was carried out. At first, 1 eq. (1.348 g, 5 mmol) of tellurium tetrachloride and 3 eq. (2.037 g, 15 mmol) of aluminum chloride were weighed into a 50 mL two-necked flask in a glove box to avoid hydrolysis of the precursor. The flask was equipped with a septum, a reflux condenser and a gas outlet at the top leading to gas washing bottles filled with sodium hydroxide solution. Argon atmosphere was maintained over the whole course of the reaction. Afterwards the educts were dissolved in 15 mL of dry benzene and the resulting yellow dispersion stirred magnetically. While the mixture was heated to 95 °C, there were several noticeable events. At around 70 °C the HCl formation started and the gas was forced up the condenser, through the gas washing bottles. This was achieved by constantly applying a slight stream of argon (balloon equipped with a needle outlet) through the septum of the flask. While reaching around 80 °C, the mixture turned grey. As soon as the benzene started to reflux, the mixture allowed to react for the next 70 min. The reaction was quenched

by carefully pouring the mixture into 20 mL of iced water. A black precipitate formed immediately and leftover aluminum chloride was hydrolyzed. After filtering the dispersion via a glass frit, the dark precipitate (~ 3.1 g) was collected and dissolved in 13 mL of boiling distilled water. The solution was hot filtrated and allowed to cool to room temperature and afterwards stored at 2 °C to form colorless needle crystals (~ 1.4 g). Recrystallization from 3 mL of a 6 : 4 mixture of ethanol and chloroform lead to colorless crystals which were washed with 10 mL of hexanes twice, followed by drying in vacuum. 1.184 g (60% of theory/83% of lit.) of Te-Cl was obtained. The triphenyl telluronium chloride was characterized via melting point determination and various NMR measurements. Additionally, a halogen test was performed to verify the chloride anions by dissolving the product in a 1 : 1 mixture of methanol and deionized water and in a different container $AgNO_3$ crystals in the same mixture of solvents. Upon mixing, a white precipitate was formed immediately (AgCl). The product was stored in the dark at 2 °C.

Analytics:

Melting point: 257.6 – 260.7 °C (lit. 249 – 250 °C)[163]

^{1}H-NMR (600 MHz, $CDCl_3$): 7.81 (d, 6H, 6x C-CH), 7.48 (t, 3H, 8x C-CH-CH-CH), 7.41 (t, 6H, C-CH-CH), 7.26 (s, $CDCl_3$)

^{13}C-NMR (150 MHz, $CDCl_3$): 135.2 (s, 6x C-CH), 131.5 (s, 3x C-CH-CH-CH), 130.4 (s, 6x C-CH-CH), 128.8 (s, 3x Te-C), 77.2 (t, $CDCl_3$)

Triphenyl Telluronium Tetrafluoroborate

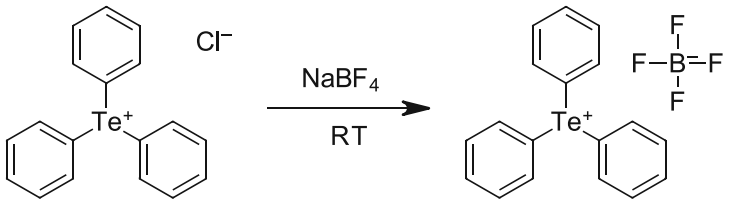

Te-Cl **Te-B**

71%

Te-Cl was used in a procedure similar to Li et al.,[129] for an ion exchange reaction. To prepare Te-B, at first 1 eq. (0.788 g, 2 mmol) of Te-Cl was dissolved in 6 mL of deionized water by gently applying heat to result in a clear solution. In the meantime, 1.05 eq. (0.231 g, 2.1 mmol) of sodium tetrafluoroborate were dissolved in 2 mL of deionized water. A clear solution was obtained after heating the mixture slightly. After both solutions were allowed to cool down to room temperature, their transparency was checked before moving on to the next step. The

clear sodium tetrafluoroborate solution was added dropwise into the clear triphenyl telluronium chloride solution. A white precipitate started to form immediately and after 15 min of reaction time the reaction mixture was filtrated via a glass frit. The solid was washed with 5 mL of deionized water twice to remove excess sodium tetrafluoroborate. After drying in vacuum, the Te-B yielded 0.633 g (71% of theory/89% of lit.) as a white powder. The triphenyl telluronium tetrafluoroborate was characterized via melting point determination and various NMR measurements. Additionally, a halogen test was performed to verify the absence of chloride anions by dissolving the product in a 1 : 1 mixture of methanol and deionized water and in a different container $AgNO_3$ crystals in the same mixture of solvents. The solution stayed transparent and no precipitate was formed. The product was stored in the dark at 2 °C.

Analytics:

Melting point: 211.5 – 215.2 °C (lit. 245 – 246 °C)[216]

^{1}H-NMR (600 MHz, $CDCl_3$): 7.64 (d, 6H, 6x C-CH), 7.61 (t, 3H, 3x C-CH-CH-CH), 7.53 (t, 6H, C-CH-CH), 7.26 (s, $CDCl_3$)

^{13}C-NMR (150 MHz, $CDCl_3$): 134.9 (s, 6x C-CH), 132.9 (s, 3x C-CH-CH-CH), 131.3 (s, 6x C-CH-CH), 123.5 (s, 4x Te-C), 77.2 (t, $CDCl_3$)

^{19}F-NMR (564 MHz, $CDCl_3$): -146.21 (s, BF_4), -146.26 (s, BF_4)

4. Onium Hexafluoroantimonates

4.1. Synthesis

4.1.1. Unmodified Cations

4.1.1.1. Diphenyl Iodonium Hexafluoroantimonate

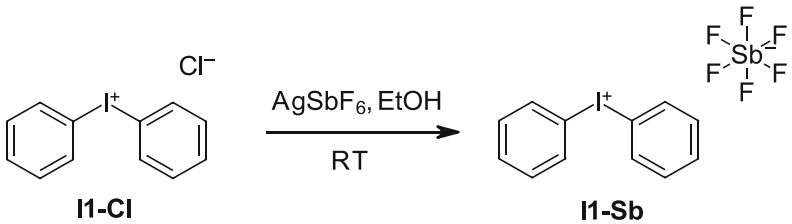

I1-Cl **I1-Sb**

73%

Diphenyl iodonium hexafluoroantimonate was synthesized in accordance to the work of Watanabe et al.[167] At first, 1.02 eq. of $AgSbF_6$ (0.252 g, 1.53 mmol) were weighed into a vial in the glove box and dissolved in 5 mL of dry ethanol. Then, 1 eq. (0.475 g, 1.50 mmol) of diphenyl iodonium chloride (I1-Cl) was weighed into a 50 mL flask and dissolved under stirring

and heating in 25 mL of dry ethanol. After the solution was allowed to cool down to room temperature, the $AgSbF_6$ solution was added dropwise to the solution of I1-Cl. The flask and the syringe were washed again with 5 mL of ethanol to ensure quantitatively transfer of the I1-Cl. A white precipitate (AgCl) was formed during this step. After a reaction time of 0.5 h at room temperature, the precipitate was filtered and the solvent was removed in vacuo. The crude product was a brownish oil, which did not crystallize. After storing the product for 24 h at 2 °C, however a gray color was observed, which turned out to be elemental silver. Therefore, the product was dissolved in 5 mL of methanol and the solution was centrifuged, therefore the silver contaminant removed. The solution was then decanted and the solvent removed in vacuo. This reaction route yielded 0.565 g (73% of theory/ 74% of lit.) of diphenyl iodonium hexafluoroantimonate. The I1-Sb was characterized melting point determination and various NMR measurements. Additionally, a halogen test was performed to verify the absence of residual chloride anions by dissolving the product in a 1 : 1 mixture of methanol and deionized water and in a different container $AgNO_3$ crystals in the same mixture of solvents. Upon mixing, no precipitate (AgCl) was formed. The product was stored in the dark at 2 °C.

Analytics:

Melting point: 104.1 – 106.4 °C (decomposition) (lit. -)

^{1}H-NMR (400 MHz, DMSO): 8.25 (d, 4H, 4x C-CH), 7.67 (t, 2H, 2x C-CH-CH-CH), 7.53 (t, 4H, C-CH-CH), 2.50 (qui, DMSO)

^{13}C-NMR (100 MHz, DMSO): 135.2 (s, 4x C-CH), 132.1 (s, 2x P-C-CH-CH-CH), 131.8 (s, 4x C-CH-CH), 116.5 (s, 2x C), 39.51 (sep, DMSO)

^{19}F-NMR (376 MHz, DMSO): -106.6 (s, SbF_6), -109.7 (s, SbF_6), -111.9 (s, SbF_6), -117.1 (t, SbF_6), -122.2 (t, SbF_6), -127.4 (s, SbF_6), -129.4 (s, SbF_6), -132.5 (s, SbF_6)

4.1.1.2. Tetraphenyl Bismuthonium Hexafluoroantimonate

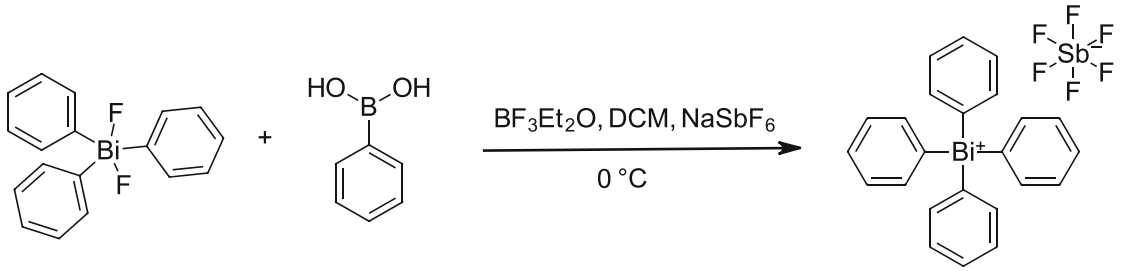

Bi1-Sb
28%

To synthesize Bi1-Sb, a reaction route according to Matano et al.[152] was carried out. The starting materials were weighed out in the glove box in order to avoid hydrolysis of the precursor. At first, 1 eq. of triphenyl bismuth difluoride (1.916 g, 4 mmol) and 1 eq. of benzene boronic acid (0.489 g, 4 mmol) were suspended in 10 mL of dry dichloromethane. The suspension was set under an argon atmosphere, cooled to 0 °C and magnetically stirred. Then 1 eq. of BF_3 diethyl etherate (0.5 mL, 4 mmol) was slowly added dropwise to the suspension, which resulted in a clear solution. After the addition, the ice bath was removed and the reaction solution was further stirred at room temperature. During the reaction some white precipitate started to form. After a total of 2 h of reaction time, a solution of 9.1 eq. of $NaSbF_6$ (9.421 g, 36.4 mmol) in 40 mL of deionized water was added dropwise to the reaction solution. The mixture was then stirred vigorously for 0.5 h. During the reaction a white precipitate started to form, which accumulated over time and did not dissolve either in the organic, nor in the aqueous layer. The white precipitate was filtrated using a glass frit and were washed around 30 mL of deionized water and 3 x 15 mL of chloroform was carried out to remove residual side product (tetraphenyl bismuthonium tetrafluoroborate). As an additional purification step the white crystals (0.985 g) were suspended in 2 x 10 mL chloroform and centrifuged afterwards. The solution was discarded and the solid dried in vacuum. This reaction route yielded 0.851 g (28% of theory/60% of lit.) of pure tetraphenyl bismuthonium hexafluoroantimonate. The Bi1-Sb was characterized via melting point determination and various NMR measurements. The product was stored in the dark at 2 °C.

Analytics:

Melting point: 290.7 °C (decomposition) (lit. 243 – 244 °C)[152]

^{1}H-NMR (400 MHz, DMSO): 7.89 (d, 8H, 8x C-CH), 7.72 (t, 8H, 8x C-CH-CH), 7.65 (t, 4H, 4x C-CH-CH-CH), 2.50 (s, DMSO)

^{13}C-NMR (100 MHz, DMSO): 144.0 (s, 4x Bi-C), 135.7 (s, 8x C-CH), 131.6 (s, 8x C-CH-CH), 131.5 (s, 4x C-CH-CH-CH), 39.51 (sep, DMSO)

^{19}F-NMR (376 MHz, DMSO): -106.6 (s, SbF_6), -109.7 (s, SbF_6), -111.9 (s, SbF_6), -117.1 (t, SbF_6), -122.63 (t, SbF_6), -127.5 (s, SbF_6), -129.5 (s, SbF_6), -132.7 (s, SbF_6)

4.1.1.3. Tris(4-methoxyphenyl) Methylium Hexafluoroantimonate

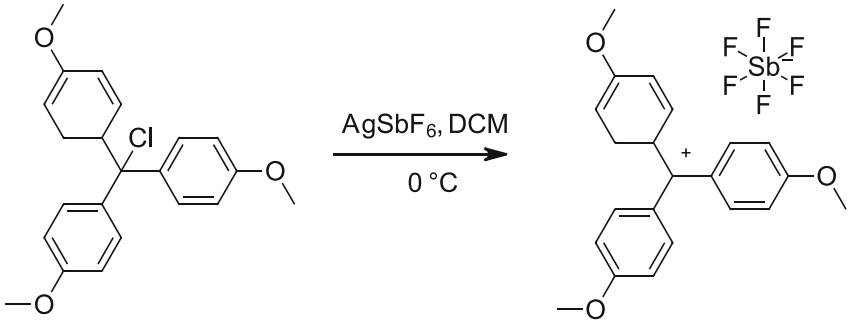

C2-Sb

78%

In order to synthesize C2-Sb, a route based on Karim et al.[133] was chosen. The first step was to weigh the starting materials in oven dried glass vials in the glove box. 1 eq. of $AgSbF_6$ (0.515 g, 1.5 mmol) and 1 eq. of tris (4-methoxypenyl) methyl chloride (0.555 g, 1.5 mmol) were each dissolved in 5 mL of dry dichloromethane. The orange tris (4-methoxyphenyl) methyl chloride solution was added dropwise to the magnetically stirred $AgSbF_6$ solution at 0 °C and the vial washed with a further 2 mL of dichloromethane to ensure quantitatively transfer of the starting material to the silver salt. When added dropwise, a white solid (AgCl) precipitated. After 2 h the reaction was stopped and the precipitate was centrifuged at 20 °C. The solution was decanted off and the solvent removed under argon atmosphere. In total the reaction yielded 0.671 g (78% of theory/-) of tris (4-methoxyphenyl) methylium hexafluoroantimonate as a deeply red colored solid. 3POMe-C- SbF_6 was characterized by various NMR measurements and a melting point determination. In addition, the stability against hydrolysis in air and water was checked via NMR. After around one minute, the result of the water stability test was negative. Direct exposure to water hydrolyzes the 3POMe-C-SbF_6 very quickly. However, the experiment conducted in air was positive. There was no noticeable hydrolysis after 1 h of exposure of the product to ambient air. Additionally, a halogen test was performed to verify the absence of residual chloride anions by dissolving the product in methanol and in a different container $AgNO_3$ crystals in methanol with a minimal

amount of deionized water to achieve a clear solution. Upon mixing, no precipitate (AgCl) was formed. The product was then stored at 2 °C in the dark under argon gas.

Analytics:

Melting point: 185.5 – 188.0 °C (lit. -)

^{1}H-NMR (400 MHz, CD_2Cl_2): 7.56 (d, 6H, 6x O-C-CH-CH), 7.27 (d, 6H, 6x O-C-CH), 5.32 (t, CD_2Cl_2), 4.10 (s, 9H, 3x O-CH_3)

^{13}C-NMR (150 MHz, CD_2Cl_2): 193.1 (s, C^+), 171.1 (s, 3x O-C), 143.4 (s, 6x O-C-CH-CH), 132.6 (s, 3x O-C-CH-CH-C), 116.9 (s, 6x O-C-CH), 57.6 (s, 3x CH_3), 54.0 (qui, CD_2Cl_2)

^{19}F-NMR (376 MHz, CD_2Cl_2): -111.2 (s, SbF_6), -114.4 (s, SbF_6), -116.6 (s, SbF_6), -121.8 (t, SbF_6), -127.6 (t, SbF_6), -132.2 (s, SbF_6), -134.2 (s, SbF_6), -137.3 (s, SbF_6)

4.1.1.4. 2,4,6-Triphenyl Pyrylium Hexafluoroantimonate

2,4,6-Triphenyl Pyrylium Chloride

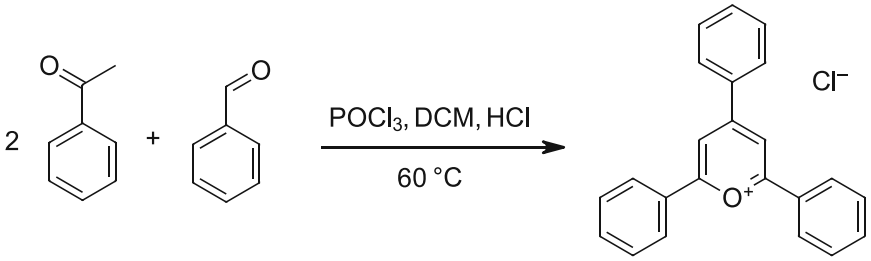

O4-Cl

39%

2,4,6-Triphenyl pyrylium chloride was synthesized in accordance to the work of Fortage et al.[168] At first, 1 eq. of benzaldehyde (1.715 mL, 16.8 mmol) and 2.5 eq. of acetophenone (4.900 mL, 42.0 mmol) were heated to 60 °C under magnetic stirring and argon atmosphere. Then 1.8 eq. of $POCl_3$ (2.8 ml, 30.0 mmol) were added dropwise, whereas the solution turned dark and HCl evolution started after around 30 min of stirring. The HCl gas was directed through two gas wash bottles (2nd filled with diluted, aqueous NaOH). As the solution became increasingly viscous, magnetic stirring was no longer possible after approximately 24 h. The reaction temperature was then kept for a total of 46 h. After the reaction time, the gummy dark brown mixture was dissolved in 42 mL of ethanol by refluxing for around 15 min. Then 1.5 eq. of concentrated HCl (2.25 mL, 25.4 mmol) were added dropwise to the boiling solution. After 5 min, the heating and stirring were stopped and the reaction solution was allowed to cool down to room temperature. Afterwards, 80 mL of diethyl ether were then added to the solution until the first solids precipitated out of solution. The mixture was stored at 2 °C for

45 min followed by the filtration of the yellow crystals via glass frit. The crystals were washed with diethyl ether until the filtrate was colorless. The filtrate, including diethyl ether from the washing step, was stored at 2 °C once more to obtain a second fraction. Finally, both fractions were combined and dried in vacuum to finally yield 2.232 g (39% of theory/57% of lit.) of 2,4,6-triphenylpyrylium chloride as yellow crystals. The O4-Cl was characterized via melting point determination and various NMR measurements. Additionally, a halogen test was performed to verify the absence of residual chloride anions by dissolving the product in a 1 : 1 mixture of methanol and deionized water and in a different container $AgNO_3$ crystals in the same mixture of solvents. Upon mixing, no precipitate (AgCl) was formed. The product was stored in the dark at 2 °C.

Analytics:

Melting point: 100.0 °C (slow decomposition) (lit. 156 - 158 °C)[217]

^{1}H-NMR (400 MHz, DMSO): 9.22 (s, 2H, 2x O^+-C-CH), 8.66 - 8.62 (m, 6H, 6x C-C-CH), 7.91 - 7.87 (m, 3H, C-C-CH-CH-CH), 7.83 – 7.78 (m, 6H, C-C-CH-CH), 2.50 (qui, DMSO)

^{13}C-NMR (100 MHz, DMSO): 170.1 (s, 2x O^+-C), 165.2 (s, 1x O^+-C-CH-C), 135.2 (s, 1x O^+-C-CH-C-C-CH-CH-CH), 135.0 (s, 2x O^+-C-C-CH-CH-CH), 132.5 (s, 1x O^+-C-CH-C-C), 130.2 (s, 2x O^+-C-CH-C-C-CH-CH), 129.9 (s, 4x O^+-C-C-CH-CH), 129.8 (s, 2x O^+-C-CH-C-C-CH), 129.2 (s, 2x O^+-C-C), 128.9 (s, 4x O^+-C-C-CH), 115.2 (s, O^+-C-CH), 39.51 (sep, DMSO)

2,4,6-Triphenyl Pyrylium Hexafluoroantimonate

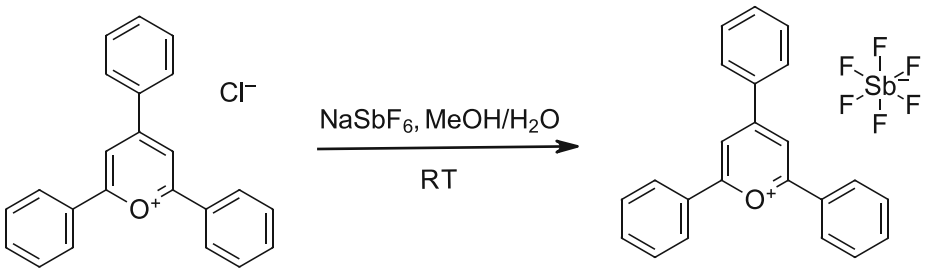

O4-Cl **O4-Sb**

74%

2,4,6-Triphenyl pyrylium hexafluoroantimonate was synthesized similar to the work of Li et al.[129] At first 1 eq. of 2,4,6-triphenylpyrylium chloride (1.728 g, 5 mmol) was dissolved in 80 mL of a 1 : 1 mixture of deionized water and methanol. In a separate flask, 1.5 eq. of $NaSbF_6$ (1.940 g, 7.5 mmol) were dissolved in 80 mL of the same solvent mixture. Then both solutions were filtered in order to separate some minor insoluble solids. Then the $NaSbF_6$ solution was

added to the magnetically stirred O4-Cl solution. Yellow solids precipitated immediately. After a reaction time of 40 min, the precipitate was filtered using a glass frit and washed three times with about 30 mL of a 1 : 1 mixture of deionized water and methanol. Finally, the 2,4,6-triphenylpyrylium hexafluoroantimonate was dried in vacuum to yield 2.007 g (73% of theory/-) as yellow crystals. The O4-Sb was characterized via melting point determination and various NMR measurements. Additionally, a halogen test was performed to verify the absence of residual chloride anions by dissolving the product in a boiling 7 : 1 mixture of methanol and deionized water and in a different container $AgNO_3$ crystals in the same boiling mixture of solvents. Upon mixing the two hot solutions, no precipitate (AgCl) was formed. The product was stored in the dark at 2 °C.

Analytics:

Melting point: 268.5 °C (decomposition) (lit. -)

^{1}H-NMR (400 MHz, DMSO): 9.17 (s, 2H, 2x O^+-C-CH), 8.60 (d, 6H, 6x C-C-CH), 7.90 - 7.86 (m, 3H, C-C-CH-CH-CH), 7.83 – 7.78 (m, 6H, C-C-CH-CH), 2.50 (qui, DMSO)

^{13}C-NMR (100 MHz, DMSO): 170.1 (s, 2x O^+-C), 165.1 (s, 1x O^+-C-CH-C), 135.2 (s, 1x O^+-C-CH-C-C-CH-CH-CH), 135.0 (s, 2x O^+-C-C-CH-CH-CH), 132.5 (s, 1x O^+-C-CH-C-C), 130.0 (s, 2x O^+-C-CH-C-C-CH-CH), 129.9 (s, 4x O^+-C-C-CH-CH), 129.8 (s, 2x O^+-C-CH-C-C-CH), 129.2 (s, 2x O^+-C-C), 128.8 (s, 4x O^+-C-C-CH), 115.2 (s, O^+-C-CH), 39.51 (sep, DMSO)

^{19}F-NMR (376 MHz, DMSO): -106.6 (s, SbF_6), -109.7 (s, SbF_6), -111.9 (s, SbF_6), -117.1 (t, SbF_6), -122.2 (t, SbF_6), -127.4 (s, SbF_6), -129.4 (s, SbF_6), -132.5 (s, SbF_6)

4.1.2. Alkoxylation of the Cations to improve Solubility

4.1.2.1. 4-Hexyloxyphenyl Triphenyl Bismuthonium Hexafluoroantimonate

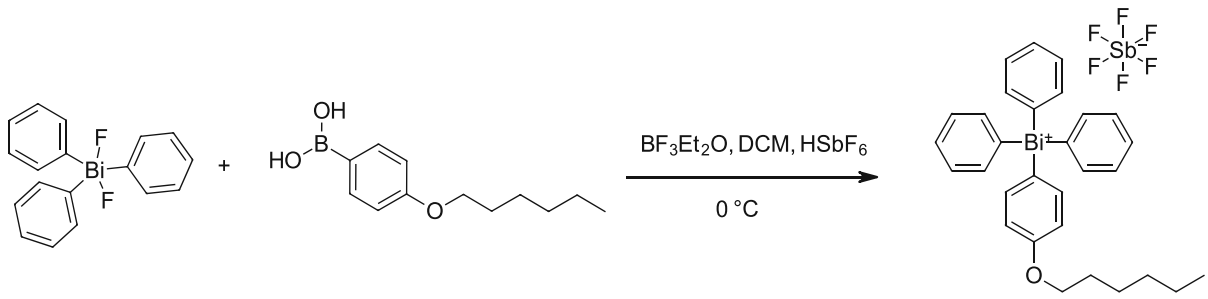

Bi2-Sb

97%

To synthesize Bi2-Sb, a reaction route according to Matano et al.[152] was carried out. First, the reactants were weighed in the glove box in order to avoid hydrolysis. 1 eq. of triphenyl

bismuth difluoride (1.196 g, 2.5 mmol) and 1 eq. of 4-hexoxyphenylboronic acid (0.556 g, 2.5 mmol) were weighed into a HD-PE bottle and dissolved in 25 mL of dry dichloromethane. The reaction solution was then magnetically stirred under an argon atmosphere and cooled to 0 °C. 1 eq. of BF_3-Et_2O (0.32 mL, 0.25 mmol) was then added dropwise and the cooling was then removed. The solution was stirred for 2 h at room temperature. Then 2 eq. of 65-70% aqueous $HSbF_6$ solution (1.87 g, 5 mmol) were added dropwise to the reaction mixture and the solution was stirred vigorously for 1 h to ensure good phase contact. After the reaction time, the layers were separated and the organic phase was washed with 2x 20 mL of deionized water to remove the remaining acids. The solvent was then removed at 60 °C in vacuum. Finally, the reaction route yielded 2.063 g (97% of theory/-) of pure 4-hexyloxyphenyl triphenyl bismuthonium hexafluoroantimonate as a viscous solid. The Bi2-Sb was characterized via various NMR measurements. The product was stored in the dark at 2 °C.

Analytics:

^{1}H-NMR (400 MHz, DMSO): 7.88 (d, 6H, 6x Bi^+-C-CH-CH-CH), 7.78 (d, 2H, 2x Bi^+-C-CH-CH-C), 7.72 (t, 6H, 8x Bi^+-C-CH-CH-CH), 7.65 (t, 3H, 3x Bi^+-C-CH-CH-CH), 7.26 (d, 2H, 2x Bi^+-C-CH-CH-C), 4.03 (t, 2H, O-CH_2), 2.50 (s, DMSO), 1.73 (qui, 2H, O-CH_2-CH_2), 1.42 (qui, 2H, O-CH_2-CH_2-CH_2), 1.35-1.27 (m, 4H, O-CH_2-CH_2-CH_2-CH_2-CH_2), 0.88 (t, 3H, CH_3)

^{13}C-NMR (100 MHz, DMSO): 161.0 (s, O-C), 143.7 (s, 3x Bi^+-C-CH-CH-CH), 137.3 (s, 2x O-C-CH), 135.6 (s, 6x Bi^+-C-CH-CH-CH), 133.2 (s, Bi^+-C-CH-CH-C), 131.6 (s, 6x C-CH-CH-CH), 131.4 (s, 3x C-CH-CH-CH), 117.6 (s, 2x O-C-CH-CH), 67.8 (s, O-CH_2), 39.51 (sep, DMSO), 30.9 (s, O-CH_2-CH_2), 28.4 (s, O-CH_2-CH_2-CH_2), 25.1 (s, O-CH_2-CH_2-CH_2-CH_2), 22.0 (s, O-CH_2-CH_2-CH_2-CH_2-CH_2), 13.9 (s, CH_3)

^{19}F-NMR (376 MHz, DMSO): -106.6 (s, SbF_6), -109.7 (s, SbF_6), -111.8 (s, SbF_6), -117.0 (t, SbF_6), -122.2 (t, SbF_6), -127.3 (s, SbF_6), -129.4 (s, SbF_6), -132.5 (s, SbF_6)

4.1.2.2. 4(4-Decyloxyphenyl)-2,6-Triphenyl Pyrylium Hexafluoroantimonate

4(4-Decyloxyphenyl)-2,6-Triphenyl Pyrylium Chloride

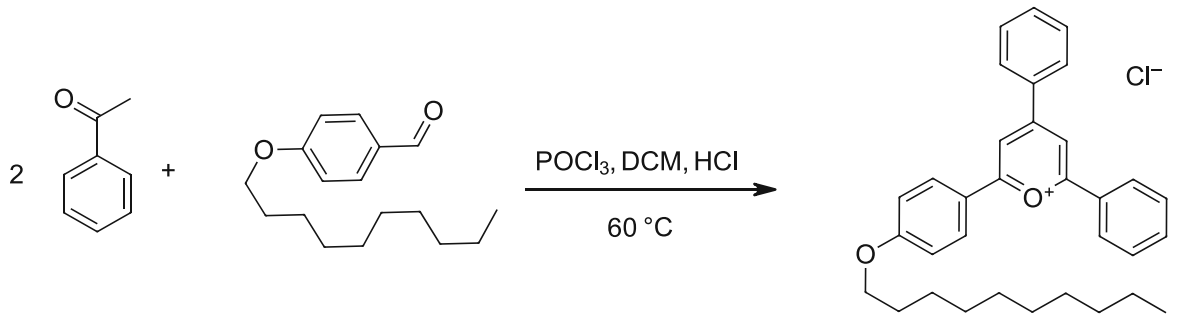

O7-Cl

45%

2,4,6-Triphenyl pyrylium chloride was synthesized in accordance to the work of Fortage et al.[168] At first, 1 eq. of 4-dodecyl benzaldehyde (1.031 g, 3.9 mmol) and 2.5 eq. of acetophenone (1.185 g, 9.8 mmol) were heated to 60 °C under magnetic stirring and argon atmosphere. Then 1.8 eq. of $POCl_3$ (0.66 ml, 7.1 mmol) were added dropwise, whereas the solution turned dark and HCl evolution started after around 30 min of stirring. The HCl gas was directed through two gas wash bottles (2nd filled with diluted, aqueous NaOH). As the solution became increasingly viscous, magnetic stirring was no longer possible after approximately 24 h. The reaction temperature was then kept for a total of 46 h. After the reaction time, the gummy dark brown mixture was dissolved in 24 mL of ethanol by refluxing for around 15 min. Then 1.5 eq. of concentrated HCl (0.52 mL, 5.9 mmol) were added dropwise to the boiling solution. After 5 min, the heating and stirring were stopped and the reaction solution was allowed to cool down to room temperature. Afterwards, 450 mL of diethyl ether were then added to the solution until the first solids precipitated out of solution. The dispersed solids were centrifuged and the diethyl ether decanted off. The solid was washed with 160 mL of diethyl ether. After this first purification step, the washing procedure was repeated 3 times to result in a total volume of 640 mL of diethyl ether as washing medium. The filtrate, including diethyl ether from the washing steps, was stored at 2 °C for 2 h to obtain even more precipitate. Both fractions were combined and dried in vacuum to finally yield 0.889 g (45% of theory/-) of 4(4-decyloxyphenyl)-2,6-triphenyl pyrylium chloride as orange crystals. The O7-Cl was characterized via melting point determination and various NMR measurements. Additionally, a halogen test was performed to verify the presence of chloride anions by dissolving the product in DMSO and in a different container $AgNO_3$ crystals in the same

solvent. Upon mixing, a precipitate (AgCl) was formed. The product was stored in the dark at 2 °C.

Analytics:

Melting point: 97.5 – 105.3 °C (lit. -)

^{1}H-NMR (400 MHz, DMSO): 9.07 (s, 2H, 2x O^{+}-C-CH), 8.74 (d, 2H, 4x O^{+}-C-CH-C-C-CH-CH), 8.57 (d, 4H, 4x C-C-CH-CH), 7.84 (t, 2H, 2x C-C-CH-CH-CH), 7.77 (t, 4H, 4x O^{+}-C-C-CH-CH), 7.29 (d, 2H, 2x O^{+}-C-CH-C-C-CH), 4.21 (t, 2H, 2x O-CH_2), 2.50 (qui, DMSO), 1.78 (qui, 2H, 2x O-CH_2-CH_2), 1.45 (qui, 2H, 2x O-CH_2-CH_2-CH_2), 1.39 - 1.24 (m, 12H, O-CH_2-CH_2-CH_2-CH_2-CH_2-CH_2-CH_2-CH_2-CH_2), 0.86 (t, 3H, CH_3)

^{13}C-NMR (100 MHz, DMSO): 168.7 (s, 2x O^{+}-C), 165.4 (s, 1x O^{+}-C-CH-C-C-CH-CH-C), 163.6 (s, 1x O^{+}-C-CH-C), 134.6 (s, 2x O^{+}-C-C-CH-CH-CH), 133.3 (s, 2x O^{+}-C-CH-C-C-CH-CH), 129.8 (s, 4x O^{+}-C-C-CH-CH), 129.3 (s, 2x O^{+}-C-C), 128.5 (s, 4x O^{+}-C-C-CH), 124.2 (s, 1x O^{+}-C-CH-C-C), 116.0 (s, 2x O^{+}-C-CH-C-C-CH), 113.1 (s, 2x O^{+}-C-CH), 68.6 (s, 1x O-CH_2), 39.51 (sep, DMSO), 31.3 (s, 1x O-CH_2-CH_2), 29.0 (s, 1x O-CH_2-CH_2-CH_2), 29.0 (s, 1x O-CH_2-CH_2-CH_2-CH_2), 28.8 (s, 1x O-CH_2-CH_2-CH_2-CH_2-CH_2), 28.7 (s, 1x O-CH_2-CH_2-CH_2 CH_2 CH_2-CH_2), 28.5 (s, 1x O-CH_2-CH_2-CH_2-CH_2-CH_2-CH_2), 25.4 (s, 1x O-CH_2-CH_2-CH_2-CH_2-CH_2-CH_2-CH_2-CH_2), 22.1 (s, 1x O-CH_2-CH_2-CH_2-CH_2-CH_2-CH_2-CH_2-CH_2-CH_2), 14.0 (s, 1x CH_3)

4(4-decyloxyphenyl)-2,6-Diphenyl Pyrylium Hexafluoroantimonate

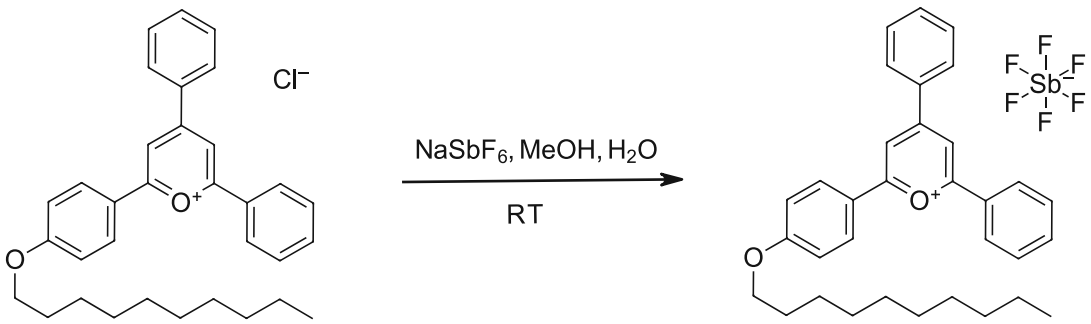

O7-Cl **O7-Sb**

63%

4(4decyloxyphenyl)-2,6-diphenyl pyrylium hexafluoroantimonate was synthesized similar to the work of Li et al.[129] At first 1 eq. of 2,4,6-triphenylpyrylium chloride (0.889 g, 1.8 mmol) was dissolved in 40 mL of a 1 : 4 mixture of deionized water and methanol under heating. In a separate flask, 1.5 eq. of $NaSbF_6$ (0.688 g, 2.7 mmol) were dissolved in 28 mL of the same solvent mixture. Then both solutions were filtered in order to separate some minor insoluble

solids. Then the $NaSbF_6$ solution was added to the magnetically stirred O7-Cl solution. Yellow solids precipitated immediately. After a reaction time of 1 h, the precipitate was filtered using a glass frit and washed three times with about 50 mL of a 1 : 4 mixture of deionized water and methanol. Finally, the 4(4decyloxyphenyl)-2,6-diphenyl pyrylium hexafluoroantimonate was dried in vacuum to yield 0.788 g (63% of theory/-) as yellow crystals. The O7-Sb was characterized via melting point determination and various NMR measurements. Additionally, a halogen test was performed to verify the absence of residual chloride anions by dissolving the product in DMSO and in a different container $AgNO_3$ crystals in the same solvent. Upon mixing the two hot solutions, no precipitate (AgCl) was formed. The product was stored in the dark at 2 °C.

Analytics:

Melting point: 174.8 – 178.8 °C (decomposition) (lit. -)

^{1}H-NMR (400 MHz, DMSO): 9.05 (s, 2H, 2x O^+-C-CH), 8.70 (d, 2H, 4x O^+-C-CH-C-C-CH-CH), 8.56 (d, 4H, 4x C-C-CH-CH), 7.85 (t, 2H, 2x C-C-CH-CH-CH), 7.78 (t, 4H, 4x O^+-C-C-CH-CH), 7.31 (d, 2H, 2x O^+-C-CH-C-C-CH), 4.23 (t, 2H, 2x O-CH_2), 2.50 (qui, DMSO), 1.79 (qui, 2H, 2x O-CH_2-CH_2), 1.46 (qui, 2H, 2x O-CH_2-CH_2-CH_2), 1.39 - 1.20 (m, 12H, O-CH_2-CH_2-CH_2-CH_2-CH_2-CH_2-CH_2-CH_2-CH_2), 0.87 (t, 3H, CH_3)

^{13}C-NMR (100 MHz, DMSO): 169.3 (s, 2x O^+-C), 166.0 (s, 1x O^+-C-CH-C-C-CH-CH-C), 164.0 (s, 1x O^+-C-CH-C), 135.1 (s, 2x O^+-C-C-CH-CH-CH), 133.6 (s, 2x O^+-C-CH-C-C-CH-CH), 130.3 (s, 4x O^+-C-C-CH-CH), 129.8 (s, 2x O^+-C-C), 129.0 (s, 4x O^+-C-C-CH), 124.6 (s, 1x O^+-C-CH-C-C), 116.5 (s, 2x O^+-C-CH-C-C-CH), 113.6 (s, 2x O^+-C-CH), 69.1 (s, 1x O-CH_2), 39.51 (sep, DMSO), 31.8 (s, 1x O-CH_2-CH_2), 29.5 (s, 1x O-CH_2-CH_2-CH_2), 29.4 (s, 1x O-CH_2-CH_2-CH_2-CH_2), 29.2 (s, 1x O-CH_2-CH_2-CH_2-CH_2-CH_2), 29.2 (s, 1x O-CH_2-CH_2-CH_2 CH_2 CH_2-CH_2), 29.0 (s, 1x O-CH_2-CH_2-CH_2-CH_2-CH_2-CH_2-CH_2), 25.9 (s, 1x O-CH_2-CH_2-CH_2-CH_2-CH_2-CH_2-CH_2-CH_2), 22.6 (s, 1x O-CH_2-CH_2-CH_2-CH_2-CH_2-CH_2-CH_2-CH_2-CH_2), 14.4 (s, 1x CH_3)

^{19}F-NMR (376 MHz, DMSO): -106.6 (s, SbF_6), -109.7 (s, SbF_6), -111.8 (s, SbF_6), -117.0 (t, SbF_6), -122.2 (t, SbF_6), -127.5 (s, SbF_6), -129.5 (s, SbF_6), -132.6 (s, SbF_6)

II. The Anionic Species of Photoacid Generators

3. Iodonium Borates

3.1. Synthesis

3.1.1. (4-Octoxyphenyl) Phenyl Iodonium Tosylate

Octyl Phenylether

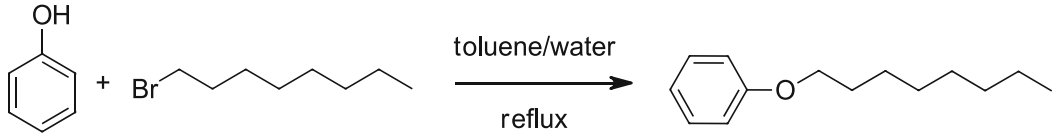

85%

To synthesize octyl phenylether, a synthesis according to a patent by Castellanos et al.[187] was carried out. At first, 1 eq. (44.89 g, 200 mmol) of 1-bromooctane, 2.39 eq. (38.62 g, 477 mmol) of phenol, 2.39 eq. (26.89 g, 478 mmol) of potassium hydroxide and 0.09 eq. (5.97 g, 18.6 mmol) of tetrabutylammonium bromide were dissolved in 100 mL of toluene and 100 mL of deionized water. The mixture was vigorously stirred and refluxed for 24 h to ensure a good phase contact between the water and the toluene. Afterwards the layers were separated and the organic layer was washed with 100 mL of 1 N NaOH, five times with 100 mL of deionized water and dried with sodium sulfate. The solvent was evaporated and the crude liquid product distilled under reduced pressure, yielding 35.248 g (85% of theory/89% of lit.) of octyl phenylether. The liquid octyl phenylether was characterized via various NMR measurements.

Analytics:

Boling Point: 124 – 126 °C (5 mbar)

^{1}H-NMR (400 MHz, DMSO): 7.26 (t, 2H, J_{HH} = 7 Hz, 2x O-C-CH), 6.92-6.87 (m, 3H, 2x O-C-CH-CH & 1x O-C-CH-CH-CH), 3.93 (t, 2H, J_{HH} = 6 Hz, O-CH_2), 2.50 (qui, DMSO), 1.69 (qui, 2H, J_{HH} = 8 Hz, O-CH_2-CH_2), 1.40 (qui, 2H, J_{HH} = 8 Hz, O-CH_2-CH_2-CH_2), 1.33-1.21 (m, 8H, O-CH_2-CH_2-CH_2-CH_2-CH_2-CH_2-CH_2), 0.86 (t, 2H, J_{HH} = 7 Hz, CH_3)

^{13}C-NMR (100 MHz, DMSO): 158.6 (s, O-C), 129.3 (s, 2x O-C-CH), 120.3 (s, 1x O-CH-CH-CH), 114.4 (s, 2x O-CH-CH), 67.2 (s, 1x O-CH_2), 39.51 (sep, DMSO), 31.2 (s, 1x O-CH_2-CH_2), 28.7 (s, 1x O-CH_2-CH_2-CH_2), 28.7 (s, 1x O-CH_2-CH_2-CH_2-CH_2), 28.6 (s, 1x O-CH_2-CH_2-CH_2-CH_2-CH_2), 25.5 (s, 1x O-CH_2-CH_2-CH_2-CH_2-CH_2-CH_2), 22.1 (s, 1x O-CH_2-CH_2-CH_2-CH_2-CH_2-CH_2-CH_2), 13.9 (s, 1x CH_3)

Hydroxy Tosyloxy Iodobenzene

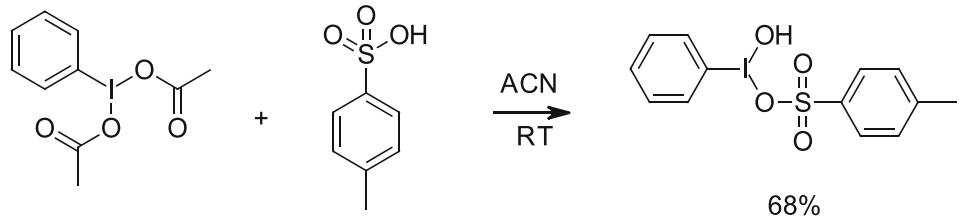

To synthesize hydroxy tosyloxy iodobenzene, a synthesis according to the work of Cross et at.[188] was carried out. At first, 1 eq. (9.638 g, 29.9 mmol) of iodobenzene diacetate and 1 eq. (5.692 g, 29.9 mmol) of 4-toluossulfoniuc acid monohydrate were suspended in 150 mL of acetonitrile. The mixture was magnetically stirred for 20 h and the solvent was removed. Afterwards the yellowish solids were washed with 3x 30 mL of water, followed by 3x 30 mL of acetonitrile and finally with 3x 30 mL of diethyl ether. The slightly yellowish crystals were dried in vacuum, yielding 8.016 g (68% of theory/72% of lit.) of hydroxy tosyloxy iodobenzene. The product was characterized via melting point determination and various NMR measurements. It was used in the next step without further purification.

Analytics:

Melting point: 137.5 – 141.5 °C (lit. 139 – 140 °C)[218]

^{1}H-NMR (400 MHz, DMSO): 8.21 (d, 2H, J_{HH} = 8 Hz, 2x I-C-CH), 7.70 (t, 1H, J_{HH} = 7 Hz, I-C-CH-CH-CH), 7.60 (t, 2H, J_{HH} = 7 Hz, 2x I-C-CH-CH), 7.48 (d, 2H, J_{HH} = 8 Hz, 2x S-C-CH), 7.12 (d, 2H, J_{HH} = 8 Hz, 2x S-C-CH-CH), 3.63 (s, 1H, OH), 2.50 (qui, DMSO), 2.29 (s, 3H, CH_3)

^{13}C-NMR (100 MHz, DMSO): 145.2 (s, S-C), 138.0 (s, CH_3-C), 137.1 (s, 2x S-C-CH), 131.1 (s, 2x I-C-CH-CH), 128.1 (s, 2x S-C-CH-CH), 127.7 (s, I-C-CH-CH-CH), 125.5 (s, 2x I-C-CH), 123.5 (s, I-C), 39.51 (sep, DMSO), 20.8 (s, CH_3)

(4-Octoxyphenyl) Phenyl Iodonium Tosylate

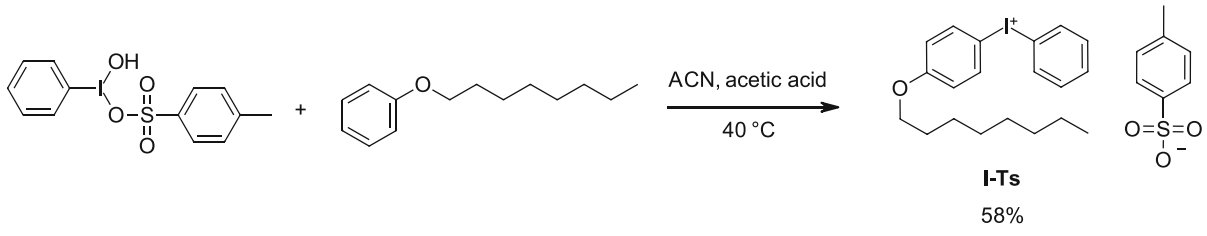

To synthesize (4-octoxyphenyl) phenyl iodonium tosylate, a synthesis similar to a patent of Castellanos et al.[187] was carried out. At first, 1 eq. (3.922 g, 10 mmol) of hydroxy tosyloxy iodobenzene, 1 eq. (2.065 g, 10 mmol) of octyl phenylether were weighed into a 50 mL flask

and mixed with 1.9 mL of acetonitrile and 0.5 mL of concentrated acetic acid. The mixture was heated up to 40 °C and the red solution magnetically stirred for 6.5 h. Then 26 mL of deionized water were added, the mixture vigorously stirred to enhance phase contact. The reaction was allowed to cool down to room temperature and stirred for 12 h. The organic layer was too viscous for efficient layer separation in a separation funnel. Therefore, the aqueous layer was removed via a pipette from the flask. To the viscous, organic layer 25 mL of deionized water were added and the mixture stirred for around one minute, followed by the removal of the aqueous layer via a pipette. This washing procedure was repeated 7x to result in a total of 200 mL of washing water. Afterwards the same washing procedure was carried out with 4 x 15 mL of diethyl ether to remove any residual non-polar starting materials. During execution of the last washing step with diethyl ether, a white precipitate started to form rapidly. If no precipitation occurs, the washing with diethyl ether can be continued. The white, sticky solids were filtrated by using a grass frit and dried in vacuum, yielding 3.341 g (58% of theory/75% of lit.) of (4-octoxyphenyl) phenyl iodonium tosylate. The I-Ts was characterized via melting point determination and various NMR measurements. It was stored in the dark at 2 °C.

Analytics:

Melting point: 122.8 – 125.8 °C (lit. -)

^{1}H-NMR (400 MHz, DMSO): 8.20 (d, 2H, 2x I^{+}-C-CH-CH-CH), 8.15 (d, 2H, 2x I^{+}-C-CH-CH-C), 7.64 (t, 1H, C-CH-CH-CH), 7.54-7.46 (m, 4H, 2x I^{+}-C-CH-CH-CH, 2x S-C-CH-CH), 7.11 (d, 2H, 2x S-C-CH), 7.05 (d, 2H, 2x I^{+}-C-CH-CH), 4.00 (t, 2H, O-CH_2), 2.50 (qui, DMSO), 2.29 (s, 3H, C-CH_3), 1.69 (qui, 2H, O-CH_2- CH_2), 1.38 (qui, 2H, O-CH_2-CH_2-CH_2), 1.33-1.18 (m, 8H, O-CH_2-CH_2-CH_2-CH_2-CH_2-CH_2-CH_2), 0.85 (t, 3H, CH_2-CH_3)

^{13}C-NMR (100 MHz, DMSO): 161.4 (s, O-C), 145.7 (s, S-C), 137.5 (s, C-CH_3), 137.3 (s, 2x I^{+}-C-CH-CH-C), 134.8 (s, 2x I^{+}-C-CH-CH-CH), 131.8 (s, C-CH-CH-CH), 131.5 (s, 2x I^{+}-C-CH-CH), 128.0 (s, 2x S-CH), 125.5 (s, 2x S-C-CH-CH), 117.7 (s, 2x I^{+}-C-CH-CH), 117.0 (s, I^{+}-C-CH-CH-CH), 105.1 (s, I^{+}-C-CH-CH-C), 39.51 (sep, DMSO), 68.0 (s, O-CH_2), 31.2 (s, O-CH_2-CH_2), 28.6 (s, O-CH_2-CH_2-CH_2), 28.6 (s, O-CH_2-CH_2-CH_2-CH_2), 28.4 (s, O-CH_2-CH_2-CH_2-CH_2-CH_2), 25.4 (s, O-CH_2-CH_2-CH_2-CH_2-CH_2), 22.0 (s, O-CH_2-CH_2-CH_2-CH_2-CH_2-CH_2), 20.8 (s, C-CH_3), 13.9 (s, CH_2-CH_3)

3.1.2. (4-Octoxyphenyl) Phenyl Iodonium Bis(trifluoromethane) Sulfonimide

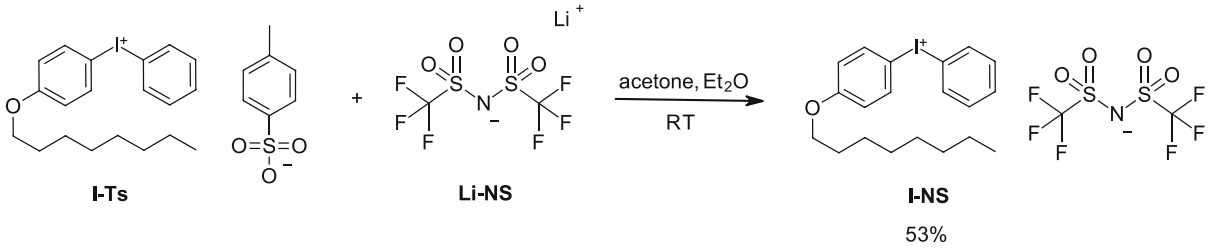

I-Ts **Li-NS** **I-NS**

53%

To synthesize (4-octoxyphenyl) phenyl iodonium bis(trifluoromethane) sulfonimide, a synthesis similar to a patent of Castellanos et al.[187] was carried out. At first, 1 eq. (1.161 g, 2 mmol) of (4-octoxyphenyl) phenyl iodonium tosylate was dissolved in 12 mL of distilled acetone by gentle heating. A clear solution was obtained. Then, 1 eq. (0.574 g, 2 mmol) of lithium bis(trifluoromethane) sulfonimide was dissolved in 12 mL of acetone. Afterwards the lithium salt solution was added into the iodonium salt solution. 30 mL of diethyl ether were added to result in a 4 : 5 mixture of acetone and diethyl ether, resulting in a cloudy dispersion after a few seconds. The formed precipitate is the byproduct lithium tosylate. The reaction mixture was stirred for 1 h and then transferred into a centrifugation tube. The white precipitate was removed via centrifugation. The solution was decanted off and the solvent was evaporated to result in a sticky solid, containing the aimed iodonium sulfonimide. In addition, the white precipitate was dried to result in 238 mg of lithium tosylate. The sticky solid was dissolved in 5 mL of acetone while heating gently. Then, 30 mL of diethyl ether were added, to result in a 1 : 6 mixture of the solvents. While stirring for 20 min, additional white precipitate started to form. Analogously to the previous workup, the mixture was centrifuged and the solution decanted off, the solvents evaporated and the sticky solid dried in vacuum. The precipitated lithium tosylate was dried again to result in 114 mg of lithium tosylate. 20 mL of diethyl ether were added to the sticky product. The solution was refluxed shortly via a heat gun to result in a cloudy dispersion, which was centrifuged, the solution decanted off and evaporated to dryness. An additional 22 mg of lithium tosylate were obtained during this purification step, due to its insolubility in diethyl ether. Therefore 374 mg of lithium tosylate precipitated in total, which were discarded at this point in time. The product was dissolved in 2 mL of acetone (tech) and flashed over ~2 g of silica gel in a glass frit. A total of 30 mL of acetone were added to perform the chromatography. The solvent was evaporated and the product dried in vacuum. Finally, 0.726 g (53% of theory/56% of lit.) of (4-octoxyphenyl) phenyl iodonium bis(trifluoromethane) sulfonimide were obtained as a highly viscous,

colorless liquid. The I-NS was characterized via various NMR measurements and was stored in the dark at 2 °C.

Analytics:

^{1}H-NMR (400 MHz, DMSO): 8.20 (d, 2H, 2x I^{+}-C-CH-CH-CH), 8.15 (d, 2H, 2x I^{+}-C-CH-CH-C), 7.64 (t, 1H, C-CH-CH-CH), 7.51 (t, 2H, 2x I^{+}-C-CH-CH-CH), 7.05 (d, 2H, 2x I^{+}-C-CH-CH), 4.00 (t, 2H, O-CH_2), 2.50 (qui, DMSO), 1.69 (qui, 2H, O-CH_2- CH_2), 1.38 (qui, 2H, O-CH_2-CH_2-CH_2), 1.32-1.17 (m, 8H, O-CH_2-CH_2-CH_2-CH_2-CH_2-CH_2-CH_2), 0.84 (t, 3H, CH_2-CH_3)

^{13}C-NMR (100 MHz, DMSO): 161.4 (s, O-C), 137.3 (s, 2x I^{+}-C-CH-CH-C), 134.8 (s, 2x I^{+}-C-CH-CH-CH), 131.8 (s, C-CH-CH-CH), 131.6 (s, 2x I^{+}-C-CH-CH), 124.3 (s, C-F_3), 121.1 (s, C-F_3), 117.9 (s, C-F_3), 117.8 (s, 2x I^{+}-C-CH-CH), 117.0 (s, I^{+}-C-CH-CH-CH), 114.7 (s, C-F_3), 105.1 (s, I^{+}-C-CH-CH-C), 39.51 (sep, DMSO), 68.1 (s, O-CH_2), 31.2 (s, O-CH_2-CH_2), 28.6 (s, O-CH_2-CH_2-CH_2), 28.6 (s, O-CH_2-CH_2-CH_2-CH_2), 28.4 (s, O-CH_2-CH_2-CH_2-CH_2-CH_2), 25.4 (s, O-CH_2-CH_2-CH_2-CH_2-CH_2-CH_2), 22.0 (s, O-CH_2-CH_2-CH_2-CH_2-CH_2-CH_2-CH_2), 13.9 (s, CH_2-CH_3)

^{19}F-NMR (376 MHz, DMSO): -78.7 (s, 2x C-F_3)

3.1.3. (4-Octoxyphenyl) Phenyl Iodonium Bis(oxalato)borate

Lithium Bis(oxalato)borate

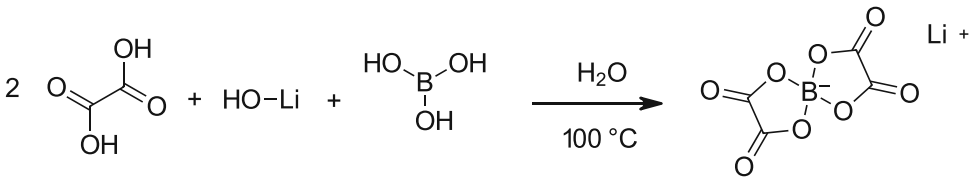

Li-B1

10%

To synthesize lithium bis(oxalatoborate), a synthesis according to a patent by Lischka et at.[192] was carried out. At first, 1 eq. (1.199 g, 50 mmol) of lithium hydroxide, 2 eq. (9.004 g, 100 mmol) of oxalic acid and 75 mL of deionized water were reacted in a 250 mL three-necked round bottom flask, equipped with a distillation apparatus. The mixture was stirred magnetically for 30 min and heated up to 30 °C due to the exothermic acid-base reaction taking place. To the clear solution, 1 eq. (3.092 g, 50 mmol) of boric acid was dissolved in 65 mL of deionized water were added over the course of 15 min. To ensure a quantitatively transfer of the boric acid, the beaker and the transfer syringe were washed with an additional 85 mL of deionized water. The mixture was heated to 100 °C internal temperature for 18 h, to distill off around 218 mL of water. Afterwards the still wet, white residue was dispersed in

10 mL of deionized water and allowed to cool down to room temperature. White crystals formed, which were filtrated, washed with 10 mL of ice-cold deionized water and dried at the rotary evaporator. Crude Li-B1 was obtained in a yield of 7.9 g. However, the pure product should be completely soluble in DMSO, which was not the case. Therefore, as a purification step, the Li-B1 was recrystallized. 7.9 g of lithium bis(oxalatoborate) were dissolved in 50 mL of boiling ethyl acetate and hot filtrated to remove any insoluble residuals. The ethyl acetate was removed at the rotary evaporator until a remaining volume of around 20 mL was reached. The solution was stored at 2 °C for several hours to let the crystals form. The white powder was filtrated, washed with 5 mL of ice-cold ethyl acetate and dried in vacuum, yielding 1.379 g (10% of theory/11% of lit.) of Li-B1. The lithium bis(oxalatoborate) was characterized via decomposition point determination and a ^{13}C-NMR measurements.

Analytics:

Melting point: 326 °C (decomposition) (lit. 314 °C)[219]

^{13}C-NMR (100 MHz, DMSO): 154.2 (s, 4x B$^-$-O-C), 40.0 (sep, DMSO)

^{11}B-NMR (128 MHz, DMSO): 7.37 (s, B)

(4-Octoxyphenyl) Phenyl Iodonium Bis(oxalato)borate

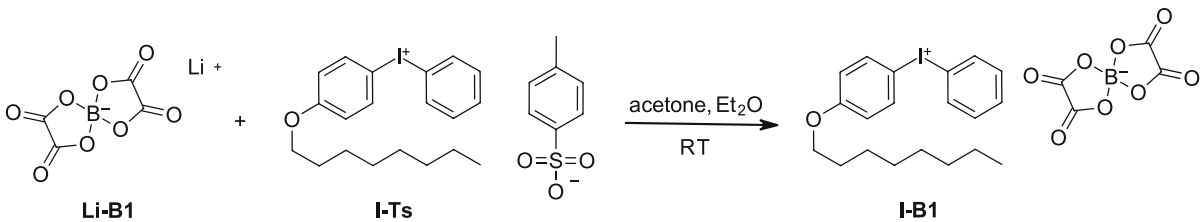

Li-B1 I-Ts I-B1

33%

To synthesize (4-octoxyphenyl) phenyl iodonium bis(oxalatoborate), a metathesis reaction similar to a patent of Castellanos et al.[187] was carried out. At first, 1 eq. (1.161 g, 2 mmol) of (4-octoxyphenyl) phenyl iodonium tosylate was dissolved in 12 mL of acetone by gentle heating. A clear solution was obtained. The, 1 eq. (0.388 g, 2 mmol) of lithium bis(oxalatoborate) was dissolved in 2 mL of acetone. Afterwards the lithium salt solution was added dropwise into the iodonium salt solution via a syringe. 3 mL of acetone as washing medium were used to quantitively transfer the lithium salt into the iodonium salt solution. Afterwards, 17 mL of diethyl ether were added to result in a 1 : 1 mixture of acetone and diethyl ether, resulting in a cloudy, white dispersion after a few seconds. The formed precipitate is the byproduct lithium tosylate. The reaction mixture was stirred for 20 min and

then transferred into a centrifugation tube. The white precipitate was removed via centrifugation. The solution was decanted off and the solvent was evaporated to result in a sticky solid, containing the aimed iodonium salt. In addition, the white precipitate was dried to result in 210 mg of lithium tosylate. The sticky solid was dissolved in 5 mL of acetone. Then, 30 mL of diethyl ether were added, to result in a 1 : 6 mixture of the solvents. While stirring for 20 min, additional white precipitate started to form. Analogously to the previous workup, the mixture was centrifuged and the solution decanted off, the solvents evaporated and the sticky solid dried in vacuum. The precipitated lithium tosylate was dried to result in 94 mg of lithium tosylate. Then, 31 mL of diethyl ether were added and the solution boiled shortly, which resulted in two layers. Therefore, 1.5 mL of acetone were added to result in a 1 : 21 mixture of the solvents. The cloudy dispersion was centrifuged, the solution decanted off and evaporated to dryness at the rotary evaporator and later on a high vacuum pump. An additional 46 mg of lithium tosylate were obtained during this purification step. The iodonium salt was transferred into a flask and 20 mL of diethyl ether and 0.5 mL of acetone were added. Two layers were formed and the mixture was boiled and stirred. Acetone was added dropwise until a one-layer system with white precipitate was obtained. During the heating procedure, some of the diethyl ether evaporated. After centrifugation, the clear solution was evaporated and the product dried in high vacuum. From the last purification step, 51 mg of lithium tosylate were obtained, resulting in a total amount of 401 mg precipitated, which were discarded at this point in time. The product was dissolved in 2 mL of acetone and flashed over ~2 g of silica gel in a glass frit. A total of 30 mL of acetone were added to perform the chromatography. Finally, 0.459 g (33% of theory/-) of (4-octoxyphenyl) phenyl iodonium bis(oxalatoborate) were obtained as a sticky, white solid. The I-B1 was characterized via various NMR measurements and was stored in the dark at 2 °C.

Analytics:

^{1}H-NMR (400 MHz, DMSO): 8.20 (d, 2H, 2x I^{+}-C-CH-CH-CH), 8.16 (d, 2H, 2x I^{+}-C-CH-CH-C), 7.66 (t, 1H, C-CH-CH-CH), 7.52 (t, 2H, 2x I^{+}-C-CH-CH-CH), 7.07 (d, 2H, 2x I^{+}-C-CH-CH), 4.01 (t, 2H, O-CH_2), 2.50 (qui, DMSO), 1.69 (qui, 2H, O-CH_2- CH_2), 1.38 (qui, 2H, O-CH_2-CH_2-CH_2), 1.32-1.18 (m, 8H, O-CH_2-CH_2-CH_2-CH_2-CH_2-CH_2-CH_2), 0.85 (t, 3H, CH_2-CH_3)

^{13}C-NMR (100 MHz, DMSO): 161.9 (s, O-C), 158.6 (s, 4x B^{-}-O-C), 137.7 (s, 2x I^{+}-C-CH-CH-C), 135.3 (s, 2x I^{+}-C-CH-CH-CH), 132.3 (s, C-CH-CH-CH), 132.1 (s, 2x I^{+}-C-CH-CH), 118.3 (s, 2x I^{+}-C-CH-CH), 117.5 (s, I^{+}-C-CH-CH-CH), 105.6 (s, I^{+}-C-CH-CH-C), 68.6 (s, O-CH_2), 40.0 (sep, DMSO),

31.7 (s, O-CH_2-$\underline{C}H_2$), 29.1 (s, O-CH_2-CH_2-$\underline{C}H_2$), 29.1 (s, O-CH_2-CH_2-CH_2-$\underline{C}H_2$), 28.9 (s, O-CH_2-CH_2-CH_2-CH_2-$\underline{C}H_2$), 25.9 (s, O-CH_2-CH_2-CH_2-CH_2-CH_2-$\underline{C}H_2$), 22.5 (s, O-CH_2-CH_2-CH_2-CH_2-CH_2-CH_2-$\underline{C}H_2$), 14.4 (s, CH_2-$\underline{C}H_3$)

^{11}B-NMR (128 MHz, DMSO): 7.37 (s, B)

3.1.4. (4-Octoxyphenyl) Phenyl Iodonium Difluoro(oxalato)borate

Lithium Difluoro(oxalato)borate

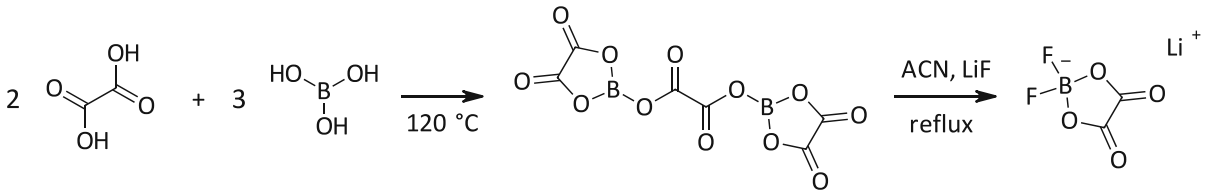

Li-B2
17%

The synthesis of oxalic acid bis(4,5-dioxo-1,3,2-dioxaborolan-2-yl)ester was carried out according to a patent by Zhang et al.[194] First, 1 eq. (9.008 g, 100 mmol) oxalic acid was reacted with 0.67 eq. (4.124 g, 66.7 mmol) boric acid heated to 120 °C under stirring. Since the mixture did not melt well, 2 mL of deionized water were added and the temperature increased to 125 °C. The resulting suspension was stirred for two hours at a pressure of 500 mbar and then step by step lowered and allowed to stir overnight under vacuum and the liberated water was distilled off. The white residue was dissolved in 40 mL acetonitrile. Since the residue did not completely dissolve, it was filtered and to the solution 1.33 eq. (3.460 g, 133.4 mmol) lithium fluoride were added. The suspension formed in the process was heated to reflux for 5 h under argon atmosphere. The white suspension was then hot filtered and the solvent was removed in vacuum. The white residue was mixed with 60 mL of a 1 : 1 mixture of acetonitrile and toluene. Insoluble remaining solids were separated off by filtration. The solvents were completely evaporated. The white solid was dissolved in 12 mL of acetonitrile with heating, then 12 mL of toluene were added and the mixture was allowed to cool to room temperature. After storage at -20 °C overnight, solids precipitated, were filtered and dried in vacuo. The white solid was dissolved in 7 mL acetonitrile with heating, then 7 mL toluene were added and the mixture was allowed to cool to room temperature. After 24 h of storage at -20 °C, crystals formed, were filtered and dried in vacuum. This yielded 1.586 g (17% of theory (23% of lit.) of (4-octyloxyphenyl) phenyl iodonium difluoro(oxalato)borate as a white solid. The product Li-B2 was characterized by various NMR measurements and stored at 2 °C with exclusion of light.

Analysis:

Melting Point: 258 °C (decomposition) (lit. -)

^{13}C-NMR (100 MHz, DMSO): 158.6 (s, 2x B$^-$-O-C), 39.51 (sep, DMSO)

^{19}F-NMR (376 MHz, DMSO): -150.70 (m, B$^-$-F$_2$), -150.75 (m, B$^-$-F$_2$)

^{11}B-NMR (128 MHz, DMSO): 2.92 (t, B)

(4-Octoxyphenyl) Phenyl Iodonium Difluoro(oxalato)borate

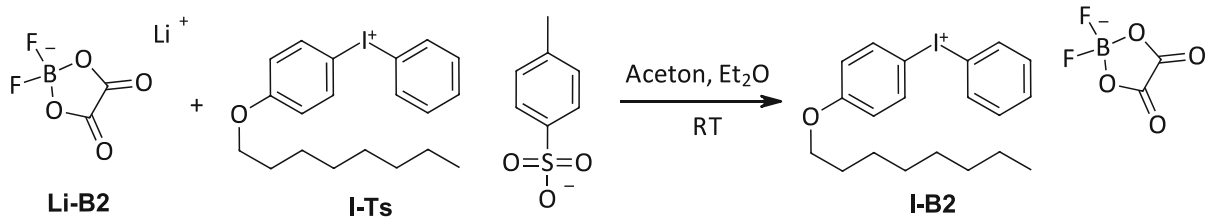

Li-B2 + **I-Ts** → **I-B2**

70%

To synthesize I-B2 a metathesis reaction based on a patent by Castellanos et al.[187] was carried out. First, 1 eq. (0.864 g, 6.0 mmol) Li-B2 was dissolved in 6.3 mL acetone and added dropwise under stirring to a solution of 1 eq. (3.484 g, 6.0 mmol) of I-Ts in 38.9 mL acetone. The resulting white suspension was stirred for 20 min, centrifuged and the solution was decanted off and the solvent was removed in vacuum. The solid white residue obtained during centrifuging corresponded to 322 mg of the by-product lithium tosylate. The yellowish oily residue was dissolved in 10 mL of acetone and mixed with 20 mL of diethyl ether, which corresponds to a solvent ratio of 1 : 2. A white precipitate formed and after 20 min the suspension was centrifuged and then dried in vacuum. The yellowish oily residue was dissolved in 7 mL acetone and then 70 mL diethyl ether were added, which corresponds to a solvent ratio of 1 : 10. After 20 min of stirring, the precipitate was centrifuged, the solution decanted and dried in vacuum. The oily residue was dissolved in 2 mL acetone and mixed with 40 mL diethyl ether, which corresponds to a solvent ratio of 1 : 20. The suspension was stirred for 20 min, centrifuged, the solution decanted and the solvents were removed in vacuum. The last step consists of adding 10 mL diethyl ether to the oily residue, resulting in a two-layer mixture. By slowly adding 2 mL of acetone, a cloudy dispersion formed, which was then centrifuged in order to separate off any lithium tosylate that was still present. A total of 1.443 g of lithium tosylate thus precipitated, which was discarded at this point in time. The solvents of the decanted solution were removed in vacuum. In order to increase the purity of the crude product and to remove I-Ts residues, flash column chromatography was carried out.

The product was dissolved in 2 mL acetone and separated chromatographically with 60 mL of acetone over a glass frit filled with ~2 g of silica gel. The solvent was then removed on a rotary evaporator and the product was dried in a fine vacuum, resulting in 2.293 g (70% of theory/-) of (4-octyloxyphenyl) phenyl iodonium difluoro(oxalato)borate as a sticky, white solid. The product I-B2 was characterized by various NMR measurements and stored at 2 °C. with exclusion of light.

Analysis:

^{1}H-NMR (400 MHz, DMSO): 8.20 (d, 2H, 2x I^+-C-CH-CH-CH), 8.15 (d, 2H, 2x I^+-C-CH-CH-C), 7.65 (t, 1H, C-CH-CH-CH), 7.53 (t, 2H, 2x I^+-C-CH-CH-CH), 7.06 (d, 2H, 2x I^+-C-CH-CH), 4.01 (t, 2H, O-CH_2), 2.50 (qui, DMSO), 1.69 (qui, 2H, O-CH_2- CH_2), 1.38 (qui, 2H, O-CH2-CH_2-CH_2), 1.33 – 1.22 (m, 8H, O-CH_2-CH_2-CH_2-CH_2-CH_2-CH_2-CH_2), 0.86 (t, 3H, CH_2-CH_3)

^{13}C-NMR (100 MHz, DMSO): 162.0 (s, O-C), 159.8 (s, 2x B^--O-C), 137.7 (s, 2x I^+-C-CH-CH-C), 135.3 (s, 2x I^+-C-CH-CH-CH), 132.3 (s, C-CH-CH-CH), 132.1 (s, 2x I^+-C-CH-CH), 118.3 (s, 2x I^+-C-CH-CH), 117.5 (s, I^+-C-CH-CH-CH), 105.6 (s, I^+-C-CH-CH-C), 68.6 (s, O-CH_2), 40.0 (sep, DMSO), 31.7 (s, O-CH_2-CH_2), 29.1 (s, O-CH_2-CH_2-CH_2), 29.1 (s, O-CH_2-CH_2-CH_2-CH_2), 28.9 (s, O-CH_2-CH_2-CH_2-CH_2), 25.9 (s, O-CH_2-CH_2-CH_2-CH_2-CH_2-CH_2), 22.5 (s, O-CH_2-CH_2-CH_2-CH_2-CH_2-CH_2-CH_2), 14.4 (s, CH_2-CH_3)

^{19}F-NMR (376 MHz, DMSO): -150.68 (s, B^--F_2), -150.75 (s, B^--F_2)

^{11}B-NMR (128 MHz, DMSO): 2.92 (t, B)

3.1.5. (4-Octyloxyphenyl) Phenyl Iodonium Tetrakis((1,1,1,3,3,3-hexafluoro-propan-2-yl)oxy)borate

Sodium Tetrakis((1,1,1,3,3,3-hexafluoro-propan-2-yl)oxy)borate

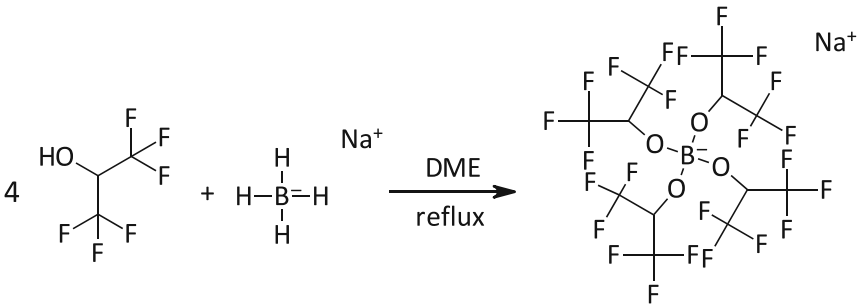

Na-B3
56%

The synthesis of sodium Na-B3 was carried out according to a patent by Kaliner et al.[197] In the first step, 1.0 eq. (0.378 g, 10 mmol) of sodium borohydride were weighed in the glove box

into a two-necked round bottom flask and mixed with 15.1 mL dimethoxy ethane. The mixture was refluxed for a few minutes. Since the sodium borohydride was insoluble even at reflux, the reaction mixture was cooled to room temperature. Over the course of 40 min, 4.3 eq. (4.5 mL, 43 mmol) of hexafluoroisopropanol were added dropwise to the suspension, which resulted in an exothermic reaction with bubble formation. After the addition was complete, the white suspension was refluxed for 4 h at 90 °C. and then allowed to cool to room temperature. The yellow, slightly cloudy reaction mixture was filtered, the solvent was removed in vacuum and the yellowish solid was dried in vacuum overnight. The reaction yielded 7.911 g of sodium tetrakis((1,1,1,3,3,3-hexafluoropropan-2-yl)oxy)borate plus residual DME as a slightly yellow solid. The Na-B3 still contains 6 eq. of DME at this point (determined by ^{1}H-NMR), which has to be accounted for in further synthesis steps. This circumstance leads to a decreased actual yield of 4.469 g (56% of theory/58% of lit.). The product was as obtained in the next reaction step, characterized by various NMR measurements and stored at 2 °C. with exclusion of light.

Analysis:

^{1}H-NMR (400 MHz, DMSO): 4.65 (s, 4H, 4x CH), 2.50 (qui, DMSO)

^{13}C-NMR (100 MHz, DMSO): 122.3 (q, 8x C-F_3), 69.5 (qui, 8x B-O-CH), 40.0 (sep, DMSO)

^{19}F-NMR (376 MHz, DMSO): -74.21 (s, 8x C-F_3)

^{11}B-NMR (128 MHz, DMSO): 1.55 (qui, B)

(4-Octyloxyphenyl) Phenyl Iodonium Tetrakis((1,1,1,3,3,3-hexafluoro-propan-2-yl)oxy)borate

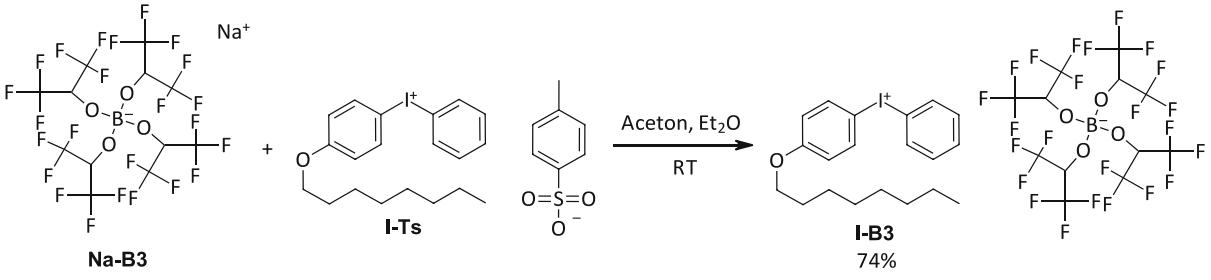

The metathesis reaction to yield I-B3 was based on a patent from Castellanos et al.[187] First, 7.887 g of Na-B3 with a molar ratio of product to dimethoxy ethane of 1 : 6 (determined by ^{1}H-NMR) were dissolved in 7 mL of distilled acetone. The actual mass of Na-B3 not accounting for DME is 4.469 g. Since I-B3 was not completely soluble in acetone, the suspension was filtered and the filter rinsed with 3 mL acetone. 0.715 g of insoluble solids remained in the

filter, which results in a corrected amount of 0.95 eq. (3.754 g, 5.3 mmol) of Na-B3 having actually dissolved in acetone. In the meantime, 1.0 eq. (3.251 g, 5.6 mmol) I-Ts was dissolved in 40 mL of distilled acetone. Now the Na-B3 solution was added dropwise to the I-Ts solution and a white precipitate being formed immediately. The suspension was stirred for 20 min and then centrifuged to result in 1.137 g of white by-product sodium tosylate. The decanted yellow solution was mixed with 25 mL diethyl ether, which corresponded to a ratio of the solvents of acetone : diethyl ether of 2 : 1. The precipitate formed and the dispersion was stirred for 20 min. The mixture was then centrifuged and the solvents of the decanted solution were removed in vacuum. The yellow viscous residue was dissolved in 5 mL of distilled acetone and mixed with 30 mL of diethyl ether (solvent ratio 1 : 6). After 20 min of stirring, the precipitate was removed by centrifugation and the solvent decanted. The solution was dried in vacuum. A total of 1.146 g of sodium tosylate thus precipitated, which was discarded at this point in time. In order to remove I-Ts residues, flash column chromatography was carried out. The viscous yellow residue was dissolved in 2 mL distilled acetone and separated chromatographically with 60 mL of distilled acetone over a glass frit filled with ~2 g of silica gel. The solvent was removed in vacuo and the product was dried vacuum overnight. Finally yielding 4.475 g (74% of theory/-) of (4-octyloxyphenyl) phenyl iodonium tetrakis((1,1,1,3,3,3-hexafluoropropan-2-yl)oxy)borate as a viscous yellowish liquid. The product I-B3 was characterized by various NMR measurements and stored at 2 °C with exclusion of light.

Analysis:

^{1}H-NMR (400 MHz, DMSO): 8.22 (d, 2H, 2x I^{+}-C-CH-CH-CH), 8.11 (d, 2H, 2x I^{+}-C-CH-CH-C), 7.64 (t, 1H, C-CH-CH-CH), 7.53 (t, 2H, 2x I^{+}-C-CH-CH-CH), 7.05 (d, 2H, 2x I^{+}-C-CH-CH), 4.71 (s, 4H, 4x B^{-}-O-CH), 4.00 (t, 2H, O-CH_2), 2.50 (qui, DMSO), 1.69 (qui, 2H, O-CH_2- CH_2), 1.39 (qui, 2H, O-CH2-CH_2-CH_2), 1.33 – 1.19 (m, 8H, O-CH_2-CH_2-CH_2-CH_2-CH_2-CH_2-CH_2), 0.85 (t, 3H, CH_2-CH_3)

^{13}C-NMR (100 MHz, DMSO): 161.9 (s, O-C), 137.7 (s, 2x I^{+}-C-CH-CH-C), 132.3 (s, 2x I^{+}-C-CH-CH-CH), 132.1 (s, C-CH-CH-CH), 131.9 (s, 2x I^{+}-C-CH-CH), 122.3 (q, 8x C-F_3), 118.2 (s, 2x I^{+}-C-CH-CH), 117.3 (s, I^{+}-C-CH-CH-CH), 106.0 (s, I^{+}-C-CH-CH-C), 105.4 (s, I^{+}-C-CH-CH-C), 69.5 (qui, 8x B-O-CH), 68.5 (s, O-CH_2), 40.0 (sep, DMSO), 31.6 (s, CH_2-CH_2-CH_3), 29.1 (s, CH_2- CH_2-CH_2-CH_3), 29.0 (s, CH_2- CH_2-CH_2-CH_2-CH_3), 28.8 (s, O-CH_2-CH_2), 25.8 (s, O-CH_2-CH_2-CH_2), 22.4 (s, CH_2-CH_3), 14.0 (s, CH_2-CH_3)

^{19}F-NMR (376 MHz, DMSO): -74.44 (s, 8x C-F_3)

^{11}B-NMR (128 MHz, DMSO): 1.55 (qui, B)

3.1.6. (4-Octyloxyphenyl) Phenyl Iodonium CN-Bis[Tris(pentafluorophenyl)borane]

Tris(2,3,4,5,6-pentafluorophenyl)borane

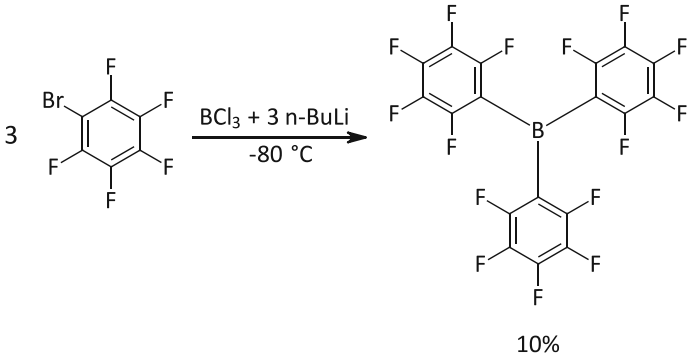

10%

Tris(2,3,4,5,6-pentafluorophenyl)borane was prepared based on the work of Fischer et al.[198] At first, 3 eq. (3.8 mL, 30 mmol) 1-bromo-2,3,4,5,6-pentafluorobenzene was dissolved in 81.5 mL hexanes and reacted with 3 eq. (12.0 mL, 30 mmol, 2.5 M in hexanes) n-butyllithium at -80 to -90 °C under argon atmosphere. The n-butyllithium was added via a syringe over the course of 15 min. The reaction mixture was stirred for 1 h within the temperature range. Then 1 eq. of boron trichloride (10 mL, 10 mmol, 1.0 M in hexanes) was added dropwise to the reaction mixture over a period of 10 min, followed by stirring of the suspension at -80 °C for 60 min. Then the mixture was allowed to warm to room temperature and stirred for 17 h. The solvents of the white suspension were removed in vacuum and the solid residue was then ground into small pieces in the glove box and transferred to a sublimation flask. The sublimation was carried out at around 2 x 10^{-2} mbar and 90 °C for around 24 h, resulting in white product at the condenser of the apparatus and a brown residue at the bottom. The brown residues were removed as best as possible in the glove box to prevent hydrolysis of the white product. The sublimation and workup processes were repeated two more times. After the second run, 1.401 g of white sublimate were obtained. The third run yielded 3 fractions of product. After around one hour there was a drop of liquid on the condenser, which was discarded. After three hours, the first fraction was removed from the cold finger, which corresponded to 98 mg of white solid. Another two hours later, the second fraction was removed from the cold finger (433 mg) and the third fraction from the edge of the flask (56 mg). NMR measurements and melting point determinations were carried out on all three fractions. The first fraction was discarded due to impurities and fraction 2 and 3 were combined. Finally, the reaction yielded 0.489 g (10% of theory/12% of lit.) of tris(2,3,4,5,6-pentafluorophenyl)-borane as a white solid.

Analysis:

Melting Point: 116.5 – 119.3 °C (lit. 125 – 127 °C)[220]

^{13}C-NMR (100 MHz, DMSO): 148.7 (d, 6x B-C-CF), 142.8 (d, 3x B-C-CF-CF-CF), 137.2 (d, 6x B-C-CF-CF), 119.9 – 119.0 (m, 3x B-C), 40.0 (sep, DMSO)

^{19}F-NMR (376 MHz, DMSO): -130.64 (d, 6x B-C-CF), -146.86 (t, 3x B-C-CF-CF-CF), 160.54 (t, 6x B-C-CF-CF)

Potassium CN-Bis[Tris(pentafluorophenyl)borane]

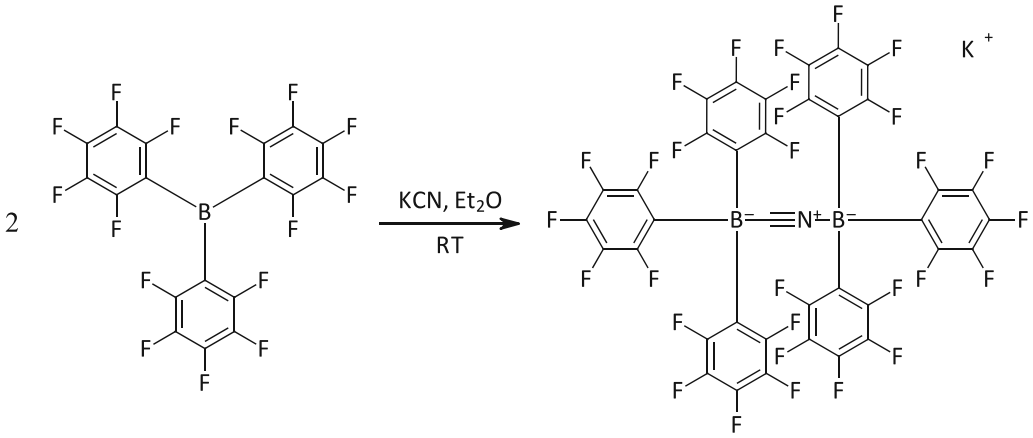

K-B4
94%

The product K-B4 was synthesized according to the work of Zhou et al.[199] First, 1 eq. (819 mg, 1.6 mmol) of tris(2,3,4,5,6-pentafluorophenyl)borane and 0.5 eq. (52 mg, 0.8 mmol) of potassium cyanide were weighed into a 25 mL flask in the glove box. Then 14 mL of dry diethyl ether were added. The dispersion was magnetically stirred for 18 h at room temperature under argon atmosphere, during which the KCN dissolved completely. Since the final material is sensitive to temperature, 25 °C were not exceeded in any step over the course of the reaction route or workup. The diethyl ether was removed in vacuum on the rotary evaporator at RT. The K-B4 product tends to foam during the solvent removal. Finally, the synthesis route yielded 820 mg (94% of theory/94% of lit.) of potassium CN-bis[tris(pentafluorophenyl)-borane] as a solid white powder. The product K-B4 was characterized various NMR measurements and stored at 2 °C with exclusion of light. Interestingly, the product seems to be stable despite temperatures above 25 °C in the absence of solvent.

Analysis:

Melting Point: 287 °C (decomposition) (lit. -)

^{13}C-NMR (100 MHz, DMSO): 149.1 (s, 12x B^--C-CF), 146.6 (s, 6x B^--C), 140.1 (s, B^--C≡N^+-B^-), 138.0 (s, 6x B^--C-CF-CF-CF), 135.4 (s, 12x B^--C-CF-CF), 40.0 (sep, DMSO)

^{19}F-NMR (376 MHz, DMSO): -132.3 (d, 6x C-B^--C-CF) -133.1 (d, 6x N^+-B^--C-CF), -157.3 (t, 3x C-B^--C-CF-CF-CF), -159.3 (t, 3x N^+-B^--C-CF-CF-CF), -163.9 (t, 6 x C-B^--1C-CF-CF), -164.9 (t, 6 x N^+-B^--C-CF-CF)

^{11}B-NMR (128 MHz, DMSO): -23.20 (s, B)

(4-Octyloxyphenyl) Phenyl Iodonium CN-Bis[Tris(pentafluorophenyl)borane]

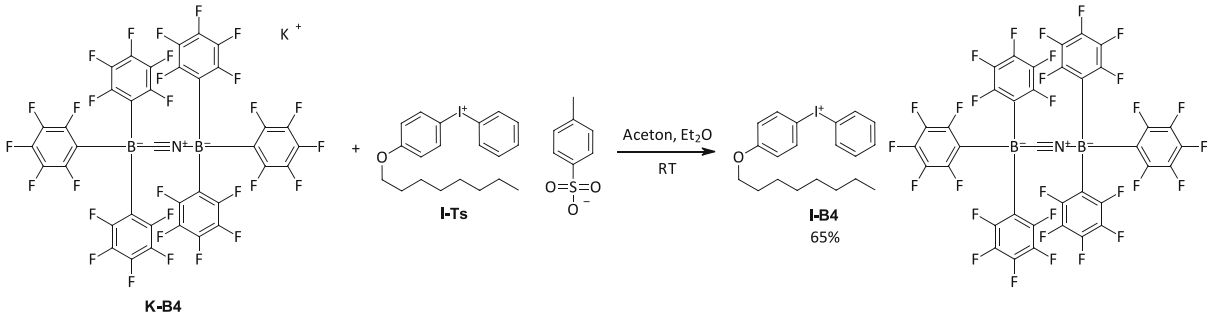

To synthesize I-B4, a metathesis reaction based on a patent by Castellanos et al.[187] was carried out. First, 0.95 eq. (517 mg, 0.48 mmol) of K-B4 were dissolved in 2 mL acetone and added dropwise to a solution of 1 eq. (290 mg, 0.50 mmol) of I-Ts in 13 mL acetone with stirring at room temperature. A gel-like precipitate was formed. The suspension was stirred for 10 min and mixed with 7.5 mL diethyl ether, which corresponds to a ratio of the solvents of acetone : diethyl ether of 2 : 1. Additional diethyl ether was added until stirring of the gel-like precipitate was possible. The suspension was stirred for 10 min, centrifuged, decanted and the solvent removed in vacuum. The yellow viscous residue was dissolved in 4 mL acetone and mixed with 20 mL diethyl ether, (solvent ratio 1 : 5). Additional diethyl ether was added until stirring of the gel-like precipitate was possible. After stirring for 10 min, the suspension was centrifuged, the solution decanted and the solvents removed in vacuum. The potassium tosylate precipitate was discarded at this point in time. In order to remove I-Ts residues, flash column chromatography was carried out. The viscous yellow residue was dissolved in 2 mL acetone and separated chromatographically with 50 mL of acetone over a glass frit filled with ~2 g of silica gel. The solvent was removed in vacuum and the residue was further dried in high vacuum overnight. A total of 477 mg (65% of theory/-) of (4-octyloxyphenyl) phenyl iodonium

CN-bis[tris(pentafluorophenyl)borane] were obtained as a sticky, colorless solid. The product I-B4 was characterized by NMR measurements and stored at 2 °C with exclusion of light.

Analytics:

^{1}H-NMR (400 MHz, DMSO): 8.20 (d, 2H, 2x I^{+}-C-CH-CH-CH), 8.15 (d, 2H, 2x I^{+}-C-CH-CH-C), 7.66 (t, 1H, C-CH-CH-CH), 7.53 (t, 2H, 2x I^{+}-C-CH-CH-CH), 7.06 (d, 2H, 2x I^{+}-C-CH-CH), 4.00 (t, 2H, O-CH_2), 2.50 (qui, DMSO), 1.69 (qui, 2H, O-CH_2- CH_2), 1.38 (qui, 2H, O-CH_2-CH_2-CH_2), 1.33-1.20 (m, 8H, O-CH_2-CH_2-CH_2-CH_2-CH_2-CH_2-CH_2), 0.85 (t, 3H, CH_2-CH_3)

^{13}C-NMR (100 MHz, DMSO): 162.0 (s, O-C), 149.1 (s, 12x B^{-}-C-CF), 146.6 (s, 6x B^{-}-C), 140.1 (s, B^{-}-C≡N^{+}-B^{-}), 138.0 (s, 6x B^{-}-C-CF-CF-CF), 137.7 (s, 2x I^{+}-C-CH-CH-C), 135.4 (s, 12x B^{-}-C-CF-CF), 135.3 (s, 2x I^{+}-C-CH-CH-CH), 132.3 (s, C-CH-CH-CH), 132.1 (s, 2x I^{+}-C-CH-CH-CH), 118.3 (s, 2x I^{+}-C-CH-CH), 117.4 (s, I^{+}-C-CH-CH-CH), 105.5 (s, I^{+}-C-CH-CH-C), 68.5 (s, O-CH_2), 40.0 (sep, DMSO), 31.7 (s, O-CH_2-CH_2), 29.1 (s, O-CH_2-CH_2-CH_2), 29.1 (s, O-CH_2-CH_2-CH_2-CH_2), 28.8 (s, O-CH_2-CH_2-CH_2-CH_2-CH_2), 25.8 (s, O-CH_2-CH_2-CH_2-CH_2-CH_2-CH_2), 22.5 (s, O-CH_2-CH_2-CH_2-CH_2-CH_2-CH_2-CH_2), 14.3 (s, CH_2-CH_3)

^{19}F-NMR (376 MHz, DMSO): -132.3 (d, 6x C-B^{-}-C-CF) -133.1 (d, 6x N^{+}-B^{-}-C-CF), -157.3 (t, 3x C-B^{-}-C-CF-CF-CF), -159.3 (t, 3x N^{+}-B^{-}-C-CF-CF-CF), -163.9 (t, 6 x C-B^{-}-C-CF-CF), -164.9 (t, 6 x N^{+}-B^{-}-C-CF-CF)

^{11}B-NMR (128 MHz, DMSO): -23.30 (s, B)

3.1.7. (4-Octyloxyphenyl) Phenyl Iodonium CN-[Tris(pentafluorophenyl)borane]

Potassium CN-[Tris(pentafluorophenyl)borane]

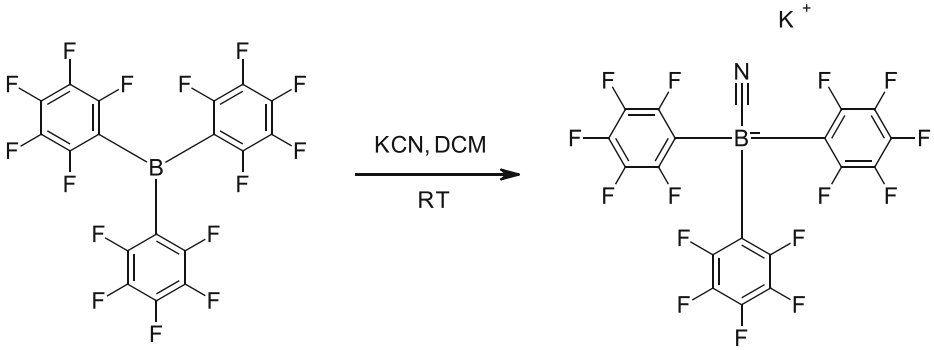

K-B5

68%

The product K-B5 was synthesized similar to Zhou et al.[199] First, 1 eq. (307 mg, 0.6 mmol) of tris(2,3,4,5,6-pentafluorophenyl)borane was weighed into a 5 mL vial in the glove box. Then 3.5 mL of dry dichloromethane were added. The mixture was stirred at room temperature

until the borane dissolved completely. In a separate vial potassium cyanide was dissolved in deionized water and 1 eq. (39 mg, 0.6 mmol, ~0.2 mL) of the solution was added to the borane solution to result in an opaque solution. After 16 h of vigorous stirring at room temperature, 0.5 mL of deionized water were added and the layers separated. The aqueous layer was washed twice with 4 mL of dichloromethane and twice with 4 mL of diethyl ether. The solvents were removed in vacuum on the rotary evaporator at RT. The product tends to foam during evaporation of the solvents. Finally, the synthesis route yielded 234 mg (68% of theory/-) of potassium CN-[tris(pentafluorophenyl)borane] as a white solid. The product K-B5 was characterized various NMR measurements and stored at 2 °C with exclusion of light.

A faster workup procedure can be executed, if high yield is preferred over high purity. This route is sometimes advantageous if the salt is used in a next step as precursor. After the 16 h of stirring, the solvents are evaporated immediately without any water addition or extraction steps. Then, the viscous liquid is dissolved in 10 mL of dichloromethane and the solvent evaporated quickly at the rotary evaporator at 30 °C. This process removes the minor amounts of water fast. Finally, K-B5 is obtained as a white solid in a yield of 99%.

Unfortunately, upscaling of the vials did not work as well, since the contact of water and dichloromethane is not that good for larger quantities. For larger scale synthesis, up to 20 of the vials were prepared simultaneously. Then the contents of the up to 20 vials were united after the 16 h stirring into one single flask for workup.

Analysis:

Melting Point: 57 °C (decomposition) (lit. -)

^{13}C-NMR (100 MHz, DMSO): 148.9 (s, B$^-$-C≡N), 146,7 (s, 3x B$^-$-C), 139.1 (s, 6x B$^-$-C- CF), 137.4 (s, 6x B$^-$-C-CF-CF), 134.9 (s, 3x B$^-$-C-CF-CF-CF), 40.0 (sep, DMSO)

^{19}F-NMR (376 MHz, DMSO): -134.7 (d, 6x B$^-$-C-CF) -162.2 (t, 3x B$^-$-C-CF-CF-CF), -165.9 (t, 6 x B$^-$-C-CF-CF)

^{11}B-NMR (128 MHz, DMSO): -4.20 (s, B)

(4-Octyloxyphenyl) Phenyl Iodonium CN-[Tris(pentafluorophenyl)borane]

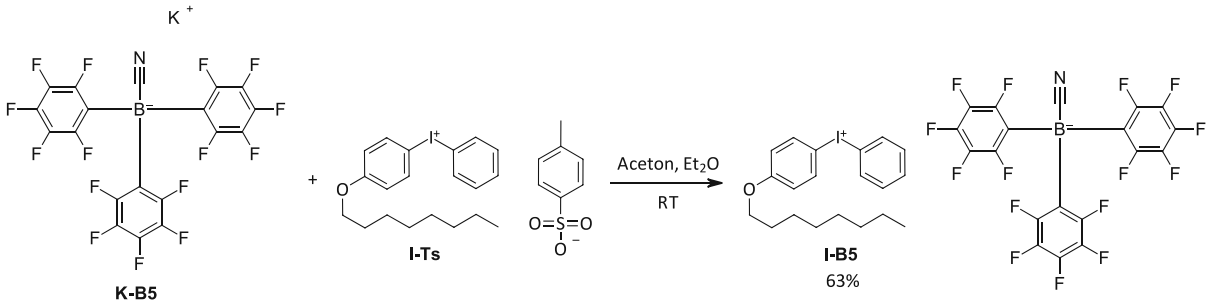

To synthesize I-B5, a metathesis reaction based on a patent by Castellanos et al.[187] was carried out. First, 0.95 eq. (255 mg, 0.44 mmol) of K-B5 were dissolved in 3 mL acetone and added dropwise to a solution of 1 eq. (267 mg, 0.46 mmol) of I-Ts in 5 mL acetone with stirring at room temperature. A gel-like precipitate was formed. The suspension was stirred for 10 min and mixed with 4 mL diethyl ether, which corresponds to a ratio of the solvents of acetone : diethyl ether of 2 : 1. Additional diethyl ether was added until stirring of the gel-like precipitate was possible. The suspension was stirred for 10 min, centrifuged, decanted and the solvent removed in vacuum. The yellow viscous residue was dissolved in 1 mL acetone and mixed with 5 mL diethyl ether, (solvent ratio 1 : 5). Additional diethyl ether was added until stirring of the gel-like precipitate was possible. After stirring for 10 min, the suspension was centrifuged, the solution decanted and the solvents removed in vacuum. The potassium tosylate precipitate was discarded at this point in time. In order to remove I-Ts residues, flash column chromatography was carried out. The viscous yellow residue was dissolved in 2 mL acetone and separated chromatographically with 30 mL of acetone over a glass frit filled with ~2 g of silica gel. The solvent was removed in vacuum and the residue was further dried in high vacuum overnight. A total of 274 mg (63% of theory/-) of (4-octyloxyphenyl) phenyl iodonium CN-[tris(pentafluorophenyl)borane] were obtained as a sticky, colorless solid. The product I-B5 was characterized by NMR measurements and stored at 2 °C with exclusion of light.

Analytics:

^{1}H-NMR (400 MHz, DMSO): 8.20 (d, 2H, 2x I^{+}-C-CH-CH-CH), 8.15 (d, 2H, 2x I^{+}-C-CH-CH-C), 7.66 (t, 1H, C-CH-CH-CH), 7.53 (t, 2H, 2x I^{+}-C-CH-CH-CH), 7.06 (d, 2H, 2x I^{+}-C-CH-CH), 4.00 (t, 2H, O-CH_2), 2.50 (qui, DMSO), 1.69 (qui, 2H, O-CH_2- CH_2), 1.38 (qui, 2H, O-CH_2-CH_2-CH_2), 1.33-1.20 (m, 8H, O-CH_2-CH_2-CH_2-CH_2-CH_2-CH_2-CH_2), 0.85 (t, 3H, CH_2-CH_3)

^{13}C-NMR (100 MHz, DMSO): 162.0 (s, O-C), 148.9 (s, B^{-}-C≡N), 146,7 (s, 3x B^{-}-C), 139.1 (s, 6x B^{-}-C- CF), 137.7 (s, 2x I^{+}-C-CH-CH-C), 137.4 (s, 6x B^{-}-C-CF-CF), 135.3 (s, 2x I^{+}-C-CH-CH-CH), 134.9

(s, 3x B⁻-C-CF-CF-CF), 132.3 (s, C-CH-CH-CH), 132.1 (s, 2x I⁺-C-CH-CH-CH), 118.3 (s, 2x I⁺-C-CH-CH), 117.4 (s, I⁺-C-CH-CH-CH), 105.5 (s, I⁺-C-CH-CH-C), 68.5 (s, O-CH_2), 40.0 (sep, DMSO), 31.7 (s, O-CH_2-CH_2), 29.1 (s, O-CH_2-CH_2-CH_2), 29.1 (s, O-CH_2-CH_2-CH_2-CH_2), 28.8 (s, O-CH_2-CH_2-CH_2-CH_2-CH_2), 25.8 (s, O-CH_2-CH_2-CH_2-CH_2-CH_2-CH_2), 22.5 (s, O-CH_2-CH_2-CH_2-CH_2-CH_2-CH_2-CH_2), 14.3 (s, CH_2-CH_3)

^{19}F-NMR (376 MHz, DMSO): -134.7 (d, 6x B⁻-C-CF) -162.2 (t, 3x B⁻-C-CF-CF-CF), -165.9 (t, 6 x B⁻-C-CF-CF)

^{11}B-NMR (128 MHz, DMSO): -4.20 (s, B)

4. Sulfonium Borates

4.1. Synthesis

4.1.1. Tris(4-((4-acetylphenyl)thio)phenyl) Sulfonium Sulfonimide

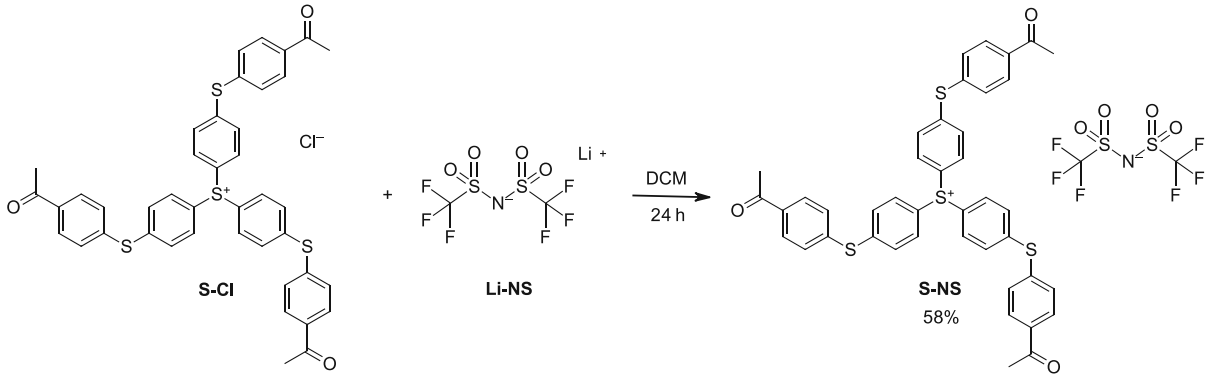

To synthesize tris(4-((4-acetylphenyl)thio)phenyl) sulfonium sulfonimide, a metathesis reaction according to a paper of Klikovits et al.[117] was carried out. At first, 1 eq. (2.966 g, 4 mmol) of tris(4-((4-acetylphenyl)thio)phenyl) sulfonium chloride was dissolved in 30 mL of dichloromethane. A clear solution was obtained. Then, 1 eq. (1.147 g, 4 mmol) of lithium sulfonimide was weighed into a 250 mL three-necked flask and mostly dissolved (still little cloudy) in 200 mL of dichloromethane by gentle heating. The solution was magnetically stirred. Afterwards the sulfonium salt solution was added dropwise into the lithium salt solution via a syringe over the course of 5 min. Additionally, 20 mL of dichloromethane were used to quantitively transfer the sulfonium salt into the flask. The reaction mixture was stirred for 18 h, while a white precipitate started to form. The white lithium chloride precipitate was removed via filtration. Solvent was removed in vacuum until around 50 mL remained. The organic layer was washed with 3 x 15 mL of deionized water and dried over sodium sulfate. The solvent was evaporated in vacuum until around 5-7 mL remained. The concentrated

solution was purified by flash column chromatography to remove sulfonium chloride starting material. The salts were separated chromatographically with 50 mL of dichloromethane over a glass frit filled with ~2 g of silica gel. Solvent was removed in vacuum. Finally, 2.319 g (58% of theory/-) of tris(4-((4-acetylphenyl)thio)phenyl) sulfonium sulfonimide were obtained as a white crystalline solid. The S-NS salt was characterized via various NMR measurements and the melting point was determined. Additionally, a halogen test was performed to verify the absence of residual chloride anions by dissolving the product in DMSO with minor amounts of deionized water and in a different container $AgNO_3$ crystals in the same solvent mixture. Upon mixing the two hot solutions, no precipitate (AgCl) was formed. It was stored in the dark at 2 °C.

Analytics:

Melting Point: 137.6 – 142.2 °C (lit. -)

^{1}H-NMR (400 MHz, DMSO): 8.02 (d, 6H, 6x S^+-C-CH), 7.74 (d, 6H, 6x O=C-C-CH), 7.62 (d, 6H, 6x O=C-C-CH-CH), 7.56 (d, 6H, 6x S^+-C-CH-CH), 2.60 (s, 9H, 3x CH_3), 2.50 (qui, DMSO)

^{13}C-NMR (100 MHz, DMSO): 197.2 (s, 3x O=C), 143.9 (s, 3x S^+-C-CH-CH-C), 136.9 (s, 3x O=C-C), 136.7 (s, 3x O=C-C-CH-CH-C), 132.6 (s, 6x S^+-C-CH-CH), 132.1 & 130.4 (s, 6x O=C-C-CH-CH), 130.4 & 128.8 (s, 6x O=C-C-CH-CH), 129.7 (s, 6x S^+-C-CH-CH), 124.6 (s, C-F_3), 122.6 (s, 3x S^+-C), 121.1 (s, C-F_3), 118.7 (s, C-F_3), 115.9 (s, C-F_3), 39.51 (sep, DMSO), 26.8 (s, 3x CH_3)

^{19}F-NMR (376 MHz, DMSO): -78.70 (s, 2x C-F_3)

4.1.2. Tris(4-((4-acetylphenyl)thio)phenyl) Sulfonium Bis(oxalatoborate)

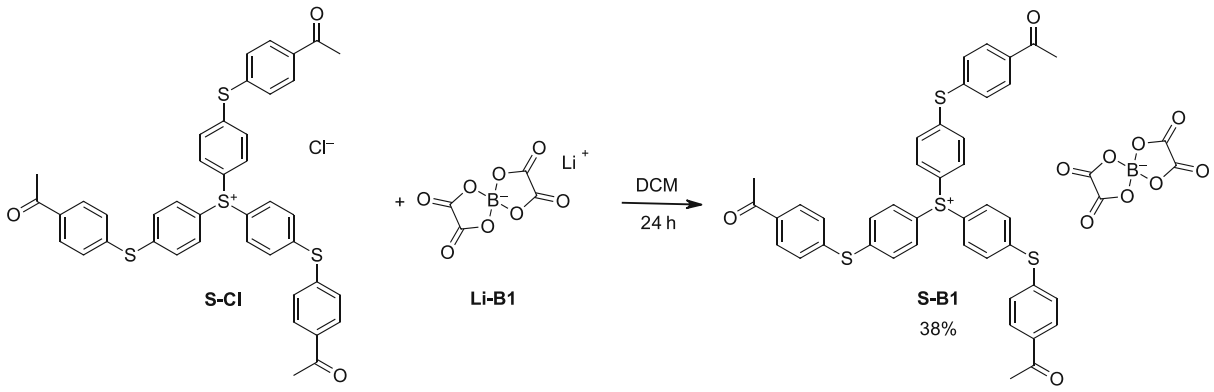

To synthesize tris(4-((4-acetylphenyl)thio)phenyl) sulfonium bis(oxalatoborate), a metathesis reaction according to a paper of Klikovits et al.[117] was carried out. At first, 1 eq. (1.613 g, 2.15 mmol) of tris(4-((4-acetylphenyl)thio)phenyl) sulfonium chloride was dissolved in 30 mL of dichloromethane. A clear solution was obtained. Then, 1 eq. (0.418 g, 2.15 mmol) of lithium

bis(oxalatoborate) was weighed into a 500 mL three-necked flask and mostly dissolved (still little cloudy) in 290 mL of dichloromethane by gentle heating. The solution was magnetically stirred. Afterwards the sulfonium salt solution was added dropwise into the lithium salt solution via a syringe over the course of 5 min. Additionally, 20 mL of dichloromethane were used to quantitively transfer the sulfonium salt into the flask. The reaction mixture was stirred for 18 h, while a white precipitate started to form slowly. The white lithium chloride precipitate was removed via filtration. Solvent was removed in vacuum until around 50 mL remained. The organic layer was washed with 3 x 15 mL of deionized water and dried over sodium sulfate. The solvent was evaporated in vacuum until around 5-7 mL remained. The concentrated solution was purified by flash column chromatography to remove sulfonium chloride starting material. The salts were separated chromatographically with 50 mL of dichloromethane over a glass frit filled with ~2 g of silica gel. Solvent was removed in vacuum. Finally, 0.731 g (38% of theory/-) of tris(4-((4-acetylphenyl)thio)phenyl) sulfonium bis(oxalatoborate) were obtained as a white crystalline solid. The S-B1 salt was characterized via various NMR measurements and the melting point was determined. Additionally, a halogen test was performed to verify the absence of residual chloride anions by dissolving the product in DMSO with minor amounts of deionized water and in a different container $AgNO_3$ crystals in the same solvent mixture. Upon mixing the two hot solutions, no precipitate (AgCl) was formed. It was stored in the dark at 2 °C.

Analytics:

R_f: 0.1 (DCM)

Melting Point: 80.4 – 84.1 °C (lit. -)

^{1}H-NMR (400 MHz, DMSO): 8.02 (d, 6H, 6x S^+-C-CH), 7.76 (d, 6H, 6x O=C-C-CH), 7.63 (d, 6H, 6x O=C-C-CH-CH), 7.56 (d, 6H, 6x S^+-C-CH-CH), 2.61 (s, 9H, 3x CH_3), 2.50 (qui, DMSO)

^{13}C-NMR (100 MHz, DMSO): 197.2 (s, 3x O=C), 158.1 (s, 2x B^--O-C), 144.0 (s, 3x S^+-C-CH-CH-C), 136.9 (s, 3x O=C-C), 136.7 (s, 3x O=C-C-CH-CH-C), 132.6 (s, 6x S^+-C-CH-CH), 132.0 & 130.7 (s, 6x O=C-C-CH-CH), 130.4 & 128.8 (s, 6x O=C-C-CH-CH), 129.6 (s, 6x S^+-C-CH-CH), 122.6 (s, 3x S^+-C), 39.51 (sep, DMSO), 26.7 (s, 3x CH_3)

^{11}B-NMR (128 MHz, DMSO): 7.37 (s, B)

4.1.3. Tris(4-((4-acetylphenyl)thio)phenyl) Sulfonium Difluoro(oxalato)borate

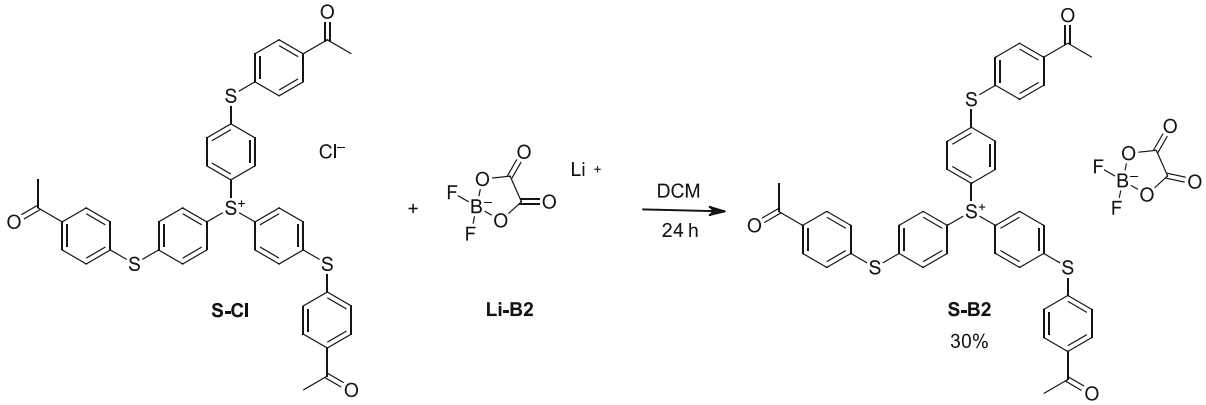

To synthesize tris(4-((4-acetylphenyl)thio)phenyl) sulfonium difluoro(oxalato)borate, a metathesis reaction according to a paper of Klikovits et al.[117] was carried out. At first, 1 eq. (1.500 g, 2 mmol) of tris(4-((4-acetylphenyl)thio)phenyl) sulfonium chloride was dissolved in 80 mL of dichloromethane. A clear solution was obtained. Then, 1 eq. (0.288 g, 2 mmol) of lithium difluoro(oxalato)borate was weighed into a 250 mL three-necked flask and mostly dissolved (still little cloudy) in 80 mL of dichloromethane by gentle heating. The solution was magnetically stirred. Afterwards the sulfonium salt solution was added dropwise into the lithium salt solution via a syringe over the course of 5 min. Additionally, 20 mL of dichloromethane were used to quantitively transfer the sulfonium salt into the flask. The reaction mixture was stirred for 18 h, while a white precipitate started to form slowly. The white lithium chloride precipitate was removed via filtration. Solvent was removed in vacuum until around 50 mL remained. The organic layer was washed with 10 mL of deionized water and dried over sodium sulfate. The solvent was evaporated in vacuum until around 3-5 mL remained. The concentrated solution was purified by flash column chromatography to remove sulfonium chloride starting material. The salts were separated chromatographically with 30 mL of dichloromethane over a glass frit filled with ~2 g of silica gel. Solvent was removed in vacuum. Finally, 0.512 g (30% of theory/-) of tris(4-((4-acetylphenyl)thio)phenyl) sulfonium difluoro(oxalato)borate were obtained as a white crystalline solid. The S-B2 salt was characterized via various NMR measurements and the melting point was determined. Additionally, a halogen test was performed to verify the absence of residual chloride anions by dissolving the product in DMSO with minor amounts of deionized water and in a different container $AgNO_3$ crystals in the same solvent mixture. Upon mixing the two hot solutions, no precipitate (AgCl) was formed. It was stored in the dark at 2 °C.

Analytics:

R_f: 0.1 (DCM)

Melting Point: 93.4 – 96.5 °C (lit. -)

^{1}H-NMR (400 MHz, DMSO): 8.02 (d, 6H, 6x S^+-C-CH), 7.76 (d, 6H, 6x O=C-C-CH), 7.63 (d, 6H, 6x O=C-C-CH-CH), 7.56 (d, 6H, 6x S^+-C-CH-CH), 2.61 (s, 9H, 3x CH_3), 2.50 (qui, DMSO)

^{13}C-NMR (100 MHz, DMSO): 197.2 (s, 3x O=C), 159.0 (s, 2x B^--O-C), 143.9 (s, 3x S^+-C-CH-CH-C), 136.9 (s, 3x O=C-C), 136.7 (s, 3x O=C-C-CH-CH-C), 132.6 (s, 6x S^+-C-CH-CH), 132.1 & 130.7 (s, 6x O=C-C-CH-CH), 130.4 & 128.8 (s, 6x O=C-C-CH-CH), 129.6 (s, 6x S^+-C-CH-CH), 122.7 (s, 3x S^+-C), 39.51 (sep, DMSO), 27.8 (s, 3x CH_3)

^{19}F-NMR (376 MHz, DMSO): -150.68 (q, B^--F_2), -150.75 (q, B^--F_2)

^{11}B-NMR (128 MHz, DMSO): 2.92 (t, B)

4.1.4. Tris(4-((4-acetylphenyl)thio)phenyl) Sulfonium CN-Bis[Tris(pentafluorophenyl)borane]

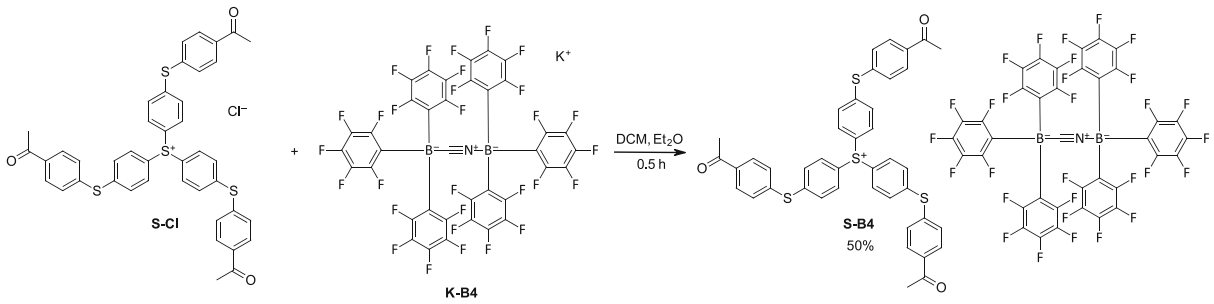

To synthesize tris(4-((4-acetylphenyl)thio)phenyl) sulfonium CN-bis[tris(pentafluorophenyl)borane], a metathesis reaction according to a paper of Klikovits et al.[117] was carried out. At first, 1 eq. (0.039 g, 0.05 mmol) of tris(4-((4-acetylphenyl)thio)phenyl) sulfonium chloride was dissolved in 0.6 mL of a 10 : 1 mixture of dichloromethane and diethyl ether. A clear solution was obtained. Then, 1 eq. (0.056 g, 0.05 mmol) of potassium CN-bis[tris(pentafluorophenyl)borane] was weighed into a 5 mL flask and dissolved in 2 mL of the same 10 : 1 mixture of solvents. The solution was magnetically stirred. Afterwards the sulfonium salt solution was added dropwise into the potassium salt solution via a syringe over the course of 5 min. The mixture was set under argon atmosphere. Additionally, 1 mL of the solvent mixture was used to quantitively transfer the sulfonium salt into the flask. The reaction mixture was stirred for 0.5 h, while a white precipitate started to form. The white potassium chloride precipitate was removed via filtration. Solvents were removed in vacuum at 25 °C until around 1 mL remained. The concentrated product solution was purified by flash column chromatography to remove

sulfonium chloride starting material. The salts were separated chromatographically with 3 mL of dichloromethane over a small glass frit filled with ~0.3 g of silica gel. Solvents were removed in vacuum at 25 °C. Finally, 0.045 g (50% of theory/-) of tris(4-((4-acetylphenyl)thio)phenyl) sulfonium CN-bis[tris(pentafluorophenyl)borane] were obtained as a white crystalline solid. The S-B4 salt was characterized via various NMR measurements and the melting point was determined. Additionally, a halogen test was performed to verify the absence of residual chloride anions by dissolving the product in DMSO with minor amounts of deionized water and in a different container $AgNO_3$ crystals in the same solvent mixture. Upon mixing the two hot solutions, no precipitate (AgCl) was formed. It was stored in the dark at 2 °C.

Analytics:

Melting Point: 70.5 – 74.8 °C (lit. -)

^{1}H-NMR (400 MHz, DMSO): 8.02 (d, 6H, 6x S^+-C-CH), 7.75 (d, 6H, 6x O=C-C-CH), 7.62 (d, 6H, 6x O=C-C-CH-CH), 7.56 (d, 6H, 6x S^+-C-CH-CH), 2.61 (s, 9H, 3x CH_3), 2.50 (qui, DMSO)

^{13}C-NMR (100 MHz, DMSO): 197.2 (s, 3x O=C), 149.1 (s, 12x B^--C-CF), 146.6 (s, 6x B^--C), 143.9 (s, 3x S^+-C-CH-CH-C), 140.1 (s, B^--C≡N^+-B^-), 138.0 (s, 6x B^--C-CF-CF-CF), 136.9 (s, 3x O=C-C), 136.7 (s, 3x O=C-C-CH-CH-C), 135.4 (s, 12x B^--C-CF-CF), 132.6 (s, 6x S^+-C-CH-CH), 132.1 & 130.4 (s, 6x O=C-C-CH-CH), 130.4 & 128.8 (s, 6x O=C-C-CH-CH), 129.7 (s, 6x S^+-C-CH-CH), 122.6 (s, 3x S^+-C), 39.51 (sep, DMSO), 26.8 (s, 3x CH_3)

^{19}F-NMR (376 MHz, DMSO): -132.3 (d, 6x C-B^--C-CF) -133.1 (d, 6x N^+-B^--C-CF), -157.2 (t, 3x C-B^--C-CF-CF-CF), -159.2 (t, 3x N^+-B^--C-CF-CF-CF), -163.8 (t, 6 x C-B^--1C-CF-CF), -164.9 (t, 6 x N^+-B^--C-CF-CF)

^{11}B-NMR (128 MHz, DMSO): -23.30 (s, B)

4.1.5. Tris(4-((4-acetylphenyl)thio)phenyl) Sulfonium CN-[Tris(pentafluorophenyl)borane]

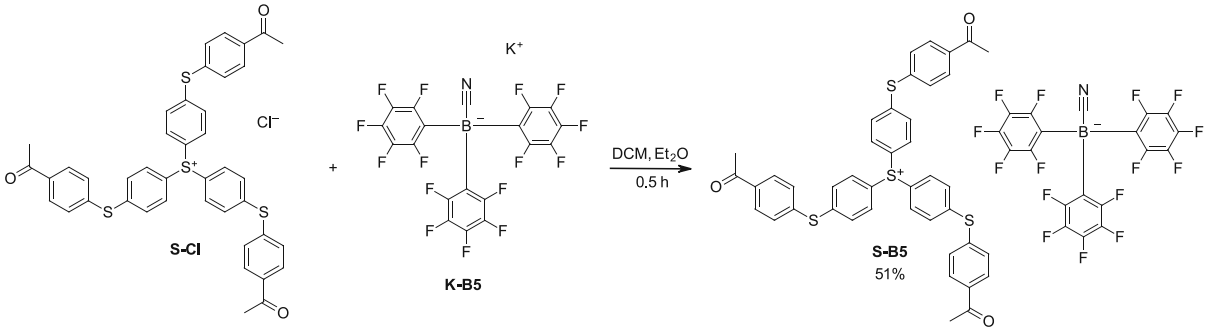

To synthesize tris(4-((4-acetylphenyl)thio)phenyl) sulfonium CN-[tris(pentafluorophenyl)borane], a metathesis reaction according to a paper of Klikovits et al.[117] was carried out. At first, 1 eq. (0.251 g, 0.34 mmol) of tris(4-((4-acetylphenyl)thio)phenyl) sulfonium chloride was dissolved in 3 mL of a 10 : 1 mixture of dichloromethane and diethyl ether. A clear solution was obtained. Then, 1 eq. (0.190 g, 0.34 mmol) of potassium CN-bis[tris(pentafluorophenyl)borane] was weighed into a 50 mL flask and dissolved in 14 mL of the same 10 : 1 mixture of solvents. The solution was magnetically stirred. Afterwards the sulfonium salt solution was added dropwise into the potassium salt solution via a syringe over the course of 5 min. The mixture was set under argon atmosphere. Additionally, 3 mL of the solvent mixture was used to quantitively transfer the sulfonium salt into the flask. The reaction mixture was stirred for 0.5 h, while a white precipitate started to form. The white potassium chloride precipitate was removed via filtration. Solvents were removed in vacuum at 25 °C until around 2 mL remained. The concentrated product solution was purified by flash column chromatography to remove sulfonium chloride starting material. A glass frit filled with ~2 g of silica gel was conditioned with dichloromethane and the around 2 mL of product solution were put onto the silica gel. Then 20 mL of dichloromethane followed by 20 mL of diethyl ether were flushed through the column to remove any impurities. Afterwards, the product was eluted with 20 mL of distilled acetone. Solvent was removed in vacuum at 25 °C. The product tends to foam during evaporation of the solvents. Finally, 0.214 g (51% of theory/-) of tris(4-((4-acetylphenyl)thio)phenyl) sulfonium CN-[tris(pentafluorophenyl)borane] were obtained as a white crystalline solid. The S-B5 salt was characterized via various NMR measurements and the melting point was determined. Additionally, a halogen test was performed to verify the absence of residual chloride anions by dissolving the product in DMSO with minor amounts of deionized water and in a different container $AgNO_3$ crystals in the same solvent mixture. Upon

mixing the two hot solutions, no precipitate (AgCl) was formed. It was stored in the dark at 2 °C.

Analytics:

Melting Point: 62.9 – 66.2 °C (lit. -)

^{1}H-NMR (400 MHz, DMSO): 8.02 (d, 6H, 6x S^{+}-C-CH), 7.75 (d, 6H, 6x O=C-C-CH), 7.62 (d, 6H, 6x O=C-C-CH-CH), 7.56 (d, 6H, 6x S^{+}-C-CH-CH), 2.61 (s, 9H, 3x CH_3), 2.50 (qui, DMSO)

^{13}C-NMR (100 MHz, DMSO): 197.2 (s, 3x O=C), 148.9 (s, B^{-}-C≡N), 146,7 (s, 3x B^{-}-C), 143.9 (s, 3x S^{+}-C-CH-CH-C), 139.1 (s, 6x B^{-}-C- CF), 137.4 (s, 6x B^{-}-C-CF-CF), 136.9 (s, 3x O=C-C), 136.7 (s, 3x O=C-C-CH-CH-C), 134.9 (s, 3x B^{-}-C-CF-CF-CF), 132.6 (s, 6x S^{+}-C-CH-CH), 132.1 & 130.4 (s, 6x O=C-C-CH-CH), 130.4 & 128.8 (s, 6x O=C-C-CH-CH), 129.7 (s, 6x S^{+}-C-CH-CH), 122.6 (s, 3x S^{+}-C), 39.51 (sep, DMSO), 26.8 (s, 3x CH_3)

^{19}F-NMR (376 MHz, DMSO): -134.7 (d, 6x B^{-}-C-CF) -162.2 (t, 3x B^{-}-C-CF-CF-CF), -165.9 (t, 6 x B^{-}-C-CF-CF)

^{11}B-NMR (128 MHz, DMSO): -4.21 (t, B)

III. Metal-Free Ring-Opening Metathesis Polymerization

3. ROMP Monomers

3.1. Synthesis

3.1.1. 5-(Butoxymehtyl)-2-norbornene

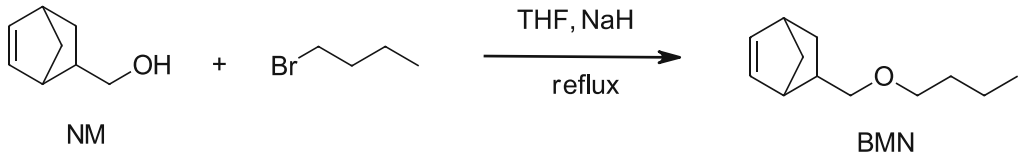

NM BMN

31%

To synthesize 5-(butoxymethyl)-2-norbornene, a synthesis according to Liu et al.[205] was carried out. At first, 4 eq. (12 g, 300 mmol) of sodium hydride (60 wt% dispersion in paraffine) were added into a two-necked flask and dissolved in 150 mL of distilled THF. Then, 1 eq. (9.376 g, 75 mmol) of NM (mixture of isomers) was added dropwise to the magnetically stirred, grey dispersion, which resulted in a slow bubble formation. After complete addition, the mixture was refluxed for 2 h, followed by the dropwise addition of 2 eq. (18.312 g, 150 mmol) of 1-bromobutane to the boiling suspension. The mixture was allowed to cool down to room temperature and stirred for 21 h. Reaction progress and the correlating absence of NM was checked via TLC (PE : EE = 10 : 1) and a R_f value of 0.77 for the product. Afterwards 50 mL of deionized water added carefully (exothermic reaction), followed by the addition of 100 mL of diethyl ether and the layers were finally separated. The organic layer was washed with 50 mL of deionized water, 50 mL of 0.5 N KOH and in the end with two times 50 mL of deionized water again. Sodium sulfate was used to dry the organic layer. The solvent was evaporated and the crude yellow liquid purified by vacuum distillation. Finally yielding 4.240 g (31% of theory/36% of lit.) of 5-(butoxymethyl)-2-norbornene as colorless liquid. The liquid BMN was characterized via various NMR measurements.

Analytics:

R_f: 0.77 (PE : EE = 10 : 1)

Boiling Point: 104 °C – 107 °C (26 mbar)

^{1}H-NMR (400 MHz, $CDCl_3$): 7.26 (s, $CDCl_3$), 6.13 - 5.88 (m, 2H, C<u>H</u>=C<u>H</u>), 3.48 - 2.71 (m, 6H, CH-C<u>H</u>$_2$-O-C<u>H</u>$_2$-C<u>H</u>$_2$), 2.40 - 0.43 (m, 12H, 7x norbornene-<u>H</u>, 1x C<u>H</u>$_2$-C<u>H</u>$_3$)

^{13}C-NMR (100 MHz, $CDCl_3$): 137.3, 136.9, 136.8 & 132.7 (s, <u>C</u>H=<u>C</u>H), 77.2 (t, $CDCl_3$), 75.7, 74.8, 71.1 & 71.0 (s, <u>C</u>H$_2$-O-<u>C</u>H$_2$), 49.6 & 45.2 (s, CH=CH-CH-<u>C</u>H$_2$), 44.2, 43.9, 42.4 & 41.7 (s, <u>C</u>H-

CH=CH-CH), 39.1 & 39.0 (s, CH-CH_2-O), 32.04 & 32.02 (s, O-CH_2-CH_2), 30.0 & 29.4 (s, O-CH_2-CH-CH_2), 19.60 & 19.58 (s, CH_3-CH_2), 14.16 & 14.15 (s, CH_3)

3.1.2. 5-(Methoxymethyl)-2-norbornene

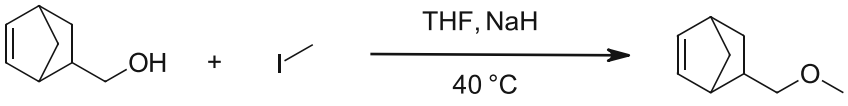

NM MMN

42%

To synthesize 5-(methoxymethyl)-2-norbornene, a synthesis similar to Lu et al.[111] was carried out. At first, 4 eq. (8.9 g, 220 mmol) of sodium hydride (60 wt% dispersion in paraffine) were dispersed in 110 mL of distilled THF in a beaker. Then, 1 eq. (6.830 g, 55 mmol) of NM (mixture of isomers) was added into a two-necked flask and magnetically stirred. Then, the grey NaH dispersion was added to the NM, which resulted in exothermic bubble formation. After complete addition, the mixture was heated to 40 °C for 4 h, followed by the dropwise addition of 2 eq. (15.555 g, 110 mmol) of iodomethane to the suspension (exothermic reaction). The mixture was allowed to stir at 40 °C for 42 h. Reaction progress and the correlating absence of NM was checked via TLC (PE : EE = 10 : 1) and a R_f value of 0.6 for the product. Afterwards 30 mL of deionized water added carefully (exothermic reaction), followed by the addition of 60 mL of diethyl ether and the layers were separated. The organic layer was washed with 30 mL of deionized water, 30 mL of 0.5 N KOH and in the end with two times 30 mL of deionized water again. Finally, the aqueous layer was re-extracted once with 30 mL of diethyl ether and the organic layers combined. Sodium sulfate was used to dry the organic layer. The solvent was evaporated and the crude yellowish liquid (not lower than 200 mbar at 40 °C). The product was purified by vacuum distillation (literature boiling point: 68 - 72 °C at 34 mbar).[221] Finally yielding 4.600 g (61% of theory/70% of lit.) of 5-(methoxymethyl)-2-norbornene as colorless liquid. The liquid MMN was characterized via various NMR measurements.

However, to further improve the purity to be suitable for ROMP applications, a column chromatography was performed. 3.186 g (42% of theory) were obtained after purification over 213 g of silica gel (PE : EE = 10 : 1) and drying in vacuum (not lower than 200 mbar at 40 °C).

Analytics:

R_f: 0.6 (PE : EE = 10 : 1)

Boiling Point: 70 °C – 72 °C (34 mbar)

^{1}H-NMR (400 MHz, $CDCl_3$): 7.26 (s, $CDCl_3$), 6.15 - 5.82 (m, 2H, CH=CH), 3.45 - 2.65 (m, 7H, CH-CH=CH-CH, CH_2-O-CH_3), 2.40 - 0.40 (m, 5H, O-CH_2-CH-CH_2, CH=CH-CH-CH_2)

^{13}C-NMR (100 MHz, $CDCl_3$): 137.3, 136.8, 136.8 & 132.6 (s, CH=CH), 77.2 (t, $CDCl_3$), 77.8, 76.9 (s, CH_2-O), 59.0 & 58.9 (CH_3), 49.6 & 45.2 (s, CH=CH-CH-CH_2), 44.1, 43.9, 42.4 & 41.7 (s, CH-CH=CH-CH), 39.1 & 38.9 (s, CH-CH_2-O), 29.9 & 29.4 (s, O-CH_2-CH-CH_2)

4. Photoredox-Mediators

4.1. Synthesis

4.1.1. Pyrylium Tetrafluoroborates

4.1.1.1. 4(4-Decyloxyphenyl)-2,6-(4-methoxyphenyl) Pyrylium Tetrafluoroborate

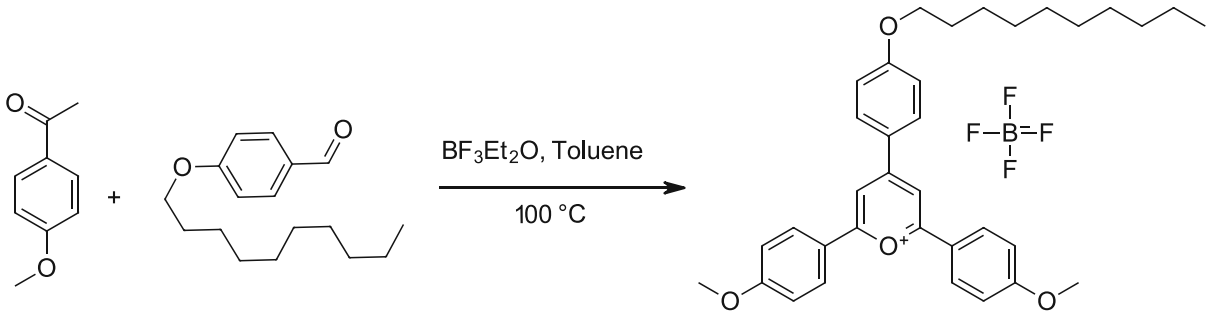

P1-B

32%

4(4-decyloxyphenyl)-2,6-(4-methoxyphenyl) pyrylium tetrafluoroborate was synthesized in accordance to the work of Breder et al.[206] At first, 1 eq. of 4-decyloxy benzaldehyde (2.364 g, 9 mmol), 2.5 eq. of 4-methoxy acetophenone (3.378 g, 22.5 mmol) and 5 mL of toluene were transferred into a three-necked round bottom flask equipped with a condenser. Magnetic stirring and argon atmosphere were applied. Afterwards, 2.4 eq. of boron trifluoride diethyl etherate (2.7 ml, 21.6 mmol) were added dropwise and the reaction heated to 100 °C. The forming gases were directed through two gas wash bottles (2nd filled with diluted, aqueous NaOH). The solution became increasingly viscous and dark red. The reaction temperature of 100 °C was then kept for a total of 18 h. After the reaction time, the dark mixture was dissolved in 10 mL of ethanol by refluxing for around 15 min. The solution was allowed to cool down to room temperature. Afterwards, 300 mL of diethyl ether were then added to the solution to precipitate the salt out of solution. The dispersed solids were centrifuged and the diethyl ether

decanted off. The solids were washed with 160 mL of diethyl ether. After this first purification step, the washing procedure was repeated 2 times to result in a total volume of 480 mL of diethyl ether as washing medium. The red solids were dried in vacuum and dissolved in 50 mL of acetone. Some insoluble parts were removed via hot filtration and the solvent evaporated to finally yield 1.762 g (32% of theory/-) of 4(4-decyloxyphenyl)-2,6-(4-methoxyphenyl) pyrylium tetrafluoroborate as red powder. The P1-B was characterized via melting point determination and various NMR measurements. The product was stored in the dark at 2 °C.

Analytics:

Melting point: 152.7 – 156.1 °C (decomposition) (lit. -)

^{1}H-NMR (400 MHz, DMSO): 8.70 (s, 2H, 2x O^{+}-C-CH), 8.55 (d, 2H, 2x O^{+}-C-CH-C-C-CH), 8.44 (d, 4H, 4x O^{+}-C-C-CH), 7.24 (d, 6H, 6x C-C-CH-CH), 4.17 (t, 2H, 2x O-CH_2), 3.95 (s, 6H, 2x O-CH_3), 2.50 (qui, DMSO), 1.78 (qui, 2H, O-CH_2-CH_2), 1.49 - 1.18 (m, 14H, O-CH_2-CH_2-CH_2-CH_2-CH_2-CH_2-CH_2-CH_2-CH_2), 0.87 (t, 3H, CH_3)

^{13}C-NMR (100 MHz, DMSO): 168.2 (s, 2x O^{+}-C), 165.2 (s, 1x O^{+}-C-CH-C-C-CH-CH-C), 165.0 (s, 2x O^{+}-C-C-CH-CH-C), 162.2 (s, 1x O^{+}-C-CH-C), 132.9 (s, 2x O^{+}-C-CH-C-C-CH), 131.1 (s, 4x O^{+}-C-C-CH), 124.7 (s, 1x O^{+}-C-CH-C-C), 121.9 (s, 2x O^{+}-C-C), 116.1 (s, 2x O^{+}-C-CH-C-C-CH-CH), 115.8 (s, 4x O^{+}-C-C-CH-CH), 111.2 (s, 2x O^{+}-C-CH), 68.9 (s, 1x O-CH_2), 56.5 (s, 2x O-CH_3), 39.5 (sep, DMSO), 31.8 (s, 1x O-CH_2-CH_2), 29.5 (s, 1x O-CH_2-CH_2-CH_2), 29.4 (s, 1x O-CH_2-CH_2-CH_2-CH_2), 29.3 (s, 1x O-CH_2-CH_2- CH_2-CH_2-CH_2), 29.2 (s, 1x O-CH_2-CH_2-CH_2 CH_2 CH_2-CH_2), 29.0 (s, 1x O-CH_2-CH_2-CH_2-CH_2-CH_2-CH_2-CH_2), 25.9 (s, 1x O-CH_2-CH_2-CH_2-CH_2-CH_2-CH_2-CH_2-CH_2), 22.6 (s, 1x O-CH_2-CH_2-CH_2-CH_2- CH_2-CH_2-CH_2-CH_2-CH_2), 14.4 (s, 1x CH_3)

^{19}F-NMR (376 MHz, DMSO): -148.2 (s, BF_4), -148.3 (s, BF_4)

4.1.1.2. 4(4-Declyoxyphenyl)-2,6(4-ethylhexanoxyphenyl) Pyrylium Tetrafluoroborate

4'(2-ethylhexanoxy)-acetophenone

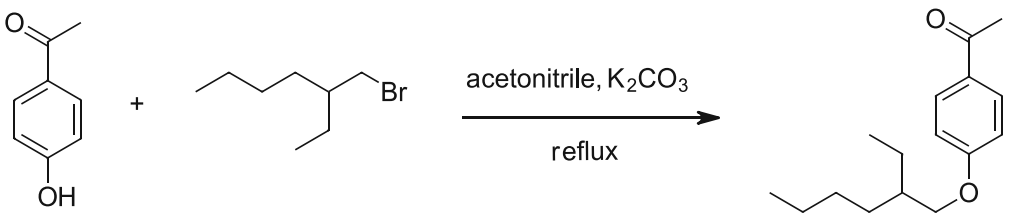

62%

To synthesize 4'(2-ethylhexanoxy)-acetophenone, a synthesis similar to Hudkins et al.[207] was carried out. At first, 1 eq. (3.400 g, 25 mmol) of 4'-hydroxyacetophenone were weighed into

a two-necked flask equipped with a septum and a condenser and dissolved in 85 mL of dry acetonitrile. Then, 3 eq. (10.516 g, 75 mmol) of potassium carbonate were added and the resulting dispersion stirred and heated to reflux. After 3 h, 1.05 eq. (4.6 mL, 26.3 mmol) of 1-bromo-2-ehtylhexane were added dropwise via syringe. The mixture was allowed to stir at reflux for 19 h. Reaction progress was checked via TLC. Since the reaction was not finished, a catalytic amount of benzyl-trimethylammonium chloride was added as a phase transfer agent. 20 h later, the reaction was stopped, the potassium carbonate filtrated off and the solvent removed in vacuum. To the residue was mixed with 50 mL of ethyl acetate, filtrated and the organic layer was washed with 3 x 25 mL of 1 N aqueous sodium hydroxide solution and one time with 25 mL of deionized water. The organic layer was dried with sodium sulfate and evaporated. The crude yellowish liquid was purified by MPLC column chromatography (213 g of silica gel, PE : EE = 9 : 1). Finally yielding 3.824 g (62% of theory/87% of lit.) of 4'(2-ethylhexanoxy)-acetophenone as colorless liquid. The product was characterized via various NMR measurements.

Analytics:

R_f: 0.8 (PE : EE = 2 : 1)

^{1}H-NMR (400 MHz, $CDCl_3$): 7.92 (d, 2H, 2x O-C-CH-CH), 7.26 (s, $CDCl_3$), 6.92 (d, 2H, 2x O-C-CH), 3.90 (d, 2H, O-CH_2), 2.55 (s, 3H, O=C-CH_3), 1.74 (qui, 1H, O-CH_2-CH), 1.55 – 1.37 (m, 4H, 2x O-CH_2-CH-CH_2), 1.26 – 1.37 (m, 4H, O-CH_2-CH-CH_2-CH_2-CH_2), 0.98 – 0.84 (m, 6H, 2x CH_3)

^{13}C-NMR (100 MHz, $CDCl_3$): 197.0 (s, C=O), 163.6 (s, C-O), 130.8 (s, 2x CH-C-C=O), 130.2 (s, C-C=O), 114.4 (s, 2x CH-C-O), 77.23 (t, $CDCl_3$), 70.9 (s, CH_2-O), 39.5 (sep, DMSO), 39.5 (s, O-CH_2-CH), 30.7 (s, O-CH_2-CH-CH_2-CH_2-CH_2-CH_3), 29.2 (s, O-CH_2-CH-CH_2-CH_2-CH_2-CH_3), 25.5 (s, CH_3-C=O), 24.0 (s, O-CH_2-CH-CH_2-CH_2-CH_2-CH_3), 23.2 (s, O-CH_2-CH-CH_2-CH_3), 14.3 (s, O-CH_2-CH-CH_2-CH_2-CH_2-CH_3), 11.3 (s, O-CH_2-CH-CH_2-CH_3)

4(4-Declyoxyphenyl)-2,6(4-ethylhexanoxyphenyl) Pyrylium Chloride

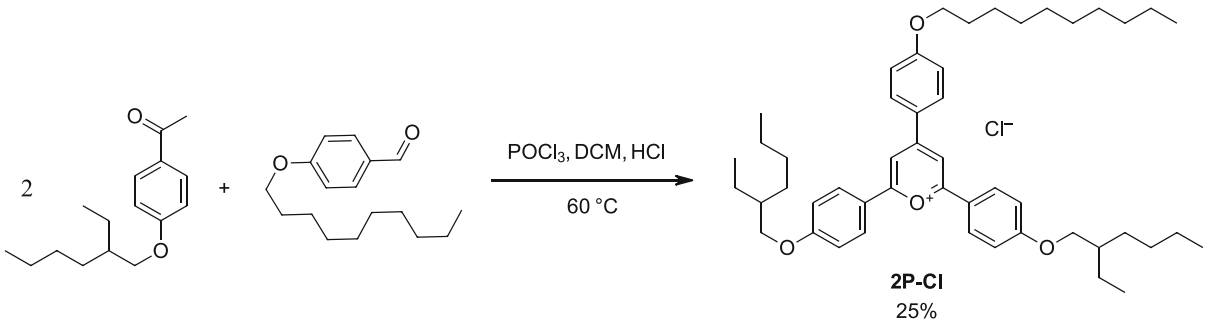

4(4-Decyloxyphenyl)-2,6(4-ethylhexanoxyphenyl) pyrylium chloride was synthesized in accordance to the work of Fortage et al.[168] At first, 1 eq. of 4-decyloxy benzaldehyde (1.05 mL, 4.5 mmol) and 2.5 eq. of 4'-ethylhexanoxy acetophenone (2.794 g, 11.3 mmol) were heated to 60 °C under magnetic stirring and argon atmosphere. Then 1.8 eq. of $POCl_3$ (0.75 mL, 8.1 mmol) were added dropwise, whereas the solution turned dark and HCl evolution started after around 10 min of stirring. The HCl gas was directed through two gas wash bottles (2nd filled with diluted, aqueous NaOH). As the solution became increasingly viscous, magnetic stirring was no longer possible after a few hours. After 24 h, 10 mL of dichloromethane were added to the sticky mixture to make magnetic stirring possible again. The reaction temperature was then kept for another 24 h. The gummy dark red mixture was dissolved in 20 mL of ethanol by refluxing for around 15 min. Then 1.5 eq. of concentrated HCl (0.6 mL, 6.8 mmol) were added to the boiling solution. After 15 min, the heating and stirring were stopped and the reaction solution was allowed to cool down to room temperature. The solution was stored at 2 °C over two days. Resulting in a separation of the mixture into a sticky residue at the bottom of the flask, which is soluble in hexanes, therefore not of interest and can be discarded, and a dark red solution. The dark red solution was decanted off into a beaker and added dropwise into the tenfold volume of hexanes (100 mL). Phase separation occurred, leaving a dark layer at the bottom and the hexanes in the upper layer. The hexanes were transferred into a separate beaker via decantation and the dark layer extracted twice with 50 mL hexanes in the beaker. After the removal of the hexanes by decantation and pipette, the dark layer discarded.

Yields can be increased by refluxing the sticky residues with 30 mL of ethanol again, followed by the extraction procedure with hexanes.

The combined hexane layers were dried in vacuum to yield a red, sticky residue. Yielding 1.008 g (25% of theory/-) of 4(4-Decyloxyphenyl)-2,6(4-ethylhexanoxyphenyl) pyrylium

chloride as a red, slightly sticky solid. The P2-Cl was characterized via melting point determination and various NMR measurements. Additionally, a halogen test was performed to verify the presence of chloride anions by dissolving the product in DMSO and in a different container $AgNO_3$ crystals in the same solvent. Upon mixing, a precipitate (AgCl) was formed. The product was stored in the dark at 2 °C.

Analytics:

^{1}H-NMR (400 MHz, DMSO): 8.76 (s, 2H, 2x O^+-C-CH), 8.58 (d, 2H, 2x O^+-C-CH-C-C-CH-CH), 8.45 (d, 4H, 4x O^+-C-C-CH-CH), 7.34 – 7.20 (m, 6H, 4x O^+-C-C-CH, 2x O^+-C-CH-C-C-CH), 4.18 (t, 2H, O-CH_2-CH_2), 4.07 (d, 4H, 2x O-CH_2-CH), 2.50 (qui, DMSO), 1.82 – 1.68 (m, 4H, 2x O-CH_2-CH; 2x O-CH_2-CH_2), 1.56 – 1.38 (m, 8H, 2x O-CH_2-CH-(CH_2)$_2$), 1.38 - 1.17 (m, 22H, 2x O-CH_2-CH-CH_2-CH_2-CH_2; O-CH_2-CH_2-CH_2-CH_2-CH_2-CH_2-CH_2-CH_2), 0.99 – 0.80 (m, 15H, 5x CH_3)

^{13}C-NMR (100 MHz, DMSO): 168.0 (s, 2x O^+-C), 165.2 (s, 1x O^+-C-CH-C-C-CH-CH-C), 164.1 (s, 2x O^+-C-C-CH-CH-C), 162.0 (s, 1x O^+-C-CH-C), 132.4 (s, 2x O^+-C-CH-C-C-CH), 130.8 (s, 4x O^+-C-C-CH), 124.7 (s, 1x O^+-C-CH-C-C), 121.4 (s, 2x O^+-C-C), 115.8 (s, 4x O^+-C-C-CH-CH), 115.4 (s, 2x O^+-C-CH-C-C-CH-CH), 111.0 (s, 2x O^+-C-CH), 70.8 (s, 2x O-CH_2-CH), 68.5 (s, 1x O-CH_2-CH_2), 39.5 (sep, DMSO), 38.5 (s, 2x CH), 31.8 (s, 1x O-CH_2-CH_2), 29.8 (s, 2x CH-CH_2), 29.5 (s, 1x O-CH_2-CH_2-CH_2), 29.4 (s, 1x O-CH_2-CH_2-CH_2-CH_2), 29.3 (s, 1x O-CH_2-CH_2- CH_2-CH_2-CH_2), 29.2 (s, 1x O-CH_2-CH_2-CH_2 CH_2 CH_2-CH_2), 29.0 (s, 1x O-CH_2-CH_2-CH_2-CH_2-CH_2-CH_2-CH_2), 28.4 (s, 2x CH-CH_2-CH_2), 25.9 (s, 1x O-CH_2-CH_2-CH_2-CH_2-CH_2-CH_2-CH_2), 22.6 (s, 1x O-CH_2-CH_2-CH_2-CH_2- CH_2-CH_2-CH_2-CH_2-CH_2), 23.2 (s, 2x CH-CH_2-CH_2-CH_2), 22.5 (s, 2x CH-CH_2-CH_3), 14.0 (s, 3x CH_2-CH_2-CH_3), 10.9 (s, 2x CH-CH_2-CH_3)

4(4-Decyloxyphenyl)-2,6(4-ethylhexanoxyphenyl) Pyrylium Tetrafluoroborate

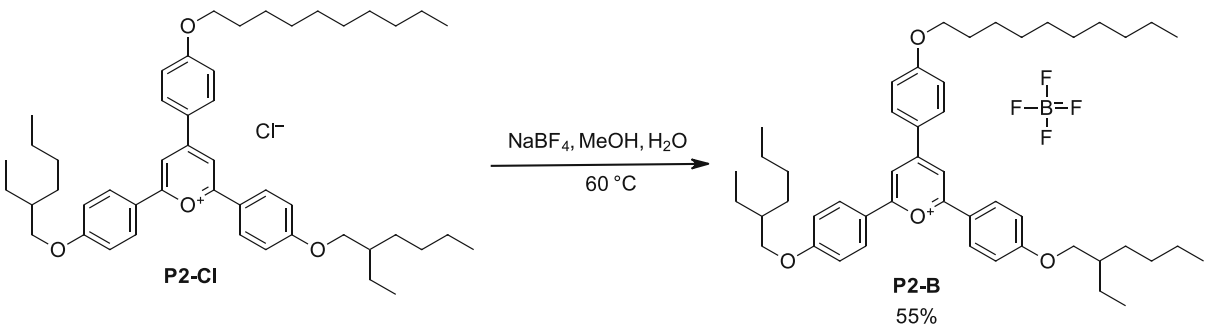

4(4-methoxyphenyl)-2,6(4-ethylhexanoxyphenyl) pyrylium hexafluoroantimonate was synthesized similar to the work of Li et al.[129] At first 1 eq. of 4(4-decyloxyphenyl)-2,6(4-ethylhexanoxyphenyl) pyrylium chloride (0.953 g, 1.3 mmol) was dissolved in 50 mL of a 1 : 12

mixture of methanol and deionized under heating. In a separate flask, 1.5 eq. of $NaBF_4$ (0.206 g, 1.9 mmol) were dissolved in 12 mL of the same solvent mixture. Both mixtures were heated to 60 °C in beakers to ensure solubility of the starting materials. The hot P2-Cl solution was transferred through a filter into a 60 °C preheated flask and magnetically stirred. Then the hot $NaSbF_6$ solution was added over a filter to the pyrylium salt solution. The filtration of both hot solutions was necessary to prevent minor impurities in the final product. Sticky solids precipitated immediately. After 10 min of reaction time at 60 °C, the heating source was removed and the mixture was allowed to cool down to room temperature over the course of one hour. The solution became increasingly lighter in color as more and more product precipitated. Since the red product was sticky, the solution was decanted off. The solids were washed three times with 10 mL of a 1 : 4 mixture of methanol and deionized water. Finally, the 4(4-decyloxyphenyl)-2,6(4-ethylhexanoxyphenyl) pyrylium hexafluoroantimonate was dried in vacuum to yield 0.561 g (55% of theory/-) as red slightly sticky solid. The P2-B was characterized via melting point determination and various NMR measurements. Additionally, a halogen test was performed to verify the absence of residual chloride anions by dissolving the product in DMSO and in a different container $AgNO_3$ crystals in the same solvent. Upon mixing the two hot solutions, no precipitate (AgCl) was formed. The product was stored in the dark at 2 °C.

Analytics:

Melting point: 63.7 – 67.4 °C (lit. -)

^{1}H-NMR (400 MHz, DMSO): 8.76 (s, 2H, 2x O^+-C-CH), 8.58 (d, 2H, 2x O^+-C-CH-C-C-CH-CH), 8.45 (d, 4H, 4x O^+-C-C-CH-CH), 7.34 – 7.20 (m, 6H, 4x O^+-C-C-CH, 2x O^+-C-CH-C-C-CH), 4.18 (t, 2H, O-CH_2-CH_2), 4.07 (d, 4H, 2x O-CH_2-CH), 2.50 (qui, DMSO), 1.82 – 1.68 (m, 4H, 2x O-CH_2-CH; 2x O-CH_2-CH_2), 1.56 – 1.38 (m, 8H, 2x O-CH_2-CH-(CH_2)$_2$), 1.38 - 1.17 (m, 22H, 2x O-CH_2-CH-CH_2-CH_2-CH_2; O-CH_2-CH_2-CH_2-CH_2-CH_2-CH_2-CH_2-CH_2-CH_2), 0.99 – 0.80 (m, 15H, 5x CH_3)

^{13}C-NMR (100 MHz, DMSO): 168.0 (s, 2x O^+-C), 165.2 (s, O^+-C-CH-C-C-CH-CH-C), 164.1 (s, 2x O^+-C-C-CH-CH-C), 162.0 (s, O^+-C-CH-C), 132.4 (s, 2x O^+-C-CH-C-C-CH), 130.8 (s, 4x O^+-C-C-CH), 124.7 (s, O^+-C-CH-C-C), 121.4 (s, 2x O^+-C-C), 115.8 (s, 4x O^+-C-C-CH-CH), 115.4 (s, 2x O^+-C-CH-C-C-CH-CH), 111.0 (s, 2x O^+-C-CH), 70.8 (s, 2x O-CH_2-CH), 68.5 (s, O-CH_2-CH_2), 39.5 (sep, DMSO), 38.5 (s, 2x CH), 31.8 (s, O-CH_2-CH_2), 29.8 (s, 2x CH-CH_2), 29.5 (s, O-CH_2-CH_2-CH_2), 29.4 (s, O-CH_2-CH_2-CH_2-CH_2), 29.3 (s, O-CH_2-CH_2-CH_2-CH_2-CH_2), 29.2 (s, O-CH_2-CH_2-CH_2-CH_2-CH_2-CH_2), 29.0 (s, O-CH_2-CH_2-CH_2-CH_2-CH_2-CH_2-CH_2), 28.4 (s, 2x CH-CH_2-CH_2), 25.9 (s, O-CH_2-CH_2-CH_2-

CH_2-CH_2-CH_2-CH_2-$\underline{C}H_2$), 22.6 (s, O-CH_2-CH_2-CH_2-CH_2- CH_2-CH_2-CH_2-CH_2-$\underline{C}H_2$), 23.2 (s, 2x CH-CH_2-CH_2-$\underline{C}H_2$), 22.5 (s, 2x CH-$\underline{C}H_2$-CH_3), 14.0 (s, 3x CH_2-CH_2-$\underline{C}H_3$), 10.9 (s, 2x CH-CH_2-$\underline{C}H_3$)

^{19}F-NMR (376 MHz, $CDCl_3$): -149.65 (s, BF_4), -149.70 (s, BF_4)

4.1.2. Pyrylium Hexafluoroantimonates and Tetraphenylborates

4.1.2.1. 4(4-Decyloxyphenyl)-2,6(4-methoxyphenyl) Pyrylium Hexafluoroantimonate

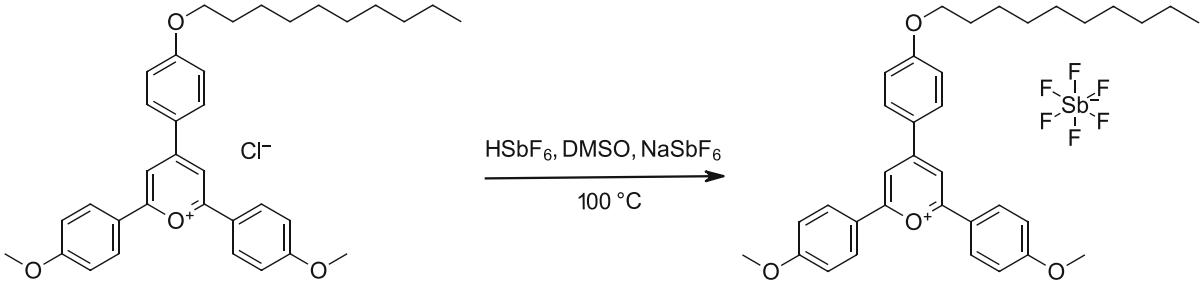

P1-Cl **P1-Sb**

57%

4(4-decyloxyphenyl)-2,6(4-methoxyphenyl) pyrylium hexafluoroantimonate was synthesized similar to a patent of Tavares. et al.[160] At first 1 eq. of 4(4-decyloxyphenyl)-2,6(4-methoxyphenyl) pyrylium chloride (0.084 g, 0.15 mmol) was dissolved in 10 mL of DMSO at 100 °C. Then 1.2 eq. of $HSbF_6$ (65 wt% in water, 0.02 mL, 0.18 mmol) were added dropwise to the pyrylium salt solution and stirred for 1 h at 100 °C. After the addition of 30 mL of deionized water, red solids precipitated. The solids were centrifuged and washed with 3 x 10 mL of a 1 : 4 mixture of water and methanol. The solids were then dried in vacuum overnight. The red solids were dissolved in 30 mL of dichloromethane and treated with 21 eq. of $NaSbF_6$ (0.815 g, 3.2 mmol). The sodium hexafluoroantimonate was dissolved in 70 mL of water and the washing procedure was conducted with 7 x 10 mL of the solution. The aqueous layer was reextracted once with 10 mL of dichloromethane and the combined organic layers were dried with sodium sulfate. The solvent was removed in vacuum. Finally, the reaction route yielded 0.065 g (57% of theory/-) of 4(4-decyloxyphenyl)-2,6(4-methoxyphenyl) pyrylium hexafluoroantimonate as red solid. The P1-Sb was characterized via melting point determination and various NMR measurements. Additionally, a halogen test was performed to verify the absence of residual chloride anions by dissolving the product in DMSO and in a different container $AgNO_3$ crystals in the same solvent. Upon mixing the two hot solutions, no precipitate (AgCl) was formed. The product was stored in the dark at 2 °C.

Analytics:

Melting point: 164.1 – 168.3 °C (lit. -)

^{1}H-NMR (400 MHz, DMSO): 8.70 (s, 2H, 2x O^{+}-C-CH), 8.55 (d, 2H, 2x O^{+}-C-CH-C-C-CH), 8.44 (d, 4H, 4x O^{+}-C-C-CH), 7.24 (d, 6H, 6x C-C-CH-CH), 4.17 (t, 2H, 2x O-CH_2), 3.95 (s, 6H, 2x O-CH_3), 2.50 (qui, DMSO), 1.78 (qui, 2H, O-CH_2-CH_2), 1.49 - 1.18 (m, 14H, O-CH_2-CH_2-CH_2-CH_2-CH_2-CH_2-CH_2-CH_2-CH_2), 0.87 (t, 3H, CH_3)

^{13}C-NMR (100 MHz, DMSO): 168.2 (s, 2x O^{+}-C), 165.2 (s, 1x O^{+}-C-CH-C-C-CH-CH-C), 165.0 (s, 2x O^{+}-C-C-CH-CH-C), 162.2 (s, 1x O^{+}-C-CH-C), 132.9 (s, 2x O^{+}-C-CH-C-C-CH), 131.1 (s, 4x O^{+}-C-C-CH), 124.7 (s, 1x O^{+}-C-CH-C-C), 121.9 (s, 2x O^{+}-C-C), 116.1 (s, 2x O^{+}-C-CH-C-C-CH-CH), 115.8 (s, 4x O^{+}-C-C-CH-CH), 111.2 (s, 2x O^{+}-C-CH), 68.9 (s, 1x O-CH_2), 56.5 (s, 2x O-CH_3), 39.51 (sep, DMSO), 31.8 (s, 1x O-CH_2-CH_2), 29.5 (s, 1x O-CH_2-CH_2-CH_2), 29.4 (s, 1x O-CH_2-CH_2-CH_2-CH_2), 29.3 (s, 1x O-CH_2-CH_2- CH_2-CH_2-CH_2), 29.2 (s, 1x O-CH_2-CH_2-CH_2 CH_2 CH_2-CH_2), 29.0 (s, 1x O-CH_2-CH_2-CH_2-CH_2-CH_2-CH_2-CH_2), 25.9 (s, 1x O-CH_2-CH_2-CH_2-CH_2-CH_2-CH_2-CH_2-CH_2), 22.6 (s, 1x O-CH_2-CH_2-CH_2-CH_2- CH_2-CH_2-CH_2-CH_2-CH_2), 14.4 (s, 1x CH_3)

^{19}F-NMR (376 MHz, DMSO): -107 to -111 (m, SbF_6)

4.1.2.2. 4(4-Decyloxyphenyl)-2,6(4-methoxyphenyl) Pyrylium Tetraphenylborate

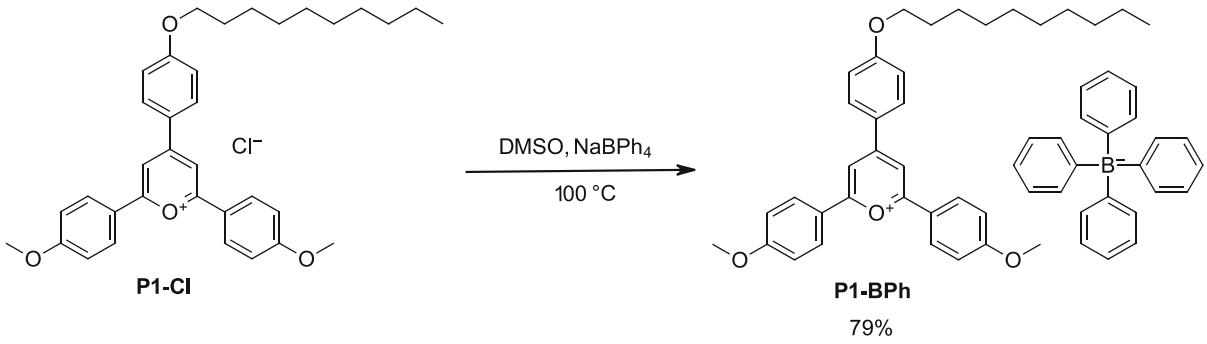

P1-Cl **P1-BPh** 79%

4(4-decyloxyphenyl)-2,6(4-methoxyphenyl) pyrylium tetraphenylborate was synthesized similar to the work of Li et al.[129] At first 1 eq. of 4(4-decyloxyphenyl)-2,6(4-methoxyphenyl) pyrylium chloride (0.395 g, 0.7 mmol) was dissolved in 20 mL of a mixture of methanol, deionized water and DMSO in a ratio of 17 : 7 : 26 respectively. Then 1.5 eq. of $NaBPh_4$ (0.363 g, 1.1 mmol) were dissolved in 15 mL of the same solvent mixture and heated to 100 °C. The sodium borate solution was hot filtrated into the pyrylium salt solution and stirred for 1 h at 100 °C. The mixture was allowed to cool down to RT and the precipitating red solids were collected via centrifugation. The solids were washed with 2 x 10 mL of the same mixture of solvents described at the beginning. The solids were then dried in vacuum overnight. To better remove any DMSO or water residues, the red solids were dissolved in 20 mL of dichloromethane and the solvent was removed in vacuum. Finally, the reaction route yielded

0.469 g (79% of theory/-) of 4(4-decyloxyphenyl)-2,6(4-methoxyphenyl) pyrylium tetrafluoroborate as a red solid. The P1-BPh was characterized via melting point determination and various NMR measurements. Additionally, a halogen test was performed to verify the absence of residual chloride anions by dissolving the product in DMSO and in a different container $AgNO_3$ crystals in the same solvent. Upon mixing the two hot solutions, no precipitate (AgCl) was formed. The product was stored in the dark at 2 °C.

Analytics:

Melting point: 119.8 – 123.5 °C (lit. -)

^{1}H-NMR (400 MHz, DMSO): 8.80 (s, 2H, 2x O^+-C-CH), 8.61 (d, 2H, 2x O^+-C-CH-C-C-CH), 8.50 (d, 4H, 4x O^+-C-C-CH), 7.32 – 7.24 (m, 6H, 6x C-C-CH-CH), 7.23 – 7.11 (m, 8H, 8x B^--C-CH-CH), 6.92 (t, 8H, 8x B^--C-CH-CH), 6.78 (t, 4H, 4x B^--C-CH-CH-CH), 4.17 (t, 2H, 2x O-CH_2), 3.95 (s, 6H, 2x O-CH_3), 2.50 (qui, DMSO), 1.78 (qui, 2H, O-CH_2-CH_2), 1.49 - 1.18 (m, 14H, O-CH_2-CH_2-CH_2-CH_2-CH_2-CH_2-CH_2-CH_2-CH_2-CH_2), 0.87 (t, 3H, CH_3)

^{13}C-NMR (100 MHz, DMSO): 168.2 (s, 2x O^+-C), 165.2 (s, 1x O^+-C-CH-C-C-CH-CH-C), 165.0 (s, 2x O^+-C-C-CH-CH-C), 164.1 & 163.6 & 163.1 & 162.6 (s, 4x B^--C), 162.2 (s, 1x O^+-C-CH-C), 135.5 (d, 8x B^--C-CH), 132.9 (s, 2x O^+-C-CH-C-C-CH), 131.1 (s, 4x O^+-C-C-CH), 125,2 (m, 8x B^--C-CH-CH), 124.7 (s, 1x O^+-C-CH-C-C), 121.9 (s, 2x O^+-C-C), 121.5 (s, 4x B^--C-CH-CH-CH), 116.1 (s, 2x O^+-C-CH-C-C-CH-CH), 115.8 (s, 4x O^+-C-C-CH-CH), 111.2 (s, 2x O^+-C-CH), 68.9 (s, 1x O-CH_2), 56.5 (s, 2x O-CH_3), 39.51 (sep, DMSO), 31.8 (s, 1x O-CH_2-CH_2), 29.5 (s, 1x O-CH_2-CH_2-CH_2), 29.4 (s, 1x O-CH_2-CH_2-CH_2-CH_2), 29.3 (s, 1x O-CH_2-CH_2- CH_2-CH_2-CH_2), 29.2 (s, 1x O-CH_2-CH_2-CH_2 CH_2 CH_2-CH_2), 29.0 (s, 1x O-CH_2-CH_2-CH_2-CH_2-CH_2-CH_2-CH_2), 25.9 (s, 1x O-CH_2-CH_2-CH_2-CH_2-CH_2-CH_2-CH_2-CH_2), 22.6 (s, 1x O-CH_2-CH_2-CH_2-CH_2- CH_2-CH_2-CH_2-CH_2-CH_2), 14.4 (s, 1x CH_3)

4.1.3. Pyrylium Hexafluorophosphates

4.1.3.1. 4(4-Decyloxyphenyl)-2,6(4-methoxyphenyl) Pyrylium Hexafluorophosphate

4(4-Decyloxyphenyl)-2,6(4-ethylhexanoxyphenyl) Pyrylium Chloride

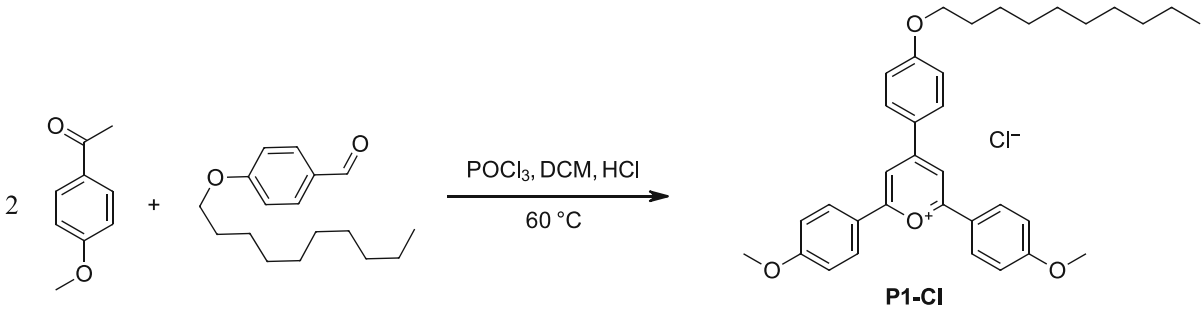

P1-Cl

45%

4(4-Decyloxyphenyl)-2,6(4-ethylhexanoxyphenyl) pyrylium chloride was synthesized in accordance to the work of Fortage et al.[168] At first, 1 eq. of 4-decyloxy benzaldehyde (2.35 mL, 10 mmol) and 2.5 eq. of 4-methoxy acetophenone (3.796 g, 25 mmol) were heated to 60 °C under magnetic stirring and argon atmosphere. Then 1.8 eq. of $POCl_3$ (1.7 mL, 18 mmol) and 8 mL of dichloromethane were added dropwise, whereas the solution turned dark and HCl evolution started after around 10 min of stirring. The HCl gas was directed through two gas wash bottles (2nd filled with diluted, aqueous NaOH). As the solution became increasingly viscous, magnetic stirring was no longer possible after a few hours. After 24 h, 20 mL of dichloromethane were added to the sticky mixture to make magnetic stirring possible again. The reaction temperature was then kept for another 24 h. The gummy dark red mixture was dissolved in 15 mL of ethanol by refluxing for around 15 min. Then 1.5 eq. of concentrated HCl (1.4 mL, 15 mmol) were added to the boiling solution. After 15 min, the heating and stirring were stopped and the reaction solution was allowed to cool down to room temperature. The solution was stored at 2 °C over 2 h. The dark red solution was transferred into a beaker and added dropwise into the tenfold volume of diethyl ether (450 mL). Red solids precipitated immediately. The red product was washed twice with 20 mL of diethyl ether and once with 20 mL of acetone in the beaker. The red product was dried in vacuum, yielding 2.517 g (45% of theory/-) of 4(4-Decyloxyphenyl)-2,6(4-methoxyphenyl) pyrylium chloride as a red solid. The P1-Cl was characterized via melting point determination and various NMR measurements. Additionally, a halogen test was performed to verify the presence of chloride anions by dissolving the product in DMSO and in a different container $AgNO_3$ crystals in the same solvent. Upon mixing, a precipitate (AgCl) was formed. The product was stored in the dark at 2 °C.

Analytics:

Melting point: 264.2 – 268.3 °C (lit. -)

^{1}H-NMR (400 MHz, DMSO): 8.70 (s, 2H, 2x O^{+}-C-C<u>H</u>), 8.55 (d, 2H, 2x O^{+}-C-CH-C-C-C<u>H</u>), 8.44 (d, 4H, 4x O^{+}-C-C-C<u>H</u>), 7.24 (d, 6H, 6x C-C-CH-C<u>H</u>), 4.17 (t, 2H, 2x O-C<u>H_2</u>), 3.95 (s, 6H, 2x O-C<u>H_3</u>), 2.50 (qui, DMSO), 1.78 (qui, 2H, O-CH_2-C<u>H_2</u>), 1.49 - 1.18 (m, 14H, O-CH_2-CH_2-C<u>H_2</u>-C<u>H_2</u>-C<u>H_2</u>-C<u>H_2</u>-C<u>H_2</u>-C<u>H_2</u>-C<u>H_2</u>), 0.87 (t, 3H, C<u>H_3</u>)

^{13}C-NMR (100 MHz, DMSO): 168.2 (s, 2x O^{+}-<u>C</u>), 165.2 (s, 1x O^{+}-C-CH-C-C-CH-CH-<u>C</u>), 165.0 (s, 2x O^{+}-C-C-CH-CH-<u>C</u>), 162.2 (s, 1x O^{+}-C-CH-<u>C</u>), 132.9 (s, 2x O^{+}-C-CH-C-C-<u>CH</u>), 131.1 (s, 4x O^{+}-C-C-<u>CH</u>), 124.7 (s, 1x O^{+}-C-CH-C-<u>C</u>), 121.9 (s, 2x O^{+}-C-<u>C</u>), 116.1 (s, 2x O^{+}-C-CH-C-C-CH-<u>CH</u>), 115.8 (s, 4x O^{+}-C-C-CH-<u>CH</u>), 111.2 (s, 2x O^{+}-C-<u>CH</u>), 68.9 (s, 1x O-<u>CH_2</u>), 56.5 (s, 2x O-C<u>H_3</u>), 39.5 (sep, DMSO), 31.8 (s, 1x O-CH_2-<u>CH_2</u>), 29.5 (s, 1x O-CH_2-CH_2-<u>CH_2</u>), 29.4 (s, 1x O-CH_2-CH_2-CH_2-<u>CH_2</u>), 29.3 (s, 1x O-CH_2-CH_2-CH_2-CH_2-<u>CH_2</u>), 29.2 (s, 1x O-CH_2-CH_2-CH_2-CH_2-CH_2-<u>CH_2</u>), 29.0 (s, 1x O-CH_2-CH_2-CH_2-CH_2-CH_2-CH_2-<u>CH_2</u>), 25.9 (s, 1x O-CH_2-CH_2-CH_2-CH_2-CH_2-CH_2-CH_2-<u>CH_2</u>), 22.6 (s, 1x O-CH_2-CH_2-CH_2-CH_2- CH_2-CH_2-CH_2-CH_2-<u>CH_2</u>), 14.4 (s, 1x <u>CH_3</u>)

4(4-Decyloxyphenyl)-2,6(4-methoxyphenyl) Pyrylium Hexafluorophosphate

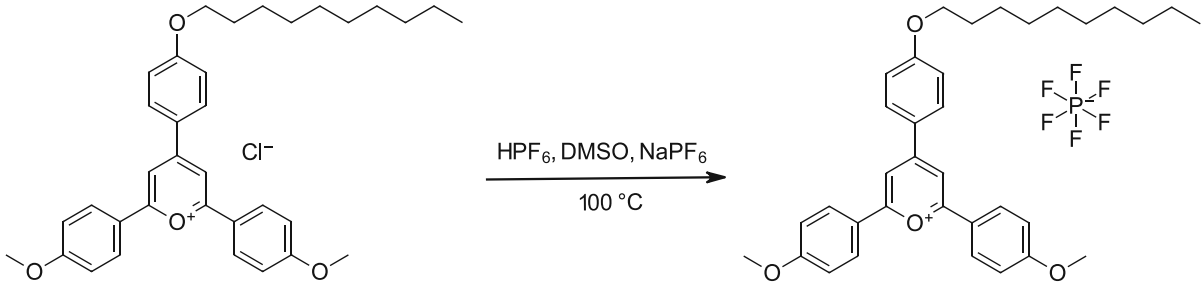

P1-Cl **P1-P**

53%

4(4-decyloxyphenyl)-2,6(4-methoxyphenyl) pyrylium hexafluorophosphate was synthesized similar to a patent of Tavares. et al.[160] At first 1 eq. of 4(4-decyloxyphenyl)-2,6(4-methoxyphenyl) pyrylium chloride (0.226 g, 0.4 mmol) was dissolved in 10 mL of DMSO at 100 °C. Then 1.2 eq. of HPF_6 (60 wt% in water, 0.08 mL, 0.5 mmol) were added dropwise to the pyrylium salt solution and stirred for 1 h at 100 °C. After the addition of 40 mL of deionized water, red solids precipitated. The solids were washed with 3 x 10 mL of a 1 : 4 mixture of water and methanol. The solids were then dried in vacuum overnight. The red solids were dissolved in 30 mL of dichloromethane and treated with 21 eq. of $NaPF_6$ (1.411 g, 8.4 mmol). The sodium hexafluorophosphate was dissolved in 70 mL of water and the washing procedure was conducted with 7 x 10 mL of the solution. The aqueous layer was reextracted once with

10 mL of dichloromethane and the combined organic layers were dried with sodium sulfate. The solvent was removed in vacuum. Finally, the reaction route yielded 0.143 g (53% of theory/-) of 4(4-decyloxyphenyl)-2,6(4-methoxyphenyl) pyrylium hexafluorophosphate as red solid. The P1-P was characterized via melting point determination and various NMR measurements. Additionally, a halogen test was performed to verify the absence of residual chloride anions by dissolving the product in DMSO and in a different container $AgNO_3$ crystals in the same solvent. Upon mixing the two hot solutions, no precipitate (AgCl) was formed. The product was stored in the dark at 2 °C.

Analytics:

Melting point: 198.6 – 200.5 °C (lit. -)

^{1}H-NMR (400 MHz, DMSO): 8.70 (s, 2H, 2x O^+-C-CH), 8.55 (d, 2H, 2x O^+-C-CH-C-C-CH), 8.44 (d, 4H, 4x O^+-C-C-CH), 7.24 (d, 6H, 6x C-C-CH-CH), 4.17 (t, 2H, 2x O-CH_2), 3.95 (s, 6H, 2x O-CH_3), 2.50 (qui, DMSO), 1.78 (qui, 2H, O-CH_2-CH_2), 1.49 - 1.18 (m, 14H, O-CH_2-CH_2-CH_2-CH_2-CH_2-CH_2-CH_2-CH_2-CH_2), 0.87 (t, 3H, CH_3)

^{13}C-NMR (100 MHz, DMSO): 168.2 (s, 2x O^+-C), 165.2 (s, 1x O^+-C-CH-C-C-CH-CH-C), 165.0 (s, 2x O^+-C-C-CH-CH-C), 162.2 (s, 1x O^+-C-CH-C), 132.9 (s, 2x O^+-C-CH-C-C-CH), 131.1 (s, 4x O^+-C-C-CH), 124.7 (s, 1x O^+-C-CH-C-C), 121.9 (s, 2x O^+-C-C), 116.1 (s, 2x O^+-C-CH-C-C-CH-CH), 115.8 (s, 4x O^+-C-C-CH-CH), 111.2 (s, 2x O^+-C-CH), 68.9 (s, 1x O-CH_2), 56.5 (s, 2x O-CH_3), 39.5 (sep, DMSO), 31.8 (s, 1x O-CH_2-CH_2), 29.5 (s, 1x O-CH_2-CH_2-CH_2), 29.4 (s, 1x O-CH_2-CH_2-CH_2-CH_2), 29.3 (s, 1x O-CH_2-CH_2-CH_2-CH_2-CH_2), 29.2 (s, 1x O-CH_2-CH_2-CH_2-CH_2-CH_2-CH_2), 29.0 (s, 1x O-CH_2-CH_2-CH_2-CH_2-CH_2-CH_2-CH_2), 25.9 (s, 1x O-CH_2-CH_2-CH_2-CH_2-CH_2-CH_2-CH_2-CH_2), 22.6 (s, 1x O-CH_2-CH_2-CH_2-CH_2- CH_2-CH_2-CH_2-CH_2-CH_2), 14.4 (s, 1x CH_3)

^{19}F-NMR (376 MHz, DMSO): -69.2 (s, PF_6), -71.1 (s, PF_6)

^{31}P-NMR (162 MHz, DMSO): -144.2 (sep, PF_6)

4.1.3.2. 4(4-Decyloxyphenyl)-2,6(4-ethylhexanoxyphenyl) Pyrylium Hexafluorophosphate

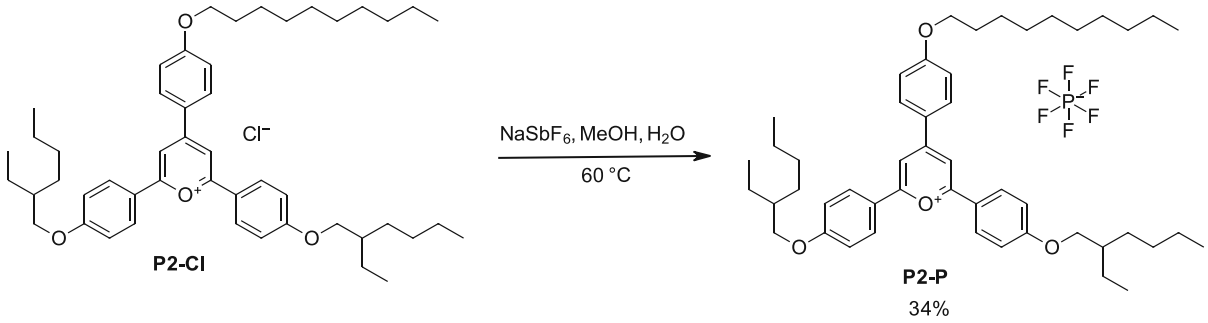

P2-Cl P2-P
34%

4-decyloxyphenyl)-2,6(4-ethylhexanoxyphenyl) pyrylium hexafluorophosphate was synthesized similar to the work of Li et al.[129]At first 1 eq. of 4(4-decyloxyphenyl)-2,6(4-ethylhexanoxyphenyl) pyrylium chloride (0.223 g, 0.3 mmol) was dissolved in 12 mL of a 1 : 40 mixture of deionized water and methanol under heating. In a separate flask, 1.5 eq. of $NaPF_6$ (0.117 g, 0.5 mmol) were dissolved in 20 mL of the same solvent mixture. The hot P2-Cl solution was transferred through a filter into a 60 °C preheated flask and magnetically stirred. Then the 60 °C hot $NaPF_6$ solution was added over a filter to the pyrylium salt solution and stirred for 1 h. After the addition of 1.8 mL deionized water, sticky solids precipitated. The solids were washed with 3 x 10 mL of a 1 : 4 mixture of water and methanol. The solids were then dried in vacuum overnight. A second fraction started to precipitate overnight and another 0.5 mL of deionized water were added. The solids were subject to the same workup as fraction one. Finally, both fractions were combined and yielded 0.087 g (34% of theory/-) of 4(4-decyloxyphenyl)-2,6(4-ethylhexanoxyphenyl) pyrylium hexafluorophosphate as red sticky solid. The P2-P was characterized via melting point determination and various NMR measurements. Additionally, a halogen test was performed to verify the absence of residual chloride anions by dissolving the product in DMSO and in a different container $AgNO_3$ crystals in the same solvent. Upon mixing the two hot solutions, no precipitate (AgCl) was formed. The product was stored in the dark at 2 °C.

Analytics:

Melting point: 53.0 – 55.0 °C (lit. -)

^{1}H-NMR (400 MHz, DMSO): 8.76 (s, 2H, 2x O^+-C-CH), 8.58 (d, 2H, 2x O^+-C-CH-C-C-CH-CH), 8.45 (d, 4H, 4x O^+-C-C-CH-CH), 7.34 – 7.20 (m, 6H, 4x O^+-C-C-CH, 2x O^+-C-CH-C-C-CH), 4.18 (t, 2H, O-CH_2-CH_2), 4.07 (d, 4H, 2x O-CH_2-CH), 2.50 (qui, DMSO), 1.82 – 1.68 (m, 4H, 2x O-CH_2-CH; 2x O-CH_2-CH_2), 1.56 – 1.38 (m, 8H, 2x O-CH_2-CH-(CH_2)$_2$), 1.38 - 1.17 (m, 22H, 2x O-CH_2-CH-CH_2-CH_2-CH_2; O-CH_2-CH_2-CH_2-CH_2-CH_2-CH_2-CH_2-CH_2-CH_2), 0.99 – 0.80 (m, 15H, 5x CH_3)

^{13}C-NMR (100 MHz, DMSO): 168.0 (s, 2x O$^+$-C), 165.2 (s, O$^+$-C-CH-C-C-CH-CH-C), 164.1 (s, 2x O$^+$-C-C-CH-CH-C), 162.0 (s, O$^+$-C-CH-C), 132.4 (s, 2x O$^+$-C-CH-C-C-CH), 130.8 (s, 4x O$^+$-C-C-CH), 124.7 (s, O$^+$-C-CH-C-C), 121.4 (s, 2x O$^+$-C-C), 115.8 (s, 4x O$^+$-C-C-CH-CH), 115.4 (s, 2x O$^+$-C-CH-C-C-CH-CH), 111.0 (s, 2x O$^+$-C-CH), 70.8 (s, 2x O-CH$_2$-CH), 68.5 (s, O-CH$_2$-CH$_2$), 39.5 (sep, DMSO), 38.5 (s, 2x CH), 31.8 (s, O-CH$_2$-CH$_2$), 29.8 (s, 2x CH-CH$_2$), 29.5 (s, O-CH$_2$-CH$_2$-CH$_2$), 29.4 (s, O-CH$_2$-CH$_2$-CH$_2$-CH$_2$), 29.3 (s, O-CH$_2$-CH$_2$-CH$_2$-CH$_2$-CH$_2$), 29.2 (s, O-CH$_2$-CH$_2$-CH$_2$-CH$_2$-CH$_2$-CH$_2$), 29.0 (s, O-CH$_2$-CH$_2$-CH$_2$-CH$_2$-CH$_2$-CH$_2$-CH$_2$), 28.4 (s, 2x CH-CH$_2$-CH$_2$), 25.9 (s, O-CH$_2$-CH$_2$-CH$_2$-CH$_2$-CH$_2$-CH$_2$-CH$_2$), 22.6 (s, O-CH$_2$-CH$_2$-CH$_2$-CH$_2$- CH$_2$-CH$_2$-CH$_2$-CH$_2$-CH$_2$), 23.2 (s, 2x CH-CH$_2$-CH$_2$-CH$_2$), 22.5 (s, 2x CH-CH$_2$-CH$_3$), 14.0 (s, 3x CH$_2$-CH$_2$-CH$_3$), 10.9 (s, 2x CH-CH$_2$-CH$_3$)

^{19}F-NMR (376 MHz, DMSO): -69.2 (s, PF$_6$), -71.1 (s, PF$_6$)

^{31}P-NMR (162 MHz, DMSO): -144.2 (sep, PF$_6$)

4.1.3.3. 4(4-Octadecyloxyphenyl)-2,6(4-methoxyphenyl) Pyrylium Hexafluorophosphate

4(4-Octadecyloxyphenyl)-2,6(4-methoxyphenyl) Pyrylium Chloride

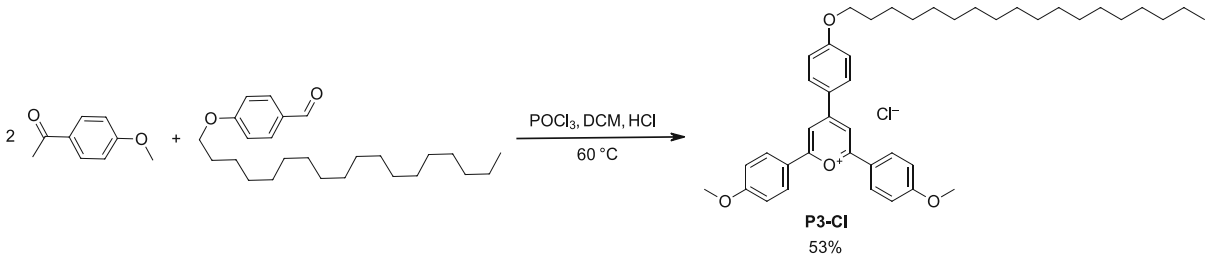

4(4-Octadecyloxyphenyl)-2,6(4-methoxyphenyl) pyrylium chloride was synthesized similar to the work of Fortage et al.[168] At first, 1 eq. of 4-octadecyloxy benzaldehyde (2.622 g, 7 mmol) and 2.5 eq. of 4-methoxy acetophenone (2.629 g, 17.5 mmol) were heated to 60 °C under magnetic stirring and argon atmosphere. 5 mL of dichloromethane were added. Then 1.8 eq. of $POCl_3$ (1.2 mL, 12.6 mmol) were added dropwise, whereas the solution turned dark red and slight HCl evolution started after around 10 min of stirring. The HCl gas was directed through two gas wash bottles (2nd filled with diluted, aqueous NaOH). After 24 h, 10 mL of dichloromethane were added to the sticky mixture to make magnetic stirring possible again. The reaction temperature was then kept for another 24 h. The gummy dark red mixture was dissolved in 20 mL of ethanol by refluxing for around 15 min. Then 1.5 eq. of concentrated HCl (1 mL, 10.5 mmol) were added to the boiling solution. After 15 min, the heating and stirring were stopped and the reaction solution was allowed to cool down to room temperature. The solution was stored at 2 °C overnight. The dark red solution was added dropwise into 200 mL of hexanes and stirred for 5 min, leaving a bright red precipitate. The brown-red colored

hexanes were decanted off and discarded. This washing procedure was repeated twice with 100 mL of hexanes and 5 min of stirring per step. The red solids were dried in vacuum to finally yield 2.512 g (53% of theory/-) of 4(4-octadecyloxyphenyl)-2,6(4-methoxyphenyl) pyrylium chloride as a bright red solid. The P3-Cl was characterized via melting point determination and various NMR measurements. Additionally, a halogen test was performed to verify the presence of chloride anions by dissolving the product in DMSO and in a different container $AgNO_3$ crystals in the same solvent. Upon mixing, a precipitate (AgCl) was formed. The product was stored in the dark at 2 °C.

Analytics:

Melting point: 132 - 136 °C (lit. -)

^{1}H-NMR (400 MHz, DMSO): 8.75 (s, 2H, 2x O^+-C-CH), 8.57 (d, 2H, 2x O^+-C-CH-C-C-CH-CH), 8.47 (d, 4H, 4x O^+-C-C-CH-CH), 7.32 – 7.19 (m, 6H, 4x O^+-C-C-CH, 2x O^+-C-CH-C-C-CH), 4.18 (t, 2H, O-CH_2-CH_2), 3.95 (s, 6H, 2x O-CH_3), 2.50 (qui, DMSO), 1.82 – 1.72 (m, 2H, 2x O-CH_2-CH_2), 1.49 – 1.41 (m, 2H, 2x O-CH_2-CH_2-CH_2), 1.41 - 1.19 (m, 28H, O-CH_2-CH_2-CH_2-CH_2-CH_2-CH_2-CH_2-CH_2-CH_2-CH_2-CH_2-CH_2-CH_2-CH_2), 0.88 – 0.80 (t, 3H, CH_3)

^{13}C-NMR (100 MHz, DMSO): 167.9 (s, 2x O^+-C), 164.8 (s, O^+-C-CH-C-C-CH-CH-C), 164.5 (s, 2x O^+-C-C-CH-CH-C), 161.9 (s, O^+-C-CH-C), 132.5 (s, 2x O^+-C-CH-C-C-CH), 130.6 (s, 4x O^+-C-C-CH), 124.3 (s, O^+-C-CH-C-C), 121.5 (s, 2x O^+-C-C), 115.7 (s, 2x O^+-C-CH-C-C-CH-CH), 115.3 (s, 4x O^+-C-C-CH-CH), 110.8 (s, 2x O^+-C-CH), 68.4 (s, O-CH_2), 56.0 (s, 2x O-CH_3), 39.5 (sep, DMSO), 31.3 (s, O-CH_2-CH_2), 29.1 – 28.4 (m, O-CH_2-CH_2-CH_2-CH_2-CH_2-CH_2-CH_2-CH_2-CH_2-CH_2-CH_2-CH_2-CH_2-CH_2), 25.4 (s, O-$(CH_2)_{15}$-CH_2-CH_2-CH_3), 22.0 (s, O-$(CH_2)_{16}$-CH_2-CH_3), 13.9 (s, CH_3)

4(4-Octadecyloxyphenyl)-2,6(4-ethylhexanoxyphenyl) Pyrylium Hexafluorophosphate

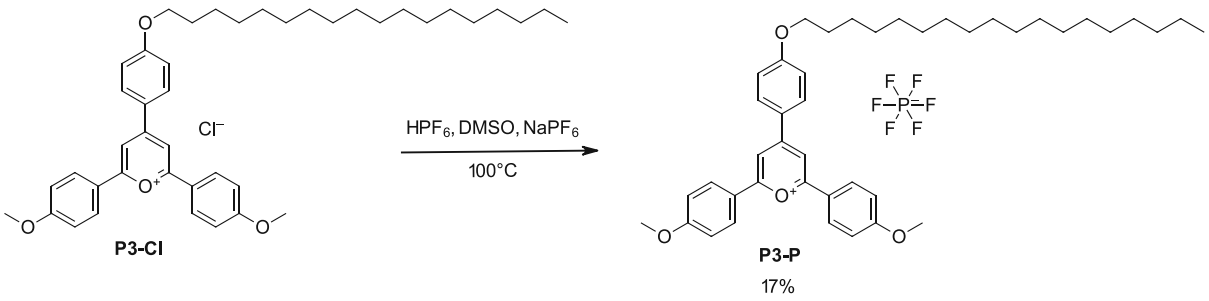

4(4-octadecyloxyphenyl)-2,6(4-ethylhexanoxyphenyl) pyrylium hexafluorophosphate was synthesized similar to a patent of Tavares. et al.[160] At first 1 eq. of 4(4-octadecyloxyphenyl)-2,6(4-ethylhexanoxyphenyl) pyrylium chloride (0.404 g, 0.6 mmol) was dissolved in 15 mL of DMSO at 100 °C. In a separate flask, 1.2 eq. of HPF_6 (60 wt% in water, 0.07 mL, 0.7 mmol) were

dissolved in 0.7 mL of DMSO. Then the HPF_6 solution was added to the pyrylium salt solution. After 1 h of reaction time at 100 °C, the heating source was removed and the mixture was allowed to warm up to room temperature. Afterwards 20 mL of deionized water were added to the DMSO mixture to start precipitating the pyrylium salt. The red solids were centrifuged and washed two times with 20 mL of water, followed by centrifugation. The pyrylium salt was pre-dried in vacuum. Then 30 mL of dichloromethane were added and removed in vacuum to better remove residual water. This drying procedure was performed over 4 days at 60 °C to result in a red solid. In the next step the red powder was transferred into a vial, 30 mL of dichloromethane were added and the vial closed. The mixture was carefully refluxed for a few seconds and then treated in the ultrasonic bath at 35 °C for 1 h followed by stirring for 18 h at RT. Now parts of the red powder were in solution, while some insoluble parts remained. The insoluble parts were filtrated off and treated with 21 eq. of $NaPF_6$ (2.116 g, 12.6 mmol). The sodium hexafluorophosphate was dissolved in 70 mL of water and the washing procedure was conducted with 7 x 10 mL of the solution. The aqueous layer was reextracted once with 10 mL of dichloromethane and the combined organic layers were dried with sodium sulfate. The solvent was removed in vacuum. Finally, the 4(4-octadecyloxyphenyl)-2,6-diphenyl pyrylium hexafluorophosphate yielded 0.082 g (17% of theory/-) as red solid. The P3-P was characterized via melting point determination and various NMR measurements. Additionally, a halogen test was performed to verify the absence of residual chloride anions by dissolving the product in DMSO and in a different container $AgNO_3$ crystals in the same solvent. Upon mixing the two hot solutions, no precipitate (AgCl) was formed. The product was stored in the dark at 2 °C.

Analytics:

Melting point: 198.5 – 201.8 °C (lit. -)

^{1}H-NMR (400 MHz, DMSO): 8.75 (s, 2H, 2x O^+-C-C<u>H</u>), 8.57 (d, 2H, 2x O^+-C-CH-C-C-CH-C<u>H</u>), 8.47 (d, 4H, 4x O^+-C-C-CH-C<u>H</u>), 7.32 – 7.19 (m, 6H, 4x O^+-C-C-C<u>H</u>, 2x O^+-C-CH-C-C-C<u>H</u>), 4.18 (t, 2H, O-C<u>H_2</u>-CH_2), 3.95 (s, 6H, 2x O-C<u>H_3</u>), 2.50 (qui, DMSO), 1.82 – 1.72 (m, 2H, 2x O-CH_2-C<u>H_2</u>), 1.49 – 1.41 (m, 2H, 2x O-CH_2-CH_2-C<u>H_2</u>), 1.41 - 1.19 (m, 28H, O-CH_2-CH_2-CH_2-C<u>H_2</u>-C<u>H_2</u>-C<u>H_2</u>-C<u>H_2</u>-C<u>H_2</u>-C<u>H_2</u>-C<u>H_2</u>-C<u>H_2</u>-C<u>H_2</u>-C<u>H_2</u>-C<u>H_2</u>-C<u>H_2</u>-C<u>H_2</u>), 0.88 – 0.80 (t, 3H, C<u>H_3</u>)

^{13}C-NMR (100 MHz, DMSO): 167.9 (s, 2x O^+-C), 164.8 (s, O^+-C-CH-C-C-CH-CH-C), 164.5 (s, 2x O^+-C-C-CH-CH-C), 161.9 (s, O^+-C-CH-C), 132.5 (s, 2x O^+-C-CH-C-C-CH), 130.6 (s, 4x O^+-C-C-CH), 124.3 (s, O^+-C-CH-C-C), 121.5 (s, 2x O^+-C-C), 115.7 (s, 2x O^+-C-CH-C-C-CH-CH), 115.3 (s, 4x O^+-

C-C-CH-CH), 110.8 (s, 2x O^+-C-CH), 68.4 (s, O-CH_2), 56.0 (s, 2x O-CH_3), 39.5 (sep, DMSO), 31.3 (s, O-CH_2-CH_2), 29.1 – 28.4 (m, O-CH_2-CH_2-CH_2-CH_2-CH_2-CH_2-CH_2-CH_2-CH_2-CH_2-CH_2-CH_2-CH_2-CH_2), 25.4 (s, O-$(CH_2)_{15}$-CH_2-CH_2-CH_3), 22.0 (s, O-$(CH_2)_{16}$-CH_2-CH_3), 13.9 (s, CH_3)

^{19}F-NMR (376 MHz, DMSO): -69.2 (s, PF_6), -71.1 (s, PF_6)

^{31}P-NMR (162 MHz, DMSO): -144.2 (sep, PF_6)

MATERIALS AND METHODS

Nuclear Magnetic Resonance

^{1}H-, ^{13}C-, ^{19}F-, ^{11}B- and, ^{31}P-NMR spectra were recorded on a BRUKER Avance DRX-400 FT-NMR spectrometer or a BRUKER DPX-600 FT-NMR spectrometer. Chemical shifts were referred in ppm and referenced on the respective NMR-solvent. The multiplicity of the signals was reported as s = singlet, d = doublet, t = triplet, or m = multiplet.

To determine the ROMP conversions via ^{1}H-NMR, the following integrals were taken after each spectrum was referred to the solvent peak (Table 11).

Table 11: Integrals selected for monomer(s) and polymer(s) after photoredox-mediated MF-ROMP in the photoreactor

System	Integral monomer(s) [ppm]	Integral polymer(s) [ppm]
N	6.27 – 5.79	2.60 – 2.39
N-MMN	6.32 – 5.77	2.86 – 2.79 (polyMMN) 2.45 – 2.27 (polyN)
DCPD	5.92 – 5.77	5.67 – 5.53

The molar amount of polymer was calculated by the use of the NMR-obtained integrals for homopolymerization experiments according to Equation 8 and for copolymerization experiments according to Equation 9.

Equation 8: Calculation of the conversion for homopolymerization experiments (N and DCPD MF-ROMP)

$$C\ [\%] = \frac{n_P}{n_P + n_M} * 100$$

$$n_P = \frac{(m_T - m_R) * \frac{m_M}{m_T}}{M_M} * I_P * F \qquad n_M = \frac{(m_T - m_R) * \frac{m_M}{m_T}}{M_M}$$

C…conversion [%]

n_P…molar amount of polymer in the photoreactor

n_M…molar amount of monomer in the photoreactor

m_T…total mass of formulation transferred into the photoreactor [g]

m_R…removed mass from photoreactor at time of sample collection (for example at t=0 m_T equals still m_R) [g]

I_P…Integral value in ^{1}H-NMR of the polymer if monomer integral is set to "1" [ ]

F…multiplicative factor for the ratio of hydrogens in the peaks of monomer and polymer (N: F=1; DCPD: F=2) [ ]

M_M…molar mass of the monomer in use (N: 94.15; DCPD: 132.20) [g mol^{-1}]

Equation 9: Calculation of the conversion for copolymerization experiments (N-MMN MF-ROMP)

$$C\ [\%] = \frac{n_{P_i}}{n_{P_i} + n_{M_i}} * 100$$

$$n_{P_i} = \sum \left(\frac{(m_T - m_R) * \frac{m_{M_i}}{m_T}}{M_{M_i}} * I_{P_i} * F_i \right) \qquad n_{M_i} = \sum \left(\frac{(m_T - m_R) * \frac{m_{M_i}}{m_T}}{M_{M_i}} \right)$$

C…conversion [%]

n_{Pi}…molar amount of each polymer in the photoreactor

n_{Mi}…molar amount of each monomer in the photoreactor

m_T…total mass of formulation transferred into the photoreactor [g]

m_R…removed mass from photoreactor at time of sample collection (for example at t=0 m_T equals still m_R) [g]

m_{Mi}…masses of individual monomers in the photoreactor (m_{Mi} m_T^{-1} leads to a constant mass ratios) [g]

I_{Pi}…Integral value in ^{1}H-NMR of the individual polymers if monomers integral is set to "1" [ ]

F_i…multiplicative factor for the individual ratios of hydrogens in the peaks of monomers and polymers (N: F=1; MMN: F=2) [ ]

M_{Mi}…molar mass of the monomers in use (N: 94.15; MMN: 138.21) [g mol^{-1}]

ATR-FTIR

ATR-FTIR was performed on a PerkinElmer Spectrum 65 FT-IR Spectrometer equipped with a Specac MKII Golden Gate Single Reflection ATR System.

The EGC was calculated utilizing the ratios between the epoxy- and the reference band of the starting formulations and the polymer samples (Equation 10).

Equation 10: Calculation of the epoxy group conversion (EPG) via integration of the IR-band at 914 cm^{-1} (epoxy group) and referring it to the aromatic ring band (828 cm^{-1}), or the phenyl ether band (1183 cm^{-1})

$$EPG\ [\%] = \left(1 - \frac{\frac{A_{P,915}}{A_{P,ref}}}{\frac{A_{F,915}}{A_{F,ref}}} \right) * 100$$

$A_{P,915}$ … integrated area of the epoxy IR-band at 914 cm^{-1} of the final polymer [ ]

$A_{P,ref}$ … integrated area of the reference IR-band at 828 or 1183 cm^{-1} of the final polymer [ ]

$A_{F,915}$ … integrated area of the epoxy IR-band at 914 cm^{-1} of the initial formulation [ ]

$A_{F,ref}$ … integrated area of the reference IR-band at 828 or 1183 cm^{-1} of the initial formulation [ ]

UV-VIS

At the Lambda 750 UV-Vis photometer wavelength from 260 to 600 nm at a slit width of 2 nm were measured and 3 mL of solution were transferred in 10 mm quartz cells.

Thin Layer Chromatography (TLC)

TLC was carried out by using TL-aluminum foils coated with silica gel (60 F245) from Merck.

Thermal DSC

DSC was conducted on a DSC 449 F1 Jupiter device from Netzsch equipped with an autosampler. The prepared formulations were weighed in 13 ± 3 mg portions into small aluminum crucibles, which were closed by a pierced lid, with a pipette. The crucible then was transported via the auto sampler into the measuring chamber, which was flushed with nitrogen (40 mL min^{-1}) to maintain an inert atmosphere. There was also a second crucible, the empty reference. The conversions were determined via Equation 11 and the R_P was calculated via Equation 12. The theoretical heats of polymerization and the monomer densities were taken from Table 12.

Table 12: Theoretical heats of polymerization ($H_{P,0}$) and densities (ρ) of the monomers

Sample	$H_{P,0}$ [J mol^{-1}]	$H_{P,0}$ [J g^{-1}]	ρ [g L^{-1}]
BADGE[222]	194000	570	1160
ECC[222]	194000	769	1170
HDDGE[222]	194000	842	1076
PC[223]	125600	1230	1210

Equation 11: Calculation of the EGC[224]

$$EGC\ [\%] = \frac{\Delta H_p}{\Delta H_{P,0}} * 100$$

ΔH_P … heat of polymerization of the sample [J g^{-1}]

$\Delta H_{P,0}$ … theoretical heat of polymerization [J g^{-1}]

Equation 12: Calculation of the rate of polymerization[225]

$$R_P\ \left[\frac{mmol}{l * s}\right] = \frac{DSC * \rho}{H_{P,0} * 1000}$$

DSC … corresponds to the heat produced per mass unit of sample [mW mg^{-1}]

ρ … density of the monomer [g L^{-1}]

$\Delta H_{P,0}$ … theoretical heat of polymerization [J g^{-1}]

PhotoDSC

Photo-DSC analysis was performed on a DSC 204 F1 Phoenix device from Netzsch equipped with an autosampler and a double-core glass-fiber light guide (diameter = 3 mm). The formulations were weighed in 12 ± 2 mg portions into small aluminum crucibles with a pipette.

The crucible then was transported via the auto sampler into the measuring chamber which was flushed with nitrogen to maintain an inert atmosphere. There was also a second crucible, the empty reference. The conversions were determined via Equation 11 and the R_P was calculated via Equation 12. The theoretical heats of polymerization and the monomer densities were taken from Table 12.

Rheology

The storage stability was determined via rheology measurements using an Anton Paar MCR 300 rheometer. Around 80 µL of formulation were used each time. The gap size between stamp and plate was set to 48 µm.

Column Chromatography

Column chromatography was carried out using a Büchi MPLC device, equipped with a control unit (C-620), a UV-photometer (C-635) and a fraction collector (C-660).

Melting Points

The measurements were performed on an automated OptiMelt device from SRS Stanford Research Systems.

RICFP

The respective formulations were then poured into a Teflon mold measuring 65 mm x 5 mm x 5 (length, width, depth) mm and then heated at one end with a focused infrared source (OPTRON IR-Spot 150 W; 10 mm focal point), which automatically switched off at 190 °C using an IR-sensor (OPTRON IN810 CF2). The frontal polymerizations were then recorded with a thermal imaging camera (OPTRIS Xi 400). From the progression of the front through the sample, the frontal velocity could then be calculated (Equation 13).

Equation 13: Calculation of the frontal velocity

$$v_F = \frac{l}{t}$$

v_F … frontal velocity [cm min^{-1}]
l … covered length of the front [cm]
t … time required to cover the length [min]

The covered length of the front was selected from a defined length after the beginning of the shape to a defined length before the end of the shape or a defined length before the front stopped. The maximum front temperature was determined by averaging the maximum front temperature at a defined length after the beginning of the mold and the maximum front temperature at a defined length before the end of the mold or the maximum front temperature a defined length before the front stopped. The front starting time ($t_{F,s}$) represents the time interval from start of the UV-irradiation until a stable frontal polymerization is established.[125] However, this value is heavily influenced by the frontal velocity. Therefore, a correction factor, the frontal boundary time ($t_{F,b}$) is introduced. This value represents the time a front visibly passed a section a defined length after the irradiation shield (distance d). This section is monitored by the IR-camera and as soon as the maximum temperature at this point is reached, $t_{F,b}$ can be determined. Knowing the frontal velocity and the distance d between the irradiation spot and the section a defined length after the irradiation shield, the frontal velocity independent front starting time can be calculated (Equation 14). For thermally initiated frontal polymerization, no front starting time was calculated.

Equation 14: Calculation of the front starting time

$$t_{F,s} = t_{F,b} - \frac{d}{v_F}$$

d … distance between irradiation spot and a defined length after the irradiation shield [cm]

For the thin film measurements, in a mold with the dimensions of 95 mm × 5 mm (length, width), which rises continuously starting from 5 mm to 0.1 mm depth, the layer thickness at which the frontal polymerization stops was measured.

Hot Lithography

Hot lithography on a Caligma 200 UV printer. All parts with direct resin contact were heated to 90 °C including the material vat, building platform and recoating unit. The light source during the printing process is represented by a 405 nm LED laser with a spot diameter of 18 µm at the surface of the material. Part layer thickness was set to 50 µm. However, the thickness of the first layer was set to 10 µm. The glass plate was equipped with a transparent Teflon foil. Energy intensity of the LED laser was set to 100%, corresponding to 1936 mJ cm^{-1} at a scan speed of 2 m s^{-1}. Resin height was set to 250 µm and hatching distance to 0.015 mm.

Scanning Electron Microscopy (SEM)

The 3D printed parts were characterized via SEM to determine layer quality. The sample morphology was imaged with a Phillips XL-30 after sputtering with a thin gold layer.

Photoreactor

The photoreactor consists of a 10 mL 2-necked flask equipped with a septum and a sealed quickfit submerged in a temostated water bath set to 25 °C. A lightguide was inserted into the quickfit. At each time 0.7 mL of the solution was transferred via syringe into an NMR-tube (0.5 mL) for the following ^{1}H-NMR analysis and into two small vials for GPC (2 x 0.1 mL).

Gel permeation chromatography (GPC)

GPC was performed with dry tetrahydrofuran (THF) containing 250 ppm or 0.5 mg mL^{-1} 3,5-di-tertbutyl-4-hydroxytoluene (BHT) stabilizer as eluent. A relative average molecular weight was determined with conventional calibration using a calibration curve of 11 narrow polystyrene standards with an average molecular weight M_w ranging from 375 g mol^{-1} to 177000 g mol^{-1}. 0.1 mL sample of the photoreactor at 10, 30 and 60 min were diluted with around 1 mL THF containing the BHT to result in a concentration of ~2-3 mg mL^{-1}. GPC was performed on a Malvern VISCOTEK TDA system fitted with a ViscotekTDA 305-021 RI + Viscodetector, a UV Detector Module 2550 for TDA 305, and a VISCOTEK SEC-MALS 9 light scattering detector. For the separation three in series-connected PSS SDC columns with particle sizes of 100 Å, 1000 Å and 100 000 Å were used with dry THF (stabilized with BHT) as eluent under isothermal conditions at 35 °C and a flow rate of 0.8 mL min^{-1}. Finally, the molecular weights M_n was calculated by the measured ratio of M_w to Đ.

Cyclic Voltammetry

The compounds were weighed into brown-glass vials and dissolved in 5 mL of a 0.5 M solution of tetraethyl ammonium tetrafluoroborate in dry acetonitrile as an electrolyte. The sample solution was bubbled with argon gas for 3 min and all experiments were performed under light protection. Achieving a concentration of 0.01 M of the tested initiators. Then 5 mL of the mixture were transferred into the IKA ElectraSyn 2.0 device containing a silver reference electrode filled with a 3 M aqueous solution of KCl, a platinum working electrode and a platinum counter electrode.

In advance of every new measurement and in between every measurement the electrodes, as well as the measurement chamber were cleaned with acetone, followed by 1 N hydrochloric acid and in the end rinsed with dry acetonitrile to ensure reproducibility.

Digital Light Microscopy

Microscopy was performed on a Keyence VHX-S550E digital multi scan microscope equipped with a Keyence VH-ZST-200 lens system (x200 – x2000 magnification).

ATTACHMENT

All successfully synthesized onium salts:

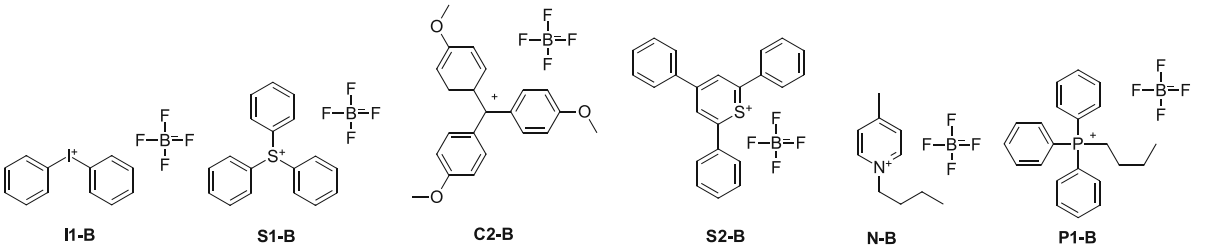

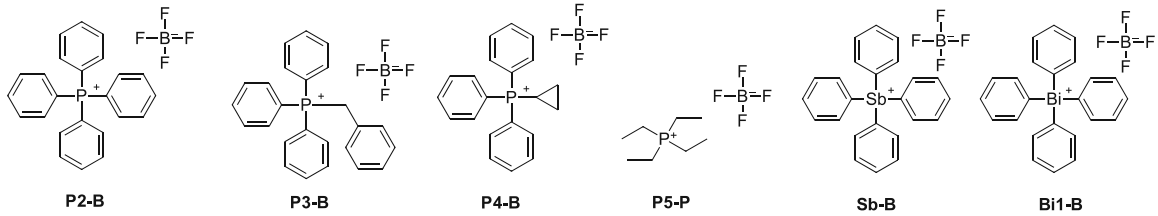

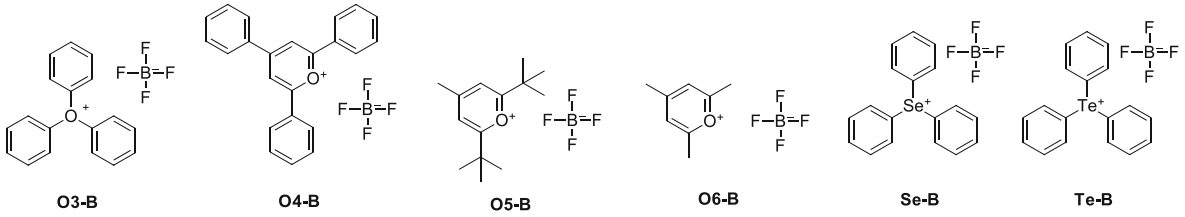

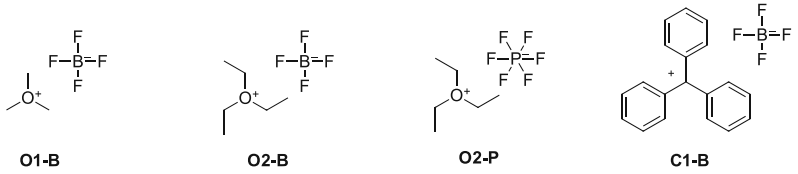

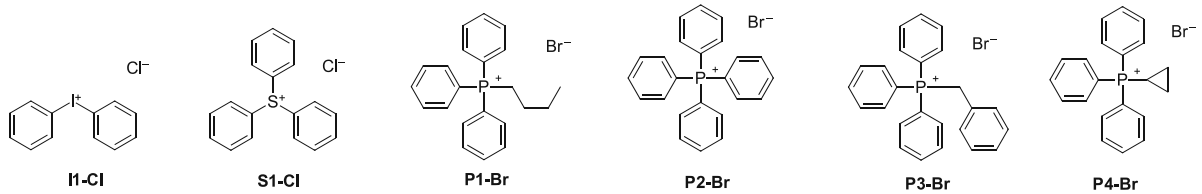

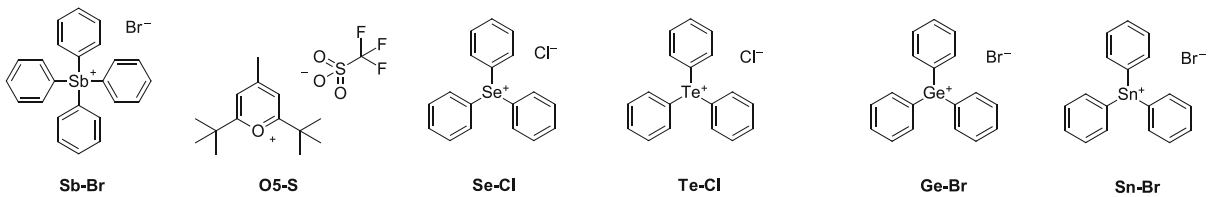

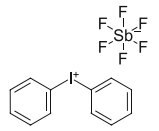

I1-Sb

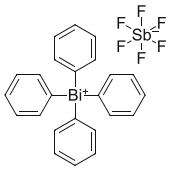

Bi1-Sb

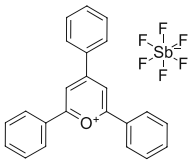

O4-Sb

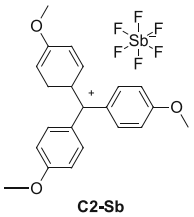

C2-Sb

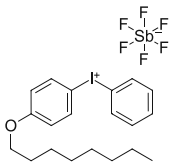

Com-I-Sb

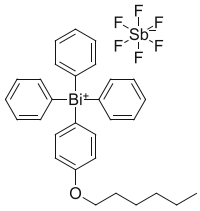

Bi2-Sb

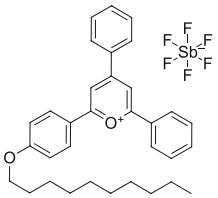

O7-Sb

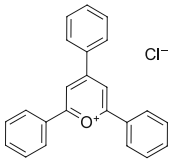

O4-Cl

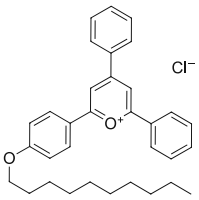

O7-Cl

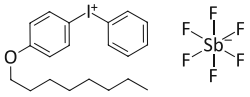

Com-I-Sb

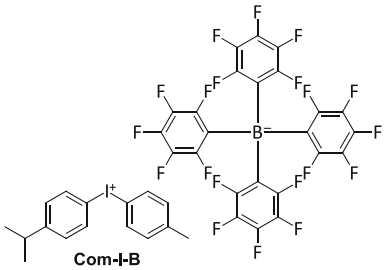

Com-I-B

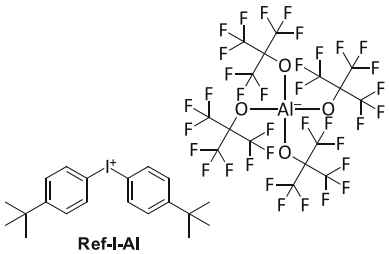

Ref-I-Al

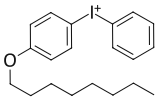

I-NS

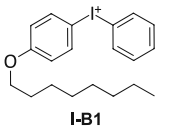

I-B1

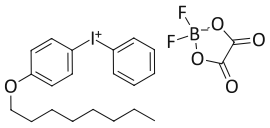

I-B2

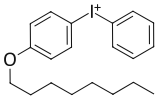

I-B3

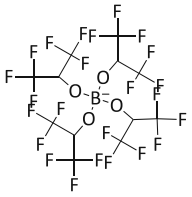

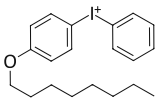

I-B4

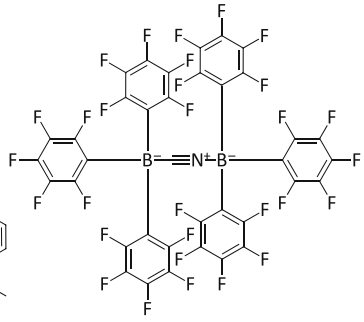

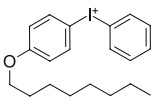

I-B5

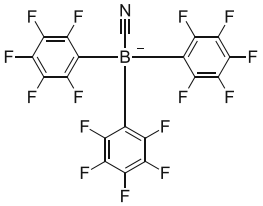

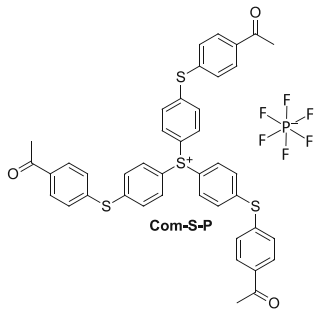

Com-S-P

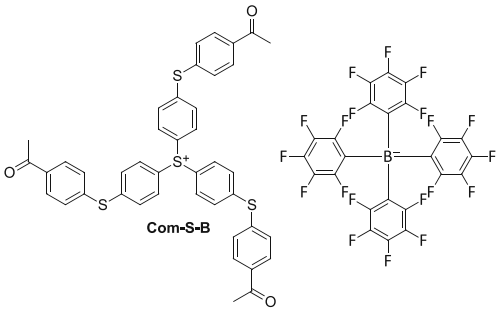

Com-S-B

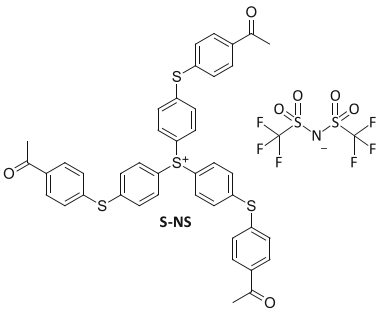

S-NS

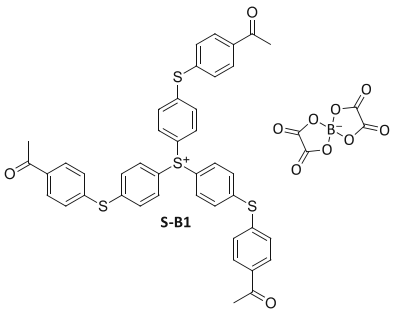

S-B1

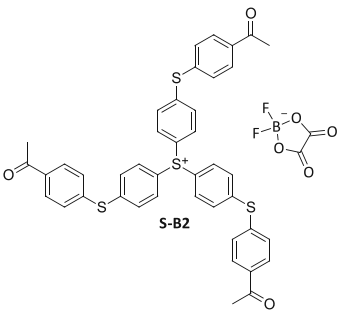

S-B2

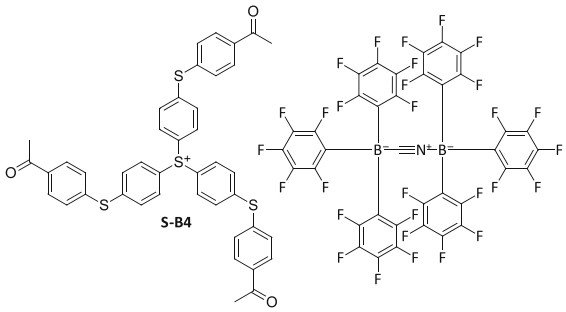

S-B4

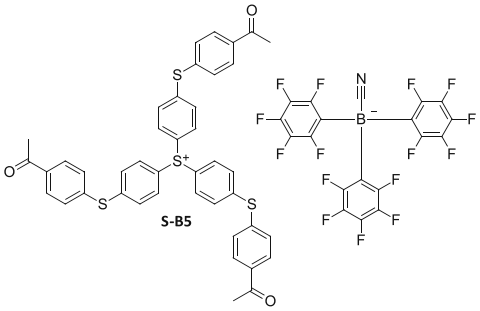

S-B5

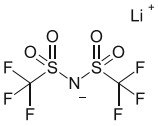

Li-NS

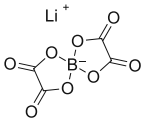

Li-B1

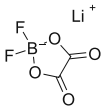

Li-B2

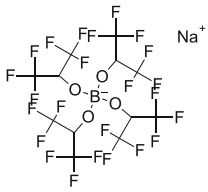

Na-B3

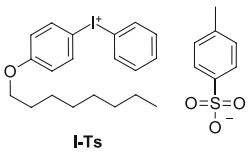

I-Ts

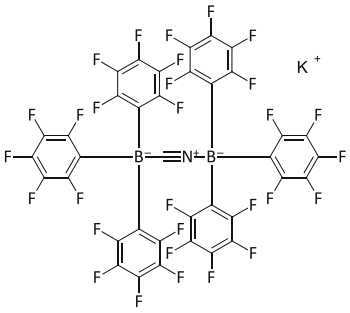

K-B4

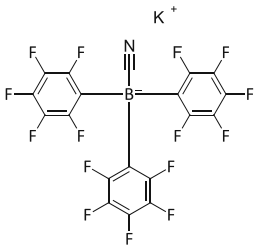

K-B5

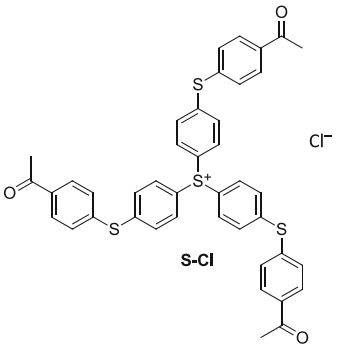

S-Cl

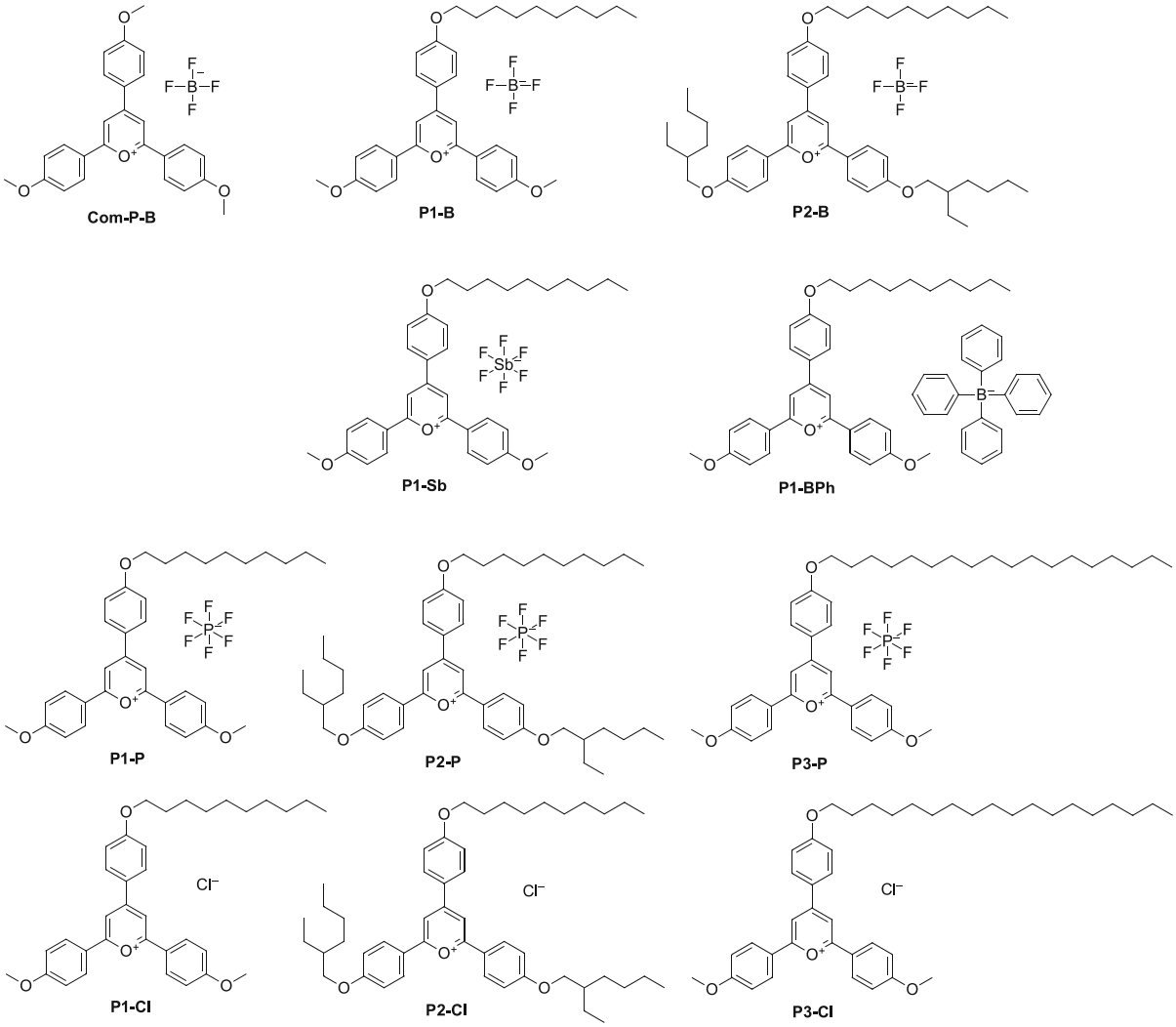

Additional figures:

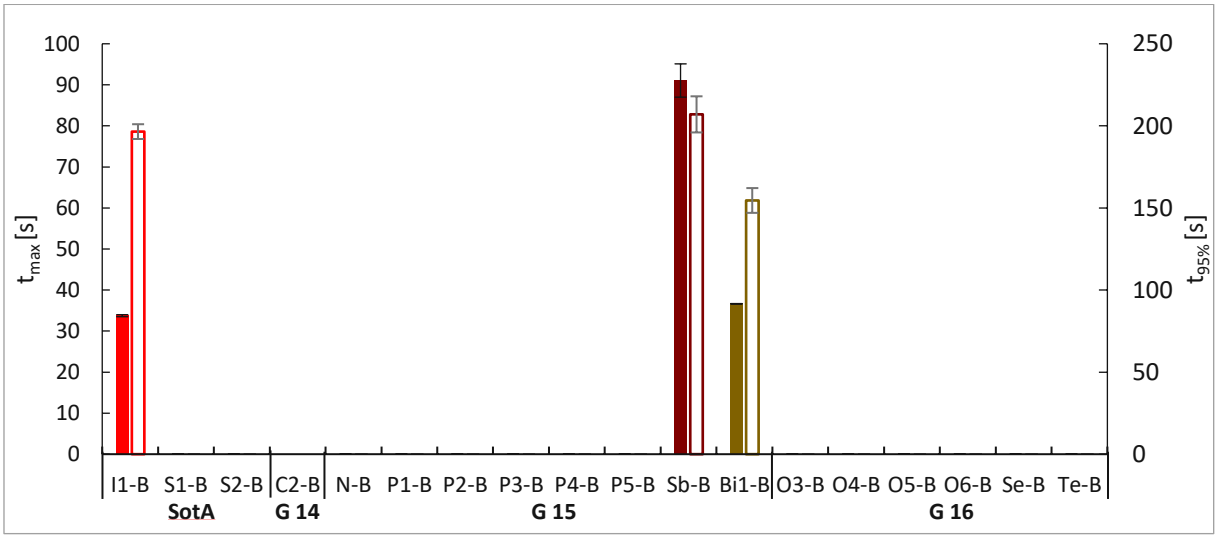

Figure 255: Time at highest exothermicity (t_{max} - full) and time until 95% of the total conversion is reached ($t_{95\%}$ – framed) in BADGE/PC with the onium tetrafluoroborates (sensitized by anthracene)

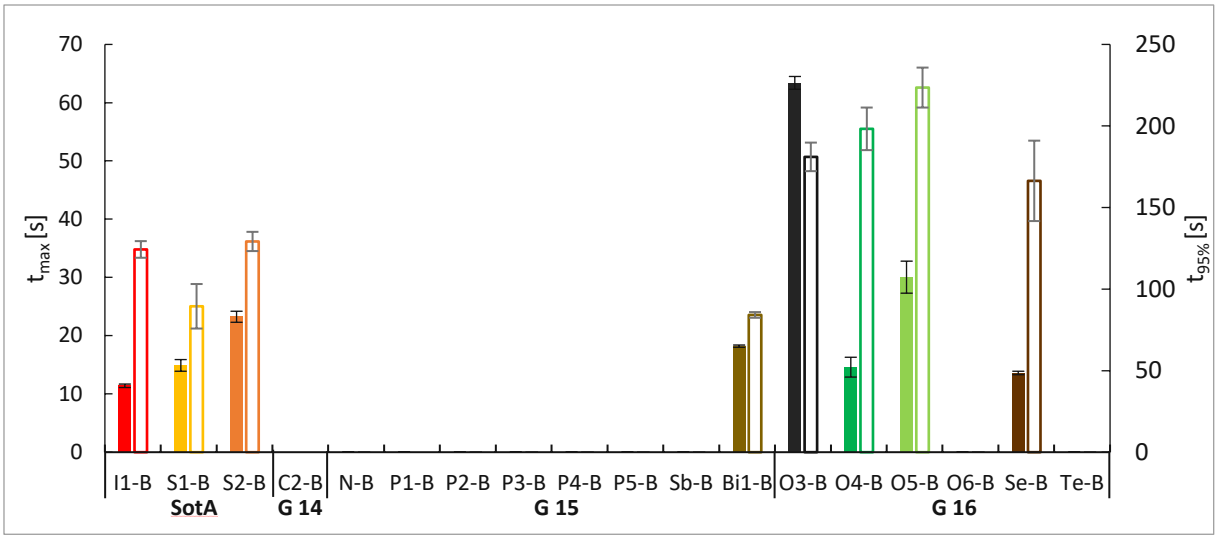

Figure 256: Time at highest exothermicity (t_{max} - full) and time until 95% of the total conversion is reached ($t_{95\%}$ – framed) in ECC/PC with the onium tetrafluoroborates (sensitized by anthracene)

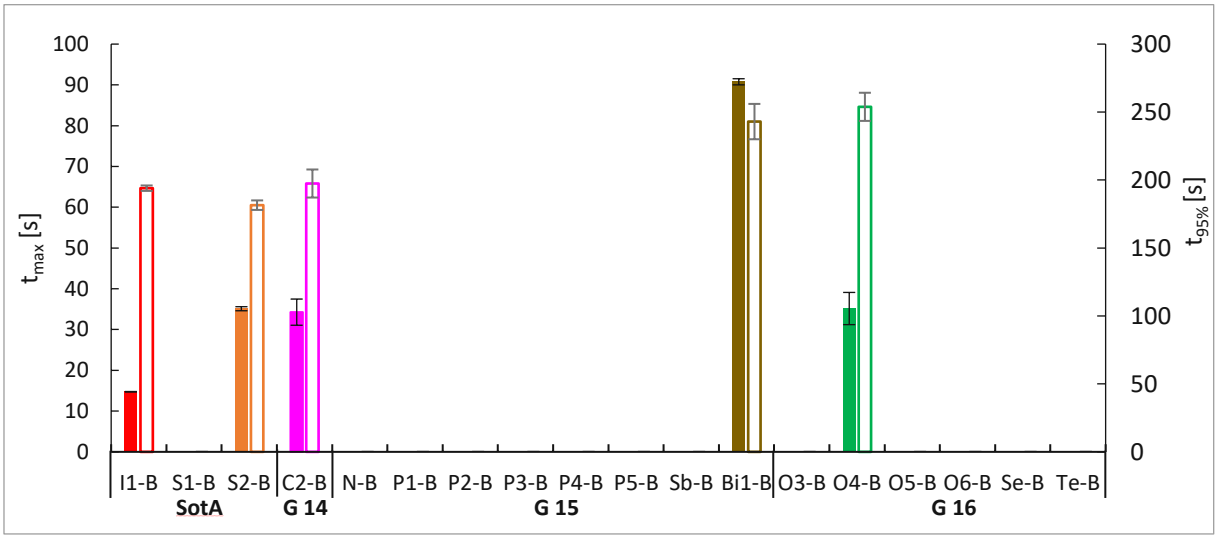

Figure 257: Time at highest exothermicity (t_{max} - full) and time until 95% of the total conversion is reached ($t_{95\%}$ – framed) in BADGE/PC with the onium tetrafluoroborates (photo-induced decomposition by Ivocerin)

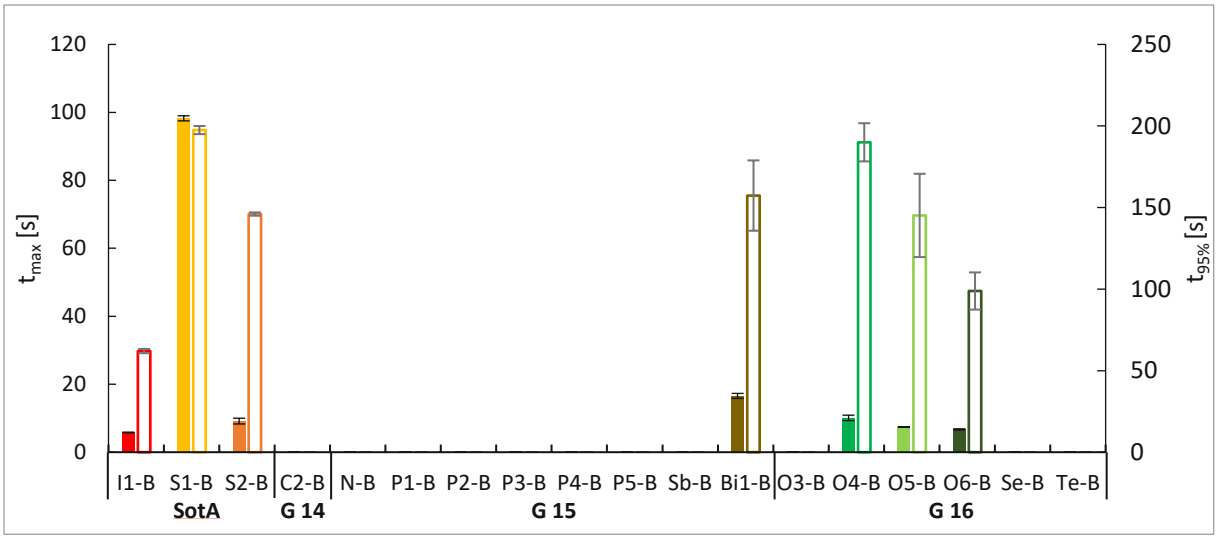

Figure 258: Time at highest exothermicity (t_{max} - full) and time until 95% of the total conversion is reached ($t_{95\%}$ – framed) in ECC/PC with the onium tetrafluoroborates (photo-induced decomposition by Ivocerin)

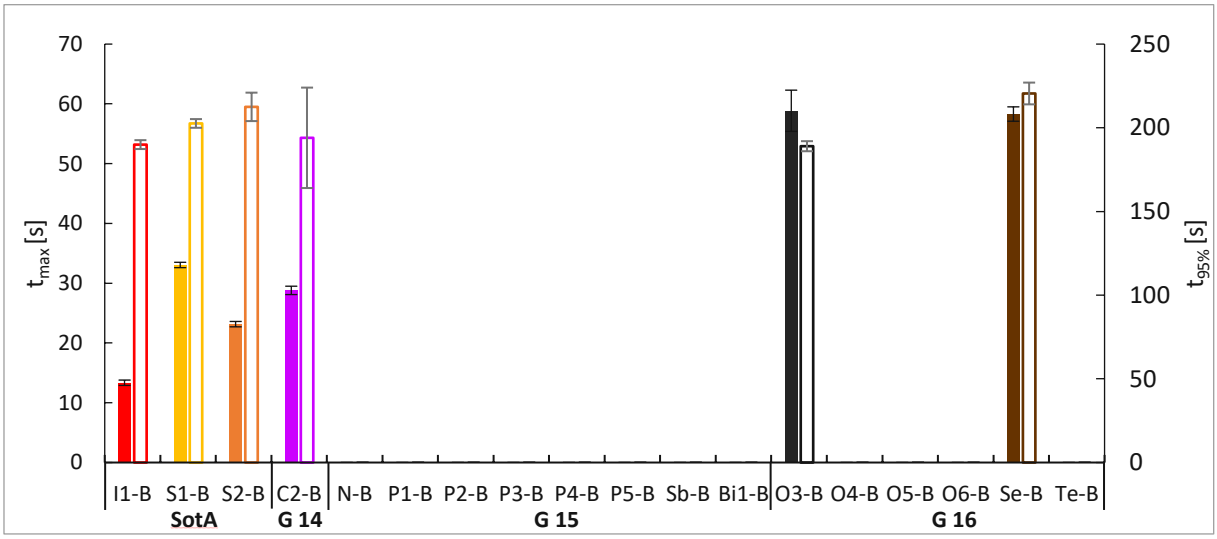

Figure 259: Time at highest exothermicity (t_{max} - full) and time until 95% of the total conversion is reached ($t_{95\%}$ – framed) in BADGE/PC with the onium tetrafluoroborates (Photoinitiation)

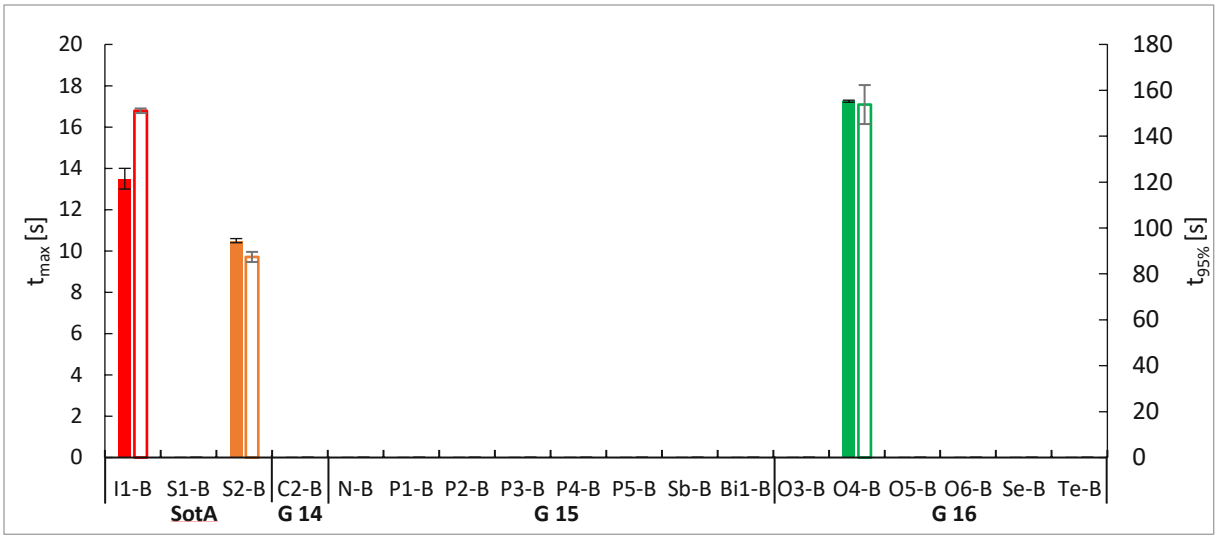

Figure 260: Time at highest exothermicity (t_{max} - full) and time until 95% of the total conversion is reached ($t_{95\%}$ – framed) in ECC/PC with the onium tetrafluoroborates (Photoinitiation)

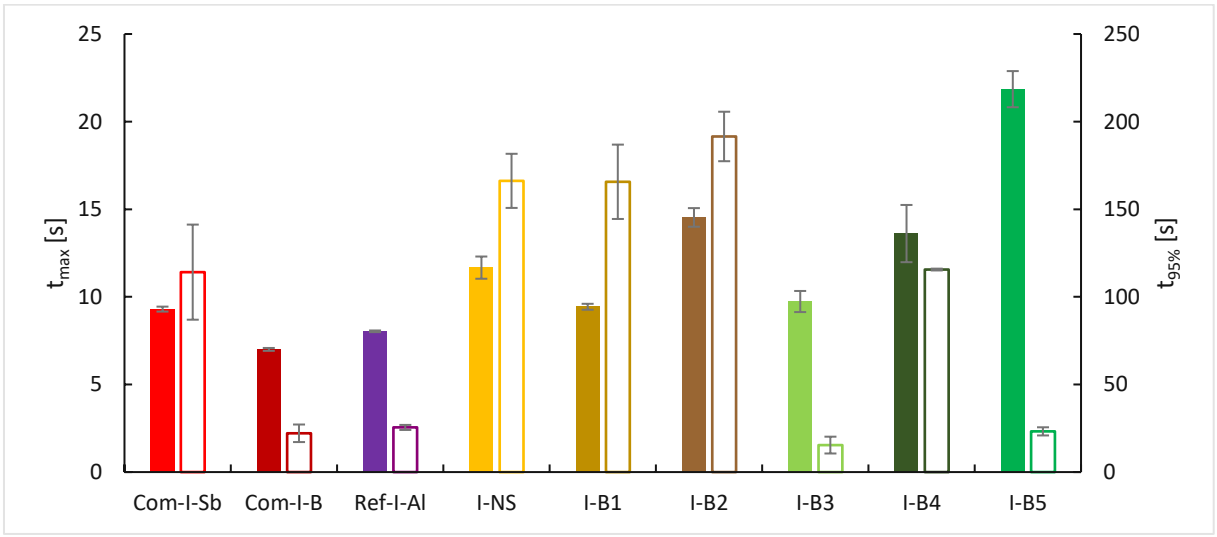

Figure 261: Time at highest exothermicity (t_{max} - full) and time until 95% of the total conversion is reached ($t_{95\%}$ – framed) in BADGE with the iodonium salts (photo-induced decomposition by Ivocerin)

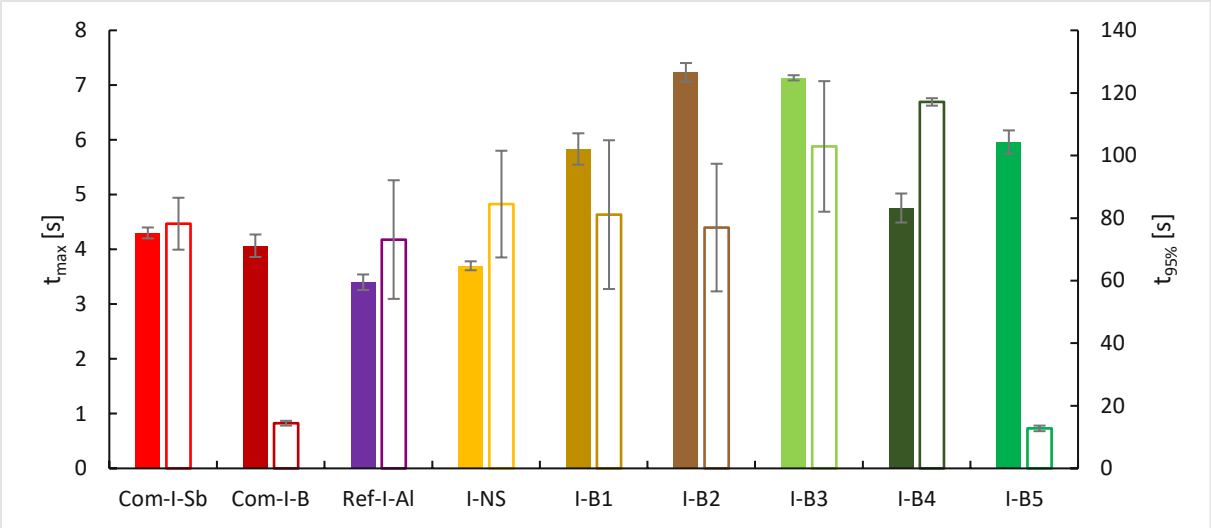

Figure 262: Time at highest exothermicity (t_{max} - full) and time until 95% of the total conversion is reached ($t_{95\%}$ – framed) in ECC with the iodonium salts (photo-induced decomposition by Ivocerin)

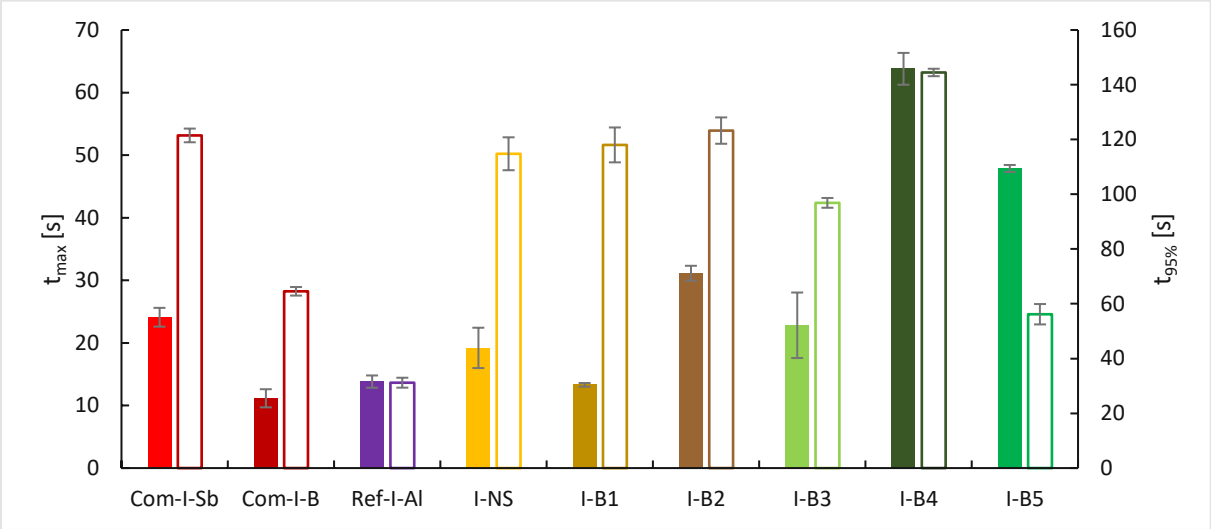

Figure 263: Time at highest exothermicity (t_{max} - full) and time until 95% of the total conversion is reached ($t_{95\%}$ – framed) in BADGE with the iodonium salts (Photoinitiation)

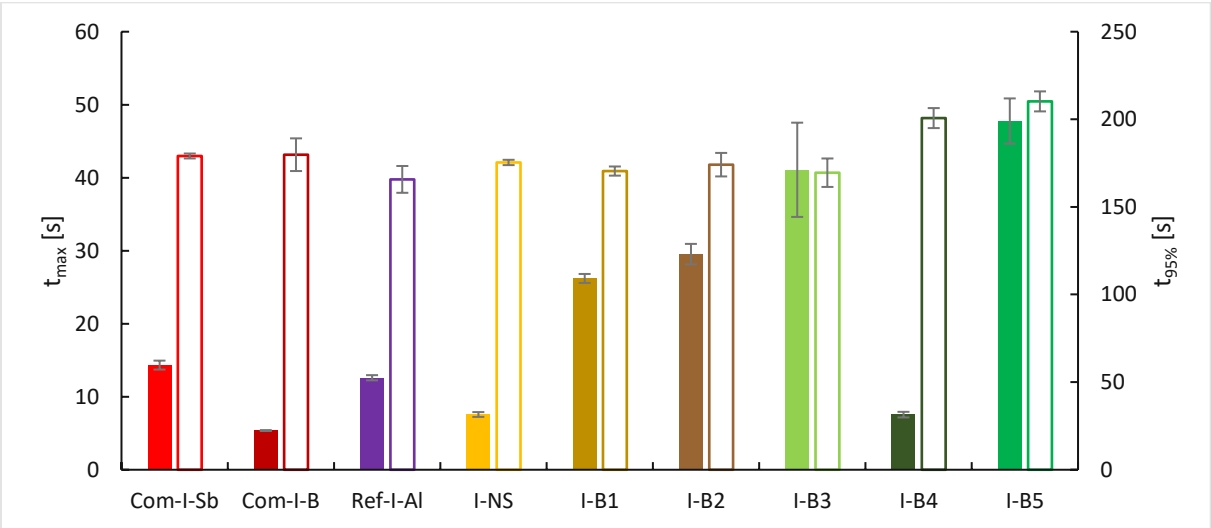

Figure 264: Time at highest exothermicity (t_{max} - full) and time until 95% of the total conversion is reached ($t_{95\%}$ – framed) in ECC with the iodonium salts (Photoinitiation)

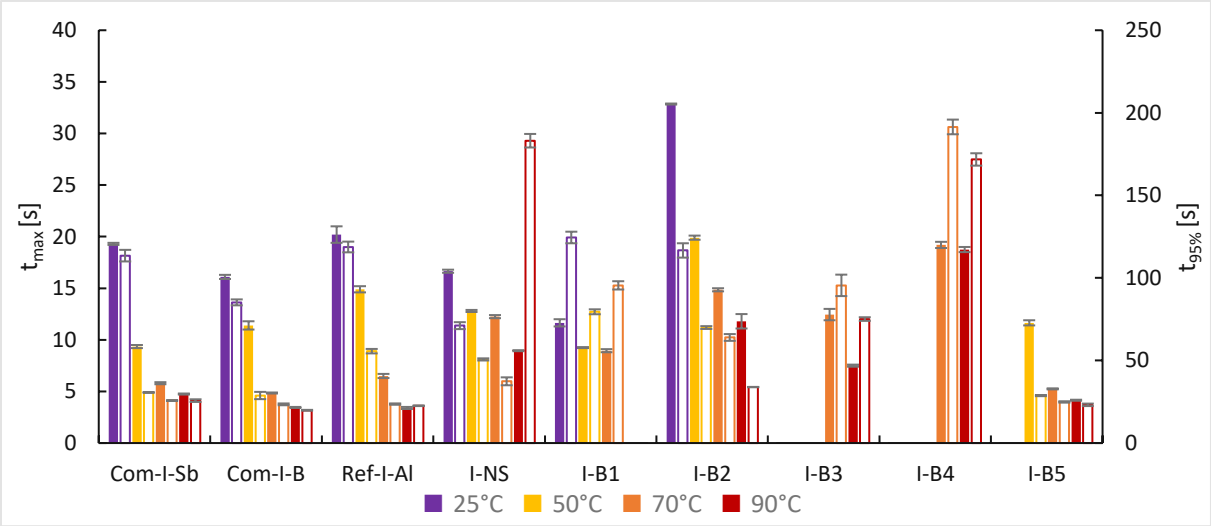

Figure 265: Time at highest exothermicity (t_{max} - full) and time until 95% of the total conversion is reached ($t_{95\%}$ – framed) in BADGE with 1 wt% of iodonium salt at 25 °C, 50 °C, 70 °C and 90 °C (Photoinitiation)

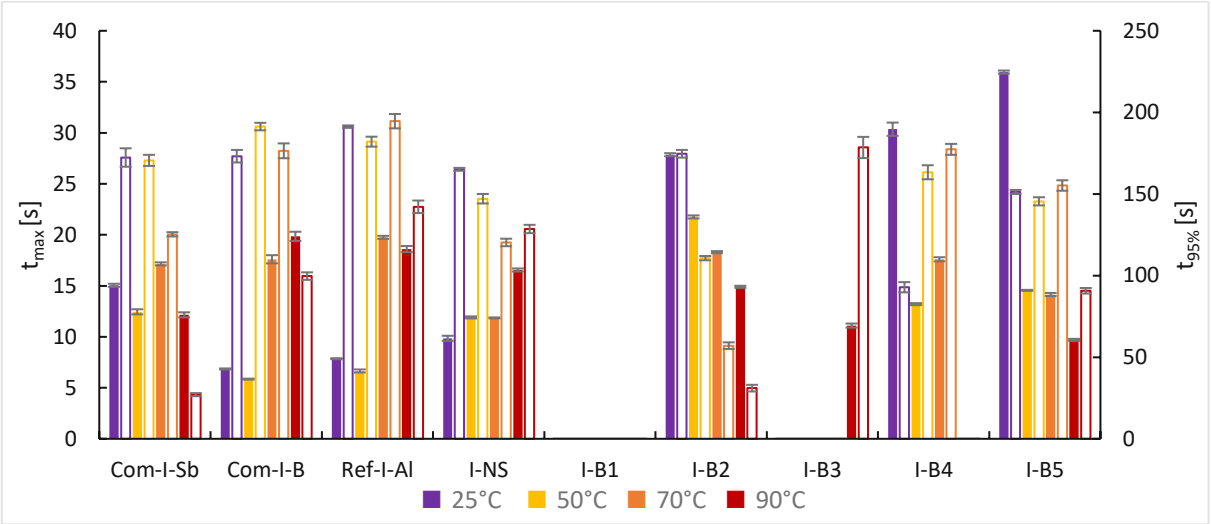

Figure 266: Time at highest exothermicity (t_{max} - full) and time until 95% of the total conversion is reached ($t_{95\%}$ – framed) in ECC with 1 wt% of iodonium salt at 25 °C, 50 °C, 70 °C and 90 °C (Photoinitiation)

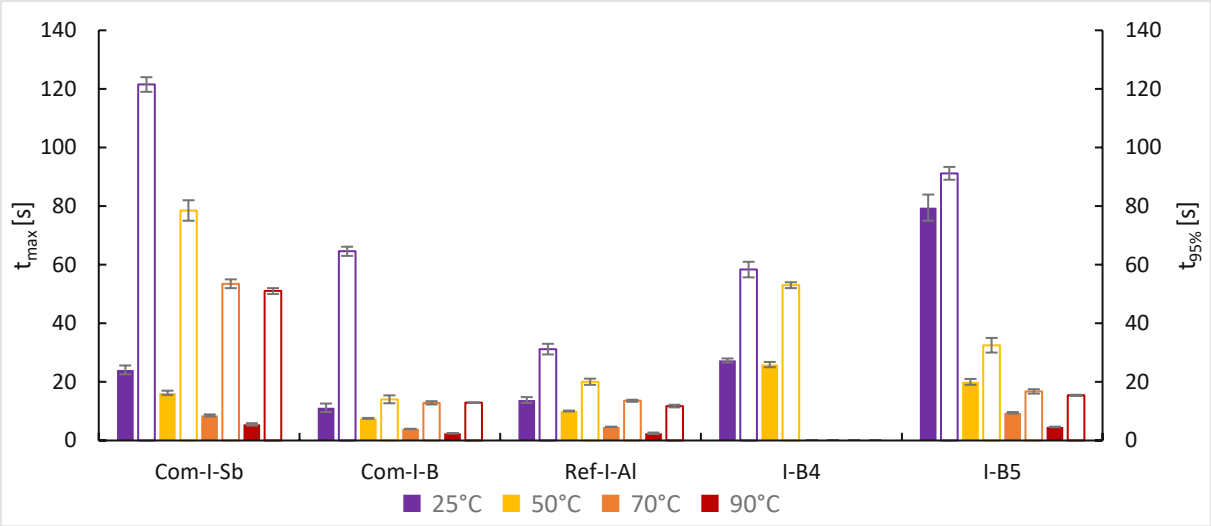

Figure 267: Time at highest exothermicity (t_{max} - full) and time until 95% of the total conversion is reached ($t_{95\%}$ – framed) in BADGE with 1 mol% of iodonium salt at 25 °C, 50 °C, 70 °C and 90 °C (Photoinitiation)

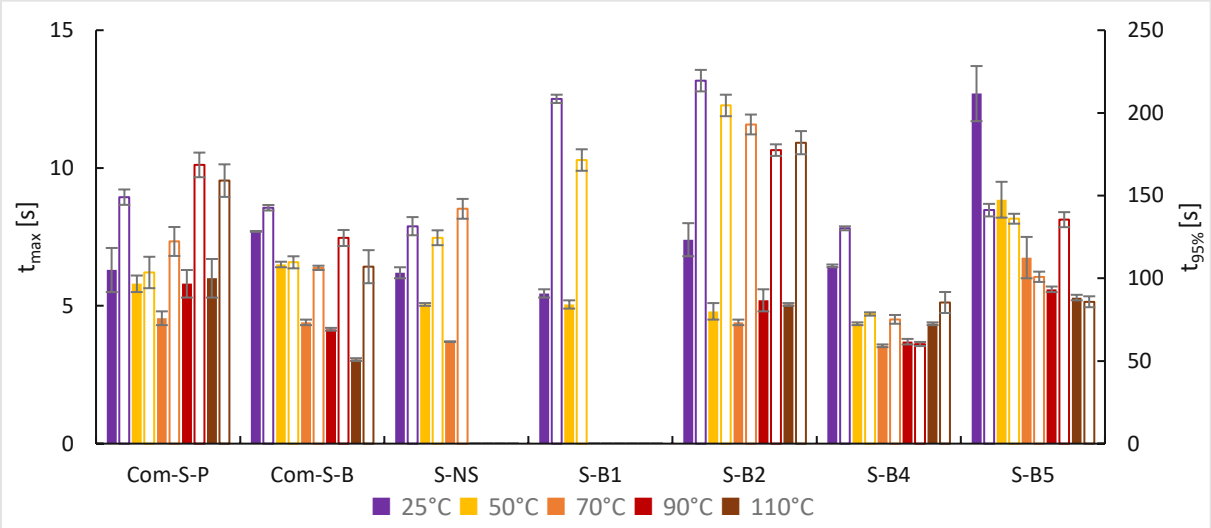

Figure 268: Time at highest exothermicity (t_{max} - full) and time until 95% of the total conversion is reached ($t_{95\%}$ – framed) in BADGE with 1 mol% of sulfonium salt at 25 °C, 50 °C, 70 °C, 90 °C and 110 °C (Photoinitiation)

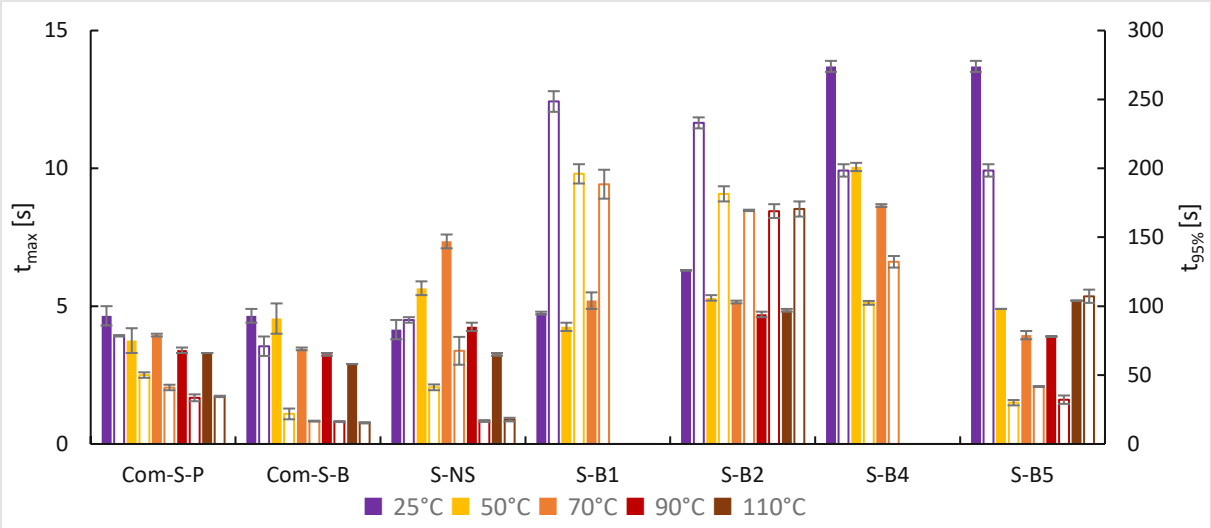

Figure 269: Time at highest exothermicity (t_{max} - full) and time until 95% of the total conversion is reached ($t_{95\%}$ – framed) in ECC with 1 mol% of sulfonium salt at 25 °C, 50 °C, 70 °C, 90 °C and 110 °C (Photoinitiation)

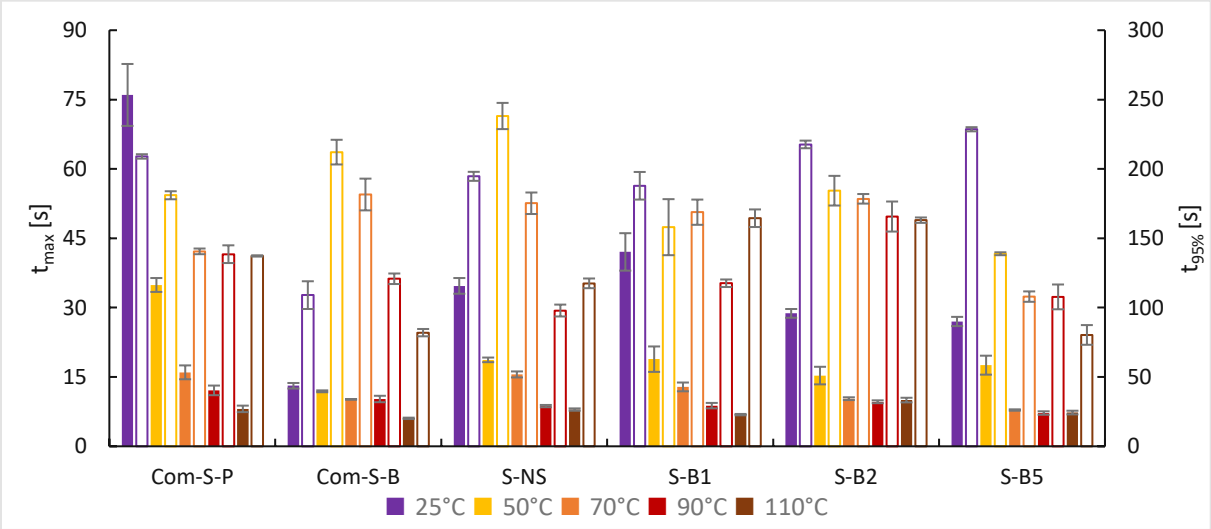

Figure 270: Time at highest exothermicity (t_{max} - full) and time until 95% of the total conversion is reached ($t_{95\%}$ – framed) in BADGE 1 mol% of sulfonium salt, 0.35 mol% DBA and 0.12 mol% EDAB at 25 °C, 50 °C, 70 °C, 90 °C and 110 °C (sensitization by DBA)

BIBLIOGRAPHY

1. Fouassier, J.-P., *Photoinitiation, Photopolymerization, and Photocuring: Fundamentals and Applications*. Hanser: Munich, 1995; p 95-106.
2. Fouassier, J. P.; Allonas, X.; Burget, D., Photopolymerization reactions under visible lights: principle, mechanisms and examples of applications. *Prog Org Coat* **2003,** *47* (1), 16-36.
3. Ligon, S. C.; Liska, R.; Stampfl, J.; Gurr, M.; Mülhaupt, R., Polymers for 3D Printing and Customized Additive Manufacturing. *Chem Rev* **2017,** *117* (15), 10212-10290.
4. Bomze, D., Radical induced Cationic Frontal Polymerization as a new and versatile Curing Technique for Epoxy Resins. *Dissertation* **2016**, 105 ff.
5. Srivatsan, T. S.; Sudarshan, T. S., Additive Manufacturing of Materials: Viable Techniques, Metals, Advances, Advantages, and Applications. **2015,** *1st ed.* (Taylor & Francis, New York), 43.
6. Raos, P.; Klapan, I.; Galeta, T., Additive Manufacturing of Medical Models--Applications in Rhinology. *Coll Antropol* **2015,** *39* (3), 667-73.
7. Associates, W. W. R., 3D Printing and Additive Manufacturing State of the Industry. *Annual Worldwide Progress Report, USA* **2018**.
8. Wang, X.; Jiang, M.; Zhou, Z. W.; Gou, J. H.; Hui, D., 3D printing of polymer matrix composites: A review and prospective. *Compos Part B-Eng* **2017,** *110*, 442-458.
9. Mondschein, R. J.; Kanitkar, A.; Williams, C. B.; Verbridge, S. S.; Long, T. E., Polymer structure-property requirements for stereolithographic 3D printing of soft tissue engineering scaffolds. *Biomaterials* **2017,** *140*, 170-188.
10. Ligon-Auer, S. C.; Schwentenwein, M.; Gorsche, C.; Stampfl, J.; Liska, R., Toughening of photo-curable polymer networks: a review. *Polym Chem-Uk* **2016,** *7* (2), 257-286.
11. Schönherr, J. A.; Baumgartner, S.; Hartmann, M.; Stampfl, J., Stereolithographic Additive Manufacturing of High Precision Glass Ceramic Parts. *Materials* **2020,** *13* (7), 1492.
12. Gmeiner, R.; Deisinger, U.; Schonherr, J.; Lechner, B.; Detsch, R.; Boccaccini, A. R.; Stampfl, J., Additive Manufacturing of Bioactive Glasses and Silicate Bioceramics. *J Ceram Sci Technol* **2015,** *6* (2), 75-86.
13. https://formlabs.com/blog/ultimate-guide-to-stereolithography-sla-3d-printing/. **Accessed 08.08.2022**.
14. Hatzenbichler, M.; Geppert, M.; Gruber, S.; Ipp, E.; Almedal, R.; Stampfl, J., DLP based light engines for additive manufacturing of ceramic parts. *Proc Spie* **2012,** *8254*.
15. Bártolo, P. J., *Stereolithography: Materials, Processes and Applications*. Springer, New York: 2011; p 1-36.
16. Noren, G. K.; Krajewski, J. J.; Murphy, E. J., Cationically curable polyurethane compositions having vinyl ether functionality. *US4996282A* **1991**.
17. Steinmann, B.; Wolf, J.-P.; Schulthess, A.; Hunziker, M., (Cyclo)Aliphatic Epoxy Compounds. *CA2112010A1* **2000**.
18. Bayer, H.; Fischer, W.; Muhrer, V.; Rogler, W.; Schoen, L., Low shrinkage photo-curable resin and its use in a stereolithography process. *DE19541075C1* **1995**.
19. Peer, G.; Dorfinger, P.; Koch, T.; Stampfl, J.; Gorsche, C.; Liska, R., Photopolymerization of Cyclopolymerizable Monomers and Their Application in Hot Lithography. *Macromolecules* **2018,** *51* (22), 9344-9353.
20. Pojman, J. A.; Moeller, M.; Matyjaszewski, K., *Polymer Science: A Comprehensive Reference*. Elsevier Science: Amsterdam: 2012; Vol. 3.

21. Chechilo, N. M.; Enikolop.Ns, Structure of Polymerization Wave Front and on Mechanism of Polymerization Reaction Spreading. *Dokl Akad Nauk Sssr+* **1974,** *214* (5), 1131-1133.
22. Pojman, J. A.; Ilyashenko, V. M.; Khan, A. M., Free-radical frontal polymerization: Self-propagating thermal reaction waves. *J Chem Soc Faraday T* **1996,** *92* (16), 2825-2837.
23. Mariani, A.; Bidali, S.; Fiori, S.; Malucelli, G.; Ricco, L., New vistas in frontal polymerization. *Macromol Symp* **2004,** *218*, 1-9.
24. Mariani, A.; Fiori, S.; Chekanov, Y.; Pojman, J. A., Frontal ring-opening metathesis polymerization of dicyclopentadiene. *Macromolecules* **2001,** *34* (19), 6539-6541.
25. Chekanov, Y.; Arrington, D.; Brust, G.; Pojman, J. A., Frontal curing of epoxy resins: Comparison of mechanical and thermal properties to batch-cured materials. *J Appl Polym Sci* **1997,** *66* (6), 1209-1216.
26. Scognamillo, S.; Bounds, C.; Luger, M.; Mariani, A.; Pojman, J. A., Frontal Cationic Curing of Epoxy Resins. *J Polym Sci Pol Chem* **2010,** *48* (9), 2000-2005.
27. Mariani, A.; Bidali, S.; Fiori, S.; Sangermano, M.; Malucelli, G.; Bongiovann, R.; Priola, A., UV-ignited frontal polymerization of an epoxy resin. *J Polym Sci Pol Chem* **2004,** *42* (9), 2066-2072.
28. Crivello, J. V.; Dietliker, K.; Bradley, G., *Photoinitiators for Free Radical Cationic & Anionic Photopolymerisation*. Wiley: Hoboken, New Jersey, 1999; p Chapter III, p.334.
29. Green, W. A., *Industrial Photoinitiators: A Technical Guide*. Taylor & Francis: Boca Raton, 2010; p Chapter Cationic chemistry, Chapter 7.
30. Bulut, U.; Crivello, J. V., Investigation of the reactivity of epoxide monomers in photoinitiated cationic polymerization. *Macromolecules* **2005,** *38* (9), 3584-3595.
31. Sangermano, M., Advances in cationic photopolymerization. *Pure Appl Chem* **2012,** *84* (10), 2089-2101.
32. Decker, C.; Moussa, K., Kinetic-Study of the Cationic Photopolymerization of Epoxy Monomers. *J Polym Sci Pol Chem* **1990,** *28* (12), 3429-3443.
33. Sipani, V.; Scranton, A. B., Dark-cure studies of cationic photopolymerizations of epoxides: Characterization of the active center lifetime and kinetic rate constants. *J Polym Sci Pol Chem* **2003,** *41* (13), 2064-2072.
34. Sangermano, M.; Cerrone, M.; Colucci, G.; Roppolo, I.; Ortiz, R. A., Preparation and characterization of hybrid thiol-ene/epoxy UV-thermal dual-cured systems. *Polym Int* **2010,** *59* (8), 1046-1051.
35. Crivello, J. V.; Dietliker, K.; Bradley, G., *Photoinitiators for Free Radical Cationic & Anionic Photopolymerisation*. Wiley: Hoboken, New Jersey, 1999; p Chapter III, p.329-373.
36. Crivello, J. V.; Lam, J. H. W., Diaryliodonium Salts - New Class of Photo-Initiators for Cationic Polymerization. *Macromolecules* **1977,** *10* (6), 1307-1315.
37. Crivello, J. V., The discovery and development of onium salt cationic photoinitiators. *J Polym Sci Pol Chem* **1999,** *37* (23), 4241-4254.
38. Roloff, A.; Meier, K.; Riediker, M., Synthetic and Metal Organic-Photochemistry in Industry. *Pure Appl Chem* **1986,** *58* (9), 1267-1272.
39. Schlesinger, S. I., Epoxy Photopolymers in Photoimaging and Photofabrication. *Polym Eng Sci* **1974,** *14* (7), 513-515.
40. Crivello, J. V.; Lam, J. H. W., Photoinitiated Cationic Polymerization with Triarylsulfonium Salts. *J Polym Sci Pol Chem* **1979,** *17* (4), 977-999.
41. Hartmann, C.; Meyer, V., Ueber eine neue Klasse jodhaltiger, stickstofffreier organischer Basen. *Ber Dtsch Chem Ges* **1894,** *27* (1), 426-432.

42. Crivello, J. V.; Lee, J. L., Recent Advances in Thermally and Photochemically Initiated Cationic Polymerization. *Polym J* **1985,** *17* (1), 73-83.
43. Pitt, H. M., Process for making sulfonium compounds. *Patent* **1957**.
44. Crivello, J. V.; Dietliker, K.; Bradley, G., *Photoinitiators for Free Radical Cationic & Anionic Photopolymerisation*. Wiley: Hoboken, New Jersey, 1999; p 421-423 (Chapter III).
45. Dadashi-Silab, S.; Doran, S.; Yagci, Y., Photoinduced Electron Transfer Reactions for Macromolecular Syntheses. *Chem Rev* **2016,** *116* (17), 10212-10275.
46. Gillespie, R. J.; Peel, T. E.; Robinson, E. A., Hammett Acidity Function for Some Super Acid Systems .1. Systems H2s04-S03, H2so4-Hso3f, H2so4-Hso3cl, and H2so4-Hb(Hso4)4. *J Am Chem Soc* **1971,** *93* (20), 5083-+.
47. Gurney, R. W., *Ionic Processes in Solution*. Dover Publications,: New York, USA, 1953.
48. Dickert, F., G. A. Olah, G. K. S. Prakash, J. Sommer: Superacids, John Wiley & Sons, New York, Chichester, Brisbane, Toronto, Singapore. *Berichte der Bunsengesellschaft für physikalische Chemie* **1987,** *91* (10), 1073-1074.
49. Hasani, M.; Amin, S. A.; Yarger, J. L.; Davidowski, S. K.; Angell, C. A., Proton Transfer and Ionicity: An 15N NMR Study of Pyridine Base Protonation. *The Journal of Physical Chemistry B* **2019,** *123* (8), 1815-1821.
50. Ansari, Y.; Ueno, K.; Angell, C. A., Protic Ionic Liquids Can Be Both Free Proton Conductors and Benign Superacids. *J Phys Chem B* **2021,** *125* (28), 7855-7862.
51. Hasani, M.; Yarger, J. L.; Angell, C. A., On the Use of a Protic Ionic Liquid with a Novel Cation To Study Anion Basicity. *Chemistry* **2016,** *22* (37), 13312-9.
52. Olah, G. A.; Prakash, G. K. S.; Sommer, J.; Molnar, A., *Superacid Chemistry*. Wiley: Hoboken, New Jersey, USA, 2009; p Chapter 2, p. 35f.
53. Haartz, J. C.; Mcdaniel, D. H., Fluoride-Ion Affinity of Some Lewis-Acids. *J Am Chem Soc* **1973,** *95* (26), 8562-8565.
54. Greb, L., Lewis Superacids: Classifications, Candidates, and Applications. *Chemistry – A European Journal* **2018,** *24* (68), 17881-17896.
55. Erdmann, P.; Leitner, J.; Schwarz, J.; Greb, L., An Extensive Set of Accurate Fluoride Ion Affinities for p-Block Element Lewis Acids and Basic Design Principles for Strong Fluoride Ion Acceptors. *Chemphyschem* **2020,** *21* (10), 987-994.
56. Muller, L. O.; Himmel, D.; Stauffer, J.; Steinfeld, G.; Slattery, J.; Santiso-Quinones, G.; Brecht, V.; Krossing, I., Simple access to the non-oxidizing Lewis superacid PhF -> Al(OR(F))(3) (R(F) = C(CF(3))(3)). *Angewandte Chemie-International Edition* **2008,** *47* (40), 7659-7663.
57. Kogel, J. F.; Sorokin, D. A.; Khvorost, A.; Scott, M.; Harms, K.; Himmel, D.; Krossing, I.; Sundermeyer, J., The Lewis superacid Al[N(C6F5)(2)](3) and its higher homolog Ga[N(C6F5)(2)](3) - structural features, theoretical investigation and reactions of a metal amide with higher fluoride ion affinity than SbF5. *Chem Sci* **2018,** *9* (1), 245-253.
58. Bohrer, H.; Trapp, N.; Himmel, D.; Schleep, M.; Krossing, I., From unsuccessful H-2-activation with FLPs containing B(Ohfip)(3) to a systematic evaluation of the Lewis acidity of 33 Lewis acids based on fluoride, chloride, hydride and methyl ion affinities. *Dalton T* **2015,** *44* (16), 7489-7499.
59. Krossing, I.; Raabe, I., Relative stabilities of weakly coordinating anions: A computational study. *Chem-Eur J* **2004,** *10* (20), 5017-5030.
60. Roth, D.; Wadepohl, H.; Greb, L., Bis(perchlorocatecholato)germane: Hard and Soft Lewis Superacid with Unlimited Water Stability. *Angewandte Chemie-International Edition* **2020,** *59* (47), 20930-20934.

61. Abdulrasoul, F. A. M.; Ledwith, A.; Yagci, Y., Thermal and Photo-Chemical Cationic Polymerizations Induced by Agpf6 in Presence of Free-Radical Initiators. *Polym Bull* **1978,** *1* (1), 1-6.
62. Yagci, Y.; Borbely, J.; Schnabel, W., On the Mechanism of Acylphosphine Oxide Promoted Cationic Polymerization. *Eur Polym J* **1989,** *25* (2), 129-131.
63. Hartwig, A.; Koschek, K.; Lühring, A., Influence of Proton Donors on the Cationic Polymerization of Epoxides. 2006; pp 205-216.
64. Klikovits, N.; Liska, R.; D'Anna, A.; Sangermano, M., Successful UV-Induced RICFP of Epoxy-Composites. *Macromol Chem Phys* **2017,** *218* (18), 1700313.
65. Sangermano, M.; Antonazzo, I.; Sisca, L.; Carello, M., Photoinduced cationic frontal polymerization of epoxy-carbon fibre composites. *Polym Int* **2019,** *68* (10), 1662-1665.
66. Green, W. A., *Industrial Photoinitiators: A Technical Guide*. Taylor & Francis: Boca Raton, 2010; p 128 (Chapter 5.4 Sensitization and Synergy).
67. Calderon, N., Ring-Opening Polymerization of Cycloolefins. *J Macromol Sci R M C* **1972,** *C 7* (1), 105-&.
68. Novak, B. M.; Risse, W.; Grubbs, R. H., The development of well-defined catalysts for ring-opening olefin metathesis polymerizations (ROMP). In *Polymer Synthesis Oxidation Processes*, Springer Berlin Heidelberg: Berlin, Heidelberg, 1992; pp 47-72.
69. Frenzel, U.; Nuyken, O., Ruthenium-based metathesis initiators: Development and use in ring-opening metathesis polymerization. *J Polym Sci Pol Chem* **2002,** *40* (17), 2895-2916.
70. Chauvin, Y., Olefin metathesis: The early days (Nobel lecture). *Angewandte Chemie-International Edition* **2006,** *45* (23), 3740-3747.
71. Grubbs, R. H., Olefin-metathesis catalysts for the preparation of molecules and materials (Nobel lecture). *Angewandte Chemie-International Edition* **2006,** *45* (23), 3760-3765.
72. Calderon, N., Olefin Metathesis Reaction. *Accounts Chem Res* **1972,** *5* (4), 127-&.
73. Tallon, M. A., Ring-Opening Metathesis Polymerization (ROMP) Using Maleic Anhydride-Based Monomers. In *Handbook of Maleic Anhydride Based Materials: Syntheses, Properties and Applications*, Musa, O. M., Ed. Springer International Publishing: Cham, 2016; pp 311-398.
74. Benson, S. W.; Cruickshank, F. R.; Golden, D. M.; Haugen, G. R.; Oneal, H. E.; Rodgers, A. S.; Shaw, R.; Walsh, R., Additivity Rules for Estimation of Thermochemical Properties. *Chem Rev* **1969,** *69* (3), 279-+.
75. Odian, G., *Principles of Polymerization*. Wiley: 2004.
76. Slugovc, C., The ring opening metathesis polymerisation toolbox. *Macromol Rapid Comm* **2004,** *25* (14), 1283-1297.
77. Bielawski, C. W.; Grubbs, R. H., Living ring-opening metathesis polymerization. *Prog Polym Sci* **2007,** *32* (1), 1-29.
78. Herisson, J. L.; Chauvin, Y., Transformation Catalysis of Olefins by Tungsten Complexes .2. Telomerization of Cyclic Olefins in Presence of Acyclic Olefins. *Makromolekul Chem* **1971,** *141* (Feb9), 161-&.
79. Benedicto, A. D.; Claverie, J. P.; Grubbs, R. H., Molecular-Weight Distribution of Living Polymerization Involving Chain-Transfer Agents - Computational Results, Analytical Solutions, and Experimental Investigations Using Ring-Opening Metathesis Polymerization. *Macromolecules* **1995,** *28* (2), 500-511.
80. Chen, Z. R.; Claverie, J. P.; Grubbs, R. H.; Kornfield, J. A., Modeling Ring-Chain Equilibria in Ring-Opening Polymerization of Cycloolefins. *Macromolecules* **1995,** *28* (7), 2147-2154.

81. Flory, P. J., Molecular size distribution in ethylene oxide polymers. *J Am Chem Soc* **1940,** *62*, 1561-1565.
82. Webster, O. W., Living Polymerization Methods. *Science* **1991,** *251* (4996), 887-893.
83. Natta, G.; Pino, P.; Corradini, P.; Danusso, F.; Mantica, E.; Mazzanti, G.; Moraglio, G., Crystalline High Polymers of Alpha-Olefins. *J Am Chem Soc* **1955,** *77* (6), 1708-1710.
84. Ziegler, K.; Holzkamp, E.; Breil, H.; Martin, H., The Mulheim Normal Pressure Polyethylene Process. *Angewandte Chemie-International Edition* **1955,** *67* (19-2), 541-547.
85. Grubbs, R. H.; Wenzel, A. G., *Handbook of Metathesis, Volume 1: Catalyst Development and Mechanism*. Wiley: 2015.
86. Fischer, E. O.; Maasbol, A., On Existence of Tungsten Carbonyl Carbene Complex. *Angewandte Chemie-International Edition* **1964,** *3* (8), 580-&.
87. Tebbe, F. N.; Parshall, G. W.; Reddy, G. S., Olefin Homologation with Titanium Methylene-Compounds. *J Am Chem Soc* **1978,** *100* (11), 3611-3613.
88. Schrock, R. R.; Fellmann, J. D., Multiple Metal-Carbon Bonds .8. Preparation, Characterization, and Mechanism of Formation of Tantalum and Niobium Neopentylidene Complexes, M(Ch2cme3)3(Chcme3). *J Am Chem Soc* **1978,** *100* (11), 3359-3370.
89. Rocklage, S. M.; Fellmann, J. D.; Rupprecht, G. A.; Messerle, L. W.; Schrock, R. R., Multiple Metal-Carbon Bonds .19. How Niobium and Tantalum Complexes of the Type-M(Chcme3)(Pr3)2cl3 Can Be Modified to Give Olefin Metathesis Catalysts. *J Am Chem Soc* **1981,** *103* (6), 1440-1447.
90. Schrock, R. R.; Murdzek, J. S.; Bazan, G. C.; Robbins, J.; Dimare, M.; Oregan, M., Synthesis of Molybdenum Imido Alkylidene Complexes and Some Reactions Involving Acyclic Olefins. *J Am Chem Soc* **1990,** *112* (10), 3875-3886.
91. Dallasta, G.; Mazzanti, G.; Natta, G.; Porri, L., Anionic-Coordinated Polymerization of Cyclobutene. *Makromolekul Chem* **1962,** *56*, 224-227.
92. Porri, L.; Rossi, R.; Diversi, P.; Lucherin.A, Ring-Opening Polymerization of Cycloolefins with Catalysts Derived from Ruthenium and Iridium. *Makromol Chem* **1974,** *175* (11), 3097-3115.
93. Sutthasupa, S.; Shiotsuki, M.; Sanda, F., Recent advances in ring-opening metathesis polymerization, and application to synthesis of functional materials. *Polym J* **2010,** *42* (12), 905-915.
94. Gilliom, L. R.; Grubbs, R. H., Titanacyclobutanes Derived from Strained Cyclic Olefins - the Living Polymerization of Norbornene. *J Am Chem Soc* **1986,** *108* (4), 733-742.
95. Schrock, R. R.; Feldman, J.; Cannizzo, L. F.; Grubbs, R. H., Ring-Opening Polymerization of Norbornene by a Living Tungsten Alkylidene Complex. *Macromolecules* **1987,** *20* (5), 1169-1172.
96. Nguyen, S. T.; Johnson, L. K.; Grubbs, R. H.; Ziller, J. W., Ring-Opening Metathesis Polymerization (Romp) of Norbornene by a Group-Viii Carbene Complex in Protic Media. *J Am Chem Soc* **1992,** *114* (10), 3974-3975.
97. Schwab, P.; France, M. B.; Ziller, J. W.; Grubbs, R. H., A Series of Well-Defined Metathesis Catalysts - Synthesis of [Rucl2(=Chr')(Pr(3))(2)] and Its Reactions. *Angewandte Chemie-International Edition* **1995,** *34* (18), 2039-2041.
98. Scholl, M.; Ding, S.; Lee, C. W.; Grubbs, R. H., Synthesis and activity of a new generation of ruthenium-based olefin metathesis catalysts coordinated with 1,3-dimesityl-4,5-dihydroimidazol-2-ylidene ligands. *Org Lett* **1999,** *1* (6), 953-956.
99. Love, J. A.; Morgan, J. P.; Trnka, T. M.; Grubbs, R. H., A practical and highly active ruthenium-based catalyst that effects the cross metathesis of acrylonitrile. *Angewandte Chemie-International Edition* **2002,** *41* (21), 4035-4037.

100. Love, J. A.; Sanford, M. S.; Day, M. W.; Grubbs, R. H., Synthesis, structure, and activity of enhanced initiators for olefin metathesis. *J Am Chem Soc* **2003,** *125* (33), 10103-10109.
101. Karlen, T.; Ludi, A.; Muhlebach, A.; Bernhard, P.; Pharisa, C., Photoinduced Ring-Opening Metathesis Polymerization (Promp) of Strained Bicyclic Olefins with Ruthenium Complexes of the Type [(Eta(6)-Arene(1))Ru(Eta(6)-Arene(2))](2+) and [Ru(Nc-R)(6)](2+). *J Polym Sci Pol Chem* **1995,** *33* (10), 1665-1674.
102. Eivgi, O.; Phatake, R. S.; Nechmad, N. B.; Lemcoff, N. G., Light-Activated Olefin Metathesis: Catalyst Development, Synthesis, and Applications. *Accounts Chem Res* **2020,** *53* (10), 2456-2471.
103. Committee for Medicinal Products for Human Use. Guidelines for the Specification Limits for Residues of Metal Catalysts or Metal Reagents. *(European Medicines Agency)* **2008**.
104. Cho, J. H.; Kim, B. M., An efficient method for removal of ruthenium byproducts from olefin metathesis reactions. *Org Lett* **2003,** *5* (4), 531-533.
105. Wang, H.; Goodman, S. N.; Dai, Q. Y.; Stockdale, G. W.; Clark, W. M., Development of a robust ring-closing metathesis reaction in the synthesis of SB-462795, a cathepsin K inhibitor. *Org Process Res Dev* **2008,** *12* (2), 226-234.
106. Maynard, H. D.; Grubbs, R. H., Purification technique for the removal of ruthenium from olefin metathesis reaction products. *Tetrahedron Lett* **1999,** *40* (22), 4137-4140.
107. Nagarkar, A. A.; Kilbinger, A. F. M., Catalytic living ring-opening metathesis polymerization (Retracted article. See vol. 10, pg. 573, 2018). *Nat Chem* **2015,** *7* (9), 718-723.
108. Vougioukalakis, G. C., Removing Ruthenium Residues from Olefin Metathesis Reaction Products. *Chem-Eur J* **2012,** *18* (29), 8868-8880.
109. Miura, T.; Kim, S.; Kitano, Y.; Tada, M.; Chiba, K., Electrochemical enol ether/olefin cross-metathesis in a lithium perchlorate/nitromethane electrolyte solution. *Angewandte Chemie-International Edition* **2006,** *45* (9), 1461-1463.
110. Okada, Y.; Chiba, K., Electron transfer-induced four-membered cyclic intermediate formation: Olefin cross-coupling vs. olefin cross-metathesis. *Electrochim Acta* **2011,** *56* (3), 1037-1042.
111. Lu, P.; Kensy, V. K.; Tritt, R. L.; Seidenkranz, D. T.; Boydston, A. J., Metal-Free Ring-Opening Metathesis Polymerization: From Concept to Creation. *Accounts Chem Res* **2020,** *53* (10), 2325-2335.
112. Ogawa, K. A.; Goetz, A. E.; Boydston, A. J., Metal-Free Ring-Opening Metathesis Polymerization. *J Am Chem Soc* **2015,** *137* (4), 1400-1403.
113. Kovacic, S.; Slugovc, C., Ring-opening Metathesis Polymerisation derived poly(dicyclopentadiene) based materials. *Mater Chem Front* **2020,** *4* (8), 2235-2255.
114. Ruiu, A.; Sanna, D.; Alzari, V.; Nuvoli, D.; Mariani, A., Advances in the Frontal Ring Opening Metathesis Polymerization of Dicyclopentadiene. *J Polym Sci Pol Chem* **2014,** *52* (19), 2776-2780.
115. Robertson, I. D.; Dean, L. M.; Rudebusch, G. E.; Sottos, N. R.; White, S. R.; Moore, J. S., Alkyl Phosphite Inhibitors for Frontal Ring-Opening Metathesis Polymerization Greatly Increase Pot Life. *Acs Macro Lett* **2017,** *6* (6), 609-612.
116. Bedford, R. B.; Hazelwood, S. L.; Limmert, M. E., Extremely high activity catalysts for the Suzuki coupling of aryl chlorides: the importance of catalyst longevity. *Chem Commun* **2002,** (22), 2610-2611.
117. Klikovits, N.; Knaack, P.; Bomze, D.; Krossing, I.; Liska, R., Novel photoacid generators for cationic photopolymerization. *Polym Chem-Uk* **2017,** *8* (30), 4414-4421.

118. Bomze, D.; Knaack, P.; Koch, T.; Jin, H. F.; Liska, R., Radical Induced Cationic Frontal Polymerization as a Versatile Tool for Epoxy Curing and Composite Production. *J Polym Sci Pol Chem* **2016,** *54* (23), 3751-3759.
119. Akhtar, S. R.; Crivello, J. V.; Lee, J. L.; Schmitt, M. L., New synthesis of aryl-substituted sulfonium salts and their applications in photoinitiated cationic polymerization. *Chem Mater* **1990,** *2* (6), 732-737.
120. Pojman, J. A., Traveling Fronts of Methacrylic-Acid Polymerization. *J Am Chem Soc* **1991,** *113* (16), 6284-6286.
121. Bynum, S.; Tullier, M.; Morejon-Garcia, C.; Guidry, J.; Runnoe, E.; Pojman, J. A., The effect of acrylate functionality on frontal polymerization velocity and temperature. *J Polym Sci Pol Chem* **2019,** *57* (9), 982-988.
122. Nason, C.; Roper, T.; Hoyle, C.; Pojman, J. A., UV-Induced frontal polymerization of multifunctional (meth)acrylates. *Macromolecules* **2005,** *38* (13), 5506-5512.
123. Zhou, J. P.; Jia, S. J.; Fu, W. L.; Liu, Z. L.; Tan, Z. Y., Fast curing of thick components of epoxy via modified UV-triggered frontal polymerization propagating horizontally. *Mater Lett* **2016,** *176*, 228-231.
124. Lecompere, M.; Allonas, X.; Marechal, D.; Criqui, A., Versatility of Pyrylium Salt/Vinyl Ether Initiating System for Epoxide Dual-Cure Polymerization: Kick-Starting Effect of the Coinitiator. *Macromol Rapid Comm* **2017,** *38* (13).
125. Bomze, D.; Knaack, P.; Liska, R., Successful radical induced cationic frontal polymerization of epoxy-based monomers by C-C labile compounds. *Polym Chem-Uk* **2015,** *6* (47), 8161-8167.
126. Tsuchimura, T., Recent Progress in Photo-Acid Generators for Advanced Photopolymer Materials. *J Photopolym Sci Tec* **2020,** *33* (1), 15- 26.
127. https://commons.wikimedia.org/wiki/File:Simple_Periodic_Table_Chart-en.svg, **acessed 23.03.2020**.
128. Korwar, S.; Burkholder, M.; Gilliland, S. E.; Brinkley, K.; Gupton, B. F.; Ellis, K. C., Chelation-directed C-H activation/C-C bond forming reactions catalyzed by Pd(II) nanoparticles supported on multiwalled carbon nanotubes. *Chem Commun* **2017,** *53* (52), 7022-7025.
129. Li, Y.; Yantian, H.; Zaosheng, L., Wuhan University of Science and Technology, One alkyl triphenyl substituted group based phosphonium salt preparation method and application. *Patent* **2017**, CN107129511, Location in patent: Paragraph 0054-0057; 0065; 0066.
130. Michaudel, Q.; Chauvire, T.; Kottisch, V.; Supej, M. J.; Stawiasz, K. J.; Shen, L. X.; Zipfel, W. R.; Abruna, H. D.; Freed, J. H.; Fors, B. P., Mechanistic Insight into the Photocontrolled Cationic Polymerization of Vinyl Ethers. *J Am Chem Soc* **2017,** *139* (43), 15530-15538.
131. Meerwein, H.; van Emster, K., Balanced isomers between bornyl chloride, isobornyl chloride and camphene chlorohydrate. *Ber Dtsch Chem Ges* **1922,** *55*, 2500-2528.
132. Jung, M. E.; Lagoutte, R.; Jahn, U., Triphenylcarbenium Tetrafluoroborate. In *Encyclopedia of Reagents for Organic Synthesis*, 2011.
133. Karim, A.; Schulz, N.; Andersson, H.; Nekoueishahraki, B.; Carlsson, A. C. C.; Sarabi, D.; Valkonen, A.; Rissanen, K.; Grafenstein, J.; Keller, S.; Erdelyi, M., Carbon's Three-Center, Four-Electron Tetrel Bond, Treated Experimentally. *J Am Chem Soc* **2018,** *140* (50), 17571-17579.
134. Kraus, C. A.; Foster, L. S., Some phenylgermanium derivatives. *J Am Chem Soc* **1927,** *49*, 457-467.

135. Olah, G. A.; Laali, K. K.; Wang, Q.; Prakash, G. K. S., *Onium Ions*. Wiley: Hoboken, 1998; p 391-424.
136. Edlund, U.; Arshadi, M.; Johnels, D., Direct Nmr Spectroscopic Evidence for Solvated Triorganostannyl Cations. *J Organomet Chem* **1993,** *456* (1), 57-60.
137. Mckinney, R. J.; Nugent, W. A., Lewis Acid Effects on Selectivity in Nickel-Catalyzed Pentenenitrile Hydrocyanation - Triorganotin Salts as Tunable Lewis Acid Promoters. *Organometallics* **1989,** *8* (12), 2871-2875.
138. Chambers, R. F.; Scherer, P. C., Phenyltin compounds. *J Am Chem Soc* **1926,** *48* (1), 1054-1062.
139. Olah, G. A.; Laali, K. K.; Wang, Q.; Prakash, G. K. S., *Onium Ions*. Wiley: 1998; p 4-95.
140. Olah, G. A.; Watkins, M., Fluorinations with Pyridinium Polyhydrogen Fluoride Reagent - 1-Fluoroadamantane. *Org Synth* **1988,** *50-9*, 628-631.
141. Boyer, N. E., Methoden der organischen chemie (houben–weyl) vol. xii, part I. Organische phosphorverbindungen, K. Sasse, E. Muller, Editors, Georg Thieme Verlag, Stuttgart, 1963. Lxxii 683 pp., DM 166; dm 149.40 for subscribers. *Journal of Polymer Science Part A: General Papers* **1965,** *3* (6), 2383-2385.
142. Schmidbaur, H., Trimethylphosphonium Methylide (Trimethyl Methylenephosphorane). In *Inorganic Syntheses*, 1978; pp 135-140.
143. Takuma, K.; Takata, T.; Endo, T., Cationic polymerization of epoxide with benzyl phosphonium salts as the latent thermal initiator. *Macromolecules* **1993,** *26* (4), 862-863.
144. Atmaca, L.; Kayihan, I.; Yagci, Y., Photochemically and thermally induced radical promoted cationic polymerization using allyl phosphonium salts. *Polymer* **2000,** *41* (16), 6035-6041.
145. TETSUO, K.; YOSHIO, A., COMPOUND, LIQUID CRYSTAL COMPOSITION, AND DISPLAY ELEMENT *Patent* **2017**, Location in patent: Paragraph 0102-0104.
146. Mathey, F.; D., V.; J.-N., V.; J.-L., P., Science of Synthesis, Compounds with One Saturated Carbon Heteroatom Bond, Product Class 12: Alkylphosphonium Salts. *General Review* **2009,** *42*, 503-594.
147. Pan, B.; Gabbaï, F. P., [Sb(C6F5)4][B(C6F5)4]: An Air Stable, Lewis Acidic Stibonium Salt That Activates Strong Element-Fluorine Bonds. *J Am Chem Soc* **2014,** *136* (27), 9564-9567.
148. Ma, Y. Q.; Li, J. S.; Xuan, Z. N.; Liu, R. C., Synthesis, characterization and antitumor activity of some arylantimony triphenylgermanylpropionates and crystal structures of Ph3GeCH(Ph)CH2CO2SbPh4 and [Ph3GeCH2CH(CH3)CO2](2)Sb(4-ClC6H4)(3). *J Organomet Chem* **2001,** *620* (1-2), 235-242.
149. Matano, Y.; Shinokura, T.; Yoshikawa, O.; Imahori, H., Triaryl(1-pyrenyl)bismuthonium salts: Efficient photoinitiators for cationic polymerization of oxiranes and a vinyl ether. *Org Lett* **2008,** *10* (11), 2167-2170.
150. Solyntjes, S.; Neumann, B.; Stammler, H. G.; Ignat'ev, N.; Hoge, B., Bismuth Perfluoroalkylphosphinates: New Catalysts for Application in Organic Syntheses. *Chem-Eur J* **2017,** *23* (7), 1568-1575.
151. Challenger, F.; Wilkinson, J. F., Organo-derivatives of bismuth. Part V. The stability of halogen, cyano-, and thiocyanoderivatives of tertiary aromatic bismuthines. *J Chem Soc* **1922,** *121*, 91-104.
152. Matano, Y.; Begum, S. A.; Miyamatsu, T.; Suzuki, H., A new and efficient method for the preparation of bismuthonium and telluronium salts using aryl- and alkenylboronic acids. First observation of the chirality at bismuth in an asymmetrical bismuthonium salt. *Organometallics* **1998,** *17* (20), 4332-4334.

153. Meerwein, H.; Hinz, G.; Hofmann, P.; Kroning, E.; Pfeil, E., The tertiary oxonium salts, I. *J Praktische Chemie* **1937,** *147* (10/12), 257-285.
154. Nesmeianov, A. N.; Tolstaia, T. P., Triphenyloxonium Salts. *Dokl Akad Nauk Sssr+* **1957,** *117* (4), 626-628.
155. Nesmeyanov, A. N.; Tolstaya, T. P., Salts of o,o'-diphenylenephenyloxonium ion. *Bulletin of the Academy of Sciences of the USSR, Division of chemical science* **1959,** *8* (4), 620-623.
156. Umemoto, T.; Adachi, K.; Ishihara, S., CF3 oxonium salts, O-(trifluoromethyl)dibenzofuranium salts: In situ synthesis, properties, and application as a real CF3+ species Reagent. *J Org Chem* **2007,** *72* (18), 6905-6917.
157. Olah, G. A.; Laali, K. K.; Wang, Q.; Prakash, G. K. S., *Onium Ions*. Wiley: 1998; p 150.
158. Flood, D. T., Fluorobenzene. *Org Synth* **1933,** *13*, 46-50.
159. Lecompère, M.; Allonas, X.; Maréchal, D.; Criqui, A., Versatility of Pyrylium Salt/Vinyl Ether Initiating System for Epoxide Dual-Cure Polymerization: Kick-Starting Effect of the Coinitiator. *Macromol Rapid Comm* **2017,** *38* (13), 1600660.
160. HOVIONE INTER. LTD; LEITAO, E. P. T. K., Lawrence, ELECTROPHILIC ALKYLATING REAGENTS, THEIR PREPARATION AND USE *Patent* **2012**, Location in patent: column 23.
161. lrgolic, K. J., Houben-Weyl Methods of Organic Chemistry. *Georg-Thieme Verlag, Stütgart* **1990,** *E12b*, 676-706.
162. Crivello, J. V.; Lam, J. H. W., Photoinitiated Cationic Polymerization by Triarylselenonium Salts. *J Polym Sci Pol Chem* **1979,** *17* (4), 1047-1057.
163. Gunther, W. H. H.; Nepywoda, J.; Chu, J. Y. C., Methods in Chalcogen Chemistry .5. New Reagent for Synthesis of Aromatic Tellurium Compounds. *J Organomet Chem* **1974,** *74* (1), 79-84.
164. Tsierkezos, N. G., Cyclic voltammetric studies of ferrocene in nonaqueous solvents in the temperature range from 248.15 to 298.15 K. *J Solution Chem* **2007,** *36* (3), 289-302.
165. Crivello, J. V.; Dietliker, K.; Bradley, G., *Photoinitiators for Free Radical Cationic & Anionic Photopolymerisation*. Wiley: Hoboken, New Jersey, 1999; p Chapter III, p 347 - 350.
166. Pappas, S. P., Photogeneration of Acid .6. A Review of Basic Principles for Resist Imaging Applications. *J Imaging Technol* **1985,** *11* (4), 146-157.
167. Watanabe, S.; Yamamoto, K.; Itagaki, Y.; Iwamura, T.; Iwama, T.; Kataoka, T., The first aryne evolution from the reactions of selenonium salts with aryllithiums. *Tetrahedron* **2000,** *56* (6), 855-863.
168. Fortage, J.; Peltier, C.; Nastasi, F.; Puntoriero, F.; Tuyeras, F.; Griveau, S.; Bedioui, F.; Adamo, C.; Ciofini, I.; Campagna, S.; Laine, P. P., Designing Multifunctional Expanded Pyridiniums: Properties of Branched and Fused Head-to-Tail Bipyridiniums. *J Am Chem Soc* **2010,** *132* (46), 16700-16713.
169. Malik, M. S.; Schlogl, S.; Wolfahrt, M.; Sangermano, M., Review on UV-Induced Cationic Frontal Polymerization of Epoxy Monomers. *Polymers-Basel* **2020,** *12* (9).
170. Castellanos, F.; Fouassier, J. P.; Priou, C.; Cavezzan, J., Synthesis, reactivity, and properties of new diaryliodonium salts as photoinitiators for the cationic polymerization of epoxy silicones. *J Appl Polym Sci* **1996,** *60* (5), 705-713.
171. Riddlestone, I. M.; Kraft, A.; Schaefer, J.; Krossing, I., Taming the Cationic Beast: Novel Developments in the Synthesis and Application of Weakly Coordinating Anions. *Angewandte Chemie-International Edition* **2018,** *57* (43), 13982-14024.
172. Krossing, I.; Raabe, I., Noncoordinating anions - Fact or fiction? A survey of likely candidates. *Angewandte Chemie-International Edition* **2004,** *43* (16), 2066-2090.

173. Nie, J.; Kobayashi, H.; Sonoda, T., Copper(II)bis((trifluoromethyl)sulfonyl)amide. A novel Lewis acid catalyst in Diels-Alder reactions of cyclopentadiene with methyl vinyl ketone. *Catal Today* **1997,** *36* (1), 81-84.
174. Aravindan, V.; Gnanaraj, J.; Madhavi, S.; Liu, H. K., Lithium-Ion Conducting Electrolyte Salts for Lithium Batteries. *Chem-Eur J* **2011,** *17* (51), 14326-14346.
175. Antoniotti, S.; Dalla, V.; Dunach, E., Metal Triflimidates: Better than Metal Triflates as Catalysts in Organic Synthesis - The Effect of a Highly Delocalized Counteranion. *Angewandte Chemie-International Edition* **2010,** *49* (43), 7860-7888.
176. Gonsior, M.; Krossing, I.; Muller, L.; Raabe, I.; Jansen, M.; van Wullen, L., PX4+, P2X5+, and P5X2+ (X = Br, I) salts of the superweak Al(OR)(4)(-) anion [R = C(CF3)(3)]. *Chem-Eur J* **2002,** *8* (19), 4475-4492.
177. Lancaster, S. J.; Walker, D. A.; Thornton-Pett, M.; Bochmann, M., New weakly coordinating counter anions for high activity polymerisation catalysts: [(C6F5)(3)B-CN-B(C6F5)(3)](-) and [Ni{CNB(C6F5)(3)}(4)](2-). *Chem Commun* **1999,** (16), 1533-1534.
178. Zhou, J. M.; Lancaster, S. J.; Walker, D. A.; Beck, S.; Thornton-Pett, M.; Bochmann, M., Synthesis, structures, and reactivity of weakly coordinating anions with delocalized berate structure: The assessment of anion effects in metallocene polymerization catalysts. *J Am Chem Soc* **2001,** *123* (2), 223-237.
179. Messe, L.; Messe, L.; Chapelat, C.; Patel, R., Photocurable compositions for preparing abs-like articles. *US2010119835A1* **2008**.
180. Lalevée, J.; Tehfe, M.-A.; Zein-Fakih, A.; Ball, B.; Telitel, S.; Morlet-Savary, F.; Graff, B.; Fouassier, J. P., N-Vinylcarbazole: An Additive for Free Radical Promoted Cationic Polymerization upon Visible Light. *Acs Macro Lett* **2012,** *1* (7), 802-806.
181. Lapin, S. C.; Snyder, J. R.; Sitzmann, E. V.; Barnes, D. K.; Green, G. D., Stereolithography using vinyl ether-epoxide polymers. *US5437964A* **1984**.
182. Sitzmann, E. V.; Anderson, R. F.; Barnes, D. K.; Patel, A. B., Increasing the useful range of cationic photoinitiators in stereolithography. *WO1996000412A1* **1994**.
183. Brandrup, J.; Immergut, E. H.; Grulke, E. A., *Polymer Handbook, 4th Edition*. Wiley: 1999; p 438.
184. Husár, B.; Hatzenbichler, M.; Mironov, V.; Liska, R.; Stampfl, J.; Ovsianikov, A., 6 - Photopolymerization-based additive manufacturing for the development of 3D porous scaffolds. In *Biomaterials for Bone Regeneration*, Dubruel, P.; Van Vlierberghe, S., Eds. Woodhead Publishing: 2014; pp 149-201.
185. Dall'Argine, C.; Hochwallner, A.; Klikovits, N.; Liska, R.; Stampf, J.; Sangermano, M., Hot-Lithography SLA-3D Printing of Epoxy Resin. *Macromol Mater Eng* **2020,** *305* (10).
186. Klikovits, N.; Sinawehl, L.; Knaack, P.; Koch, T.; Stampfl, J.; Gorsche, C.; Liska, R., UV-Induced Cationic Ring-Opening Polymerization of 2-Oxazolines for Hot Lithography. *Acs Macro Lett* **2020,** *9* (4), 546-551.
187. Castellanos, F.; Cavezzan, J.; Fouassier, J.-P., Onium Borates/Borates of Organometallic Complexes and Cationic Initiaton of Polymerization therewith. *Patent* **1993**, 4-5.
188. Cross, D. J.; Kenny, J. A.; Houson, I.; Campbell, L.; Walsgrove, T.; Wills, M., Rhodium versus ruthenium: contrasting behaviour in the asymmetric transfer hydrogenation of alpha-substituted acetophenones. *Tetrahedron-Asymmetr* **2001,** *12* (12), 1801-1806.
189. Wang, D. X.; Garra, P.; Fouassier, J. P.; Lalevee, J., Silane/iodonium salt as redox/thermal/photoinitiating systems in radical and cationic polymerizations for laser write and composites. *Polym Chem-Uk* **2020,** *11* (4), 857-866.

190. Herzig, T.; Schreiner, C.; Gerhard, D.; Wasserscheid, P.; Gores, H. J., Characterisation and properties of new ionic liquids with the difluoromono[1,2-oxalato(2-)-O,O ']borate anion. *J Fluorine Chem* **2007,** *128* (6), 612-618.
191. Zugmann, S.; Moosbauer, D.; Amereller, M.; Schreiner, C.; Wudy, F.; Schmitz, R.; Schmitz, R.; Isken, P.; Dippel, C.; Muller, R.; Kunze, M.; Lex-Balducci, A.; Winter, M.; Gores, H. J., Electrochemical characterizaiton of electrolytes for lithium-ion batteries based on lithium difluoromono(oxalato)borate. *J Power Sources* **2011,** *196* (3), 1417-1424.
192. Lischka, U.; Wietelmann, U.; Marion, W., Lithium-bisoxalatoborat, Verfahren zu dessen Hersetllung und dessen Verwendung. *Patent* **1999**, 4, DE19829030C1.
193. Xia, L.; Lee, S.; Jiang, Y.; Xia, Y.; Chen, G. Z.; Liu, Z., Fluorinated electrolytes for li-ion batteries: The lithium difluoro (oxalato) borate additive for stabilizing the solid electrolyte interphase. *ACS omega* **2017,** *2* (12), 8741-8750.
194. Zhang, S.; Xu, C.; Jow, T. R., Metal borate synthesis process. Google Patents: 2010.
195. Ping, Q.; Xu, B.; Ma, X.; Tian, J.; Wang, B., An iron oxyborate Fe 3 BO 5 material as a high-performance anode for lithium-ion and sodium-ion batteries. *Dalton Transactions* **2019,** *48* (17), 5741-5748.
196. Li, A.; Xu, L.; Li, S.; He, Y.; Zhang, R.; Zhai, Y., One-dimensional manganese borate hydroxide nanorods and the corresponding manganese oxyborate nanorods as promising anodes for lithium ion batteries. *Nano Research* **2015,** *8* (2), 554-565.
197. Kaliner, M.; Rupp, A.; Krossing, I.; Strassner, T., Tunable Aryl Alkyl Ionic Liquids with Weakly Coordinating Tetrakis ((1, 1, 1, 3, 3, 3-hexafluoropropan-2-yl) oxy) borate [B (hfip) 4] Anions. *Chemistry–A European Journal* **2016,** *22* (29), 10044-10049.
198. Fischer, M.; Schmidtmann, M., B (C 6 F 5) 3-and HB (C 6 F 5) 2-mediated transformations of isothiocyanates. *Chem Commun* **2020,** *56* (46), 6205-6208.
199. Zhou, J.; Lancaster, S. J.; Walker, D. A.; Beck, S.; Thornton-Pett, M.; Bochmann, M., Synthesis, structures, and reactivity of weakly coordinating anions with delocalized borate structure: the assessment of anion effects in metallocene polymerization catalysts. *J Am Chem Soc* **2001,** *123* (2), 223-237.
200. Taschner, R.; Knaack, P.; Liska, R., Bismuthonium- and pyrylium-based radical induced cationic frontal polymerization of epoxides. *Journal of Polymer Science* **2021,** *59* (16), 1841-1854.
201. Mete, Y.; Seidler, K.; Gorsche, C.; Koch, T.; Knaack, P.; Liska, R., Cationic photopolymerization of cyclic esters at elevated temperatures and their application in hot lithography. *Polym Int* **2022,** *71* (9), 1062-1071.
202. Hong, S. H.; Grubbs, R. H., Highly active water-soluble olefin metathesis catalyst. *J Am Chem Soc* **2006,** *128* (11), 3508-3509.
203. Leguizamon, S. C.; Cook, A. W.; Appelhans, L. N., Employing Photosensitizers for Rapid Olefin Metathesis Additive Manufacturing of Poly(dicyclopentadiene). *Chem Mater* **2021**.
204. Wang, W. B.; Chen, M.; Pang, W. M.; Li, Y. G.; Zou, C.; Chen, C. L., Palladium-Catalyzed Synthesis of Norbornene-Based Polar-Functionalized Polyolefin Elastomers. *Macromolecules* **2021,** *54* (7), 3197-3203.
205. Liu, S. F.; Chen, Y. W.; He, X. H.; Chen, L.; Zhou, W. H., Stable Crosslinked Vinyl-Addition-Type Polynorbornene Graft Copolymer Proton-Exchange Membranes. *J Appl Polym Sci* **2011,** *121* (2), 1166-1175.
206. Rode, K.; Palomba, M.; Ortgies, S.; Rieger, R.; Breder, A., Aerobic Allylation of Alcohols with Non-Activated Alkenes Enabled by Light-Driven Selenium-pi-Acid Catalysis. *Synthesis-Stuttgart* **2018,** *50* (19), 3875-3885.

207. Hudkins, R. L.; Raddatz, R.; Tao, M.; Mathiasen, J. R.; Aimone, L. D.; Becknell, N. C.; Prouty, C. P.; Knutsen, L. J. S.; Yazdanian, M.; Moachon, G.; Ator, M. A.; Mallamo, J. P.; Marino, M. J.; Bacon, E. R.; Williams, M., Discovery and Characterization of 6-{4[3-(R)-2-Methylpyrrolidin-1-yl)propoxy]phenyl}-2H-pyridazin-3-one (CEP-26401, Irdabisant): A Potent, Selective Histamine H-3 Receptor Inverse Agonist. *J Med Chem* **2011,** *54* (13), 4781-4792.
208. Kraszkiewicz, L.; Skulski, L., Facile syntheses of symmetrical diaryliodonium salts from various arenes, with sodium metaperiodate as the coupling reagent in acidic media. *Synthesis-Stuttgart* **2008,** (15), 2373-2380.
209. Makarova, L. G.; Nesmeianov, A. N., The decomposition and formation of onium salts and the synthesis of organoelemental compounds through onium compounds. I. Two types of decomposition of diphenyliodonium salts. *Dokl Akad Nauk Sssr+* **1945,** *50*, 617-626.
210. Kharchenko, V. G.; Chalaya, S. N.; Noritsina, M. V.; Kulikova, L. K., Synthesis and antimicrobial activity of thiapyrylium salts. *Khimiko-Farmatsevticheskii Zhurnal* **1976,** *10* (1), 80-83.
211. Schlosser, M., Phosphororganische Verbindungen. I. Eine Methode Zur Darstellung Selektiv Deuterierter Verbindungen. *Chem Ber-Recl* **1964,** *97* (11), 3219.
212. Swamy, K. C. K.; Kumar, N. N. B.; Balaraman, E.; Kumar, K. V. P. P., Mitsunobu and Related Reactions: Advances and Applications. *Chem Rev* **2009,** *109* (6), 2551-2651.
213. Moiseev, D. V.; Malysheva, Y. B.; Shavyrin, A. S.; Kurskii, Y. A.; Gushchin, A. V., Study of homo- and cross-coupling competition in the reaction of triarylbismuth(V) dicarboxylates with methyl acrylate in the presence of a palladium catalyst. *J Organomet Chem* **2005,** *690* (16), 3652-3663.
214. Matano, Y.; Azuma, N.; Suzuki, H., Synthesis, X-Ray Structure and Reactions of (2-Oxoalkyl)Triarylbismuthonium Salts. *J Chem Soc Perk T 1* **1994,** (13), 1739-1747.
215. Wittig, G.; Fritz, H., *Tetraphenyl-Tellur. *Annalen Der Chemie-Justus Liebig* **1952,** *577* (1), 39-46.
216. Rainville, D. P.; Zingaro, R. A., The Reactions of Selenium Tetrachloride and Tellurium Tetrachloride with Some Trivalent Aryl Organometallic Halides. *J Organomet Chem* **1980,** *190* (3), 277-288.
217. Pchelintseva, N. V.; Chalaya, S. N.; Kharchenko, V. G., Synthesis of 2,4-Dichloro-2-Pentene-1,5-Diones. *Zh Org Khim+* **1990,** *26* (9), 1854-1856.
218. Ye, C. F.; Twamley, B.; Shreeve, J. M., Straightforward syntheses of hypervalent iodine(III) reagents mediated by selectfluor. *Org Lett* **2005,** *7* (18), 3961-3964.
219. An, Y. X.; Zuo, P. J.; Cheng, X. Q.; Liao, L. X.; Yin, G. P., The effects of LiBOB additive for stable SEI formation of PP13TFSI-organic mixed electrolyte in lithium ion batteries. *Electrochim Acta* **2011,** *56* (13), 4841-4848.
220. Lee, H. S.; Yang, X. Q.; Xiang, C. L.; McBreen, J.; Choi, L. S., The synthesis of a new family of boron-based anion receptors and the study of their effect on ion pair dissociation and conductivity of lithium salts in nonaqueous solutions. *J Electrochem Soc* **1998,** *145* (8), 2813-2818.
221. Haigh, D. M.; Kenwright, A. M.; Khosravi, E., Ring opening metathesis polymerisations of norbornene and norbornadiene derivatives containing oxygen: a study on the regeneration of Grubbs catalyst. *Tetrahedron* **2004,** *60* (34), 7217-7224.
222. Brandrup, J.; Immergut, E. H.; Grulke, E. A., *Polymer Handbook, 4th Edition*. Wiley: 1999; p II/374.
223. Abdul-Karim, R.; Hameed, A.; Malik, M. I., Ring-opening polymerization of ethylene carbonate: comprehensive structural elucidation by 1D & 2D-NMR techniques, and selectivity analysis. *Rsc Adv* **2017,** *7* (19), 11786-11795.

224. Menczel, J. D.; Prime, R. B., *Thermal Analysis of Polymers: Fundamentals and Applications*. Wiley, Hoboken, New Jersey, USA: 2014; p Chapter 2.
225. Flory, P. J., *Principles of Polymer Chemistry*. Cornell University Press: Munich, 1953.